Orebody Modelling for Exploration: The Western Mineralisation, Broken Hill

Mohammad Lotfolah Hamedani

B.S. (Honours) in Accounting
B.S. (Honours) in Mining Engineering (Exploration)
M.S. in Mining Engineering (Exploration)

Geology and Geophysics
School of Earth and Environmental Sciences
The University of Adelaide

Thesis submitted as fulfilment of the requirements for the degree of Doctor of Philosophy in the Faculty of Science, University of Adelaide

March 2011

CHAPTER 1

Regional and Local Geology and the Aims of this Study

1.1 Introduction

The world's largest Zn-Pb-Ag deposit (Figure 1.1), Broken Hill, in far western New South Wales, was discovered in September 1883 by a German noble man who called himself Charles Rasp (Sainisch-Plimer 1999). The Broken Hill orebody is in the Palaeoproterozoic Curnamona Province, formed at 1686 ± 5 Ma, underwent multiphase intense deformation and high grade metamorphism at 1600 Ma (Olarian Orogeny) and less intense metamorphism in the 500 Ma (Delamerian Orogeny). It is an 8 km long linear mass that has the shape of a boomerang that plunges both NE and SW. It crops out at the centre where some 80 Mt of sulphide rocks have been lost by weathering and erosion (Plimer 1984). The orebody has produced over 250 million tonnes of high-grade ore originally containing 28 Mt Pb, 24 Mt Zn and 1 billion oz[1] Ag with estimated revenue in today's Australian dollars of $ 300 billion. The wealth generated from Broken Hill led to the industrialisation of Australia and the formation of the world's two largest mining companies, BHP Billiton and Rio (Blainey 1968). Satellite images of the Broken Hill Mine are provided in supplementary files to this thesis.

The Broken Hill deposit is associated with hundreds of small Broken Hill-type deposits in the Willyama Supergroup (Stevens 2003). The main Broken Hill deposit and hundreds of Broken Hill-type deposits have the same lead isotope signature thereby suggesting similar formation processes (Gulson et al. 1985; Stevens 2003) whereas the small Pinnacles Zn-Pb-Ag deposit has a Pb isotope signature suggesting that it is some 10 Ma older than the main Broken Hill deposit (Parr, Stevens & Carr 2003) yet formed by the same process. The Broken Hill ore deposit is in a world-class metallogenic province wherein there more than 4,000 pits and shafts have been sunk for a diversity of commodities such as Zn, Pb, Ag, Cu, Au, W, Sn, Be, U and non-metallic minerals. The world's largest zinc-lead deposit is in a province where most rocks are enriched in Zn and Pb, sulphide deposits of a number of types are common and soils derived from sulphide-bearing rocks and silicate rocks produce a metal-enriched regolith.

[1] **Ounces**

Figure 1.1: Contained grade and tonnage of metals for stratiform Zn-Pb deposits. The Broken Hill deposit is the largest Zn-Pb known deposit in the world (redrawn from Large et al. 2005).

1.2 Curnamona Province

The Curnamona Province extends across eastern South Australia and western New South Wales (Figure 1.2). It is ovoid in shape, has an area of about 50,000 km^2 and is divided into eight domains (Conor & Preiss 2008). It comprises Palaeoproterozoic metasediments, metavolcanics and chemical metasediments (Willyama Supergroup) intruded by early Mesoproterozoic granites and, in places, covered by early Mesoproterozoic volcanic rocks (Robertson et al. 1998). Neoproterozoic sequences unconformably overlie the older rocks of the Curnamona Province. There is a temporal stratigraphic correlation (~1720–1640 Ma) between the Broken Hill and the Olary Domains and many geochronological studies have correlated stratigraphic units between the two Domains (e.g. Clarke, Burg & Wilson 1986; Willis et al. 1983).

Figure 1.2: The eight Domains of the Curnamona Province (from Conor et al. 2006).

PIRSA have compiled 1:25,000 sheets of the Olary Domain collated from a 10-year integrated 1:10,000 outcrop lithological and structural mapping program by honours students from The University of New England, The University of Newcastle and The University of Melbourne. There has been limited mapping of the Moolawatana Domain by students and much of the mapping has been undertaken by Teale (unpublished). Because of the lack of detailed geochronological information and absence of some important stratigraphic successions of the Broken Hill Group within the Olary Domain (e.g. Parnell Formation; Freyers Metasediments; Hores Gneiss; Figure 1.3; Page et al. 2005), the stratigraphic correlations are somewhat loose. It is the unit that contains Broken Hill-type mineralisation that is absent from the Olary Domain and possibly the Moolawatana Domain.

With U-Pb geochronological dating of detrital zircon, the age constraints of depositional sediments and important magmatic and metamorphic events are limited to predominantly felsic rocks and the timing of mafic rocks may not be determined precisely as some may be intrusive (Yamashita, Creaser & Villeneuve 2000). This is the case in the

Broken Hill Domain. A combination of Sm-Nd isotope and monazite U-Pb with the detrital zircon U-Pb dating may provide more accurate age constraint. The Willyama Supergroup in the south Curnamona Province is divided on lithological and geophysical characteristics into the Olary, Broken Hill and Redan Domains (Conor et al. 2006; Figure 1.2).

The Broken Hill Domain has few intercalated metavolcanics from top to bottom of the stratigraphy and has undergone several intense Olarian (~1600 Ma) deformation events coeval with high-grade metamorphism and, accordingly, a precise age for the stratigraphic sequence of the Willyama Supergroup is difficult to determine with great accuracy.

Figure 1.3: Stratigraphy and geochronology of the exposed Willyama Supergroup in the Broken Hill Block, Euriowie Block and Redan Sub-Block. The Parnell Metadolerites are dated at 1686 Ma (from Stevens 2009).

Some different stratigraphic successions in the Broken Hill Domain have overlapping detrital zircon ages, despite the fact that they are not juxtaposed. This may indicate unconformities. For example, quartz-albite rocks sequences of the Himalaya Formation in the Thackaringa Group have overlapping detrital zircon ages with major granitic gneiss sills adjacent to the Broken Hill ore deposit yet the two units are spatially separate (Raetz, Krabbendam & Donaghy 2002). Inherited refractory zircon cores in magmatic zircon grains result from partial to complete melting of older sediments or magmatic rocks. The dominant population of inherited zircon ages derive from weathering of older source rocks, magmatism or xenocrysts hence the maximum age of deposition cannot be precisely constrained because there is no certainty that the samples analysed contain the youngest zircon present in a population (Page & Laing 1992). Although unconformities, disconformities and layer-parallel thrusts have not been recognised at Broken Hill, this does not mean they do not exist. Notwithstanding these limitations, for the purposes of this study, the Broken Hill Domain geochronology used is that of Raetz, Krabbendam & Donaghy (2002) is used.

The Geological Survey of New South Wales constructed a stratigraphy and later validated this with geochronology (Figure 1.3). This stratigraphy is constantly being revised (albeit slightly), has a predictive basis and can be used in the field. Its strengths are that the mapping was fact outcrop mapping done by an integrated team who used the same lithological nomenclature. Because of lack of exposed basement and erosion of the top of the Willyama Supergroup in the Broken Hill Domain, its overall thickness is not known precisely and it is estimated between 6-7 km (Stevens et al. 1983; Willis et al. 1983). SHRIMP geochronological studies of detrital zircons (Page et al. 2005; Page & Laing 1992; Page, Stevens & Gibson 2005; Raetz, Krabbendam & Donaghy 2002) and stratigraphy (Willis et al. 1983) show deposition of the Willyama Supergroup took place from $\leq$ 1710 Ma at the base to $\leq$ 1642 $\pm$ 5 Ma at the top (Nutman & Gibson 1998; Page, Stevens & Gibson 2005; Stevens 2000; Stevens et al. 1988).

The weakness of the NSW Geological Survey stratigraphic mapping is that there was no structural mapping hence deformational interpretation is based on lithology and not measured structural fabrics. Furthermore, the Parnell Formation was mapped as a stratigraphic unit rather than Allendale Metasediments intruded by mafic sills at a

buoyancy level. However, the mafic rocks which define the Parnell Formation are intrusive (James, Pearce & Oliver 1987; Phillips, Archibald & Wall 1985; Stevens 2009). Stevens (1998) argued that it is not clear whether the amphibolite rocks of the Parnell Formation occurred during deposition of the Willyama Supergroup or younger deposition or whether the amphibolite rocks are related to sub-volcanic events. More recent geochronology shows that the amphibolites of the Parnell Formation (Figure 1.3) were intruded as high Fe- and Ti-tholeiitic basalts (Raveggi et al. 2007) into wet sediments at 1685 ± 5 Ma thereby establishing geothermal systems (Plimer 2006b; Stevens 2003).

1.3 The Willyama Supergroup

Over a fifteen-year period, the Geological Survey of New South Wales mapped the Broken Hill Domain at 1:12,500 scale maps and published geological maps at 1:25,000 scale. Supporting geophysical, regolith, metallogenic and summary maps were published at 1:25,000, 1:50,000, 1: 100,000, 1:250,000 and 1:1,000,000 scales. The Willyama Supergroup in the Broken Hill Domain is dominated by rocks interpreted as metamorphosed highly deformed clastic metasediments (Andrews 1922; Gustafson, Burrell & Garretty 1950; Willis et al. 1983) that formed in an intra-continental rift succession (Willis et al. 1983). The metasediments show features interpreted as sedimentary structures such as bedding, graded bedding, cross bedding, ripples and pull-apart structures (Laing, Marjoribanks & Rutland 1978; Slack et al. 1993; Willis et al. 1983). The metasediments are intruded by pre-, syn- to post-deformational felsic and mafic magmatic rocks and, where magmatism is bimodal at 1686 ± 5 Ma, there are occurrences of Broken Hill-type Zn-Pb-Ag mineralisation and associated pre-metamorphic alteration (Conor & Preiss 2008; Parr & Plimer 1993; Phillips, Archibald & Wall 1985; Plimer 1975, 1986).

The Broken Hill orebody is hosted by the Broken Hill Group, a unit that varies in thickness from 300 to 2000 m, but mostly between 1000 m and 1500 m. The depositional age of the Broken Hill Group is estimated between the ages of the Plumbago Formation (1693 ± 3 Ma) in the Olary Domain and the Hores Gneiss (1685 ± 3 Ma) in the Broken Hill Group (Page et al. 2005). The main conclusions from studies of the Broken Hill Domain (Conor & Preiss 2008; Laing 1996a; Phillips, Archibald & Wall 1985; Plimer 1985; Slack & Stevens 1994; Stevens 1986; Stevens et al. 1988; Willis et al. 1983) were that the Broken Hill orebody was deposited in a deep-water intra-cratonic rift.

Since that time, Stevens (2003), Feldman (2004), Plimer (2006b) and Damm (2008) have reinterpreted the area as a shallow water intra-continental rift setting on the basis of detailed sequence stratigraphy of the metasediments. Plimer (2006b) suggested that the depositional setting was a shallow fresh water intra-cratonic continental rift lake. Outside the precinct of the orebody, the uppermost unit of the Broken Hill Group (Hores Gneiss) is dominated by felsic gneiss whereas the Hores Gneiss enclosing the Broken Hill orebody is thicker, dominated by clastic metasediments and has very minor units of felsic gneiss. This may support the view that the Broken Hill orebody formed in a depression or rift (Plimer 2006b). Although major transgressive retrograde shear zones were mapped, it is surprising that no thrusts were recognised because it is expected that nappe (F_1; Laing, Marjoribanks & Rutland 1978) and isoclinal (F_2; Laing, Marjoribanks & Rutland 1978) folding would produce thrusts.

1.4 The Broken Hill ore deposit

The Broken Hill ore deposit is hosted by metasediments that have undergone variable degrees pre-metamorphic hydrothermal alteration to quartz-, garnet- and gahnite[2]-rich assemblages (Groves et al. 2008; Haydon & McConachy 1987; Heimann et al. 2009; Plimer 1979). The initial fluid conduit for the Broken Hill ore deposit is in the southern part of the field between The Zinc Corporation and New Broken Hill Consolidated Mines (Groves et al. 2008; Plimer 1979). The ore deposit (Figure 1.4) comprises the following Lodes and Lenses:

- **C Lode:** a Zinc Lode and a transgressive footwall alteration zone (Groves et al. 2008; Plimer 1979),
- **B Lode:** a basal Zinc Lode (Groves et al. 2008; Hodgson 1974; Johnson & Klingner 1975; Plimer 1979; Segnit 1961; Stilwell 1959),
- **A Lode:** two manganoan Zinc Lodes (Groves et al. 2008; Johnson & Klingner 1975; Plimer 1979),
- **1 Lens:** a Zinc orebody (Groves et al. 2008; Johnson & Klingner 1975),
- **2 Lens:** a Lead orebody (Groves et al. 2008; Johnson & Klingner 1975; Mackenzie 1968; Plimer 1979), and

[2] **(Zn, Fe) Al_2O_4**

- **3 Lens:** a Lead orebody and an upper most mass (Groves et al. 2008; Johnson & Klingner 1975; Plimer 1979).

In Broken Hill, the Silver City, was established on the secondary silver ore derived from 2 and 3 Lens and it was only late in the history that the Zinc Lodes were exploited. Stratigraphically equivalent to the Zinc Lodes is the Western Mineralisation, a poorly defined low- to medium-grade sulphide mass discovered in 1913 by BHP[3] (Blampain & Plimer 2006; Gentle 1968; Plimer 2006b). In the 1950s, Broken Hill South cut a haulage drive from Browne Shaft to No 7 Shaft through the Western Mineralisation for sampling, drilling and access and, in the 1970s, MM&M[4] Ltd. extracted a 1,500 tonne Western Mineralisation ore parcel for trial milling. Stratigraphically equivalent to the Western Mineralisation on the eastern limb of the Broken Hill Antiform is a quartz-, garnet-, gahnite and sulphide-bearing zone (Eastern Mineralisation) that has yet to be explored (Plimer 2006b). It is the Western Mineralisation that is the subject of this study, it is open at depth, it has high-grade zones, possibly at zones of dilation (Plimer 2006b) to the south and to the north and mining will commence in 2011 at the CBH Resources Ltd Rasp Mine. B Lode, A Lode, 2 Lens and 3 Lens comprise the greatest tonnage of sulphide rocks at Broken Hill (Table 1.1).

Table 1.1: Size and grades of the Broken Hill orebodies and the Western Mineralisation (Plimer 2006b; Stevens 2003).

Orebody	Tonnage	Lead grade	Zinc grade	Silver grade
3 Lens	79 Mt	14 % Pb	14 % Zn	250 g/t Ag
2 Lens	85 Mt	14 % Pb	11 % Zn	100 g/t Ag
1 Lens	10 Mt	8 % Pb	20 % Zn	50 g/t Ag
A Lode	53 Mt	4 % Pb	10 % Zn	40 g/t Ag
B Lode	46 Mt	5 % Pb	17 % Zn	40 g/t Ag
C Lode	11 Mt	3 % Pb	5 % Zn	20 g/t Ag
The Western Mineralisation	17 Mt	2.2 % Pb	3.2% Zn	28 g/t Ag

[3] **Broken Hill Proprietary Company**
[4] **Minerals, Mining and Metallurgy Limited**

NOTE:
This figure is included on page 9 of the print copy of the thesis held in the University of Adelaide Library.

Figure 1.4: Open pits on CML7[5] from which carbonate, sulphate and sulphide ores were extracted from 1883-2001 (from CBH Resources Ltd).

The BHP open pit is adjacent to Delprat Shaft and the Block 14 Pit is immediately SW of the Blackwood Pit. During the 1980s, secondary minerals were mined from Kintore, Block 14 and Blackwood Pits and primary sulphide ores were mined from No 7 Shaft, Blackwood Pit and Browne Shaft. Tribute mining in the 1990s of secondary and primary minerals in Block 14 Pit was undertaken by Mr. Craig Williams of Pinnacles Mines Pty Ltd. This study concentrates on the upper part of the Western Mineralisation on CML7.

1.4.1 Mine sequence stratigraphy

A different stratigraphy for the metasediments enclosing the Broken Hill orebody has been compiled by the mining companies because the regional geological mapping was not undertaken in the mines area, the scale of regional mapping was different from the scale of mapping in the mines area and there are subtle facies relationships associated with the Broken Hill orebodies, although hosted by recognisable stratigraphic units (Tables 1.2 and 1.3). Geological cross-sections of the Broken Hill orebodies have been provided in supplementary files to this thesis. The Broken Hill orebodies occur in Unit 4.7 and

[5] **Consolidated Mining Lease Number 7 or the Broken Hill Rasp Project**

there is substantial pre-metamorphic hydrothermal alteration of Units 4.6 - 4.1 with known orebodies and mineralisation in Units 4.5 and 3.5 and widespread Broken Hill-type mineralisation in Units 4.6, 4.5, 4.4, 4.3 and 4.1 (Plimer 2006b). In the Broken Hill Mines area, sulphide rocks are present at the tops of Units 4.7, 4.5, 4.4, 4.3 and 4.1 with the main Broken Hill Lodes present in Unit 4.7. There are minor iron formations in Units 4.6 and 4.8 which are oxidative facies before and after sulphide rock deposition in Unit 4.7.

Table 1.2: Regional and mine stratigraphic subdivisions of the Willyama Supergroup (from CBH Resources Ltd).

Table 1.3: Summary of Units 4.8, 4.7 and 4.6 in Suite 4, average unit thickness and range of unit thickness (simplified from Haydon & McConachy 1987).

NOTE:
This table is included on page 11 of the print copy of the thesis held in the University of Adelaide Library.

There have been a number of attempts to understand the depositional environment of the Broken Hill Domain (Slack & Stevens 1994; Willis et al. 1983), the southern segment of the Broken Hill orebody (Haydon & McConachy 1987) and the central

[6] Banded Iron Formation
[7] Local term for foliated garnet- K-feldspar-biotite-quartz bearing gneiss
[8] See Section 1.6.3
[9] Local term for garnet-rich K-feldspar-sillimanite-quartz bearing psammopelite
[10] Green plumbian orthoclase containing Pb in its atomic structure

segment of the Broken Hill orebody (Feldman 2004). Haydon and McConachy (1987) used conventional mining company diamond drill core logging of lithology, geotechnical and engineering aspects combined with down-hole gamma ray logging. During high grade metamorphism, there is a decrease in porosity and permeability; there is massive dewatering which removed K and U from Broken Hill rocks (Ahmad & Wilson 1982), two generations of K- and U-rich pegmatites formed during the Olarian Orogeny (Laing, Marjoribanks & Rutland 1978) and retrogression has resulted in the removal of K (Phillips 1980). Despite these problems, Haydon and McConachy (1987) were able to validate the stratigraphy obtained from conventional logging and they suggested that the Broken Hill orebody formed by the replacement of shallow water deltaic sediments.

In the Western Mineralisation, metasediments show sharply truncated graded bedded stratigraphy, characterised by coarse grained sillimanite-almandine[11] at the top and fine grained quartz-feldspar at the base. Kitchen (2001) showed from only one Western Mineralisation diamond drill core that the thickness of metapsammitic beds increased up stratigraphy beneath the Western Mineralisation. Feldman (2004) tried a more conventional sequence stratigraphic approach and measured the $\frac{\text{metapelite}}{\text{metapsammite}}$ ratio metre-by-metre in 20 Western Mineralisation diamond drill cores. Feldman's work was limited by the number of available drill cores at the time; he attempted to establish structure contours for one of the stratigraphic marker horizons (Unit 4.6 metapelite) and attempted to deduce the environment of deposition for the sequences beneath the Broken Hill orebody.

Despite limited data, Feldman (2004) concluded that there were three upward-coarsening sediment cycles in the Broken Hill Group and that metapsammite horizon also became thicker towards the top of each cycle. This has been validated by additional core logging by Plimer (2006b) and Damm (2008). Massive metapelite of Unit 4.6 is characterised by high a Al content (crenulated sillimanite, biotite, almandine), no quartz and no feldspar. Unit 4.6 metapelite is used as sedimentary marker horizon (Blampain & Plimer 2006; Haydon & McConachy 1987; Plimer 2006b). It contains a remarkably stratigraphically continuous thin marker BIF with quartz, almandine, magnetite, gahnite, hyalophane and sulphides. The stratigraphic bottom of Unit 4.6 (and 4.8) is very sharp boundary and it is different from other lithological boundaries in the Broken Hill Group

[11] $Fe_3Al_2(SiO_4)_3$

which tend to be gradational or cyclical. This suggests a sudden change in depositional environment which may be coincident with sudden deepening, formation of depositional basin, intrusion of amphibolite and the establishment of geothermal system (Plimer 2006b).

1.4.2 Rock types of the Broken Hill ore deposit

1.4.2.1 Metasediments

Metasediments of the Broken Hill deposit comprise metamorphosed clastic sedimentary rocks with minor chemical sediments such as chert, oxide-facies, BIF, pelite, psammite, psammopelite, much interlamination, bedding, graded bedding and other sedimentary structures. Major metasediments of the Broken Hill Group contain HFSE[12], Y[13] and REEs[14] that originated from the erosion of anorogenic granite and rhyolitic to rhyodacitic rocks with A type chemistry (Slack & Stevens 1994). Local stratigraphic sequences of quartz-feldspar ± biotite ± garnet gneisses in the Broken Hill Group (e.g. Potosi-type gneiss) are assumed as source of the metasediment (Slack & Stevens 1994).

In Broken Hill region, Hores Gneiss dominated by felsic gneiss (Stevens & Barron 2002) whereas, in the mines area, the Hores Gneiss dominated by upward coarsening cycles of sediments and very minor felsic gneiss. This suggests that the mines area was a topographic low, graben or rift into which clastic sediment was deposited whereas the Hores Gneiss in the Broken Hill region was an area with little clastic deposition. The main constituents of metapelite, metapsammites and metapsammopelites in the Broken Hill comprises sillimanite, quartz, biotite, ± garnet, ± K-feldspar, ± plagioclase and ± cordierite. These rocks are more chloritised down-hole (i.e. up stratigraphy). Metapelites contain much more sillimanite and mica in comparison with metapsammopelite and metapsammites.

1.4.2.2 Pegmatite

The main constituents of pegmatites comprise quartz, ± feldspar (plagioclase and K-feldspar), ± garnet, ± biotite, ± chlorite, ± plumbian orthoclase. Pegmatites may be foliated, unfoliated, boudinaged and brecciated.

---

[12] **High Field Strength Elements**
[13] **Yttrium**
[14] **Rare Earth Elements**

1.4.2.3 Lode horizon rocks

Lode horizon rocks typically comprise the following rock types:

1. Blue quartz lode comprising blue quartz, ± gahnite, ± minor garnet,

2. Quartzite lode comprising quartz , ±gahnite, ± garnet, ± feldspar, ± biotite and ± tourmaline, and

3. Garnet quartzite, garnetite and garnet envelope (Spry & Wonder 1989; Wonder, Spry & Windom 1988, p.228), medium-coarse grained rocks contains Mn-rich almandine, ± gahnite, ± biotite and ± feldspar. The altered garnet-bearing rocks contain a variety of minerals such as blue quartz, hedenbergite[15], gahnite and sulphide minerals.

A package of metasediment, garnet quartzite, garnetite, blue quartz-gahnite lode and pegmatite are spatially associated with all sulphide orebodies of the Broken Hill deposit (Burton 1998; Johnson & Klingner 1975).

1.4.2.4 Amphibolite

Amphibolites were high Fe- and Ti-tholeiitic basalts typical of triple point magmas in the mid ocean ridge and they show in situ differentiation (Brick 2005; Brown et al. 1983; James, Pearce & Oliver 1987) from feldspathic tops to more mafic base in accord with younging directions in the metasediments. Amphibolites have also undergone pre-metamorphic hydrothermal alteration (Phillips, Archibald & Wall 1985).

1.4.2.5 Potosi Gneiss

Potosi Gneiss is a local name for foliated garnet-feldspar-biotite-quartz bearing gneiss (Raetz, Krabbendam & Donaghy 2002). It occurs in both Unit 4.4 and 4.7. Plimer (2006b) argued that Potosi Gneiss proximal to the Broken Hill mines may be an altered rock in comparison with other lithological units of Hores Gneiss in Unit 4.7. In Broken Hill Mine, there is trend from the garnet-bearing feldspathic psammite and the garnet-plagioclase gneiss into blue quartz -garnet ± biotite ± pyrrhotite ± chalcopyrite rock. The Potosi Gneiss appears in the lowermost part of the Parnell Gneiss which overlies the Allendale Metasediments and is overlain by the Freyers Metasediments (Conor & Preiss 2008).

---

[15] $CaFeSi_2O_6$

1.5 Tectonism

1.5.1 Olarian Orogeny

In the Olarian Orogeny (Tables 1.4 to 1.6), F_1 folds are nappe-like isoclinal folds with rarity of hinges and well-developed high grade metamorphism (M_1) and axial plane schistosity (S_1) (Hobbs et al. 1984; Laing 1996b; Laing, Marjoribanks & Rutland 1978; Marjoribanks et al. 1980; Plimer 2006b; Stevens 1986; Willis et al. 1983). The F_1-M_1 age is the same in the Broken Hill, Olary and Moolawatana Domains suggesting that the Olarian Orogeny was a widespread regional event. Pegmatites and granites (especially in the Olary Domain) show that there was melting but there may have been less melting in the Broken Hill Domain because the rocks are higher metamorphic grade hence more anhydrous (Phillips 1980; Stevens 1986). Some minor granitic rocks in the Euriowie Inlier of the Broken Hill Domain show low metamorphic grade.

Table 1.4: Summary of the major deformation (D), metamorphism (M), schistosity (S) and P-T conditions during D_1 and D_2 of the Olarian Orogeny.

Event Name	Event label	Deformation features	Structure and foliation	Mineral assemblage	P-T conditions
Olarian Orogeny (~1600-1500 Ma) (White et al. 1995)	D_1 / M_1 1600 Ma (Page & Laing 1992; Stevens 1999)	Appearance of regional nappe-like isoclinal folds F_1 (Hobbs et al. 1984; Laing 1996b; Laing, Marjoribanks & Rutland 1978; Marjoribanks et al. 1980; Plimer 2006b; Stevens 1986; Willis et al. 1983). Pegmatite intrusion cross cutting Lode horizon (Morland & Webster 1998; Webster 1996).	Axial plane schistosity (S_1) parallel to bedding within-metapelite and metapsammopelite (Laing, Marjoribanks & Rutland 1978; Morland & Webster 1998) Weak foliation in psammitic rocks.	Sillimanite-garnet-quartz feldspar	Max. T=750-800°C and P=5-6 kbar (Phillips 1980; Stevens 1986)

F_2 folds are open isoclinal form coeval high grade metamorphism resulting in axial plane S_2 sillimanite and crenulations of S_1 sillimanite (Laing, Marjoribanks & Rutland 1978) at 1600-1590 Ma (Page & Laing 1992). Harrison and McDougall (1981) and Lu et al. (1996) report an Ar age of about 1250 Ma that suggests a thermal event for the Broken Hill and the Olary Domains respectively. However, no associated deformation event has been recognised. The thermal system is an enigmatic regional event (because it appeared in the Broken Hill and the Olary Domains) and many ages could have been reset in the 500 Ma Delamerian Orogeny.

Table 1.5: Summary of the major deformation (D), metamorphism (M), schistosity (S) and P-T conditions during D_2 of the Olarian Orogeny.

Event Name	Event label	Deformation features	Structure and foliation	Mineral assemblage	P-T conditions
Olarian Orogeny (~1600-1500 Ma) (White et al. 1995)	D_2 / M_2 (~1600-1590 Ma) (Nutman & Ehlers 1998; Page & Laing 1992; Page, Stevens & Gibson 2000)	Macroscopic and microscopic upright folding (Laing, Marjoribanks & Rutland 1978; Webster 1996). Intrusion of pegmatite during D_2	Appearance of three major F_2 folds within the mines site: The Hanging Wall Synform, the Broken Hill Antiform and the Broken Hill Synform (Laing, Marjoribanks & Rutland 1978) Development of foliation (sillimanite) and lineation in high-grade ore zones within droppers[16] (Hodgson 1974; Maiden 1975; Webster 1993). Refolding of pegmatites of D_1 by F_2 and development of S_2 axial plane pegmatite (Laing, Marjoribanks & Rutland 1978).	Sillimanite-garnet-quartz feldspar	Max. T=750-800°C and Max. P=5-6 kbar (Phillips 1980; Stevens 1986).

[16] A local term to describe a sulphide projection up or down the axial plane schistosity

F_3 folds are coeval lower grade metamorphism because of occurrence of muscovite-defined schistosity suggesting isobaric cooling (Page & Laing 1992; Stevens 1986). Haydon and McConachy (1987) and Laing (1996b) suggest F_3 remobilised sulphides whereas Plimer (1984) suggests that F_3 is the last phase whereby there is major sulphide remobilisation were remobilised in even later events.

Table 1.6: Summary of the major deformation (D), metamorphism (M), schistosity (S) and P-T conditions during D_3 of the Olarian Orogeny.

Event Name	Event label	Deformation features	Structure and foliation	Mineral assemblage	P-T conditions
Olarian Orogeny (~1600-1500 Ma) (White et al. 1995)	D_3 (1556 ±10 Ma) (Tonelli, Woodhead & Hergt 2003)	Development of minor F_3 folds with open to monoclinal folds close to retrograde shear zones (White et al. 1995).	Development retrograde Shear zones (Laing, Marjoribanks & Rutland 1978). Development of the Globe Vauxhall, Retrograde British, De Bavay Shear zones (White et al. 1995) Cross cutting the Main Line of Lode (White et al. 1995) and the Main Shear (Rothery 2001)	Development of quartz, sericite and biotite assemblages within shear zones (Morland & Webster 1998).	Greenschist facies T=550-600°C and P=5-5.5 kbar (Phillips 1980)

At least two types of dolerite dykes dated at 830 Ma (dyke swarms and gabbroic intrusions) are known in the Broken Hill Domain (Stevens et al. 1988). These are the same age as the dyke swarms in South Australia (Gairdner Dyke Swarm) and the same age as the initiation of the breakup of Rodinia (Li, Zhang & Powell 1995; Zhao & McCulloch 1993). This suggests the Broken Hill and Olary Domains underwent extension at this time. In the Broken Hill orebody, drill holes have intersected epidotised tholeiitic dolerite dykes in the central part of deposit, including the Western Mineralisation, and Unit 4.7 at depth

(Plimer 2006a). The sample cores of the Western Mineralisation within Unit 4.7 shows N- and NW- trending epidotised tholeiitic dolerite dykes. Rare sulphide minerals were present within the dolerite samples that transgress the Western Mineralisation. Dolerite samples were not considered in detail for this study. Dolerite dykes intruded massive sulphide rocks of 2 and 3 Lens resulting in fragmentation and garnetisation (Plimer 1984).

1.5.2 Delamerian Orogeny

The Delamerian Orogeny (Table 1.7) consists of two folding events (D_5 and D_6) coeval low grade metamorphism (Corbett & Phillips 1981). In the high grade metamorphic grade rocks of the Broken Hill Domain, the high grade shear zones may have been rejuvenated, new shear zones may have been initiated and there may have been a little hydration and resultant retrograde metamorphism of silicate rocks. Shear zones that cut the orebody (e.g. British Shear Zone) displace the orebody and remobilise Ag and Pb towards the shears (Plimer 1984). Sulphide rocks with tholeiitic dolerite clasts shows that the orebody must have moved during the Delamerian Orogeny (Plimer 2006b).

Table 1.7: Summary of the major deformation (D), metamorphism (M), schistosity (S) and P-T conditions during D_5 and D_6 of the Delamerian Orogeny.

Event Name	Event label	Deformation features	Structure and foliation	Mineral assemblage	P-T conditions
Delamerian Orogeny (~520-485 Ma) (Hand, Rutherford & Barovich 2003)	D_5 & D_6 (Corbett & Phillips 1981)	Reactivation of retrograde shear zone associated with post D_4 (Phillips 1980) and cross cutting pre-existing shear structure. Brittle fault system developed within the mineralised zone (Webster 1996). Sulphide minerals were remobilised through the reactivation of retrograde shear zones as veins (White et al. 1995).	Weak foliation developed throughout the deposit (White et al. 1995).	Development of siderite, muscovite, chlorite, sericite and quartz along faults, shears, vugs and joints (Morland & Webster 1998).	Greenschist facies metamorphism T=350°C and P=2 kbar (Phillips 1980)

1.6 Characteristics of the Broken Hill orebodies

The Broken Hill orebodies comprise four Zinc ores (Zn > Pb) and two Lead ores (Pb > Zn) as well as some non-outcropping mineralised zones (e.g. the Western Mineralisation and the Centenary Mineralisation). These are closely correlated with each other over a strike length of more than 8.5 km along the Main Line of Lode and some minor discontinuous orebodies occur over a strike length of 25 km. On scales of 1:2000 and smaller, the Broken Hill ore deposits are considered as stratiform or stratabound that underwent major and minor multiphase deformation (Plimer 2006b). Lawrence (1968), Walters (1996) and Walters and Bailey (1998) suggested high-grade metamorphism increased the grain size of ore minerals of the Broken Hill deposit and led to localised metasomatic remobilisation. A cataclastic texture is common in most of sulphide rocks of the Broken Hill orebodies and it is characterised by angular to rounded clasts of wall rocks including metapelite, metapsammite, quartz, plumbian orthoclase, garnetite, garnet quartzite, quartz-gahnite rocks (Blampain & Plimer 2006; Plimer 1984).

1.6.1 Partial melting

1.6.1.1 Orebody

There are arguments as to whether partial melting has any role in sulphide ore formation of the Broken Hill deposit. The concept of partial melting of massive sulphide deposits was developed by Frost, Mavrogenes and Tomkins (2002), Lawrence (1967), Tomkins, Pattison and Frost (2007) and Vokes (1971). Sparks and Mavrogenes (2005) argued that presence of inclusions of sulphide minerals in garnet from garnetite indicate the partial melting of the enclosing garnet. However, Spry, Plimer and Teale (2008) claimed that this is not correct because P-T conditions of the Curnamona Craton (upper greenschist-lower amphibolite) were too low for this melting. Moreover, mineralogical observations show that some of the sulphide inclusions formed in open system such as fractures of quartz and garnet or along the boundaries. Spry, Plimer and Teale (2008) argue that the sulphide inclusions were derived from hydrothermal processes during retrograde metamorphism rather than partial melting.

1.6.1.2 Wall rocks

Wall rocks of the Broken Hill orebodies comprise intermittent garnetite and quartz garnetite. Mavrogenes et al. (2004) argue that enrichment of Mn in garnetite and quartz

garnetite are associated with partial melting. They suggested the reaction of Mn-rich sphalerite on wall rocks as the reason for the increase in Mn content in the wall rocks of Broken Hill deposit. However, although such a process consumes Mn, in nature, sphalerite does not have such a high Mn content hence there is problem of mass balance. Furthermore, Mn rims have formed during the low metamorphic grade Delamerian Orogeny when P-T conditions were far too low for sulphide rock melting (Plimer 2006b). Another problem for interpretation by Mavrogenes et al. (2004) is that Mn-rich garnetite and garnet quartzite are located near the Pb-rich ores of the Broken Hill deposit rather than Zn-rich ores (problem of distribution of garnetite; Spry, Plimer & Teale 2008).

Spry, Plimer and Teale (2008) suggest exhalation and inhalation effects at or near the sea floor as the reason of the Fe- and Mn-rich wall rocks of Broken Hill. Garnet quartzites of the Western Mineralisation are significantly more within the structural hanging wall rather than the structural footwall and they are interlayered with major unaltered pelitic and psammopelitic units. The hanging wall of the Western Mineralisation also shows a range of weak to intense alteration.

1.6.2 The Eastern Mineralisation

The Eastern Mineralisation is characterised by quartz-orange garnet[17]-hedenbergite, cataclastic sulphide veins (e.g. quartz-galena ± chalcopyrite-sphalerite veins) and bleached clasts of pelite and sulphide veinlets (Blampain & Plimer 2006; Plimer 2006a). The major differences of the Eastern Mineralisation with the west of the lease area are the presence of stratigraphic units of magnetite-bearing amphibolite, Potosi Gneiss and metasediments and the absence of the stratigraphic marker Unit 4.6 and its BIF (Blampain & Plimer 2006).

1.6.3 The Western Mineralisation

The Western Mineralisation located in Unit 4.7 and its basal unit, Potosi Gneiss No.1 (Figure 1.5) is equivalent to stratigraphic spotted psammopelite. The orebody was formed within syn-metamorphic quartz veins and it is characterised as stringers of sulphide, disseminated ore and remobilised sulphide ore (Plimer et al. 2003). The remobilisation is a significant geological factor of the Western Mineralisation that should

[17] **They are mainly spessartine (Sparks & Mavrogenes 2005)**

be considered when the statistical results of the Western Mineralisation are interpreted. The Potosí Gneiss No. 1 is overlain by thin sequences of blue quartz lode and garnet quartzite followed by interval sequences of metapelite and metapsammopelite which underlying the Western Lode limb (Haydon & McConachy 1987). The garnet quartzite lenses of the Western Mineralisation thin out and grade laterally to metapsammopelite rich-garnet from downdip to updip of the Western Mineralisation (Haydon & McConachy 1987). Above the Globe Vauxhall Shear Zone, Unit 4.7 is capped by thin and continuous Potosi Gneiss (Potosí Gneiss No.2).

NOTE:
This figure is included on page 21 of the print copy of the thesis held in the University of Adelaide Library.

Figure 1.5: Cross-section shows the Western Mineralisation, the Centenary Mineralisation and their stratigraphic positions (redrawn from Haydon & McConachy 1987).

The Western Mineralisation comprises three stratabound sequences (Leyh 2000; Spry, Plimer & Teale 2008), a downdip extensions of A Lode with high abundant spessartine[18] ± rhodonite[19] unit equivalent to garnet quartzite (Haydon & McConachy 1987), a hedenbergite-rich unit equivalent to B Lode (Gentle 1968) and a quartz-gahnite-bearing sequence equivalent to C Lode. In this study, the silicate minerals and rock types of the three stratabound units where intersected the sulphide rocks are quantified to understand whether there is a quantitative relationship between the silicate minerals and mineralisation. There is a distinct gradation of metapelite and feldspathic metapsammopelite into garnet-bearing metapelite and garnetite in the stratigraphic footwall of both C Lode and the Western Mineralisation.

The Western Mineralisation is terminated downdip by the Globe Vauxhall Shear Zone which has a high angle to bedding. It consists of several closely-spaced shear zones within a wide-retrogressed zone (Figure 1.5). The Centenary Mineralisation is located structurally beneath the Globe Vauxhall Shear Zone and may be equivalent to the Western Mineralisation or may be in the upper segment of Unit 4.5. The Centenary Mineralisation zone appears mostly within blue quartz lode, garnet gangue and calc-silicate gangue in addition to garnet quartzite.

1.6.4 Mineral chemistry and alteration

Mineral chemistry of the Broken Hill ore deposit differs from other known base metal massive sulphide ore deposits because of deformation, remobilisation and chemical fractionation during the Olarian and Delamerian Orogenies. Some of the fundamental differences are:

1. The lack of pyrite (FeS_2) in the Broken Hill orebodies and yet the abundance of pyrite in the Broken Hill Block, e.g. Thackaringa Group (Plimer, 1977) indicate that the Broken Hill orebody has originally a low S content and that S could not have been released during granulite facies metamorphism,

2. The lack of barite ($BaSO_4$) and other sulphates in most Broken Hill-type deposits (e.g. Pinnacles) and the presence of hyalophane-celsian rocks in the Broken Hill Domain stratigraphically equivalent to barite rocks in the Olary Domain,

[18] **$Mn_3Al_2(SiO_4)_3$**
[19] **$MnSiO_3$ often contains minor Ca, Fe and Mg**

3. The low Cu and Au content of the massive sulphide rocks with slight enrichment in the garnet-rich rocks associated with 3 Lens. These Cu and Au enrichments are associated with enrichment in As, Ag, Mo and W,

4. The high Mn, Ca, halide (F, I and Br) and phosphorus content (Plimer 1984), and

5. The high U content of immediate wall rocks (Plimer 1979).

The stratigraphically lowermost of the Broken Hill orebodies is characterised by enrichment of Zn, Cu, Bi, P, Ni and Ca and depletion of Pb, Ag, Mn, Sb, As and F in comparison with stratigraphic uppermost of the Broken Hill (Haydon & McConachy 1987; Johnson & Klingner 1975; Plimer 1979; Spry, Plimer & Teale 2008). Hydrothermal alteration of oxides and Pb, Zn, U, S and Fe increase toward the Broken Hill orebodies are characterised by depletion in Na_2O, CaO, Sr, MgO and enrichment in SiO_2, K_2O, Rb, MnO, Pb, Zn, U, S, P_2O_5 and total Fe and TiO_2 (Plimer 1979). Moreover, during this hydrothermal alteration, the ratio of $\frac{Rb}{Sr}$ increased from less than 500 m from the orebodies to 30-100 m at the orebodies (Plimer 1979). In this study, the spatial distribution and variation of 10 elements of the Western Mineralisation are plotted and interpreted.

There has been little isotopic work undertaken on the sulphide masses at Broken Hill (apart from Pb and S) and previous work has been geologically unconstrained. The literature does not show that any authors have ever considered that the formation of the Broken Hill orebody may have been a long-lived geothermal process whereby earlier sulphide masses were replaced by later sulphide masses, as is seen in Kuroko-type deposits. This suggests that rather than zonation from C Lode to 3 Lens viewed through the Principle of Superposition, earlier Zinc orebodies (e.g. A Lode) may be replaced by later Pb-Mn rich fluids.

1.7 Unsolved problems and research questions of the Broken Hill orebodies

The development of mining operations and the evolution of knowledge, scientific matters concerning the Broken Hill orebody will always be contentious. The greatest geological problem at Broken Hill is that, although there have been generations of mine and exploration geologists, there has been no consistent system of rock nomenclature and qualitative core logging and hence there is no detailed stratigraphic, structural, geophysical

and geochemical model of the Broken Hill orebody. Core logging has been non-numerical and subjective and it has suffered from generations of geologists qualitatively logging core differently.

To gain an understanding of the stratigraphic setting of the Broken Hill ore deposit, there needs to be a consistent coherent logging system for Broken Hill and, although the Southern Operations (NBHC, Zinc Corporation, Pasminco and now Perilya), Broken Hill South, CBH Resources, North Broken Hill and the Geological Survey of NSW have all had logging systems and nomenclature, these systems are all different are not able to be used for correlation. This research project was undertaken on the Western Mineralisation on CML7 in order to address the following unsolved problems:

a. The Western Mineralisation has been documented using conventional qualitative core logging and previous collected samples [geological, geotechnical, engineering and AAS[20], wet chemical, ICP-OES[21] assaying, XRF[22], EMPA[23] and ICP-MS[24]] of oriented and non-oriented core. No geophysical logging has been undertaken and the previous quantitative information was not well integrated so that it could be used simply for a variety of statistical analysis and thus the maximum information has not been extracted from core.

b. Conventional qualitative core logging is separated from mineral chemistry and geophysical data which is commonly undertaken by mine geologists rather than research scientists. Logging is constrained to a number of rock types (metapelite, metapsammopelite, metapsammite, BIF, amphibolite, garnet amphibolite, Potosi Gneiss, felsic gneiss and pegmatite), these rock types are not related to mineral chemistry or whole rock geochemistry (hence subtle pre-metamorphic alteration is ignored) and assays are only undertaken where visible sulphides are present. Assays are on a different scale to lithological logs and they are added as a flitch later with Micromine™ and Vulcan™ models for mining. Such a diversity of information on different scales cannot be evaluated simultaneously. However, the

[20] Atomic Absorption Spectrophotometry
[21] Inductively Coupled Plasma-Optical Emission Spectrometry
[22] X-Ray Fluorescence
[23] Electron Microprobe Analysis
[24] Inductively Coupled Plasma Mass Spectrometry

processes undertaken at the Rasp Mine are standard industry practice for the economic mining of sulphide orebodies and do not allow the easy use of the data for performing different statistical methods and providing quantitative core log diagrams and bar diagrams.

c. Geostatistical methods are used at the Rasp Mine to validate assay data, to test the veracity of data, to construct economic mining models and to calculate resources and reserves but the quantitative core log data can be evaluated using a variety of classic bivariate and multivariate statistical methods to improve quality of interpretation. There have been a number of due diligence and ore resource/reserve studies undertaken by CBH Resources Ltd and their consultants. However, the answers sought in such studies were commercial and not scientific hence were unable to address some of the unsolved problems above.

d. There is a lack of a quantitative understanding of the spatial relationship and structural continuity of geological, geochemical and geophysical features of the Western Mineralisation. The spatial and structural characteristics of the Broken Hill ore deposit including the Western Mineralisation resulted from a multiphase evolving geothermal system that has undergone a superimposition of a multiphase tectonism and deformation. The events created hydrothermal alteration, induced sulphide flow structures in silicate rocks, remobilised sulphide minerals, distilled some elements from the sulphide rocks and changed the orebody morphology. Spatial models of quantitative core log data of the Western Mineralisation can address the following unknown issues:

1. The nature and morphology of geochemical zonation haloes,
2. Spatial texture of sulphide minerals,
3. Classification of geochemical anomalies,
4. Separation of threshold values from background and anomalous levels for different elements,
5. Identification of geochemical and mineralogical zonation patterns,
6. Spatial anisotropy,

7. Spatial pattern of magnetic susceptibility,
8. Detection of geochemical pathfinders of Pb and Zn, and
9. Identification of geochemical zonation sequence in different directions of the orebody.

During this study, there were a number of validation questions that were considered in the research. Some of the questions are:

1. Were the various type of data sets (geology, geochemistry and geophysics) used accurate and can results from different statistical methods be compared?
2. How were samples collected?
3. What sample intervals were used and how were these samples related to each other?
4. Were different data sets cross checked, re-analysed and validated?
5. How was qualitative geological data integrated with quantitative geochemical data, bearing in mind that these data sets were collected on different scales?
6. Why should such data be integrated?

The aim of this project is to analyse and interpret these old data sets (assay) and integrate data sets generated during this study (geophysics, lithology, mineralogy and sulphide textures) by univariate, bivariate, multivariate analysis and geostatistical methods to evaluate the degree of uncertainty of the interpretations. As the Rasp Mine is in the planning stage, these interpretations will be timely as ore resource calculations show that there is high, medium and low grade ore yet there is no predictive methodology for grade.

CHAPTER 2

Quantitative Core Logging in the Western Mineralisation

2.1 Introduction

There has been more than 100 years of drilling at CML7 in Broken Hill on seven different grid systems in feet, fathoms and metres. Most cores are not preserved, there are no logs of many of the holes from the 19th and early 20th Centuries and only some of this data is preserved as assay plots on maps. It is only in the last 40 years that core has been stored in dedicated core facilities. On CML7, none of the core from drilling by previous CML7 mining companies is preserved (BHP, Sulphide Corporation, Block 10 Silver Mining Company, BHP Block 14 Company, North Broken Hill, South Broken Hill and Minerals Mining and Metallurgy) and there is only partial preservation of core from Normandy Mining Ltd's exploration activities. CML7 was acquired by Redfire Resources N.L. (now CBH Resources Ltd) in 2001 and all drill core since that time is preserved. Another 4,500 m of underground drilling of the Western Mineralisation from the Rasp Mine decline is taking place at present. Fanned holes drilled westerly are designed to infill areas where drilling used in this study was sparse. This new drilling is to convert resources to reserves to make the project more bankable and to more closely define the Western Mineralisation for stope design.

Assay values from underground drilling from the 1000', 1150', 1250' and 1480' levels by BH South Ltd in the 1950s and 1960s are plotted but no duplicate samples remain, no core remains and the core was not geologically mapped. No grade control underground drill core is preserved and some of these data sets are plotted onto old maps. Because the 127 years of continuous mining on CML7 has been by numerous operators with different economic constraints, the only data on the Western Mineralisation used in this study was that of CBH Resources Ltd because core is available for validation and cross checking. Nevertheless, there have been 4 geologists (Pascal Blampain, John Collier, Ian Plimer, Catherine Errock) who have logged CBH Resources Ltd core and relogged the Normandy Mining Ltd core over the last decade. There was an attempt by Blampain to standardise nomenclature and logging techniques hence there is a high degree of internal consistency for qualitative logging.

The Western Mineralisation sample cores were not logged by CBH Resources Ltd for ore texture, ore modal mineralogy, ore structure and magnetic susceptibility but the data collected in this study was integrated with metre-by-metre assay data, mineralogical and lithological logs of CBH Resources Ltd.

This chapter addresses the uncertainties associated with conventional core logging (as shown by the Western Mineralisation) and introduces a numerical approach for the quantification of visual estimates of minerals, rock types and textures and the relationship of this data to mine assay data. These relationships are shown on Western Mineralisation drill collar maps (Figure 2.1) and 3D visualisation of sample locations (Figure 2.2). Satellite imagery of the Western Mineralisation has been provided in supplementary file to this thesis.

2.2 Maps

2.2.1 Drill collar locations

The 54 CBH Resources Ltd surface drill holes into the Western Mineralisation are shown on Figure 2.1. In Figure 2.1, four drill holes 3230, 3231, 3232 and 3233 are related to Normandy Mining Ltd's previous exploration activities and other drill holes are related to the Western Mineralisation's exploration activities. The drill hole numbers of the Western Mineralisation were named by a prefix "WMDD[1]" (e.g. WMDD4001) but in this thesis, only the drill hole numbers (e.g. 4001) are used in figures and text.

Surface drill locations were 1,500.7 m in the south (drill hole 4052), 2,562.3 m in the north (drill hole 4034), and 9,249.9 m in the west (drill hole 4042) to 9,531.88 m in the east (drill hole 4054). Horizontal angles relative to strike were calculated on a local CBH Resources Ltd graticule system hence true north is different from grid north. Therefore, azimuth of the Broken Hill Mine toward northing is slightly different from the geographical azimuth at the Broken Hill district. There are now 31 CBH Resources Ltd underground holes drilled from the Rasp Decline into the Western Mineralisation. Some of the underground drill cores have assay values and only their assay values have been used in this study.

[1] **Western Mineralisation Diamond Drill core**

Based on the existing standard collar location map of CBH Resources Ltd, the northing and easting data were converted to local territory and for this purpose values of 1,000 and 10,000 were added to the original values of the north and east of the Western Mineralisation respectively. Moreover, the easting values are increasing from the west toward the east in the collar map. In this collar map, the contour lines show the relative surface level of the drill holes in metres. The perimeter of the collar map is 2900 m and the surface area corresponds to 385,000 m^2.

There is a number of surface drill holes that were drilled from the same collar but with different dips and they produced a series of fanned holes. In Figure 2.1, this can be seen in several cases where a single point is attributed to different drill holes. Furthermore, Figure 2.1 shows that most drill holes in the Western Mineralisation drilled along a strike of approximately 15° toward NE from the local north coordinate of the CBH Resources Ltd.

The surface drill holes were drilled in an irregular pattern (Figure 2.1). This arrangement of drill sites was chosen because of logistical problems such as vicinity of the Western Mineralisation to the City of Broken Hill and interference with existing buildings, roads and railways (see the satellite imagery of the collar locations of the surface drill holes in supplementary files to this thesis). Moreover, the drill hole numbers in the collar map are not in a regular order and were named by CBH Resources Ltd based on the chronological order of drilling.

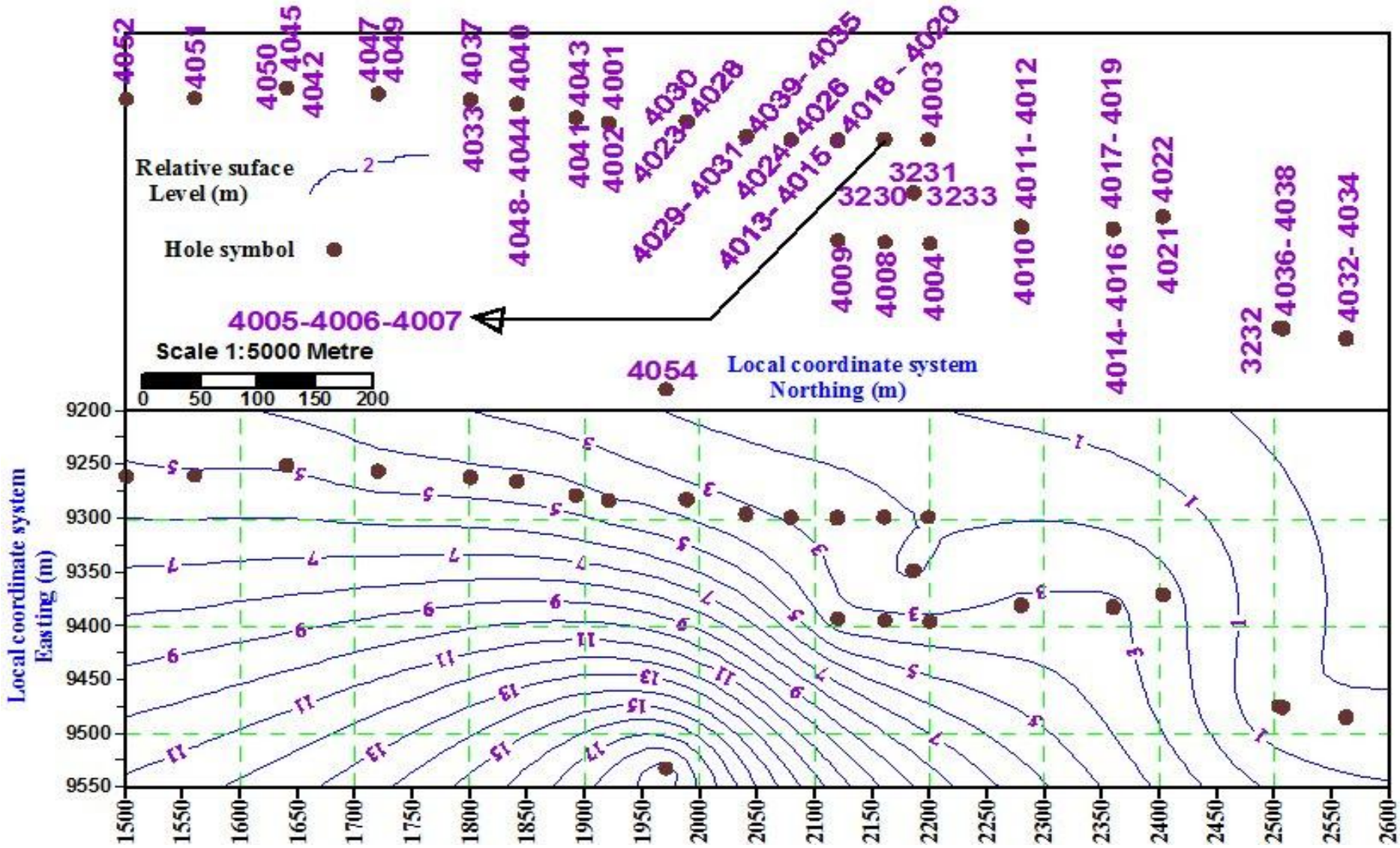

Figures 2.1: Collar locations of the surface drill holes and relative surface levels of the Western Mineralisation.

2.2.2 Three-dimensional visualisation of the analysed sample locations

Sample locations of the Western Mineralisation were plotted on a 3D grid (Figure 2.2). The 3D sample locations shown are for the drill cores selected for both assaying and detailed geological examination in this study. The 3D sample locations are provided at a scale of 1:6,000 m for all directions (northing, easting and elevation). In Figure 2.2, the elevation is increasing upwards in contrast with depth. The top elevation (10,222.33 m) shows the start of sampled drill hole 4032 and the bottom elevation (9,691.69 m) is related to the end of sulphide mineralised sample in drill hole 4052. Total depth between start and end of sampled drill hole 4032 and 4052 respectively is 530.64 m. The local elevation values were summed at 10,000 in accord with the base map of the CBH Resources Ltd for the Western Mineralisation.

The sampled drill locations were gradually deeper towards the south-western corner of the 3D map (Figure 2.2). The magnetic azimuth calculated from the local grid azimuth is plus 43°. The depth of surface drill holes varies from 141 m to 698.8 m and the three drill holes in Normandy Mining (3232, 3231 and 3230) were deeper with a hole end depth of 830.8 m. However, there are no assay values available beyond 530 m depth in any of the drill holes.

The length of underground drill holes ranges from 107.3 m to 402.4 m. The dip of surface drill holes varies from -47° to -88° and the dip of underground drill holes ranges between +10 and -90. It should be noted that term dip, in this section is a mining concept. Negative dip indicates moving down from the horizontal surface level and positive dip means moving up towards the horizontal surface level.

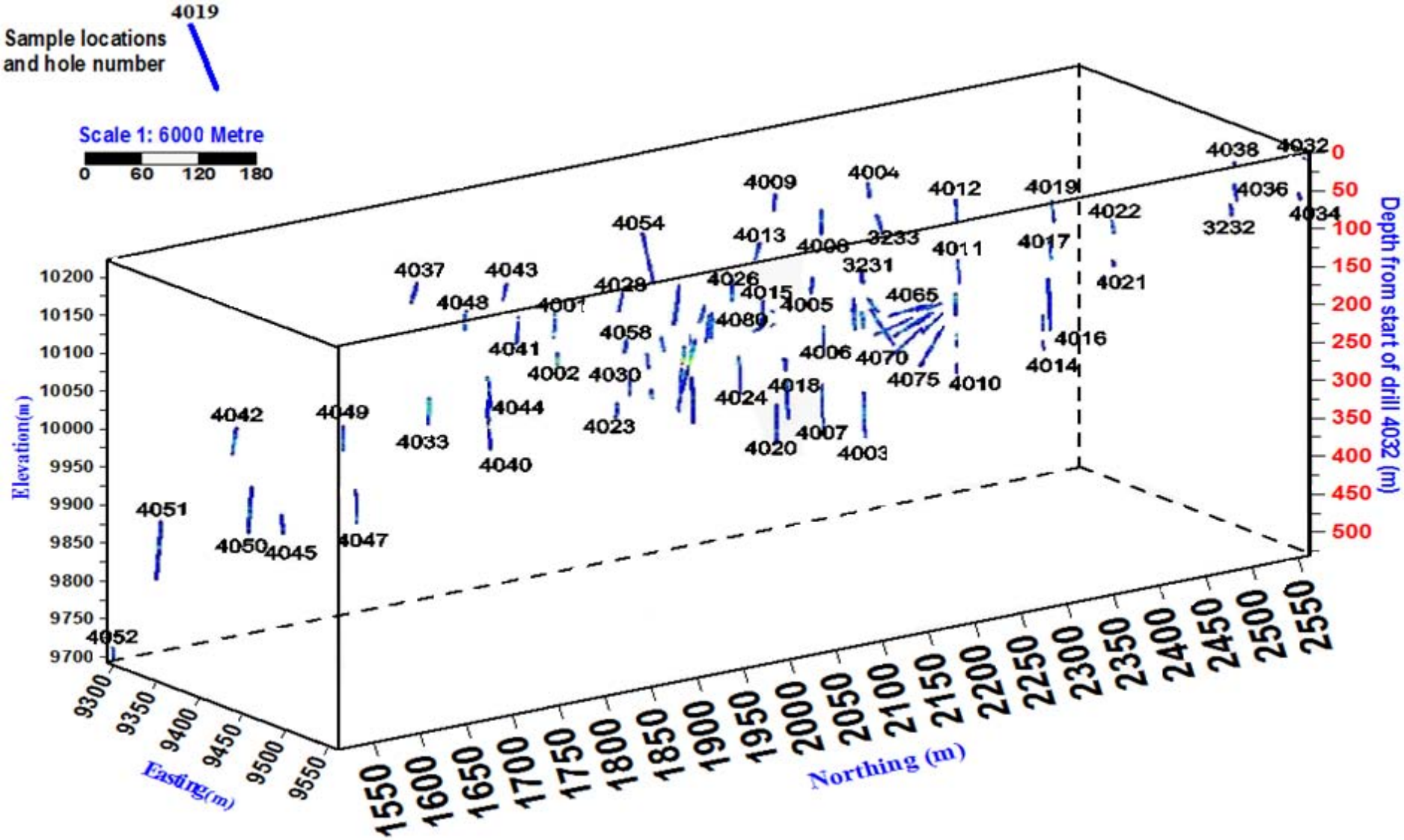

Figure 2.2: A 3D visualisation of the sulphide mineralised sample locations in the Western Mineralisation.

2.3 Geological information resulted from core logging in the Western Mineralisation

2.3.1 The conventional core logging

In mines, a set of quantitative data and descriptive geological information is provided for each drill hole. The quantitative data usually consists of the core size, azimuth and dip of drill holes, collar location of drill holes and depth of the major rock type, rock quality designation (RQD), recovery percentage, rock strength, orientation reliability and fracture density as well as specific gravity. Descriptive geological information is commonly provided for petrography and dominant sulphide and silicate minerals, texture, alteration or weathering, deformation and metamorphic minerals from macroscopic visual examination.

The recovery percentage of the core intervals is calculated by measuring the total length of core (using the tape measure) that has been marked up as percentage over the one metre interval. An empirical method for estimating core recovery is RQD and it is calculated by summation of the length of all pieces of cores if they are individually greater than a length of 100 mm. For example, if the core is recovered in pieces that are all longer than 100 mm, the RQD is 100 % whereas if some pieces are shorter than 100 mm, the RQD will decrease. The RQD value provides general information regarding the degree of jointing and faulting in the rock mass. It is the procedures that are utilised by CBH Resources Ltd as their conventional qualitative core logging of the Western Mineralisation (Table 2.1).

Table 2.1: An example of the conventional core log for drill hole 4008 from surface to 56.5 m. This drill core was logged by a senior geologist (Blampain).

NOTE:
This table is included on page 34 of the print copy of the thesis held in the University of Adelaide Library.

Although later information of the provided core logs of the Western Mineralisation was transferred to sophisticated software package such as Micromine^{TM}, Vulcan^{TM} and Surpac^{TM}. The conventional core investigation data suffers from the following weaknesses:

1. Non-uniformity of observation and missed information,
2. Geological information is qualitative (or descriptive),
3. Geological information is provided for different length of core samples, and

4. Absence of assay values and geophysical results (e.g. magnetic susceptibility and specific gravity) in the conventional core logs for evaluation of internal consistency and coherency.

The geological information of core samples of the Western Mineralisation has not been based on variation of the sulphide mineralisation, but is based on variation of rock type intervals. In this case, attribution of a large length of core (e.g. 20 m) to one rock type may be useful for description of the non-mineralised core intervals (barren units) and low grade sulphide rocks, but in the rich-sulphide rocks (economic ore zones or productive zones) cause loss of quality and quantity of the geological information. Moreover, it is not clear where the reported geological information over a long length of core relates to any particular part of the core. Core investigation in equal length core sections increases the number of investigated geological samples and improves the quality of geological observations.

2.3.2 The quantitative core logging

The aim of this project is to construct comprehensive and quantitative geological information for 1,928 m of core samples of 54 surface drill holes to supplement the qualitative logs of CBH Resources Ltd. The first step was to identify major geological parameters for providing a quantitative core logging. The following geological information was selected for this study:

1. Silicate mineral assemblages: green feldspar, pink garnet[2], orange garnet, red garnet[3], hedenbergite, rhodonite, white quartz, gahnite and blue quartz.

2. Sulphide minerals assemblages: galena, sphalerite, chalcopyrite, pyrrhotite, pyrite and arsenopyrite, and

3. Rock types: dolerite, garnet quartzite (quartz garnetite), quartzite lode, pegmatite, metapelite, metapsammite, metapsammopelite and blue quartz lode

- **Blue quartz lode**

The term blue quartz lode (blue quartz ± gahnite ± minor garnet) has been used in most internal mining reports of the Broken Hill Mine and the conventional core logs of the Western Mineralisation as a rock type. This rock type appears broadly distributed in the

[2] They are mainly pink almandine [$Fe_3Al_2(SiO_4)_3$]-pyrope [$(Mg_3Al_2(SiO_4)_3$]
[3] They are mainly spessartine (Sparks & Mavrogenes 2005)

stratigraphic package of the Broken Hill orebodies. Blue quartz lode has also been used in some papers (e.g. Morland & Webster, 1998; Plimer, 2006b). In this study, in a few core samples, the major host rock was not blue quartz lode but the samples containing a small volume percentage of blue quartz. In these cases, it was accounted for as a mineral. Therefore, the volume percentage of blue quartz was quantified both for rock group (blue quartz lode) and for mineral group (blue quartz). Nevertheless, in most cases, the abundance of the blue quartz lode was estimated similar to the blue quartz in mineral group.

2.3.3 Quantification of minerals and rock types

In the Western Mineralisation, each one-metre core section was examined in smaller parts based on variation of rock types and mineral content. The average volume percent of the individual minerals and rock types were reported for each one-metre core sample. For quantification of minerals and rock types, they were classified into the three following groups based on their grain sizes, distribution and texture.

2.3.3.1 Quantification of minerals and rock types in group one

Group one includes all the investigated rock types of this study and some coarse grain silicate minerals (e.g. green feldspar, white quartz, blue quartz and garnets) and sulphide minerals (e.g. galena, sphalerite and pyrrhotite) in high grade sulphide mineralised samples (Figure 2.3). Major textures of sulphide minerals in this group comprise: massive, brecciated, high grade veins, stringer and network.

Figure 2.3: Coarse sulphide minerals including galena (grey), sphalerite (black), chalcopyrite (yellow) and white quartz in a cataclastic massive sulphide rock of the Western Mineralisation (drill hole 4033 at 353.2 m). The structural position of cataclastic ore is unknown and may well remain so until further underground mining commences.

In Figure 2.3, the sulphide and silicate minerals have entirely occupied the clear part of each metre split core and rock type. Minerals are visually identifiable by their high continuity and massive textures. In this group, the amount of minerals ranges from 10 to 65 vol. % [4]. The volume percent of rocks was estimated using a tape measure. However, in some samples, any obvious boundary between two different rock types was equivocal because the boundary is gradational (e.g. metapsammopelite as a transitional rock between metapelite and metapsammite). Furthermore, the volume percentage of rock types is biased when the core axis to bedding angle approaches parallelism. In highly mineralised samples, the estimation of sulphide mineral content is problematic because an intergrowth of several sulphide and silicate minerals masks the mineral lustre. In order to reduce this error, the cores were viewed both wet and dry.

2.3.3.2 Quantification of minerals in group two

Group two consists of some silicate minerals including pink garnet, red garnet, orange garnet, hedenbergite, rhodonite and gahnite. Minerals of this group are characterised by a regular dissemination of grains, equal crystal size and distinct colour along one metre core intervals (e.g. Figure 2.4). The quantifying process in this group was performed based on mineralogical comparison charts of Figure 2.5 (Terry & Chilingar 1955). In this group, the amount of minerals varies between 5 and 50 vol %.

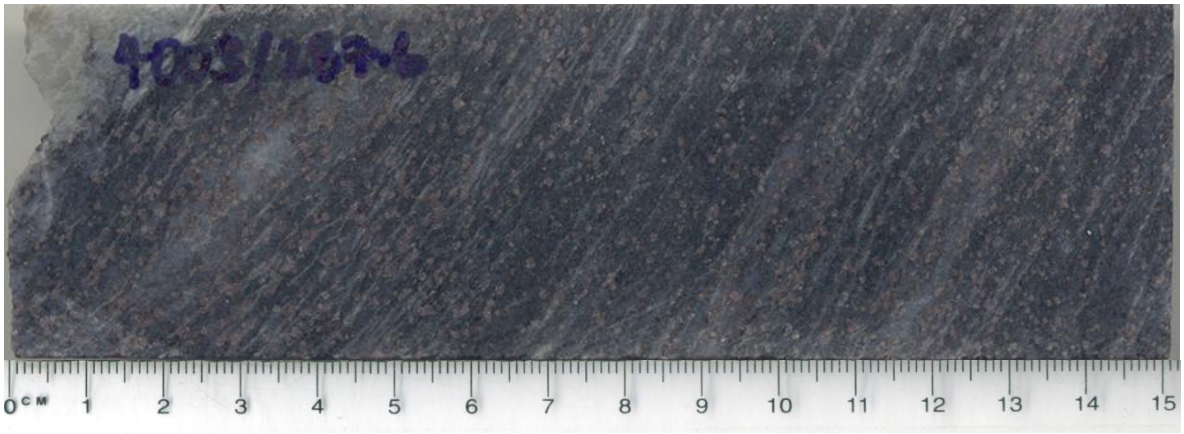

Figure 2.4: Distribution of pink garnet (red crystals) within garnet quartzite in drill hole 4003, between 287.6 m and 287.75 m.

[4] **Volume percent**

NOTE:
This figure is included on page 38 of the print copy of the thesis held in the University of Adelaide Library.

Figure 2.5: Comparison charts for estimating volume percentage of minerals based on their grain size and abundance (from Terry & Chilingar 1955).

2.3.3.3 Quantification of minerals in group three

The third group comprises mostly sulphide minerals such as galena, sphalerite, pyrite, chalcopyrite and pyrrhotite. Sulphide minerals of this group are characterised by irregular distribution (cluster form), low grade veins and unequal crystal size (Figure 2.6).

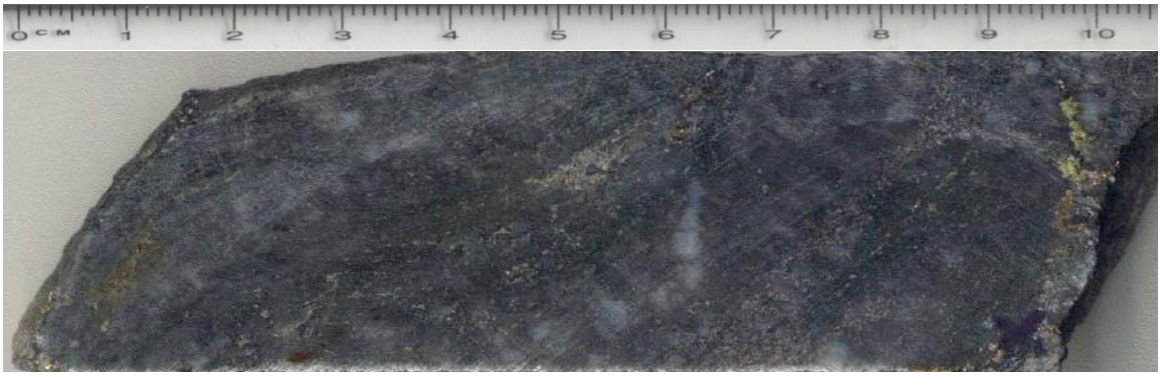

Figure 2.6: Low grade veins of chalcopyrite and other sulphide minerals within garnet quartzite in drill hole 4003 at 317.9 m.

In this group, sulphide minerals comprise less than 5 vol. % of the Western Mineralisation. These sulphide minerals are not economically significant. However, estimation of minerals of this group produce great information about ore mineral zonation pattern that sometimes functions as pathfinder for tracking mineralised zones. The spatial structure of the ore mineral zonation pattern depends on distinguishing both parts of low and high grade sulphide mineralised zones of the Western Mineralisation.

2.3.4 Some effective parameters and considerations in the quantitative core logging

Estimating volume percentage of minerals and rock types is an empirical method that depends on the geological, mineralogical and human parameters. Some of the parameters have been outlined in Table 2.2.

Table 2.2: Effective parameters in quality of the quantitative core logging.

Mineralogical parameters	**Equal or unequal distribution of minerals, grain size, texture, colour and the proportions of minerals in mineral mixtures.**
Human parameters	**These parameters may have indirectly significant effects on the quantification process. It can be improved by development of practical core logging, concentration, identification of local rock types and quick classification of samples based on the known local rock types.**
Geological parameters	**Geological complexity such as the number of minerals, rock types and textures present in a core sample.**

Based on the practical experience of this study, some considerations (Table 2.3) have shown to be a useful for minimizing uncertainties during quantification of minerals and rock types.

Table 2.3: Useful considerations for quantification of minerals and rock types.

The quantitative core investigation can be improved if carried out by one person for the sample set in order to get a coherent core logging.
Previous experience of conventional core logging helps to improve speed of the quantitative core logging.
Using split cores for visual examination helps to identify minerals better and improve the quantitative estimate of minerals and rock types.
Paying attention to information recorded in the conventional core logs improves quantitative core logging for the samples.
Quantification of galena and sphalerite in the presence of Pb and Zn assays respectively may produce a bias in visual grade estimation and visual modal mineralogical estimation.
Identification of important physical properties of each mineral (e.g. shape, size, lustre, colour, textures, associated minerals, textural continuity, distribution, cleavage, crystal form and enveloping rocks) increases the reliability of visual recognition and estimation of minerals.
Using daylight and a hand lens.
It is essential to examine sulphide minerals in dry core because wet core exacerbates sulphide mineral lustre and affects modal estimation.
Silicate minerals and rock types of wet core are more consistent.
Magnetic susceptibility should be measured on dry samples.
It is necessary to perform visual estimation of minerals and rocks for a set of similar samples during a continuous period of time; otherwise, there is the possibility of losing coherency.
Random checking of the quantified minerals or rock types in previous samples in order to increase accuracy, precision and reduce the risk of human error.
If the results of assay data are available, the estimated galena and sphalerite can be reconciled with Pb and Zn assays respectively.

2.3.5 Quantification of textures for sulphide minerals of the Western Mineralisation

There are some textural descriptions in the conventional core logging of the Western Mineralisation by CBH Resources Ltd but the conventional core logs do not show clearly in which part of the drill cores they were observed. In the Western Mineralisation, dominant textures within rich sulphide samples were network and massive (suggesting remobilisation) whereas in low grade sulphide rocks, the major textures were disseminated, vein and laminated.

The stringer texture was present in both high grade and low grade sulphide samples. An indicator was used for quantification of the sulphide textures. In this method, a value of one was given to occurrence of each texture that was seen within each metre core. Based on this, spatial probability of occurrence of textures was calculated in Chapters 6 and plotted in Chapter 8. Identification of textures may be indirectly helpful for prediction of dilution effects in mining when, for example, a high grade sulphide zone has unexpected textural changes that will affect grade control.

One good example of application of the indicator in geological study is related to De Geoffroy and Wignall (1972). They quantified visually rock types, minerals and structural geology in several porphyry deposits of Cu and Mo in the Cordilleran Belt in order to identify their similarities and differences. They processed their results with character analysis but character analysis does not indicate the volume percentage of minerals or rock types.

2.3.6 Previous visual quantification methods in geosciences

Visual quantification of the Western Mineralisation is not limited to this study and core samples were quantified visually for recovery percent, RQD and fracture density for which all the data is purely empirical. For example, in the Western Mineralisation, fracture density quantification, the quantity of bedding and jointing was measured over one metre intervals.

2.4 Geochemical data of the Western Mineralisation

In the Western Mineralisation, the selected intervals of drill cores for assaying comprise sulphide mineralised rocks, poorly mineralised zones and to some extent their enclosing unmineralised host rocks. The core samples were cut with a diamond saw along their long axis and one half of the core was retained in the core tray and other parts of the split cores of different lengths (between 0.5 and 1.75 m) were sent for assaying. In the Western Mineralisation, the surface drill core samples of CBH Resources Ltd were assayed by ICP-OES for 10 elements [Pb %, Zn %, Fe %, S %, Cu %, Ag (ppm), Cd (ppm), Sb (ppm), Bi (ppm), As (ppm)] and the underground samples assayed for 8 elements [Pb %, Zn %, Fe %, S %, Ag (ppm), As (ppm), Sb (ppm) and Bi (ppm)].

2.4.1 Sample size reconciliation

Western Mineralisation drill core was HQ (63.5 mm[5]) and NQ size (47.6 mm[9]), core was halved for assaying and re-sampling and metallurgical bench testing left quarter core. One large diameter PQ core (85 mm[9]) was drilled for metallurgical testing and the entire core was used. With coarse grained sulphides, stringers and transgressive zones of sulphides, it is quite probable that each half core interval would give different assay data. In order to reduce such uncertainties and biased geochemical data, equivalent sample support is required otherwise it has to be shown that there is no relationship between the element concentration, core diameter and the length of core analysed.

2.4.1.1 Equivalent core diameter

Different core diameters are used for surface and underground drilling. Western Mineralisation surface holes started as HQ until the base of weathering (10-45 m) allowing tighter directional control. Once in hard rock, core diameter was reduced to NQ. Larger core diameter has better recovery however it is more expensive to drill and more difficult to handle. Variable core diameter in the evaluation of the Western Mineralisation may increase uncertainties. All sulphide mineralised core samples of this study were selected from NQ parts of the surface drill holes apart from holes 4001, 4002, 4031 and 4048 that were HQ size. The 23 underground Western Mineralisation drill holes from drill cuddies[6] in the Rasp Decline were LTK60 size (45.2 mm[9]).

If different core diameters are used for grade estimation, it is possible that the grade may not be accurate. Equivalent sample sizes are essential for accurate statistical analysis and comparison of element concentration because increase of sample volume (V) leads to decrease of variance (S^2, where S is standard deviation) of element concentration.

Hazen's study in 1967 (cited in Wellmer 1998, p.24) based on experimental drilling project undertaken at the Climax molybdenite mine near Denver (Colorado) suggested an empirical formula [Equation (2.1)] that shows **the sample volume-variance product** should be constant within a given orebody.

$$\mathbf{S^2 \times V = Constant} \qquad \textbf{(2.1)}$$

[5] Core (inside) diameter

[6] A mining term for a storage area or drill site off the main drive or decline

According to Equation (2.1), two samples with equal support collected in a close distance from one type of mineralisation have similar variance for a measured variable (e.g. element concentration). Koch and Link's study in 1970 (cited in Wellmer 1998, p.24) experimented the sample volume-variance [Equation (2.1)] for several core diameters (BQ to HQ) and they found that the variances of element concentration reduces with a much smaller proportion relative to degree of increase in their sample volumes.

In nature, the Hazen's equation may not be accurate if the distance between two samples increases because it is possible the average trend of mineralisation and grade change rapidly. Although the Hazen's equation for different distance of samples does not strictly occur in nature and specific geological properties impact on this approach, the sample volume-variance relationship [Equation (2.1)] is used for comparison of sample series with different support and possible correction (Wellmer 1998). In the Western Mineralisation, Hazen's equation was used for conversion of the HQ and LTK60 core diameters to the NQ core diameter at the same drilling position. In this case, there were fewer problems of a large distance between two samples that caused the increase in uncertainty of grade variation of mineralisation.

The Western Mineralisation is not a vein or disseminated mineralisation but it is a stratabound ore zone which is geometric, textural and grade variation. However, core logging shows that such variations are rare over a few centimetres around drill holes. Equation (2.2) is used for comparing sample volume of $\mathbf{V_1}$ with concentration variance of $\mathbf{S_1^2}$ and sample volume of $\mathbf{V_2}$ with concentration variance of $\mathbf{S_2^2}$. It is a consequent of Hazen's equation that suggests the variance of concentration inversely changes with proportion of the sample volume but the product of volume-variance is constant approximately (Wellmer 1998, p.24).

$$\mathbf{S_1^2 \times V_1 = S_2^2 \times V_2} \qquad \textbf{(2.2)}$$

All assayed parts of HQ and LKT60 drill holes were considered as a long core sample for converting to equivalent length of NQ core sample. In Table 2.4, Equations (2.3) and (2.4) are used for calculation of standard deviation of an equivalent NQ core sample from standard deviation of the HQ and the LTK60 core size. It should be noted that

the length of equivalent NQ drill cores is the same for the initial HQ and LTK60 drill cores. Therefore, the length (l) is eliminated in methodical conversion of Table 2.4.

Table 2.4: Calculation of standard deviation of an equivalent NQ core sample from standard deviation of the HQ and the LTK60 core size.

$$\pi \times r^2 \times l = V$$

$$\pi \times \frac{d^2}{4} \times l = \frac{V}{2} \rightarrow \text{Split Core}$$

$$S_{HQ}^2 \times V_{HQ} = S_{NQ}^2 \times V_{NQ}$$

$$S_{NQ} = S_{HQ} \times \sqrt{\frac{V_{HQ}}{V_{NQ}}} = S_{HQ} \times \frac{d_{HQ}}{d_{NQ}} = S_{HQ} \times \frac{63.5}{47.6}$$

$$S_{NQ} = 1.33403 \times S_{HQ} \quad (2.3)$$

$$S_{NQ} = S_{LTK60} \times \sqrt{\frac{V_{LTK60}}{V_{NQ}}} = S_{LTK60} \times \frac{d_{LTK60}}{d_{NQ}} = S_{LTK60} \times \frac{45.2}{47.6} \quad (2.4)$$

where r = Radius, l = Length of a core sample, d = Core diameter and V = Core volume

In theory, the mean grade of HQ and LTK60 samples should be considered the same for NQ samples by conversion using the volume-variance comparison line (VVC line; Figure 2.7; Wellmer 1998). If the mean of concentration of the two samples is not the same, according to Wellmer (1998), it must be assumed a systematic error and bias in drill samples. In this case, construction of the VVC line is not appropriate for this conversion or sample correction.

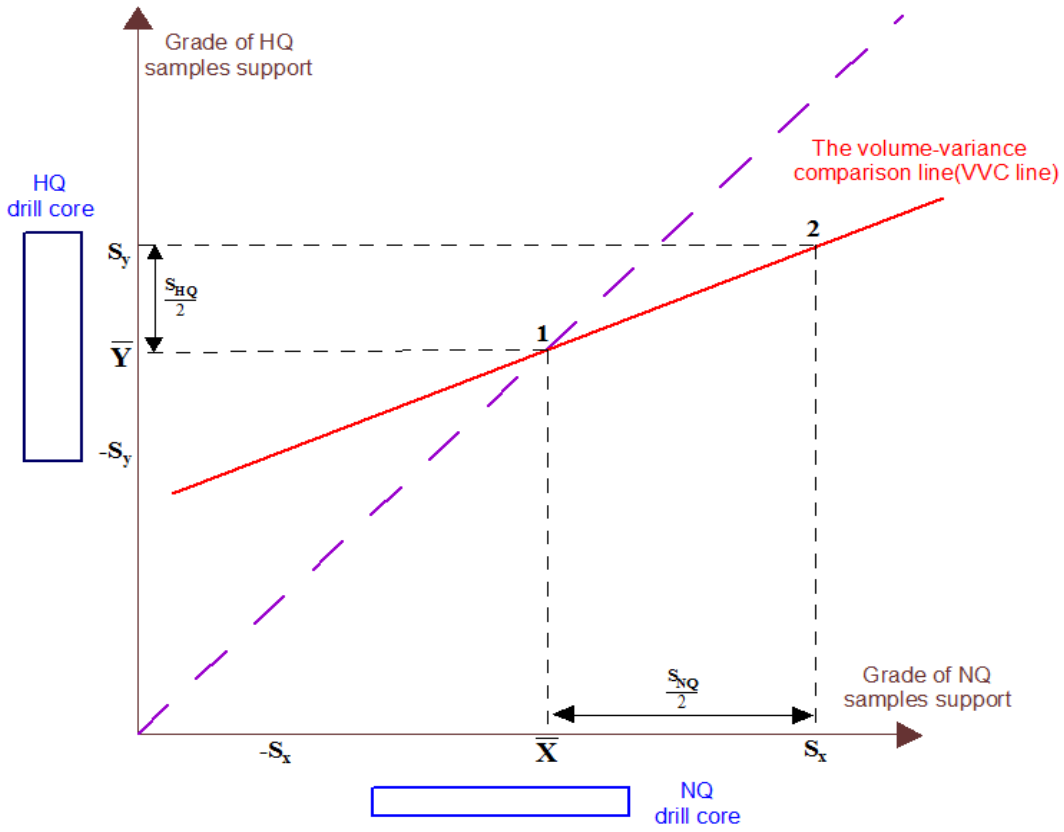

Figure 2.7: The VVC line for comparing the variances of an element concentration between HQ and NQ samples support (redrawn from Wellmer 1998). S_x and S_y are standard deviations of concentrations for NQ and HQ samples support respectively. $\overline{X}$ and $\overline{Y}$ are the mean concentrations for NQ and HQ samples support respectively.

In Figure 2.7, the mean concentration $\overline{Y}$ of the HQ samples was considered equal to the mean concentration $\overline{X}$ of the NQ samples. The two mean points of $\overline{X}$ and $\overline{Y}$ in horizontal and vertical axis respectively determine one point (1) of the VVC line. The nature and dimension of the standard deviation are the same as the mean value and can be added or subtracted to a mean value. Two points of S_x and S_y can be calculated from the standard deviation of concentration of the NQ drill core and its equivalent standard deviation of the HQ drill core respectively using Equations (2.5) and (2.6).

$$S_x = \overline{X} + \frac{S_{NQ}}{2} \quad (2.5)$$

$$S_y = \overline{Y} + \frac{S_{HQ}}{2} \quad (2.6)$$

The VVC line can be constructed by two points 1 and 2 (on red line in Figure 2.7) resulting from intersections (dashed black lines) of two points $(\overline{X}, \overline{Y})$ and (S_x, S_y). This process is performed in Excel to calculate intercept and slope of the VVC line for part of an assayed drill core. The process of volume-variance comparison may produce a few negative concentration values for NQ core. The negative data cannot be used for concentration and the simplest solution is to set them to zero. This is a reasonable solution provided the negative concentration values are not too many and their magnitude is not too large. The consequence of the elimination of negative concentration values has led to a minor decrease in resulting variance and small increase in resulting mean. In the Western Mineralisation, the small number of HQ drill cores after converting to NQ drill cores showed a few minor negative values related to low concentration values.

2.4.1.2 Equivalent length of core

According to the theory of volume-variance relationship, the length of a sample has an indirect relationship with the variance of concentration (grade). It does not mean that the difference between a few centimetres and a couple of metres core is the same as the difference of their variances of concentration. The core sections of different length should not just be integrated in geostatistical estimates and statistical analysis and they need "regularisation". The regularisation is a term used for compositing assayed core samples to a permanent interval length (e.g. one metre). The basic regularisation method combines core samples to equal length of composites and assigns a single concentration to each composite based on a weighted average of the length of core samples of the original component concentration (Smith 1999). There are several mathematical methods for regularisation and compositing of concentration (e.g. Dutter 2003). In this research, regularisation was performed by the subprogram "Data recomposition" in the Geostatistics for Windows software package (Dowd & Xu 2006).

2.4.2 Inclination of drill hole

The position of some points of each drill hole along the depth is characterised by their collar and survey. In the Western Mineralisation, the collar of each point of drill hole contains the following information:

- Easting location with negative signs and the values were summed at 10,000,

- Northing location with positive signs and the values were summed at 1,000, and

- Relative level (RL) with positive signs and the values were summed at 10,000. The RL values in contrast to depth values decrease from surface to depth. However, the RL values reduce with a smaller proportion relative to increase of the length of drill hole at depth because of inclination of the drill hole.

The survey of each point of a drill hole includes the following information:

- Azimuth or bearing with positive signs,
- Dip with positive signs for drilling up relative to the horizontal surface and negative signs for drilling down relative to the horizontal surface, and
- Hole depth with positive signs.

In the Western Mineralisation, the actual collar and survey of some points of each drill hole have been reported at different depths between 20 to 65 m relative to each other. The spatial coordinates (easting, northing and elevation) for start and end of each core sample were calculated using Visual Basic for Application (VBA; Microsoft Corporation 2006) programming in Excel and the program was named "Analyse" (Appendix A). The program estimates the collar and survey of each point of interest at depth for a drill hole based on interpolation. In the Analyse program, the entry data comprises the measured collar and survey values of some points at different depths of each drill hole and some depths of interest which we want to calculate their collar and survey values. These data sets should be entered in their corresponding columns defined by titles in Excel sheet (1) of the Analyse program (Appendix A). The entry data in column of depth should be sorted so that the lowest values change at the top of the column. In this program, positive dip values were considered for drilling toward down the surface level.

Therefore, in the Excel sheet (2) of the Analyse program, the start and end of each core section for which we want to know the coordinates should be entered in column (1) below title of "From" and column (2) below title of "To" respectively. In the VBA program of Analyse, the variables of "tot=" and "tot1=" should be adjusted by number of rows in the first column of the Excel sheets (1) and (2) respectively. The output data is produced in the Excel sheet (2) of the Analyse program and include spatial coordinates of start and

end of each selected interval core samples. In Analyse program, easting, northing and elevation of each sample are calculated by Equations (2.7), (2.8) and (2.9) in Table 2.5.

Table 2.5: Formulae used for calculation of the easting, northing and elevation of the samples of the Western Mineralisation.

$$East_{i+1} = East_i - (Depth_{i+1} - Depth_i) \times Sin(\frac{Dip_{i+1} - 90}{I}) \times Sin(\frac{Bear_{i+1}}{I}) \quad (2.7)$$

$$North_{i+1} = North_i - (Depth_{i+1} - Depth_i) \times Sin(\frac{Dip_{i+1} - 90}{I}) \times Cos(\frac{Bear_{i+1}}{I}) \quad (2.8)$$

$$RL_i = (Depth_{i+1} - Depth_i) \times Cos(\frac{90 - Dip_{i+1}}{I}) \quad (2.9)$$

where

$I = \frac{180}{\pi} = 57.295779531$,

$i = 0$, $i = i + 1$

In Excel sheet (1), for checking accuracy of the resulting coordinates, the real distance [Equation (2.10)] and the estimated distance [Equation (2.11)] are both calculated for each interval core samples along depth (Table 2.6) and their results should be equal to each other.

Table 2.6: Formulae used for calculation of the real and estimated depth of the samples in the Western Mineralisation.

$$Real\ distance = Depth_{i+1} - Depth_i \quad (2.10)$$

$$Estimated\ distance = \sqrt{(East_{i+1} - East_i)^2 + (North_{i+1} - North_i)^2 + (Rl_{i+1} - Rl_i)^2} \quad (2.11)$$

where i=2 (i.e. the second raw of the Excel sheet).

2.4.3 Recovery percentage

The total length of core is measured using a tape measure and then marked up as a percentage over one metre core intervals. The resulting percentage is recorded next to relevant depth interval in core. The recovery percentage should be reviewed to identify the occurrence of friable and unconsolidated minerals along the core samples as well as to determine the amount of core loss (during drilling, core washing and core cutting) particularly in the mineralised part of the cores.

The result of core loss leads to a systematic downward bias and under-reporting of the assay values or the ore mineral grade. Core loss will increase significantly if the cores intersect high grade ore. In the Western Mineralisation, because almost all core samples comprise consolidated rocks and minerals, more than 99 % of assayed core samples showed 100 % recovery and the rest of them had 95 % recovery. Hence, in this research there was no considerable core loss which needed correction.

2.5 Data Compositing

The reported assay values and specific gravity data were recomposited into each one metre NQ sample and the resulting data was integrated with the quantitative minerals and rock type data and the measured average magnetic susceptibility (AMS)[7] and maximum magnetic susceptibility (MMS)[7]. In this research, the following data set produced:

1. Thirty one geological variables of 1,928 surface core samples comprising 59,768 geological sample values,

2. Three physical parameters (specific gravity, MMS and AMS) of 1,928 surface core samples comprising 5,784 physical parameter sample values,

3. Ten element concentrations of 1,928 surface core samples comprising 19,280 assayed sample values,

4. Eight element concentrations of 1,287 underground core samples comprising 10,288 assayed sample values, and

5. In total, 77 drill cores in the Western Mineralisation treated for the data compositing of 95,120 sample values.

In the quantitative core log data, the rows denote the selected core sections (observations) and the columns show the rock types, sulphide and silicate minerals, sulphide textures, element concentrations, magnetic susceptibility and specific gravity. The columns were classified into two of the following independent groups so that each group adds up to 100 percent:

[7] **Details of magnetic susceptibility measurements are explained in Section 4.4**

1. Group of minerals assemblage: The volume percent of sulphide and silicate minerals were estimated and their summation was theoretically 100 percent. However, in many cases, the total was not 100 percent because of the remaining volume percent of other silicate minerals in the samples (see the data base of this thesis), and

2. Group of rock types: The volume percent of different rock types plus the volume percent of sulphide minerals should be 100 percent. Most samples (one metre core sample) of the Western Mineralisation comprise one or two rock types and a few core samples consist of more than three rock types (see the data base of this thesis).

The coordinates of northing, easting and elevation for start, middle and end of each sample interval were calculated for use in variogram analysis and spatial modelling (Chapters 6 to 8). The quantitative geological, geochemical and geophysical values were attributed to the middle of each core sample for reasons of consistent mathematical or statistical treatment of data. The quantitative core log data has been provided in supplementary files to this thesis.

2.6 Discussion about the conventional core logs 4003, 4004 and 4031

The conventional core logs of the Western Mineralisation describe only lithological and mineralogical variation with depth and the assay results were usually well much after the core has been logged and hence could not be used to assist logging. The conventional core logs would have been combined at a later stage with the assay results using Vulcan^{TM} or Micromine^{TM} at the Rasp Mine and the assay data does not appear on the primary qualitative core logs (Tables from 2.9 to 2.11). Drill holes 4003 and 4004 were selected as example of poor quality of information about the sulphide mineralised sections. There are many similar conventional core logs in the Western Mineralisation that provide little geological information for sulphide rich segments of their drill holes. Drill hole 4031 was selected for this section because it is enriched highly in Pb and Zn and it is an example for good quality conventional core logging of the sulphide intervals. Tables 2.7 and 2.8 shows codes were used for rock types and minerals respectively in the conventional core logs:

Table 2.7: Lithological codes used in the conventional core logs.

Brec = Brecciated rock	**Pe = Metapelite**	**Pm = Metapsammopelite**
Gq = Garnet quartzite	**Peg = Pegmatite**	**Ps = Metapsammite**
Luq = Blue quartz Lode	**Pq = Potosi gneiss**	**L = High grade sulphide mineralised lode**

Table 2.8: Mineralogical codes used in the conventional core logs.

Apy = Arsenopyrite	**Epi = Epidote**	**Gfld = Green feldspar**	**Rho = Rhodonite**
Bio = Biotite	**F = Fluorite**	**Gr = Graphite**	**Ser = Sericite**
Blq = Blue quartz	**Feld = Feldspar**	**Hed = Hedenbergite**	**Sill = Sillimanite**
Cc = Calcite	**Gah =Gahnite**	**Po = Pyrrhotite**	**Sl or Sph = Sphalerite**
Chl = Chlorite	**Gar = Garnet**	**Py = Pyrite**	**Mus = Muscovite**
Cpy = Chalcopyrite	**Gn or Gal = Galena**	**Q = Quartz**	

2.6.1 The conventional core log 4003

Table 2.9 describes that the content of galena is higher than sphalerite between 344.5 and 364.5 m of this drill hole and the amount of pyrrhotite is higher than pyrite and chalcopyrite.

Table 2.9: The conventional core log of the sulphide rich segment of drill hole 4003 from 308.1 to 364.5 m. This drill core was logged by Blampain and a new graduate (Collier).

2.6.2 The conventional core log 4004

Table 2.10: The conventional core log of the sulphide rich segment of drill hole 4004 from 123.7 to 177 m. This drill core was logged by Collier.

NOTE:
This table is included on page 52 of the print copy of the thesis held in the University of Adelaide Library.

Table 2.10 describes the major rock types (metapsammopelite and blue quartz lode), the minor rock types (metapelite, metapsammite and pegmatite) and the sulphide minerals (galena, sphalerite and pyrrhotite) between 123.7 and 177 m of the drill hole. However, Table 2.10 did not report the detailed locations or volume percentages of the rock types and sulphide minerals. Table 2.10 describes the following ratios between 137.4 and 158 m depth:

$$\frac{\text{galena}}{\text{sphalerite}} > 1, \text{ and}$$

$$\frac{\text{pyrrhotite}}{\text{pyrite}} > 1.$$

Table 2.10 also describes the following ratio between 158 and 177 m:

$$\frac{\text{galena}}{\text{sphalerite}} < 1.$$

2.6.3 The conventional core log 4031

Table 2.11: The conventional core log of the sulphide rich segment of drill hole 4031 from 292.6 to 332.3 m. This part of drill core was logged by a Director of CBH Resources Ltd (Plimer).

NOTE:
This table is included on page 53 of the print copy of the thesis held in the University of Adelaide Library.

Table 2.11 describes the location and texture of sulphide minerals in more detail at different depths. In this table, garnet quartzite and pegmatite comprise the major rock types within the sulphide mineralised samples.

2.7 Discussion about the quantitative core logs 4003, 4004 and 4031

In this study, the quantitative core logs were prepared for variation of 44 geological, geochemical and geophysical variables for the investigated samples of the Western Mineralisation.

2.7.1 The quantitative core log 4003

In Figures 2.8 and 2.9, the concentrations of Pb, Zn, Cd, S, Fe and to some extent Cu, sphalerite and galena show similar anomalous peaks and variation trends. Some of the maximum element concentrations within the sulphide rich segments of this drill hole are:

14.93 % Zn @[8] 334 m,
5.9 % Pb @ 335 m,
10.17 % Fe @ 361 m, and
153 ppm Cd @ 334 m.

The average concentration of Sb and Bi are 50 ppm but Sb concentration shows some anomalous peaks between 334 and 336 m and between 339 and 341m.

Some of the anomalous contents of galena and sphalerite are (Figure 2.8):

50 vol. % sphalerite @ 333 m, and
5 vol. % galena @ 335 m.

Some of the anomalous contents of silicate minerals are (Figure 2.9):

20 vol. % hedenbergite @ 347 m,
23 vol. % hedenbergite @ 348 m,
30 vol. % hedenbergite @ 349 m and 350 m, and
15 vol. % orange garnet @ 345 m and 346 m.

In drill hole 4003, the main textures of sulphide minerals are vein, disseminated and laminated. The abundance of rock types from surface to depth in sequential order are garnet quartzite, pegmatite, metapelite and metapsammopelite. There is no obvious relationship between variation of rock types and variation of galena, sphalerite, Pb and Zn from surface to depth. However, the abundance of pink garnet and gahnite shows a correlation with the appearance of garnet quartzite. Also, the orange garnet is abundant in pegmatite.

[8] The symbol "@" was used to mark the start of the depth for a core sample

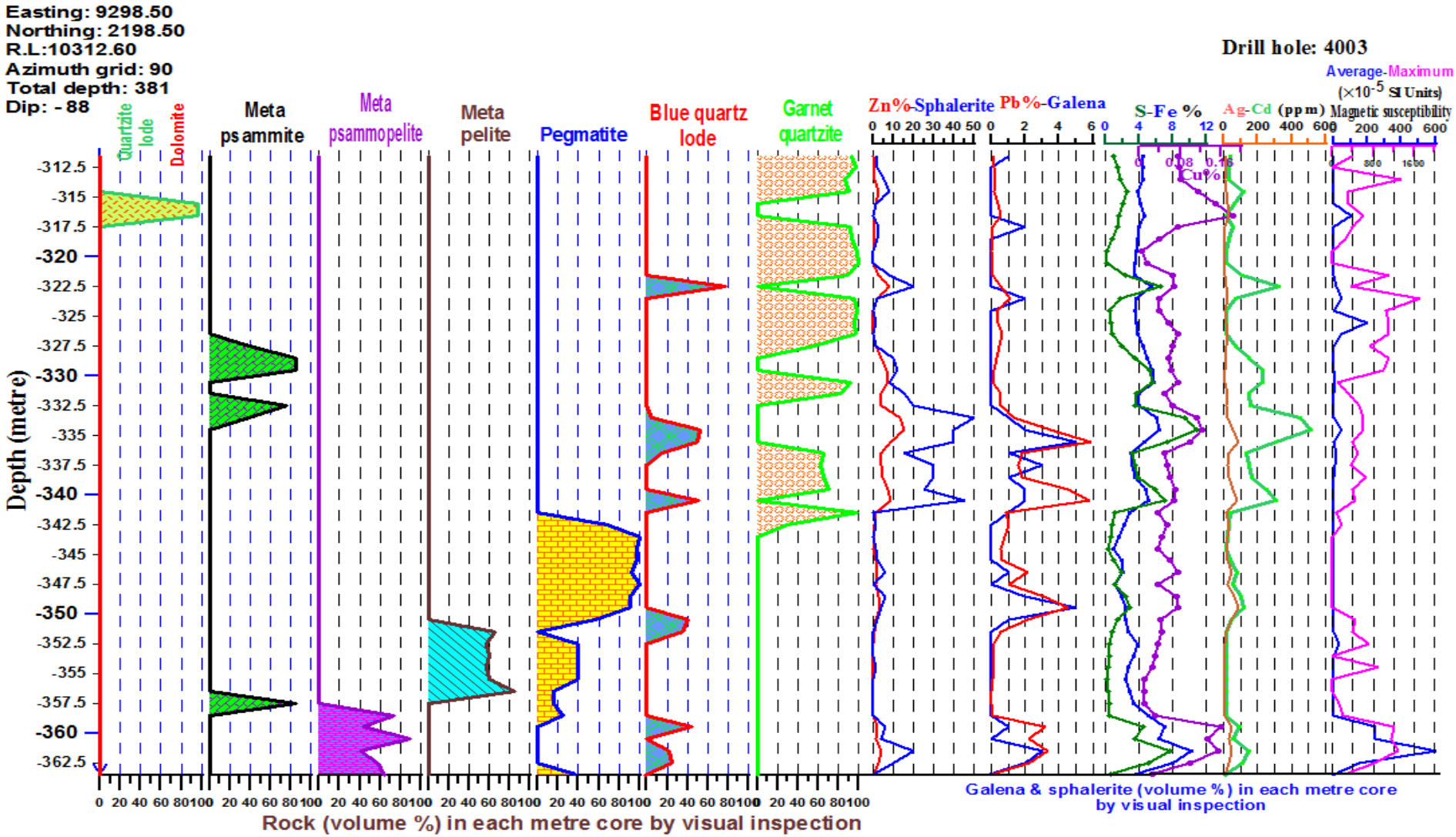

Figure 2.8: The quantitative core log of 18 parameters (rock types, minerals content, elements concentrations and magnetic susceptibility) for the investigated samples of drill hole 4003.

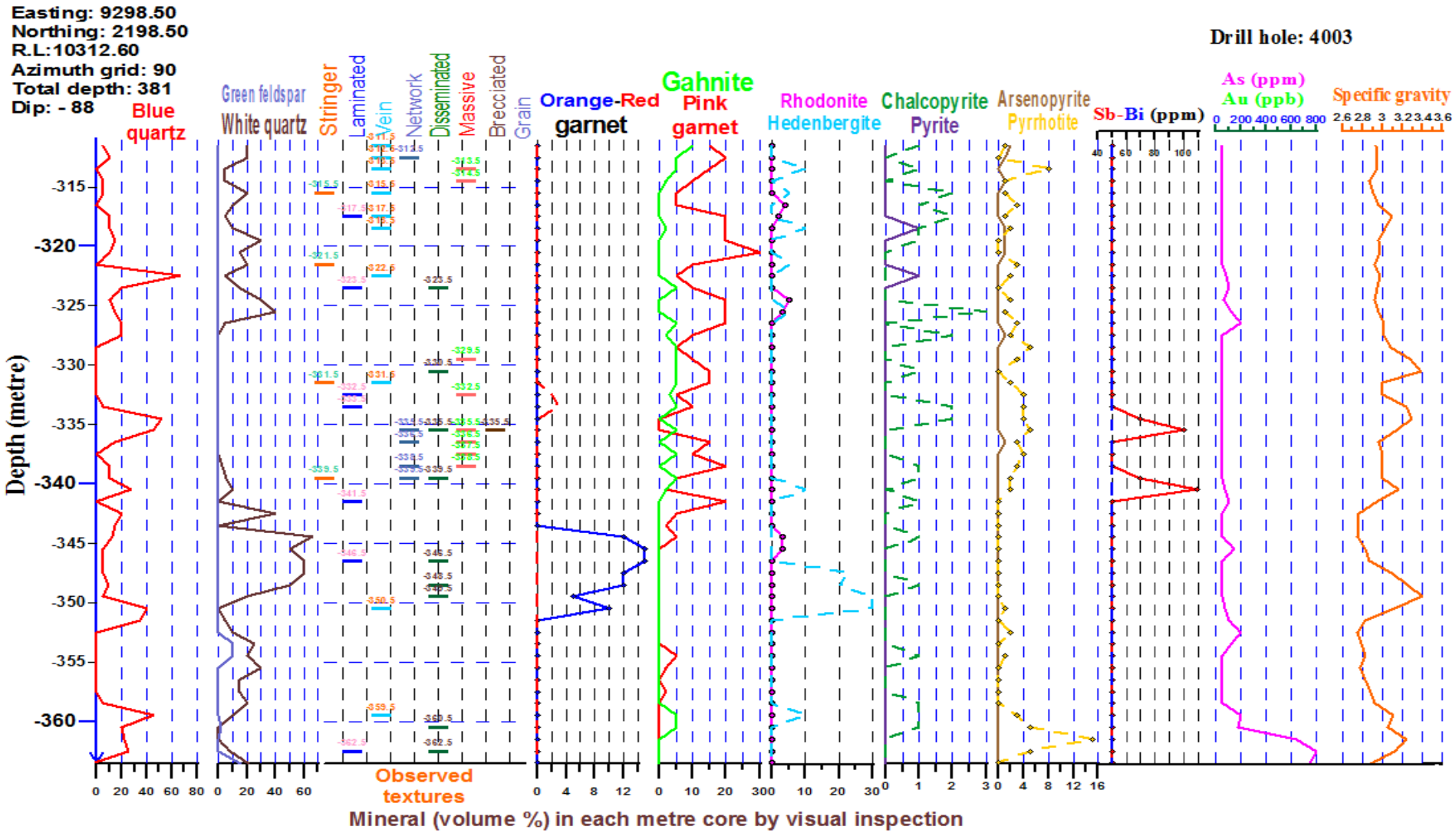

Figure 2.9: The quantitative core log of 26 parameters (sulphide textures, minerals content, elements concentration and specific gravity) for the investigated samples of drill hole 4003.

2.7.2 The quantitative core log 4004

Figures 2.10 and 2.11 show similar variation trends for the following elements and minerals:

Zn and sphalerite,
Pb and galena, and
S, Cu, Cd and Fe.

Figures 2.10 and 2.11 show high enrichment of Cd, As and Zn at some depths. For example,
210 ppm Cd @ 143 m,
293 ppm Cd @ 144 m,
195 ppm Cd @ 150 m,
6050 ppm As @144 m, and
6.1 % Zn @ 144 m.

The average concentration of As greatly increased within the analysed samples of drill hole 4004 and reached 1485 ppm.

High grade sphalerite appeared within the following depths (Figure 2.10):

16 vol. % sphalerite @ 144 m, and
26 vol. % sphalerite @ 150 m.

It is noteworthy that major sulphide minerals occurred within blue quartz in this drill hole. The abundance of pink garnet increased in garnet quartzite, metapelite and metapsammopelite. The dominant rock type for 4004 is blue quartz lode with minor metapsammite and metapsammopelite.

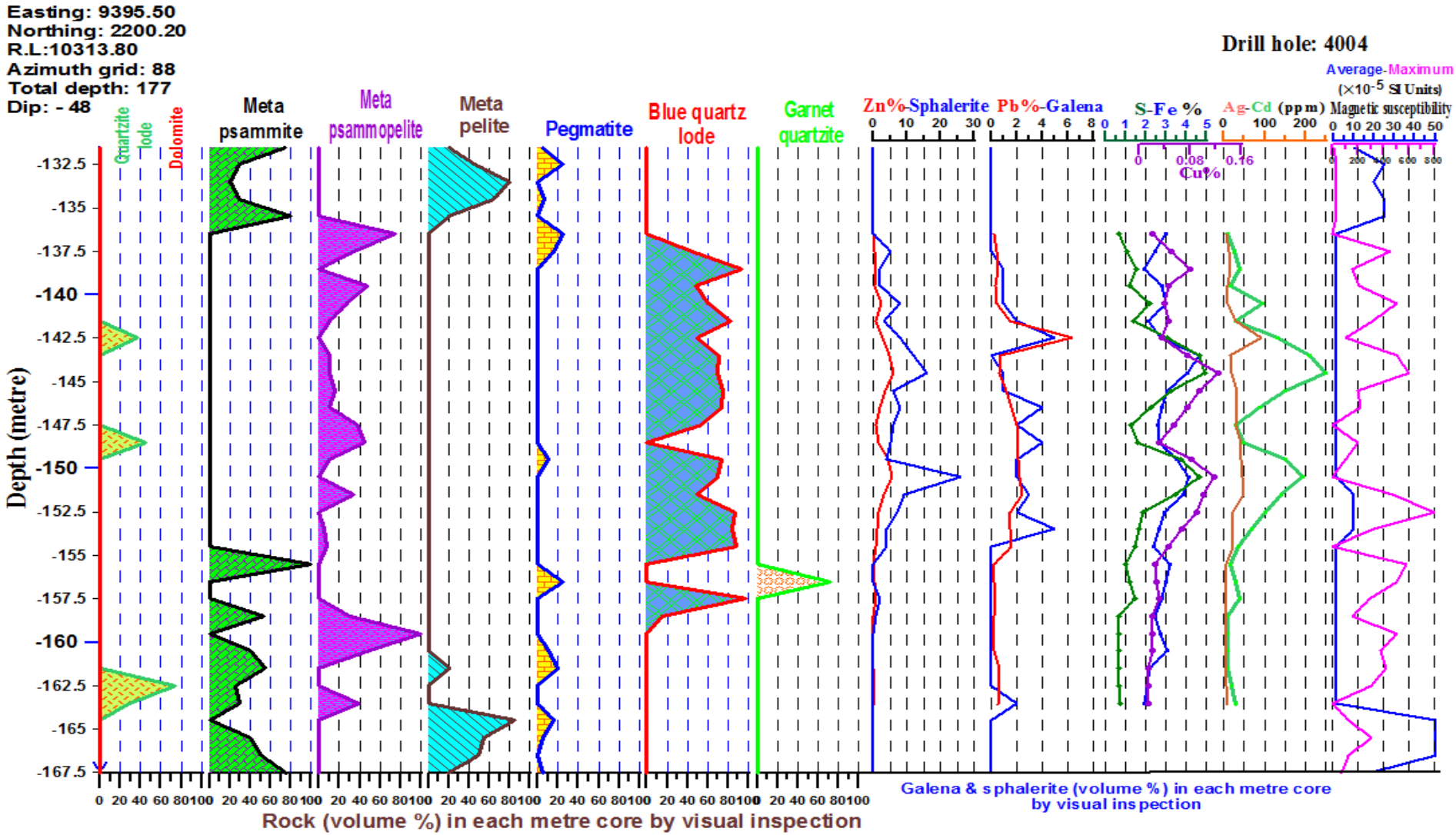

Figure 2.10: The quantitative core log of 18 parameters (rock types, minerals, elements and magnetic susceptibility) for the investigated samples of drill hole 4004.

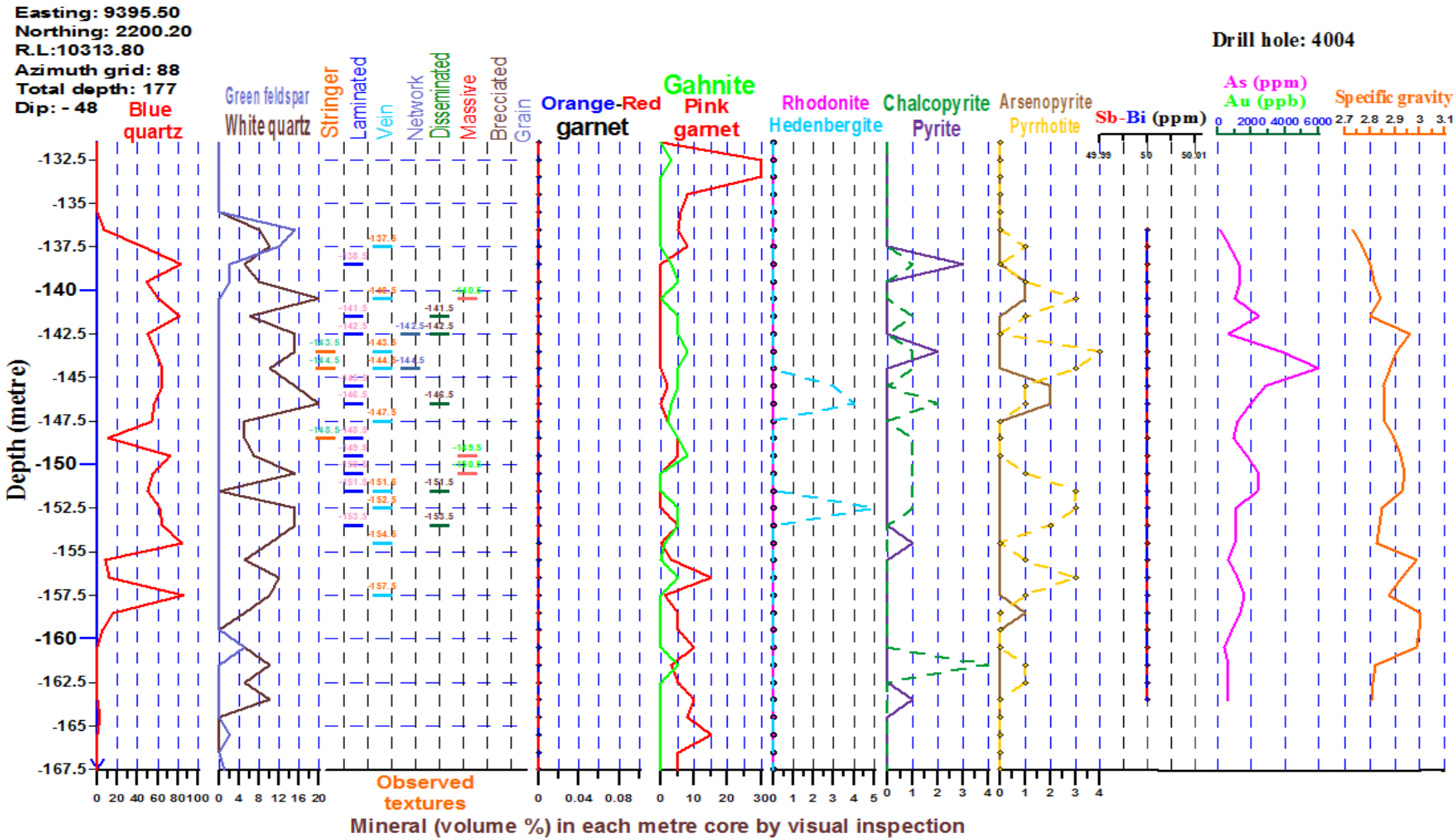

Figure 2.11: The quantitative core log of 26 parameters (sulphide textures, minerals content, elements concentration and specific gravity) for the investigated samples of drill hole 4004.

2.7.3 The quantitative core log 4031

In Figures 2.12 and 2.13, there are some similarities in variations and peak anomalies between the following elements and minerals:
Zn, Pb, sphalerite and galena, and
S, Ag and Cd.

In general, variation of all elements shows anomalous peak when approaching sulphide-bearing intervals. Some of the anomalous concentrations of Zn, Pb and Ag within this drill hole are (Figures 2.12 and 2.13):

28.10 % Zn @ 305 m,
26.87 % Zn @ 314 m,
26.47 % Zn @ 315 m,
25.07 % Zn @ 316 m,
27.84 % Pb @ 315 m,
36.68 % Pb @ 316 m, and
3773 ppm As @ 302 m
The average concentration of Sb and Bi is 50 ppm.

Some of the anomalous contents of sulphide minerals were at the following depths (Figures 2.12 and 2.13):

65 vol. % sphalerite @ 315 m,
10 vol. % galena @ 315 m, and
8 vol. % pyrrhotite between 302 and 304 m.
The abundance of the sulphide minerals decreased significantly after 317 m.

Some of the anomalous contents of orange garnet and red garnet are (Figures 2.12 and 2.13):
10 vol. % orange garnet @ 331 m, and
8 vol. % red garnet @ 302 m.

The dominant rock type within the investigated samples of drill hole 4031 is garnet quartzite and mineralisation shows a regular relationship with it. In Figure 2.13, almost all textures are equally visible in the sulphide-bearing sections of 4031. The specific gravity increases within the sulphide-rich zones.

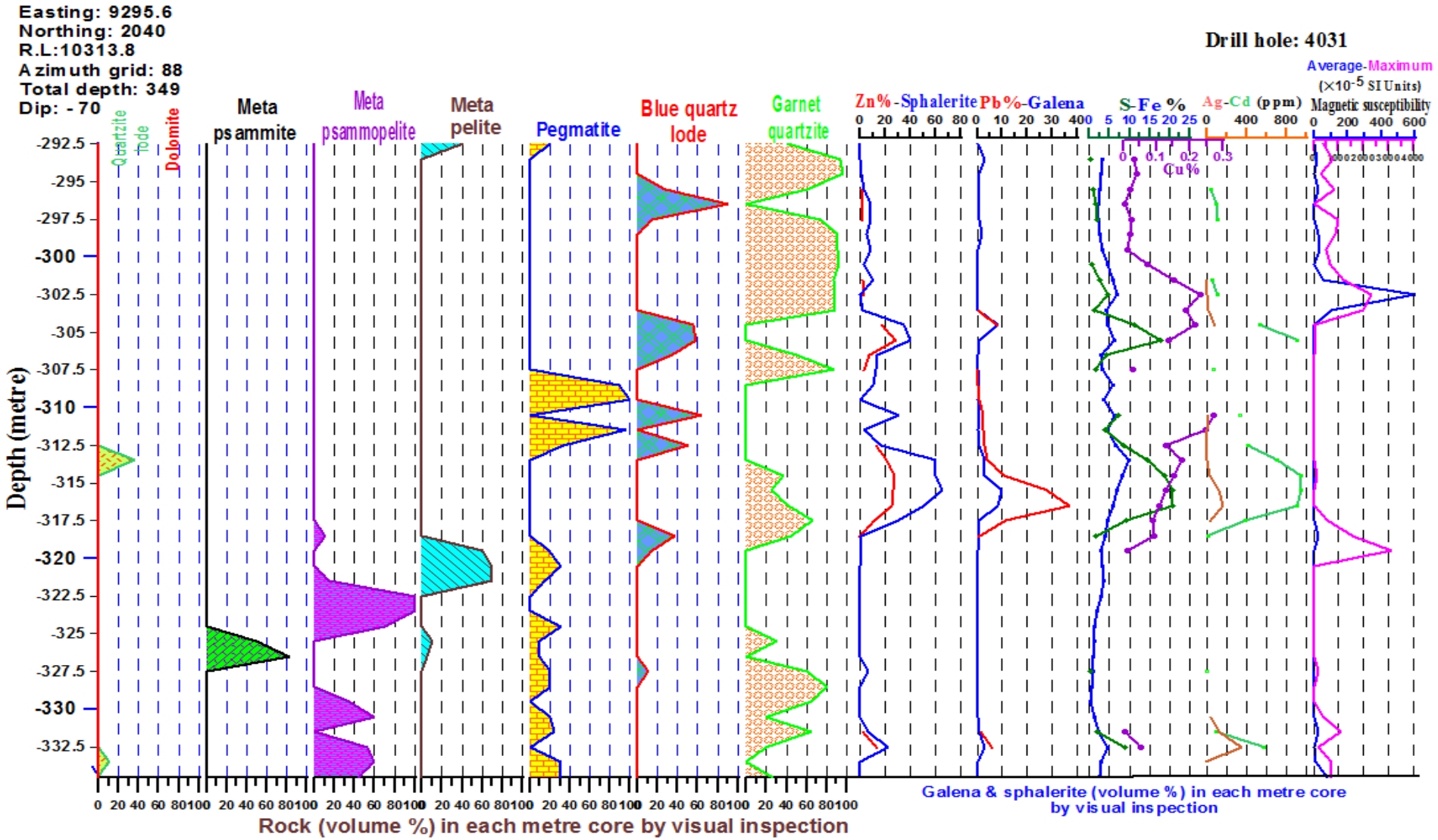

Figure 2.12: The quantitative core log of 18 parameters (rock types, minerals content, elements and magnetic susceptibility) for the investigated samples of drill hole 4031.

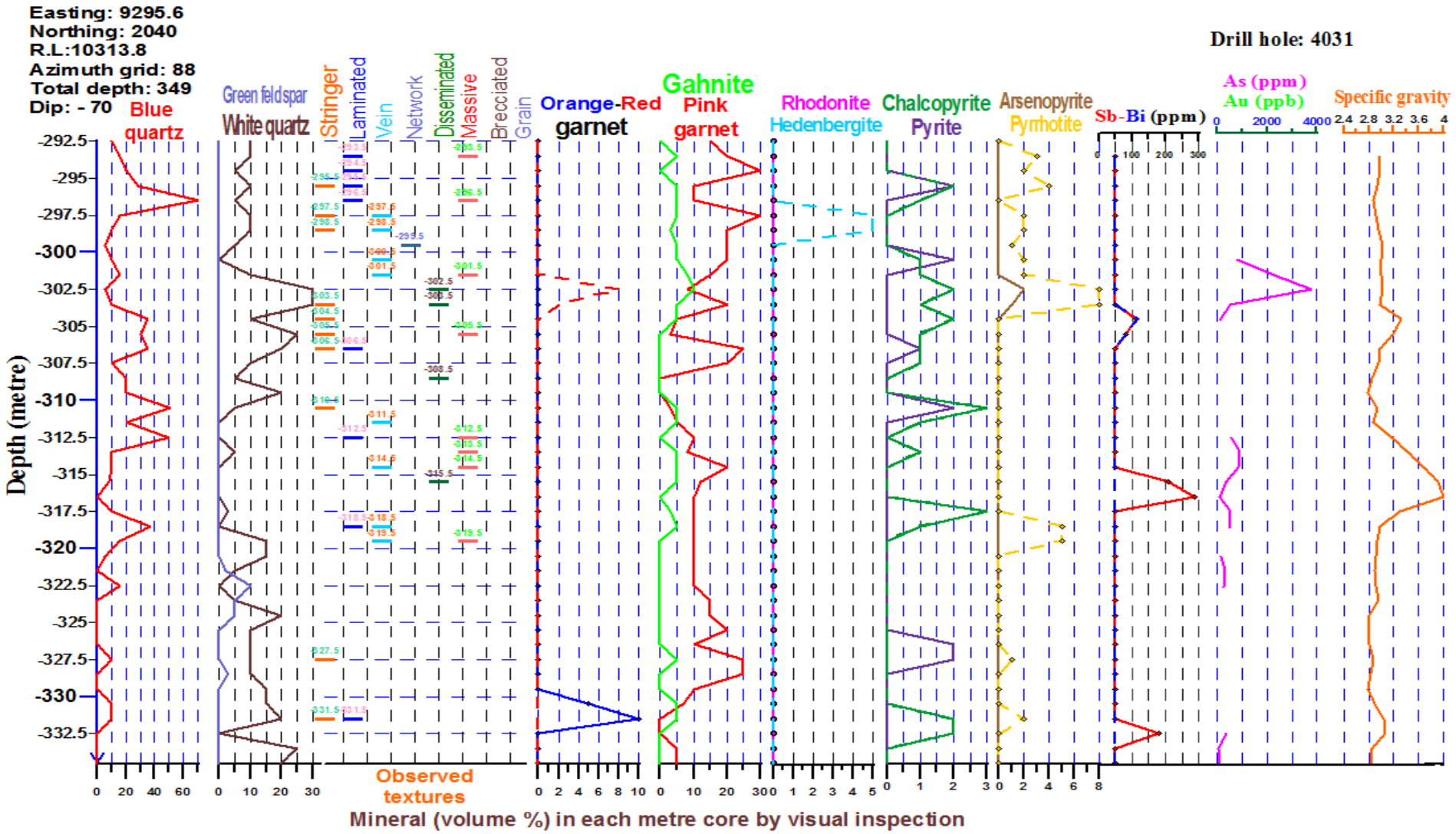

Figure 2.13: The quantitative core log of 26 parameters (sulphide textures, mineral content, elements and specific gravity) for the investigated samples of drill hole 4031.

2.8 Summary

The conventional core logging of the Western Mineralisation and other orebodies of Broken Hill have focused only on descriptive geological information for different length of drill cores and they are suffering from lack of quantitative geological information within the sulphide mineralised samples. In this study, 31 important geological variables including sulphide and silicate minerals, rock types and textures were quantified for sulphide mineralised samples and the magnetic susceptibility of 1,928 samples has been measured. The coordinates of the investigated samples were shown in the collar and the spatial maps respectively (Figures. 2.1 and 2.2).

The theory of sample volume-variance relationship was used for converting assay values of HQ and LTK60 cores to NQ cores and different lengths of assayed samples were recomposited into the equal length of samples in order to integrate the assays data with the quantitative geological information and the magnetic susceptibility measurements. The final data base comprises 44 quantitative variables for every investigated sample. Finally, this chapter compared and contrasted some conventional core logs against their respective quantitative core logs to demonstrate the resulting quality of information.

CHAPTER 3

Quantitative Core-Log Analysis for the Western Mineralisation

3.1 Introduction

In qualitative or descriptive core logging, geologists are limited to conventional or empirical core logging methods for their geological interpretation. In exploration, the time lag between qualitative core logging for geology, sample analysis for assay and preparation of a 3D block model is limited by the progress and quality of mining geology research and exploration. As mentioned in Chapter 2, conventional core logging cannot fill this gap because of the many difficulties that exist with its qualitative geological information and poor capacity to present intricate and detailed relationships between geological features and geochemical variation. Further, if just a few element concentrations of a mineralisation (e.g. Pb, Zn and Ag) are integrated for construction of a 3D block model, the final model will be only useful for mining engineers to estimate tonnage and grade of the orebody and mineral processing issues. However this may not be of much use for evaluating geological or geochemical characteristics of a specific type of mineralisation.

The quantitative core-log data set constructed in the previous chapter allows evaluation of geological information raised from drill cores in a short time and in a numerical format. The quantitative core log data set can be updated in real time, regardless of access to assay results and it can be analysed at that stage for geological interpretation. The quantitative core-log analysis enables the geologist to select relevant core samples for more detailed geological investigation.

The aim of this chapter is to statistically evaluate geological and geochemical information derived from samples of drill cores using univariate analysis of descriptive statistics. The univariate analysis is applied to the quantitative core log data set in order to describe the data and what is going on the processes of assay values, quantitative mineralogy and lithology. The univariate analysis involves the examination of a single variable at a time (e.g. variation of Zn among the assayed samples). The results are presented in the form of statistical diagrams, comparative bar diagrams and statistical tables. Moreover, in this chapter, different types of correlation coefficients are used to measure the degree of relationships between rocks types and Pb+Zn of the Western Mineralisation and examine the validity and reliability of the estimated galena+sphalerite with Pb+Zn.

The classic statistics of this chapter were calculated by SPSS (SPSS Inc. 2009) and Minitab (Minitab Inc. 2007) software packages.

3.2 Descriptive statistics

Descriptive statistics are deductive approaches that help us simplify large data sets of quantitative core logs in a sensible way to recognise drill core samples of interest. This analysis provides a flexible way to examine geological and geochemical data without preconceptions. In some circumstances (e.g. when the data set is so large), relying on geological observation without considering an application of descriptive statistics may cause biased results, with the loss of important detail or the distortion of the original data. For this purpose, some univariate analyses of the descriptive statistics were used in this chapter (Table 3.1).

Descriptive statistics have a strong reliance on graphical visualisation and the application of descriptive statistics in geology is a powerful tool for:

1. Focusing on significant geological and geochemical indications and comparing and contrasting them,
2. Providing deeper understanding of the variables,
3. Examining accuracy and precision of the variables, and
4. Summarizing a large data set to simplify information.

However, descriptive statistics cannot alone provide definite answers for geological and geochemical characteristics; such answers require our final geological judgment. This chapter aims to concentrate on the application of classic statistical methods rather than their theoretical mathematics. More details of the theoretical mathematics can be found in statistical books such as Hoaglin, Mosteller and Tukey (1983) and Tukey (1977).

Table 3.1: A summary of descriptive statistics used in this chapter.

Arithmetic mean	**Arithmetic mean (or mean in this study) is often used for measures of central tendency and indicates that quantitative data tends to cluster around a single value representing the centre of the data. For skewed data, the arithmetic mean is pulled in the direction of the heavier tail and in this case is not a true representation of the centre. Therefore, in a skewed distribution, calculation of the median is preferable.**
Median	**Median describes the middle of the range of data and separates the higher half of a population from the lower half. Compared to the mean, the median is less sensitive to outliers and skewed data and thus often provides a more informative measure of the centre.**
Confidence interval	**A confidence interval for the mean shows the reliability of a value within an estimated range of values and demonstrates the domain of the variation of the mean value. A confidence interval is always calculated for a particular percentage confidence level (e.g. 95 % confidence interval). The ideal confidence interval should be narrower or closer to the estimated mean value because the distance between a lower and higher confidence interval indicates the amount of uncertainty for a true mean value. A confidence interval for the mean is not a robust statistic for skewed data and in these cases, the measurement of confidence interval for the median is more appropriate.**
Coefficient of variation (COV)	**The COV is a measure of relative variability, equal to the standard deviation divided by the mean and the result usually is multiplied by 100. As COV is a dimensionless value, it is a useful tool for comparison of the different dispersion of data with significant different means. Dispersion in COV refers to the spread of the data around the mean value and it is calculated by the standard deviation. A greater COV for a variable indicates a higher variability of the variable relative to its mean.**
Skewness	**Skewness is a measure of how much a data set does not have a symmetrical distribution. Non-skewed distribution or normal distribution has a skewness value of zero. A positive skewness value (value greater than zero) has a distribution tail that points to the right, which indicates right skewed data. A negative skewness value has a distribution tail that points to the left.**
Quartiles	**Quartiles are values that divide total samples of data into four equal parts that help to evaluate distribution of a data set and central tendency. The first quartile (Q_1) shows 25 % of a data set is less than or equal to the Q_1 value. The second quartile (median) indicates 50 % of a data set is less than or equal to the median value and the third quartile (Q_3) shows 75 % of a data set is less than or equal to the Q_3 value.**
95 % probability (HiP) & 5 % probability (LoP)	**The amounts of 5 % of sample values that lie at the high end of the total analysed samples show a higher value than the 95 % probability of the values of the total samples (high probability or HiP). In fact, the 95 % of total samples have values less than or equal to the HiP value. In a data set, approximately 5 % of all data sets which contain higher values relative to HiP value may be suspected to be outlier data. In contrast, the amounts of the 5% of sample values that are lower than or equal to 5 % value of the total samples (low probability or LoP) may be considered as background values.**

3.3 Bar diagram

In this chapter, several bar diagrams were constructed in order to demonstrate the variation of the elements (Figures 3.3 to 3.9) and variation of galena and sphalerite (Figure 3.11) within the analysed samples of each drill core in the Western Mineralisation. The bar diagrams are composed of vertical bars for each drill core that represent minimum and maximum sample values of an element (or a mineral). Marked on each vertical bar are mean, median, LoP and HiP values. A significant difference between HiP and LoP values for an element (or mineral) indicate that it has a large variation between the analysed samples of the drill core. In a normal distribution, minimum and maximum values of the vertical bar should be close to LoP and HiP of the vertical bar respectively.

3.4 Statistical results for element concentrations of the Western Mineralisation

The statistical results of the total analysed samples have been given in Table 3.2 and plotted in Figures 3.1 and 3.2. Some statistical points of the table are explained in this section.

- **The amount of concentration**

The mean concentration of As is more than three times its median concentration. In Table 3.2, the HiP concentration of As is 22.8 times its Q_3 concentration. Table 3.2 also shows that Ag has the lowest overall mean and median concentrations. In the Western Mineralisation, Ag is largely incorporated in an atomic lattice of galena and it also occurs in tetrahedrite, pyrargyrite, polybasite, argentite, stephanite, dyscrasite, allargentum, antimonial silver and native silver. According to Table 3.2, the maximum concentrations of Fe and Bi are more than three times their HiP concentrations. This indicates that 149[1] samples are enriched significantly in Fe and 144 samples contain high Bi content.

- **Skewness**

The skewness of elements in Table 3.2 indicates that the 10 elements have positive skewed distribution. This indicates that the number of samples containing low concentrations for each element is much higher than those containing high concentrations for that element. In Table 3.2, As has the highest skewness.

[1] **Calculated by 0.05 × the number of samples containing Fe concentrations in Table 3.2**

- **COV**

According to the COV results of Table 3.2, As has the highest variability around its mean concentration and Fe has the lowest variation relative to its mean concentration. Comparison of the COV values of Zn and Pb in Table 3.2 shows that the variability of Zn around its mean concentration is 5.7 % [2] more than the variability of Pb around its mean concentration within their total analysed samples.

- **Similarities and differences**

In Table 3.2, Bi and Sb have some similar values in the number of samples, COV, median, Q3 and the maximum but they have some differences between their values of minimum, Q_1, HiP and skewness. Figures 3.1 and 3.2 show some similarities in distribution of the following elements:

- Zn and Pb,
- Fe and S,
- Bi and Sb, and
- Ag, As and Cd.

Figure 3.1 also shows that the dispersion of Cu within the analysed samples is to some extent similar to Ag, As and Cd in Figure 3.2 but with a wider dispersion.

The statistical results of the analysed samples in surface and underground drill cores have been given in Tables 3.3 and 3.4 respectively. Some important statistical results of the Tables are explained in this section.

[2] **Calculated by** $\frac{\mathbf{COV(Zn) - COV(Pb)}}{\mathbf{COV(Pb)}} \times \mathbf{100}$ **from Table 3.2**

Table 3.2: Descriptive statistics for element concentrations within the total analysed samples.

Elements (Unit)	Number of Samples	Mean	COV	Minimum	Q_1	Median	Q_3	HiP	Maximum	Skewness
Zn (%)	3013	1.98	180.1	0.0025	0.12	0.62	2.3	34.4	35.4	3.9
Pb (%)	2909	1.5	170.4	0.0025	0.18	0.60	1.76	27.8	36.7	4.7
Cu (%)	1794	0.052	89.3	0.00005	0.02	0.04	0.07	0.247	0.4	2
Fe (%)	2998	3.1	43.6	0.24	2.34	2.9	3.67	8.5	27.44	3.6
S (%)	2965	1.86	108.4	0.02	0.52	1.2	2.54	20.6	20.88	2.8
Ag (ppm)	3003	17.1	153.6	0.048	2.60	8.3	21.02	299.6	508.5	5.7
Cd (ppm)	1077	74.2	144.5	4.39	10	33.1	94.07	944.9	944.9	3.6
As (ppm)	2947	311.9	222.7	6.6	50	100	292.5	6681.5	11700	6.6
Sb (ppm)	2886	36.2	80.7	0.50	6.65	50	50	280.9	516.4	2.8
Bi (ppm)	2886	33.9	88	0.08	2.45	50	50	150	501.6	1.97

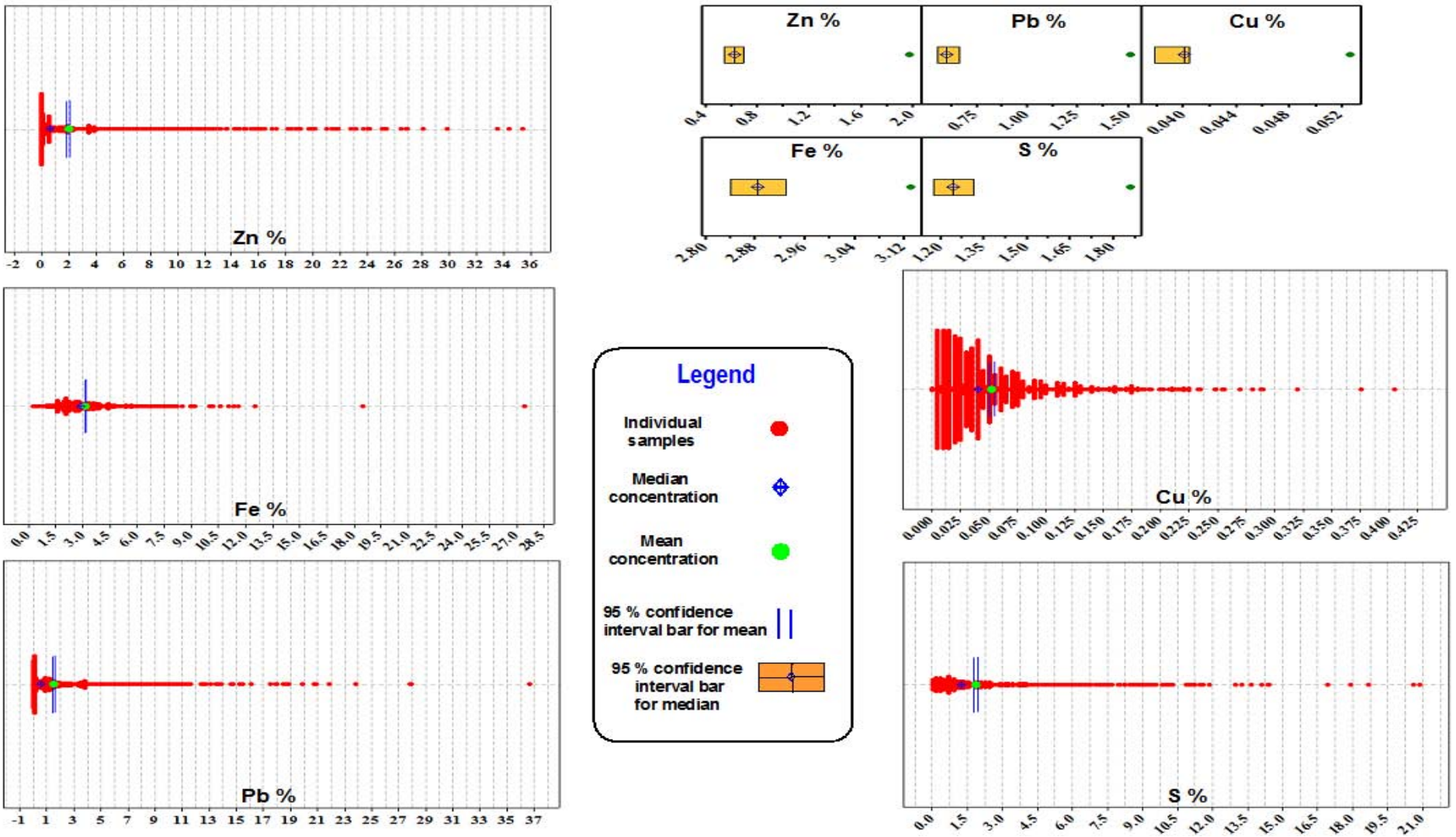

Figure 3.1: Descriptive statistics of Zn, Fe, Pb and S. The scale of horizontal axes is based on the percentage, and the number of samples of each element contributing in each graph has been given in Table 3.2.

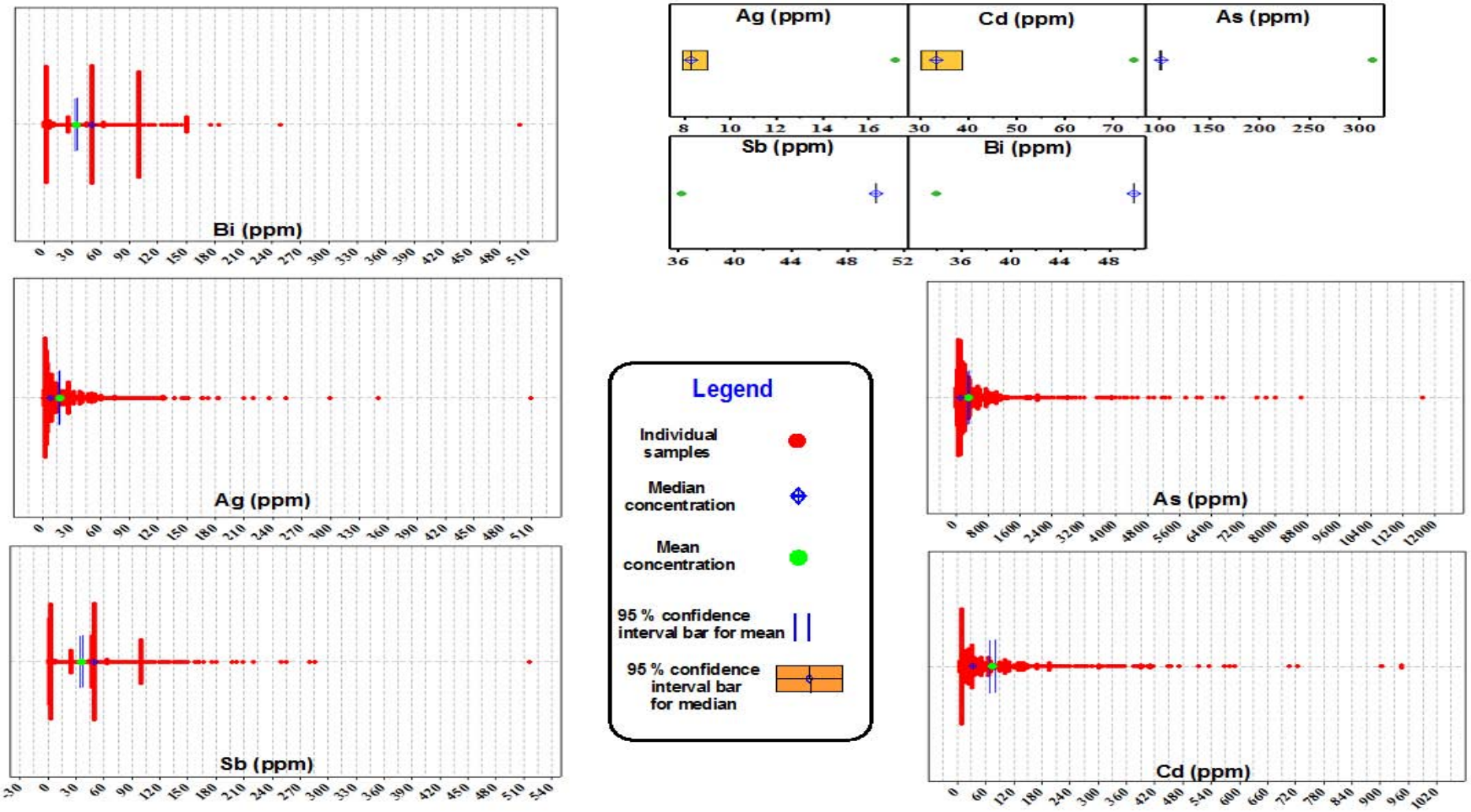

Figure 3.2: Descriptive statistics for Bi, Ag, Sb and As. The scale of horizontal axes is based on ppm and the number of samples of each element contributing in each graph has been given in Table 3.2.

Table 3.3: Descriptive statistics for 10 element concentrations within the analysed samples of surface drill holes.

Elements	Total samples	Mean	COV	Minimum	Q_1	Median	Q_3	Maximum	Skewness
Zn (%)	1809	1.69	177.2	0.0025	0.08	0.56	1.97	28.1	3.8
Pb (%)	1810	1.36	177.5	0.0025	0.13	0.55	1.64	36.7	5.5
Cu (%)	1794	0.05	89.3	0.00005	0.02	0.04	0.07	0.4	2
Fe (%)	1789	2.97	42.5	0.24	2.18	2.74	3.5	11.6	1.5
S (%)	1756	1.94	116.6	0.02	0.53	1.24	2.5	20.9	3
Ag (ppm)	1794	16.91	144.1	0.048	2.9	8.48	20.99	350.3	4.35
Cd (ppm)	1077	74.25	144.5	4.39	10	33.13	94.07	944.9	3.6
As (ppm)	1738	349.4	214.6	11.9	50	100	325	11700	6.2
Sb (ppm)	1677	52.47	27.5	25	50	50	50	286.3	7.5
Bi (ppm)	1677	54.66	31.4	25	50	50	50	249.3	4

Table 3.4: Descriptive statistics for 10 element concentrations within the analysed samples of underground drill holes.

Elements	Total samples	Mean	COV	Minimum	Q_1	Median	Q_3	Maximum	Skewness
Zn (%)	1204	2.4	175.7	0.06	0.16	0.72	2.87	35.38	3.6
Pb (%)	1099	1.7	159.4	0.073	0.24	0.72	2	27.93	3.7
Fe (%)	1209	3.4	43.7	1.06	2.57	3.07	3.8	27.44	5.6
S (%)	1209	1.7	90.4	0.062	0.49	1.22	2.63	11.05	1.4
Ag (ppm)	1209	17.4	165.9	0.68	2.3	8.18	21.73	508.5	6.8
As (ppm)	1209	258	233.6	6.6	35.5	95.7	236.5	8646.6	7.3
Sb (ppm)	1209	13.6	216.7	0.50	2.38	4.4	12.96	516.41	7.3
Bi (ppm)	1209	5	334	0.086	1.45	2.15	4.35	501.63	22

- **The amount of concentration**

Tables 3.3 and 3.4 show that the mean and median concentrations of Zn, Pb and Fe in surface drill cores are smaller than the underground drill cores. In contrast, the surface drill cores contain higher mean and median concentrations of As, Sb, Bi and S.

- **Skewness**

Comparison of the skewness of Sb and Bi between Table 3.3 and Table 3.4 shows that Sb has almost similar skewness within both surface and underground drill cores. However, the skewness of Bi in underground drill cores (22 in Table 3.4) is 5.5 times that of surface drill cores. In Table 3.4, there are significant differences between maximum (501.63 ppm) and Q_3 (4.35 ppm) concentrations of Bi within the underground drill cores.

- **COV**

The COV results of Tables 3.3 and 3.4 show that the relative variability of Sb and Bi within the underground samples is 7.8 and 10.6 times those elements within the surface samples respectively. However, Zn, Fe and Pb show small differences of variation relative to their mean values between the underground and surface samples.

According to the COV results of Tables 3.3 and 3.4, the variations of Zn and Pb within the samples of the surface drill cores are respectively 0.8 % and 11.3 % higher than the samples of underground drill cores. The relative variability of Fe relative to its mean concentration is almost the same in both of the surface and the underground drill cores. The COV of Fe in the underground drill cores is also less than the COV results of other elements.

- **Similarities and differences**

The descriptive statistics of Bi and Sb show significant differences between the analysed samples of surface (Table 3.3) and underground (Table 3.4) drill cores. Moreover, Sb and Bi in the surface drill cores have many similar values in their descriptive statistical results, but in contrast they have many different statistical results within the analysed samples of underground drill cores.

3.4.1 Interpretation of the bar diagrams of elements for the surface drill cores

- **Pb, Zn and Ag**

In Figure 3.3, the trend variation of mean and median concentrations of Pb and Ag strongly resemble each other in each drill core. This is natural because major Ag has been concentrated in the atomic structure of galena in the Western Mineralisation.

In comparison with the overall mean and median concentrations of Ag, Zn and Pb in surface drill cores (Table 3.3),

1. Drill cores 4002, 4031 and 4033 contain higher mean and median concentrations of Zn. Moreover, Zn shows high variation within the analysed samples of the drill cores (see Figure 3.3). This is because of significant differences between their minimum and HiP concentrations. In those drill cores, the HiP concentrations of Zn are close to the maximum concentrations of Zn. Sphalerite is the major sulphide mineral within the drill cores. Although Zn occurs in sphalerite, gahnite and silicates, acid dissolution and ICP-OES analysis only determined Zn in sphalerite,

2. Drill cores 4002 and 4031contain higher mean and median concentrations of Pb, and

3. Drill cores 4002 4005 and 4031 contain higher mean and median concentrations of Ag.

- **S**

The trend variation of S (Figure 3.4) is very similar to the trend variation of Zn (Figure 3.3). This is natural in the Western Mineralisation because the major sulphide mineral containing S is sphalerite. Sulphur has also been concentrated in the atomic structure of a variety of sulfosalt minerals (e.g. gudmundite, bournonite, stephanite, polybasite, pyrargerite, stibnite and tetrahedrite). The concentration of S (like Zn) shows great variation within the analysed samples of drill cores 4002, 4031 and 4033 because of significant differences between their minimum and HiP concentrations. The drill cores also contain higher overall mean and median concentration of S in comparison with those values in other surface drill cores (Table 3.3).

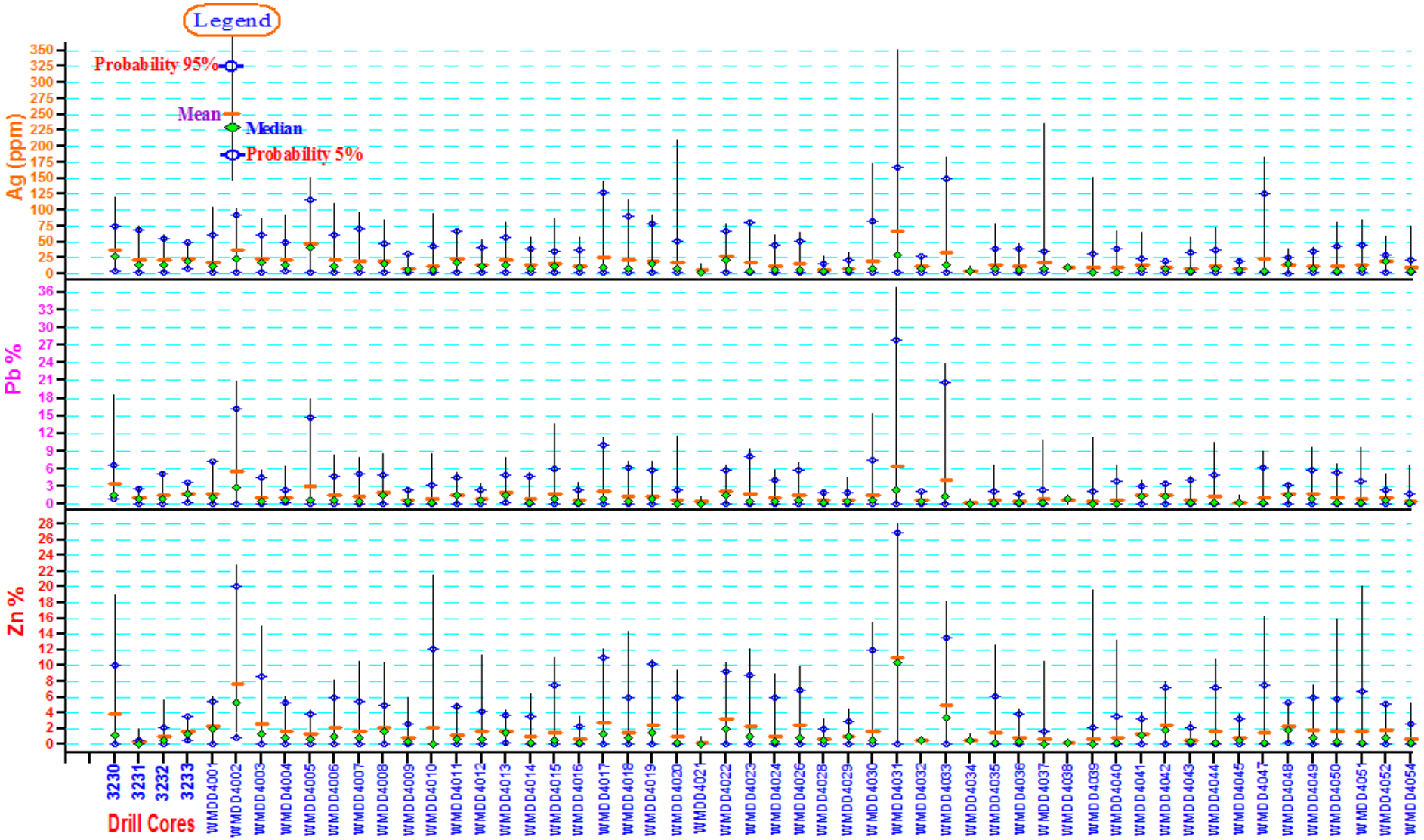

Figure 3.3: Descriptive statistics for Zn, Pb and Ag within the analysed samples of each surface drill core.

- **Fe**

In comparison with the overall mean and median concentrations of Fe (Table 3.2) drill cores 4002, 4003, 4031, 4033 and 4052 (Figure 3.4) contain higher mean and median concentrations of Fe. Pyrrhotite is a major sulphide mineral containing Fe in the Western Mineralisation and other minor sulphide and sulfosalt minerals containing Fe are pyrite, arsenopyrite, löllingite, gudmundite and tetrahedrite. Galena and sphalerite samples of the Western Mineralisation contain high Fe. Iron in silicates was not analysed.

- **Cu**

Figure 3.4 displays high mean and median concentrations of Cu among drill cores 3230, 4002, 4022, 4031 and 4052. The concentration of Cu also shows high variation within the analysed samples of drill cores 4001, 4019, 4020, 4030, 4031, 4045 and 4049 because of their higher HiP concentrations relative to the HiP concentrations of other drill cores. In the Western Mineralisation, chalcopyrite is a major sulphide mineral containing Cu. Cupper has also been incorporated in the atomic structure of a variety of sulphide minerals (e.g. galena, sphalerite and gudmundite) and sulfosalt minerals (e.g. tetrahedrite, tennantite and bournonite).

- **Cd**

In Figure 3.5, the drill core 4031 contains the highest mean and median concentrations of Cd followed by drill cores 4022 and 4042. The mean and median concentrations of Cd in drill core 4031 are almost 5 and 10 times the overall mean and median concentrations of Cd respectively within the analysed samples of surface drill cores (Table 3.3). In the Western Mineralisation, Cd has been concentrated in the atomic structure of sphalerite.

- **As**

In Figure 3.5, the median concentration of As in drill cores 4004, 4032 and 4052 is about 10 times the overall median concentration of As (100 ppm) in Table 3.3. In Figure 3.5, significant differences between the minimum and HiP concentrations of As within the analysed samples of drill core 4048 indicate a high variation of As. In the Western Mineralisation, the major minerals containing rich As are arsenopyrite and löllingite but As has also been concentrated in the atomic lattice of galena, sphalerite, pyrite and other minor sulphide minerals.

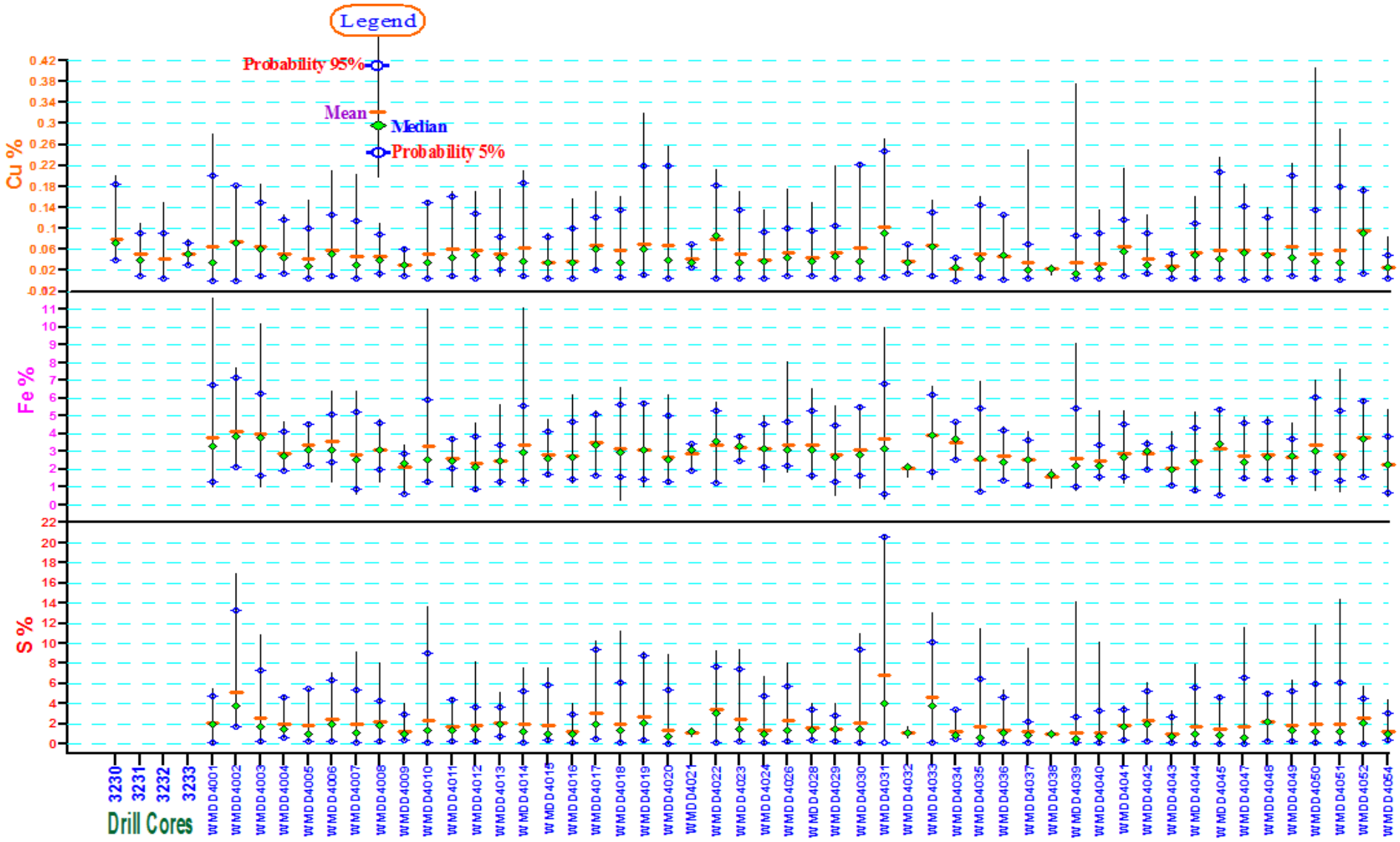

Figure 3.4: Descriptive statistics for S, Fe and Cu within the analysed samples of each surface drill core.

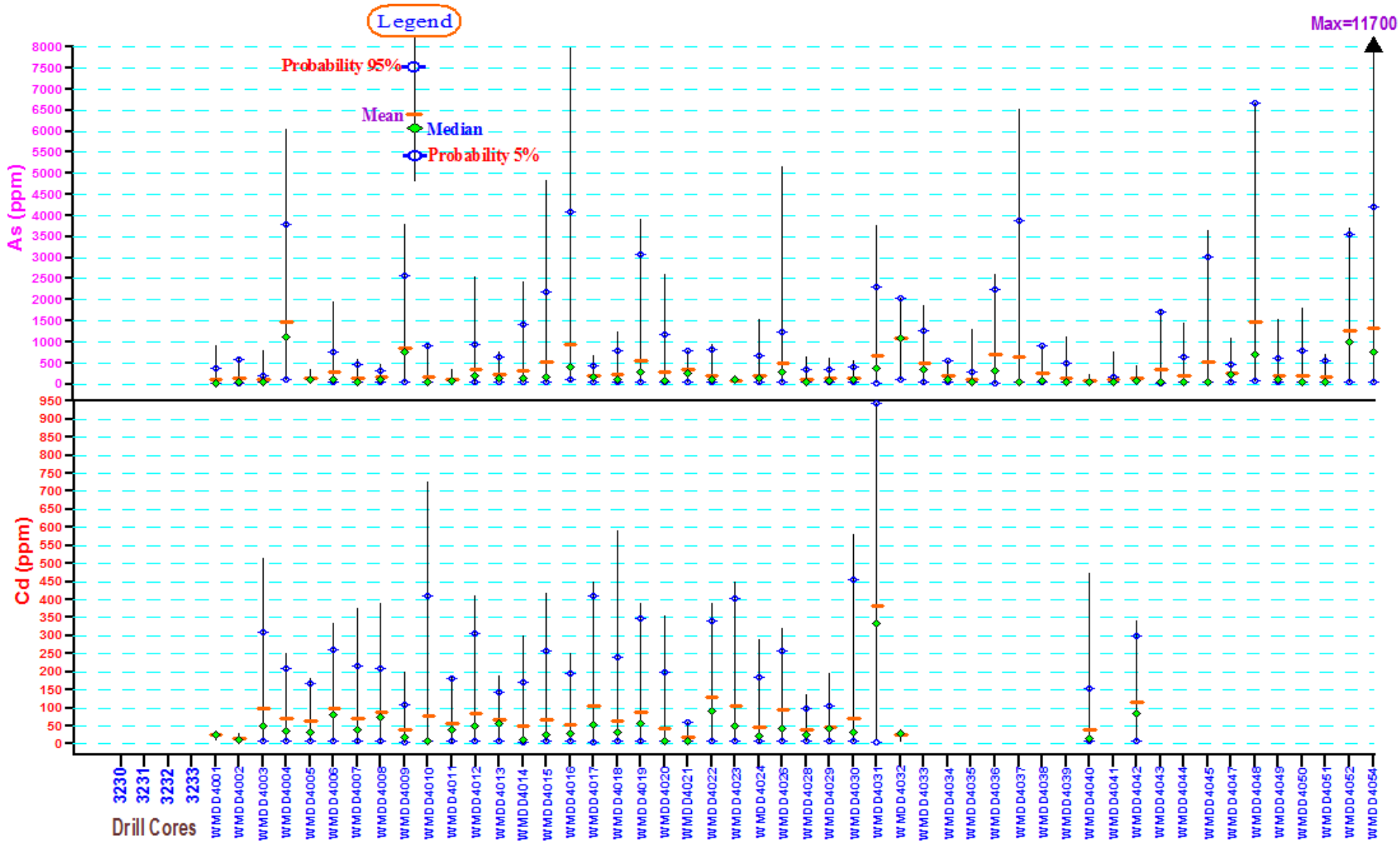

Figure 3.5: Descriptive statistics for Cd and As within the analysed samples of each surface drill core.

- **Bi and Sb**

In Figure 3.6, most of the drill cores have mean and median concentrations of ~50 ppm for Bi and Sb. However, there are some drill cores, such as 4015, 4033, 4034 and 4036, where the mean and the median concentrations of Bi are significantly greater than those of Sb.

In comparison with the overall mean and median concentrations of Bi in surface drill cores (54.66 ppm and 50 ppm respectively in Table 3.3), drill cores 4002, 4006, 4015, 4017, 4033, 4034 and 4036 contain higher mean and median Bi concentrations. In the Western Mineralisation, Bi has been concentrated significantly in the atomic structure of galena, sphalerite, pyrrhotite and other minor sulphide minerals

In comparison with the overall mean and median concentrations of Sb in surface drill cores (52.47 ppm and 50 ppm respectively in Table 3.3), drill cores 4002, 4006 and 4017 contain higher mean and median Sb concentrations. In the Western Mineralisation gudmundite is the major mineral containing Sb. However, Sb occurred either in the form of minor sulfosalt minerals (e.g. tetrahedrite, pyrargyrite and bournonite) or within the atomic structure of galena, sphalerite, pyrrhotite, pyrite and other minor sulphide minerals.

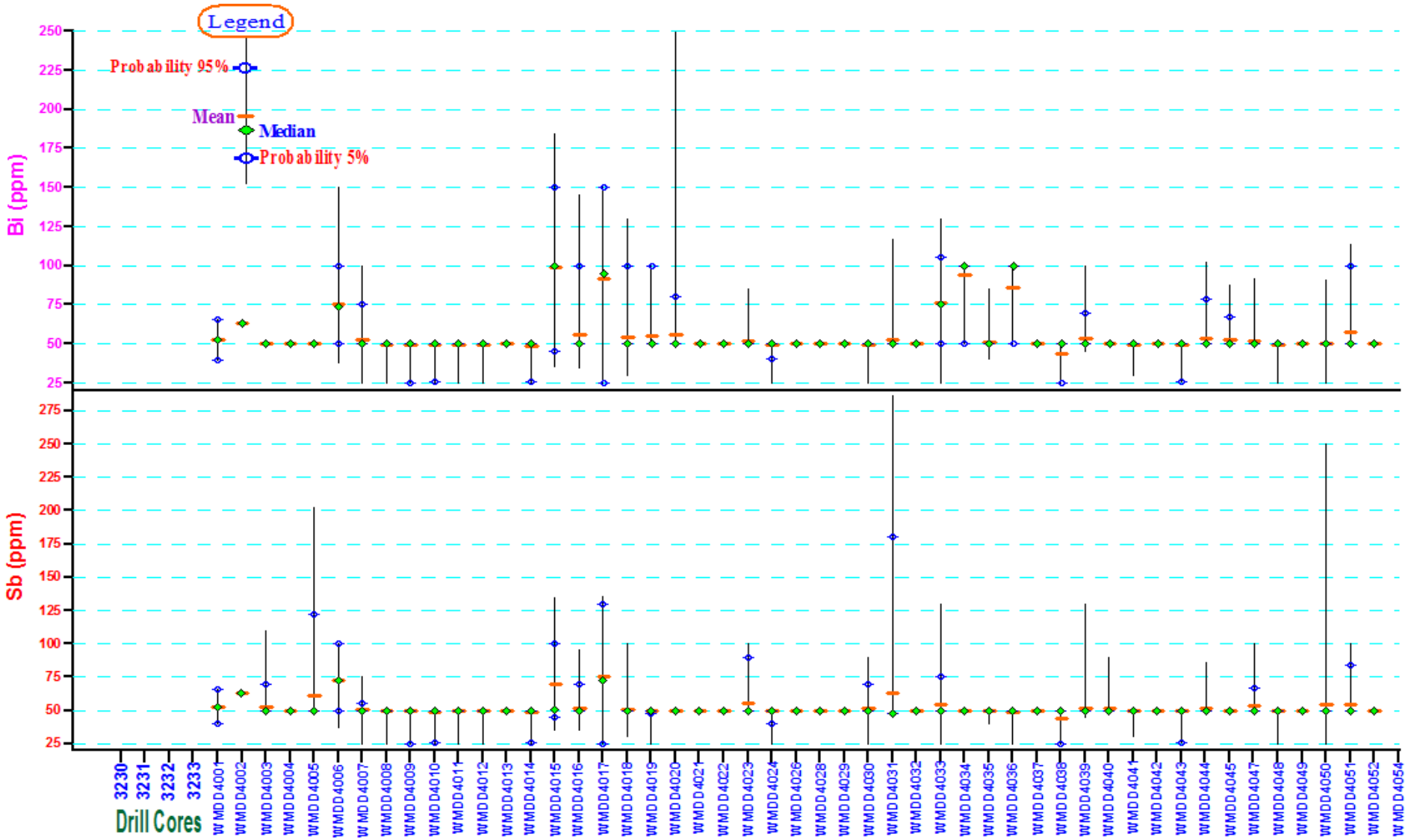

Figure 3.6: Descriptive statistics for Bi and Sb within the analysed samples of each surface drill core.

3.4.2 Interpretation of the bar diagrams of elements for the underground drill cores

- **Zn and Pb**

Figure 3.7 shows some similar trend variations of mean and median concentrations between Zn and Pb. Drill cores 4062 and 4064 contain high mean and median concentrations of Zn and Pb. There are significant differences between minimum and HiP concentrations of Pb and Zn in drill cores 4063, 4079 and 4080. This indicates high variations of Pb and Zn within the analysed samples of the underground drill cores.

- **Fe**

Drill core 4067 has the highest HiP and maximum concentrations of Fe among all existing surface (Figure 3.4) and underground (Figure 3.7) drill cores. Iron has high mean and median concentrations within the analysed samples of underground drill cores 4063, 4064, 4066, 4067, 4071 and 4080.

- **S, Ag and As**

In Figure 3.8, the trend variation of mean and median concentrations of S is comparable with those of Zn and Pb (Figure 3.7) in the corresponding underground drill cores. However, the trend variation of mean and median concentrations of Ag and As in Figure 3.8 does not vary in the same fashion. Sulphur displays high mean and median concentrations in drill cores 4062, 4064 and 4080. Silver and As show maximum variation within the analysed samples of drill cores 4059 and 4071 respectively.

- **Bi and Sb**

The mean and median concentrations of Bi and Sb are very much lower among the underground drill cores (Figure 3.9) relative to surface drill cores (Figure 3.6) and vary more distinctly among the underground drill cores relative to the surface drill cores. Drill cores 4059, 4063 and 4079 reveal high variations of Sb within their analysed samples because of their significant difference of minimum and HiP concentrations. Drill cores 4068, 4071, 4074 and 4079 shows great variations of Bi within their analysed samples.

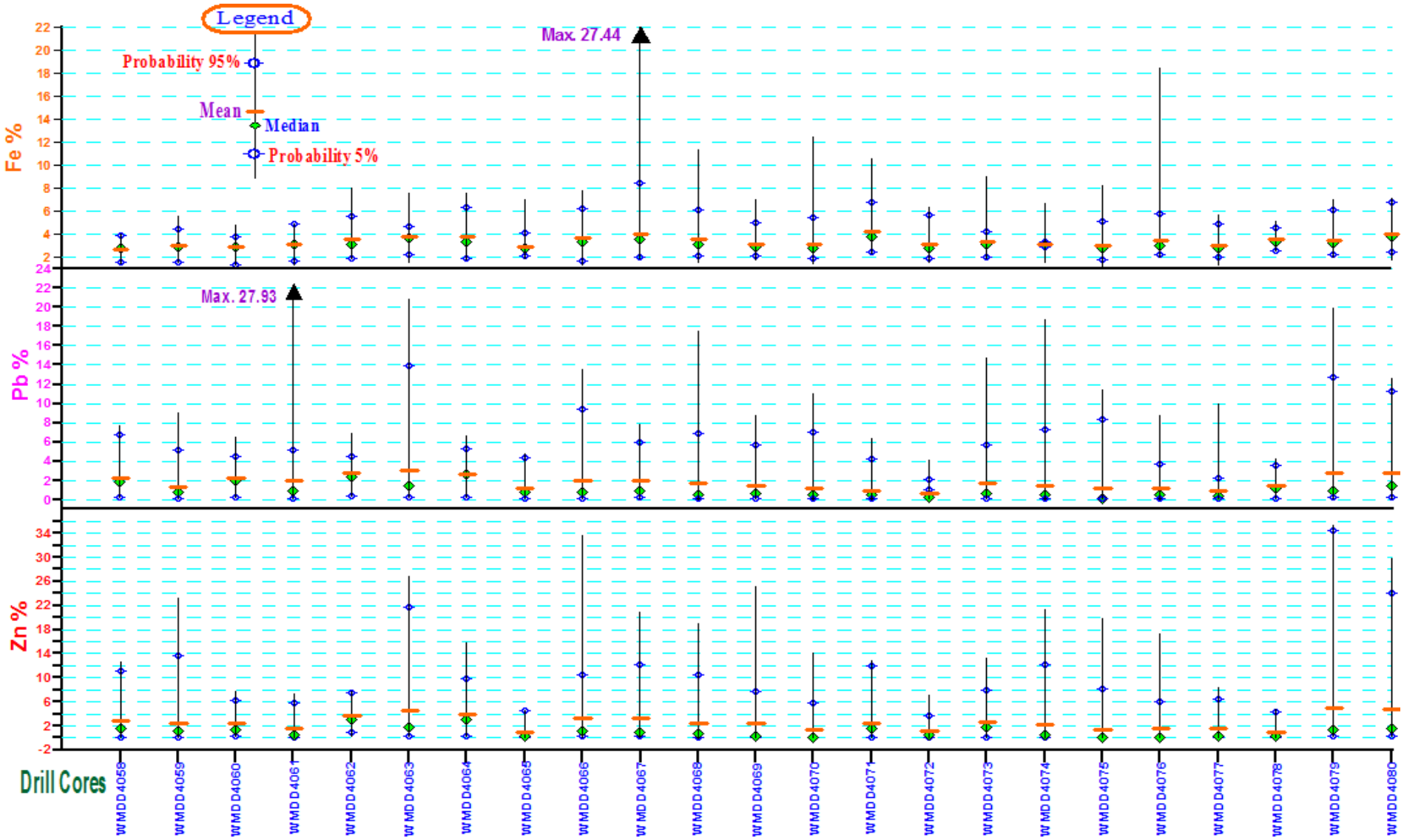

Figure 3.7: Descriptive statistics for Zn, Pb and Fe within the analysed samples of each underground drill core.

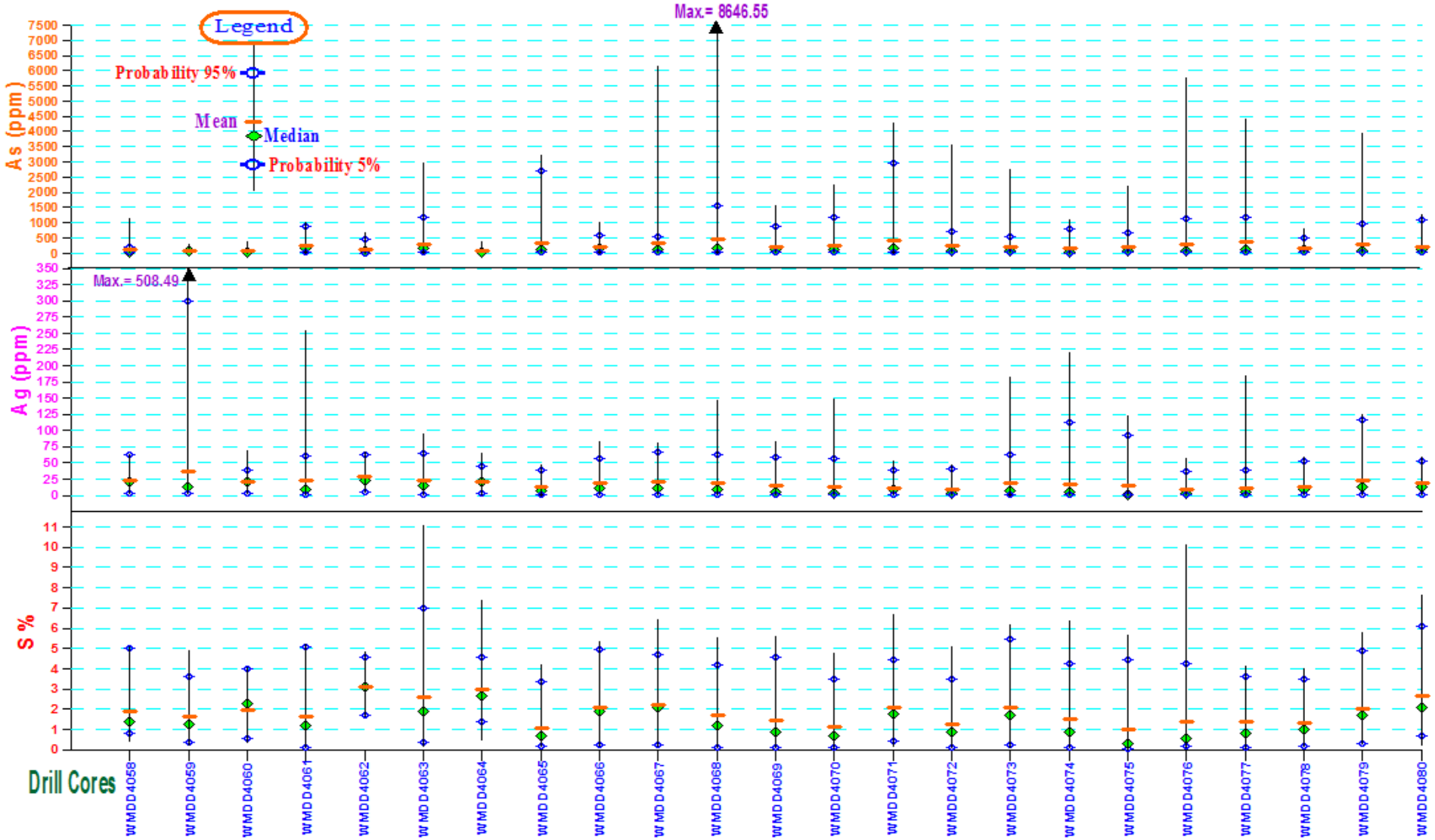

Figure 3.8: Descriptive statistics for S, Ag and As within the analysed samples of each underground drill core.

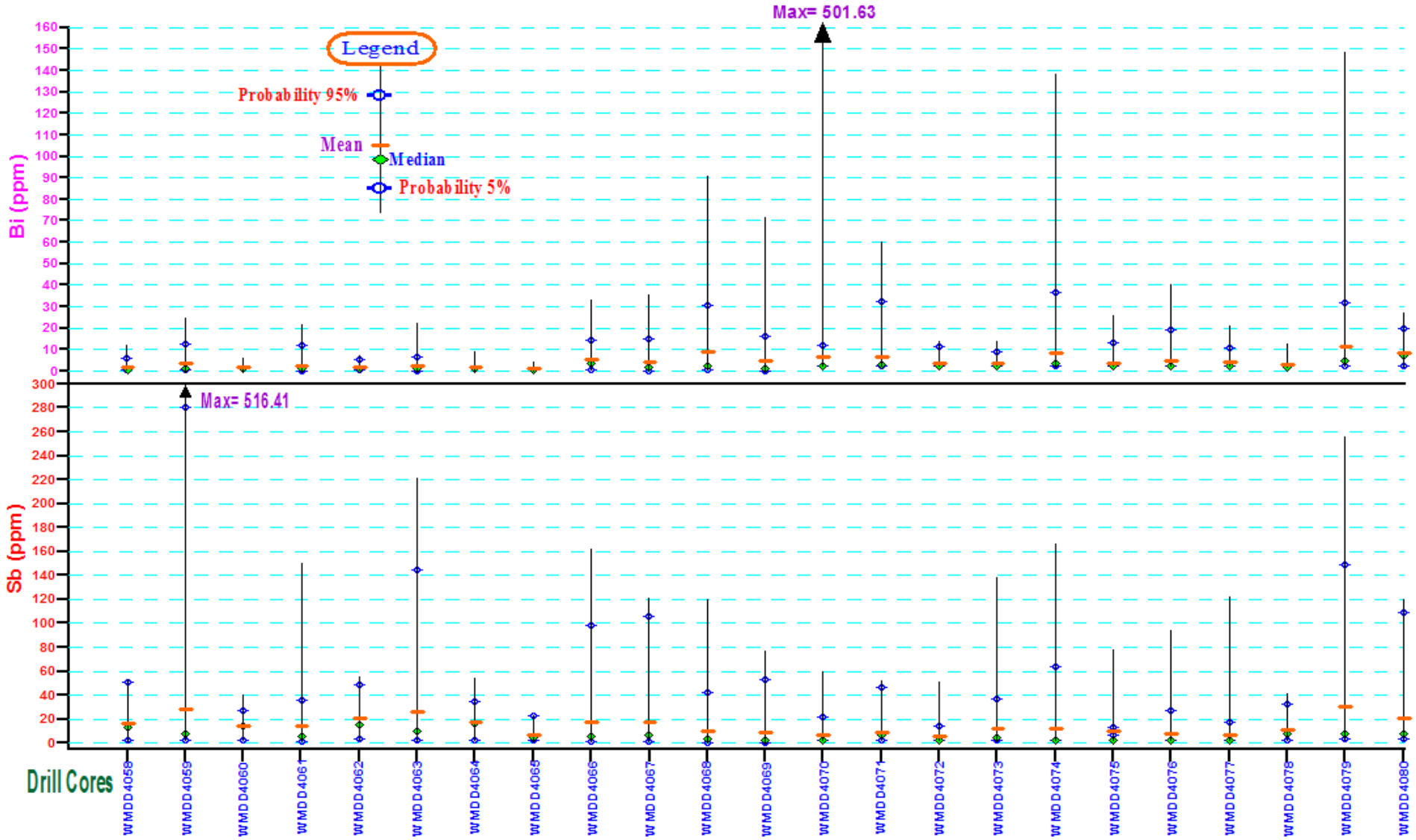

Figure 3.9: Descriptive statistics for Sb and Bi within the analysed samples of each underground drill core.

3.4.3 Discussion of the statistical results and the bar diagrams of elements

In Tables 3.2, 3.3 and 3.4, a higher COV value for an element (e.g. As in Table 3.2) relative to other elements may indicate that the element has been affected more than other elements by retrogression, remobilisation and general cooling of the orebody. In the case of As, it may have even been added during the Olarian Orogeny as a result of metamorphic fluid reacting with a redox boundary (i.e. the Western Mineralisation; Plimer 2006b). The overall mean and median concentrations of elements in Tables 3.2 to 3.4 does not provide the detailed statistical information about the variation of every element within each drill core. The bar diagrams of element concentrations provide a better opportunity to visualise some of the descriptive statistics for drill cores and evaluate their differences and similarities.

Differences between HiP and the minimum concentration of an element within the analysed samples of a drill core can better evaluate variation of the element in comparison with the difference between maximum and minimum concentrations of the element. For example, in Figure 3.3, the analysed samples of drill core 4031 contain a maximum Zn value of 28 % and a HiP of 27 %; that means 95 % of the total analysed samples contain less than or equal to 27 % Zn concentration and this is very close to 28 %. However, drill core 4039 with a maximum of 19.67 % contains a Zn concentration of less than 2 % for 95 % of the analysed samples. A bar diagram of COV can also compare the relative variation of an element concentration (or volume percentage of mineral) within different drill cores (Figure 3.13).

In the bar diagrams, drill cores with similar collar locations (fanned drill holes; Figure 2.1) show very different mean and median concentrations for some elements. For example, As in drill core 4048 (Figure 3.5) has several times higher mean, median and HiP concentrations in comparison with those of drill cores 4040 and 4044. This indicates that the variation of As changes rapidly in a small scale of space around the drill holes and there is a significant spatial anisotropic that controls variation of As even in very closely spaced drill holes. Therefore, quantification of the spatial anisotropic for each element concentration (or volume percentage of mineral) can better reveal the spatial distribution and structural variation of the element (or the mineral) within the orebody. More details are provided in Chapters 6 and 7.

The concentrations of Zn, Fe and Pb vary less than other elements relative to their mean values in the samples of surface and underground drill cores. This is probably because the elements comprise the major percentage of sulphide minerals in the Western Mineralisation.

3.5 Statistical results for sulphide and silicate minerals of the Western Mineralisation

The statistical results of sulphide and silicate minerals have been given in Tables 3.5 and 3.6 and plotted in Figure 3.10 and bar diagram of galena and sphalerite in Figure 3.11. Since the total investigated samples of the Western Mineralisation are limited to the sulphide mineralised area, the number of samples containing silicate minerals in Table 3.6 is a result of sampling bias. Some important results of Tables 3.5 and 3.6 are outlined below.

Table 3.5: Descriptive statistics for sulphide minerals.

Sulphide minerals (Vol. %)	Number of samples	Mean	COV	Min.	Q_1	Median	Q_3	Max.	Skewness
Galena	904	3.5	146.8	1	1	2	4	50	5
Sphalerite	1031	7.	127	1	2	4	8	65	3.1
Chalcopyrite	883	1.8	62.5	1	1	1	2	10	1.9
Pyrrhotite	995	3.2	103.3	1	1	2	4	40	4.5
Arsenopyrite	111	1.8	49.4	1	1	2	2	5	1
Pyrite	87	1.8	63.7	1	1	1	2	8	2.5

Table 3.6: Descriptive statistics for silicate minerals.

Sulphide minerals (Vol. %)	Number of samples	Mean	COV	Min.	Q_1	Median	Q_3	Max.	Skewness
Gahnite	777	6.3	67.6	1	4	5	8	35	2.1
White quartz	1275	8.9	108.3	1	3	5	10	70	3
Green feldspar	263	5.8	93.2	1	2	5	8	30	2.3
Pink garnet	1261	13.6	65.3	1	5	10	20	50	0.6
Red garnet	64	3.7	68.5	1	2	3	5	15	2.3
Orange garnet	101	11.1	76	1	4	10	15	40	1
Hedenbergite	197	10	94.9	1	5	5	10	60	2.6
Rhodonite	56	6.7	73.7	1	3	5	10	20	1.3
Blue quartz	1520	30	94.5	1	5	15	54	100	0.8

- **The abundance of minerals**

According to Tables 3.5, the investigated sulphide minerals in order of abundance are: **sphalerite > pyrrhotite > galena > chalcopyrite > arsenopyrite > pyrite.**

According to Tables 3.6, the investigated silicate minerals in order of abundance are: **blue quartz > white quartz > pink garnet > gahnite > green feldspar > hedenbergite > orange garnet > red garnet > rhodonite.**

According to Table 3.5, the number of pyrrhotite-bearing samples is almost 9 and 11 times that of the samples containing pyrite and arsenopyrite respectively. Pyrrhotite will be discussed in more detail in Chapter 4.

- **The volume percentage of minerals**

According to Table 3.5, the mean and median volume percentages of sphalerite are two times those of galena. Pyrrhotite has a higher mean and median volume percentage relative to those of pyrite and chalcopyrite but the median volume percentage of pyrrhotite is the same as that of arsenopyrite. In Figure 3.11, sphalerite has high mean and median values in drill cores 3230, 4002, 4031and 4033 and galena shows high mean and median volume percentages in drill cores 4005, 4033 and 4044.

- **Skewness**

Tables 3.5 and 3.6 show that all minerals have a positive skewed distribution and galena has maximum skewness followed by pyrrhotite.

- **COV**

Comparison of the COV results in Tables 3.5 shows that the volume percentage of galena has maximum variability relative to its mean volume percentage. Comparison of the COV results in Tables 3.6 shows that the volume percentage of gahnite has minimum variability relative to its mean volume percentage. In Table 3.5, pyrrhotite has a higher COV value in comparison with chalcopyrite, pyrite and arsenopyrite. This indicates that the volume percentage of pyrrhotite changes significantly more than the volume percentages of chalcopyrite, pyrite and arsenopyrite around its mean value.

- **Similarities**

Figure 3.10 shows some similarities between the dispersions of galena, sphalerite and pyrrhotite. In Figure 3.10, some minerals with a low number of samples (e.g. arsenopyrite, pyrite, chalcopyrite and hedenbergite) do not show a continuous dispersion. This is mostly because the minerals were quantified based on a discrete format (i.e. 1, 2, 3…) rather than a continuous format (e.g. 2.35) in the element concentration.

Comparison of Figure 3.11 with Figure 3.3 shows many similarities in trend variation of mean and median values between the following minerals and elements:

1. Sphalerite (Figure 3.11) and Zn (Figure 3.3), and
2. Galena (Figure 3.11) and Pb (Figure 3.3).

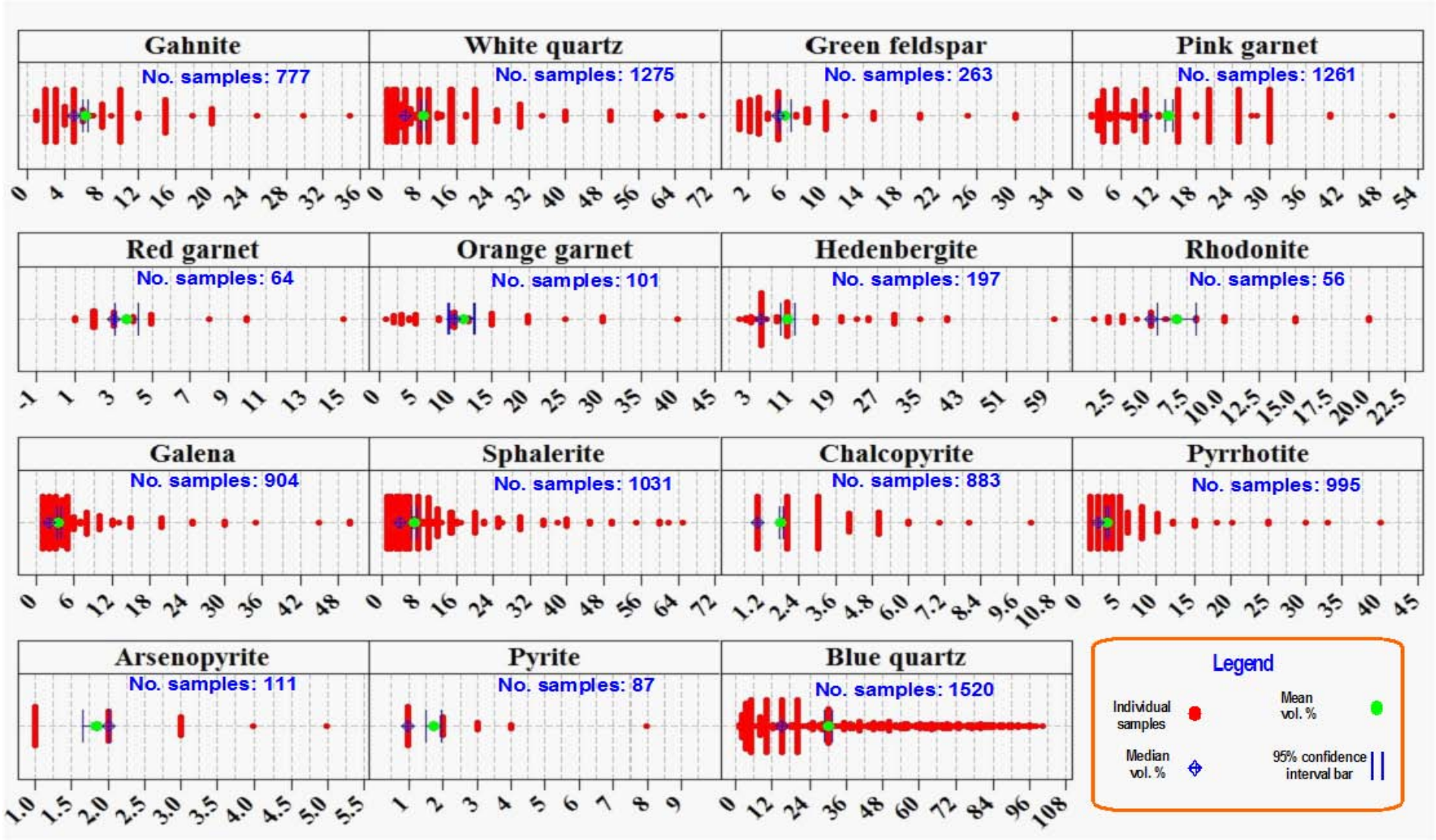

Figure 3.10: Descriptive statistics for sulphide and silicate minerals. The scale of horizontal axes is based on volume percentage.

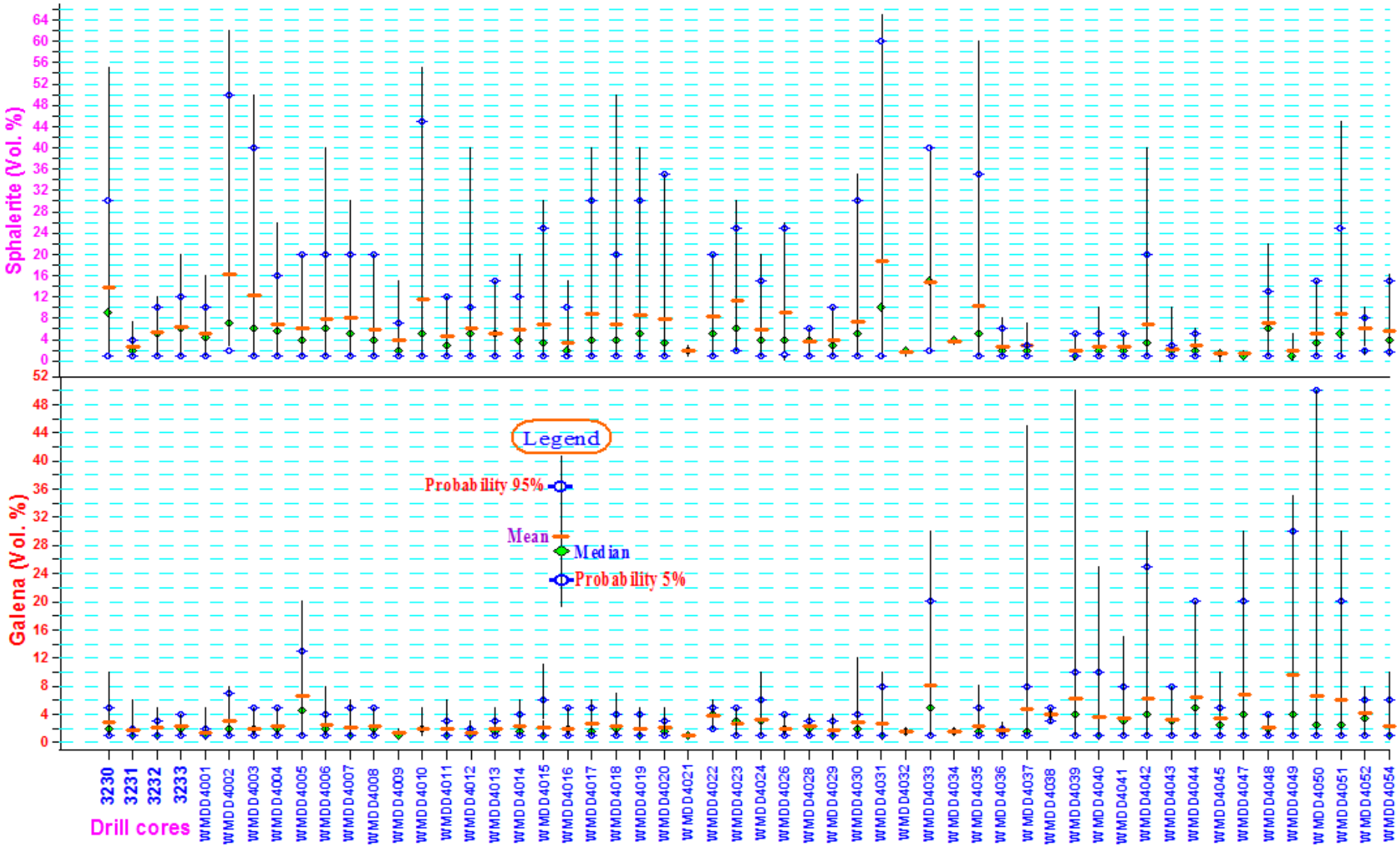

Figure 3.11: Descriptive statistics for galena and sphalerite within the analysed samples of each surface drill core.

3.5.1: Discussion of the statistical results and the bar diagram of minerals.

In comparison with massive pyrite deposits within the Broken Hill Block [e.g. Big Hill cobaltian pyrite, Thackaringa Group (Plimer 1977)] the lack of pyrite within the investigated samples of the Western Mineralisation suggests that the orebody is originally sulphur-poor. Previous studies (Groombridge 2003; Kitchen 2001; Patchett 2003; Sproal 2001) showed that the galena and sphalerite samples of the Western Mineralisation were highly enriched in Fe. This indicates a low sulphur system for formation of the orebody of the Western Mineralisation. Plimer (1977, 2006a) claimed that the Broken Hill orebodies have been unsaturated with S and the excess Pb and Zn have contributed to the composition of silicate minerals such as gahnite, zincian garnet, zincian biotite, zincian staurolite, zincian chlorite, zincian sericite, plumbian orthoclase, native lead, dyscrasite, native silver, native lead, zincian manganese olivine, safflorite and löllingite. This study also shows that the number of samples containing gahnite and green feldspar are relatively substantial within the investigated samples of the Western Mineralisation. However, weak acid digestion of sulphides for ICP-OES analysis would not have dissolved base metal-bearing silicates and gahnite.

The low volume percentage and lack of arsenopyrite within the investigated samples may be another reason for the deficiency of primary S in the Western Mineralisation. Spry, Plimer and Teale (2008, p.232) suggested the chemical reaction (3.1) as a possibility for formation of composite arsenopyrite-löllingite mineral[3] in the Broken Hill deposit.

$$2FeAs_2 + 2FeS + S_2 = 4FeAsS \qquad (3.1)$$

The chemical reaction (3.1) shows that the generation of arsenopyrite during metamorphism needs to consume S rather than production of S.

Despite the lack of pyrite and arsenopyrite (Table 3.5), chalcopyrite was presented in a larger number of samples of the Western Mineralisation. This may indicate that the dispersal of chalcopyrite (or minerals containing Cu) is controlled by different parameters. Plimer (2006b) argued that in both the Olary and Broken Hill Domains, Cu was remobilised during the Olarian Orogeny and participated at redox boundaries such as iron

[3] **Löllingite forms core and arsenopyrite forms rim of the composition mineral**

formations or sulphide rocks. The spatial distribution of chalcopyrite and Cu will be discussed in Chapters 6 to 8.

According to Table 3.6, the number of samples containing orange garnet, hedenbergite, rhodonite and red garnet is very low within the total investigated samples. It is possible that those silicate minerals were occurred naturally very low or they were unstable over a long period and thus decomposed to other silicate minerals such as pink garnet and gahnite.

Mineralogy of the investigated samples of the surface drill core shows:

1. An interdigitation of lode horizons (quartz-gahnite, quartz-garnet),
2. Replacement of metapsammite by quartz-gahnite and sulphides,
3. Replacement of metapelite by garnet rocks and ore types similar to C Lode (quartz-gahnite-sphalerite-galena),
4. B Lode (quartz-hedenbergite-red garnet-sphalerite-galena), and
5. A Lode (quartz-orange garnet-rhodonite-galena-sphalerite).

The above observations suggest multiphase ore deposition in the Western Mineralisation.

3.6 Evaluating the precision of the variation of galena+sphalerite against the variation of Pb+Zn

The most important aspect of the quantitative core logging is how precisely the variation of galena+sphalerite is correlated with the variation of Pb+Zn within the investigated samples. The two important factors for determination of precision are reliability and validity.

- **Reliability**

Reliability refers to the reproducibility of the measurement in experimental studies and the possible capacity for detecting agreements or internal consistency within measurements. In fact, two data sets can show a high correlation coefficient but it is possible they have little agreement and internal consistency in the variation of data. In this study, reliability was measured by the following approaches (Garson 2010; Hopkins 2000a):

1. Comparing the trend variation of mean and median concentrations for Pb+Zn and galena+sphalerite within the corresponding drill cores (Section 3.6.1),

2. Comparing the COVs of Pb, Zn and Pb+Zn with the COVs of galena, sphalerite and galena+sphalerite respectively within the corresponding drill cores (Section 3.6.1), and

3. Calculation of Spearman correlation coefficient[4] and Cronbach's alpha (UCLA: ATS 2007; Yaffee 2003; Tables 3.9 and 3.10).

- **Validity**

Validity refers to the amount of correlation between the value of the measurement and its true value. In this study, the values of Pb+Zn are considered as true values and it is important to know the extent of the correlation between the estimated values of galena+sphalerite and the values of Pb+Zn. Also, the degree of validity was calculated by the Pearson correlation coefficient[5] (Hopkins 2000b) for logarithmic data (Table 3.8). But as mentioned earlier a high PCC between Pb+Zn and galena+sphalerite does not mean that the trend variation of Pb+Zn in drill cores is the same as the trend variation of galena+sphalerite. A summary of statistical terms used in this section has outlined in Table 3.7.

[4] **SCC**
[5] **PCC**

Table 3.7: Different types of correlation coefficients and their statistical terms.

Correlation coefficient	**The correlation coefficients are normally reported as R= (a value between -1 and +1); squaring the R value makes it easier to understand. The square of the correlation coefficient multiplied by 100 [Equation (3.1)] describes the percentage of variation in one variable in related to the variation of another variable.** $$R^2_{jk} \times 100 \quad (3.1)$$ **Equation (3.1) is equal to percentage of variance in common between X_j and X_k. As a matter of routine it is the squared correlations that should be interpreted. This is because the correlation coefficient shows the existence of more co-variation between two elements than actually exists, and this problem gets worse as the correlation approaches zero.**
Significance level	**Significance level indicates how likely the correlations reported may be due to chance in the form of random sampling error. The significance level is important, if the data set is very small. A significance level of 0.05 for a correlation coefficient means that there is (1-0.05) or 95 % certainty of the possibility of being a true correlation coefficient and a significance level of 0.01 for a correlation coefficient means that there is (1-0.01) or 99 % certainty of the possibility of being a true correlation coefficient (Creative Research Systems 1982).**
parametric & non-parametric	**There are both parametric and non-parametric statistical methods for measuring the correlation coefficient. In parametric statistics it is supposed that the data set comes from random data with normal distribution and that the parameters of the distribution can be inferred by parametric statistics. In contrast, non-parametric statistics make no assumptions about the randomness of the data and normal distribution and they are less sensitive to outlier effects and skewed data.**
PCC	**PCC requires linearity of the relationship between the data and if the actual relationship is non-linear, it may change the real degree of the correlation coefficient. Skewness of distribution (pbarrett.net 2001) and outliers can affect linear relationships - this is the case for most of the geochemical data. If the distribution of the data set is log-normal, logarithmic data is preferable for the calculation of PCC (non-parametric method).**
SCC	**SCC is a non-parametric method that can also be used for calculation of the non-linear correlation coefficient. Spearman's approach is a form of rank order calculation based on the median between all pairs of data in a scale that is also a type of measure of reliability (Garson 2010).**
Cronbach's alpha	**Cronbach's alpha is not a statistical test but it is the most common form of reliability coefficient or internal consistency based on the average correlation among the data set. It is calculated in SPSS under the function of Analysis→Scale→Reliability Analysis.** **In this study, the dialog of the Reliability Analysis was adjusted for the model of "Two-Way Random Effects", consistency results and Cronbach's alpha. In the Two-Way Random Effects model, both judges and measures effects are random.**

3.6.1 Comparison of the variation of Pb+Zn with variation of galena+sphalerite

Comparison of Figure 3.11 with Figure 3.3 shows that there are several similar trend variations between galena and Pb and between sphalerite and Zn. However, in drill core 4031 (Figure 3.11), the mean and median volume percentage of galena is very low, although one would expect it to be higher in regard to its corresponding assay value (Pb) in this drill core (Figure 3.3). This may have occurred due to the difficulty of visual separation of galena from sphalerite and silicate minerals during the quantitative core logging. This may especially be the case, when sphalerite appears as the major ore sulphide mineral in a sample and its lustre masks the lustre of galena. This may be the general case for the quantitative core logging of other polymetallic sulphide minerals as well and it is the weakness of visual modal mineral mapping.

In this case, construction of a comparative bar diagram for variation of Pb+Zn and galena+sphalerite is more reliable for the detection of possible human error. Especially, in high grade sulphide mineralised samples, the concentration of Pb+Zn is supposed to be high, but if it is considerably lower than expected, it may be a result of one or more of the following mistakes in:

1. Reporting assay data,
2. Quantification of the ore sulphide minerals, or
3. Attributing the assay data to the wrong core sample.

Therefore, the comparison of bar diagrams of Pb+Zn and galena+sphalerite (Figures 3.12 and 3.13) provides a more efficient tool for detection of potential mistakes at the preliminary stage of data collection before data processing starts. This process improves the degree of reliability of the important assay data (e.g. Pb and Zn in the Western Mineralisation). Figure 3.13 shows many similarities in COVs of the following pair variables:

1. Pb+Zn and galena+sphalerite,
2. Zn and sphalerite, and
3. Pb and galena.

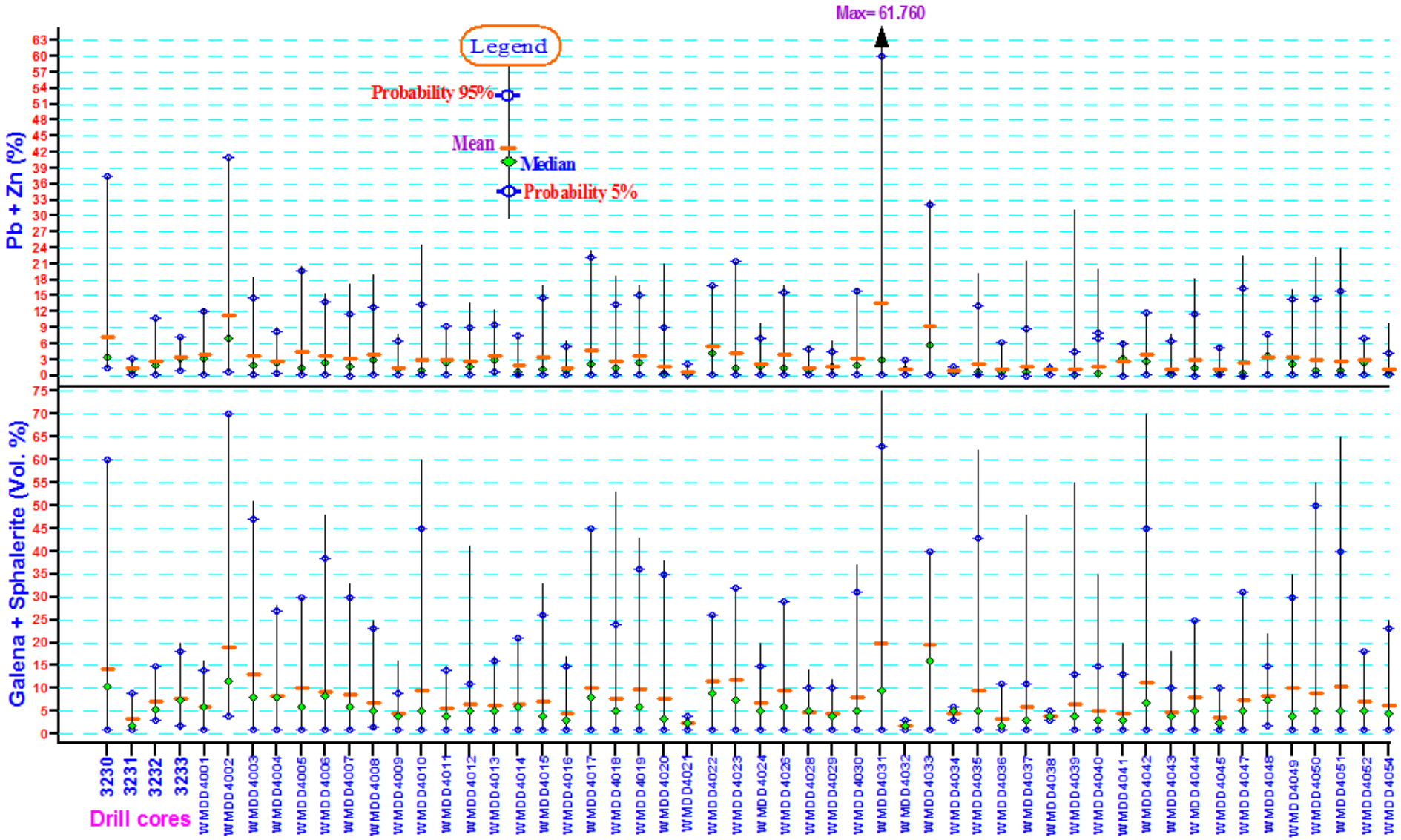

Figure 3.12: Descriptive statistics for galena and sphalerite and Pb+Zn within the analysed samples of each surface drill core.

Figure 3.13: Comparison of the COV of Pb+Zn, Zn and Pb with the COV of galena+sphalerite, sphalerite and galena respectively.

3.6.2 Probability plot

The construction of a probability plot is a means of identification of the normal distribution of a data set. The probability plots in Figure 3.14 were constructed for 1,219 samples containing Pb+Zn and galena+sphalerite. For construction of a probability plot, the data set should be arranged in ascending order; the largest data will be plotted at a lower percentage than 100 % and this makes it possible for some future data of Pb+Zn concentrations and galena+sphalerite (vol. %) with larger values than the current largest values to be located at a higher point in the order (Hart & Hart 2010). In Figure 3.14, the estimated cumulative probabilities were calculated by the method of Median Rank (Benard) with the formula $\frac{i-0.3}{n+0.4}$ in which " n " is equal to the number of samples and "i" is equal to the rank-order of each value (i.e. i = 1 indicates the smallest value and i = n for the largest). More details can be found in the "help" section of the Minitab software (Minitab Inc. 2007).

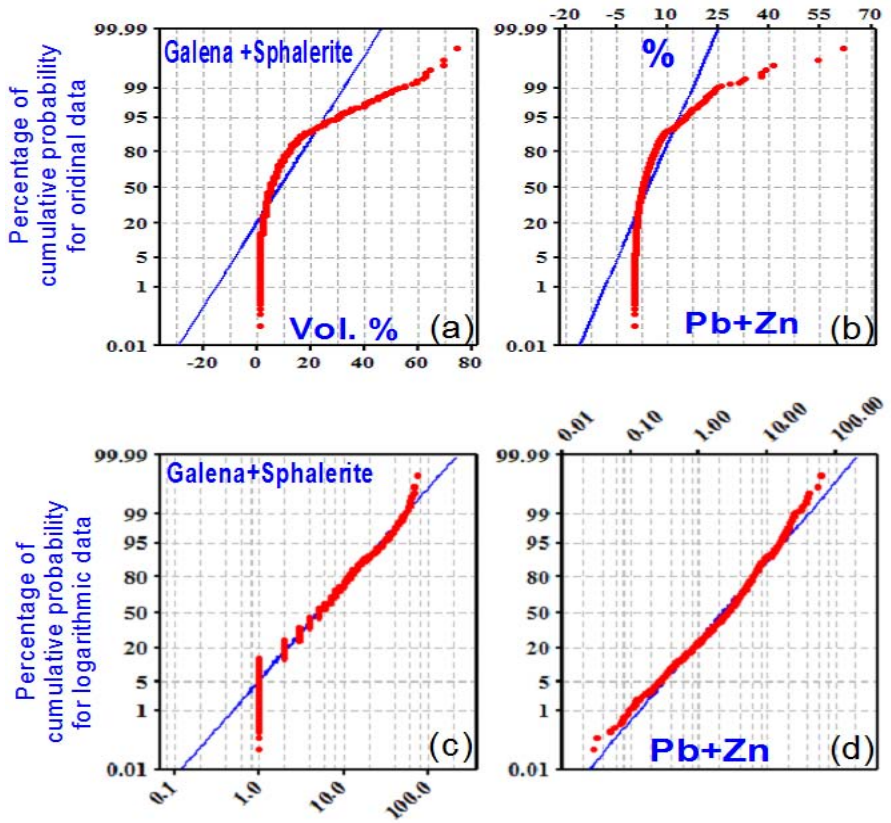

Figure 3.14: (a) and (b) are related to the original data of Pb+Zn and galena+sphalerite. The red curves show the experimental percentage of Pb+Zn concentrations and the volume percentage of galena+sphalerite against their respective estimated values of cumulative probability. The straight blue lines show the theoretical percentage of cumulative probability for near-normal distribution of the variables. (c) and (d) are related to the logarithmic data of Pb+Zn and galena+sphalerite.

3.6.3 The results of correlation coefficients

In the Western Mineralisation, galena and sphalerite were observed only in 1,219 out of 1,849 samples containing Pb and Zn. This means that 630[1] samples did not show evidence of galena or sphalerite visually but they do have low assay values for Pb or Zn. When considering this issue, PCC, SCC and alpha coefficients were calculated for the two groups of 1,219 and 1,849 samples in order to evaluate the degree of reliability and validity of the quantitative core log data.

In order to calculate correlation coefficient for 1,849 samples, a very small value of 0.000,1 was considered for the value of galena+sphalerite in 630 samples that do not have any values for volume percentage of galena+sphalerite (Tables 3.8 to 3.10). Also, because some volume percentages of galena+sphalerite are equal to one and the logarithm of one is equal to zero, for calculation of PCC, the original data plus 0.000,1 were considered for log-transformation (Table 3.8). According to Figures 3.14c and 3.14d, the logarithmic data of Pb+Zn and galena+sphalerite show near-normal distributions and PCC can be applied to the logarithmic data for evaluating the degree of validity between variation of Pb+Zn and galena+sphalerite (Table 3.8).

Table 3.8: The results of PCC for logarithmic (data+0.000,1).

Minerals / Elements	Galena+Sphalerite	Galena+Sphalerite
Pb+Zn	0.72*	0.45*
Number of samples	1219	1849
R^2 %	51.8	20.2

*The significance level (2-tailed) is 0.01

Table 3.9: The results of SCC for the original data.

Minerals / Elements	Galena+Sphalerite	Galena+Sphalerite
Pb+Zn	0.73*	0.78*
Number of samples	1219	1849
R^2 %	53.3	60.1

*The significance level (2-tailed) is 0.01

[1] 1,819-1,219

Table 3.10: The results of Cronbach's alpha for the original data.

Cronbach's alpha	Number of samples
0.814	1219
0.818	1849

3.6.4 Interpretation of the correlation coefficients

- **PCC**

PCC in Table 3.8 shows a relatively high level of correlation (0.72) between the variation of Pb+Zn and galena+sphalerite in 1,219 samples but when 1,849 samples are considered the PCC shows a low level of correlation (0.45) between the pair values of Pb+Zn and galena+sphalerite. The PCC result shows a strong validity between variations of galena+sphalerite and Pb+Zn within the 1,219 investigated samples. In Table 3.8, the result of R^2 % for 1,219 samples means that the 51.8 % of variation of galena+sphalerite can be estimated by the variation of Pb+Zn and the result of R^2 % for 1,849 samples means that only 20.2 % of variation of galena+sphalerite can be estimated by the variability of Pb+Zn.

- **SCC**

SCC in Table 3.9 shows a relatively high level of correlation (0.73) between the variation of Pb+Zn and galena+sphalerite for 1,219 samples. Even when 1,849 samples are considered the value of SCC increases from 0.73 to 0.78 between the pair values of Pb+Zn and galena+sphalerite. This shows high internal consistency between the variation of galena+sphalerite and Pb+Zn for two types of abundant samples.

- **Alpha coefficient**

The alpha coefficient in Table 3.10 also shows a high level of internal consistency or reliability between the variation of galena+sphalerite and Pb+Zn for two types of abundant samples.

3.7 Exploration signature of lithologies in the Broken Hill Domain

In the Broken Hill Domain, garnet quartzite, garnetite, blue quartz-gahnite lode and pegmatite show obvious spatial relationships with over 400 minor deposits of Broken Hill

Type (BHT) deposits including the main Broken Hill orebody (Spry, Teale & Heimann 2003). Although, there are many competing ideas about the origin of these rock types in the Broken Hill Domain of the Curnamona Province, these rock types are considered widely as exploration guides to BHT deposits (Spry, Teale & Heimann 2003). The question is whether it is possible to evaluate quantitatively the degree of relationship of the lithologies of the Western Mineralisation with variation of Zn+Pb and whether the rock types can be judged as major controlling factors of the mineralisation.

3.7.1 Statistical results for rock types of the Western Mineralisation

The results of SCCs of the investigated rock types with Pb+Zn and their descriptive statistics are given in Table 3.11 and Figure 3.15 respectively. Table 3.11 shows at a glance whether rock types vary with Pb+Zn perfectly, or nearly perfectly, and whether positively or negatively.

Table 3.11: A summary of SCC results, significance levels (2-tailed) and abundance of rock types.

Elements / Rock types	Zn + Pb	Elements / Rock types	Zn + Pb
Quartzite lode	- 0.04	Pegmatite	0.3**
Sig. (2-tailed)	0.772	Sig. (2-tailed)	0.000
Number of samples	56	Number of samples	339
Metapsammite	- 0.13*	Blue quartz lode	-0.006
Sig. (2-tailed)	0.033	Sig. (2-tailed)	0.880
Number of samples	271	Number of samples	635
Metapsammopelite	- 0.43**	Garnet quartzite	-0.29**
Sig. (2-tailed)	0.000	Sig. (2-tailed)	0.000
Number of samples	447	Number of samples	644
Metapelite	- 0.53**		
Sig. (2-tailed)	0.000		
Number of samples	129		

* Correlation is significant at the 0.05 level (2-tailed)

** Correlation is significant at the 0.01 level (2-tailed)

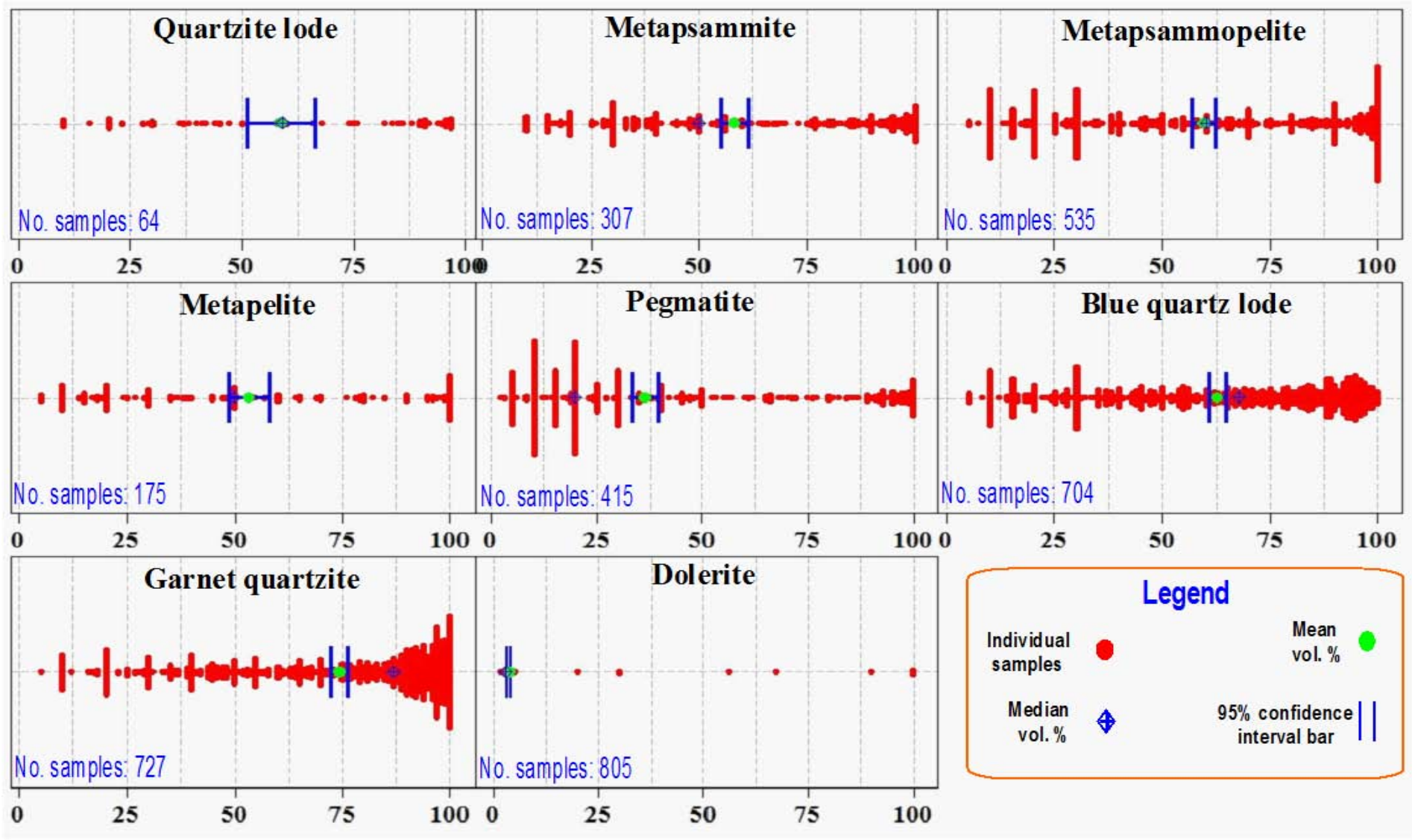

Figure 3.15: Descriptive statistics for rock types within the 1,928 investigated samples. The scale of horizontal axes is based on volume percentage.

In Table 3.11, the variation of metapelite and metapsammopelite show a low correlation with variation of Pb+Zn in opposite direction. It is not possible to compare directly the SCC values of the rock types in Table 3.11 with each other because they were calculated for different numbers of rock samples. The variations of the quartzite lode and blue quartz lode are independent of the variation of Pb+Zn and there is no internal relationship or consistency between them (Table 3.11).

3.7.2 Discussion of the correlation coefficient of the rock types with Pb+Zn

The results of SCC (Table 3.11) indicate that variations of the rock types within the investigated samples have very low to low levels of relationship with the variation of Pb+Zn. The results do not mean that the rock types are not suitable as an exploration guide to the Western Mineralisation and variogram analysis for the rock types should be calculated to understand the spatial relationship of the rock types with Pb and Zn. This will be discussed in Chapters 6 and 8.

3.8 Summary

Descriptive statistics of assay data showed some similarities in the frequency distribution of Zn-Pb, Fe-S, Bi-Sb and Ag-As-Cd. There are also some similarities in the trend variation of mean and median concentrations of Pb-Ag and Zn-S in the bar diagram of surface drill cores. Drill cores 4002 and 4031 contain high mean and median concentrations of Zn, Pb and Ag. In the underground drill cores, there are some similar trend variations among the mean and median values of Zn, Pb and S. The analysed samples of drill cores 4062 and 4064 contain higher mean and median concentrations of Zn and Pb relative to those within the analysed samples of the underground drill cores.

The mean and median concentrations of Zn, Pb and Fe within the surface drill cores are less than those within the underground drill cores. In contrast, the mean and median concentrations of As, Sb, Bi and S within the surface drill cores are more than those within the underground drill cores. In the bar diagrams, drill cores with similar collar locations (fanned drill holes) show significantly different mean and median concentration for some elements. This suggests that spatial anisotropic parameters control the spatial distribution and structural variation of the elements within the orebody.

Figures 3.12 and 3.13 show that the variation of galena+sphalerite has many similarities with the variation of Pb+Zn. According to the descriptive statistics, the mean and median volume percentages of sphalerite are twice those of galena in the Western Mineralisation. There are some similarities among dispersion of galena, sphalerite and pyrrhotite.

The PCC, SCC and alpha coefficients were relatively high between the variation of Pb+Zn and galena+sphalerite for the 1,219 samples containing galena+sphalerite. When 1,849 samples containing Pb+Zn were considered, the PCC value decreased but the values of SCC and alpha coefficients increased. The results of SCC showed very low to low internal relationships between the variation of Pb+Zn and the variation of rock types.

CHAPTER 4

The Relationship of Magnetic Pyrrhotite with the Orebody of the Western Mineralisation

4.1 Introduction

The Western Mineralisation contains pyrrhotite. It is the only magnetic mineral in the Western Mineralisation. There has been no quantitative mineralogical and statistical approach on the magnetic properties and their variation within the Broken Hill orebodies. A knowledge of the relationship between magnetic pyrrhotite and the orebody will be useful for the development of the Western Mineralisation. It would be useful if a geophysical interpretation could be integrated with geochemical information to improve ore targeting.

One way in which geophysical methods could be incorporated would be via aeromagnetic surveys, which are useful to outline an orebody's magnetic properties (Clark 1997).The resulting aeromagnetic maps can also be applied to ore mineral tracking and drill targeting at a scale suitable for exploration . However, a high-resolution aeromagnetic survey has never been conducted over the Western Mineralisation owing to the proximity of the City of Broken Hill and the large amount of magnetic noise above the Western Mineralisation (e.g. steel structures, galvanised iron buildings, pipes, railway lines and power lines).

Regional magnetic surveys in the Broken Hill area have shown the stratigraphic distribution of magnetite-bearing amphibolite, felsic rocks and metasediments, minor thin discontinuous banded iron formations comprising quartz-magnetite-spessartine-fluorapatite and the Broken Hill orebody (Figure 4.1). Godber and Bishop (2006) recommended a ground magnetic survey in order to understand the detailed magnetic properties of the lithologies that contain magnetic minerals such as pyrrhotite and magnetite. The existing drill cores provide an opportunity to conduct such a survey.

Figure 4.1: Aeromagnetic map of the Broken Hill Mine site and its surrounding area Scale: 3.8 km length (from New South Wales Department of Primary Industries 1995).

This chapter uses previous data set of chemical composition of pyrrhotite samples of the Broken Hill orebodies (Groombridge 2003; Kitchen 2001; Patchett 2003; Sproal 2001; Tully 2002) in order to establish a relationship between the Broken Hill orebodies and pyrrhotite. In this chapter, the quantitative core log of the Western Mineralisation is used for performing conventional statistical analysis to demonstrate statistically the quality of the relationship between volume percentage of pyrrhotite and the magnetic susceptibility of rocks within the orebody.

The data set was divided into two groups and they are productive samples (galena+sphalerite ≥ 1 vol. %) and barren samples (galena+sphalerite = 0). Statistical tests were performed in each group to examine the hypothesis whether the magnetic pyrrhotite is enriched significantly in the productive units within the Western Mineralisation. The correlation coefficient was calculated to determine the extent of the relationship between the variations of volume percentage of pyrrhotite, its magnetic susceptibility and the volume percentage of galena+sphalerite.

Contour plots and coefficient of variation (COV) and core logging models were constructed in order to evaluate the variation of ore sulphide minerals present with the variations of pyrrhotite abundance and its magnetic susceptibility. In view of the lack of detailed magnetic surveys of the Western Mineralisation, this magnetic susceptibility investigation and the quantification of pyrrhotite enable us to understand better the subsurface pyrrhotite distribution, different types of pyrrhotite and magnetic variation within the Western Mineralisation. The spatial distribution of magnetic susceptibility and pyrrhotite are discussed in Chapters 6 and 8.

4.2 Characteristics of pyrrhotite

Pyrrhotite has a variable composition of $Fe_{(1-x)}S$ that $0 \leq x \leq 0.13$ (De Villiers and Liles, 2010) and has monoclinic, hexagonal and orthorhombic polytypes. In nature, pyrrhotite occurs in various superstructures (superlattice) that are represented by the axial lengths of NiAs-type unit cell of "A" and "C" that they are equal to 3.44 Å[1] and 5.70 Å respectively. However, different structures of the pyrrhotite group are presented based on "C" (Table 4.1). Pyrrhotite has a variable $\frac{Fe}{S}$ ratio (Table 4.1). The pure FeS iron rich member of pyrrhotite is troilite (hexagonal). Arnold (1967) stated that natural pyrrhotite is commonly a mixture of monocline and hexagonal polytypes.

[1] Ångstrom

Table 4.1: Atomic percentage of Fe in pyrrhotite polytypes (from Carpenter & Bailey 1973; Clark 1997; Kontny et al. 2000; Kruse & Ericsson 1988; Yund & Hall 1969).

Fe % , (Chemical formula)	Crystal system	Superlattice dimension	Name
~ 50.0, (FeS)	Hexagonal	$\sqrt{3}$A, 2C	2C pyrrhotite, Troilite
~ 46.67- (Fe_7S_8)	Monoclinic	$2\sqrt{3}$ A, 2A, 4C	4C pyrrhotite, Magnetic pyrrhotite, Ferromagnetic Weiss-type pyrrhotite
~ 47.37- (~Fe_9S_{10})	Hexagonal	2A, 5C	5C pyrrhotite
~ 47.83- (~$Fe_{11}S_{12}$)	Pseudohexagonal	2A, 6C	6C pyrrhotite
~ 47.6- (~$Fe_{10}S_{11}$)	Orthorhombic	2A, 2B, 11C	11C pyrrhotite (a mixture of 5C and 6C)
47.4→47.8 (Fe_9S_{10}→$Fe_{11}S_{12}$)	Orthorhombic or Monoclinic	2A, 2B, nC $4.8 \leq n \leq 6$	nC pyrrhotite

Monocline pyrrhotite is the only ferromagnetic pyrrhotite with an approximate crystallographic structure of Fe_7S_8 (Zapletal 1992). It has a 4C superstructure. The magnetic property of monocline pyrrhotite is related to cation vacancies in its crystal structure. The vacancies decrease the overall crystal symmetry. Hence, the monoclinic pyrrhotite commonly contains more defects than hexagonal forms and is therefore more magnetic (Kontny et al. 2000). At temperatures above ~320° Celsius (Centigrade) pyrrhotite loses its magnetism and, under suitable oxygen fugacities, may convert to magnetite (Clark 1997; Rochette et al. 1990). The occurrences of pyrrhotite can be considered as an important indicator of redox and temperature in metamorphic, magmatic and diagenetic rocks (Rochette et al. 1990).

Hexagonal and other antiferromagnetic forms of pyrrhotite produce little magnetic susceptibility in rocks (Dekkers 1988) and they cannot carry remnant magnetism (Zapletal 1992). However, monoclinic pyrrhotite is important mineral for identification of remnant magnetisation and susceptibility anisotropy during geological times (Clark 1997) and it can

provide information regarding Palaeomagnetic characteristics, thermal evolution of the ancient magnetisation and the genesis of pyrrhotite.

4.3 Pyrrhotite in the Broken Hill Domain

Scott, Both and Kissin (1977) and Bryndzia, Scott and Spry (1988) suggested that hexagonal pyrrhotite in the Broken Hill orebody is a primary iron sulphide mineral formed during high-grade metamorphism, whereas monoclinic pyrrhotite is a retrograde or post-metamorphic product of primary hexagonal pyrrhotite. This indicates that crystallography of pyrrhotite (changing from non-magnetic to magnetic pyrrhotite) was influenced by the metamorphic evolution of the Broken Hill deposit.

Experimental studies of Scott, Both & Kissin (1977) showed that primary iron-rich pyrrhotite formed at high temperature within metamorphic rocks of the Broken Hill Domain and the Broken Hill orebodies. It is hexagonal pyrrhotite with exsolved troilite. During cooling metamorphosed rocks, the primary pyrrhotite inverted to hexagonal pyrrhotite + monoclinic pyrrhotite and further inverted during retrogression to monoclinic pyrrhotite + pyrite (Scott, Both & Kissin 1977, p.1415; Figure 4.2).

In nature, the conversion of hexagonal pyrrhotite to monocline pyrrhotite requires losing Fe and gaining S. Scott, Both and Kissin (1977) suggested that in the Broken Hill deposit, the reaction of pyrrhotite and sphalerite during syn- to post- metamorphism events resulted in releasing Fe and S from hexagonal pyrrhotite and sphalerite respectively. During the chemical interaction and metamorphic evolution, the hexagonal pyrrhotite was converted to monocline pyrrhotite while losing Fe and gaining S from sphalerite (Scott, Both & Kissin 1977).

In the more advanced oxidation stages, the loss of iron from hexagonal pyrrhotite may result in the occurrence of pyrite, marcasite and finally hematite or magnetite (Scott, Both & Kissin 1977). Plimer (1977) stated that the presence of primary pyrite within metapelites and metapsammites of several areas of the Broken Hill Domain (e.g. Stirling Vale, Pyrite Hill and Thackaringa) indicates that pyrite is stable at the maximum metamorphic grade of granulite facies and it did not convert to pyrrhotite. This suggests that the primary pyrrhotite and troilite in the Broken Hill orebody formed because there

was not enough sulphur to form pyrite. The presence of abundant sulphur-poor Zn, Pb, Ba and Ag minerals at Broken Hill supports such a view.

Figure 4.2: Different phases of Fe-S system in relation to variation of temperature and atomic percentage of Fe. (redrawn from Scott, Both & Kissin 1977).

In the Western Mineralisation, pyrrhotite bearing-rocks occur in association with the following minerals (Kitchen 2001):

1. Exsolution lamellae along crystallographic planes within sphalerite,
2. Exsolution lamellae along curved grain boundaries between galena and sphalerite,
3. Pyrrhotite-filled veinlets and brittle deformational fractures within chalcopyrite and sphalerite,
4. Pyrrhotite interstitial to muscovite, replacement of muscovite and cleavages fillings in muscovite, and

5. Pyrrhotite replacement by chlorite which has resulted in decomposition of pyrrhotite to marcasite.

4.3.1 Evaluation of chemical properties of pyrrhotite among the Broken Hill orebodies

There are several previous sets of EMPA analyses of pyrrhotite from the Western Mineralisation and other Broken Hill orebodies (Table 4.2). There has been no study to compare and contrast the chemical variation of pyrrhotite in the Broken Hill orebodies. In this chapter, the data sets of others on pyrrhotite chemistry are used (Table 4.2). One method was the visualisation of variation of the average atomic percent of Fe and S for pyrrhotite samples from different orebodies (Figures 4.3 and 4.4). Another useful method is correspondence analysis[2] that categorises the orebodies based on major and minor elements of pyrrhotite samples and visualise their inter-relationships on two-dimensional maps (Figures 4.5 to 4.7). A three-dimensional model of association of different chemical composition of pyrrhotite was interpreted by three correspondence maps[2]

Table 4.2: EMPA analyses of pyrrhotite from the Western Mineralisation and the Line of Lode from CML7.

Reference	Orebody	Number of pyrrhotite samples and drill holes
Kitchen (2001)	The Western Mineralisation	10 samples from 4001 and 4002
Patchett (2003)	The Western Mineralisation	34 samples from 4003
Sproal (2001)	C Lode and 2 Lens	47 samples from C Lode and 27 samples from 2 Lens
Tully (2002)	A and B Lodes, 1 Lens and Kintore Pit	15 and 16 samples from A and B Lodes respectively, 5 samples from 1 Lens and 5 samples from Kintore Pit
Groombridge (2003)	2 and 3 Lenses 2 Lens South	3 and 4 samples from 2 and 3 Lenses respectively and 5 samples from south of 2 Lens

4.3.1.1 Variation of Fe and S in pyrrhotite samples of the Broken Hill orebodies

In Figures 4.3 and 4.4, individual pyrrhotite samples were marked by red points and the blue rhombic points represent the mean atomic percent of Fe and S. In Figure 4.3, some pyrrhotite samples of B and C Lodes and the Western Mineralisation have atomic percent

[2] See the explanations of Table 4.6

of Fe equal to monoclinic pyrrhotite. Figures 4.3 and 4.4 show none of the orebodies have troilite. However, the pyrrhotite samples of the orebodies have been collected from only a few drill cores over a limited distance and more pyrrhotite samples would be needed to check the presence of troilite. Pyrrhotite samples of the Western Mineralisation show a broader variation in the atomic percentage of S (between 49.33 and 54.51) and Fe (between 45.29 and 49.51) than the other Broken Hill orebodies (Figures 4.3 and 4.4).

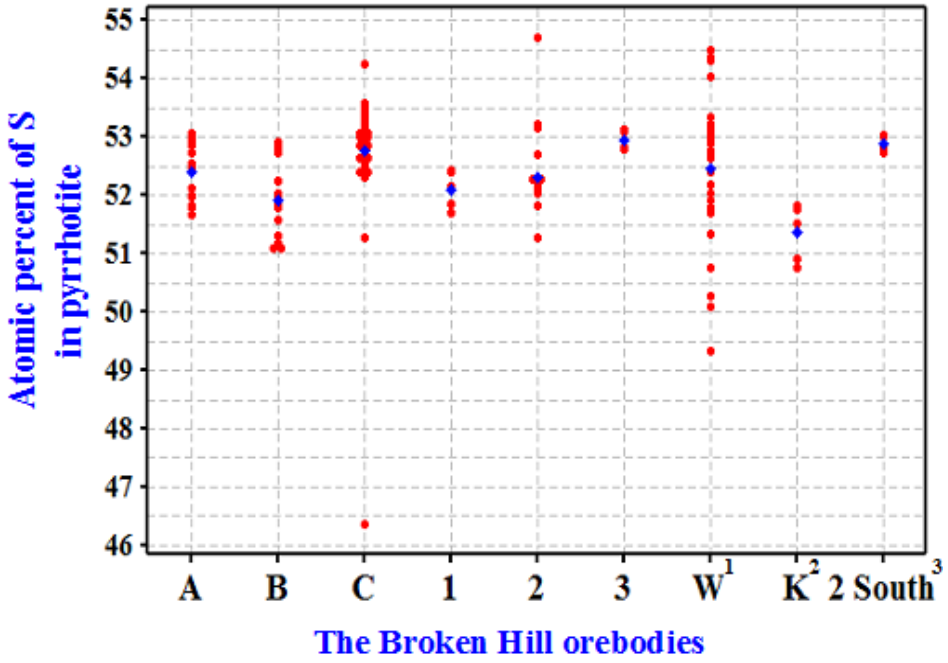

Figure 4.3: Atomic percentage of S in pyrrhotite samples of the Broken Hill orebodies.
([1]The Western Mineralisation, [2]Kintore Open Pit, [3]2 Lens South)

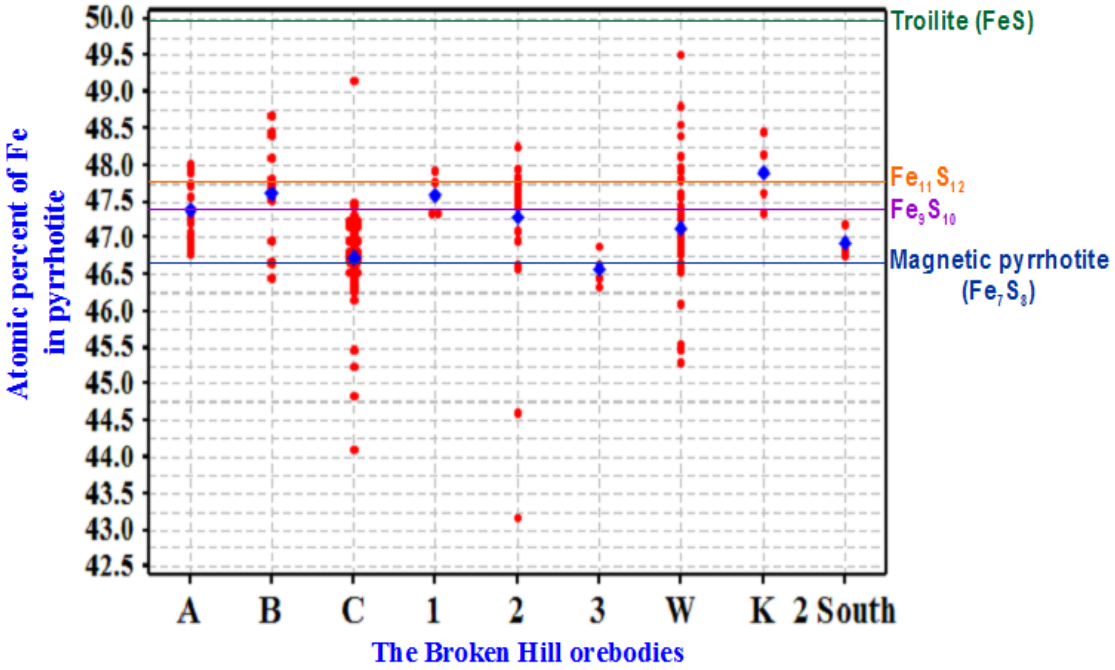

Figure 4.4: Atomic percentage of Fe in pyrrhotite samples of the Broken Hill orebodies.

4.3.1.2 Correspondence analysis for pyrrhotite samples of the Broken Hill orebodies

There are many references about mathematical theory and application of correspondence analysis e.g. Adachi (2003), Benzercri (1992), Clausen (1998), Ender (2010), Greenacre (1984, 2007), SAS Institute Inc. (1999), Social Research Update (1995), Teil and Cheminee (1975), Valenchon (1982) and Van de Geer (1993a, 1993b) but the major aim of correspondence analysis in this study is to show inter-relationship of elements of pyrrhotite samples with the Broken Hill orebodies on two-dimensional correspondence maps. Correspondence analysis is an exploratory method and non-parametric technique that has no distribution assumptions, but it needs positive data values. It is a geometric method to represent the inter-relationships of the rows and columns of a two-way contingency table (Table 4.3) in a two-dimensional map (e.g. Figure 4.4) or a low-dimensional space.

Table 4.3 shows categorical variables in a matrix format and in this Table, Fe and S comprise the major average atomic percent of pyrrhotite and the other 8 elements incorporate as minor element in atomic structure of pyrrhotite. There are significant differences between average values of major and minor elements in Table 4.3. These differences create difficulties for correspondence analysis because the variable with the greatest variance will produce the highest influence on the outcome. One way for avoiding this problem is performing correspondence analysis only with minor elements of pyrrhotite (all elements of Table 4.3 without Fe and S) and another way is using standardisation that the most universal method of standardisation is z-transformation.

Table 4.3: A contingency table of the average percentage of elements in pyrrhotite samples within the Broken Hill orebodies.

Element / Orebody	S	Fe	Cu	Zn	As	Ag	Cd	Sb	Pb	Bi
A Lode	52.38	47.3	0.008	0.011	0.085	0.006	0.009	0.007	0.005	0.18
B Lode	51.93	47.62	0.011	0.288	0.087	0.007	0.004	0.004	0.003	0.022
C Lode	52.79	46.75	0.0231	0.035	0.076	0.009	0.006	0.003	0.094	0.016
1 Lens	52.12	47.60	0.002	0.079	0.096	0.003	0.026	0.003	0.003	0.005
2 Lens	52.72	47.00	0.0535	0.074	0.089	0.011	0.004	0.003	0.001	0.007
3 Lens	52.97	46.58	0.0192	0.313	0.083	0.006	0.007	0.002	0.007	0.004
Western Mineralisation	52.27	47.32	0.0427	0.196	0.062	0.008	0.008	0.004	0.009	0.021

The z-transformation is calculated by subtraction of the mean value $(\overline{X})$ of each column from each value (X) of the column and the resulting value of the column is divided by the standard deviation (S) of the column [Equation. (4.1)].

$$z = \frac{x - \overline{x}}{s} \qquad (4.1)$$

The z-transformation of values of Table 4.3 produces some negative values that could not be analysed by correspondence analysis. It requires the addition of a minimum constant value (e.g. 2) to all the values of Table 4.4 to change them to positive values (Table 4.5). Although, with small changes of the constant value (e.g. addition of 4 instead of 2 to values of Table 4.4), the relative distance of points[3] will change inside a correspondence map but the overall inter-relationships of the points will almost remain comparable. In this case, if a great constant value is selected (e.g. 20 instead of 2), the correspondence map will change significantly. Some statistical terms are broadly used in correspondence analysis are explained in Table 4.6.

[3] **See the explanations of Table 4.6**

Table 4.4: The z-transformed values of Table 4.3.

Element / Orebody	S	Fe	Cu	Zn	As	Ag	Cd	Sb	Pb	Bi
A Lode	-0.130	0.511	-0.782	-1.067	0.199	-0.485	-0.043	2.048	-0.375	0.578
B Lode	-1.382	1.071	-0.621	1.185	0.386	-0.103	-0.700	0.038	-0.434	1.106
C Lode	0.860	-1.047	0.024	-0.872	-0.605	0.660	-0.384	-0.229	2.260	0.420
1 Lens	-0.886	1.023	-1.102	-0.514	1.227	-1.632	2.190	-0.631	-0.434	-1.137
2 Lens	0.678	-0.438	1.648	-0.555	0.610	1.577	-0.700	-0.564	-0.470	-0.780
3 Lens	1.356	-1.461	-0.183	1.388	0.068	-0.294	-0.227	-0.967	-0.299	-1.176
The Western Mineralisation	-0.495	0.341	1.017	0.436	-1.886	0.278	-0.135	0.306	-0.246	0.988

Table 4.5: The z-transformed values+2 of Table 4.4.

Element / Orebody	S	Fe	Cu	Zn	As	Ag	Cd	Sb	Pb	Bi	Row totals
A Lode	1.869	2.511	1.217	0.932	2.199	1.514	1.956	4.048	1.624	2.578	20.45
B Lode	0.617	3.071	1.378	3.185	2.386	1.896	1.299	2.038	1.565	3.106	20.54
C Lode	2.860	0.952	2.024	1.127	1.394	2.66	1.615	1.77	4.26	2.42	21.08
1 Lens	1.113	3.023	0.897	1.485	3.227	0.367	4.190	1.368	1.565	0.862	18.10
2 Lens	2.678	1.561	3.648	1.444	2.610	3.577	1.299	1.435	1.529	1.219	21.00
3 Lens	3.356	0.538	1.816	3.388	2.068	1.705	1.772	1.032	1.7	0.823	18.20
The Western Mineralisation	1.504	2.341	3.017	2.436	0.113	2.278	1.864	2.306	1.753	2.988	20.60
Column totals	14	14	14	14	14	14	14	14	14	14	140

Table 4.6: A summary of statistical terms used in correspondence analysis.

Points	**Demonstration of elements and orebodies of Table 4.3 in a correspondence map.**
Dimension	**In Table 4.5, pyrrhotite samples collected from each orebody are associated with 10 element concentrations. Therefore, each orebody can be defined by variation of the 10 elements in a 10-dimensional space.**
Scores in dimension	**Scores show the coordinates of points in a correspondence map and each point is determined by a score in relation to the scale of each dimension of a correspondence map.**
Inertia	**Variance in correspondence analysis is called inertia. Inertia is "the weighted sum of chi-square distance between each profile and the mean profile" (Ender 2010, p. 1).**
Mass	**Mass is the marginal proportion of the row and column variables that is used to weight the point profiles for calculation of point distance. So that the sum of all table entries is equal to 1.0 (StatSoft Electronic Statistics Textbook 2010) and the row and column values are standardised for producing a correspondence map. For example, in Table 4.5, each column total value will be divided by the total of sum value for the columns, i.e., 140.**
Chi-square method	**Determination of distances between the points provides all information about all similarities among them. In correspondence analysis, the distances between points are measured by chi-square method rather than the Euclidian distance. The resulting distance matrix is used as entry data of the principal component analysis[1]. The chi-square (Friendly 1995) is a weighted profile distance, where the weight is the mass of the row or column values (Table 4.7).**
The total inertia	**The sum of all the eigenvalues is named the total inertia or the total variance explained by the dimension. The total inertia is calculated by the total chi-square value (29.952 in Table 4.7) divided by the total of the sum (140 in Table 4.5).**
Correspondence analysis	**The correspondence analysis is a method for decomposing the total inertia in order to identify a lower-dimensional space for any given points. This analysis makes easier interpretation of the internal relationships of the points.**
Percentage of proportional inertia (PPI)	**In Table 4.8, PPI is calculated by $\frac{\text{Inertia of each dimension}}{\text{Total inertia}} \times 100$. For example, the proportional inertia of the first dimension in Table 4.8 accounts for 37.82 % of the total inertia (21.39 %).**
Correspondence map	**Visual presentation of the contribution of points to dimensions and contribution of the dimensions to categorisation of the points and detection of their internal-relationships. Each correspondence map accounts for part of the total variation of the points within two dimensional spaces (Figures 4.5 and 4.7).** **For measuring distances of row and column values, a symmetrical normalisation was used in this study because the principal coordinate of row and column values have slightly different scale. In a correspondence map, relative distance of points from each other and the scores of points are important parameters for interpretation (Section 4.3.1.3).**

[1] See the explanation of the principal component analysis in Section 5.7

Table 4.7: Chi-square distances of Table 4.5.

Element / Orebody	S	Fe	Cu	Zn	As	Ag	Cd	Sb	Pb	Bi	Total
A Lode	0.015	0.106	0.335	0.606	0.012	0.138	0.004	1.963	0.087	0.139	3.404
B Lode	1.005	0.504	0.223	0.622	0.054	0.012	0.277	0.000	0.117	0.539	3.352
C Lode	0268	0634	0.003	0.457	0.242	0.144	0.115	0.054	2.196	0.046	4.160
1 Lens	0.268	0.813	0.460	0.058	1.110	1.149	3.131	0.108	0.033	0.496	7.627
2 Lens	0.159	0.138	1.140	0.205	0.124	1.039	0.305	0.211	0.155	0.370	3.845
3 Lens	1.296	0.903	0.000	1.351	0.034	0.007	0.001	0.341	0.008	0.546	4.487
The Western Mineralisation	0.150	0.038	0.445	0.069	1.840	0.023	0.019	0.029	0.046	0.418	3.076
Total	3.162	3.136	2.606	3.368	3.415	2.513	3.852	2.706	2.641	2.553	29.952

Table 4.8: The results of decomposition of Table 4.5 into six dimensions.

Analysis of Contingency Table					
Dimensions	Inertia	Chi-square	Proportion of inertia	PPI	Percentage of cumulative inertia
1	0.0809		0.3782	37.82	37.82
2	0.0533		0.2493	24.93	62.75
3	0.0320		0.1495	14.95	77.69
4	0.0215		0.1007	10.07	87.76
5	0.0149		0.0696	6.96	94.72
6	0.0113		0.0528	5.28	100
Total	0.2139	29.952			

4.3.1.3 Correspondence maps for pyrrhotite samples

Figures 4.5 to 4.7 display symmetrical plots of the elements of pyrrhotite samples and the Broken Hill orebodies. Figure 4.5 shows 62.75 %[5] of the total chemical variation of pyrrhotite samples within the Broken Hill orebodies. In Figure 4.5, dimension 1 separates the plane from its zero value into two parts, positive and negative. C Lode, 2 Lens, S, Ag and Cu lie at the extreme end of the positive scale and 1 Lens, Fe and Cd are at the extreme end of the negative scale of dimension 1.

Dimension 2 separates the plane from its zero value into two parts, positive and negative. Bi, Sb and the Western Mineralisation lie at the extreme end of the negative scale and 1 and 3 Lenses, As, Cd and S lie at the extreme end of the positive scale. Both the first and second dimensions discriminates Fe-rich pyrrhotite from S-rich pyrrhotite.

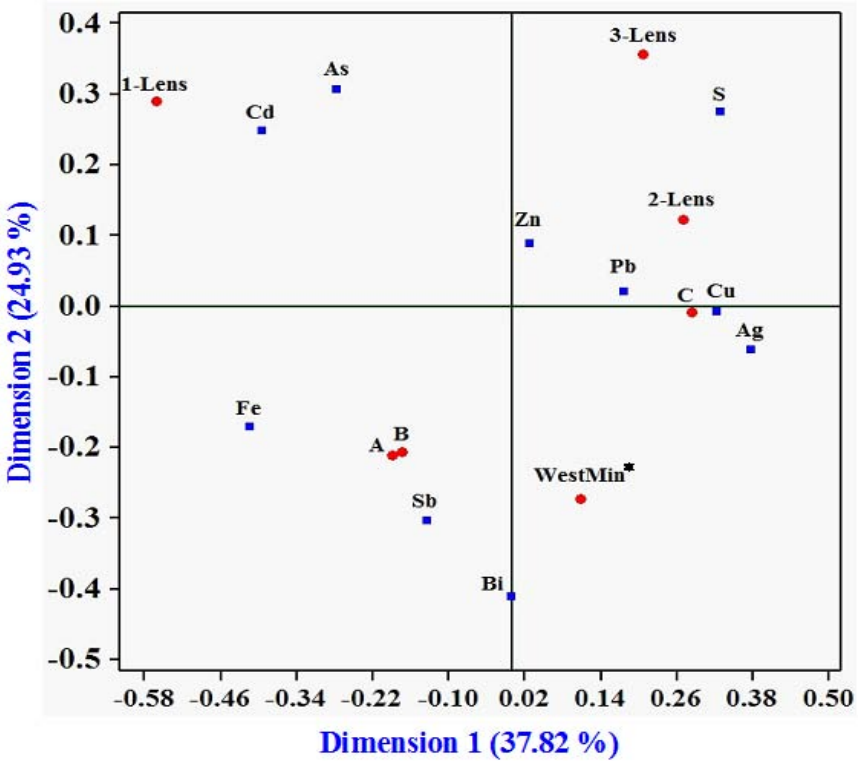

Figure 4.5: Correspondence map in relation to dimensions 1 and 2 for pyrrhotite.
(* The Western Mineralisation)

In Figure 4.6, the correspondence map of dimensions 1 and 3 jointly accounts for 52.77 % of the total chemical variation of pyrrhotite within the Broken Hill orebodies. Dimension 3 separates C Lode and Pb-rich pyrrhotite from Zn- rich pyrrhotite.

[5] **Calculated by PPI (dimension 1) + PPI (dimension 2) from Table 4.7**

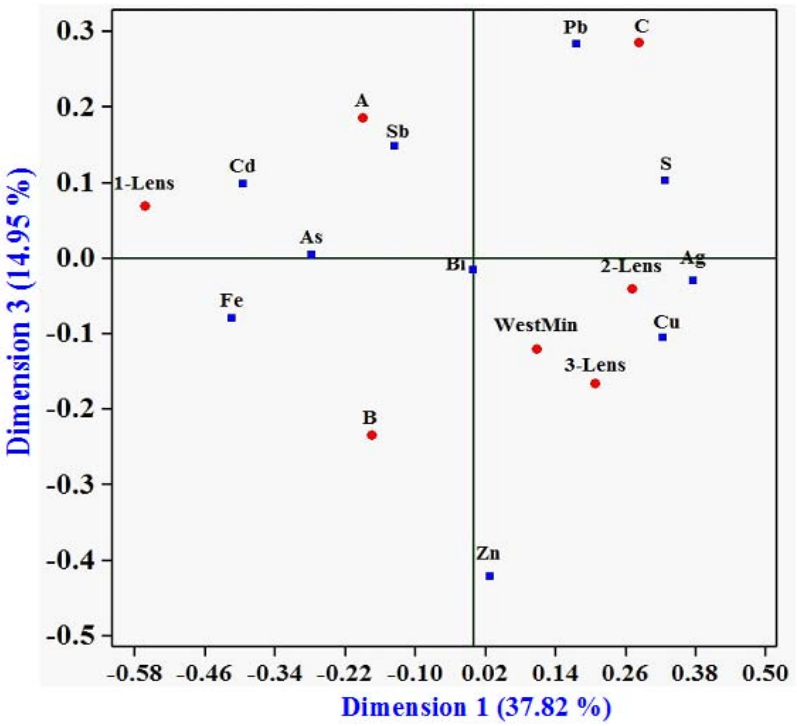

Figure 4.6: Correspondence map in relation to dimensions 1 and 3 for pyrrhotite.

In Figure 4.7, the plane of dimensions 2 and 3 accounts for 39.88 % of the total chemical variation of pyrrhotite within the Broken Hill orebodies.

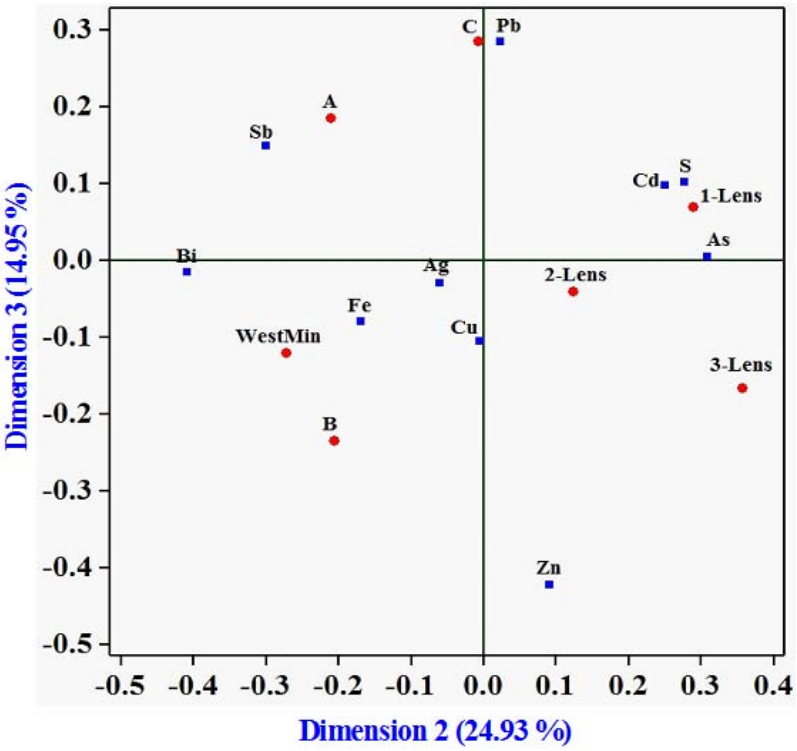

Figure 4.7: Correspondence map in relation to dimensions 2 and 3 for pyrrhotite.

Together Figures 4.5 to 4.7 provide a three-dimensional model[6] that shows 77.69 % [7] of total variation of pyrrhotite within the Broken Hill orebodies and their results are outlined below:

- A Lode contains Sb-rich pyrrhotite samples,
- B Lode contains Fe-rich pyrrhotite samples,
- C Lode contains Pb-rich pyrrhotite samples,
- 1 Lens contains Cd-rich pyrrhotite samples,
- 2 Lens contains Cu- and Ag-rich pyrrhotite samples,
- 3 Lens contains S-rich pyrrhotite samples, and
- The Western Mineralisation contains Bi- and Sb-rich pyrrhotite samples.

4.4 Magnetic susceptibility measurements in the Western Mineralisation

In order to interpret the down-hole variation of magnetic susceptibility in conjunction with variation of volume percentage of galena, sphalerite and pyrrhotite in the Western Mineralisation, a total of 54 exploration drill cores were investigated. These magnetic measurements were taken in CBH Resources' core shed aiming to systematically quantify the magnetic properties in 1,928 samples of the surface drill cores. The split cores comprised the sulphide mineralised areas and their enclosing non-mineralised rocks. The magnetic susceptibility is the intrinsic property that depends on the magnetic mineral content and also on the size and orientation of magnetic particles present in a sample. The magnetic susceptibility does not however depend on the strength of the geomagnetic field in which lithologies occurred.

The hand held magnetic susceptibility metre model Digital Fugro GMS-2 (Figure 4.8) was used in this study. The GMS-2 is a high sensitivity portable instrument with a detection range between 1×10^{-5} SI to 10 SI values and a resolution of 1×10^{-5} SI value. Therefore, values less than 1×10^{-5} SI are outside the detection range of the GMS-2 and are automatically assigned a value of 1×10^{-5} SI. The frequency of 760 Hz in this Model indicates that this instrument is not susceptible to the effects of high conductivity in some samples. When high magnetic susceptibility was shown, the instrument was frequently zeroed to avoid drift. The magnetic survey took place in a temperature range of about 10º-15° Celsius.

[6] A combination of three correspondence maps in relation to dimensions 1, 2 and 3
[7] Calculated by PPI (dimension 1) + PPI (dimension 2) + PPI (dimension 3) from Table 4.7

Magnetic susceptibility has been measured to derive the range of magnetic degrees for different rock types and the associated sulphide mineral assemblage exhibit at intervals of one metre. The magnetic susceptibility measurements should show variation of the magnetic properties and magnetic intensity from edge to the centre of the Western Mineralisation. The following magnetic susceptibility values were measured in the Western Mineralisation:

4.4.1 Average magnetic susceptibility (AMS)

Each 10 cm piece of one metre interval core sample was measured three times. The AMS values of the core were determined for the one metre core sample. It was expressed as AMS observed per metre and generally reflected lithological unit.

4.4.2 Maximum magnetic susceptibility (MMS)

Owing to the presence of disseminated pyrrhotite in each one metre interval core sample, MMS was measured at one point in each one metre core sample. It was expressed as MMS observed for a particular point in each sample.

Figure 4.8: A Magnetic Susceptibility Metre model Digital Fugro GMS-2.

4.5 Descriptive statistics for magnetic susceptibility, pyrrhotite, Pb+Zn and galena+sphalerite

In Table 4.9, maximum values of AMS and MMS are in the range of 10^{-3} SI[8] (e.g. 5500×10^{-5} SI = 5.5×10^{-3} SI) and are associated with paramagnetic minerals such as olivines, pyroxenes with positive susceptibility maximum of approximately 10^{-3} SI value (Clark 1997). The maximum AMS value of 1500×10^{-5} was measured in drill core 4010 at the depth of 256 m which contained 10 vol. % of pyrrhotite in a blue quartz lode. The MMS values of samples were up to 5500×10^{-5} or 0.055 SI. As mentioned earlier, the 1,928 investigated samples of the Western Mineralisation were divided into two groups (Table 4.10) and their statistical results are given in Table 4.11. Table 4.11 shows that the mean values of pyrrhotite, AMS and MMS within productive samples are much greater than the barren samples. This indicates that the mean volume percentage of magnetic pyrrhotite is different between the two groups of samples in Table 4.10.

Statistical tests can then be used to test if the mean values of pyrrhotite and MMS of barren and productive samples are indeed coming from two distinct distributions. The differences of the two mean values of pyrrhotite and MMS between the barren and productive samples may be significant or may be by chance. In statistics, when a result is called significance, it is not possible to have occurred by chance. This issue can be evaluated by further statistical tests.

4.5.1 Statistical tests

Depends on the distribution of data, statistical tests can be carried out by parametric or non-parametric analysis. In parametric approach, data is supposed to come from a normal distribution and parameters of the distribution can be inferred by parametric statistics. In contrast, the non-parametric approach has no assumption about the distribution and it is less sensitive to the effects of outliers.

[8] International System of Units (metric system)

Table 4.9: Descriptive statistics for magnetic susceptibility, pyrrhotite, Pb+Zn and galena+sphalerite within the analysed samples of surface drill holes.

Variables (Unit)	Number of samples	Mean	COV	Minimum	Q_1	Median	Q_3	Maximum	Skewness
Pyrrhotite (Vol. %)	997	3.175	103.43	1	1	2	4	40	4.55
Galena+sphalerite (Vol. %)	1246	8.393	121.06	1	2	5	10	75	2.9
Pb+Zn (%)	1823	3.033	160.66	0.005	0.31	1.3	3.671	61.76	4.23
AMS (SI)	1928	34.2×10^{-5}	220.48	1×10^{-5}	1×10^{-5}	1×10^{-5}	30×10^{-5}	1500×10^{-5}	6.47
MMS (SI)	1928	407.1×10^{-5}	132.61	1×10^{-5}	1×10^{-5}	232.5×10^{-5}	600×10^{-5}	5500×10^{-5}	2.88

Table 4.10: Two groups of samples used in this study.

Ore sulphide minerals	Number of samples	Name of group
galena+sphalerite $\geq$ 1 vol. %	1246	Productive
galena+sphalerite = 0 vol. %	682	Barren

Table 4.11: Descriptive statistics for magnetic susceptibility, pyrrhotite, Pb+Zn and galena+sphalerite in barren (B) and productive (P) samples.

Variables	Number of samples	Mean	COV	Minimum	Q_1	Median	Q_3	Maximum	Skewness
Pyrrhotite (B)	207	2.754	97.49	1	1	2	3	20	2.67
Pyrrhotite (P)	790	3.284	104	1	1	2	4	40	4.73
Galena+sphalerite (P)	1246	8.393	121.06	1	2	5	10	75	2.9
Pb+Zn (B)	604	0.544	177.15	0.005	0.09	0.20	0.58	10.75	4.98
Pb+Zn (P)	1219	4.266	129.38	0.027	1.05	2.59	5.22	61.76	3.73
AMS (B)	682	22.8×10^{-5}	248.93	1×10^{-5}	1×10^{-5}	1×10^{-5}	30×10^{-5}	600×10^{-5}	5.18
AMS (P)	1246	40.4×10^{-5}	205.75	1×10^{-5}	1×10^{-5}	5×10^{-5}	50×10^{-5}	1500×10^{-5}	6.43
MMS (B)	682	253.1×10^{-5}	171.31	1×10^{-5}	1×10^{-5}	60×10^{-5}	340×10^{-5}	4000×10^{-5}	3.21
MMS (P)	1246	491.7×10^{-5}	116.52	1×10^{-5}	80×10^{-5}	340×10^{-5}	750×10^{-5}	5500×10^{-5}	2.79

The student's t-test is a parametric statistical method for the comparison of the mean values of two independent groups (Everitt 2006) provided if the number of samples between the two sample groups does not differ greatly. However, according to Figures 4.9 and 4.10, the distribution of AMS, MMS, pyrrhotite and galena+sphalerite are not normal for raw and logarithmic data. Moreover, the number of productive samples (1246) is 1.8 times that of the barren samples (682) samples. Therefore, the non-parametric approach is able to provide a better mechanism to determine statistically whether the productive group differs significantly with barren group in the amount of magnetic pyrrhotite.

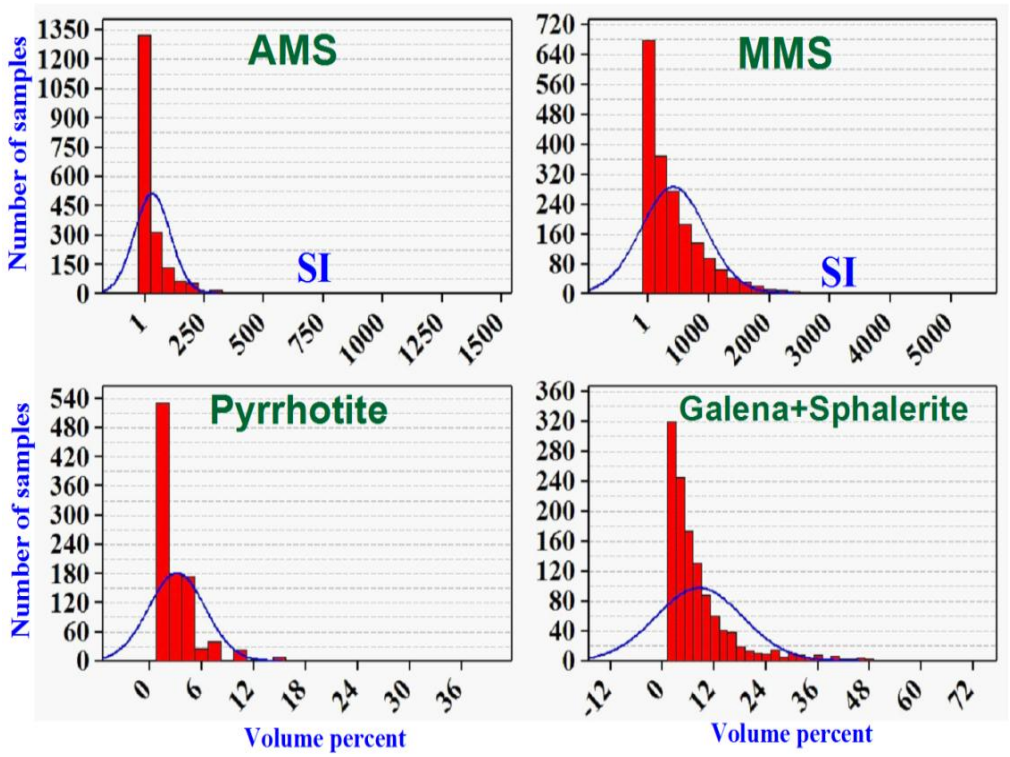

Figure 4.9: Positive skewed distributions for original data of MMS, AMS, pyrrhotite, Pb+Zn and galena+sphalerite. The red areas show the experimental distributions of MMS, AMS, pyrrhotite and galena+sphalerite and the blue curves are their respective theoretical (estimated) normal distributions.

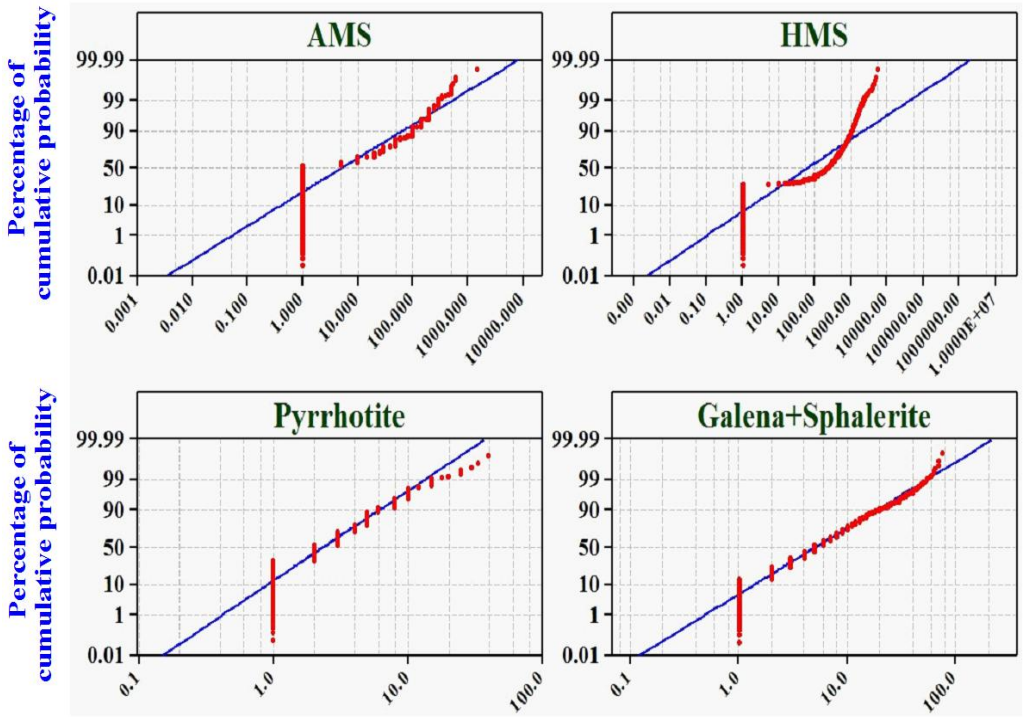

Figure 4.10: Probability graphs for logarithmic data of MMS, AMS, pyrrhotite and galena+sphalerite. The red curves show the experimental logarithmic values of the variables against their respective estimated percentage of cumulative probability and the straight blue lines show the theoretical percentage of cumulative probability for near-normal distribution of the variables.

Statistical tests give geologists a tool to make a quantitative assessment of statistical significant differences of two sample groups. If there is a significant difference between the two sample groups, it would confirm that the magnetic pyrrhotite or magnetic property can be considered as a geophysical indicator for tracking galena and sphalerite in the Western Mineralisation. The aim is to assess whether there is enough evidence to accept the null hypothesis about two sample groups or to reject the null hypothesis (alternative hypothesis).

4.5.1.1 Hypothesis of the non-parametric statistical tests

1. The null hypothesis is that the median values of AMS, MMS and pyrrhotite are the same for both barren and productive samples, and

2. Alternative hypothesis is that the median values of AMS, MMS and pyrrhotite differ between barren and productive samples.

4.5.1.2 P value or significance level (1-tailed or 2-tailed)

1. If the P value of data < 0.01, it will indicate that the data provides statistically significant evidence of a difference between the barren group and the productive group with 99 % confidence level.
2. If the P value of data > 0.01, it will conclude that the data does not provide statistically significant evidence of a difference between the barren group and the productive groups with 99 % confidence level.

In this section, only the outcomes of the non-parametric statistical tests are presented. A comprehensive description of the mechanism of the statistical tests for independent groups is in the support section of the SPSS (SPSS Inc. 2009) software package.

4.5.2 Wilcoxon Mann-Whitney U Test

In the case of independent groups, the Mann-Whitney U Test (Wilcoxon, 1945) is the most widely-used significance test for comparing two independent samples based on locations of the ranks and this test can evaluate whether two independent samples relate to the same distribution (the null hypothesis) or not (the alternative hypothesis). In the Mann-Whitney Test (Tables 4.12 and 4.13), significant values (2-tailed) and Mont Carlo Sig.[9] are less than 0.01. This indicates that AMS, MMS values and volume percentage of pyrrhotite differ significantly between the two groups of productive and barren in the Western Mineralisation (at the 99 % confidence level).

Table 4.12: The mean rank of AMS, MMS and pyrrhotite between the barren and the productive groups using the Mann-Whitney Test.

Mann-Whitney Test	Group	N*	Mean Rank	Sum of Ranks
AMS	Barren	682	856.88	583533.5
	Productive	1246	1022.55	1274094.5
MMS	Barren	682	756.50	515174.5
	Productive	1246	1077.41	1342453.5
Pyrrhotite	Barren	207	437.54	90571.5
	Productive	790	515.10	406931.5

*Number of samples

[9] Mont Carlo Significance

Table 4.13: The results of the Mann-Whitney Test.

Test Statistics		AMS	MMS	Pyrrhotite
Mann-Whitney U		351312.5	282953.5	69043.5
Wilcoxon W		583533.5	515174.5	90571.5
Z		-6.768	-12.228	-3.543
Asymp. Sig. (2-tailed)		0.000	0.000	0.000
Monte Carlo Sig. (2-tailed)	Lower Bound	0.000*	0.000*	0.000*
	99 % confidence level	0.000	0.000	0.000
	Upper Bound	0.000	0.000	0.001

* Based on 10,000 sampled tables with starting seed 2,000,000

4.5.3 Kolmogorov-Smirnov Z Test

The Kolmogorov-Smirnov Z test (Table 4.14) detects differences in both the locations and shapes of the distributions. This test measures the maximum absolute difference between the observed cumulative distribution functions in both groups. When the differences are large enough to be significant, the two distributions are considered different. In Table 4.14, the 99 % confidence level is smaller than 0.01 in the lower and upper bound that indicate the two groups differ in either shape or location.

Table 4.14: Two-Sample Kolmogorov-Smirnov Frequencies Test.

Two-Sample Kolmogorov-Smirnov Test		AMS	MMS	Pyrrhotite
Most Extreme Absolute Differences		0.147	0.295	0.157
	Positive	0.000	0.000	0.010
	Negative	-0.147	-0.295	-0.157
Kolmogorov-Smirnov Z		3.095	6.196	2.006
Asymp. Sig. (2-tailed)		0.000	0.000	0.001
Monte Carlo Sig. (2-tailed)		0.000*	0.000*	0.000*
99 % confidence level	Lower Bound	0.000	0.000	0.000
	Upper Bound	0.000	0.000	0.000

* Based on 10,000 sampled tables with starting seed 2,000,000

4.5.4 Moses Test of Extreme Reactions

The Moses Test is used in experimental studies to assess whether the experimental variable affects subjects in either a positive or a negative direction, creating a polarising effect. The Moses Test compares extreme responses of one sample with another sample obtained from a control group (in this study, barren group). If the probability associated

with the Moses test is less than the desired significance level (in this study $P < 0.01$) then it can be concluded that the two samples differ. In general, the Kolmogorov-Smirnov Z Test check the middle of the distribution for differences in central tendency and do not take account of the extreme low and high values. So it is possible when two different distributions (e.g. one normal and another polarised at the two extreme) are compared with each other and show similar central tendency that might not be found to be significantly different by the Mann-Whitney U Test and the Kolmogorov-Smirnov Z Test, while the Moses Test checks the tails of the distribution for differences in extreme tendencies (Table 4.15).

Table 4.15: Moses Extreme Reactions Test Frequencies at the 99 % confidence level.

Moses Test	Group	N
AMS	Barren (Control)	681
	Productive (Experimental)	1246
MMS	Barren (Control)	681
	Productive (Experimental)	1246
Pyrrhotite	Barren (Control)	207
	Productive (Experimental)	790

Test Statistics	AMS	MMS	Pyrrhotite
Observed Control Group Span	1418	1661	827
Sig.(1-tailed)	0.000	0.000	0.000
Trimmed Control Group Span	1212	1487	771
Sig.(1-tailed)	0.000	0.000	0.000
Outliers Trimmed from each end	34	34	10

In Table 4.15, the barren group was defined as the control group. P values or Sig.[10] (1-tailed) for AMS, MMS and pyrrhotite are below 0.01, thus indicating that the two groups of barren and productive units differ significantly at 99 % confidence level. The significance levels (1-tailed) in the trimmed group are the same as the observed group and this confirms that even if the outlier samples are removed, these two groups of barren and productive areas differ with respect to their AMS, MMS and pyrrhotite values. According to the results of non-parametric statistical tests, there is enough evidence to suggest that pyrrhotite abundance and AMS and MMS values are significantly different between productive and barren samples in the Western Mineralisation.

4.6 Bar diagrams of magnetic susceptibility and pyrrhotite

In bar diagram of AMS (Figure 4.11), the drill cores 4028 and 4052 have higher mean and median values relative to other drill cores and this indicates higher concentration

[10] **Significance level**

of magnetic minerals in these drill cores. When considering HiP value, drill cores 4010 and 4028 show maximum AMS variation. In Figure 4.11, when considering HiP value, the high variations of MMS are present within drill cores 4010, 4014 and 4031. Drill cores 4001, 4028, 4033 and 4052 reveal high mean and median values of MMS. The trends of mean variations of AMS and MMS are roughly similar (Figure 4.11). In Figure 4.11, drill cores 4028, 4033, 4045 and 4052 have high mean and median volume percentage of pyrrhotite within the surface drill cores.

The greatest variation of pyrrhotite is present in drill core 4050 followed by drill core 4030. The mean and median trend variations of pyrrhotite show similarity in a few drill cores with AMS and MMS values. For example, the mean and median values of AMS, MMS and pyrrhotite are high in drill cores 4028, 4033 and 4052 thus indicating an increase of magnetic pyrrhotite abundance within the drill cores. It is evident from Figure 4.12 that every drill core shows distinct variation for AMS, MMS, specific gravity, galena+sphalerite and Pb+Zn. There are significant similarities between the following variations:

- MMS and pyrrhotite, and
- Pb+Zn and galena+sphalerite.

In Figure 4.12, there are several similar trends of COV for AMS, MMS, specific gravity, galena+sphalerite and Pb+Zn in drill holes: 3231, 4010, 4011, 4012, 4015, 4026, 4028, 4031, 4032, 4037, 4038, 4039, 4040, 4052 and 4054.

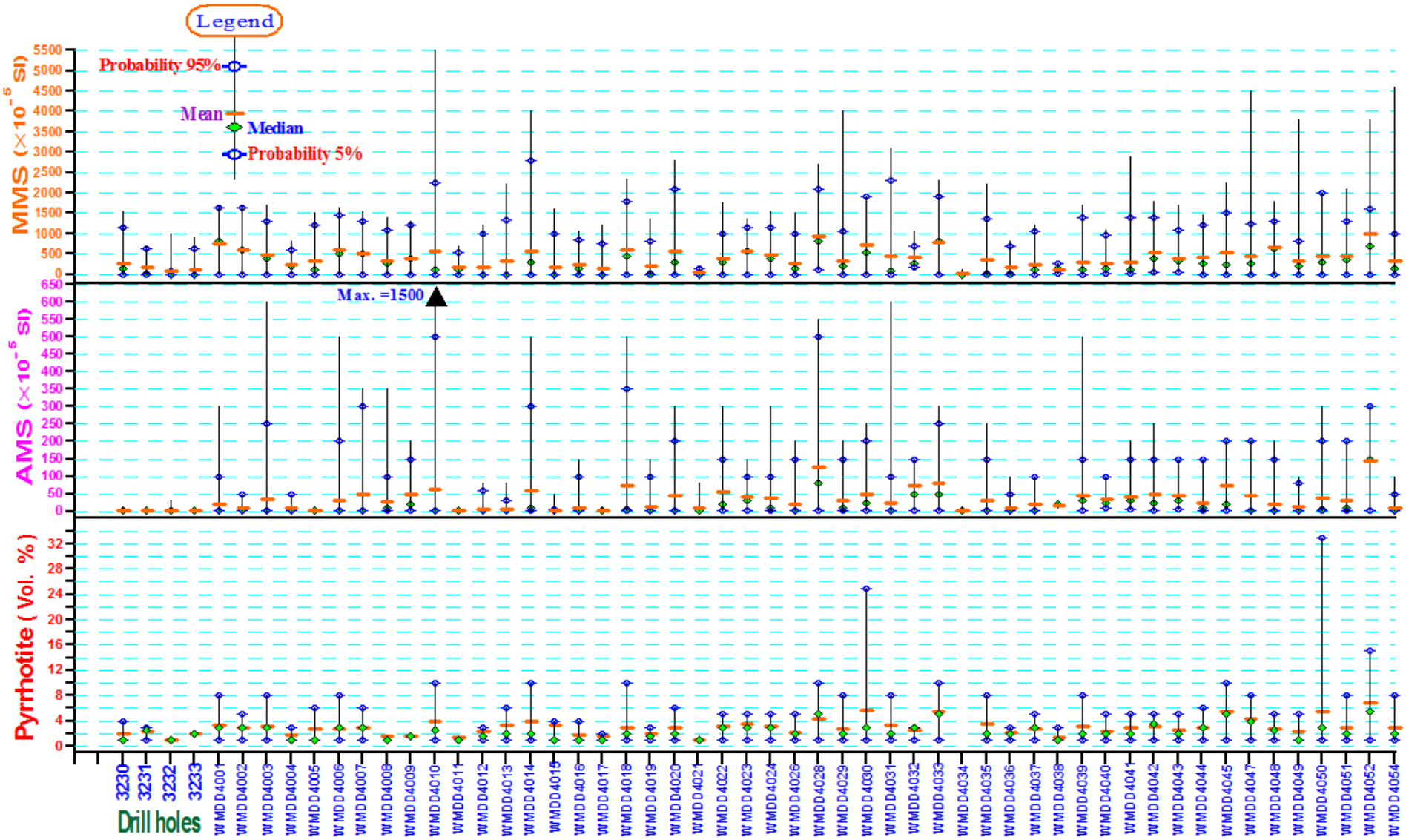

Figure 4 .11: Statistical parameters of pyrrhotite and AMS and MMS within the investigated samples of surface drill holes.

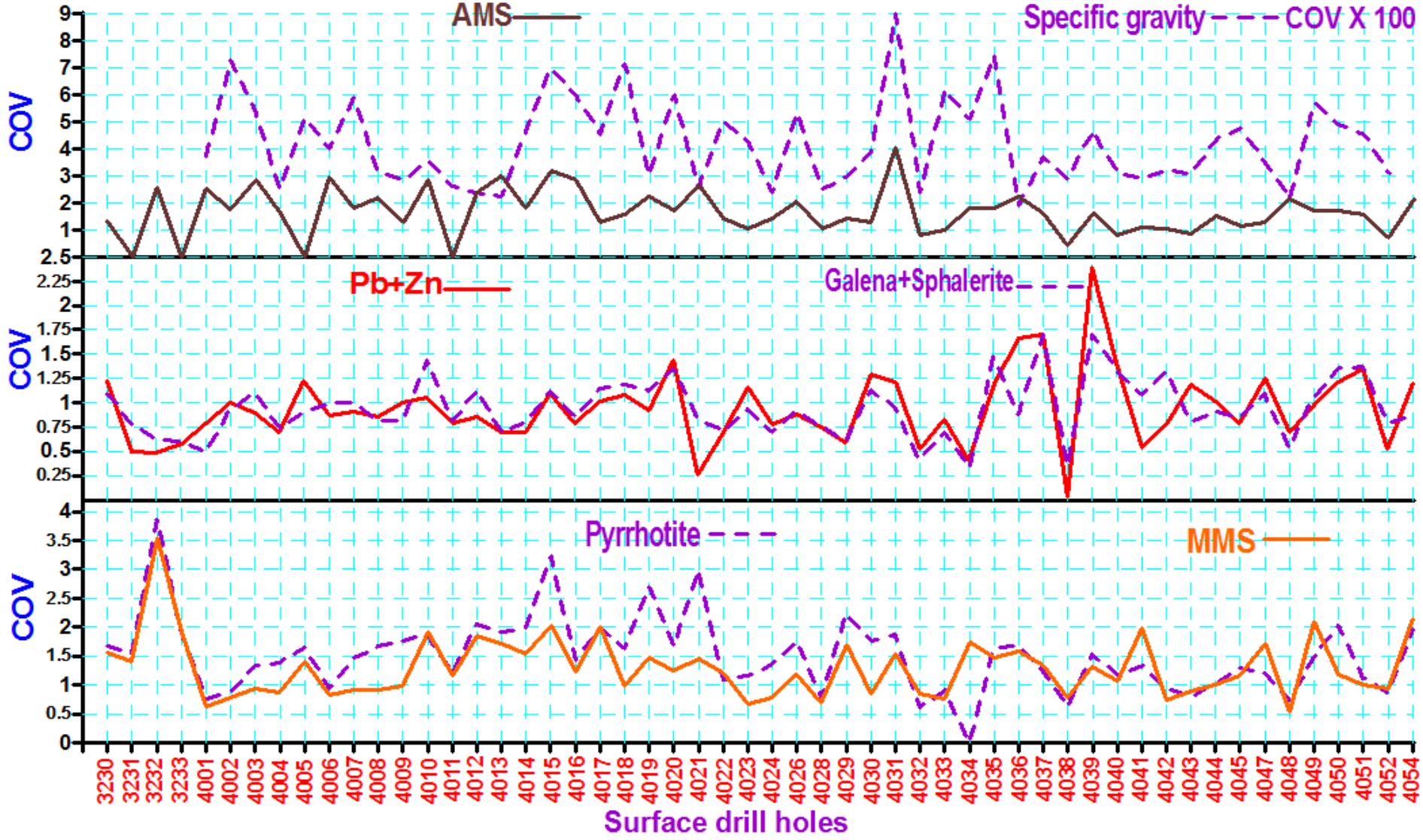

Figure 4.12: Comparison of the COV of pyrrhotite, Zn+Pb and AMS with that of MMS, sphalerite+galena and specific gravity.

4.7 Results of correlation coefficient

According to Figures 4.9 and 4.10, the distribution of original and logarithmic data of AMS, MMS, pyrrhotite and galena+sphalerite is not normal and non-parametric correlation methods such as Spearman correlation coefficient[1] (Table 4.16) and Kendall correlation coefficient[2] (Table 4.17) are preferable because they do not require any assumption for distribution. Since comparison of the correlation coefficient of AMS, MMS and pyrrhotite, requires the same number of samples, 790 samples that have values simultaneously for AMS, MMS and pyrrhotite were used to accommodate this requirement.

Table 4.16: The results of SCC for 790 samples.

Spearman	AMS	MMS	Pyrrhotite	Galena+Sphalerite
AMS	1.000	0.459*	0.483*	0.060
Sig. (2-tailed)	.	0.000	0.000	0.093
MMS	0.459*	1.000	0.648*	0.202*
Sig. (2-tailed)	0.000	.	0.000	0.000
Pyrrhotite	0.483*	0.648*	1.000	0.217*
Sig. (2-tailed)	0.000	0.000	1.000	0.000
Galena+Sphalerite	0.060	0.202*	0.217*	1.000
Sig. (2-tailed)	0.093	0.000	0.000	.

*Correlation is significant at the 0.01 level (2-tailed)

Table 4.17: The results of KCC for 790 samples.

Kendall	AMS	MMS	Pyrrhotite	Galena+Sphalerite
AMS	1.000	0.345*	0.387*	0.043
Sig. (2-tailed)	.	0.000	0.000	0.095
MMS	0.345*	1.000	0.507*	0.139*
Sig. (2-tailed)	0.000	0.000	0.000	0.000
Pyrrhotite	0.387*	0.507*	1.000	0.166*
Sig. (2-tailed)	0.000	0.000	.	0.000
Galena+Sphalerite	0.043	0.139*	0.166*	1.000
Sig. (2-tailed)	0.095	0.000	0.000	.

*Correlation is significant at the 0.01 level (2-tailed)

[1] SCC
[2] KCC

4.7.1 Interpretation of the correlation coefficients

In Tables 4.16 and 4.17, the significance level (2-tailed) between AMS and galena+sphalerite is more than 0.01 and it implies that there is less than (1- 0.01) or 99 % certainty for chance of being a true correlation coefficient.

The non-parametric correlations in Tables 4.16 and 4.17 show 64.8 % and 50.7 % correlation coefficients respectively between pyrrhotite (vol. %) and MMS (SI). In Tables 4.16 and 4.17, the result of correlation coefficient of MMS and pyrrhotite with galena+sphalerite show values close to each other. For example, in the SCC (Table 4.16), there is a 20.2 % correlation coefficient between MMS and galena+sphalerite versus 21.7 % correlation coefficient between pyrrhotite and galena+sphalerite. This indicates the relationship of high magnetic pyrrhotite with the galena and sphalerite.

4.8 Appraisal of internal relationships among magnetic susceptibility, pyrrhotite, galena+sphalerite and Pb+Zn relative to depth

There are major cases of internal relationships among variation of galena+sphalerite, Pb+Zn, pyrrhotite, AMS, MMS, specific gravity relative to depth among the 54 drill cores of the Western Mineralisation (Figures 4.13 to 4.17).

The results of observed internal relationships among the variables outline below:

1. The MMS values are anomalous in the presence of magnetic pyrrhotite and the trend of intensity of AMS values is partially analogous with MMS signatures,

2. The down hole variation of MMS values, pyrrhotite abundance and specific gravity values intensify within galena+sphalerite and Pb+Zn. It is unlikely that their marked variations may be directly attributed to lithology variations,

3. The range of MMS values and volume percentage of pyrrhotite vary from 2×10^{-3} SI to 20×10^{-3} SI and from 3 to12 (vol. %) respectively within galena+sphalerite. The range of specific gravity changes from 2 to 4, and

4. The MMS values and volume percentage of pyrrhotite display considerable fluctuation in places where the sample contains rich sulphide ore. In more detail, the following

compatibilities are shown among MMS values, pyrrhotite anomalies and galena+sphalerite content.

4.1. In most core logs, the commencement and termination of the signals of MMS and pyrrhotite anomalies roughly are consistent with the presence of sulphides (Figures 4.13 and 4.14),

4.2. In a few places, there is a partial shift or complete delay phase between the start and termination of one anomaly of MMS against the presence of sulphide ore. For example, in drill core 4014 (Figure 4.15), the anomaly of sulphide ore begins to appear immediately after termination of the MMS and pyrrhotite anomalies. Drill core 4005 (Figure 4.16) shows a delay phase and just part of the anomaly of MMS and the presence of sulphide ore overlap each other, and

4.3. In some drill cores, for example, 4044 (Figure 4.17), there are some depths where MMS anomalies are appeared in the absence of sulphide ore anomaly and vice versa. The displacement and absence of sulphide ore (galena+sphalerite) against MMS and pyrrhotite anomalies may be because pyrrhotite is ductile and during the Olarian Orogeny may have been remobilised out of sulphide rocks into the enclosing silicate rocks.

Textures in Figures 4.13 to 4.17 are associated to all sulphide minerals including pyrrhotite. However, among the investigated samples of the Western Mineralisation, pyrrhotite was present in various macroscopic textures such as stringer, disseminated, brecciated, network, massive, crystalline and veinlets. Where adjacent to galena and sphalerite, pyrrhotite is mostly disseminated, laminated and stringer, but further away from galena and sphalerite the dominant textures are massive and network. Moreover, to some extent the fine grained pyrrhotite reveals higher magnetic susceptibility and anisotropy (changing of magnetic intensity at different directions) than pyrrhotite with massive and network textures. The quantitative core log diagrams of this chapter have been provided in supplementary files to this thesis.

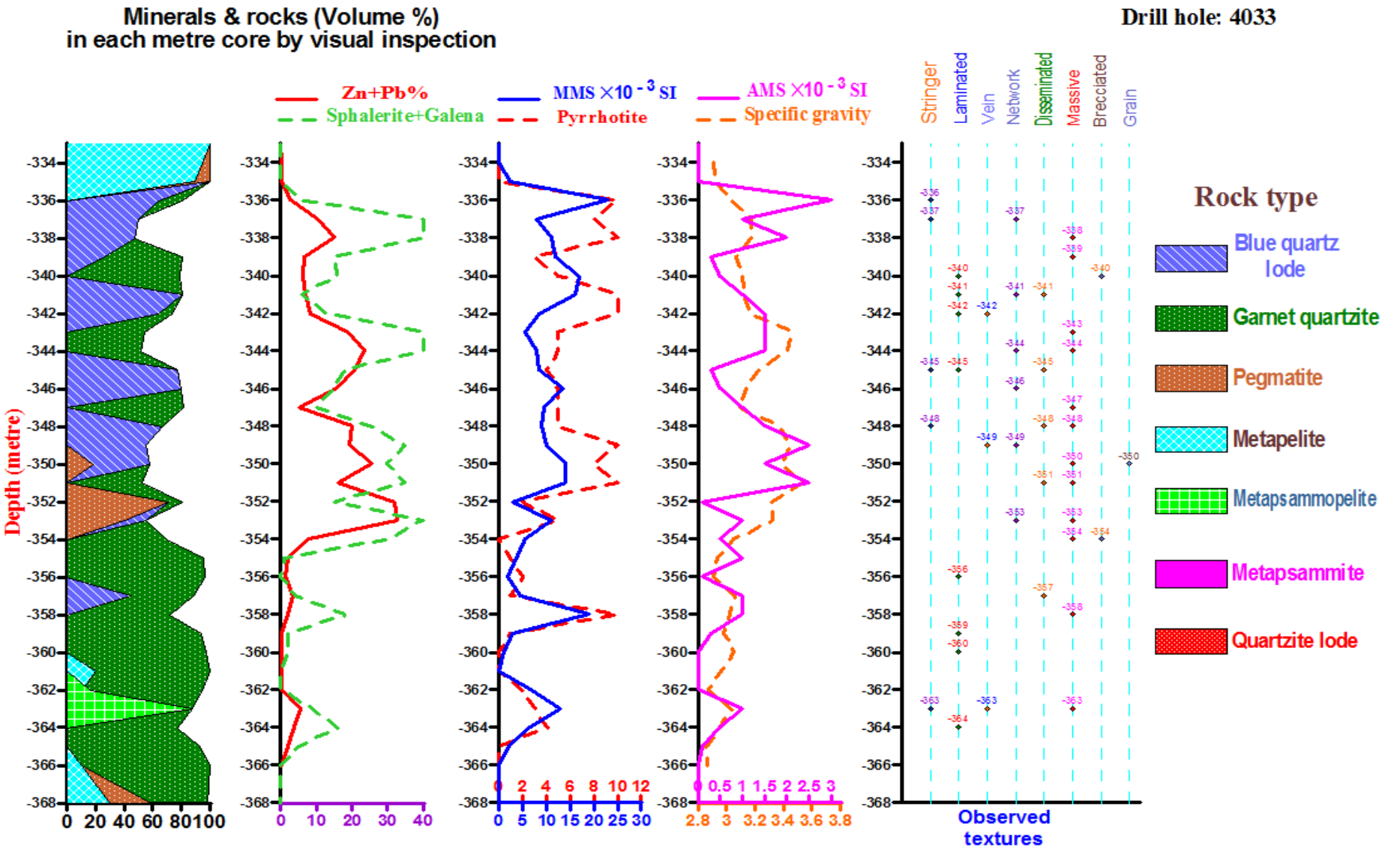

Figure 4.13: The quantitative core log for the investigated samples of drill hole 4033.

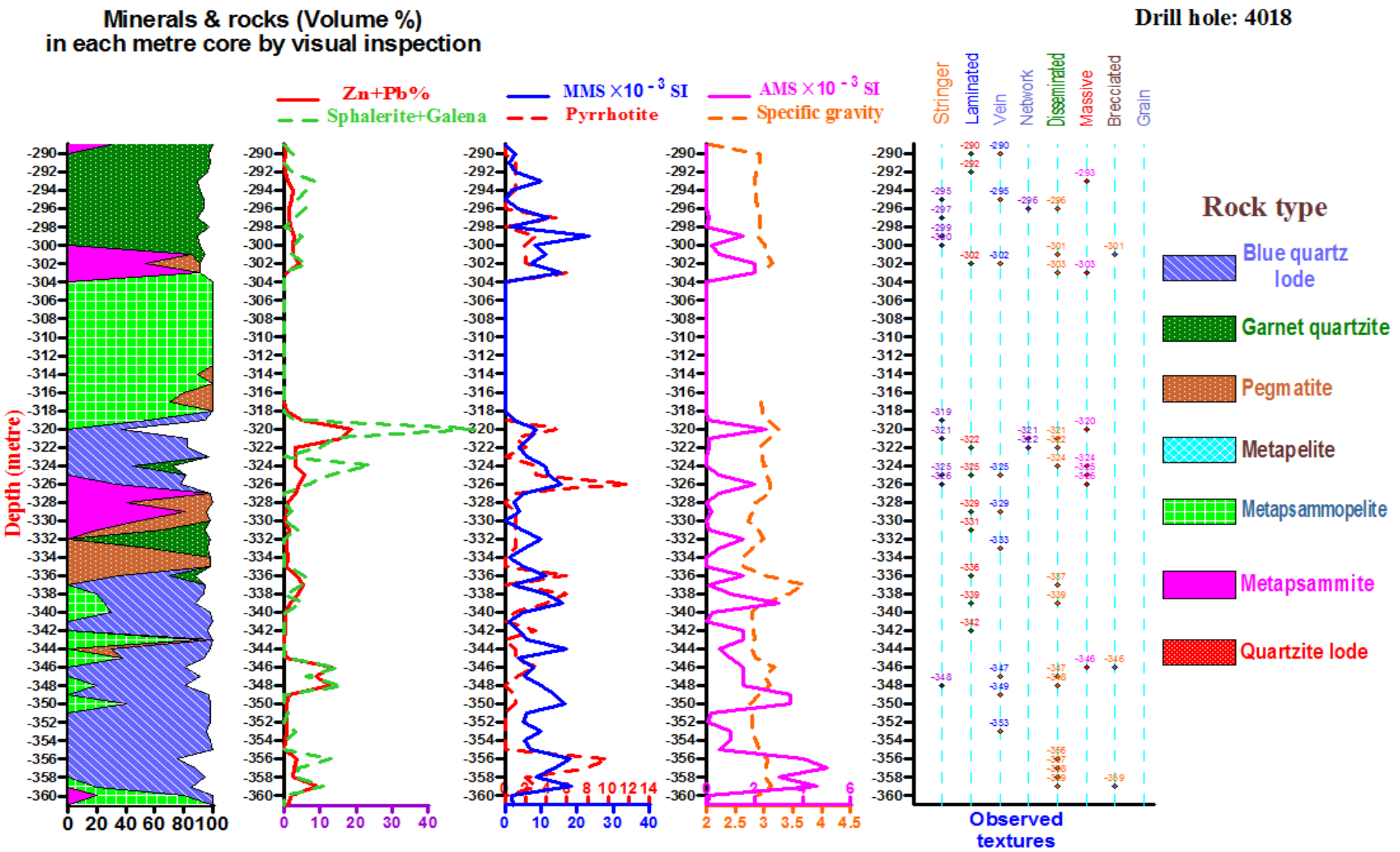

Figure 4.14: The quantitative core log for the investigated samples of drill hole 4018.

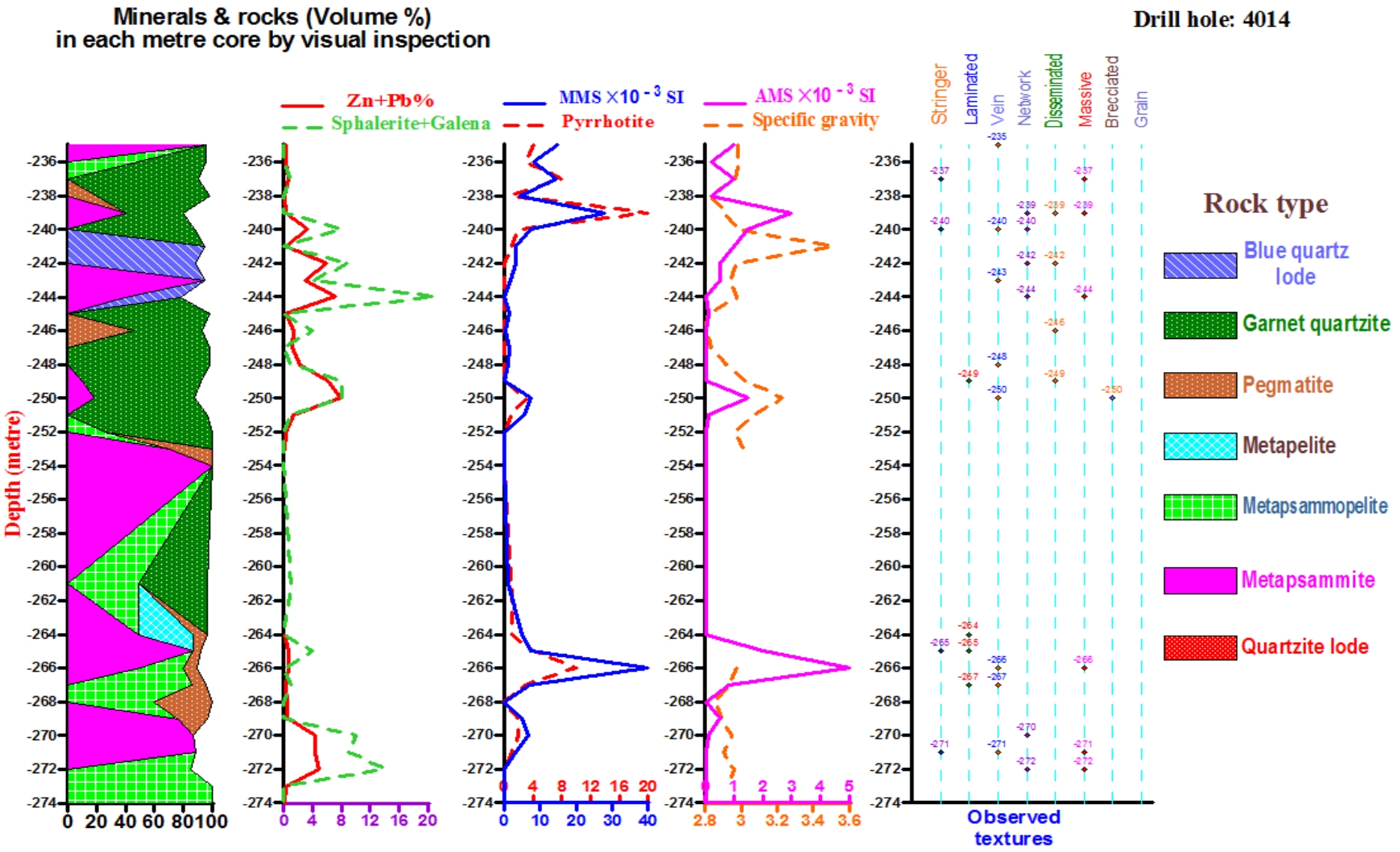

Figure 4.15: The quantitative core log for the investigated samples of drill hole 4014.

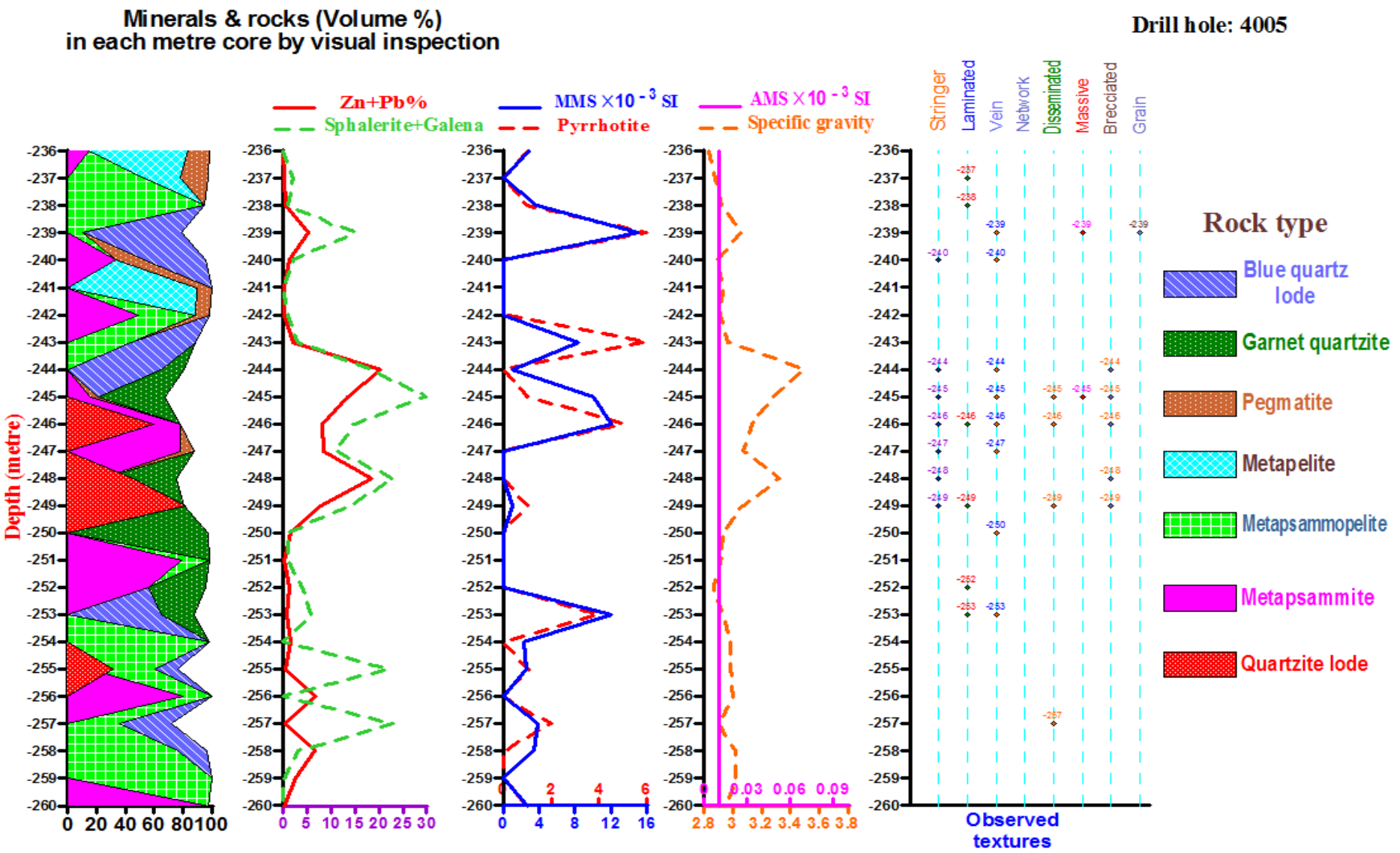

Figure 4.16: The quantitative core log for the investigated samples of drill hole 4005.

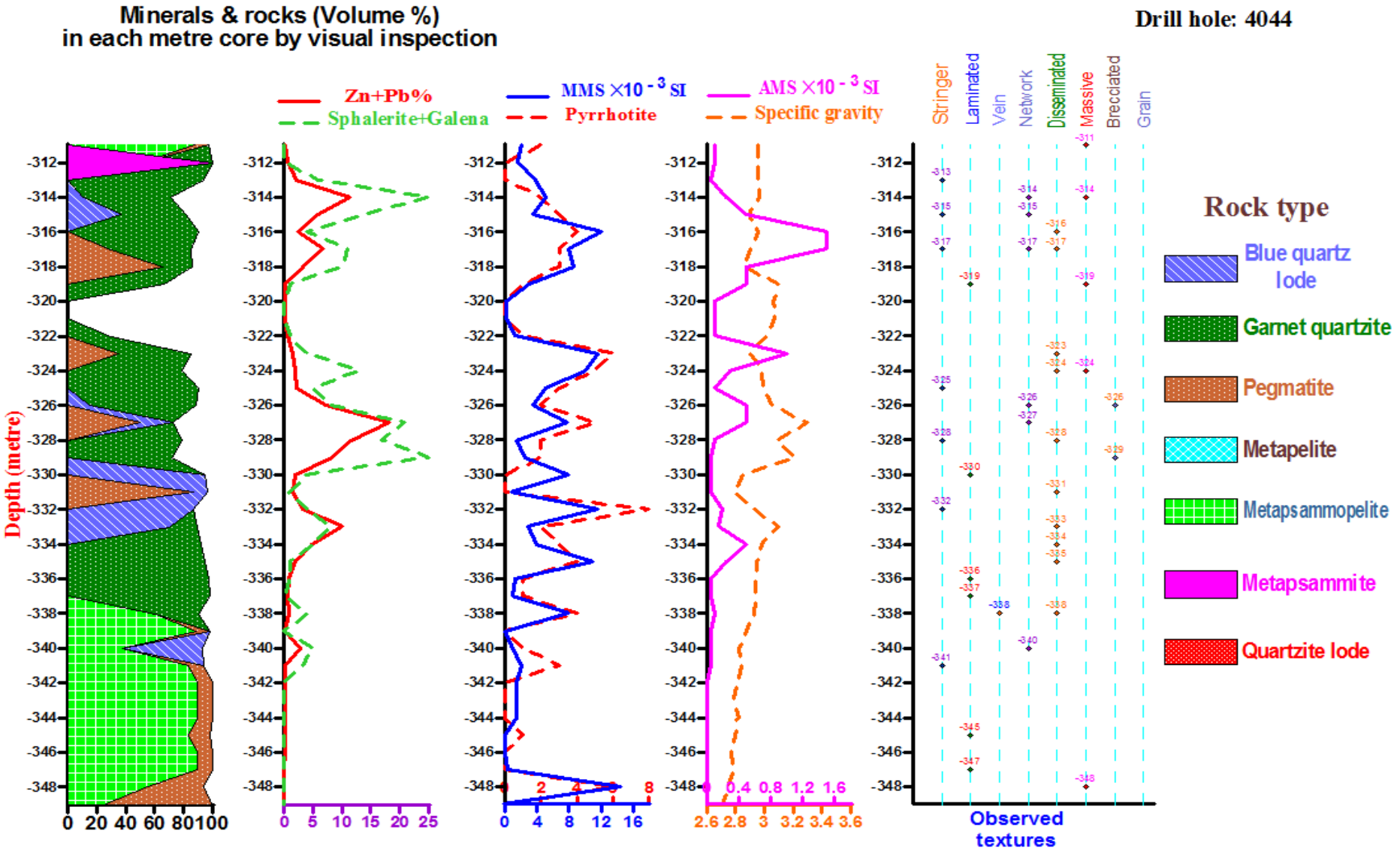

Figure 4.17: The quantitative core log for the investigated samples of drill hole 4044.

4.9 Contour plots

Contour plots are a useful tool for displaying anomalies. For example, contour plots of galena+sphalerite and Pb+Zn in the parameter space of AMS and pyrrhotite (Figures 4.18a and 4.18b) show an anomaly of galena+sphalerite and Pb+Zn that appears between 2 to 12 volume percent of pyrrhotite and between 1×10^{-3} SI and 6×10^{-3} SI value of AMS. In Figure 4.18a, another anomaly occurs between 12 and 19 volume percent of pyrrhotite and measures that are higher than 4×10^{-3} SI values for AMS.

In Figure 4.18c, the major anomalies of galena+sphalerite appear between 2 and 15 volume percent of pyrrhotite and between 3×10^{-3} SI and 20×10^{-3} SI of MMS values. In Figure 4.18d, the anomalies of Pb+Zn appear between volume percent of 4 and 12 of pyrrhotite and for MMS between 4×10^{-3} SI to 16×10^{-3} SI. In Figure 4.18d, another anomaly of Pb+Zn appears in the range of more than 35 volume percent pyrrhotite and the dominant MMS is between 0.01×10^{-3} SI and 27×10^{-3} SI. This second anomaly occurs in a few samples that are not covered by the major data set.

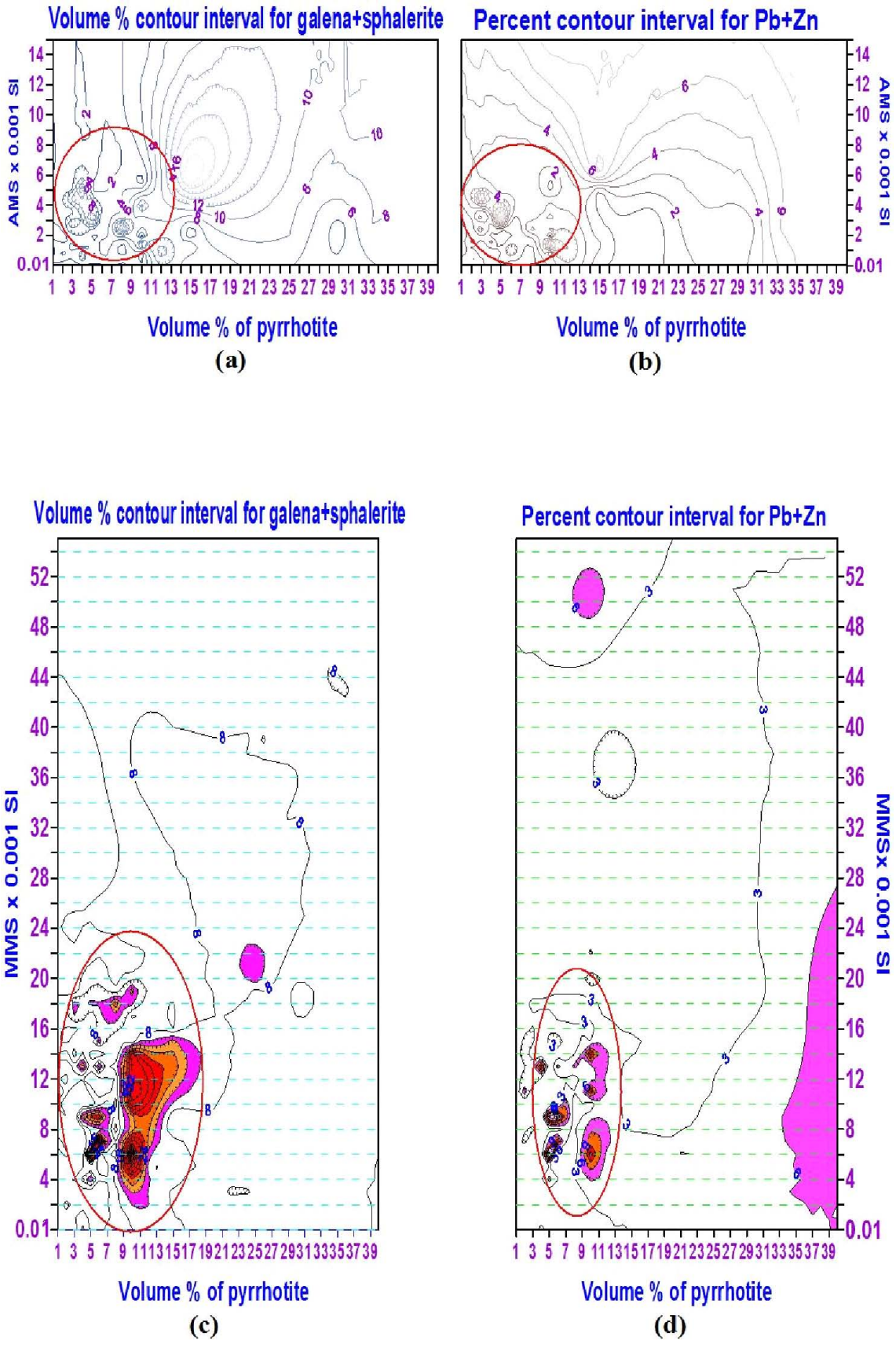

Figure 4.18: (a) and (b) show the contour plots of galena+sphalerite (vol. %) and Pb+Zn (%) respectively within the parameter space of AMS (SI) and pyrrhotite (vol. %). (c) and (d) show the contour plots of galena+sphalerite (vol. %) and Pb+Zn (%) respectively within the parameter space of MMS (SI) and pyrrhotite (vol. %).

4.10 Summary

This chapter investigated variation of magnetic pyrrhotite and its relationships with galena and sphalerite and tried to understand whether magnetic susceptibility and occurrences of pyrrhotite can be used as an exploration tool for tracking ore in the Western Mineralisation. In order to interpret the down-hole variation of magnetic susceptibility in conjunction with variation of galena (vol. %), sphalerite (vol. %) and pyrrhotite (vol. %), a total 1,928 samples of 54 exploration drill cores were investigated. The data set was then divided into two groups, productive and barren, based on the quantity of summation of galena and sphalerite.

The outcomes of this study show that samples containing galena or sphalerite have considerably more magnetic pyrrhotite than the samples without galena and sphalerite. Thus, an understanding of the variation of pyrrhotite abundance and the geological significance of its magnetic patterns provide a link between the mineralisation and the geometrical configuration of the orebody.

Simple correspondence analysis performed in this study to show a picture of internal relationships between chemical composition of pyrrhotite samples and the Broken Hill orebodies. The result of 3D correspondence map shows that pyrrhotite samples of the Western Mineralisation contain higher Bi and Sb in comparison with the other Broken Hill orebodies.

Previous collected pyrrhotite samples from the Western Mineralisation shows chemical formula of either magnetic pyrrhotite or non-magnetic pyrrhotite. The results of the COVs show significant similarities between variations of pairs of MMS and pyrrhotite, Pb+Zn and galena+sphalerite. The statistical tests of this chapter suggest that pyrrhotite abundance, AMS and MMS values are significantly difference between productive and barren samples of the Western Mineralisation.

The results of quantitative core logging suggest in most cases, the commencement and termination of the signals of MMS and pyrrhotite anomalies in depth roughly is consistent with the presence of sulphide ore anomalies. However, a partial shift or complete delay between the start and termination of one anomaly of MMS against a presence of galena+sphalerite are seen in some drill cores and in some cases, there are

some depth intervals of anomalous MMS without a concurrent galena+sphalerite anomaly and vice versa.

The result of contour plot in relation to occurrence of the ore sulphide minerals suggests that the major anomalies of galena+sphalerite appear between volume percents of 3 and 15 of pyrrhotite and between 2×10^{-3} SI and 20×10^{-3} SI of MMS values.

Ultimately, the statistical results provide quantitative information about variation of pyrrhotite (vol. %) and its magnetic properties within sulphide ore minerals which has the potential to improve ore targeting. Further geophysical magnetic survey is recommended in the Western Mineralisation so as to extend the results of this chapter and down hole magnetic susceptibility measurements may be a tool for assessing a "near miss"[1] in a drill hole.

[1] **When one is drilling for a sulphide target and gets close, then there are features that suggest how close you were to it.**

CHAPTER 5

Multi-Element Relationships: The Western Mineralisation

5.1 Introduction

Unlike geophysical data, geochemical data is stochastic in nature and multivariate statistical analysis is in general used for their evaluation. Geochemical data often suffers from several shortcomings, such as the detection limit problem, constrained data range (Aitchison 1986; Le Maitre 1982), abnormal or multi-modal populations or strongly skewed distributions (pbarrett.net 2001) and the presence of outliers (Filzmoser, Reimann & Garrett 2005). Most classical statistics are based on assumptions that random variables are following Gaussian distributions (Reimann & Filzmoser 2000), independent and unconstrained in Euclidean real space. Multivariate statistical analysis can be used to develop geochemical exploration models and identify mineral paragenesis and mineral generations through:

1. The analysis of multi-element interactions,
2. The recognition of significant controlling factors,
3. The reduction of the geochemical dimensions,
4. The mass balance recognition, or
5. Statistical chemical equilibrium analysis

There are abundant publications regarding the geochemical characteristics and the origin of the Broken Hill orebody based on interpretation of thermodynamic, sulphide melting, isotopic data, element concentrations and geological observations (e.g. Frost, Mavrogenes & Tomkins 2002; Mavrogenes et al. 2004; Phillips 1980; Phillips & Wall 1981; Ryall 1979; Spry, Plimer & Teale 2008; Stevens, Prins & Rozendaal 2005; Tomkins, Pattison & Frost 2007). However, the application of multivariate statistical analyses in relation to an orebody such as that at Broken Hill is still an area seriously under-researched. In this chapter, there is a description of a variety of bivariate and multivariate statistical analyses that were applied to detect and quantify the underlying structure of geochemical variations of sulphide minerals. The methods are useful for identification of the controlling chemical factors of sulphide ore formation in the framework of a multi-influence elemental model.

The detailed statistical analyses include:

1. Categorising chemical composition of galena and sphalerite samples of the Broken Hill orebodies in order to identify the inter-relationship between the orebodies and the chemical composition of the minerals,

2. Application of the compositional (closed) data analysis to make independent the constrained geochemical data sets created from 10 element concentrations (Section 5.3.2),

3. Calculation of correlation coefficients for pairs of element concentrations,

4. Appraisal of multi-element relationships and the underlying structures, and

5. Evaluation of the biplot of the average atomic percentage of elements in the galena and sphalerite samples in order to understand mineral generation.

The statistical analysis in this study was conducted by the following software programs:

1. Minitab software for performing simple correspondence analysis,

2. SPSS software for performing principal component analysis (PCA),

3. Matlab software (The MathWorks Inc. 2006) for programming of a 3D biplot, and

4. CoDaPack3D (Thió-Henestrosa 2008) a freeware module for conducting compositional data analysis and construction of the 3D biplot.

5.2 The comparison of mineral chemistry of galena and sphalerite samples

Galena (PbS) and sphalerite (ZnS) are the major sulphide minerals of the Broken Hill orebodies. The long term effect of deformation and metamorphism has caused galena and sphalerite to show different percentages of major elements (Pb in galena, Zn in sphalerite and S in both of them) and different minor substitution of Pb in sphalerite, Zn in galena, and different traces of Fe, Ag, Sb, Bi, Cd, Cu, Zn, Mn, Co and As in samples containing both minerals. In this section, the average atomic percentages of elements in galena and sphalerite samples collected by Kitchen (2001), Sproal (2001), Tully (2002), Groombridge (2003) and Patchett (2003) are compared (Tables 5.1 and 5.2). All these samples were analysed by the CAMECA 50X electron microprobe at The University of Melbourne.

Table 5.1: Average atomic percentage of elements in galena samples of the Broken Hill orebodies.

Researcher	The number of samples	Elements / Orebody	S	Pb	Fe	Cu	Zn	As	Ag	Cd	Sb	Bi
Tully (2002)	38	A Lode	48.488	51.076	0.039	0.042	0.04	0.017	0.085	0.077	0.065	0.001
Tully (2002)	31	B Lode	48.7	50.967	0.032	0.036	0.041	0.021	0.033	0.08	0.034	0.001
Sproal (2001)	50	C Lode	49.174	50.401	0.0701	0.0267	0.1059	0.0205	0.0377	0.0591	0.0279	0.0006
Tully (2002)	48	1 Lens	48.49	51.078	0.038	0.039	0.127	0.012	0.035	0.077	0.053	0.001
Sproal (2001)	37	2 Lens	49.5466	49.9982	0.0295	0.0514	0.1314	0.0079	0.0463	0.0737	0.0784	0.0006
Groomridge (2003)	19											
Groomridge (2003)	13	3 Lens	50.0185	49.6685	0.0037	0.0450	0.0377	0.0114	0.0753	0.0645	0.0748	0.0006
Patchett (2003)	66	WestMin*	49.1263	49.6982	0.4733	0.0437	0.2129	0.1896	0.0615	0.0509	0.2156	0.0694
Kitchen (2001)	33											

*The Western Mineralisation

Table 5.2: Average atomic percentage of elements in sphalerite samples of the Broken Hill orebodies.

Researcher	The number of samples	Elements / Orebody	S	Zn	Fe	Cu	As	Ag	Cd	Sb	Pb	Bi
Tully (2002)	11	A Lode	49.714	41.555	8.383	0.013	0.025	0.028	0.155	0.003	0.003	0.028
Tully (2002)	15	B Lode	49.99	39.862	9.8	0.014	0.024	0.009	0.086	0.004	0.003	0.013
Sproal (2001)	54	C Lode	49.7008	40.3973	8.9898	0.0244	0.0282	0.0083	0.114	0.0045	0.0021	0.0169
Tully (2002)	8	1 Lens	49.824	41.231	8.304	0.081	0.035	0.014	0.39	0.002	0.003	0.047
Sproal (2001)	9	2 Lens	50.3501	41.1261	8.3224	0.0305	0.0232	0.0072	0.0989	0.0056	0.0073	0.0172
Groomridge (2003)	12											
Groomridge (2003)	12	3 Lens	50.3507	39.2434	10.260	0.0107	0.0217	0.0056	0.0884	0.0082	0.0003	0.0105
Patchett (2003)	75	WestMin	49.8832	40.8076	8.8394	0.0208	0.0171	0.0108	0.1155	0.0038	0.0116	0.022
Kitchen (2001)	31											

The results of comparison of the Western Mineralisation with the other Broken Hill orebodies are outlined below using Tables 5.1 and 5.2:

1. The average atomic percentages of Bi, As, Fe, Sb and Zn in the galena samples of the Western Mineralisation are at least 69.4, 9, 6.75, 2.75 and 1.6 times those of the Broken Hill Lodes and Lenses respectively (Table 5.1),

2. The average atomic percentage of Pb in the sphalerite samples of the Western Mineralisation is at least 1.59 times that of the Broken Hill Lodes and Lenses (Table 5.2), and

3. The average atomic percentage of As in the sphalerite samples of the Broken Hill Lodes and Lenses is at least 1.27 times that of the Western Mineralisation (Table 5.2).

5.2.1 Correspondence analysis for galena samples within the Broken Hill orebodies

The Broken Hill orebodies are categorised based on the major and minor elements of galena and sphalerite samples using simple correspondence analysis. This method was described earlier in Section 4.3.1.2. In this section similar procedures of correspondence analysis were performed on the data of Tables 5.1 and 5.2. In the data sets of Tables 5.1 and 5.2, there are significant differences between the average values of major and minor elements. This will produce significant differences between the variance of the major and minor elements that consequently will affect greatly the result of correspondence analysis. In order to solve this problem, the data sets of Tables 5.1 and 5.2 need to be standardised using a z-transformation [Equation (4.1)].

During the z-transformation of data of Table 5.1, some negative values were produced (Table 5.3) that could not be analysed by correspondence analysis, and therefore a minimum constant value of 2 was added to all the data of Table 5.3 to change them to positive values (Table 5.4). The reason for this was explained earlier in Section 4.3.1.2. The result of decomposition of the data set of Table 5.4 into six dimensions (components) is given in Table 5.5. In Table 5.4, galena samples collected from each orebody are associated with 10 element concentrations in a 10-dimensional space. The correspondence analysis decomposes the total variation of galena into a lower-dimensional space for the 10 element concentrations. This makes it easier to understand the internal relationships between the Broken Hill orebodies and the different chemical compositions of galena.

Table 5.3: The z-transformed values of Table 5.1.

Element / Orebody	S	Pb	Fe	Cu	Zn	As	Ag	Cd	Sb	Bi
A Lode	-1.03	1.04	-0.35	0.18	-0.91	-0.34	1.52	0.74	-0.21	-0.37
B Lode	-0.66	0.87	-0.39	-0.58	-0.89	-0.28	-0.98	1.02	-0.69	-0.37
C Lode	0.17	-0.02	-0.17	-1.77	0.09	-0.29	-0.75	-0.89	-0.79	-0.38
1 Lens	-1.03	1.05	-0.36	-0.19	0.42	-0.42	-0.88	0.74	-0.39	-0.37
2 Lens	0.82	-0.65	-0.41	1.39	0.49	-0.48	-0.34	0.44	0.0002	-0.38
3 Lens	1.65	-1.17	-0.56	0.57	-0.94	-0.43	1.05	-0.40	-0.05	-0.38
The Western Mineralisation	0.08	-1.12	2.25	0.40	1.74	2.26	0.39	-1.64	2.16	2.26

Table 5.4: The z-transformed values+2 of Table 5.3.

Element / Orebody	S	Pb	Fe	Cu	Zn	As	Ag	Cd	Sb	Bi
A Lode	0.96	3.04	1.64	2.18	1.08	1.65	3.52	2.74	1.79	1.63
B Lode	1.34	2.87	1.60	1.42	1.1	1.71	1.01	3.01	1.3	1.63
C Lode	2.17	1.98	1.83	0.22	2.1	1.7	1.24	1.1	1.2	1.61
1 Lens	0.96	3.046	1.64	1.8	2.42	1.58	1.11	2.74	1.6	1.63
2 Lens	2.82	1.35	1.59	3.39	2.49	1.52	1.66	2.44	2	1.61
3 Lens	3.65	0.83	1.43	2.57	1.05	1.57	3.05	1.6	1.94	1.61
The Western Mineralisation	2.08	0.88	4.25	2.4	3.74	4.26	2.39	0.35	4.16	4.27

Table 5.5: The results of decomposition of Table 5.4 into six dimensions.

Dimensions	Inertia	Proportion of inertia	Percentage of proportional inertia (PPI)	Percentage of cumulative inertia
1	0.0751	0.4693	46.93	46.93
2	0.0458	0.2864	28.64	75.57
3	0.0194	0.1210	12.10	87.68
4	0.0154	0.0961	9.61	97.28
5	0.0043	0.0267	2.67	99.95
6	0.0001	0.0005	0.05	100.00
Total	0.16			

5.2.2 Correspondence maps for galena samples

5.2.2.1 Interpretation of Figure 5.1

Figure 5.1 shows 75.57 % [1] of the total chemical variation of galena within the Broken Hill orebodies.

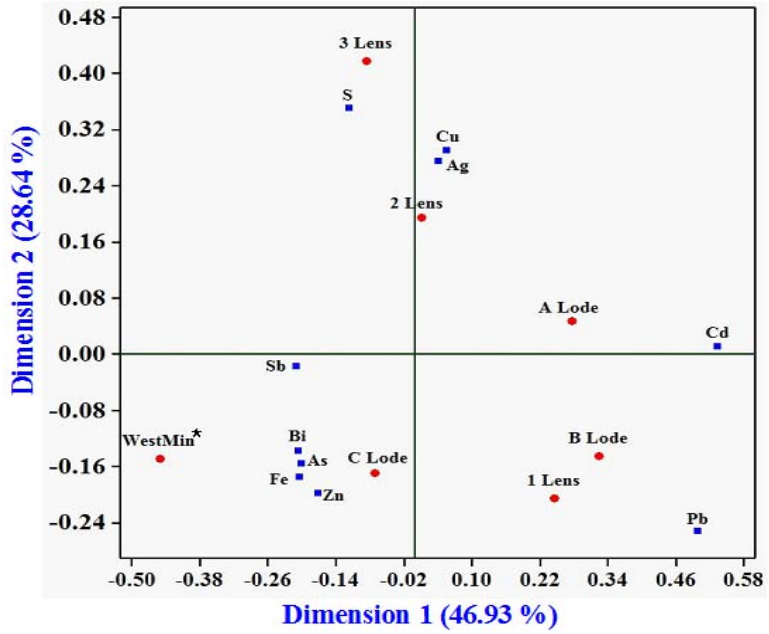

Figure 5.1: Correspondence map in relation to dimensions 1 and 2 for galena.
(*The Western Mineralisation)

1 Dimension 1

In Figure 5.1, geochemical processes that can be inferred from dimension 1 separate the map at zero value into two parts, positive and negative. Pb- and Cd-rich galena, A, B Lodes and 1 Lens lie on the positive scale of dimension 1 and the Western Mineralisation (WestMin in map), C Lode, 3Lens, Bi-, Sb-, Fe-, Zn-, As- and S-rich galena lie on the negative scale of dimension 1.

[1] **Calculated by PPI (dimension 1) + PPI (dimension 2) from Table 5.5**

2 Dimension 2

Dimension 2 separates 2, 3 Lenses (Pb Lenses) and Cu-, S- and Ag-rich galena from the Western Mineralisation, B, C Lodes, 1 Lens and Pb-, Bi-, Fe-, Zn- and As- rich galena samples.

3 Discriminator

Dimension 1 acts as a good discriminator of Cd- and Pb- rich galena from the Western Mineralisation. Dimension 2 acts as a good separator of S-, Cu-, Ag-rich galena from the Western mineralisation

5.2.2.2 Interpretation of Figure 5.2

In Figure 5.2, the correspondence map of dimensions 1 and 3 jointly accounts for 59.03%[1] of the total chemical variation of galena samples.

4 Dimension 3

Dimension 3 is a good discriminator for separating C Lode, 2 Lens, Zn- and S-rich galena from Ag-rich galena and A Lode.

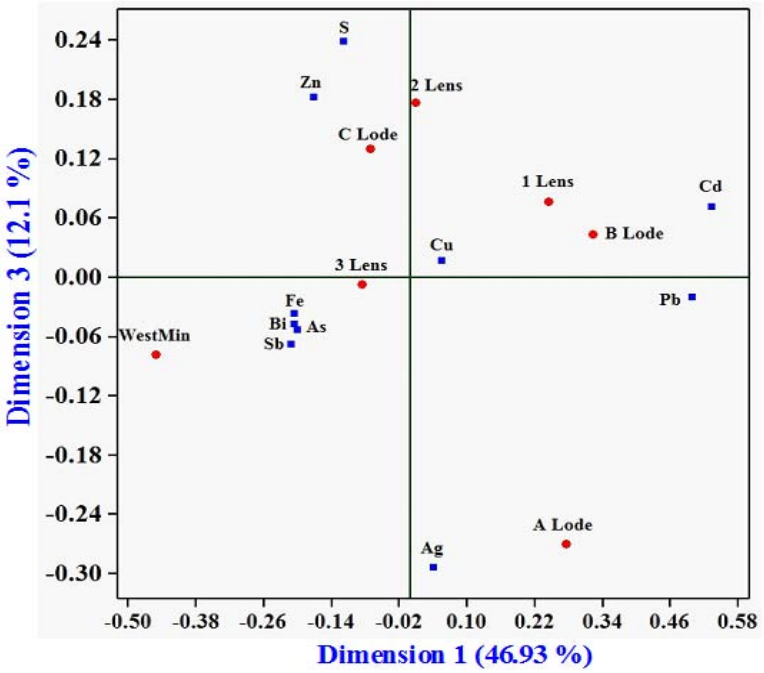

Figure 5.2: Correspondence map in relation to dimensions 1 and 3 for galena.

5.2.2.3 Interpretation of Figure 5.3

In Figure 5.3, the correspondence map of dimensions 2 and 3 accounts for 40.74% of the total chemical variation of galena.

[1] **Calculated by PPI (dimension 1) + PPI (dimension 3) from Table 5.5**

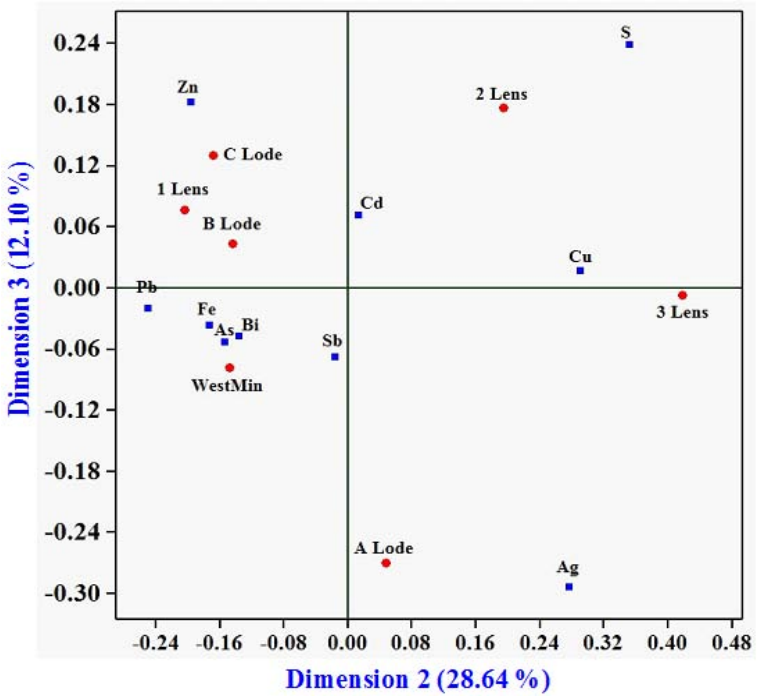

Figure 5.3: Correspondence map in relation to dimensions 2 and 3 for galena.

5.2.2.4: Interpretation of a combination of Figures 5.1 to 5.3

Together Figures 5.1 to 5.3 provide a three-dimensional[1] model that explains 87.68 %[2] of the total chemical variation of galena within the Broken Hill orebodies and their inter-relationships are outlined below:

- A Lode contains Ag-rich galena samples,
- B Lode contains Pb- and Cd-rich galena samples,
- C Lode contains Zn-rich galena samples,
- 1 Lens contains Pb-rich galena samples,
- 2 Lens contains S-rich galena samples,
- 3 Lens contains Cu-rich galena samples, and
- The Western Mineralisation contains Bi-, Fe-, As- and Sb-rich galena samples.

5.2.3: Correspondence analysis for sphalerite samples

The z-transformed values of Table 5.2 and the z-transformed values plus 2 for sphalerite are given in Tables 5.6 and Table 5.7 respectively. The result of decomposition of Table 5.7 into 6 dimensions is given in Table 5.8.

[1] **A combination of three correspondence maps in relation to dimensions 1, 2 and 3**
[2] **Calculated by PPI (dimension 1) + PPI (dimension 2) + PPI (dimension 3) from Table 5.5**

Table 5.6: The z-transformed values of Table 5.2.

Orebody \ Element	S	Pb	Fe	Cu	Zn	As	Ag	Cd	Sb	Bi
A Lode	-0.93	1.15	-0.78	-0.60	0.02	2.12	0.05	-0.72	-0.34	0.47
B Lode	0.06	-0.90	1.05	-0.56	-0.15	-0.37	-0.58	-0.22	-0.34	-0.73
C Lode	-0.98	-0.25	0.005	-0.13	0.59	-0.46	-0.33	0.02	-0.58	-0.42
1 Lens	-0.54	0.76	-0.88	2.17	1.81	0.28	2.21	-1.22	-0.34	2.008
2 Lens	1.36	0.63	-0.85	0.11	-0.30	-0.61	-0.46	0.57	0.77	-0.39
3 Lens	1.36	-1.65	1.65	-0.69	-0.56	-0.82	-0.56	1.87	-1.05	-0.93
The Western Mineralisation	-0.32	0.24	-0.18	-0.28	-1.39	-0.13	-0.31	-0.32	1.89	-0.006

Table 5.7: The z-transformed values+2 of Table 5.6.

Orebody \ Element	S	Zn	Fe	Cu	As	Ag	Cd	Sb	Pb	Bi
A Lode	1.06	3.16	1.22	1.4	2.02	4.12	2.05	1.28	1.65	2.48
B Lode	2.06	1.1	3.05	1.44	1.84	1.63	1.41	1.78	1.65	1.27
C Lode	1	1.75	2	1.86	2.59	1.53	1.67	2.02	1.42	1.58
1 Lens	1.45	2.76	1.12	4.17	3.8	2.28	4.21	0.78	1.65	4
2 Lens	3.37	2.64	1.14	2.11	1.7	1.39	1.53	2.58	2.77	1.6
3 Lens	3.37	0.35	3.65	1.3	1.43	1.18	1.43	3.87	0.95	1.07
The Western Mineralisation	1.67	2.25	1.81	1.71	0.61	1.86	1.68	1.68	3.9	2

Table 5.8: The results of decomposition of Table 5.7 into six dimensions.

Dimensions	Inertia	Proportion of inertia	PPI	Percentage of cumulative inertia
1	0.1029	0.5535	55.35	55.35
2	0.0404	0.2175	21.75	77.10
3	0.0235	0.1266	12.66	89.76
4	0.0116	0.0626	6.26	96.02
5	0.005	0.0271	2.71	98.73
6	0.0024	0.0127	1.27	100.00
Total	0.1859			

5.2.4 Correspondence maps for sphalerite samples

5.2.4.1 Interpretation of Figure 5.4

Figure 5.4 shows 77.1 % of chemical variation of sphalerite samples within the Broken Hill orebodies in relation to dimensions 1 and 2.

- **Dimension 1**

In Figure 5.4, geochemical processes that can be inferred from dimension 1 separate Fe-, Sb- and S-rich sphalerite and 3 Lens at the extreme end of the negative scale from A Lode, 1 Lens, Zn-, Ag-, Bi-, Cd-rich sphalerite at the extreme end of the positive scale.

- **Dimension 2**

Dimension 2, on the other hand, separates the Western Mineralisation and Pb-rich sphalerite samples from 1 Lens and As-rich sphalerite samples.

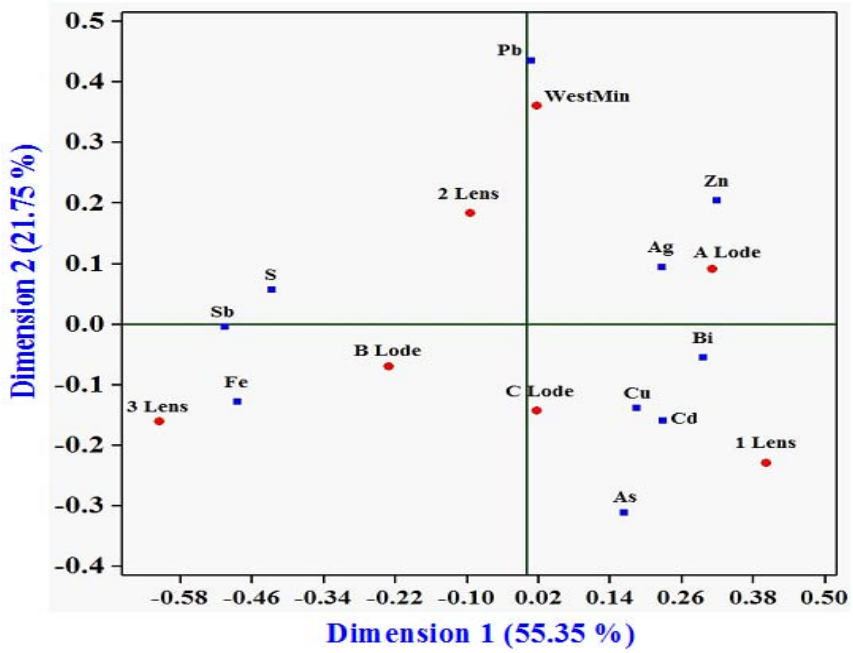

Figure 5.4: Correspondence map in relation to dimensions 1 and 2 for sphalerite.

5.2.4.2 Interpretation of Figure 5.5

In Figure 5.5, the correspondence map of dimensions 1 and 3 jointly accounts for 68 % of the total chemical variation of sphalerite samples.

- **Dimension 3**

Dimension 3 discriminates A Lode and Ag-rich sphalerite at the extreme end of the positive scale from 1 and 2 Lenses, Cu-, Pb- and S-rich sphalerite samples at the extreme end of the negative scale.

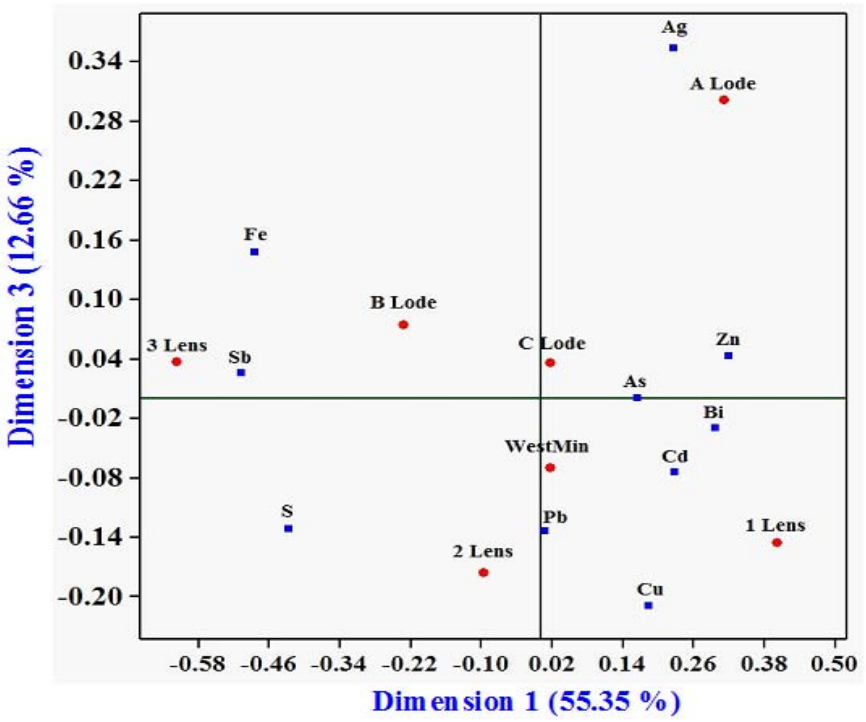

Figure 5.5: Correspondence map in relation to dimensions 1 and 3 for sphalerite.

5.2.4.3 Interpretation of Figure 5.6

In Figure 5.6, the correspondence map of dimensions 2 and 3 accounts for 34.41 % of the total chemical variation of sphalerite.

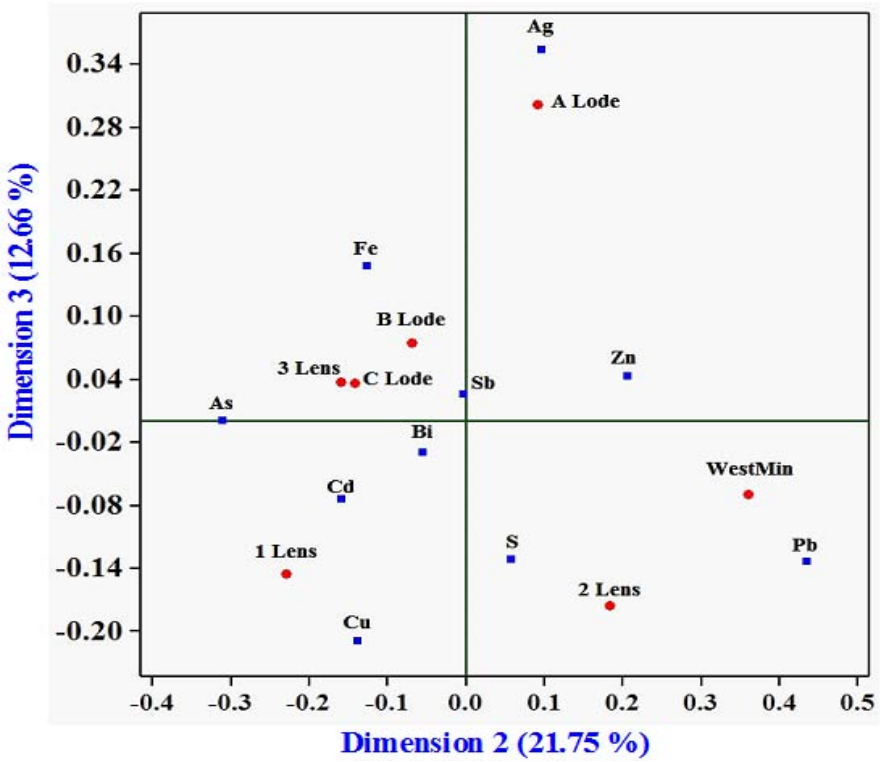

Figure 5.6: Correspondence map in relation to dimensions 2 and 3 for sphalerite.

5.2.4.4 Interpretation of a combination of Figures 5.4 to 5.6

Together Figures 5.4 to 5.6 provide a three-dimensional model that explains 89.76 %[1] of the total chemical variation of sphalerite within the orebody of the Broken Hill deposit and their inter-relationships can be summarized as follows:

- A Lode contains Ag-rich sphalerite samples,
- B Lode contains Fe- and Sb-rich sphalerite samples,
- C Lode contains As-rich sphalerite samples,
- 1 Lens contains Cd- , Bi- and Cu-rich sphalerite samples,
- 2 Lens contains Pb- and S-rich sphalerite samples,
- 3 Lens contains Sb- and Fe-rich sphalerite samples, and
- The Western Mineralisation contains Pb-rich sphalerite samples.

There is a temptation in exploration to think that the "next" Broken Hill will be identical to the main Broken Hill deposit on the Line of Lode. The result of correspondence analysis for galena and sphalerite shows that such a view is not valid. The chemical mineralogy of the Broken Hill Domain is similar to:

[1] **Calculated by PPI (dimension 1) + PPI (dimension 2) + PPI (dimension 3) from Table 5.8**

1. The Eastern Fold Belt of the Mount Isa Inlier where IOCG deposits (e.g. Ernest Henry),
2. Iron formation Cu-Au deposits (e.g. Starra line, Osborne),
3. Co-As deposits (e.g. Mount Cobalt),
4. Pb-Ag-Zn deposits (e.g. Pegmont, Cannington), and
5. Mo-Re deposits (e.g. Merlin)

Another "Broken Hill" may not even have an abundance of gahnite and garnet rocks. There may even be a Mount Isa-type Pb-Zn deposit at Broken Hill in the cover rocks. What is known about the Broken Hill Domain is that it contains the largest Zn-Pb-Ag deposit in the world, that there are thousands of minor deposits of different commodities and that the area is a major metallogenic province. This suggests that the Broken Hill Zn-Pb-Ag deposit is not an orphan.

5.3 Assay data used for multivariate statistical analysis

Some core samples (1,059) of the Western Mineralisation have equal assay data for the concentration of the following ten elements: Zn, Pb, Cu, Fe, S, Ag, Cd, As, Sb and Bi. The 1,059 samples have been cut from surface drill cores 4003 to 4032, 4040 and 4042. Some of the element concentrations including Sb, As, Bi, Cd and Ag were measured based on parts per million (ppm). Their values were converted to percentages so all assay values have the same unit, hence simplifying the analysis. The data base has been provided in supplementary file to this thesis.

5.3.1 Statistical distributions of assay values

The statistical distributions in terms of histograms of the raw data of the ten elements are displayed in Figure 5.7 and their corresponding probability plots are given in Figure 5.8. In Figure 5.7, all histograms except for Fe show strongly positive skewed distributions that indicate that the proportion of a low concentration of elements is much higher than that of a rich concentration of elements. The distribution of Bi and Sb show that they have an approximately constant concentration value. It is clear from Figures 5.7 and 5.8 that the data for the element concentrations does not follow normal distributions. They will have to be transformed to normal distributions first for effective bivariate analysis. The reason for this has been explained in Table 3.7.

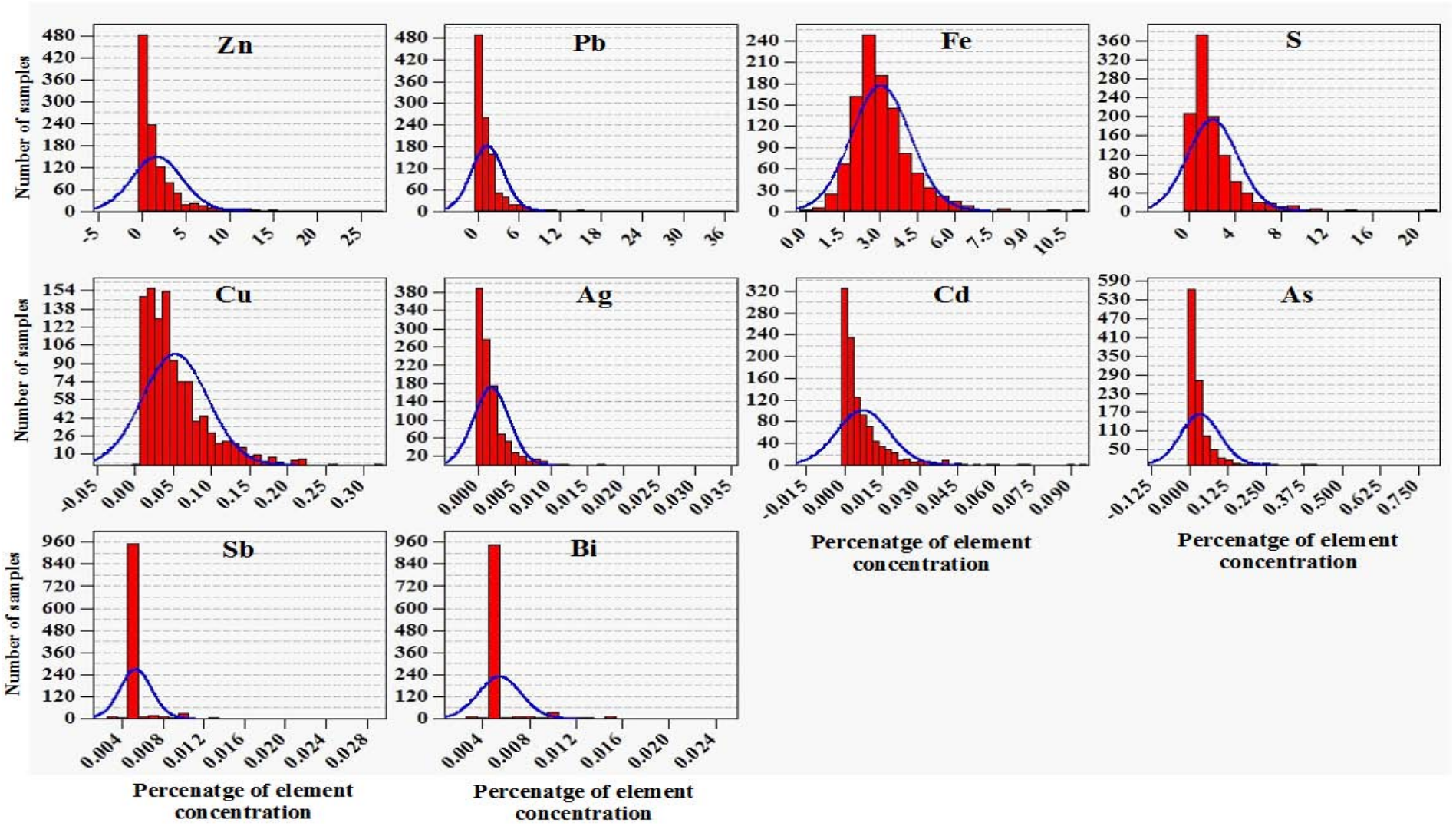

Figure 5.7: Statistical distributions for 1,059 samples of each element. The red area shows the experimental histogram for percentages of each element concentration and the blue curve shows the theoretical normal distribution model for each percentage of element concentration.

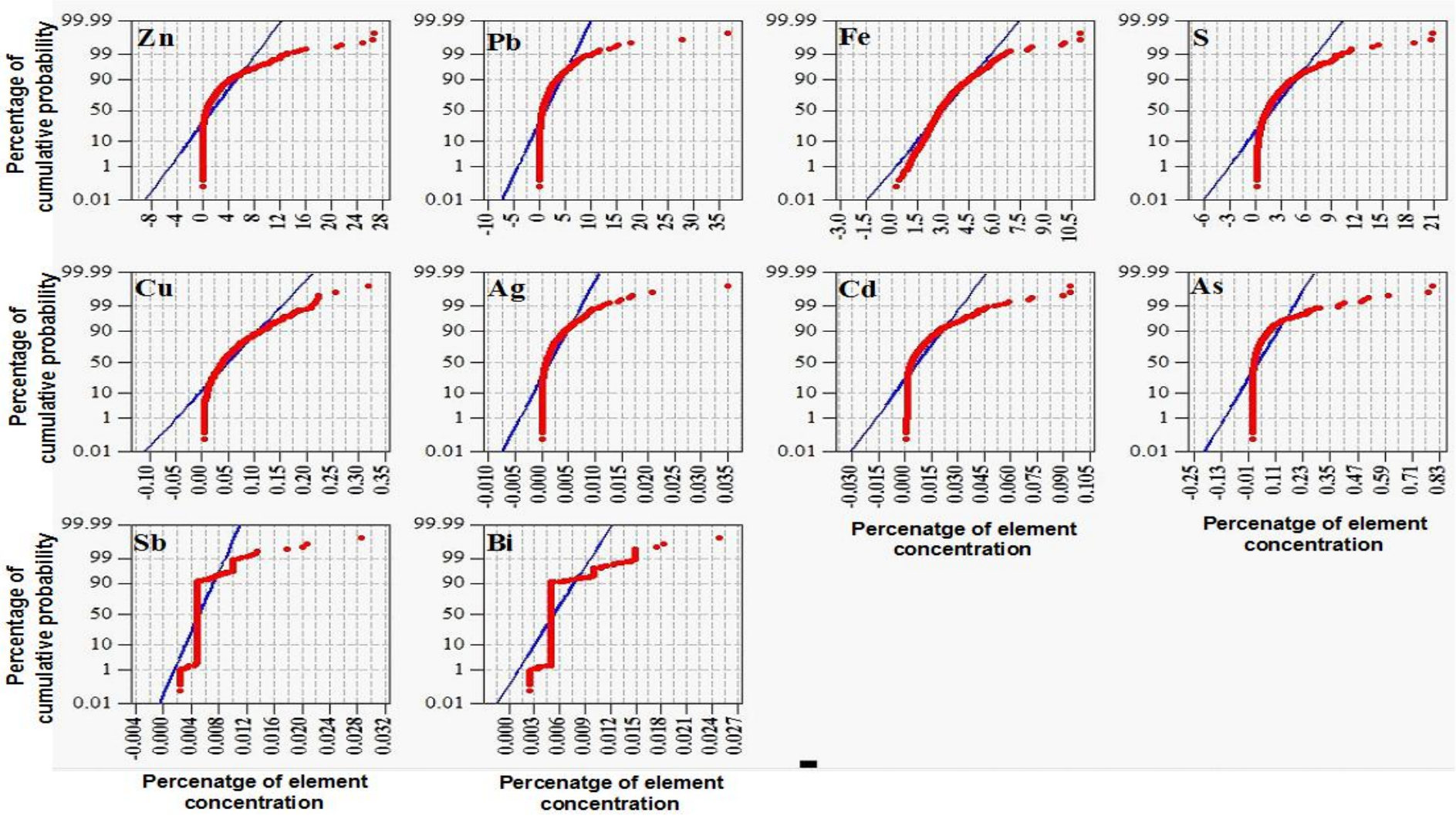

Figure 5.8: Probability graphs for 1,059 samples of each element. The red curve shows the experimental cumulative percentage of each element concentration and the straight blue line shows the theoretical percentage of cumulative probability for near-normal distribution of the elements.

5.3.2 Compositional data analysis

Compositional data is used in subjects such as geochemistry, petroleum chemistry and environmental issues (Labus 2005). Compositional data is multivariate data defined as a vector X with components of non-negative values $X_1,\ldots, X_D$ that sum up to a constant, usually 100 percent. As a consequence, elements of compositional data are not independent. For example, if one of the elements is enriched, other elements must be depleted to retain the geochemical mass balance (100%)[1]. Therefore, conventional statistics applied to raw closed geochemical data may produce incorrect outcomes.

A sample space for D-part compositional data (e.g. D=10 for current data set), S^D, is called "Simplex" (Aitchison 1986). If D=3, a ternary diagram can show clearly the different contributions of three elements for the closed data and if D=4, a tetrahedron diagram can display the different contributions of four elements for the closed data (Figure 5.9). However, there is no satisfactory way to evaluate and demonstrate the contribution of more than 4 elements in ternary and tetrahedron diagrams.

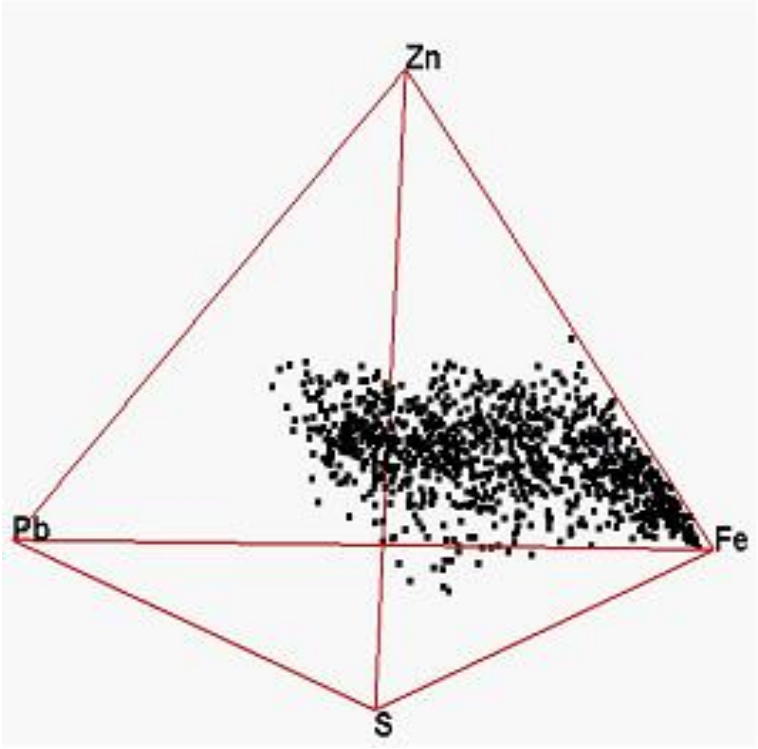

Figure 5.9: Contribution of 4 element concentrations within 1,059 samples of the Western Mineralisation in a tetrahedron model.

[1]**This problem is called closure effect (Filzmoser, Hron & Reimann 2009, p.627).**

Aitchison (1986) introduced logarithms of ratios (log-ratio) to convert compositional data into an unconstrained form in the real space R^D. The transformed data avoids the closure effect and the transformation is appropriate for elements that are measured in percentages. The following three log-ratios are used for the transformation of data into the real space (R^D):

1. Additive log-ratio (alr) transformation: value of each element (x) is divided by the value of a selected element (x_D) before taking the logarithm i.e.:

$$\mathbf{x} \in \mathbf{S^D} \rightarrow \mathbf{Y} \in \mathbf{R^{D-1}}$$

$$\mathbf{Y = alr(x)} = \left[\log \frac{x_1}{x_D}, \log \frac{x_2}{x_D}, ..., \log \frac{x_{D-1}}{x_D} \right]$$

2. Centred log-ratio (clr) transformation: value of each element (x) is divided by the geometric mean (m_g) of the data before taking the logarithm i.e.:

$$\mathbf{x} \in \mathbf{S^D} \rightarrow \mathbf{Y} \in \mathbf{R^D} \qquad \text{for } i = 1,..., D.$$

$$\mathbf{Y = clr(X)} = \left[\log \frac{x}{m_g} \right] = \left[\log \frac{x_1}{m_g}, \log \frac{x_2}{m_g}, ..., \log \frac{x_D}{m_g} \right]$$

Where m_g is the geometrical mean defined as $\mathbf{m_g} = \sqrt[D]{\Pi_{i=1}^{D} x_i}$.

3. Isometric log-ratio (ilr) transformation: the transformed vector is defined by sequential binary partition that solves the problem of data collinearity resulting from clr-transformation (Egozcue & Pawlowsky-Glahn 2005; Egozcue et al. 2003) i.e.:

$$\mathbf{x} \in \mathbf{S^D} \rightarrow \mathbf{Y} \in \mathbf{R^{D-1}} \qquad \text{for } i = 1,..., D-1$$

$$\mathbf{Y = ilr(x)} = \left[\sqrt{\frac{i}{i+1}} \log \frac{\sqrt[i]{\Pi_{j=1}^{i} x_j}}{x_{i+1}} \right]$$

5.3.3 Data preparation

The assays data of the Western Mineralisation, whose natural sample space is Simplex, were transformed into a Euclidean real space using a centred log-ratio transformation (clr) described above. The clr-transformation was selected to retain the same number of components in the transformed vector as that in the original compositional data. After the transformation, elements in the transformed data set become independent. The normality of the transformed data is checked in Figures 5.10 and 5.11. The normal data sets resulting from clr-transformation are also useful for calculation of a Pearson correlation coefficient (PCC) because it helps to detect a possible non-linear relationship between element concentrations and thus reduce the influence of possible outliers. The clr-transformed data has been provided in supplementary file to this thesis.

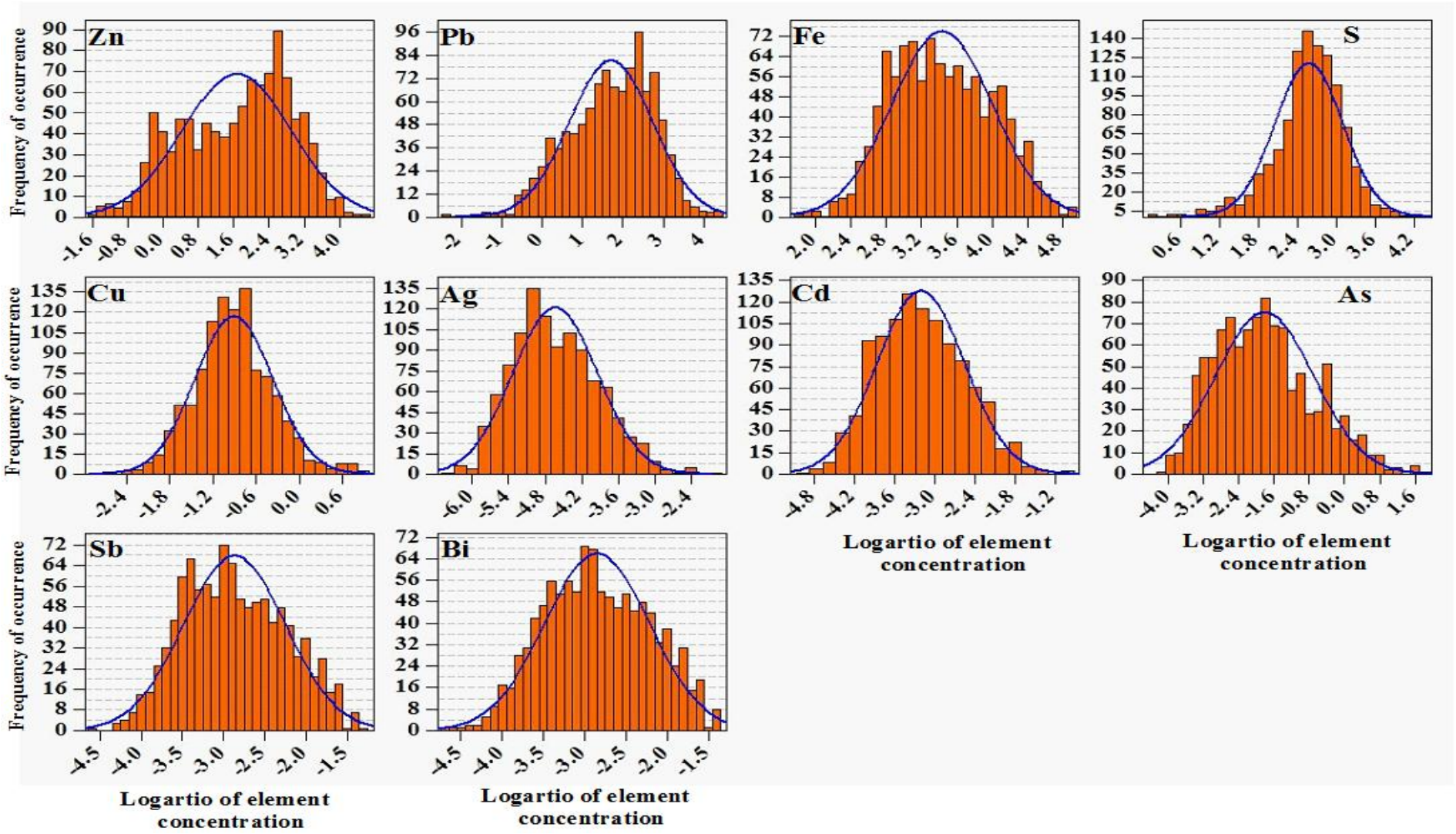

Figure 5.10: Histograms of the 1,059 clr-transformed data for each element. The red areas show the experimental histogram of the elements and the blue curves shows the theoretical normal distribution models for the elements.

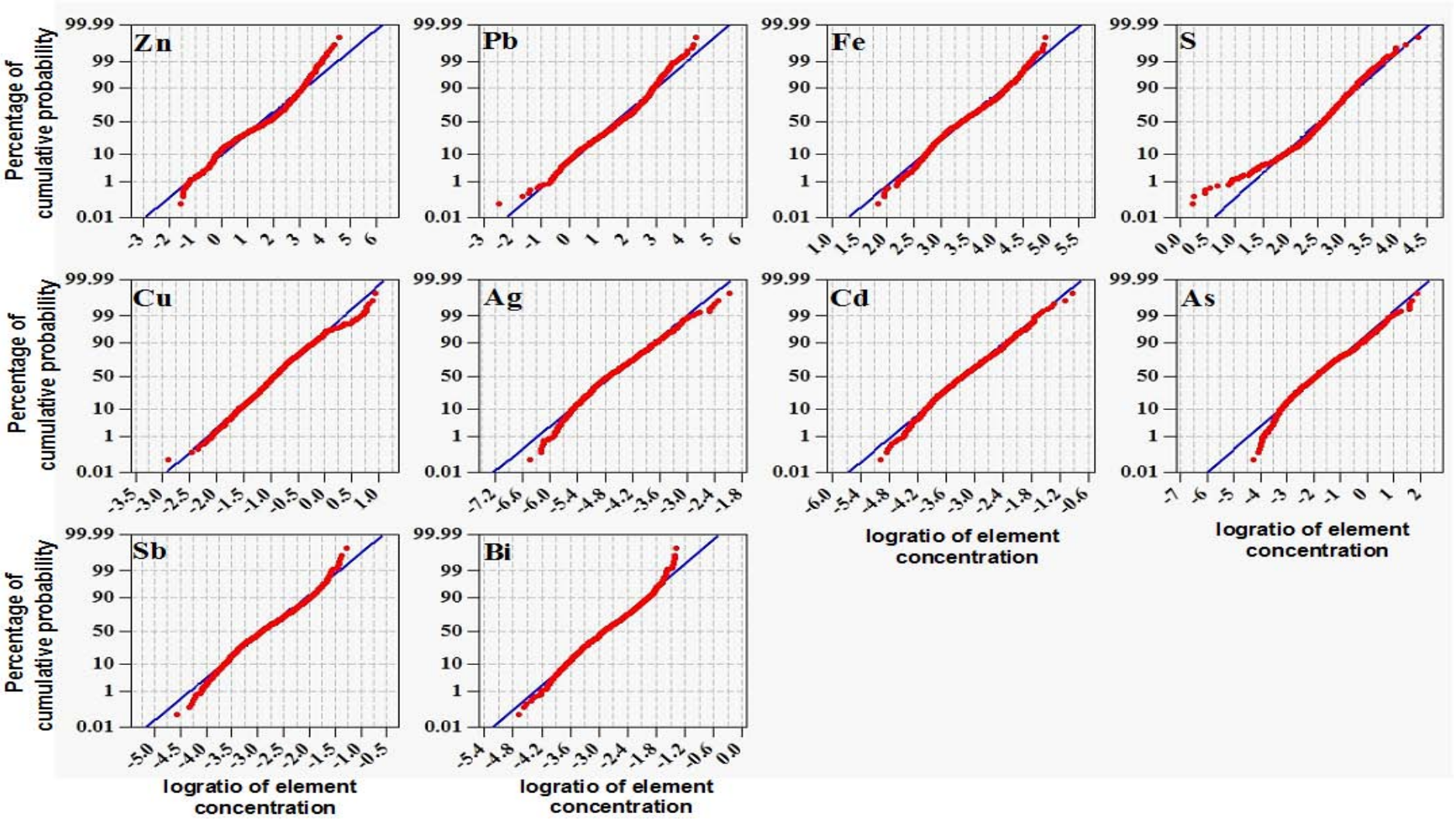

Figure 5.11: Probability graphs of the 1,059 clr-transformed data for each element. The red curves show the experimental percentage of cumulative probability for each element and the straight blue lines show the theoretical percentage of cumulative probability for near-normal distribution of the elements.

5.4 Results of bivariate analysis

The results of PCC for pair element concentrations are given in Table 5.9. Table 5.10 shows the results of $R^2 \times 100$ for elements of Fe, Cd, Ag, Sb and Bi in relation to Zn and Pb calculated from Table 5.9. The detailed description of the R-square has been given in Table 3.7.

Table 5.9: The results of PCC for the 1,059 clr-transformed data.

Elements	Zn	Pb	Cu	Fe	S	Ag	Cd	As	Sb	Bi
Zn	1	0.342**	-0.075*	-0.700**	0.607**	0.148**	0.789**	-0.477**	-0.781**	-0.776**
Sig. (2-tailed)		0.000	0.014	0.000	0.000	0.000	0.000	0.000	0.000	0.000
Pb	0.342**	1	-0.098**	-0.685**	0.258**	0.668**	0.155**	-0.386**	-0.638**	-0.643**
Sig. (2-tailed)	0.000		0.001	0.000	0.000	0.000	0.000	0.000	0.000	0.000
Cu	-0.075*	-0.098**	1	0.052	0.279**	-0.048	-0.230**	-0.140**	-0.121**	-0.103**
Sig. (2-tailed)	0.014	0.001		0.088	0.000	0.121	0.000	0.000	0.000	0.001
Fe	-0.700**	-0.685**	0.052	1	-0.371**	-0.538**	-0.446**	0.247**	0.789**	0.774**
Sig. (2-tailed)	0.000	0.000	0.088		0.000	0.000	0.000	0.000	0.000	0.000
S	0.607**	0.258**	0.279**	-0.371**	1	0.021	0.475**	-0.418**	-0.668**	-0.670**
Sig. (2-tailed)	0.000	0.000	0.000	0.000		0.488	0.000	0.000	0.000	0.000
Ag	0.148**	0.668**	-0.048	-0.538**	0.021	1	0.061*	-0.358**	-0.435**	-0.452**
Sig. (2-tailed)	0.000	0.000	0.121	0.000	0.488		0.047	0.000	0.000	0.000
Cd	0.789**	0.155**	-0.230**	-0.446**	0.475**	0.061*	1	-0.531**	-0.536**	-0.555**
Sig. (2-tailed)	0.000	0.000	0.000	0.000	0.000	0.047		0.000	0.000	0.000
As	-0.477**	-0.386**	-0.140**	0.247**	-0.418**	-0.358**	-0.531**	1	0.294**	0.314**
Sig. (2-tailed)	0.000	0.000	0.000	0.000	0.000	0.000	0.000		0.000	0.000
Sb	-0.781**	-0.638**	-0.121**	0.789**	-0.668**	-0.435**	-0.536**	0.294**	1	0.955**
Sig. (2-tailed)	0.000	0.000	0.000	0.000	0.000	0.000	0.000	0.000		0.000
Bi	-0.776**	-0.643**	-0.103**	0.774**	-0.670**	-0.452**	-0.555**	0.314**	0.955**	1
Sig. (2-tailed)	0.000	0.000	0.001	0.000	0.000	0.000	0.000	0.000	0.000	

* Correlation is significant at the 0.05 level (2-tailed).
** Correlation is significant at the 0.01 level (2-tailed).

Table 5.10: R^2 % for some elements of the Western Mineralisation.

Elements	Zn	Pb
Fe	49 %	47 %
Cd	62 %	2.4 %
Ag	14.8 %	66.8 %
Sb	60 %	40 %
Bi	60 %	41 %

The results of Table 5.9 and 510 are outlined below.

1. Positive correlations range from 0.021(between Ag and S) to 0.955 (between Sb and Bi),
2. Negative correlations change from -0.048 (between Ag and Cu) to -0.781(between Sb and Zn),
3. Elements of Bi, Sb, As, Fe and Cu are negatively correlated with Pb, Zn, S, Ag and Cd in this orebody,
4. The degree of correlation between Cu and other elements is generally very low,
5. There are strong positive correlations between Pb and Ag and between Zn and Cd,
6. Pb and Zn both have strong negative correlation with Fe, Sb and Bi,
7. Zn shows moderate positive correlation with S while Pb shows weak correlation with S, and
8. Sb and Bi have strong positive correlations with each other and also with Fe, while Sb and Bi both have strong negative correlations with S.
9. Table 5.10 shows that 60 % of the variability of the Zn concentration is negatively correlated with the variation of Sb or Bi. According to Table 5.10, Sb and Bi are negatively correlated with 40 % and 41 % of the variability of Pb respectively.

5.4.1 Interpretation of the PCC results

Silver and Cd contributed in the form of solid solution to the atomic structure of galena and sphalerite respectively in the Western Mineralisation. Low correlation coefficients of Cu with other elements indicate that enrichment or depletion of other elements did not influence the degree of variability of Cu and vice versa. It is possible Cu originated from a secondary geochemical process with a different source because the major sulphide minerals of the orebody are galena and sphalerite. The low relationship of Cu with Pb and Zn in the Western Mineralisation is similar to almost all of the Australian sedimentary exhalative Pb-Zn-Ag deposits (McArthur River, Century, Hilton, George Fisher and Cannington) that contain a Cu-content. However, the Mount Isa deposit in the north of Australia has a spatial relationship with rich Cu-bearing sulphide minerals (Large et al. 2005).

5.5 Linear multivariate regressions (LMR)

The LMR allows for prediction of the behaviour or variability of individual elements such as Pb and Zn concentrations based on other elements as predictors. Moreover, the LMR shows how well a predictor element can represent the variability of Pb or Zn concentrations. The result of the LMR shows the most economical exploration model for prediction of Pb and Zn concentrations by measuring the minimum number of predictor elements. Thus, it is important to determine whether all of the predictor elements are equally important to predict the variability of Pb or Zn and if not which of them has more priority for the predication of the Pb and Zn concentrations. The method of LMR is also used in exploration of gold (Bellehumeur & Jébrak 1993).

It is obvious that the number of predictor elements for Zn (or Pb) can increase if we have access to more than 9 element concentrations associated with the Western Mineralisation but as mentioned earlier only some of them may be considered as good predictor elements of Pb and Zn. The resulting predictor elements of Pb and Zn can be calculated by variogram analysis so as to understand whether the predictor elements are suitable as "pathfinder" or "indicator" elements (Levinson 1974, pp.54-55; Peters 1987, p.403) for tracking galena and sphalerite in the Western Mineralisation or similar Pb-Zn sulphide orebodies. More details about pathfinder elements are given in Section 7.3 where the spatial zonation of geochemical haloes is discussed for the Western Mineralisation.

In this study, a stepwise multiple regressions analysis using SPSS was carried out to evaluate the contribution of all predictor variables for a prediction model of Pb or Zn concentrations in the Western Mineralisation. In this process, the nine predictor elements of Pb, Fe, S, Cd, Ag, Sb, Bi, As and Cu for Zn and the nine predictor elements of Zn, Fe, S, Cd, Ag, Sb, Bi, As and Cu for Pb were added one by one to the regression model and their accumulative effects on Pb and Zn predictions are calculated. Correlated elements will make positive contributions to the regression model and they will be retained in the model. The assessment can be done using a desired "Adjusted R Square". The aim is to select a model with a higher Adjusted R Square and a lesser number of predictor elements. Some of the statistical terms of the LMR are briefly described below:

1. The selected predictor elements may show correlation with Pb or Zn but they need not necessarily have a strong correlation with the other predictor elements. Otherwise, a strong correlation between some of the predictor elements may

obscure the relative contributions of each predictor element to the success of the model. This can be checked using the collinearity diagnostics section of SPSS. The collinearity diagnostics measure the tolerance and Variance Inflation Factor (VIF) value. The results are presented in the prediction models of Pb and Zn. A value less than 0.01 for tolerance and more than 10 for VIF implies a strong correlation between predictor elements, meaning they have the collinearity problem, and

2. The beta value represents the intensity of influence of each predictor element on the variation of Pb and Zn. A large beta value indicates a higher impact of the predictor element on variations of Pb and Zn. The beta value is defined in units of the standard deviation. For example, a negative beta value of -0.274 of Fe for Pb (Table 5.11) indicates that a positive change of one standard deviation in Fe will result in a negative change of 0.274 standard deviations in Pb.

5.5.1 Results of LMR for Pb

A significant model with three predictor elements emerged in the third model (Table 5.11) that is characterised by $\mathbf{F_{713.787,\ 438.092} = 572.974}$ and $\mathbf{p < 0.0005}$, where 713.787 and 438.092 in F (Fisher test) are sum of the squares for regression and residual respectively. The Adjusted R Square is 0.619 and collinearity statistics are: Tolerance ($0.3 < X < 1$) and VIF < 3.

Table 5.11: Significant predictor elements of Pb in the third model of LMR analysis.

Elements	Beta	*p-value*
Fe	**-0.275**	***p < 0.0005***
Ag	**0.410**	***p = 0.0005***
Bi	**-0.245**	***p* < 0.0005**

Elements of Fe, Ag and Bi are part of the third prediction model for Pb with the Adjusted R Square of 61.9 % indicating that the variability of Fe, Ag and Bi taken together as an exploration model for Pb can predict 61.9 % of the variability (variance) of the Pb concentration in the Western Mineralisation.

5.5.2 Interpretation of LMR results for Pb

The Adjusted R Square improved when more elements were added successfully to the model. The final LMR model for Pb contains the following predictor elements in decreasing order of their significant contributions: Fe, Ag, Bi, Zn, As, Cu, Cd, Ag and Sb. Sulphur made little contribution to the prediction of Pb and therefore it was not included in the final model. In comparison with the bivariate analysis (Table 5.9), the following conclusions can be drawn based on LMR analysis of the Pb:

1. Iron and Bi concentrations have a negative impact (negative beta) on the variability of the Pb concentration. The same conclusion was also reached based on Table 5.9, and

2. Antimony concentrations did not appear in the third model as predictor elements for Pb though it was in the last model but with little contribution (small beta). On the contrary, Sb shows a strong negative correlation coefficient with Pb from the bivariate analysis (Table 5.9).

From Table 5.1, the average atomic percentage of Fe, As, Bi and Sb in galena samples of the Western Mineralisation is higher than the other Broken Hill orebodies. The result of LMR analysis suggests Fe, Ag and Bi are appropriate predictor elements for the prediction of Pb variation in the Western Mineralisation.

5.5.3 Results of LMR for Zn

For Zn concentration, the third model (Table 5.12) is characterised by $\mathbf{F_{1317.403,\ 296.121} = 572.974}$ and $\boldsymbol{p < 0.0005}$, adjusted R square of 0.816 and collinearity statistics: Tolerance ($0.5 < X < 1$) and VIF < 2.

Table 5.12: Significant predictor elements of Zn in the third model of LMR analysis.

Elements	Beta	*p-value*
Cd	**0.487**	***p < 0.0005***
Sb	**-0.578**	***p = 0.0005***
Ag	**-0.134**	***p* < 0.0005**

Elements that contribute to the quality of the prediction model for Zn are (in decreasing order of importance): Cd, Sb, Ag, Fe, As, Pb, Cu and Bi.

5.5.4 Interpretation of LMR results for Zn

A linear combination of the three elements Cd, Sb and Ag can provide a good predictor model (81.6 %) for Zn concentration in the Western Mineralisation and similar mineralisation.

1. The LMR model for Zn shows that Ag has a negative correlation (negative beta) with Zn in contrast to the correlation coefficient in Table 5.9 where it shows a weak positive correlation of Ag with Zn,

2. Bismuth has only a minor contribution to the final prediction model for Zn and consequently this model suggests that Bi is not an appropriate predictor element for tracking the variability of Zn concentration, while in Table 5.9, the Bi and Zn show a strong negative correlation, and

3. Sulphur content is not recognised as a significant predictor in the final model (9) for Zn and was thus removed from the model.

Based on these assessments, it can be concluded that LMR is more suitable for identifying the major predictor elements for tracking ore minerals and Pearson correlation coefficient should be used with care in geological interpretation.

5.6 Cluster analysis

Cluster analysis (Davis 1973; Hartigan 1975; Templ, Filzmoser & Reimann 2008) is an investigative multivariate data analysis that can be used to classify geochemical variables or samples. Cluster analysis can support the development of geochemical models

by identifying multi-element relationships or by clustering element concentrations based on the amount of their percentage of similarities. Furthermore, it reduces the number of variables that need to be considered in subsequent analysis and provides a visual description of combined variables that is easier to understand than results obtained through more traditional analysis such as PCA.

Cluster analysis needs to specify a final partitioning by selecting the number of sub-clusters (user defined) and the problem is to select an optimum number of sub-clusters for partitioning (Fraley & Raftery 1988). It is possible to group the elements into 1 to n[7] clusters, a procedure that is called "hierarchical" clustering. Hierarchical clustering provides n cluster solutions and the user should make a decision which model is the most appropriate. The principal aim of cluster analysis in the Western Mineralisation is to divide element concentrations into a number of groups to better understand the multivariate behaviour and the structures of multi-element interactions. A good cluster analysis attempts to classify the elements into groups with high levels of similarity while at the same time the differences between the individual groups are kept as large as possible.

5.6.1 Distance measures for cluster analysis

Cluster analysis uses distance measures to quantify the similarity among the element concentrations in a multivariate space based on the entered assayed samples. The "distance" in cluster analysis is not the same as a geographical distance among samples and the important issue is how best they can measure distance between the elements. Several distance measures exist in this method such as Euclidean, Manhattan, Ward, Gower (Gower 1966), Canberra (Lance & Williams 1966), the random forest proximity (Breiman 2001) and the correlation coefficient. The Euclidian is a straight-line distance in geometry that is calculated by the root of the sum of the squares and the Manhattan is the sum of linear distances.

More detail about distance measures and examples can be found in Arabie, Hubert and De Soete (1996), Gordon (1999), Mark and Roger (1984) and Swan and Sandilands (1995). However, there are no theoretical reasons to prefer one of the distances over the other. In this thesis, the correlation coefficient of the elements was used as the distance measure for quantifying the amount of similarity of 10 element concentrations.

5.6.2 Cluster algorithm

After selection of a distance measure (e.g. correlation distance) a cluster algorithm should be selected in order to determine cluster membership for each element based on their distance measures. The cluster algorithms can be "divisive" or "agglomerative". A divisive method starts with all elements in one cluster and the cluster gradually splits the

[7] **Maximum n is equal to the number of variables (i.e. elements)**

smaller groups step by step. In contrast, in the agglomerative technique, at first each element forms its own cluster and this process continues for "n" single element clusters and then the number of clusters is reduced by joining the two closest elements and continues to find another similar element for gradually joining the first two or two other elements. This procedure will proceed until one large cluster is formed.

There are several algorithms for linking two clusters, such as average linkage, complete linkage, single linkage, median linkage, centroid linkage and so on. In this study, the agglomerative average linkage distance was selected for the calculation of the cluster algorithm. The average linkage algorithm calculates the mean of all distances of two elements between the elements of two sub-clusters and then combines two sub-clusters with the minimum average distance into one new cluster.

5.6.3 Result of cluster analysis for the 1,059 clr-transformed data

Cluster analysis was calculated for the 1,059 clr-transformed data using the average linkage algorithm and correlation coefficient distance (Figure 5.12).

Figure (5.12) shows the following three main groups for 10 elements:

1. Group 1 (red colour): Zn, Pb, S, Ag and Cd,
2. Group 2 (green colour): Cu, and
3. Group 3 (blue colour): Fe, As, Sb and Bi.

It is possible to define two main groups instead of three for the cluster algorithm in Figure 5.12 and the percentage of similarity among the 10 elements does not change but Cu will be considered as part of the group 3. The horizontal line in the dendrogram (Figure 5.12) represents the similarity level between two or more elements while the vertical line indicates the distance level or differences. For example, the elements of Sb and Bi in group 3 shows the highest similarity level with 97.7 %, whereas all elements of the groups 1 and 2 reveal the lowest similarity (26.30 %) with all elements of the group 3.

Minor abundance of chalcopyrite, pyrrhotite, pyrite, gudmundite, tetrahedrite[8] and arsenopyrite in the Western Mineralisation may relate to the amount of dissimilarities of Fe, Cu, As and S in Figure 5.12.

[8] **$(Cu, Fe, Ag, Zn)_{12}Sb_4S_{13}$**

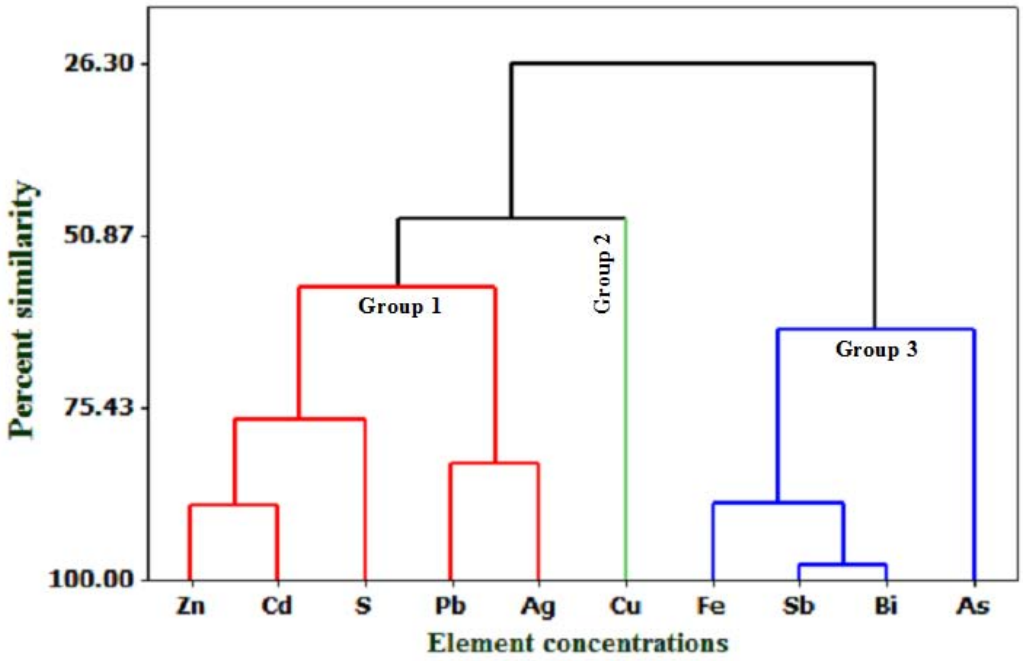

Figure 5.12: Hierarchical horizontal cluster algorithm with three main groups for 1,059 clr-transformed data of each element.

According to Figure 5.12, there are a high percentage of similarities among the following elements:

1. Zn-Cd with 89.4 %,
2. Pb-Ag with 89 %,
3. Fe-Sb-Bi with 83.4 %, and
4. S-Zn-Cd with 77 %.

Some of those similarities between the elements are seen in the sulphide minerals of the Western Mineralisation e.g. sphalerite containing Cd and galena containing Ag.

5.7 Principal Component Analysis (PCA)

PCA is a non-spatial multivariate procedure that is most commonly applied with the intention of recognising a small number of interesting sub-dimensional elements, which may then be examined by spatial approaches, exploring for spatial patterns and correlations. The aim of PCA is to reduce the complexity and dimensions of variables to a smaller number of uncorrelated principal components (Anderson 1984; Johnson & Wichern 1992; Rencher 1995). PCA helps to describe the greatest degree of variance for the lowest amount of the uncorrelated variables. In geochemical study, the goal of PCA is to facilitate the interpretation and explanation of the underlying data structure from large

assay data. Moreover, PCA investigates the degree of continuity or clustering of samples and identifies element concentrations whose significance is that they can be broken down into some distinct groups.

5.7.1 Result of PCA

The 1,059 clr-transformed data of each element of the Western Mineralisation were examined by a subprogram of the PCA and correlation matrix in SPSS 17. The correlation matrix is preferred over the covariance method if the element concentrations are measured by different scales (e.g. percentage and ppm) and need to be standardised. For solving this problem, in the subprogram of PCA, the standardisation part of the program was selected. In comparison to factor analysis, PCA deals with the total variation in the correlation matrix rather than part of it and does not require showing if the PCA is appropriate for structural detection of the data.

In Table 5.13, PC_1 explains 51.6 % of the variance of ten element concentrations and it is thus a relatively important PC, while the other PCs have less important roles in describing the variation of ten element concentrations.

Table 5.13: Summary of PCs in the Western Mineralisation.

PCs[9]	Eigenvalues	Percentage of proportional variance (PPV)	Percentage of cumulative variance (PCV)
PC_1	5.1594	51.6	51.6
PC_2	1.5696	15.7	67.3
PC_3	1.2503	12.5	79.8
PC_4	0.9561	9.6	89.4

A combination of PC_1, PC_2, PC_3 and PC_4 provides sufficient detail about major geochemical variation (89.4 %) in the Western Mineralisation, rather than studying ten geochemical elements and their behaviours individually. It should be noted that additional PCs, such as PC_5 and PC_6, if used, should increase overall variance. The increment in the variance will be case dependent but in general smaller and smaller contributions will be expected, see Figure 5.13.

[9] **Principal Components**

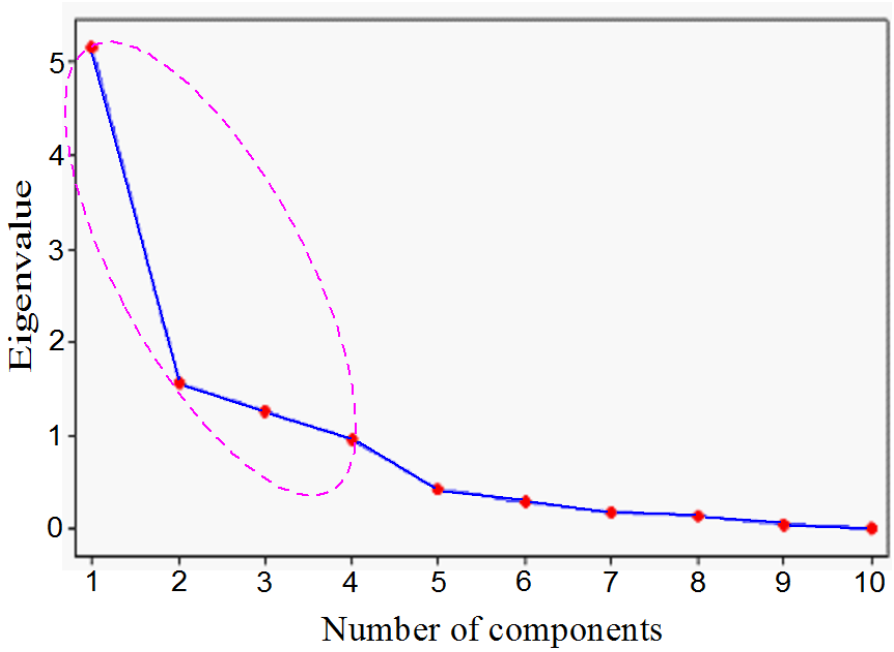

Figure 5.13: The scree plot of eigenvalues versus number of PCs.

Figure 5.13 represents the relative size of each eigenvalue in descending order versus the number of the respective PC. It shows visually which of the 10 PCs accounted for most of the variability in the Western Mineralisation. The first component shows maximum variance and the successive components make an increasingly smaller contribution to the total variance. According to the Figure, the first four eigenvalues explain the major geochemical variations of the Western Mineralisation. It should be noted that the remaining accumulated 11.6 % variances cannot be explained by the results of the first four PCs and the remaining six PCs fulfil only a small portion of the accumulated 11.6 % variances. Hence, each of them contributes only minimally to the variation of the element concentrations and cannot be interpreted meaningfully. Those PCs constitute random variations or an unsystematic chemical process within the sulphide orebody of the Western Mineralisation.

Spry, Plimer and Teal (2008) suggested that the Western Mineralisation is a stratabound deposit formed by the replacement of sediments at the top of an upward-coarsening sequence beneath an aquifer cap (Unit 4.6). If this were the case, sulphide bearing ore must have pulsated numerous times between the deposition of C Lode and A Lode and they can be interpreted as geochemical variations evident from the PCs of this study (Table 5.13). The Western Mineralisation has also a variation in grade and zonation and Plimer (2006b) argued that the intersection of F3 and F4 structures created dilation

during the Olarian Orogeny. Plimer (2006b) also suggested that more ductile minerals such as galena and pyrrhotite might have flowed into these dilation zones. The geochemical variations evident from the PCs of this study can also be attributed to the dilation zones.

5.7.2 The amount of PC loadings

In Table 5.14, the PC loadings denote the degree of correlation between individual element concentrations and the PCs (i.e. PC_1, PC_2, PC_3 and PC_4). Thus, elements with higher PC loadings in each PC play more roles in geochemical variation of the PC and have more potential for mineralisation. For example, in Table 5.14, Zn has maximum positive PC loading in PC_1 (0.857) in comparison with the weights of other elements in PC_1 and even the weights of Zn in PC_2, PC_3 and PC_4.

Table 5.14: PC loadings[10] of 10 elements for each PC (Table 5.13) of the Western Mineralisation.

PCs loading / Elements	PC_1 loading	PC_2 loading	PC_3 loading	PC_4 loading
Zn	**0.857**	**0.346**	**- 0.224**	**- 0.063**
Pb	**0.697**	**- 0.584**	**0.056**	**0.071**
Cu	**0.029**	**0.221**	**0.929**	**0.057**
Fe	**- 0.842**	**0.271**	**0.073**	**0.228**
S	**0.681**	**0.479**	**0.302**	**- 0.051**
Ag	**0.511**	**- 0.724**	**0.083**	**0.266**
Cd	**0.677**	**0.460**	**- 0.449**	**0.180**
As	**- 0.549**	**- 0.147**	**- 0.055**	**- 0.810**
Sb	**- 0.932**	**0.008**	**- 0.122**	**0.269**
Bi	**- 0.936**	**0.010**	**- 0.106**	**0.238**

This indicates a strong correlation of Zn with geochemical variation of PC_1. Therefore, major sulphide mineralisation containing Zn (sphalerite) should occur during geochemical variation evident from PC_1 in the Western Mineralisation.

In regards to the sulphide mineralogy of the Western Mineralisation, the elements with absolute PC loading values ≥ 0.4 in Table 5.14 are considered to have potential for mineralisation or are considered to have a significant influence on the geochemical variation of the PCs. According to the absolute PC loading values ≥ 0.4, the following elements have major chemical contributions to each PC:

[10] **Weights of elements in each PC**

1. PC_1: Bi, Sb, Zn, Fe, Pb, S, Cd, As and Ag,
2. PC_2: Ag, Pb, S and Cd,
3. PC_3: Cu and Cd, and
4. PC_4: As.

5.7.3 The sign of PC loadings of the elements

Interpretation of the PC loadings of the elements in Table 5.14 based on their signs (i.e. negative or positive) depends on dominant sulphide minerals in the Western Mineralisation. For example, the positive PC_1 loadings of Zn and Pb in PC_1 (with 51.6 % contribution in the sulphide mineralisation; Table 5.13) should be interpreted as sulphide mineralisation that is consistent with the dominant sulphide mineralogy (galena and sphalerite) of the Western Mineralisation.

- **Elements with the positive PC_1 loadings**

In Table 5.14, the positive loadings of Zn, Pb, Cu, Ag, Cd and S indicate the following possibilities:

1. These elements initially may tend to incorporated as a major constituent of the mineral compositions of the Western Mineralisation (e.g. Pb in galena or Zn in sphalerite),

2. These elements may be as mineral inclusions containing the elements inside other major minerals (e.g. chalcopyrite in galena), or

3. These elements are incorporated into the atomic lattice of other minerals (solid solution) as trace elements. This is most likely when the amount of an element concentration is naturally very low to form an independent mineral. For example, the average concentration of Cd is very low against the average concentrations of Zn and Pb in the Western Mineralisation (Table 3.2).

The negative PC loadings of those elements are interpreted as dilution effects or depletion or removal of those elements from sulphide bearing fluids during geochemical variation evident from the PC.

- **Elements with the negative PC_1 loadings**

In PC_1 of Table 5.14, the semi-metallic elements of As, Bi and Sb and metallic element of Fe have negative PC loadings indicating that these elements tend to be incorporated in the atomic structure of other minerals (solid solution). In contrast, positive weight values of the elements indicate that those elements trend to form independent sulphide minerals (e.g. pyrite) and sulfosalt minerals (e.g. tetrahedrite) during geochemical variations evident from the PCs.

5.7.4 Interpretation of PCs

- **PC_1**

In Table 5.14, PC_1 separates the elements of Zn, Pb, S, Ag and Cd with positive PC_1 loadings from the elements of Fe, As, Sb and Bi with negative PC_1 loadings. According to Table 5.13, major sphalerite and galena of the Western Mineralisation occurred during the processes that can be inferred from the PC_1 loadings of the elements.

- **PC_2**

In Table 5.14, PC_2 separates the elements of Zn, Cu, Fe, S and Cd with positive PC_2 loadings from the elements of Pb, Ag and As with negative PC_2 loadings. PC_2 has week positive correlations with Fe and Cu and moderate positive correlation with S, Pb and Zn.

- **PC_3**

PC_3 is characterised by highly distinct contrasts between Cu and Cd. Cu has the significant positive loading (0.929 in Table 5.14) in PC_3 that means a strong correlation with the geochemical variation evident from PC_3.

- **PC_4**

In Table 5.14, PC_4 was affected dominantly by As content because As is the only element with a highly negative PC_4 loading that has a strong correlation with PC_4. In contrast, the PC_4 loading of S is very low which suggests S content was not effective in the sulphide mineral formation during the geochemical variation evident from PC_4. This suggests that the lack of S content should have been replaced by excess As.

5.7.5 Interpretation of elements within PCs

- **Zn**

Maximum positive PC_1 loading is associated with Zn and this element also has a positive PC_2 loading in contrast with a negative PC_2 loading of Pb (Table 5.14). This is consistent with a higher abundance of sphalerite relative to galena in the Western Mineralisation.

- **Pb**

Major Pb-rich sulphide minerals (such as galena) had to be produced during the geochemical variation evident from PC_1. Pb shows smaller PC_1 loading (0.697 in Table 5.14) relative to that of Zn (0.857 in Table 5.14) that means smaller potential for mineralisation relative to Zn. PC_2 loading of Pb is a negative value (-0.584 in Table 5.14) that means the removal of Pb from sulphide mineralisation. According to Table 5.14, PC_3 and PC_4 loadings of Pb are so small that this indicates no linear relationship with geochemical variations evident from PC_3 and PC_4. Therefore, major galena should be produced during the processes that can be inferred from the loading of PC_1, but the amount of galena is smaller than sphalerite in the Western Mineralisation.

- **S**

Table 5.14 shows that the PC loading of S is reduced when comparing PC_1 to PC_3. This indicates the reduction of potential for sulphide mineralisation from PC_1 to PC_3 and there is no linear correlation between S content and the geochemical variation of other elements in PC_4.

- **Cu**

Copper has a minimum PC_1 loading (0.029 in Table 5.14) that suggests Cu concentration is not correlated with PC_1. Accordingly, there is a lack of incorporation of Cu during the formation of major galena and sphalerite minerals in the Western Mineralisation. This result is consistent with the mineralogy of the Western Mineralisation and Cu occurred there in the following form of minerals:

1. Chalcopyrite as major Cu-bearing sulphide mineral,

2. Incorporation of Cu in the atomic structure (solid solution) of sulphide minerals (e.g. gudmundite, galena, sphalerite and pyrrhotite) and sulfosalt minerals (e.g. tetrahedrite, tennantite and bournonite), and

3. Appearance in form of inclusion in other sulphide minerals. Spry, Plimer & Teale (2008, p.234) explained the presence of lamellar twins and inclusions of chalcopyrite along the cleavage and twinplanes of galena samples within the Broken Hill orebodies and they claimed that the inclusions of chalcopyrite have been generated from post-peak modification to mineral assemblage involving galena and sphalerite.

- **Fe**

Iron has a high negative PC_1 loading (-0.842 in Table 5.14) which indicates a strong negative correlation of Fe with the geochemical variation of PC_1. Iron in PC_1 has strongly concentrated in the atomic structure of major and minor sulphide minerals. This result of PC_1 is very consistent with the result of a high average atomic percentage of Fe within the atomic structures of major sulphide minerals of the Western Mineralisation (see the results of Fe concentration in Tables 5.1 and 3.2).

- **Cd and Ag**

In Table 5.14, the PC_1 loadings of Cd and Ag, being 0.677 and 0.511 respectively, show a good positive correlation with PC_1 that suggests the occurrence of minerals containing Cd and Ag resulting from geochemical variation of PC_1. Cadmium also shows a moderate positive correlation with geochemical variation of elements in PC_2. In contrast, Ag reveals a strong negative correlation with PC_2. This indicates a removal of Ag concentration during the geochemical variation evident from PC_2. In the Western Mineralisation, Cd and Ag contributed mostly to the atomic structure of sphalerite and galena respectively rather than forming major independent minerals. This may be because of the low amount of Cd and Ag (Table 3.2).

- **Bi and Sb**

In Table 5.14, Bi and Sb show strong negative correlations with PC_1 and they are incorporated significantly in the atomic lattice of galena (Table 5.1) and other sulphide minerals of the Western Mineralisation.

- **As**

Arsenic also has a moderate negative PC_1 loading and high negative PC_4 loading (Table 5.14). This indicates that during the processes associated with PC_1 and PC_4, arsenic may be highly concentrated in the atomic structure of sulphide minerals (e.g. galena; Table 5.1). Plimer (2006b) stated that it is possible that As, Mo, W and Au were added to sulphide rocks during the Olarian Orogeny.

5.7.6 Maps of PC loadings

A map of PC loadings visualises distances between elements (points) in ratios to the two dimensional space of two specific PCs. The maps of PC loadings help us to understand the following issues:

1. Identification of the relative real distances of elements in different dimensional spaces,
2. Evaluation of the probability of occurrence of mineral paragenesis, and
3. Identification of the potential mineralisation during the geochemical interaction of the two PCs.

- **Similarity of the map of PC loadings to correspondence maps**

They both aim to reduce dimensional spaces and chemical complexity. This helps to better interpret the multi-influences of elements.

- **Differences between the map of PC loadings and correspondence maps**

The map of PC loadings is used to show the relationship of one type of variable (e.g. elements) within two PC spaces at one time; however, a correspondence map is used to show the relationships between two different types of variable (e.g. the Broken Hill orebodies with the elements of a mineral) simultaneously within two dimensional spaces.

Important factors for interpretation of the maps of PC loadings are**:**

1. The total variance of each map that indicates the degree of total mineralisation during the effect of geochemical interaction between two PCs,
2. The magnitude value of PC loading for each element that indicates the degree of potential for mineral formation of the element within the map in comparison with the other elements, and
3. Distances of elements (points) from each pair of PCs in each map that reveal the possible mineral paragenesis or occurrence of different minerals during the geochemical interactions of the two PCs.

5.7.6.1 Map of PC_1 loading and PC_2 loading (Figure 5.14)

- **Chemical variation**

PC_1 loading and PC_2 loading jointly account for 67.3 %[11] of the total geochemical variation in the Western Mineralisation.

- **Position of important elements relative to PC_1 loading scale**

By dividing this map into two parts from the zero value of the PC_1 loading scale, the group of elements Fe, Bi, Sb and As lies at the extreme end of the negative scale of the PC_1 loading and the group of elements Pb, Zn, Cd, S and Ag lies at the extreme end of the positive scale of the PC_1 loading. In this map, there is an intense polarization or divergence between the two groups of elements on the negative and positive sides of the PC_1 loading scale. This is because of the relatively high distances between the two groups of elements.

- **PC_1 loading as a chemical discriminator**

In Figure 5.14, it is obvious that PC_1 loading acts as a good geochemical discriminator between the elements Zn-Pb-Ag-Cd-S and Bi-Sb-Fe-As in the Western Mineralisation.

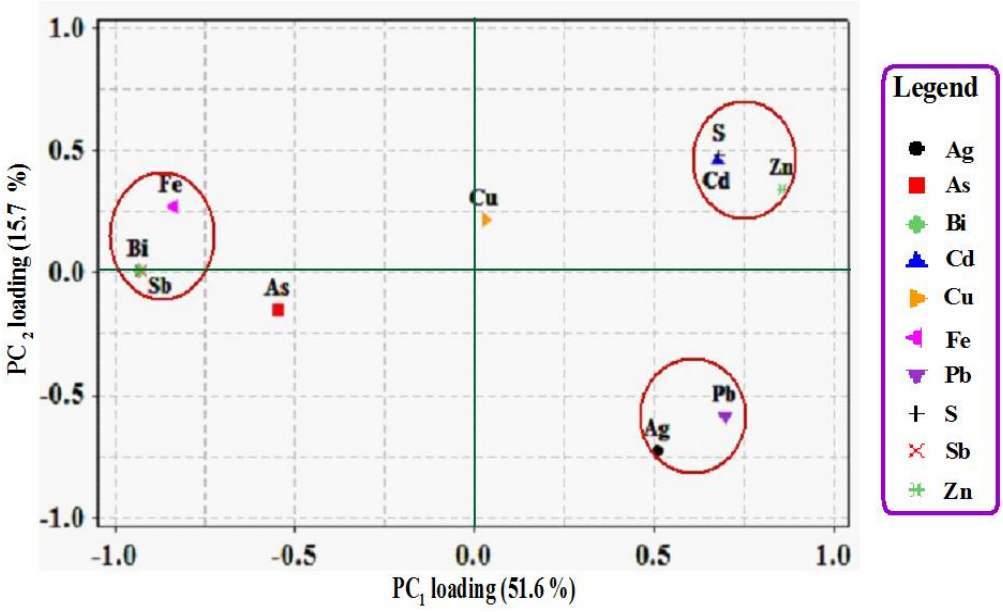

Figure 5.14: Map of PC_1 loading, PC_2 loading and the legend of 10 elements.

[11] **Calculated by PPV (PC_1) + PPV (PC_2) from Table 5.13**

- **Position of important elements in relation to PC_2 loading scale**

If Figure 5.14 is divided into two parts from the zero value of the PC_2 loading scale, it shows distinct polarization between the group elements of Pb-Ag at the extreme end of the negative scale of the PC_2 loading and the group elements of S-Zn-Cd at the extreme end of the positive scale of the PC_2 loading. This result is very consistent with the chemical composition of the sphalerite and galena samples collected from the Western Mineralisation because the sphalerite samples (Table 5.2) contain a higher average atomic percentage of Cd and S relative to the galena samples (Table 5.1). In contrast, the galena samples (Table 5.1) contain more Ag relative to the sphalerite samples (Table 5.2).

The occurrence of arsenopyrite and löllingite[12] can be associated with the geochemical interaction between PC_2 loading and PC_1 loading. However, the abundance of these minerals is very low in the Western Mineralisation because PC_2 has only 15.7 % contribution to sulphide mineralisation of the orebody.

5.7.6.2 Map of PC_1 loading and PC_3 loading (Figure 5.15)

- **Chemical variation**

PC_1 loading and PC_3 loading account for 64.1 %[13] of the total geochemical variation.

- **Position of important elements in relation to PC_3 loading scale**

PC_3 loading is characterised by significant loading of Cu, which is positioned at the upper end of the positive scale of the PC_3 loading and to a lesser extent Cd at the lower end of negative scale of the PC_3 loading.

Figure 5.15 also shows that the geochemical interaction between PC_3 loading and PC_1 loading can produce arsenopyrite and löllingite. However, PC_3 has only 12.5 % contribution to sulphide mineralisation of the orebody.

[12] **$FeAs_2$**
[13] **Calculated by PPV (PC_1) + PPV (PC_3) from Table 5.13**

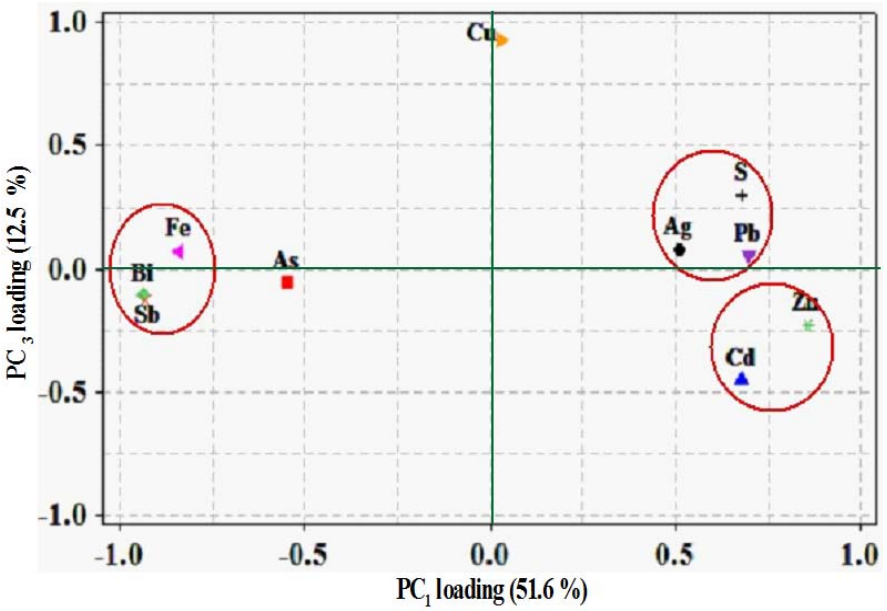

Figure 5.15: Map of PC_1 loading and PC_3 loading.

5.7.6.3 Map of PC_1 loading and PC_4 loading (Figure 5.16)

- **Chemical variation**

PC_1 loading and PC_4 loading account for 61.2 %[14] of the total geochemical variation of the Western Mineralisation.

- **PC_4 loading as a chemical discriminator**

PC_4 loading clearly separates As (at the extreme end of negative scale of the PC_4 loading) from the rest of the elements.

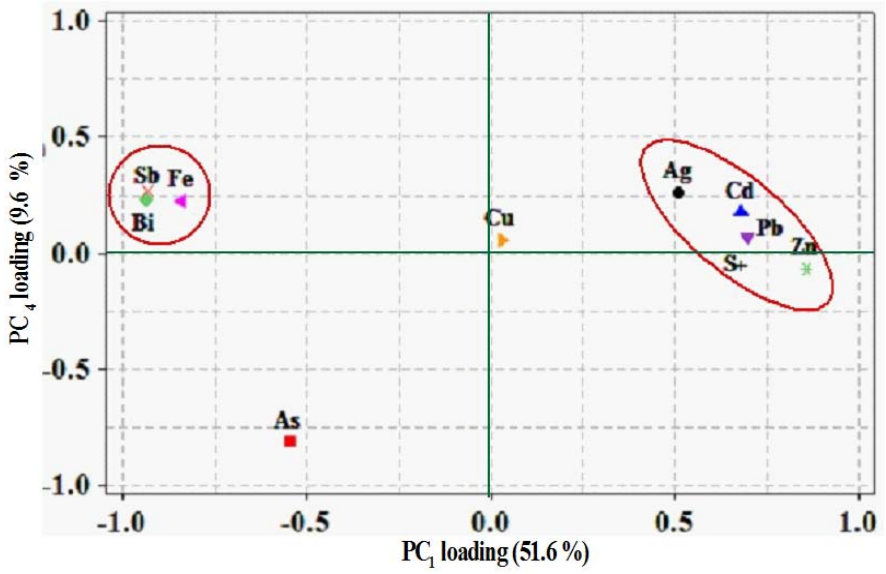

Figure 5.16: Map of PC_1 loading and PC_4 loading.

[14] **Calculated by PPV (PC_1) + PPV (PC_4) from Table 5.13**

5.7.6.4 Map of PC_2 loading and PC_3 loading (Figure 5.17)

- **Chemical variation**

PC_2 loading and PC_3 loading only account for 28.2 %[15] of the total geochemical variation of the Western Mineralisation.

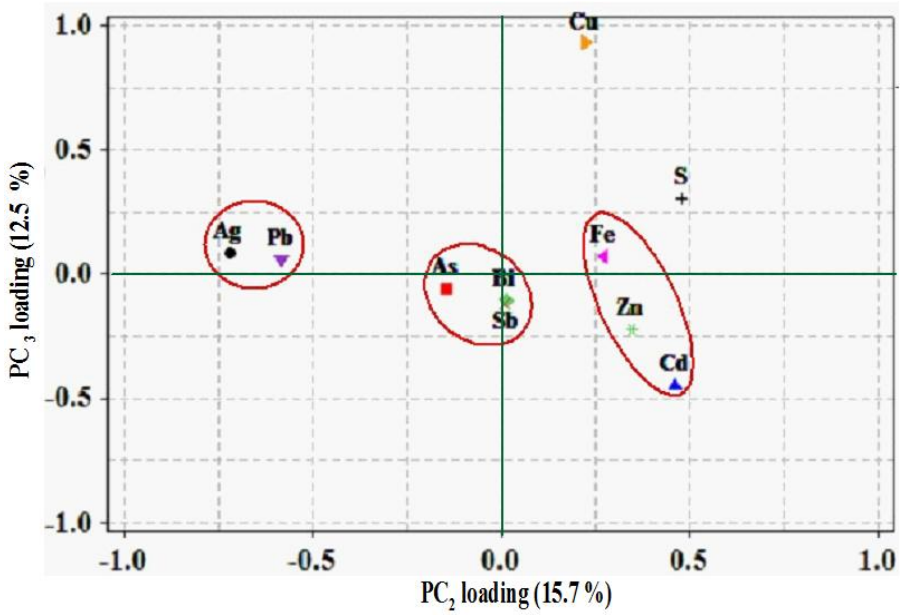

Figure 5.17: Map of PC_2 loading and PC_3 loading.

- **PC_2 loading as a chemical discriminator**

Based on this map, PC_2 loading again separates the elements of Pb and Ag from the elements of Zn, S and Cd. PC_3 loading appears to act as a discriminator of Cu from other elements.

5.7.6.5 Map of PC_2 loading and PC_4 loading (Figure 5.18)

- **Position of important elements in relation to PC_2 scale**

As shown in Figure 5.14 and 5.17, PC_2 loading in Figure 5.18 also shows the positive loading of Zn as opposed to the negative loading of Pb in relation to the PC_2 loading scale. This model highlights more enrichment of sphalerite relative to galena that is very consistent with the Western Mineralisation.

[15] **Calculated by PPV (PC_2) + PPV (PC_3) from Table 5.13**

- **Paragenesis**

In Figure 5.18, the distance between Cu and the group elements of Fe, S, Sb, Zn, Cd and Bi is small. This indicates that, during the geochemical interaction of PC_2 loading with PC_4 loading, there was potential for occurrence of chalcopyrite, tetrahedrite and gudmundite. However, they are minor minerals in the Western Mineralisation and this conclusion is consistent with the present interpretation of this map. This is because the map shows the elements have contributed only 25.3 % of the total chemical variation of the Western Mineralisation and also that the elements show very weak loadings in this map (i.e. low potential for occurrence of minerals with those elements).

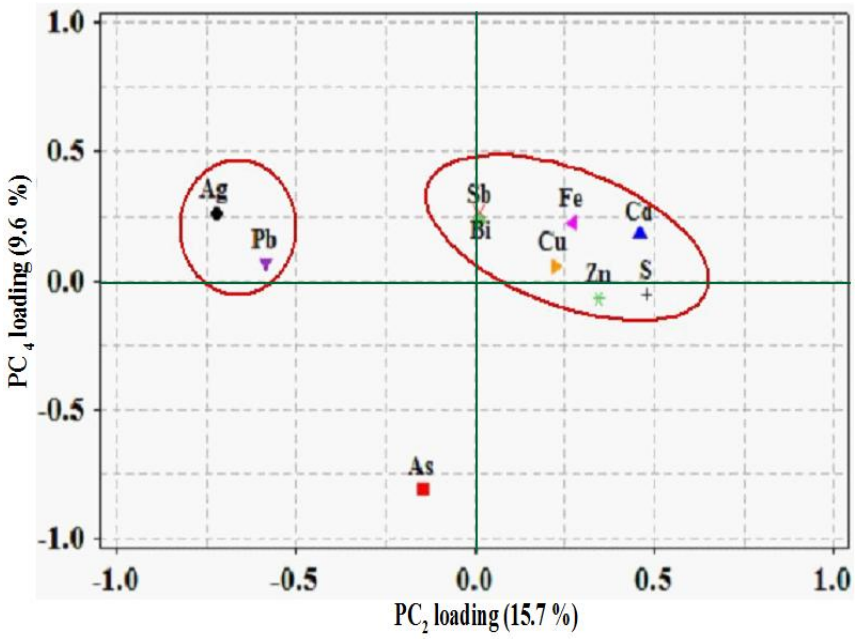

Figure 5.18: Map of PC_2 loading and PC_4 loading.

5.7.6.6 Map of PC_3 loading and PC_4 loading (Figure 5.19)

- **Chemical variation**

PC_3 loading and PC_4 loading account for 22.1%[16] of the total geochemical variation of the Western Mineralisation.

- **PC_4 loading and PC_3 loading as chemical discriminators**

In this map, PC_4 loading separates As from other elements and PC_3 loading appears to be a discriminator of Cu from other elements.

[16] **Calculated by PPV (PC_3) + PPV (PC_4) from Table 5.13**

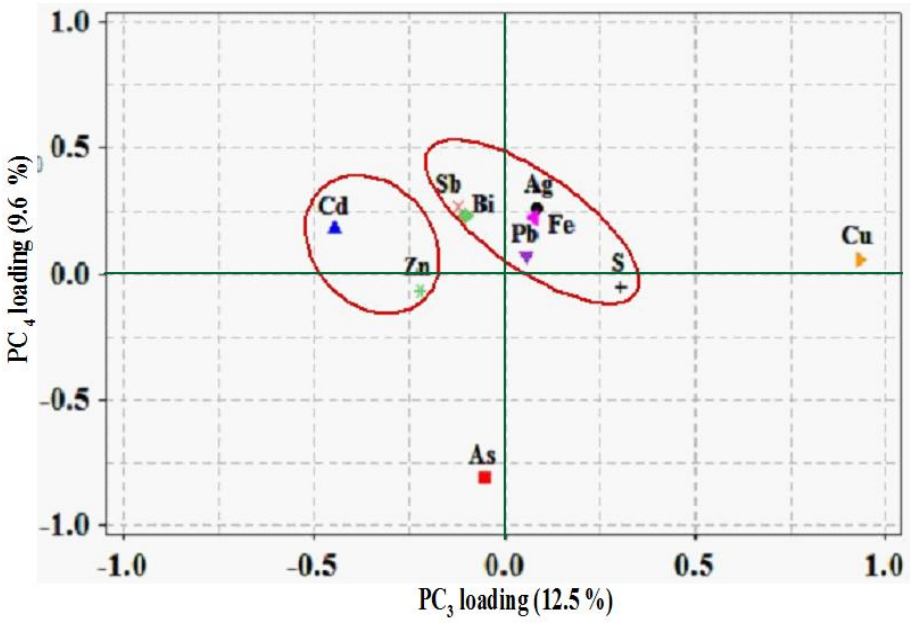

Figure 5.19: Map of PC_3 loading and PC_4 loading.

5.7.7 Map of PC scores

A map of PC scores visualises the distribution of samples (observations) in ratios of two dimensional spaces of specific PCs. The projections of samples in different maps that resulted from two different PCs, constitute the possibility for evaluating the probability distribution of samples based on the geochemical interaction of the two PCs (Figure 5.20). The k^{th} PC score of a sample is calculated by Equation (5.1):

$$\textbf{PC score}_{ik} = \sum_{j=1}^{10} (\textbf{PC loading}_{jk} \times \textbf{Element concentration}_{j}) \qquad \textbf{(5.1)}$$

In Equation (5.1), the PC score is calculated for the i^{th} sample (i =1 to 1,059 in this data set) and the k^{th} PC (k =1 to 4), and j (j = 1 to 10) is the PC loading and element concentration respectively listed in Table 5.14. For example, the PC score for PC_1 is calculated as:

PC score $_{i\,1}$ = 0.857 × Zn + 0.697 × Pb + 0.029 × Cu - 0.842 × Fe + 0.681 × S + 0.511 × Ag + 0.677 × Cd - 0.549 × As - 0.932 × Sb - 0.936×Bi

Where Zn, Pb, Cu, Fe, S, Ag, Cd, As, Sb and Bi are the clr-transformed element concentrations for sample i.

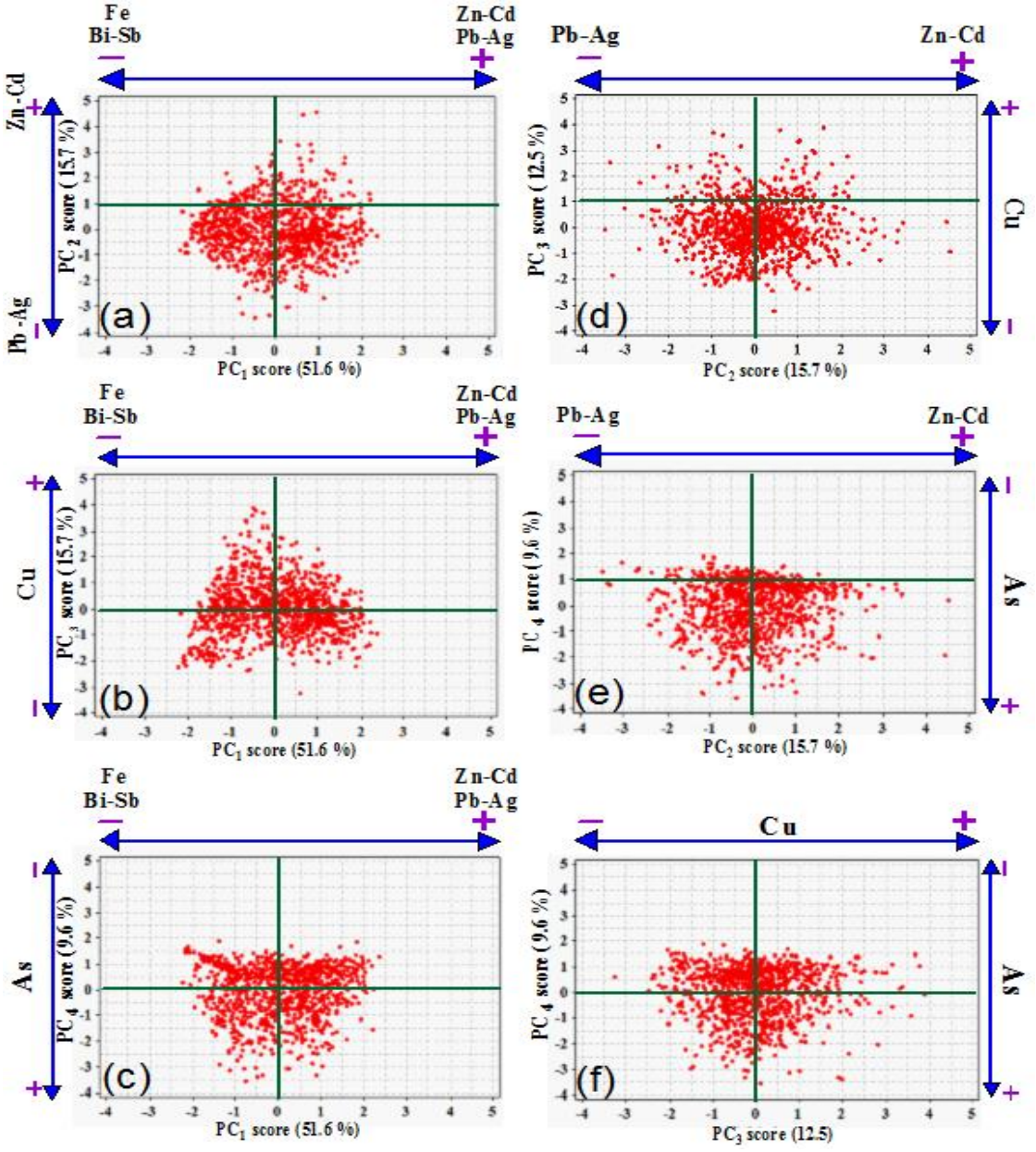

Figure 5.20: Maps of PC scores for 1,059 clr-transformed sample data of each element using SPSS.

In Figures 5.20, the signs of "+" and "-" represent the enrichment and depletion of samples respectively relative to the elements marked in each map. In Figure 5.20, the elements marked in each map are based on the results of maps of PC loadings in Sections 5.7.6.1 to 5.7.6.6. As an example, Figure 5.20d demonstrates that samples located at the extreme end of the positive scale of the PC_2 score are enriched in Zn and Cd and depleted in Pb and Ag. PC_2 score in this map tends to separate Zn- and Cd-rich samples (at the

positive scale of PC_2 score) from Pb- and Ag- rich sulphide samples (at the negative scale of PC_2 score). The distribution of samples in Figure 5.20d does not show a linear relationship relative to PC_2 score and PC_3 score. This indicates that almost all of the samples are independent from the two PCs. The data sets of PC scores have been provided in supplementary file to this thesis.

5.7.8 Biplots of PC loadings and PC scores for 1,059 samples of the Western Mineralisation

One of the most popular statistical approaches for the visualisation of compositional data sets in geochemistry is seen in ternary diagrams. It can be used effectively to evaluate the variability of three element concentrations or three oxide elements. However, the technique has difficulty in handling more than three components (Aitchison 1986), such as is the case in this study. For this reason, biplot diagrams are used for this study instead of ternary diagrams. Biplots (Aitchison & Greenare 2002; Gabriel 1971; Greenacre 2010) can display samples (points), element concentrations (vectors) and their degrees of correlation in a diagram. It is a very efficient tool to visualise multiple element concentrations (more than 3 elements) and samples in a low dimensional space.

In a biplot, the lengths and directions of vectors are important for its interpretation. The cosine of the angle between two vectors approximates the amount of correlation between the two element concentrations. The length of a vector represents the standard deviation of the element concentration. A short length of a vector for an element concentration in a biplot indicates that the element is relatively constant in the data set, whereas a long one indicates a greater relative variation of the element (Labus 2005). The 1,059 clr-transformed values of this chapter were used for the construction of biplots of 10 element concentrations and 1,059 samples in relation to for PC_1 and PC_2 loadings using Minitab software (Figures. 5.21 and 5.22).

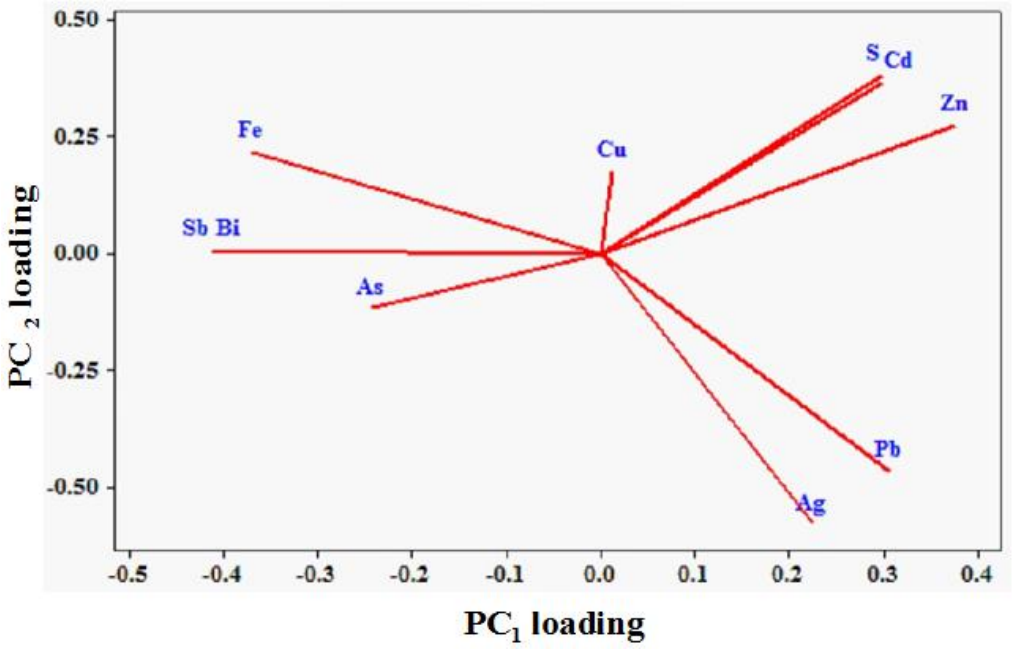

Figure 5.21: Biplot for 10 element concentrations of the Western Mineralisation in relation to PC_1 loading and PC_2 loading.

According to the measurement of vectors in Figure 5.21, Bi and Sb have larger vectors or higher geochemical variability relative to the other eight elements and Cu shows the lowest geochemical variability in the Western Mineralisation.

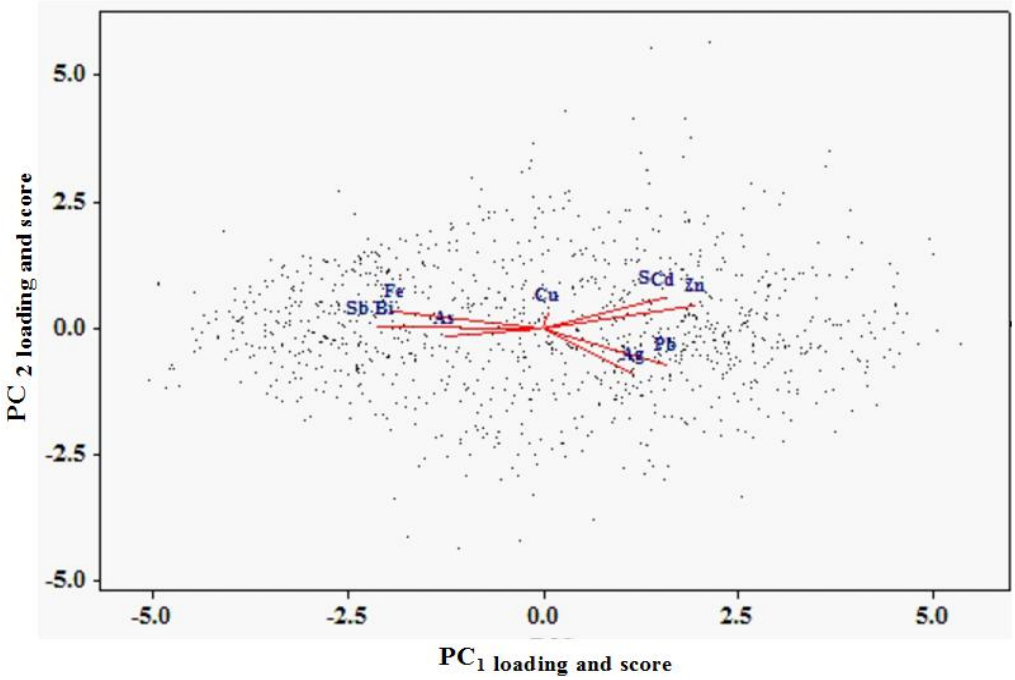

Figure 5.22: Biplot for a combination of 1,059 samples (Figure 5.20a) and 10 element concentrations (Figure 5.21) in relation to $PC_{1\ \text{loading and score}}$ and $PC_{2\ \text{loading and score}}$.

The distance between two vertices is approximately proportional to the variance of their log-ratios, ln (X_i / X_j). The vertices of Fe, Sb, Bi and As are close to each other which indicates the geochemical variation of these elements are closely correlated. Figures 5.21 and 5.22 demonstrate the following four groups of correlated elements in association with their PCs loadings:

1. Group 1: Zn, Cd and S have positive PC_1 and PC_2 loadings,
2. Group 2: Pb and Ag have positive PC_1 loadings and negative PC_2 loadings,
3. Group 3: Fe, As, Bi and Sb display clear negative PC_1 loadings, and
4. Group 4: Cu shows a clear positive PC_2 loading and very low correlation with other elements.

5.8 Three-dimensional biplots for chemical composition of galena and sphalerite samples of the Western Mineralisation

3D biplots can also be generated in relation to element concentrations and sample distribution using the software packages of Matlab and CoDaPack3D for Excel. In these software packages, it is possible to rotate orthogonally the whole biplot in space and demonstrate the distribution of samples and elements within different angles. The spatial rotation helps to separate different distributed samples within elements into suitable angles. This helps to identify possible mineral generation, mineral alteration and remobilisation of one or more elements.

For this investigation, 92 galena and 103 sphalerite samples from Kitchen (2001) and Patchett (2003) were used. Kitchen's samples were collected from drill cores 4001 and 4002 and Patchett's samples were collected from drill core 4003. The galena and sphalerite samples were analysed by measuring the atomic percentage of 11 elements using EMPA. The measured elements in galena and sphalerite have been shown in Figures 5.23 and 5.25 respectively. The data sets of Kitchen and Patchett have been provided in a supplementary file to this thesis.

5.8.1 Procedure for preparation of data for the CoDaPack3D

In the CodaPack3D, when introducing the geochemical data, the summation of the atomic percentage of the elements should be 100. However, the summation does not always reach 100 percent and calculation is required to find the remaining percentage

value. That remaining value is calculated by the subtraction of the summation of other percentage element concentrations from 100. The title row of each column in a standard spreadsheet of CoDaPack3D was labelled according to the element concentrations and the remaining percentage value. The atomic percentage of 11 element concentrations and the remaining percentage value of each sample were inputted in columns of a standard spreadsheet of CoDaPack3D. This program calculates the clr-transformation of the constrained geochemical data automatically and generates a 3D biplot.

Current CoDaPack3D does not show visually the three axes of PC_1, PC_2 and PC_3 in a 3D biplot (Figures 5.23a, 5.24a, 5.25a and 5.26a) but by programming in Matlab software can show the PCs scales (Figures 5.23b, 5.24b, 5.25b and 5.26b). It should be noted that a 3D biplot is not limited only to three PCs in a tetragonal model and a 3D biplot can be defined and interpreted for more than three PCs, for example in a pentagonal or hexagonal model.

5.8.2 Galena

Figures 5.23 and 5.24 show the same 3D biplot for galena but viewed from different angles to give a sense of distance between vectors and show their real lengths. Samples inside the red line of Figures 5.23a or 5.24a comprise a small number of galena samples identified by the influence of chemical variation of Fe and Zn. Figures 5.23 and 5.24 show two types of galena generation containing Zn- and Fe-rich galena (samples inside the red line) and Zn- and Fe-poor galena. The following observations can be drawn from Figures 5.23 and 5.24 which are consistent with the results from previous analyses:

1. Strong positive correlation among Pb, Bi and S,
2. Strong positive correlation between Zn and Fe,
3. Strong negative correlation of Fe and Zn other eight elements,
4. Moderate positive correlation of Ag, Sb and As,
5. Moderate positive correlation of Co and Cd,
6. Strong negative correlation of Cd with Ag, Sb and As,
7. Strong negative correlation of Co with Ag, Sb and As, and
8. High atomic variation of Zn, Fe and Cd in galena samples.

Table 5.15: Summary of decomposition galena samples into seven PCs based on variation of eleven elements.

PCs	PPV	PCV
PC_1	26	26
PC_2	19	45
PC_3	14	59
PC_4	12	71
PC_5	10	81
PC_6	10	90
PC_7	8	98

According to Table 5.15, a combination of PC_1, PC_2 and PC_3 explain 59 % of geochemical variation of galena samples in the Western Mineralisation.

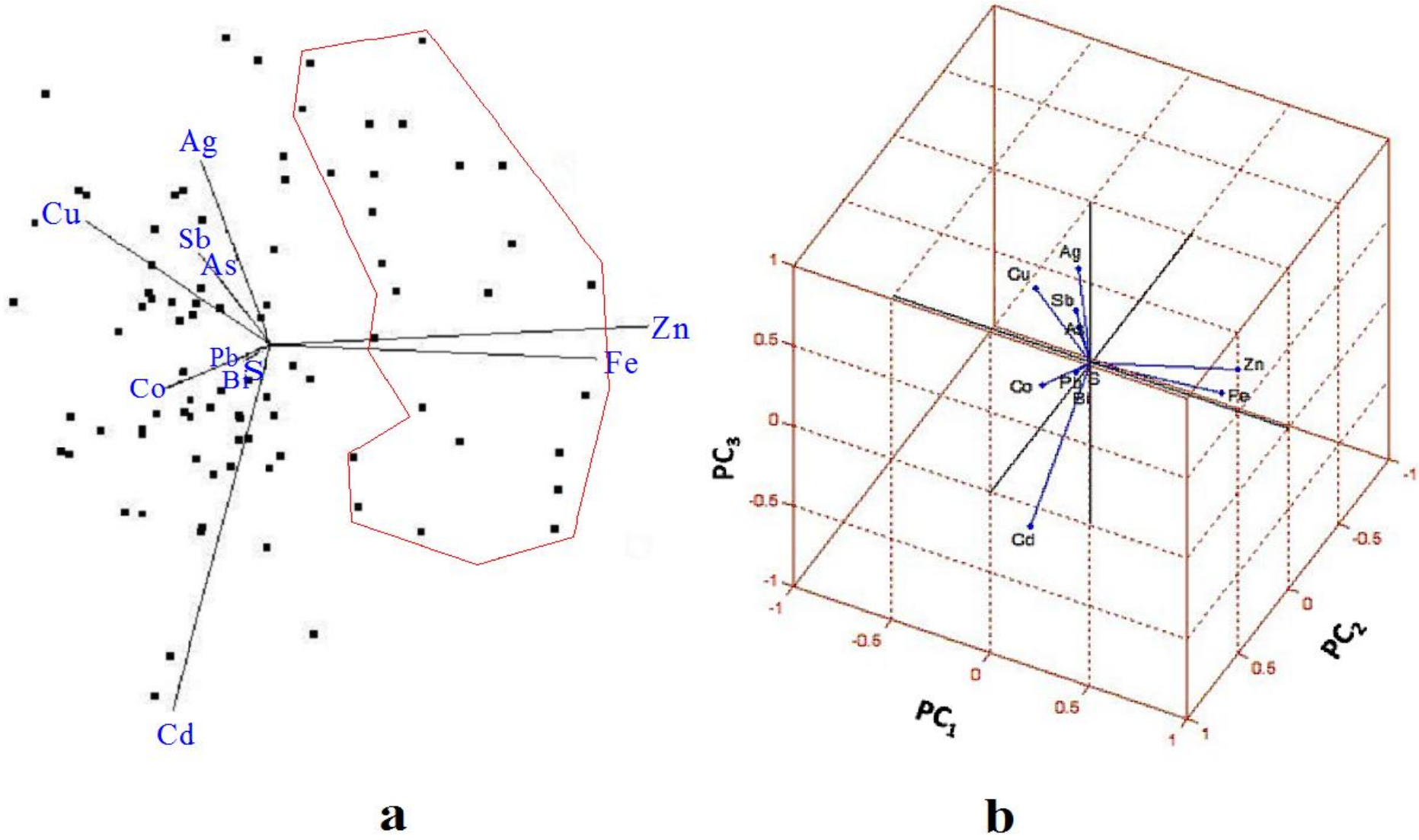

Figure 5.23: (a) the 3D biplot of galena samples of the Western Mineralisation and (b) the axes of the 3D biplot in relation to three PCs.

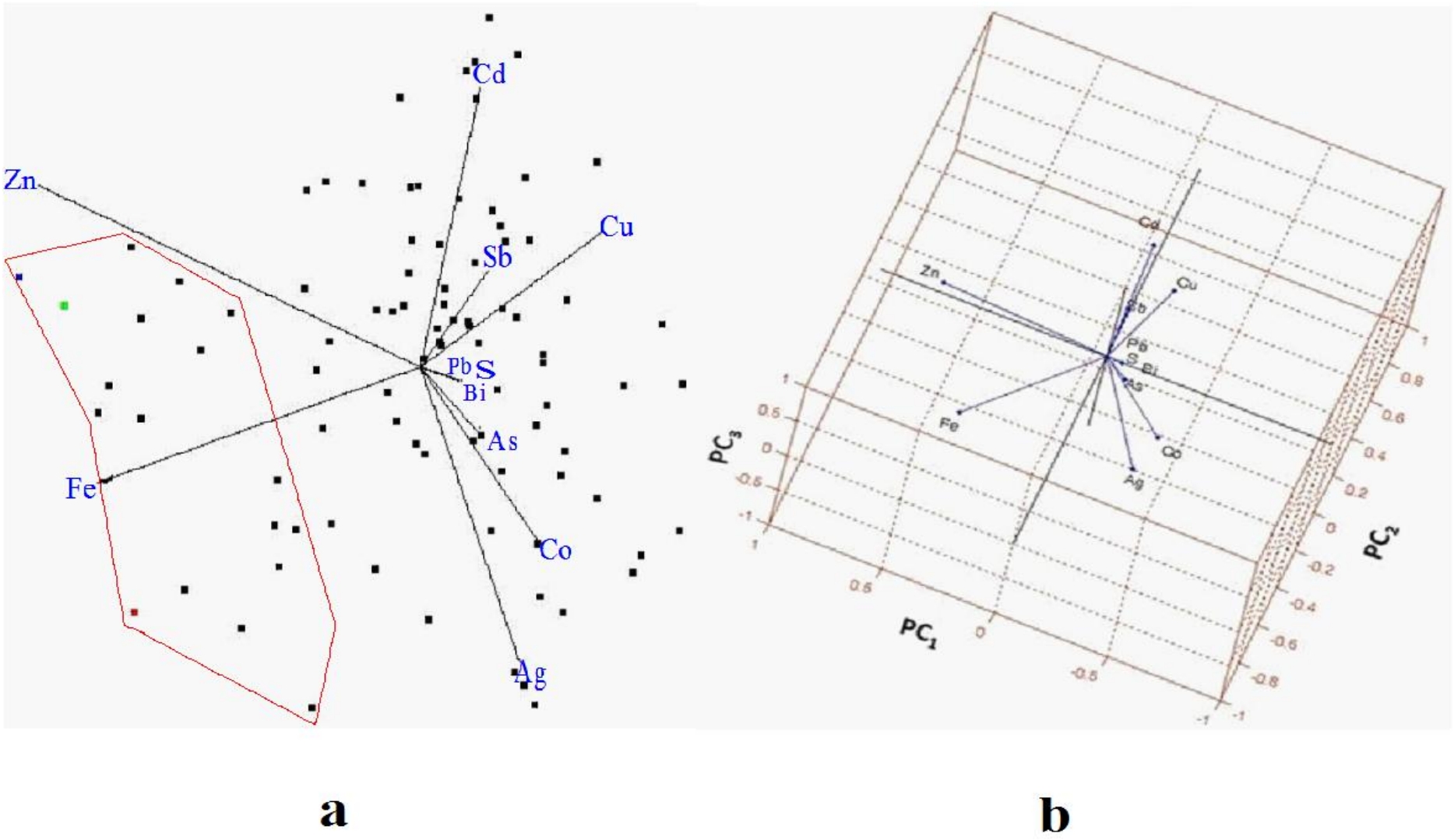

Figure 5.24: (a) the same plot as that of Figure 5.22a, but viewing from a different angle and (b) the axes of the 3D biplot in relation to three PCs.

5.8.3 Sphalerite

The biplot of the sphalerite samples is given in Figures 5.25 and 5.26. They show clearly two generations of sphalerite samples in the Western Mineralisation. One generation of sphalerite samples was strongly affected by the chemical variation of Bi (samples inside the red region) and they were enriched in Bi. The following observations can be drawn from Figures 5.25 and 5.26:

1. Strong positive correlation among Zn, Cd, Fe and S,
2. Strong positive correlation among Pb, Co and Cu,
3. Strong positive correlation among Ag and Sb,
4. Strong negative correlation of Bi with the other 9 elements,
5. Strong negative correlation of Ag with Co, Pb and Cu,
6. Strong negative correlation of Sb with Co, Pb and Cu, and
7. High atomic variation of Bi in sphalerite samples.

Again, these observations agree well with the results from previous analyses.

Table 5.16: Summary of decomposition sphalerite samples into seven PCs based on variation of eleven elements.

PCs	PPV	PCV
PC_1	29	29
PC_2	16	45
PC_3	15	60
PC_4	12	72
PC_5	11	83
PC_6	9	92
PC_7	7	99

According to Table 5.16, a combination of PC_1, PC_2 and PC_3 accounts for 60 % of geochemical variation of sphalerite in the Western Mineralisation.

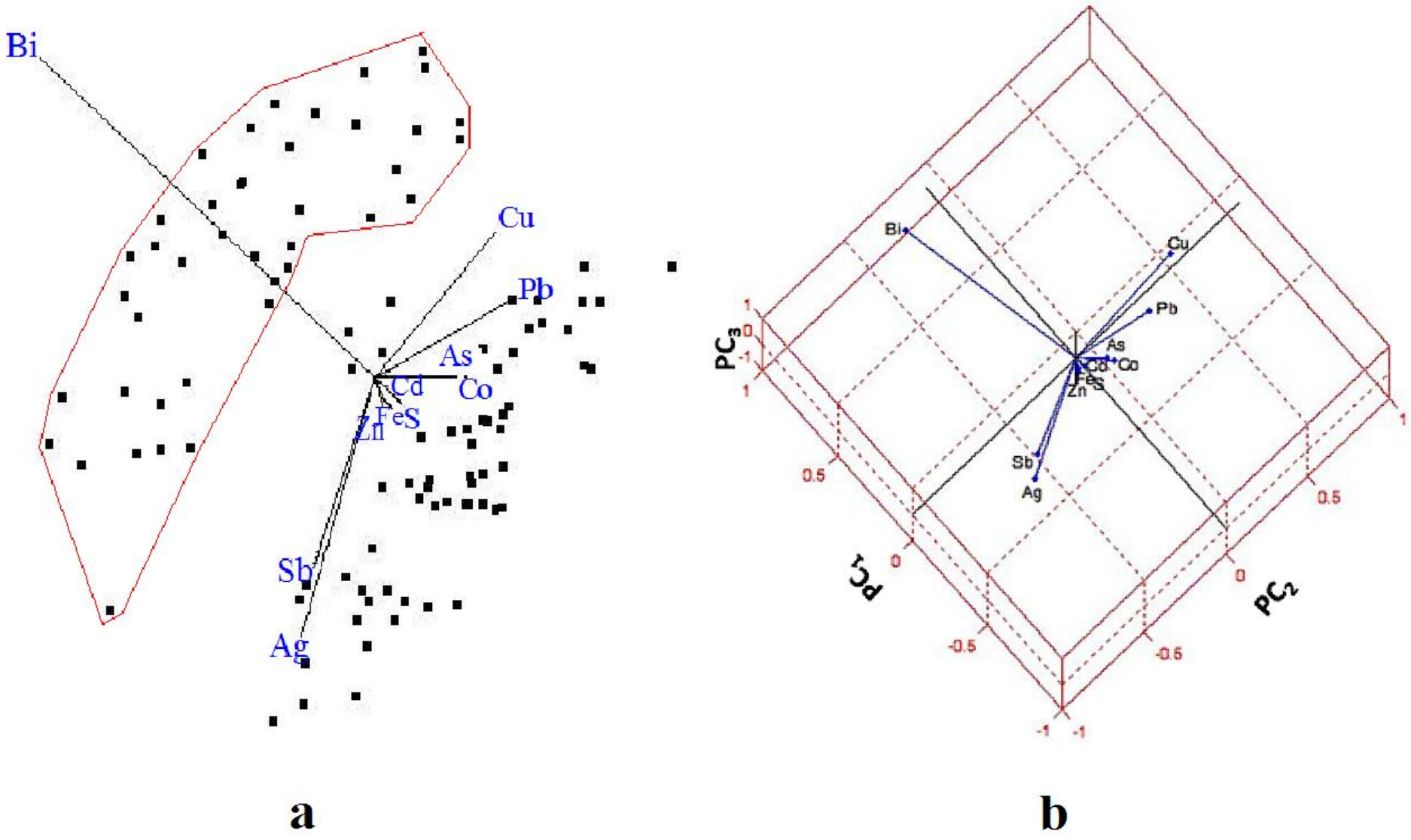

Figure 5.25: (a) the 3D biplot of sphalerite samples of the Western Mineralisation and (b) the axes of the 3D biplot in relation to three PCs.

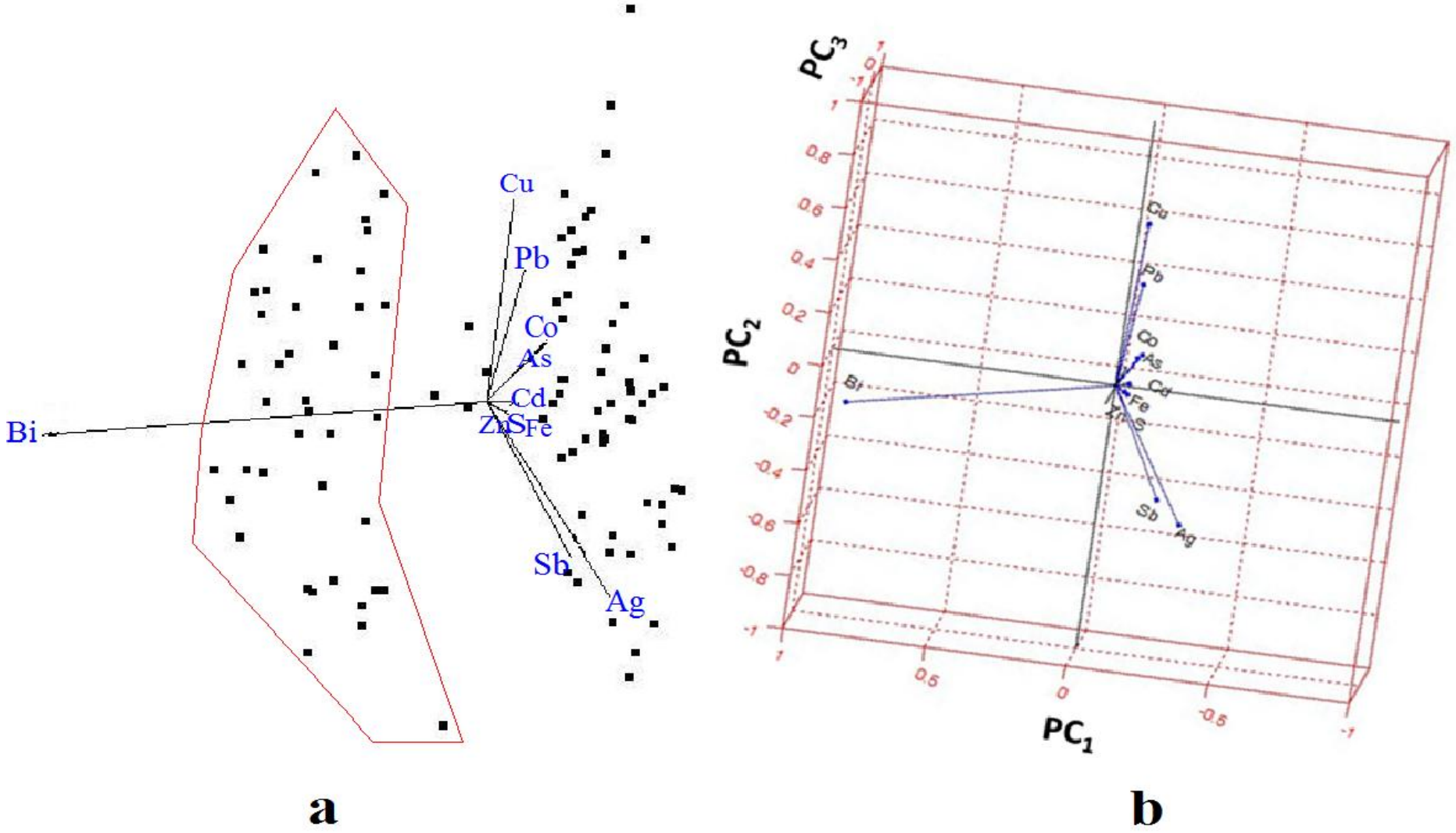

Figure 5.26: (a) the same plot as that of Figure 5.25a but viewing from a different angle and (b) the axes of the 3D biplot in relation to three PCs.

5.9 Summary

In this chapter, simple correspondence analysis was used to provide a picture of the internal relationships between the chemical composition of the galena samples and the Broken Hill orebodies and between the chemical composition of the sphalerite samples and the Broken Hill orebodies. Bivariate and multivariate analyses were calculated for 1,059 assayed samples of each element concentration. In order to generate unconstrained data, the compositional data of elements were transformed to a clr log-ratio. The clr transformed data of the elements also showed normal distributions. The following conclusions can be drawn from the analyses conducted in this chapter:

1. The results of 3D correspondence maps showed that galena samples of the Western Mineralisation contain higher Bi, Fe, As and Sb, and sphalerite samples of the Western Mineralisation contain higher Pb in comparison with the other Broken Hill orebodies,

2. According to bivariate analysis, Zn showed a strong positive correlation with Cd and high negative correlations with Fe, Sb and Bi. Lead showed a strong positive correlation with Ag and high negative correlations with Fe, Sb and Bi,

3. Based on multiple linear regressions:

3.1 The three key predictor elements for Pb are Fe, Ag and Bi concentrations with an Adjusted R Square value of 0.619,

3.2 The three key predictor elements for Zn are Cd, Sb and Ag concentrations with an Adjusted R Square value of 0.816, and

3.3 This means that chemical variation of Pb and Zn in the Western Mineralisation can be estimated by chemical variation of Fe, Ag, Bi, Sb and Cd.

4. The cluster algorithm grouped 10 elements based on their similarity. Three groups were identified: group 1 shows high similarity among the elements of Zn, Pb, S, Ag and Cd; group 2 contains Cu only; and group 3 shows high similarity among the elements of Fe, As, Sb and Bi,

5. PCA was used to reduce the chemical complexity of 10 elements (10 dimensional spaces or 10 components) into four dimensional spaces or four PCs. The following four PCs were derived:

5.1: PC_1: Bi, Sb, Zn, Fe, Pb, S, Cd, As and Ag,
5.2: PC_2: Ag, Pb, S and Cd,
5.3: PC_3: Cu and Cd, and
5.4: PC_4: As.

6. The four PCs were considered as major geochemical discriminators for the sulphide mass of the Western Mineralisation: PC_1 separated Zn and Pb from the other elements, PC_2 separated Zn from Pb, PC_3 discriminated Cu from the other nine elements and finally PC_4 act as a good discriminator for As,

7. The biplot of PC_1 and PC_2 classified ten elements into the following groups (Section 5.7.6):

7.1: Group-1: Zn, Cd and S,
7.2: Group-2: Pb and Ag,
7.3: Group-3: Fe, As, Bi and Sb, and
7.4: Group-4: Cu.

8. The 3D biplot of chemical composition of galena samples of the Western Mineralisation showed two generations of Zn- and Fe- rich galena and Zn- and Fe-poor galena samples, and

9. The 3D biplot of chemical composition of sphalerite samples of the Western Mineralisation revealed two generations of Bi- rich and poor sphalerite samples.

CHAPTER 6

Variogram Analysis for the Western Mineralisation

6.1 Introduction

Statistical analysis for variables which are spatially correlated uses geostatistics rather than classical statistics. The technique uses a model (variogram) that describes the spatial geological or geophysical continuity of the variables of mineralised zone. The variogram model can be constructed provided there are sufficient samples available, generally the case for a mining operation. The geostatistical approach enables the quantification of structural and random variations of the variables in space, and more importantly the approach retains the effects of significant anomalous samples and therefore helps to identify the anomalous locations.

Combining variogram models with techniques, such as kriging or simulation, geostatistics can then be used to generate the 3D block model for the orebody. Compared with classical statistics, such as multivariate regression, the block model is a more effective tool to visualise the continuity and distribution of grade variables in space. In general, mining engineers' main interests are to model only economic elements in the mineralisation (e.g. Pb, Zn and Ag or combination of them) in order to estimate tonnage and grade of future production. For example, at Broken Hill, uneconomic elements such as Bi, As, Sb, Fe are usually not considered for any geostatistical analysis unless they are treated as contaminant elements in the final product (for which the smelter may charge a penalty).

In this chapter, 136 directional variogram and down-hole variogram models were calculated for 43 variables (assays, minerals, rock types, magnetic susceptibility, specific gravity and sulphide textures) measured in the Western Mineralisation. The software used for these calculations is Geostatistics for Windows (Dowd & Xu 2006), a geostatistical package developed at The University of Adelaide. The variogram models derived are then used for the estimation of 43 block models using ordinary kriging. The specific objective of this chapter is to determine variogram parameters of the 43 measured variables, including the degree of spatial variability and grade continuity, the directional anisotropy and the proportion of between the structural and random variations of the variables.

6.2 Variography

Variography is a common tool and starting point for quantifying spatial variations of grade variables in a coherent model for orebody characteristics (Guibal 2001). It essentially describes the spatial correlation of a variable of interest such as the anomalous enrichment of a valuable element in an ore deposit. Variography comprises the direct experimental variogram calculation from sample data and an appropriate variogram model fitted to the experimental data. The experimental variogram is calculated by averaging the squared difference of the grade values over all pairs of sample data with the specified distance and direction i.e. Equation (6.1):

$$\gamma^*(\mathbf{h}) = \frac{1}{2}\frac{1}{n}\sum_{i=1}^{n}\left[g(x_i) - g(x_i + h)\right]^2 \qquad (6.1)$$

Where

$\gamma^*(\mathbf{h})$ = experimental variogram value

h = distance vector which is a directional distance

n = number of pairs of samples at a given distance h

$\mathbf{g}(x_i)$ = grade value at location x_i

$\mathbf{g}(x_i+\mathbf{h})$ = grade value at distance h from location x_i

The experimental variogram thus calculated is in general erratic. A smoothed functional form $\gamma(h)$ is in generally used to describe the relationship which is the variogram model. Common models include spherical scheme, Gaussian model and exponential model. Parameters for $\gamma(h)$ are derived based on the best-of-fit principle (Figure 6.1). For this application, the variogram models are defined for the following three domains:

1. Domains based on geological information, such as minerals, rock types and textures of sulphide minerals,
2. Domains based on element concentrations, and
3. Domains based on magnetic susceptibility and specific gravity.

It should be noted that variogram models may not necessarily be the same based on different domains. For example, the variogram models and parameters of galena are not the same as Pb concentration in the Western Mineralisation (Appendix B) and their respective images in Chapters 7 and 8 show different boundaries.

6.2.1 Variogram model-spherical scheme

In minerals applications, the variogram of grade values near the origin (i.e. zero distance) in general appears to be a linear. It increases with distance and eventually reaches a stable value (or fluctuating around a stable value) which is termed the sill value of the variogram. The sill value, in stationary case, is also equal to the total variance. The distance when the variogram reach the sill value is termed the range of the variogram. The initial variogram value when $h \rightarrow 0$ [Equation (6.1)] is termed the nugget variance.

The proportion of the nugget variance with the sill value is termed "nugget effect" (Dowd 2006a, p.81), which together with the slope of the variogram are the two most significant factors affecting the outcome of the kriging estimation. A variogram model fitting this type of variogram behaviour is called the spherical model (see the red dashed curve in Figure 6.1). Spherical model is the most popular variogram model used in minerals application. In Figure 6.1, three structural components are fitted to achieve the best-of-fit.

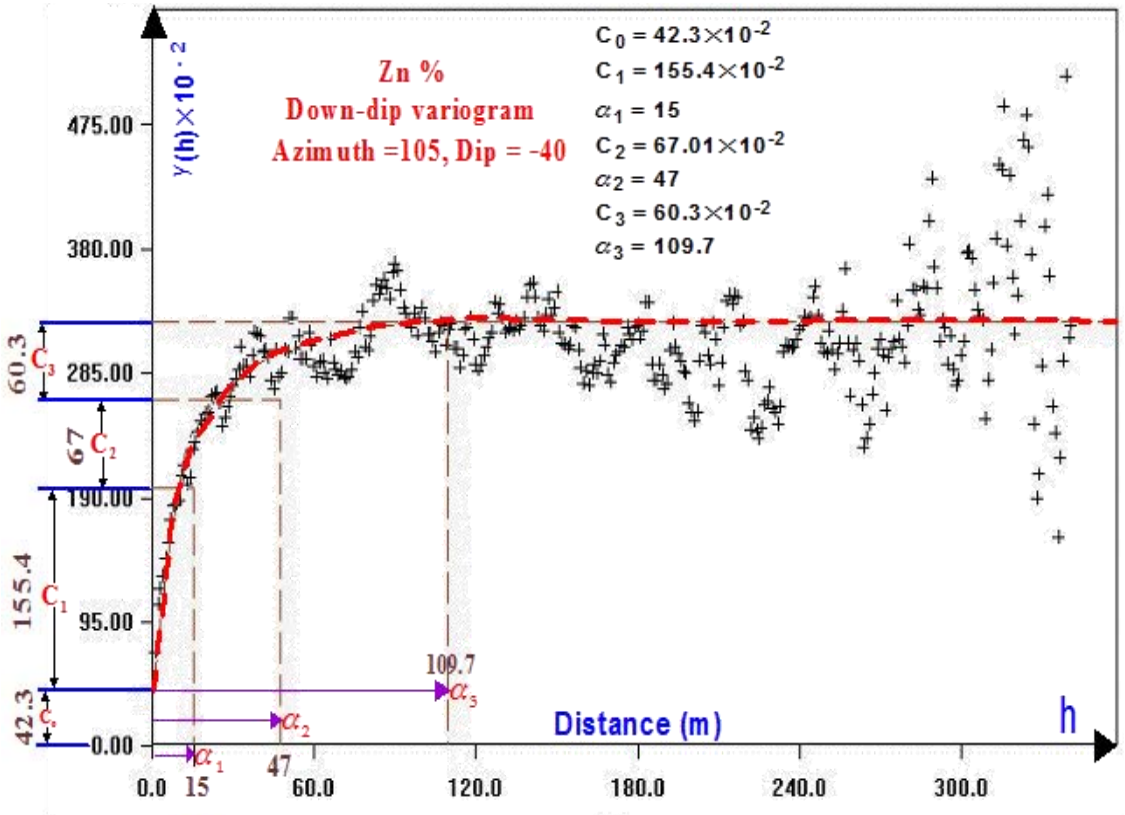

Figure 6.1: An experimental variogram ("+") and a fitted spherical model (red dashed curve) for Zn concentration of the Western Mineralisation and its variogram parameters.

Formulae used for calculation of the three structural components and the ranges of influence for a variogram model is given in Table 6.1.

Table 6.1: Formulae for calculation of variogram models with three structural components.

$$\gamma(\mathbf{h}) = \mathbf{C_0} + \mathbf{C_1} \times \mathbf{F(h,\alpha_1)} + \mathbf{C_2} \times \mathbf{F(h,\alpha_2)} + \mathbf{C_3} \times \mathbf{F(h,\alpha_3)} \quad \textbf{for} \quad \mathbf{0 < h \le \alpha_1}$$

$$\gamma(\mathbf{h}) = \mathbf{C_0} + \mathbf{C_1} \times \mathbf{F(h,\alpha_1)} + \mathbf{C_2} \times \mathbf{F(h,\alpha_2)} + \mathbf{C_3} \times \mathbf{F(h,\alpha_3)} \quad \textbf{for} \quad \mathbf{0 < h \le \alpha_1}$$

$$\gamma(\mathbf{h}) = \mathbf{C_0} + \mathbf{C_1} + \mathbf{C_2} \times \mathbf{F(h,\alpha_2)} \quad \textbf{for} \quad \mathbf{\alpha_1 < h \le \alpha_2}$$

$$\gamma(\mathbf{h}) = \mathbf{C_0} + \mathbf{C_1} + \mathbf{C_2} + \mathbf{C_3} \times \mathbf{F(h,\alpha_3)} \quad \textbf{for} \quad \mathbf{\alpha_2 < h \le \alpha_3}$$

$$\gamma(\mathbf{h}) = \mathbf{C_0} + \mathbf{C_1} + \mathbf{C_2} + \mathbf{C_3} \quad \textbf{for} \quad \mathbf{h \ge \alpha_3}$$

$$\mathbf{F(h,a_i)} = \left\{ \frac{\mathbf{3}}{\mathbf{2}} \times \frac{\mathbf{h}}{\boldsymbol{\alpha}_\mathbf{i}} - \frac{\mathbf{1}}{\mathbf{2}} \times \left(\frac{\mathbf{h}}{\boldsymbol{\alpha}_\mathbf{i}} \right)^{\mathbf{3}} \right\}$$

where C_i and a_i are the structural variance and the corresponding range for the i^{th} structure and i=1, 2, 3 , C_0 = The nugget variance , C_1, C_2, C_3 = The structural variance, $C_0+C_1+C_2+C_3$=Total variance or sill value of the variogram, α_1, α_2 = The range of influence , α_3 = The full range of influence

Nugget variance describes random variation of uncertain phenomena at small scale. Sampling errors and geological discontinuity will also contribute to the value of nugget variance. A high nugget effect is the case when the nugget variance is greater than 50 % of the total variance[1] (Dominy, Stephenson & Annels 2001). In this case, the application of geostatistics will not have significant improvement in estimation over classical statistics. In this application, the nugget effect for all 43 variables (element concentrations, minerals, rocks and geophysical measurement) are significantly smaller than 50 %.

6.2.2 The range of influence

The range of influence is an indication of the extent of spatial correlations. The maximum range is identified in a variogram model at the maximum distance when the variogram value reaches the sill (e.g. a_3 in Figure 6.1). The spatial correlation of the concentration at a distance greater than the maximum range of the variogram model is considered to be non-existence (Walter, Christensen & Simmelsgaard 2002).

[1] **Sill value**

6.2.3 Advantages of application of geostatistics versus classic statistics

Compared with geostatistics, classical statistics assume spatial independence of grade values i.e., any spatial correlation is disregarded. The variogram in this case is a horizontal line (Figure 6.2a) which equals to the total variance of the variable. This type of variogram model is termed the "pure nugget effect" (Carrasco 2010; Dominy, Stephenson & Annels 2001) with zero range of correlation. In this case, the search neighbourhood imposed in geostatistics for block estimation is irrelevant as no correlation is considered at any scale (Vann, Jackson & Bertoli 2003). In geostatistics, the general appearance of the variogram is shown in Figure 6.2b. The value of the variogram starts at a lower value and it will increase gradually with distance until it reaches the sill value, which is the total variance of the variable. The value of variogram smaller than the total variance indicates that there is spatial correlation for the distance as variogram is indirectly proportional to correlation.

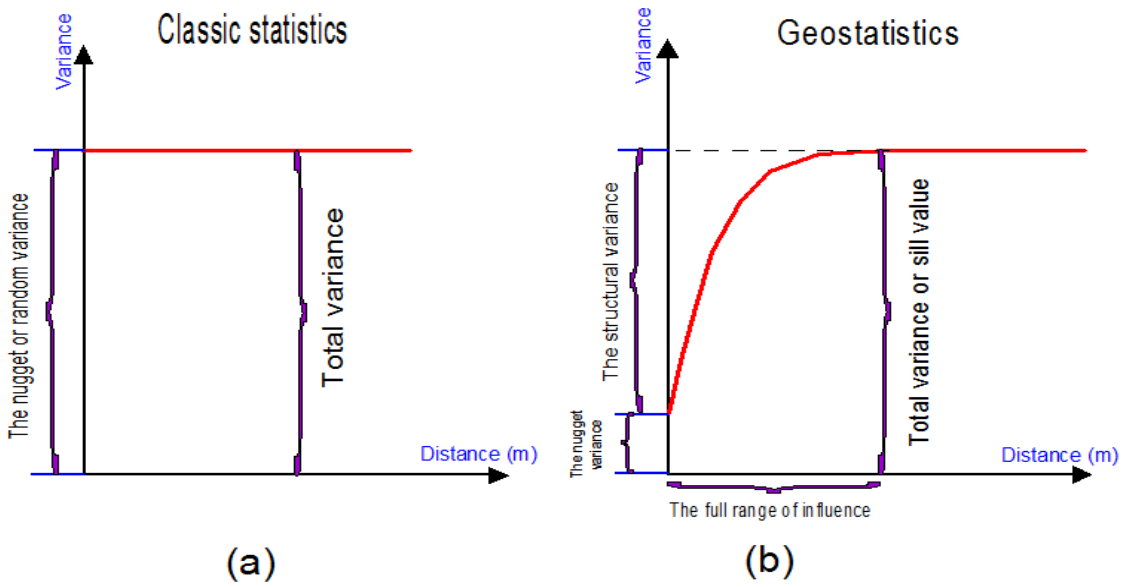

Figure 6.2: The change of variance (the red line) versus distance in (a) classic statistics and in (b) geostatistics.

6.2.4 Variogram calculations

A variogram is directional. In order to calculate variogram at different directions, the following parameters should be defined:

1. The direction of variogram (azimuth and dip angles, or trend and plunge of the directional line). The directions of variograms are defined by an azimuth angle that is measured horizontally clockwise from north (0 to 360 degrees) and a dip angle that

is measured from the horizontal plane (-90 to 90 degrees) as positive (if the dipping direction is in the positive elevation direction).

2. Conical search angle (0-90 degrees) and maximum search distance. In practice, it is unlikely pairs of samples will be aligned exactly in the variogram direction. It is then necessary to determine an approximate tolerance angle θ for capturing pairs of samples in a particular direction. This tolerance angle θ help classify any pairs of samples within $\pm \frac{\theta}{2}$ either side of a specified direction as being in that direction (Figure 6.3). This angle is termed the angle of regularisation. Maximum search distance will effectively turn the conical search into a truncated conical search (Figure 6.3).

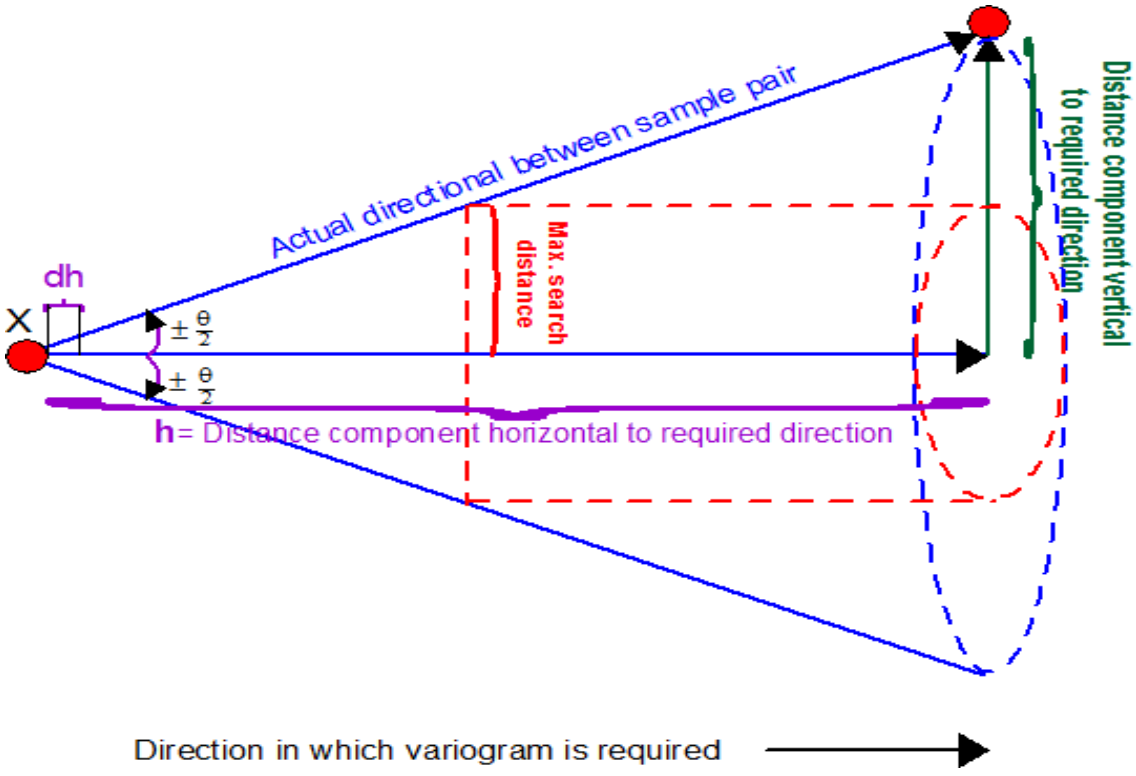

Figure 6.3: Conical search volume and effect of direction approximation in a cone.

3. Lag distance for variogram. In Figure 6.3, all sample locations falling within a slice of width "dh" on the top of the cone are considered to be at a lag of "h" from sample "X".

6.2.4.1 Down-hole variogram

Down-hole variograms refer to the variograms calculated along each drill hole. As samples are aligned closely with each drill hole, the variograms calculated in general will be the best candidates for identifying possible variogram structures. The down-hole variogram also help derive a more reliable estimate for the nugget variance for the related three-dimensional variogram model, which is in general difficult based on erratic three-dimensional experimental variogram (Guibal 2001).

In order to work out variogram in a particular direction closely aligned with the drill hole direction, drill holes are classified (projected) on cross-sections and directions on the cross-sectional plane. The average of individual down-hole variograms is calculated for each specified direction within each specified cross-section and then those directional variograms are averaged over all cross-sections to determine the global average directional variograms of the entire mineralised zone or some specified part of it (Dowd 2006b, p 32). The drilling section of the Western Mineralisation is perpendicular to the strike of the mineralisation. The alignment of drill cores along drilling section makes easier to calculate directional variograms with minimum distance and angle approximations. The down-hole variograms in this case are calculated based on cross-sections perpendicular to the strike direction of the mineralisation (NNE-SSW).

6.2.4.2 Three-dimensional (3D) variograms in different directions

The ultimate purpose of variogram modelling is to construct the three dimensional variogram structures that quantify the 3D spatial correlation. The full 3D variogram model can be constructed based on directional variograms calculated along different directions. The common representation for a 3D variogram model is using an ellipsoid with different lengths of axes, representing different variogram ranges in the three main axes: major, intermediate and minor. Major axis is the direction of longest range (maximum continuity) in the direction and minor axis is the direction of the shortest range (minimum continuity). In minerals applications, major axis normally coincides with the strike-plunge direction of the orebody, intermediate axis with the down-dip direction and minor axis with the cross-dip direction. This is also the case for the Western Mineralisation based on its 3D variogram calculations.

6.2.4.3 Problem with raw data of the Western Mineralisation for calculation of variogram models

All raw element concentrations except for Fe and some minerals and rocks produce highly positively skewed distributions (Figures 6.4 and 6.5) and their experimental variograms calculated directly from raw assay values are very noisy in all directions (e.g. Figure 6.6) which make very difficult to derive suitable variogram models. In this study, therefore non-linear transformation was applied to help derive the final variogram models to be used. The transformation used in this case is lognormal transformation.

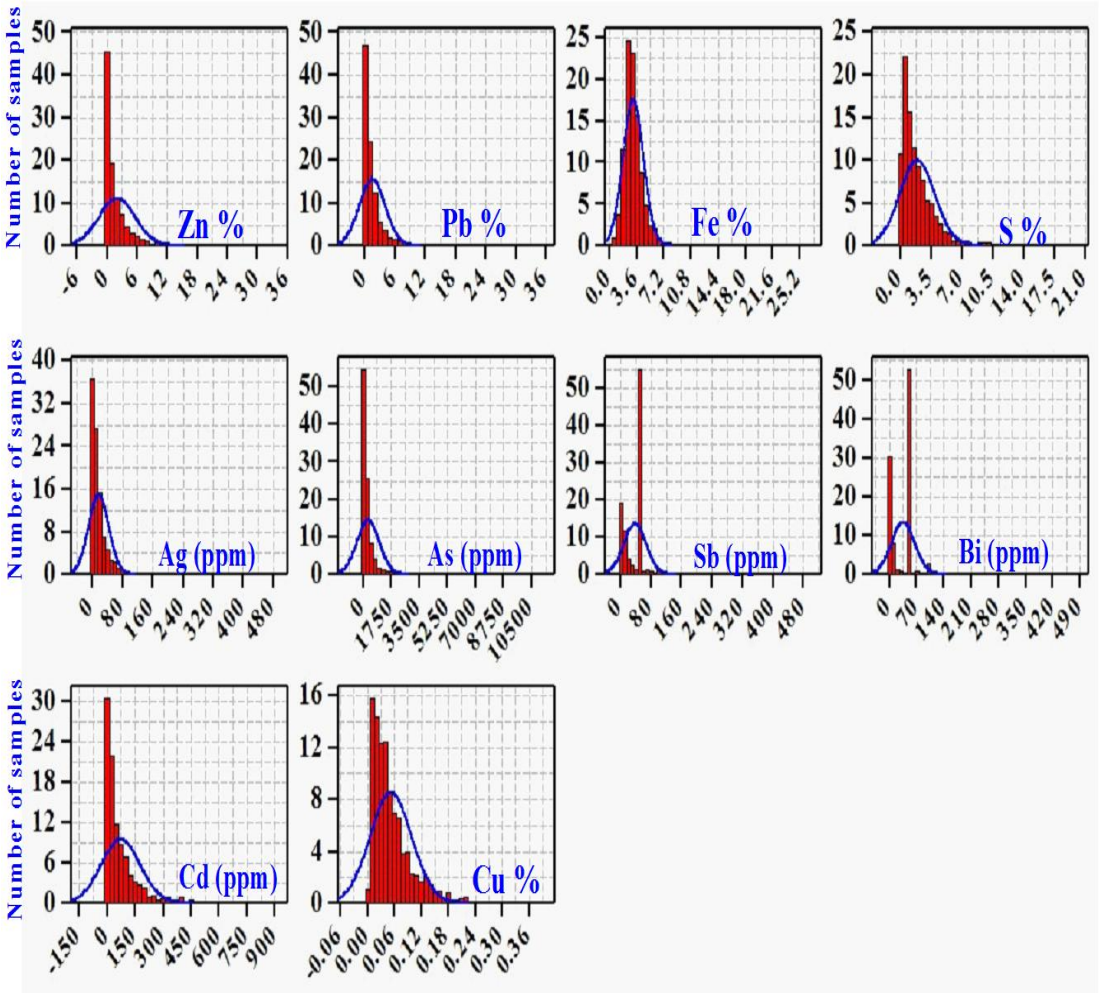

Figure 6.4: The histograms of raw element concentration. The red areas show the experimental histograms of the element concentrations and the blue curves show the theoretical normal distribution fitted for those elements.

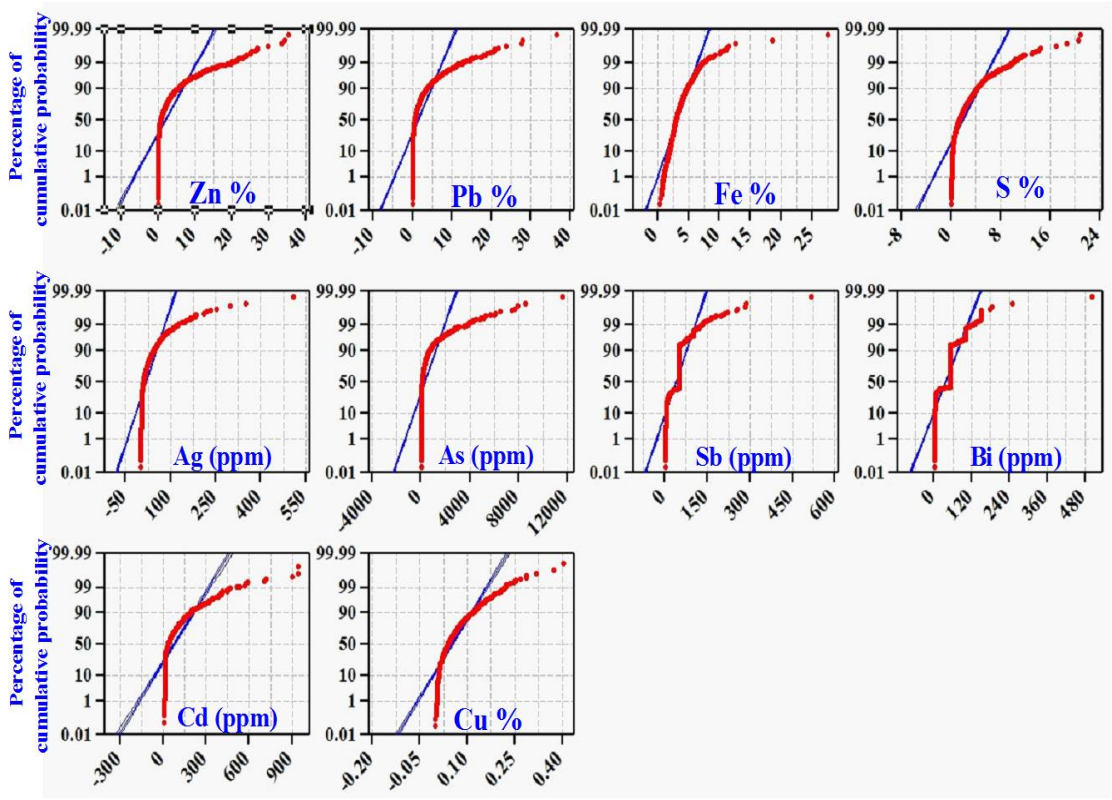

Figure 6.5: The probability plots of the raw element concentrations versus the percentage of cumulative probability of the element concentrations (red curves). The discrepancy from straight lines (blue lines) means the departure from normal distribution.

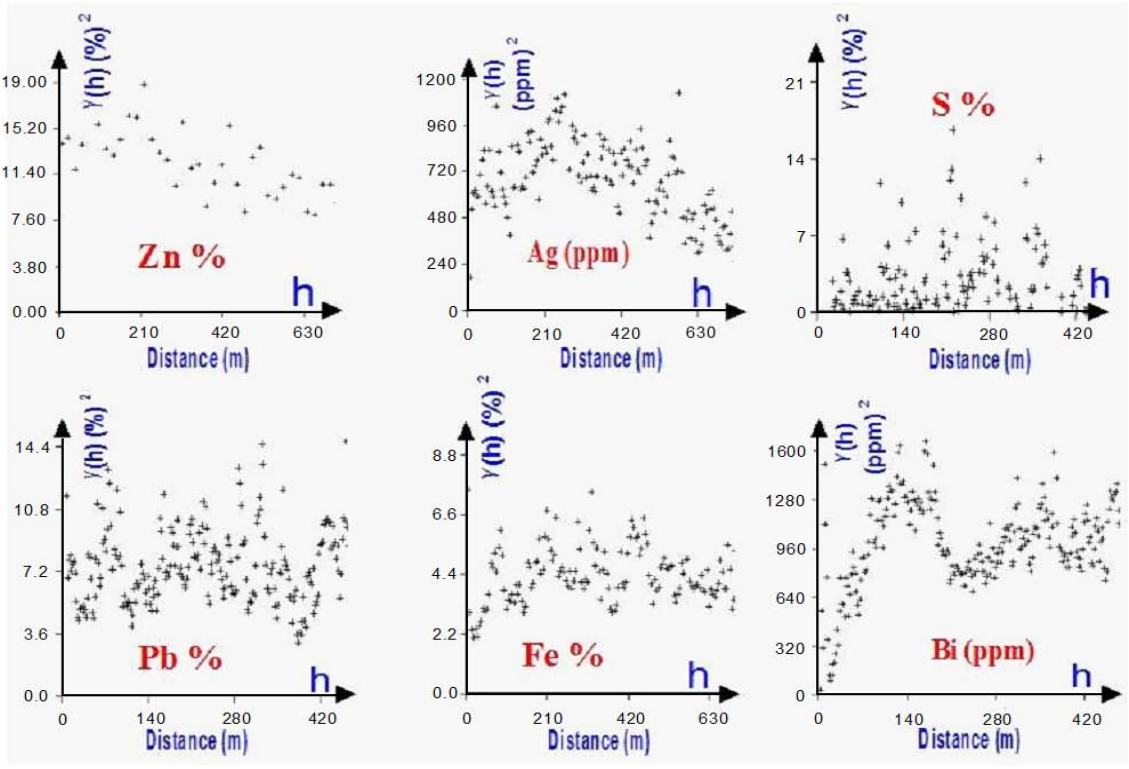

Figure 6.6: Some examples of the erratic experimental variograms that were produced by the strike-plunge variogram of the raw data of Zn, S, Pb, Fe, Ag and Bi.

6.2.4.4 Logarithmic transformation of data

Logarithmic transformation of the data involves taking simple logarithms of the sample values. Variograms are then calculated based on the transformed values. Because of the non-linear relationship, the transformation usually helps reveal the spatial correlation as it in general reduces the effect of outliers. The transformation in most cases also alleviates the proportional effect.

6.2.4.5 Back-transformation

The problem here is that only variograms for raw data can be used in linear geostatistics. The variograms modelled in logarithmic scale must be back-transformed to raw data scale. The simplest approach for the back transformation is to assume that the ranges of influence and the nugget effects in both scales are identical and only differences are in their sill values (Dowd 2006b, p 53). The variances in raw data scale are taken as the sill values for the variograms for the raw data based on stationary assumption. This back-transformation is only approximate as the transformation is non-linear (Dowd 2006b). Equation (6.2) is used for calculation of the structural components for the variogram model in raw data scale based on the above approach:

$$\frac{C_i}{\sigma^2_{\text{Logarithmic data}}} \times \sigma^2_{\text{Raw data}} \qquad (6.2)$$

Where $\sigma^2_{\text{Logarithmic data}}$ = Sill value of the variogram of logarithms of data

$\sigma^2_{\text{Raw data}}$ = The variance of raw data in classic statistic

C_i = The nugget variance (i=0) and the structural variance (i=1, 2, 3,…).

Table 6.2 shows an example of calculation of the approximate variogram model. Appendix B provides the detailed descriptions of the variogram parameters used.

Table 6.2: The approximate variogram model of Pb in raw data scale for the strike-plunge direction resulted from the variogram model of the logarithms of the data.

$$\sigma^2_{\text{Logarithm, Pb}} = C_0 + C_1 + C_2 = 22.9\times10^{-2} + 130\times10^{-2} + 100\times10^{-2} = 252.9\times10^{-2}$$

$$\sigma^2_{\text{Raw data, Pb}} = 6.59\ (\%)^2$$

$$\frac{C_{0,\text{Pb}}}{\sigma^2_{\text{Logarithm, Pb}}}\times\sigma^2_{\text{Raw data, Pb}} = \frac{22.9\times10^{-2}}{252.9\times10^{-2}}\times6.59\ (\%)^2 = 0.60\ (\%)^2$$

$$\frac{C_{1,\text{Pb}}}{\sigma^2_{\text{Logarithm, Pb}}}\times\sigma^2_{\text{Raw data, Pb}} = \frac{130\times10^{-2}}{252.9\times10^{-2}}\times6.59\ (\%)^2 = 3.40\ (\%)^2$$

$$\frac{C_{2,\text{Pb}}}{\sigma^2_{\text{Logarithm, Pb}}}\times\sigma^2_{\text{Raw data, Pb}} = \frac{100\times10^{-2}}{252.9\times10^{-2}}\times6.59\ (\%)^2 = 2.62\ (\%)^2$$

6.3 The strike, plunge and dip of the orebody in the Western Mineralisation

The strike, plunge and dip of the orebody of the Western Mineralisation were estimated for 3D visualisation of the sulphide sample locations (Figure 2.2), observations of structural geology and variogram analysis. The primary estimated ranges were:

1. **Strike direction of the orebody**: between 5º and 25º from north,
2. **Plunge of the orebody**: between 15º and 35º from horizontal plane, and
3. **Dip of the orebody**: between 30° and 50° from horizontal plane.

Figure 6.7 shows an average intersection of the mineralisation zone in a couple of dashed red planes in the Western Mineralisation which was simplified to depict the possible strike, plunge and dip of the orebody. Therefore, the spatial outline of the orebody is not a symmetrical plane. In Figure 6.7, plunge and dip are used as a term of structural geology. In structural geology, plunge is used for lineation (e.g. fold hinges, mineral lineations, cleavage and bedding intersections) and dip is used for planar features. Plunge and dip in structural geology always have positive values. More accurate orientation angles for the orebody of the Western Mineralisation (Figure 6.8) were determined based on derived directional variogram models for the three perpendicular planes of strike-plunge, down-dip and cross-dip (Figure 6.9).

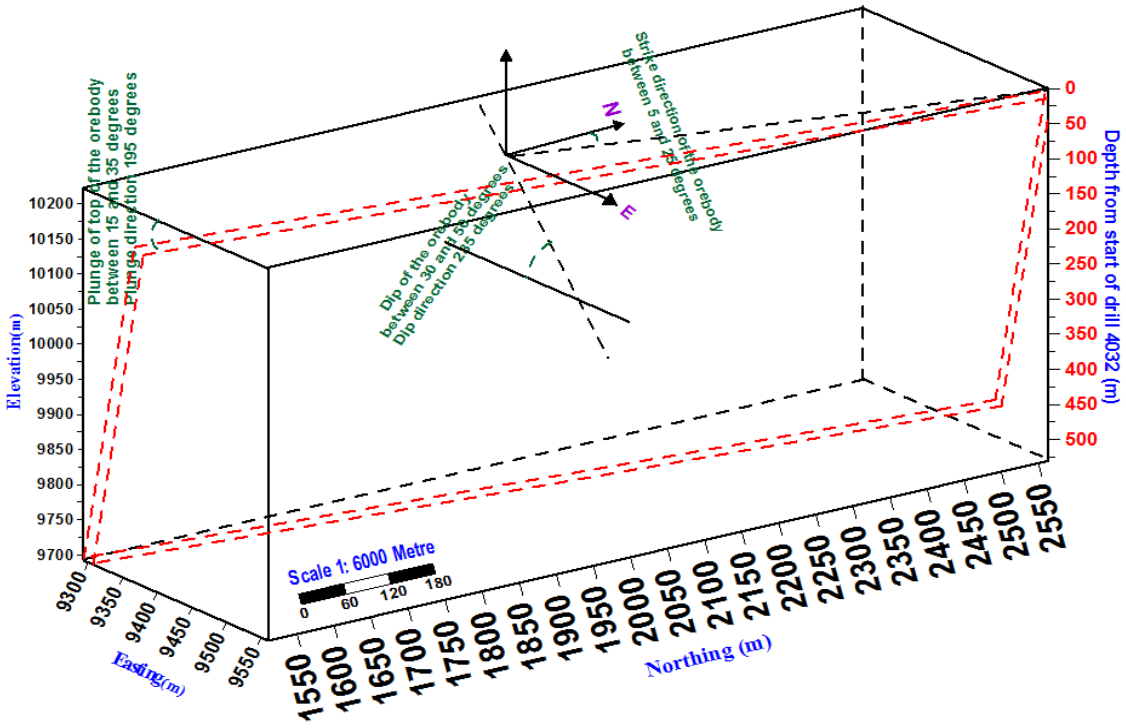

Figure 6.7: The possible ranges of strike, plunge and dip for the Western Mineralisation.

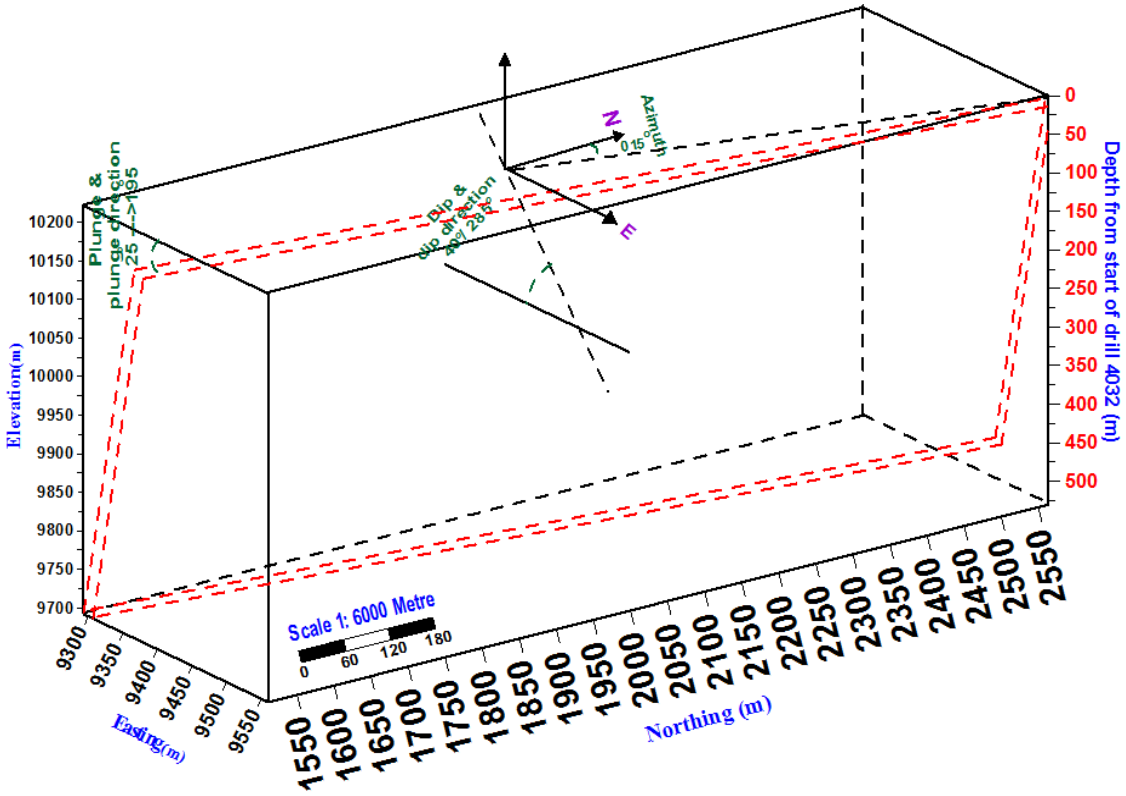

Figure 6.8: The Western Mineralisation is characterised by a strike direction of 15°, a plunge of 25° and a plunge direction of 195° (in structural geology, it is defined by 25°→195°) and a dip of 40° and a dip direction of 285° (in structural geology is defined by 40° / 285°).

On the strike-plunge plane, the variogram ranges construct the ellipse as shown in Figure 6.9a. The major axis of the ellipse is the strike-direction of the orebody (azimuth 15°) and the minor axis is the dip-direction (285°). In the down-dip plane (Figure 6.9b), the variogram model will have an ellipse with the major axis representing the strike-direction of the 3D variogram model and the minor axis of the ellipse is in the intermediate axis. The intermediate axis of the 3D variogram model in the down-dip direction is worked out to be 40^{o}. On the cross-dip plane (Figure 6.9c), the major axis of the ellipse is in the intermediate axis direction of the ellipse and the minor axis represents the cross-dip variogram range.

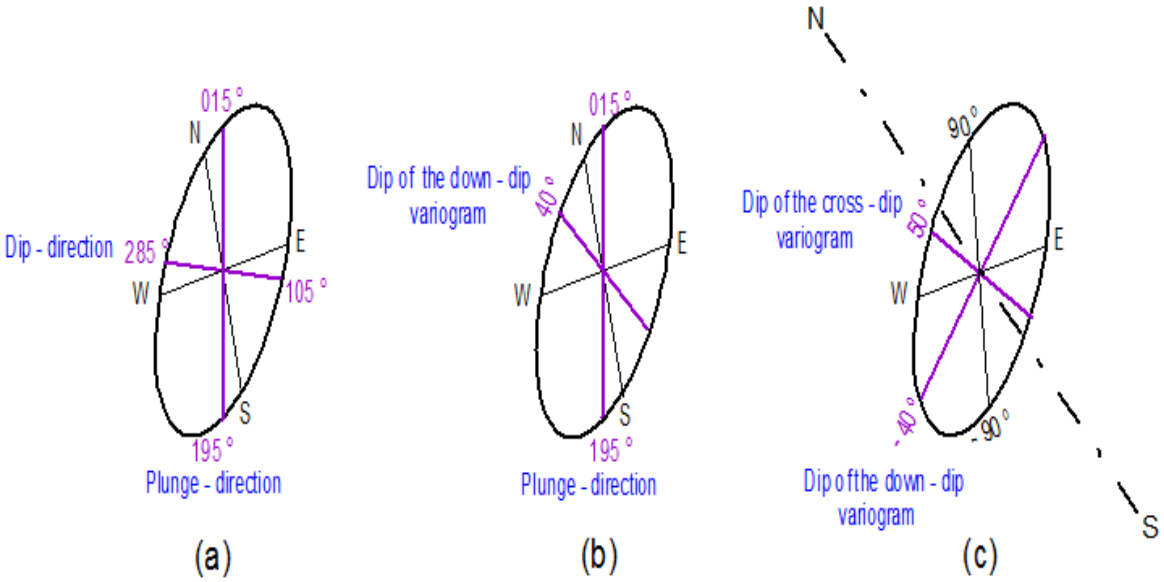

Figure 6.9: (a) shows a horizontal plane ellipse that is used for displaying the strike-direction of the strike-plunge variogram and dip-direction of the down-dip variogram. (b) shows the vertical plane ellipse for the dip angles of the down-dip (-40°) variogram and strike-direction of the strike-plunge variogram and (c) displays the vertical plane ellipse for the dip angles of the cross-dip (50°) and the down-dip (-40°) variograms.

It should be noted that a directional variogram model with an azimuth angle of X° is identical to the variogram model with the azimuth angle of X°+180°, provided the sign of the dip angle for the direction is also reversed.

6.4 The use of variogram ranges for the design of the optimal sampling grid

A simple application of the derived variogram ranges is in the design of the optimal sampling grid which is cost effective. The optimal sampling grid derived based on the variogram models from the Western Mineralisation can help the design of an optimal

sampling grid for similar Zn-Pb-Ag type of mineralisation within the Broken Hill district or in other areas. Once the full 3D variogram model is constructed, it is possible to calculate the optimal distance between sampling drill holes. As a rule of thumb, $\frac{2}{3}$ of the variogram range is usually considered an appropriate distance to capture the spatial grade continuity of mineralisation (Flatman & Yfantis 1984, p.346). In practice, it is unlikely variogram anisotropies will coincide exactly with the coordinate system (easting, northing and elevation) used and the calculated sampling grid will have to be adjusted accordingly. The optimal surface geochemical sample spacing for detecting anomalous concentration and geochemical zonation in the Western Mineralisation are calculated and shown in Tables 6.3 and 6.4.

Table 6.3: An appropriate surface geochemical sampling grid for Pb, S, Bi, Fe and Zn when the real dip of orebody is not clear for the Western Mineralisation.

The full range of influence (metre)	Elements				
	Pb	S	Bi	Fe	Zn
The full range of influence at the strike direction=15°	304.36	227.49	190.97	179.26	149.84
The full range of influence at the strike direction=105°	151.27	39.31	130.19	84.30	104.09
The full range of influence at the strike direction=15° × $\frac{2}{3}$	202.91	151.66	127.31	119.51	99.89
The full range of influence at the strike direction=105° × $\frac{2}{3}$	100.85	26.21	86.79	56.20	69.39
Anisotropy ratios	2.01	5.79	1.47	2.13	1.44

As discussed above, the longer variogram range on the plane is in the strike-plunge direction and the shorter range is in the cross-dip direction.

Table 6.4: An appropriate surface geochemical sampling grid for Cd, Cu, Sb, As and Ag when the real dip of orebody is not clear for the Western Mineralisation.

The full range of influence (metre)	Elements				
	Cd	Cu	Sb	As	Ag
The full range of influence at the strike direction=15°	115.92	100.85	79.00	51.98	33.58
The full range of influence at the strike direction=105°	84.13	66.08	19.61	15.17	15.63
The full range of influence at the strike direction=15° × $\frac{2}{3}$	77.28	67.23	52.67	34.65	22.39
The full range of influence at the strike direction=105° × $\frac{2}{3}$	56.09	44.05	13.07	10.11	10.42
Anisotropy ratios	1.38	1.53	4.03	3.43	2.15

For example, in order to detect the extension of geochemical halo zoning for Zn in the Western Mineralisation, the optimal surface sampling grid should be about 100 m (99.89 m in Table 6.3) along the azimuth of 15° and 69 m (69.39 m in Table 6.3) along the azimuth of 105° (Figure 6.10). Tables 6.3 show that S has the greatest variogram anisotropy ratio. This indicates that spatial continuity of S concentration in the strike direction of 105° is 5.75 times that of the strike direction of 15° in the Western Mineralisation

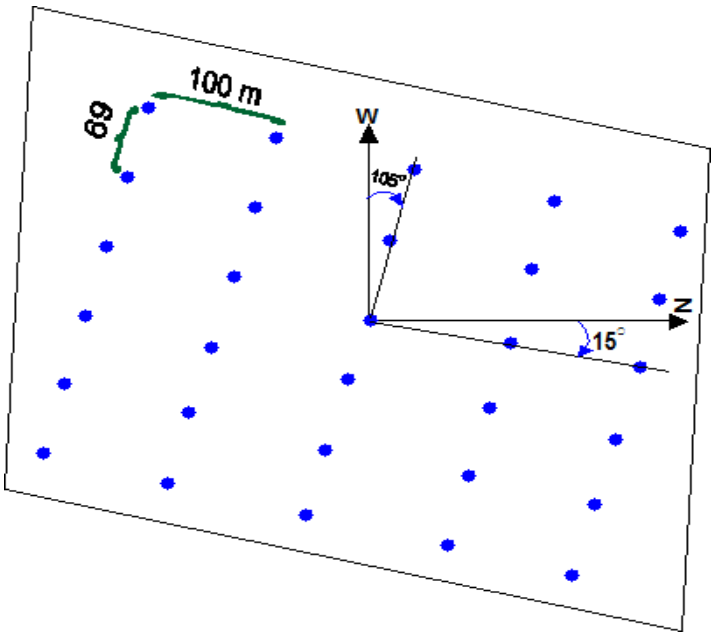

Figure 6.10: A schematic geochemical sampling grid for detection of Zn concentration.

It should be noted that different variogram anisotropies are detected for different elements in the Western Mineralisation. An overall optimal sampling grid in this case will be a compromise considering variograms for all elements, if the spatial variations for all elements are to be appropriately quantified. If all ten elements are considered in this example, the optimal sampling grid will be 10 m in the strike direction of 105° (the minimum range for As in Table 6.4) and 22 m in the strike direction of 15° (the minimum range for Ag in Table 6.4),

6.5 Comparison of variogram parameters of the Western Mineralisation with other Pb and Zn deposits

One way to characterise the spatial structures and variations of mineralisation is application of variogram parameters (range of influence, nugget effect and sill values) derived for the elements concerned. Deposits with more irregular grade variations such as gold or vein type deposits may have a large nugget effect and a short range of influence. Relatively uniform deposits such as stratabound sedimentary Pb-Zn mineralisation are characterised by very low nugget variance and a large variogram range. Figure 6.12 compares published variogram parameters from other types of lead and zinc sulphide deposits such as Irish, Mississippi Valley-type deposits (MVT), sedimentary exhalative deposits (Sedex) and vein-type Pb-Zn deposits with variogram parameters of the Western Mineralisation.

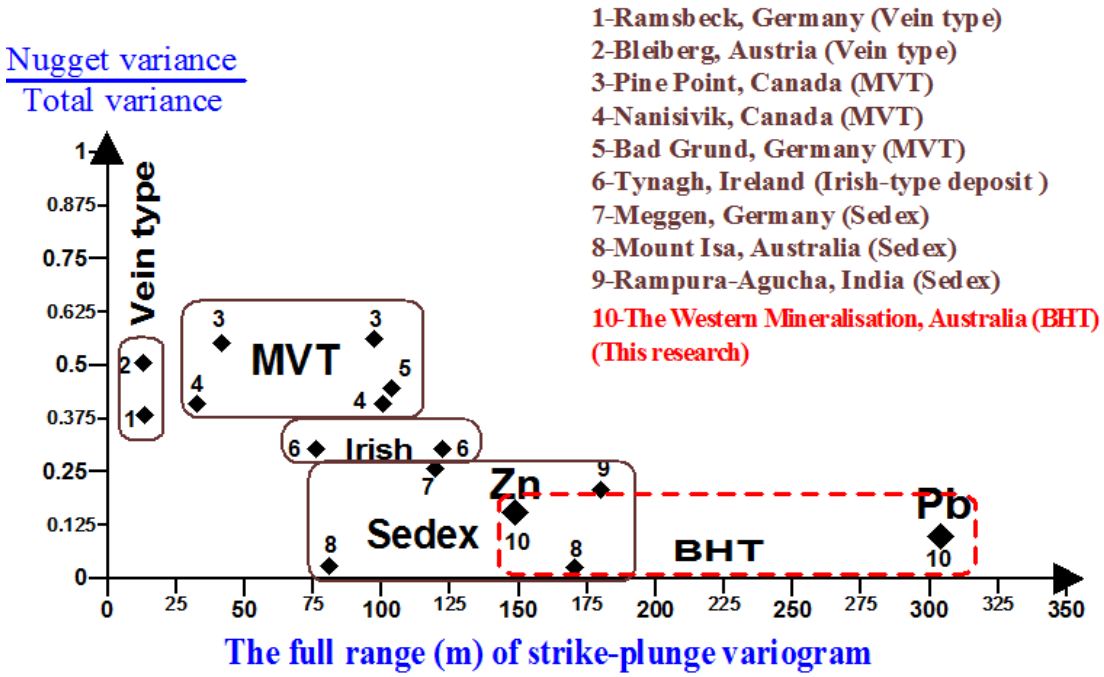

Figure 6.12: The nugget effect ($\frac{C_0}{Sill}$) versus the full range of variogram for Zn and Pb concentrations (modified from Wellmer 1998).

Figure 6.12 shows that the Western Mineralisation is a more continuous mineralisation and has higher degree of spatial correlation relative to other lead and zinc sulphide ore deposits. Therefore, the use of geostatistical analysis for the Western Mineralisation is more appropriate technique in comparison with classic statistical methods. In Figure 6.12, the Western Mineralisation has a long range of influence and the nugget effect is only higher than the Mount Isa deposit in Australia. It should be noted that relative nugget effect is also related to the composite length (size) of core samples. Smaller nugget effect will be obtained for larger sample size (Guibal 2001).

6.6 Variogram anisotropy of different elements in the Western Mineralisation

Variogram anisotropy reveals different spatial variability of the elements in different directions. The anisotropy can be represented by an ellipsoid where the major axis is in the direction of the longest range and the minor axis is in the direction of the shortest variogram range. In general, the longest variogram range coincides with the strike-plunge direction of the orebody, the intermediate range with the down-dip direction and the shortest variogram range with the cross-dip direction. However, this is not necessarily to be always the case. In the following discussion, the variogram ellipsoids for different elements are plotted using the following conventions (Figures 6.13 and 6.14):

1. Strike-plunge and down-dip variograms make SD ellipse (red ellipse),
2. Strike-plunge and cross-dip variograms make SC ellipse (violet ellipse), and
3. Down-dip and cross-dip variograms make DC ellipse (blue ellipse).

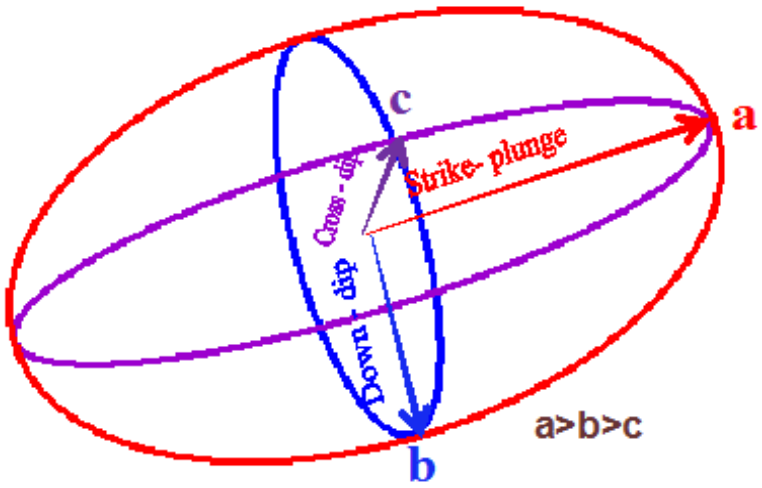

Figure 6.13: The anisotropy ellipsoid (Rose diagram) with three directional and dimensional ellipses.

Where

"**a**" is the full range of influence derived based on the strike-plunge variogram,

"**b**" is the full range of influence derived based on the down-dip variogram, and

"**c**" is the full range of influence derived based on the cross-dip variogram.

The comparison of the variogram ellipsoids for different elements in the Western Mineralisation are shown in Figure 6.14.

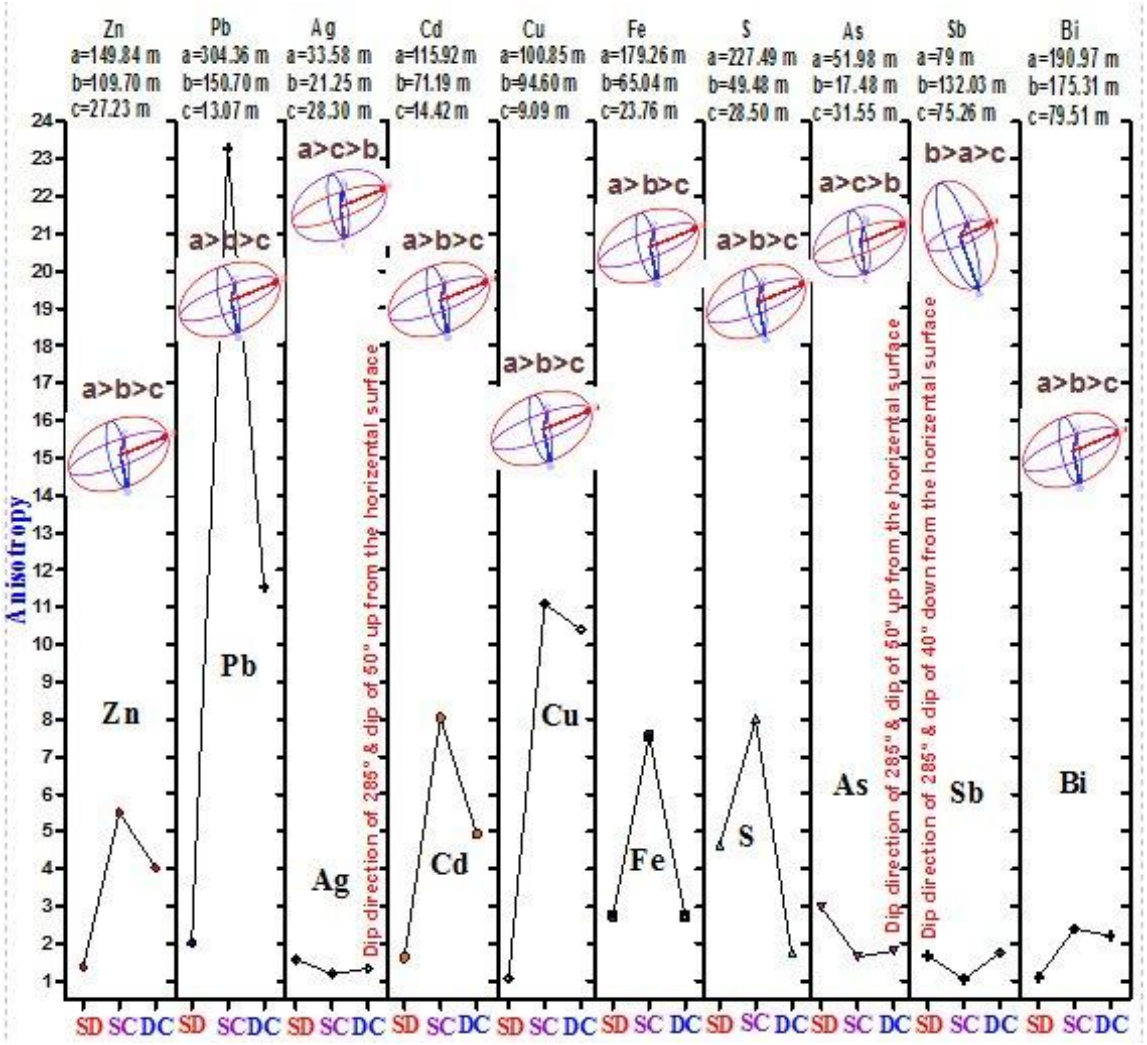

Figure 6.14: Comparison of geometrical ellipsoids (Rose diagrams) of compositional parameters, their radii and anisotropy ratios.

Further analysis reveals the following three distinct sets of anisotropies:

1. **a > b > c:** the largest range **"a"** is in the azimuth direction of 195° and plunge of 25° which coincides with the strike-plunge direction of the orebody. The shortest range **"c"** is in the cross-dip direction which is at the azimuth of 285°. Elements in the category include Zn, Pb, Cd, Cu, Fe, S and Bi,

2. **a > c > b:** the largest range **"a"** is in the azimuth direction of 195° and plunge of 25° which coincides with the strike-plunge direction of the orebody. The shortest range **"b"** is in the down-dip direction. Elements in the category include Ag and As, and

3. **b > a > c:** the longest range **"b"** is in the down-dip direction of the orebody and the shortest range is in the cross-dip direction. Only the element of Sb is under this category.

Anisotropy ratios can also be calculated for all the elements by Equation (6.3) in Table 6.5. These ratios can help to analyse the spatial continuity of the elements. For this exercise, the ratios are calculated for each ellipse of Figure 6.14 by dividing the major radius of ellipse by its minor radius. For example, the anisotropy ratios of Zn (Figure 6.14) are calculated in Table 6.5.

Table 6.5: Formula used for calculation of the anisotropy ratios and its results for Zn concentration of the Western Mineralisation.

$$\textbf{Anisotropy ratio of each ellipse} = \frac{\textbf{Max. radius of the ellipse}}{\textbf{Min. radius of the ellipse}} \qquad \textbf{(6.3)}$$

$$\textbf{At SD ellipse} \rightarrow \frac{a}{b} = \frac{149.8}{109.7} = 1.4$$

$$\textbf{At SC ellipse} \rightarrow \frac{a}{c} = \frac{149.8}{27.2} = 5.5$$

$$\textbf{At DC ellipse} \rightarrow \frac{b}{c} = \frac{109.7}{27.2} = 4$$

The anisotropy ratios thus measure the ratios of the spatial correlation along the major radius to the spatial correlation along the minor radius on the corresponding plane. For instance, in the case of the SD ellipse, the anisotropy ratio of S is 4.6 indicating that the extent of spatial correlation of S along the major radius with direction of 015° from north and plunge of 25° is 4.6 times its minor radius with direction of 285° from north and plunge of 40°. For the SC ellipse, the anisotropy ratios of Pb, Cu, Cd, S, Fe and Zn are generally high. The highest value of 23 is observed for Pb. For the DC ellipse, the ratios show high values for Pb, Cu, Cd and Zn. The highest value is 11.53 for Pb in this ellipse. Bismuth, Sb, As and Ag have lower anisotropy ratios in comparison with those of the other elements.

6.7 Evaluation of similarity levels among 10 elements of the Western Mineralisation based on their radii in Figure 6.14

Cluster analysis was used for evaluation of the similarity levels. In this exercise, the values of a, b and c of each element in Figure 6.14[2] were used as input data into cluster algorithm. The method of average linkage and correlation coefficient distance was applied in the cluster algorithm using Minitab software. In this method, the 10 elements were subdivided into groups based on their radii in such a way that the full ranges of elements inside each group are similar. The result is shown in Figure 6.15.

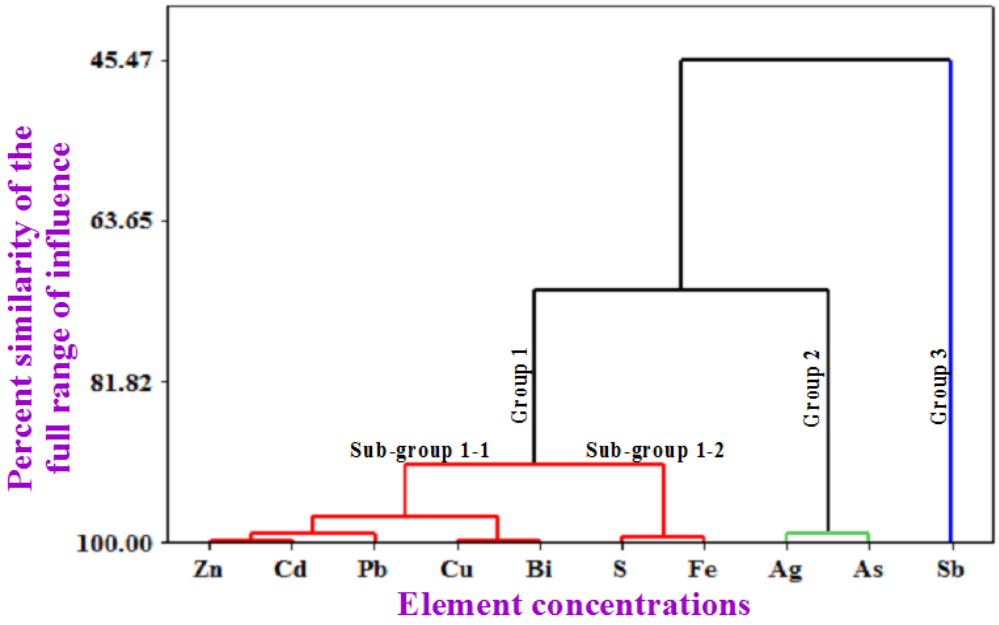

Figure 6.15: The similarity levels among 10 elements based on their radii of a, b and c within their Rose diagrams[3].

According to Figure 6.15, the first similarity level was divided into three following groups:

1. Group 1: Zn, Cd, Pb, Cu, Bi, S and Fe,
2. Group 2: Ag and As, and
3. Group 3: Sb.

In Figure 6.15, Sb has minimum similarity level (45.47 %) with the other elements of two groups, followed by Ag and As (group 2) that have 71.45 % similarity with the elements of group one. Ag and As are at one group possibly because their radii of ellipsoids are in the same category of a > c > b and Sb is separated from other elements by the cluster algorithm because its radius of ellipsoid (b > a > c) is in a different category to

[2] **Extracted from their three dimensional variogram models in Appendix B**
[3] **Their full ranges of the three- dimensional variogram models**

all the other elements. Group one is divided into two distinct sub-groups consisting of Zn-Cd-Pb-Cu-Bi and S-Fe at the 91.13 % similarity level.

6.8 Variogram validation (cross-validation) of the Western Mineralisation

The variogram models of the Western Mineralisation were validated using the cross-validation technique implemented in the Geostatistics for Windows software package. The method involves a back-estimation process where each sample is removed in turn from the data set and the value at the sample location is estimated from the remaining sample data by kriging using the fitted variogram model. By doing so, the exact errors of the estimations are known as both the true value and the estimate at sample locations. Statistics of the estimation errors can then be used to quantify the suitability of the variogram model and to adjust, if necessary, the parameters. For an unbiased estimator, a preliminary requirement for estimation, the average value of the estimation error[4] must be zero. If proper variogram model is used, the mean squared error[5] should be close to the mean kriging variance[6]. The cross-validation results for Zn are shown in Figure 6.16. Validation results for other variables (assay, minerals, rocks and geophysical data) are given in Appendix C.

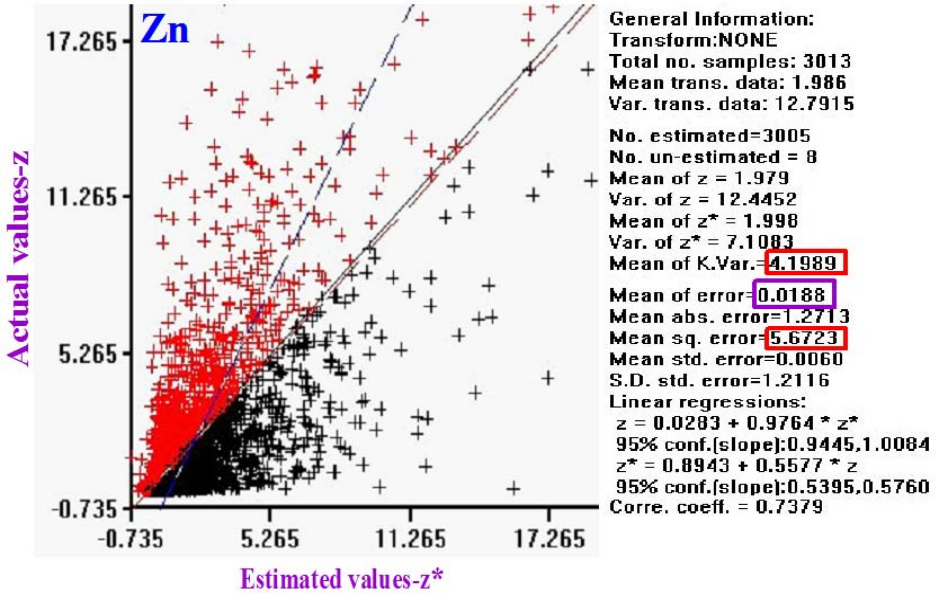

Figure 6.16: A scatter plot of the pairs of estimated values and actual values, the linear regressions and the statistical calculations for the example of Zn concentration of the Western Mineralisation.

[4] **Mean of error in Figure 6.16**
[5] **Mean sq. error in Figure 6.16**
[6] **Mean of K.Var. in Figure 6.16**

The following three groups of cross-validation analyses have been conducted in this research:

1. **Group 1**-geochemical elements: the cross-validations show the variogram models used are in general appropriate as very low average errors and moderate to high correlation coefficients (more than 50 %) between true values and kriging estimates are observed. It should be noted that the average errors for As, Bi, Sb, Ag and Cd are in ppm scale and in absolute terms they are actually very small,

2. **Group 2**-most geological variables and magnetic susceptibility: the results show relatively moderate to high correlation coefficients (between 30 % and 60 %) and small average errors. It should be noted because the values of minerals and rock types are estimated from visual inspection of drill cores, therefore sampling errors are expected to be high. This is reflected in the greater scatter in the cross-validation output, and

3. **Group 3**-some geological variables: the results show low correlation coefficients (less than 30 %), but still with very small average estimation error. Some examples in this group are visual estimates of the content of pyrite, arsenopyrite and red garnet (Appendix C). Their low correlation coefficients are possibly due to a low number of samples available for variogram modelling and poor value resolution (e.g. all values of a kind of mineral are between 1 % and 3 %). Sampling errors may also have significant effect on the outcome. Therefore, the estimations of group 3 are considered to be a rather subjective process and the use of geostatistics does not make them more objective. However, they may help improve subjective decisions and geological interpretation (Carras 2001).

6.9 Final variogram parameters used for estimation of a block model for the Western Mineralisation

After cross-validation, 43 variogram models are finalized which are to be used for the block estimation to be described in Chapters 7 and 8. For each variogram model, the following parameters are finalised:

6.9.1 Nugget variance (C_0) and other structural components of variance

For example, the variance terms for Pb are:

$$\mathbf{C_0 = 0.6\,(\%)^2}$$
$$\mathbf{C_1 = 3.4\,(\%)^2}$$
$$\mathbf{C_2 = 2.6\,(\%)^2}$$

6.9.2 The longest ranges of influence (a) for each variogram structure

For instance, a_1 and a_2 for Pb are:

$$\mathbf{a_1 = 30\,m}$$
$$\mathbf{a_2 = 304\,m}$$

6.9.3 The rotation angles of the three main axes against the coordinate system used

These are defined by three angles. Angle 1 is the rotation against the elevation axis to orientate the northing in the projected major axis direction (projected on the horizontal plane) of the variogram ellipsoid (15°). Angle 2 is the rotation against the rotated easting axis to orientate the northing in the true direction of the major axis of the ellipsoid (-25°). Angle 3 is the rotation against the major axis (the rotated northing) to orientate the easting in the intermediate axis direction of the ellipsoid (-40º).

6.9.4 Two anisotropy ratios

The two anisotropic ratios, together with the three rotation angles described above, define the directional anisotropy of the variogram model. Anisotropic ratio 1 is the ratio between the intermediate range and the longest range and ratio 2 is the ratio of shortest range against the longest range. For example, the anisotropic ratios 1 and 2 for Pb are calculated in Table 6.6 (Appendix B):

Table 6.6: Calculation of the anisotropic ratios 1 and 2 for Pb concentration.

The anisotropic ratio 1:	$\frac{a_{1,\text{Down-dip}}}{a_{1,\text{ Strike-plunge}}} = \frac{15.9}{30.5} = 0.52$ $\frac{a_{2,\text{Down-dip}}}{a_{2,\text{ Strike-plunge}}} = \frac{150.7}{304.3} = 0.49$ a_1 = The first range of influence a_2 = The second range of influence
The anisotropic ratio 2:	$\frac{a_{1,\text{Cross-dip}}}{a_{1,\text{Strike-plunge}}} = \frac{3.3}{30.5} = 0.11$ $\frac{a_{2,\text{Cross-dip}}}{a_{2,\text{Strike-plunge}}} = \frac{13}{304.3} = 0.04$ a_1 = The first range of influence a_2 = The second range of influence

6.10 Block Model

6.10.1 Orebody outline

The first step in the construction of block model is to define an orebody wireframe (skin) which is then filled with blocks that divide up the orebody. The orebody skin are constructed from orebody outlines defined on cross-sections based on drill hole projection on the cross-sections. During the 3D wireframe construction process, the Dijkstra algorithm method was selected in the Geostatistics for Windows as the algorithm ensure the surface reconstructed is optimal in the sense that the surface area is minimised (Xu & Dowd 2001).

6.10.2 Kriging parameters

Data search strategy and search parameters are also important for the successful implementation of a kriging estimation regime. In this research, the largest variogram range, together with the anisotropic parameters described above, are used to define the data search neighbourhood for the kriging estimation. For example, 304 m is used to define the search radius for the estimation of Pb as that is the largest range for the variogram for Pb. For discrete block representation, 4×4×4 points are used.

6.10.3 Block size determination

The use of appropriate block size is important for deriving a suitable block model to be used. If the block size is too large, the resolution of orebody representation will be too low, and to the contrary, if the block size is too small, the variation of estimated block values will be greatly reduced (over-smoothed). The determination of a suitable block size, however, is not an easy issue. From the geostatistical point of view, a suitable block size is ultimately determined by the sample spacing. From the mining operation point of view, the block size ideally should be identical to the actual selective mining unit to be used in the mining operation. The actual spatial continuity of the grad values also plays a part in the final decision. In the following section, it will try to find a suitable block size based only on geostatistics.

Kriging variance in this case can be used as an effective tool to derive a suitable block size. For smaller block size, correlations between samples and block will be lower and the kriging variance is expected to be higher. A suitable block size can be found by examining the variation of kriging variance against different block sizes. As a rule of thumb, a suitable block size will be one that has the smallest possible size under the condition that the kriging variance is reasonable compared with larger block sizes. The results of kriging variances against different block size for three elements are given in Table 6.7 and Figure 6.17 below. Based on these investigations, the block size of $20 \times 20 \times 10$ m (or the volume of 4000 m^3) is considered to be the most suitable.

Table 6.7: The selected discretisation grid, the corresponding volume and the mean value of kriging variance for three elements of Pb, Zn and Bi.

Discretisation grid (m)	Volume (m^3)	The mean value of kriging variance		
		Pb ($\%^2$)	Zn($\%^2$)	Bi (ppm^2)
5 ×5×10	250	3.49	8.11	951.11
10 ×10×10	1000	2.97	7.16	895.35
15 ×15×10	2250	2.72	6.36	847.79
20 ×20×10	4000	2.36	5.78	810.85
25 ×25×10	6250	2.31	5.32	780.7
30 ×30×10	9000	2.19	5	752.06
40 ×40×10	16000	2.1	4.52	714.48
50 ×50×10	25000	2.05	4.21	679.04

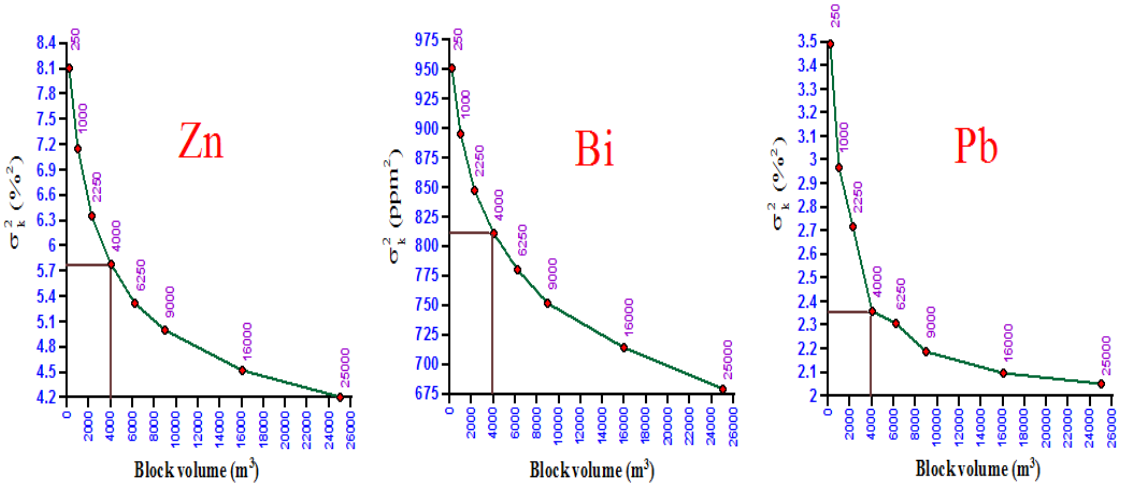

Figure 6.17: Visualisation of the mean value of kriging variance estimation versus different block volumes for Zn, Pb and Bi.

It is interesting to note that the average drilling spacing in the Western Mineralisation is about 50 m and it is unusual for a block model with block size smaller than half of the drilling spacing. This is only suitable for cases where the variogram shows a low nugget effect and large correlation range i.e. mineralisation with high grade continuity, such as the case for the Western Mineralisation. The block size of 20×20×10 m is also suitable in this case for the identification of geochemical halo pattern, spatial variation of minerals, rocks and geophysical features which will be discussed in Chapters 7 and 8. The 43 block model as defined will produce in total of 424 horizontal and vertical cross-sections cutting through the orebody at different elevation and directions. Those cross-sections will be examined in more detail in Chapters 7 and 8 for spatial variability of all the 43 variables concerned.

6.10.4 Optimal number of samples for kriging estimation

In general, fewer number of samples used for kriging will produce higher kriging (estimation) variance than greater number of samples, provided samples are all within the correlation range to the point to be estimated. However large number of samples will increase the computation cost and in some cases the improvement is negligible due to the screen effect of kriging. In this context, the number of samples to be used for kriging can be optimised. This can also be done by cross-validation. For this study, the cross-validations for the elements are run using 10, 20, 30, 40, 50, 60 and 70 numbers of samples. The average estimation errors for different cases are plotted against the number of

samples used, as shown in Figure 6.18 for some selected elements and Appendix D for all elements, where the optimal numbers are marked with red circles.

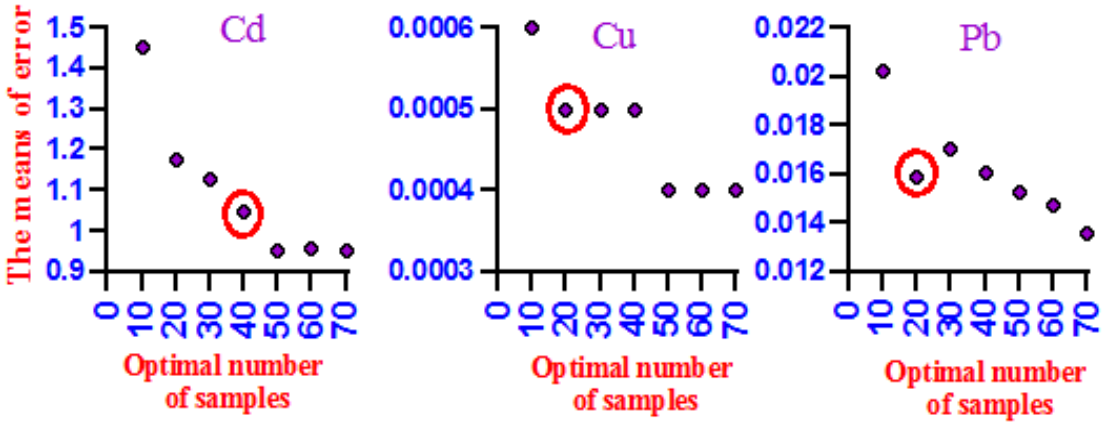

Figure 6.18: Average estimation errors versus the number of samples used for kriging for the elements of Cd, Cu and Pb.

6.10.5 The univariate ordinary kriging

The current study uses only linear geostatistics, in particular, univariate ordinary kriging, for all the estimations. Linear kriging is commonly referred to as the BLUE (Best Linear Unbiased Estimator) estimator. This is the most commonly used geostatistical estimation technique in the mining industry. More detailed discussions of the technique and other linear and non-linear techniques can be found in Armstrong (1998), hil s and Delfiner (1999), Goovaerts (1997), Kelkar (2002), Lloyd (2006), Olea (1999), Webster and Oliver (2007) and Yarus and Chambers (1994). Multivariate geostatistics is not used in the current study, although some multivariate statistics were discussed in Chapter 5. This is mainly due to the time constraint and the large number of variables involved. It could be a future research topic in its own right.

6.11 Summary

Variogram analysis is a very useful tool to help quantify the spatial correlation and spatial variations for the variables concerned in the current study. In this chapter, the geostatistical techniques were used to identify the anisotropic characteristics of the variables, the continuity of the spatial variations and the similarity analysis of the variables. A total of 136 directional variograms (three dimensional and down-hole) for 43 variables of the Western Mineralisation were calculated, modelled and cross-validated (Appendices B and C). The models were then used to construct the three-dimensional variogram models (ellipsoids) for all 43 variables. These models were used to help the

interpretation of geological, geochemical and geophysical data and will be used in the next chapters for kriging estimations.

Ten elements were selected to evaluate their degree of similarity based on their variogram parameters and their spatial anisotropic characteristics. The result showed that the 10 elements can be classified in three similar groups, including:

1. Group 1: Zn, Pb, S, Fe, Cu, Cd and Bi,
2. Group 2: Ag and As, and
3. Group 3: Sb.

The variogram parameters for Pb and Zn in the Western Mineralisation were compared with those of other similar significant Pb-Zn deposits and the result showed that Pb and Zn concentrations in the orebody of the Western Mineralisation have a higher degree of spatial correlation or greater degree of continuity. This indicates that application of a spatial correlation tool, such as geostatistics rather than the classical statistics in this case is a more appropriate choice for the modelling of the variables.

The variogram ranges of ten elements in the Western Mineralisation were also used to derive the optimal sampling grid for this mineralisation, which is found to be 22 m in the strike-plunge direction and 10 m in the cross-dip direction of the orebody. The analysis as described has not been performed before at Broken Hill or similar types of deposits. The study is the first to have comprehensive analyses of combined geological, geophysical and geochemical characteristics for an unmined orebody.

Suitable variogram models for all 43 variables were calculated, modelled and cross-validated to produce suitable models to be used in the kriging estimation. For a few minerals, such as pyrite, arsenopyrite and red garnet, appropriate variogram models could not be produced due to insufficient number of samples.

The kriging parameters for the linear estimation method chosen were also optimised. The optimal numbers of samples to be used for kriging were found by examining the kriging variance against the number of samples used. The optimal block size to be used to construct the block model for the deposit was found to be 20×20×10 m, which was calculated by examining the variation of kriging variance versus different block sizes.

CHAPTER 7

Spatial Geochemical Models for the Western Mineralisation

7.1 Introduction

The study of spatial models of mineral deposits based on archived data of drill core from mine sites enables geologists to recognise and evaluate the scale of spatial correlation of each type of mineralisation using geological, geochemical and geophysical information. Thus, exploration guidelines for similar deposits can be developed on the base of existing data and their quantitative statistical interpretation. In spatial geochemical models, element concentrations are treated as spatial variables i.e. their variations are location dependent. A spatial geochemical model of an orebody can present significant support to exploration geochemistry when it is used for identification of the following issues:

1. Geometrical properties of geochemical haloes (e.g. distribution, size, orientation, shape and dimension),
2. The spatial variability of geochemical haloes with depth in different cross-sections,
3. Separation of threshold[1] level from background and anomalous concentrations, and
4. Identification of zonation sequence in different directions.

In this study, Western Mineralisation drill cores provide a valuable opportunity to evaluate dispersion and zonation of the primary geochemical haloes and their geological and geophysical associations for this type of Zn and Pb mineralisation. Since the spatial geochemical model of the Western Mineralisation is derived directly from its mineralised samples at different depths, it provides useful information for future geochemical survey. This approach is widely used in mining operations for the estimation of in situ mineral resource/reserve in relation to grade-tonnage of the orebody. However, it is still a rare practice to use the spatial models for the appraisal of zonation patterns of the orebody. More details concerning the geochemical halo zoning can be found in Beus and Grigorian (1977), Chen, Huang and Liang (2008), Chen and Zhao (1998), Grigorian (1974), Gundobin (1984), Huang and Zhang (1989), Kashirtseva (1967), Lawrie and Hinman (1998), Liu and Xu (1995) and Walters (1998).

[1] **Minimum anomalous value**

The specific geochemical characteristics of the Western Mineralisation may be controlled by its structural environment (dislocations, faults and fractures) and formation of strike equivalent Broken Hill deposit. However, the different orebodies at the Broken Hill deposit may be generated and controlled by different geological and geochemical parameters with different scaling properties. For example, based on this study it is difficult to define a universal zonation halo system valid for the entire Broken Hill deposit. The main purposes of spatial geochemical modelling in this chapter are:

1. Construction of cross-sections for evaluating geochemical halo patterns of Pb, Zn, As, Cu, Fe, S, Sb, Bi, Ag and Cd in different directions,
2. Separation of the concentration range of threshold values from its background and anomalous levels in the orebody of the Western Mineralisation,
3. Quantitative comparison of the dimensional distribution patterns, orientation and anisotropies of the 10 geochemical haloes in order to determine zonation sequence of the orebody, and
4. Identification of pathfinder (indicator) elements associated with Pb and Zn ore of the Western Mineralisation.

7.2 Construction of cross-sections for evaluating geochemical halo patterns

A zonation of a geochemical halo has a spatial nature and vectorial context that can be defined by the three following parameters:

1. Dimension (space),
2. Direction, and
3. Element concentration.

The halo zonation can be a distinct spatial representation of the effects of the ore-bearing solution (Beus & Grigorian 1977) plus any effects of secondary redistribution and remobilisation (e.g. metamorphism and deformation). In order to study of the geochemical haloes and the zonation patterns of the steeply dipping mineralised zone of the Western Mineralisation, the following types of sections (Beus & Grigorian 1977) were constructed inside the 3D block models of the 10 elements:

1. **Transverse sections** to show the variation of halo patterns in the horizontal sections (Figure 7.1),

2. **Longitudinal sections** to show the variation of halo patterns in north-south vertical sections along the strike of the mineralised zone (Figure 7.2), and
3. **Axial sections**[2] to show the variation of halo patterns along east-west vertical sections (Figure 7.3).

For identification of transverse zonation, the spatial models of the 10 element concentrations of the Western Mineralisation were intersected by transverse (horizontal) directions at an elevation of 10218 m close to the surface and an elevation of 9848 m next to the bottom of the 3D mineralised sample locations and two cross-sections between them at 10078 m and at 9958 m (Figure 7.1).

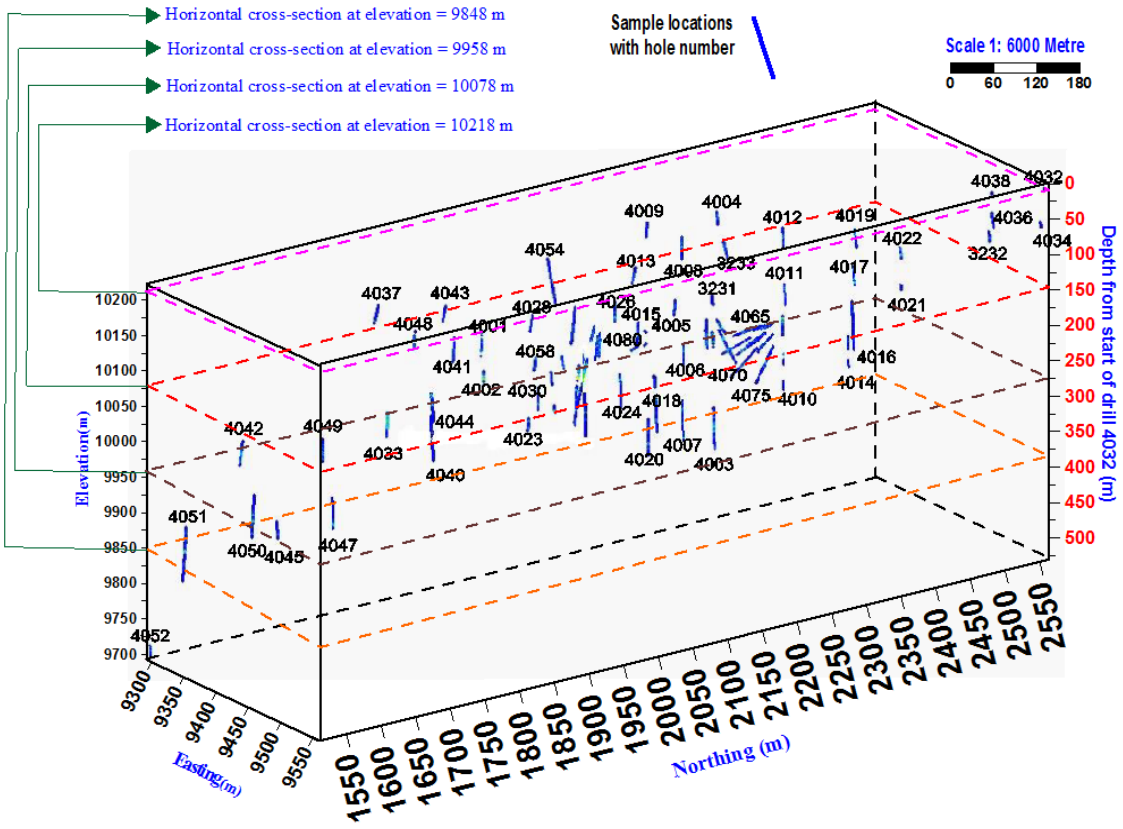

Figure 7.1: The position of four transverse (horizontal) sections (dashed red rectangles) and locations of the mineralised drill core intersections.

For demonstrating of the longitudinal zonation, 3D block models of the 10 element concentrations were cut vertically along north-south directions by two cross-sections at east = 9357 m and east = 9467 m. In general, two longitudinal sections were mapped for each of the spatial models (Figure 7.2).

[2] **Vertical zonation**

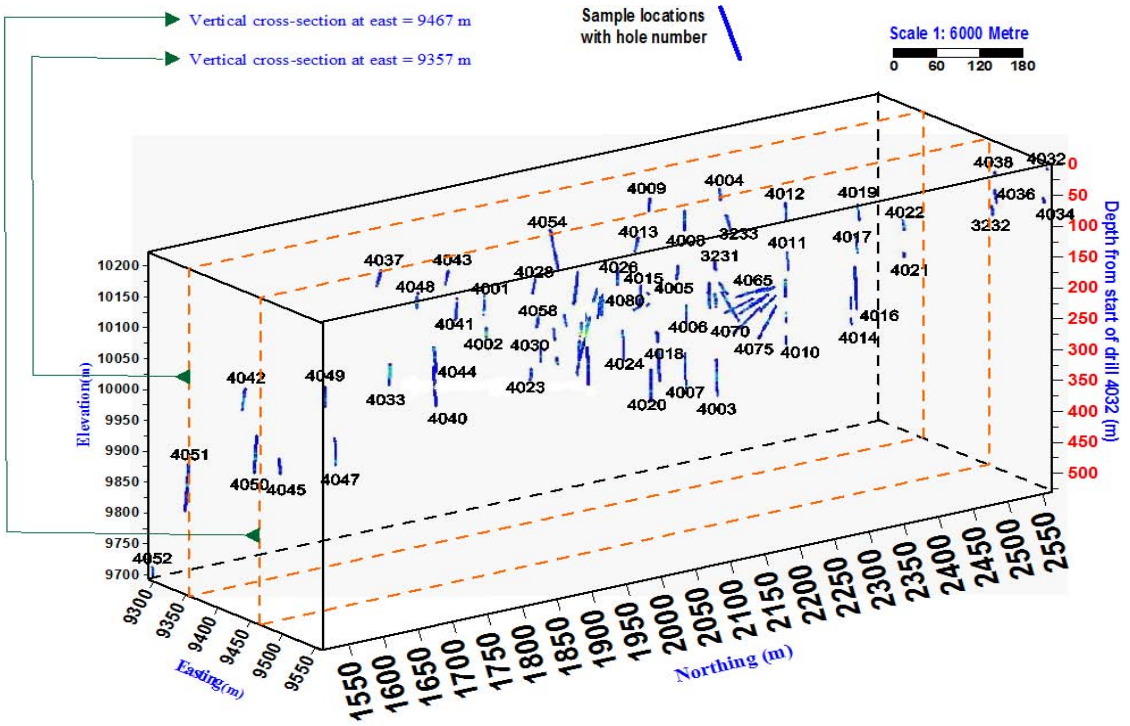

Figure 7.2: The mineralised sample locations and the position of two longitudinal sections (dashed orange rectangles).

For identification of the axial zonation, 3D block models were cut vertically in east-west direction at north = 1639 m and north = 2109 m (Figure 7.3).

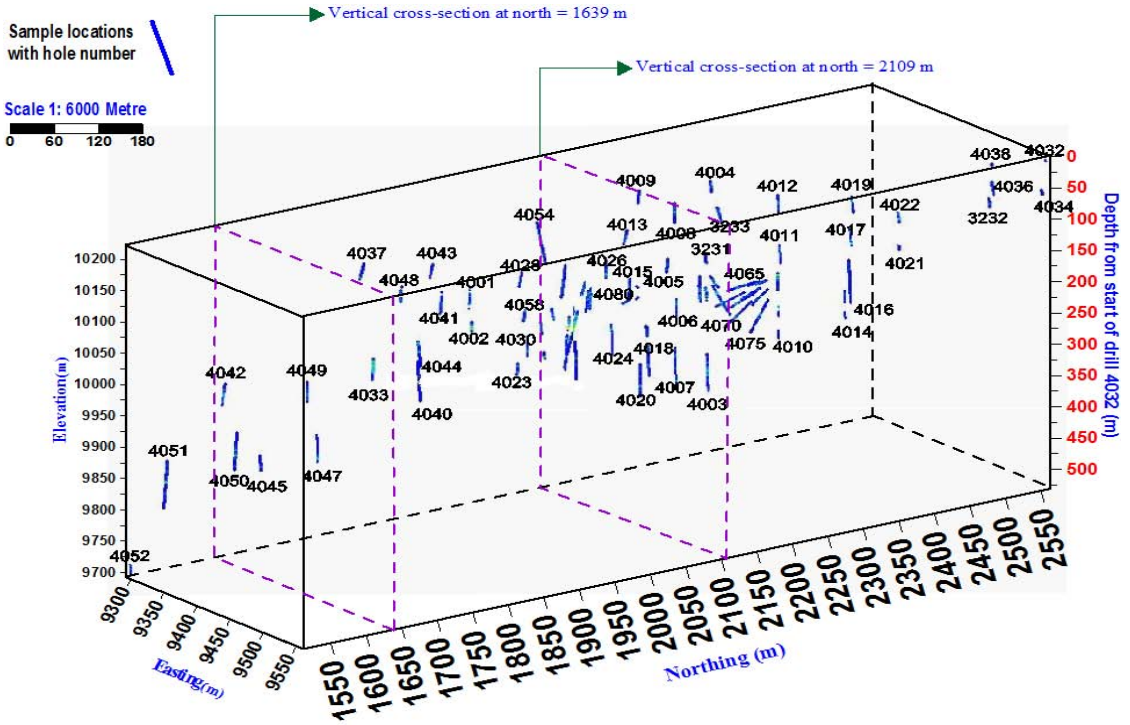

Figure 7.3: The position of two axial sections and the locations of intersection of mineralisation (dashed violet rectangles).

The positions of the cross-sections inside the 3D block model were selected so that they intersect the maximum number of core samples and also to be located at an appropriate distance from each other. It should be noted that all variogram parameters of the three-dimensional block models were presented in Appendix B where 3D block models were constructed and can be used to generate cross-sections in any additional directions of interest for further interpretation.

7.3 Separation of threshold values from background and anomalous levels

An important aspect in exploration geochemistry is the determination of threshold levels for pathfinder elements. Pathfinder elements may appear as principal constituents of a mineral (e.g. Pb in galena) or in the form of solid solution in a mineral (e.g. Ag in galena). In general, the pathfinder elements must be measured economically and highly accurately and precisely (Graham et al. 2009). Furthermore, a pathfinder element (Levinson 1974, pp.54-55; Peters 1987, p.403) for Pb and Zn within those cross-sections should be evaluated for the following characteristics:

1. It should show a broader and wider dispersal halo or higher mobility relative to elements representing the ore (i.e. Pb and Zn haloes in the Western Mineralisation; DMTC-The Delta Mine Training Center 2009; Taylor et al. 1984). This should be examined in different cross-sections because the extent of each element may vary considerably according to the various directions and locations of mineralisation,

2. The structural distribution of the pathfinder elements should be similar to and coherent with the Pb and Zn haloes,

3. The concentration of pathfinder elements should be determined with reference to anomalism, threshold and background levels, and

4. The geometrical patterns of pathfinder element distribution should be determined for different directions and depth.

There are several previous case studies for separation of geochemical anomaly from threshold and background level using aspatial[3] statistical method (classic statistics) and spatial statistical methods (geostatistics) or a combination of them, including probability graphs, univariate and multivariate analysis (Govett et al. 1975; Grigorian &

[3] **Non-spatial**

Ziaii 1997; Miesch 1981; Sinclair 1974, 1976; Stanley 1988; Stanley & Sinclair 1989), fractal concentration-area method (Cheng 1999; Cheng, Agterberg & Ballantyne 1994; Cheng, Agterberg & Bonham-Carter 1996; Cheng, Xu & Grunsky 2000), the multifractal inverse distance weighted (Lima et al. 2003), the element concentration-distance method (Li, Ma & Shi 2003) and finally, spatial statistical methods such as kriging, moving average procedures and spatial factor analysis (Grunsky & Agterberg 1988).

The spatial methods (geostatistical framework) such as moving averages and kriging have largely overtaken non-spatial methods because of consideration of sample size, sample locations, the scale of structural relationship of intrinsic variables and the degree of spatial continuity of mineralisation as well as their anisotropism.

For determination of local or regional threshold, the following situations can be considered, depending on the number and location of samples within the mineralisation or non-mineralisation area and their amount of concentrations:

1. The first situation arises in regional geochemical prospecting for detecting secondary haloes (e.g. in soil and regolith). In this situation, most often the number of samples representing the regional background concentration is greater than the anomalous samples and recognition of a reliable regional anomalous grade is a very difficult practice. The regional background levels are usually spread broadly over an area and reflect regional geological processes with a wide-range of correlations. In this case, it would be necessary to separate the regional threshold concentration from a large number of background grades and to define this as maximum deviation from the regional background contents, and

2. Unlike the above situation, when a large number of samples are extracted from a mineralisation zone at different depths, the local threshold level should be separated from a large number of local anomalous samples. In this case, the local threshold level is deduced to be the minimum local anomalous content appearing in a mineralisation zone and the local anomalous grades are confined to the mineralised samples with a narrow-range of correlations. For this situation, the application of the spatial statistical methods is more efficient.

For determination of local threshold in the Western Mineralisation, a similar concept of concentration-area (Cheng, Agterberg & Ballantyne 1994) was integrated with a

3D kriged block model for each element. The combination of concentration-area and 3D kriged block model provide a very powerful and robust technique for geochemical anomaly separation and for minimising misclassification of threshold concentrations and background levels.

7.3.1 Procedure of separating threshold from background in the Geostatistics for Windows software

Figures 7.4 to 7.7 show 10 geochemical haloes of the Western Mineralisation in different sections with a colour index distinguishing background level and threshold grade. The method used for detection of threshold level relies on adjusting the colour index of the Geostatistics for Windows software between minimum concentration (blue area) and a relative maximum concentration (red area) for each of the 10 elements. In this method, the relative maximum concentration of each element is changed manually in the colour index until the red area becomes the largest area (Figures 7.4 to 7.7). In this situation, a slightly increase or decrease of the relative maximum concentration causes an extreme reduction of the red area. The largest red area for each of the 10 elements was obtained from implementation of the above procedure at eight different cross-sections to identify the commonest threshold level among them.

In colour indices of Figures 7.4 to 7.7, the minimum concentration of elements are not zero except for Pb, Zn and Cu in the Western Mineralisation and this suggests the elements will have larger dispersal haloes if geochemical sampling or the drilling network spread is broader in the vicinity of the Western Mineralisation. Although the local threshold level can be specified to the value of red colour of each element in Figures 7.4 to 7.7; however, because the regional threshold concentration is always lower than the local threshold concentration, so a range of concentrations between green and red (in colour index of Figures 7.4 to 7.7) were considered arbitrarily as the threshold concentrations range for each element, rather than one specific concentration.

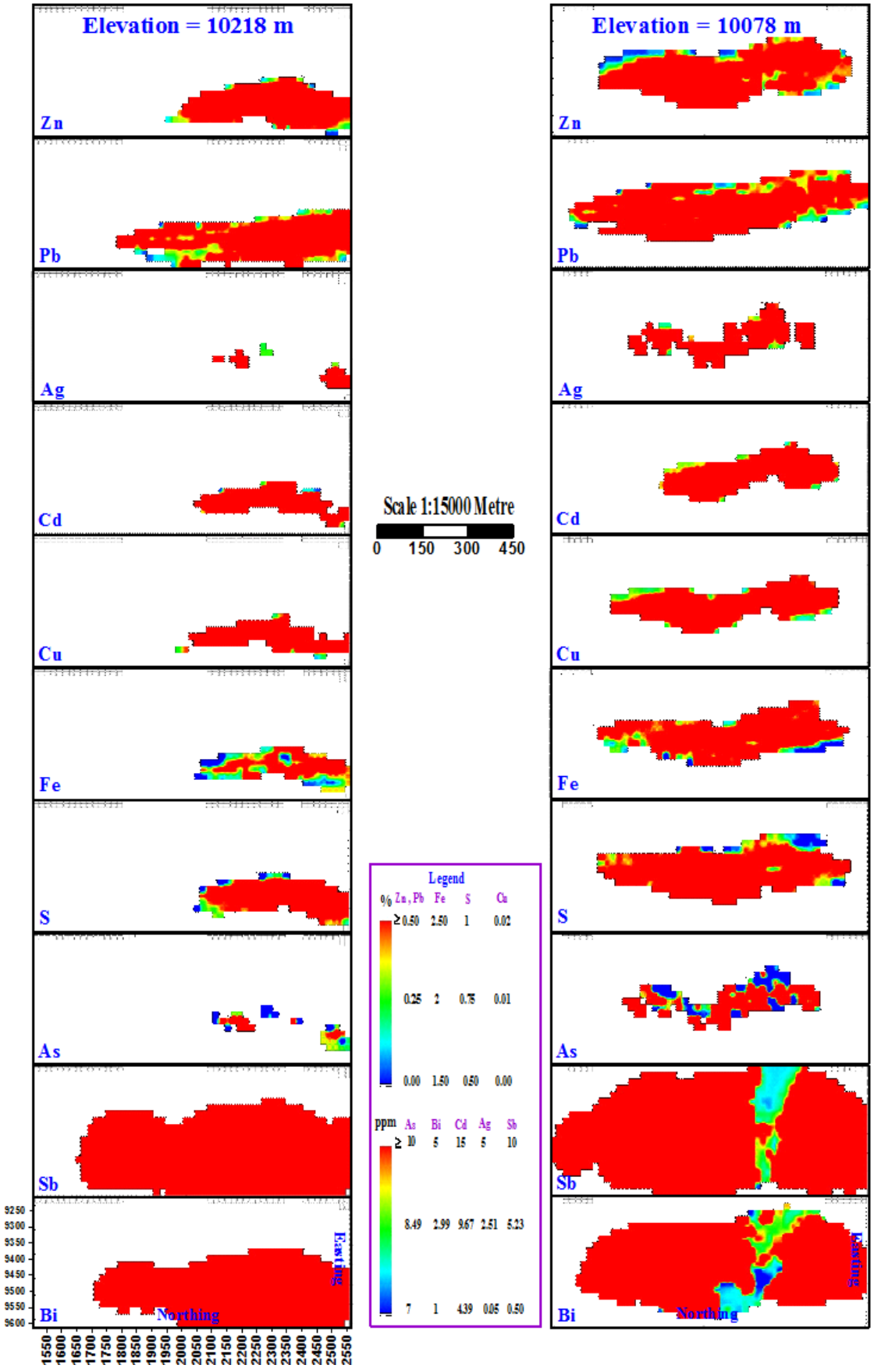

Figure 7.4: The transverse sections of 10 geochemical haloes between background and local threshold levels (elevation=10218 m and elevation=10078 m).

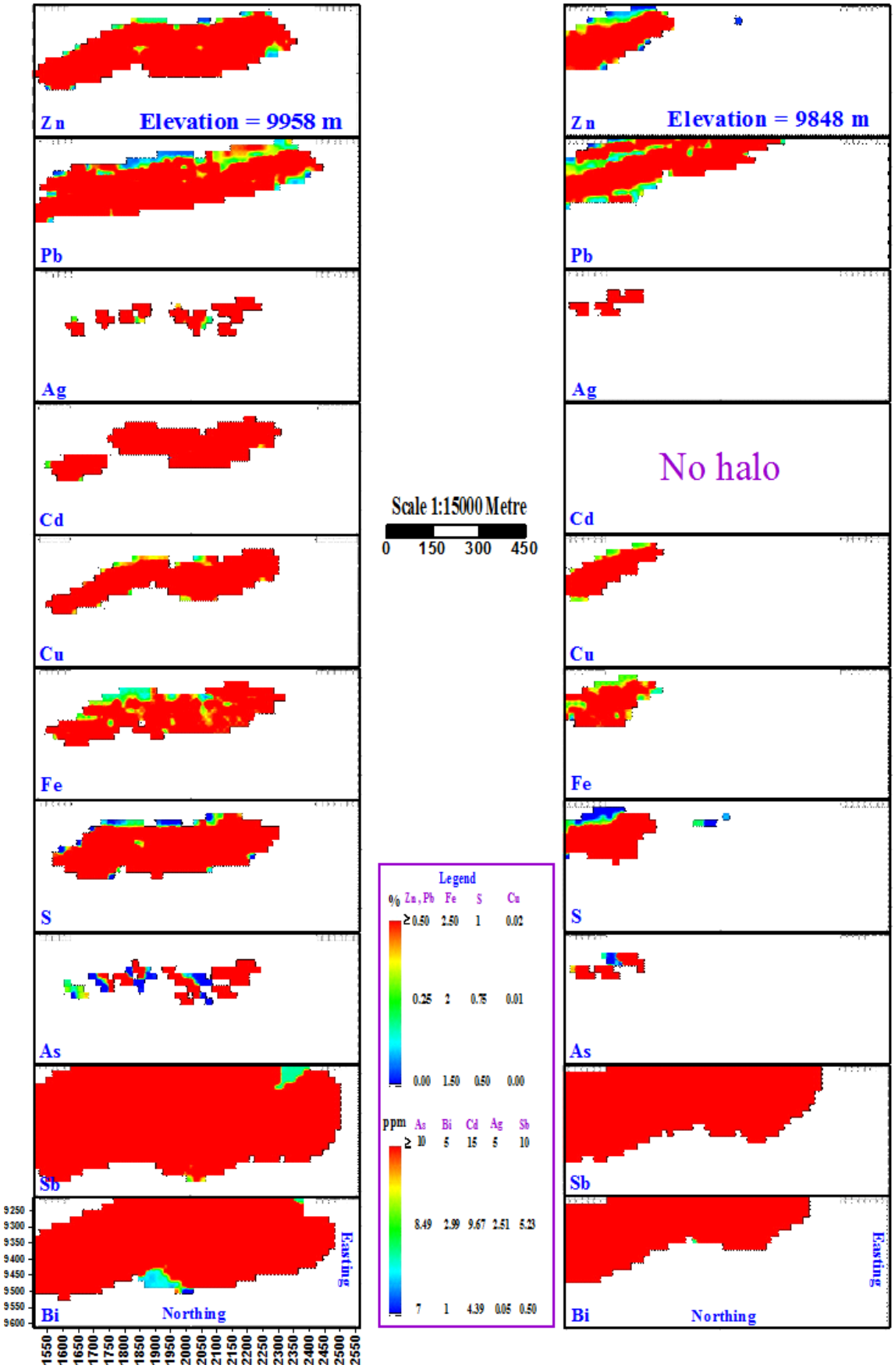

Figure 7.5: The transverse sections of 10 geochemical haloes between background and local threshold levels (elevation=9958 m and elevation=9848 m).

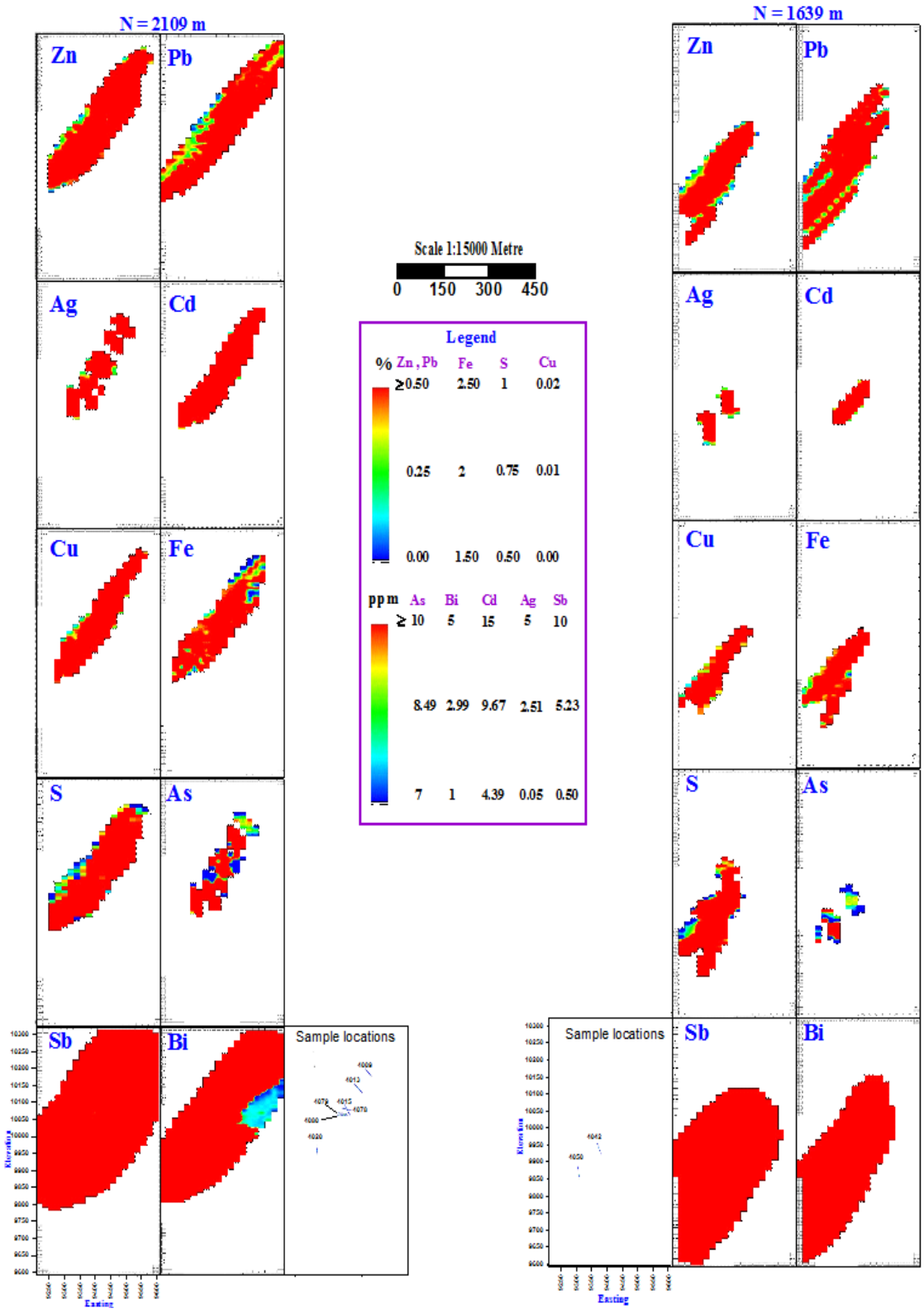

Figure 7.6: The E-W axial sections of 10 geochemical haloes between background and local threshold levels at N=2109 m and N=1639 m.

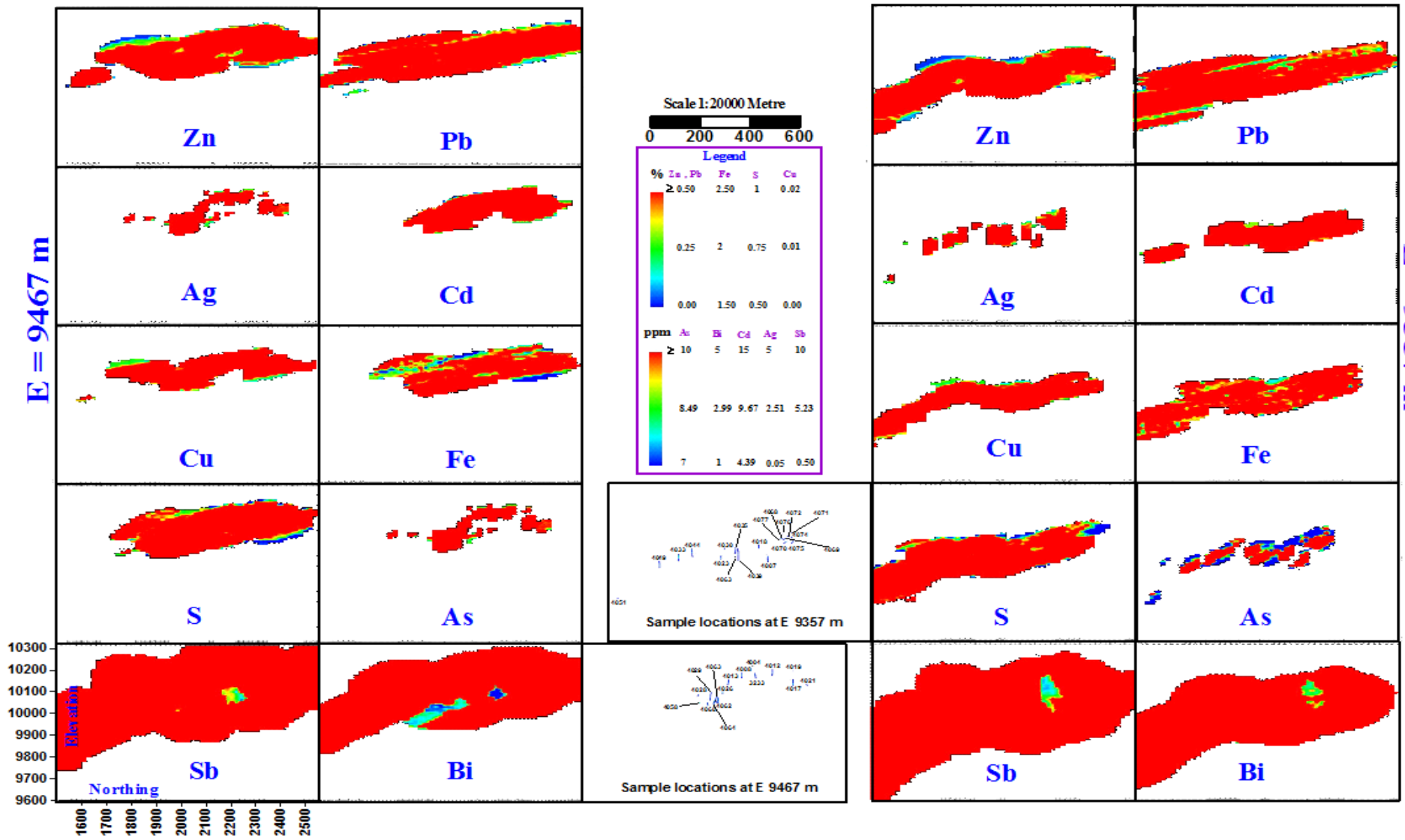

Figure 7.7: The N-S longitudinal sections of 10 geochemical haloes between background and local threshold levels at E=9467 m and at E=9357 m.

The geochemical haloes in Figure 7.6 are characterised by an approximately 40° dip toward the west. Figure 7.7 show that the geochemical haloes have a southward-dip of about 25°. Although all the 10 geochemical haloes of the Western Mineralisation are related to common geological features, geochemical environment, structure and lithostratigraphy, they delineated various distinct intensifications and expansion dispersal halo patterns with changes of depth and distance (Figures 7.4 to 7.7).

Antimony and Bi delineate maximum and most pronounced geochemical haloes in all cross-sections. In addition, the orientation and distribution shape of Sb and Bi haloes display a good conformity with the shape of Pb and Zn haloes. Therefore, they can be considered as possible pathfinder elements for exploration of Pb and Zn in the Western Mineralisation and similar types of mineralisation. Although there is a loose correlation between lode horizon rocks (quartz-gahnite, quartz-garnet, plumbian orthoclase, tourmalinite etc), such a correlation could not be determined in this statistical study. These lode horizon rocks are commonly interpreted as proximal to sulphides and their presence demonstrates a near miss. However, this may be flawed and the use of predictor elements such as Sb and Bi may be more fruitful.

7.4 Quantitative comparison of the geometrical characteristics of the geochemical halo patterns at different cross-sections of the Western Mineralisation

The geometrical dimensions of the 10 analysed elements within the Western Mineralisation are distinctive and can be compared quantitatively with each other. For this purpose, the maximum width and maximum length of each geochemical halo were measured and their anisotropy ratios were calculated for each cross-section (Figures 7.4 to 7.7). The anisotropy ratio for each geochemical halo was calculated from the ratio of the maximum length of the geochemical halo to its maximum width. The maximum length and maximum width were measured in that part of the threshold ranges of each element that was marked by colours in the range from green to red.

In Figures 7.4 to 7.7, a few geochemical haloes such as As and Ag display discontinuous dispersal haloes in their images. In these cases, the maximum length of their haloes was measured in exactly the same way as continuous geochemical haloes regardless of the gaps in their haloes. This is mostly because the need to understand the maximum

dispersion and absolute distance that the elements are able to migrate and disperse within a mineralisation zone.

7.4.1 Geometrical characteristics of transverse (horizontal) zoning haloes at different elevations (or depths of the orebody).

The information on Tables 7.1 and 7.2 are important exploration guides for identifying sequences of the zonation of haloes along depth of the orebody, tracking primary and secondary geochemical haloes of Pb and Zn sulphide ore similar to the Western Mineralisation. According to those Tables, the following general sequence of geochemical zonation (7.1) can be concluded from around the Western Mineralisation or on non-mineralised rocks [left elements in geochemical zonation (7.1)] to the centre of mineralisation zone [right elements in geochemical zonation (7.1)] in the Western Mineralisation:

Sb - Bi – Pb - Zn - (Cu, Cd, Fe, S) - (Ag, As) **(7.1)**

The sequence of elements inside the parentheses of geochemical zonation (7.1) may change with the depth of mineralisation.

Table 7.1: Maximum lengths, maximum widths and anisotropy ratios on the transverse sections at different elevations (Figures 7.4 and 7.5).

Elevations	Transverse sections	Length (m)	Width (m)	Anisotropy ratio
10218 m	Sb	900	300	3.00
	Bi	855	240	3.56
	Pb	780	165	4.73
	Zn	600	165	3.64
	Cu	585	120	4.88
	Cd	510	105	4.86
	Fe	495	120	4.13
	S	495	135	3.67
	Ag	450	67.5	6.67
	As	435	75	5.80
10078 m	Sb	1050	375	2.80
	Pb	990	180	5.50
	Bi	960	300	3.20
	S	840	180	4.67
	Zn	840	180	4.67
	Fe	840	135	6.22
	Cu	750	135	5.56
	As	660	135	4.89
	Ag	615	135	4.56
	Cd	585	150	3.90
9958 m	Sb	990	360	2.75
	Bi	975	285	3.42
	Pb	945	165	5.73
	Zn	855	180	4.75
	Fe	780	165	4.73
	Cd	765	142.5	5.37
	Cu	765	135	5.67
	S	750	165	4.55
	As	630	120	5.25
	Ag	630	105	6.00
9848 m	Sb	840	300	2.80
	Bi	795	255	3.12
	Pb	735	195	3.77
	Zn	360	157.5	2.29
	Fe	315	142.5	2.21
	Cu	315	120	2.63
	S	300	135	2.22
	Ag	255	78	3.27
	As	240	45	5.33
	Cd	No halo	No halo	No halo

Table 7.2: The sequence of geochemical haloes based on their maximum lengths, maximum widths and anisotropy ratios resulted from Table 7.1.

Zonation sequence along the transverse sections	Elevation	Maximum lengths
	10218 m	Sb > Bi > Pb > Zn > Cu > Cd > Fe = S > Ag > As
	10078 m	Sb > Pb > Bi > S = Zn = Fe > Cu > As > Ag > Cd
	9958 m	Sb > Bi > Pb > Zn > Fe > Cd = Cu > S > As = Ag
	9848 m	Sb > Bi > Pb > Zn > Fe = Cu > S > Ag > As
	Elevation	Maximum widths
	10218 m	Sb >Bi > Pb = Zn > S > Cu = Fe > Cd > As > Ag
	10078 m	Sb > Bi > Pb = Zn = S > Cd > Fe = Cu = As = Ag
	9958 m	Sb > Bi > Zn > Pb = Fe = S > Cd > Cu > As > Ag
	9848 m	Sb > Bi > Pb > Zn > Fe > S > Cu > Ag > As
	Elevation	Anisotropy ratios
	10218 m	Ag > As > Cu > Cd > Pb > Fe > S > Zn > Bi > Sb
	10078 m	Fe > Cu > Pb > As > S = Zn > Ag > Cd > Bi > Sb
	9958 m	Ag > Pb > Cu > Cd > As > Zn > Fe > S > Bi > Sb
	9848 m	As > Pb > Ag > Bi > Sb > Cu > Zn > S > Fe

Figure 7.8 shows the results of Tables 7.1 to 7.2.

- **Maximum length**

According to Figures 7.8a, b, c, d, group (i) includes elements of Sb, Bi and Pb with greater lengths than groups (ii) and (iii). Group (ii) consists of Zn, Cu, S and Fe with greater lengths than group (iii) which contains As and Ag. Apart from Figure 7.8b, Cd can be attributed to group (ii).

- **Maximum width**

According to Figures 7.8e, f, g, h, elements of group (i) have greater widths and wider distribution relative to the elements of group (ii).

- **The anisotropy ratios**

The anisotropy ratios in Figures 7.8i, j, k, l compare the amount of dispersion of each element in two directions. In Figures 7.8i, j, k, l, Sb and Bi have relatively constant anisotropy ratios at four elevations. The anisotropy ratio of Sb varies between 2.75 and 3 and for Bi between 3.12 and 3.56. Accordingly, Sb and Bi are showing very low anisotropy ratios at all elevations and this highlights their greater dispersion within and around the Western Mineralisation in all directions and depths relative to other elements. At elevation 9848 m, Pb, Zn, Cu, S, Fe and Ag show a much lower anisotropy ratio relative to other elevations. This is because the maximum lengths of geochemical haloes are highly reduced at this depth while their maximum widths only vary a little.

- **Pathfinder elements**

In Figures 7.8a, c, d, e, f, g, h, at all elevations, Sb and Bi display a greater length and width relative to Pb and Zn. At elevation 10078 m (Figures 7.8b and 7.8f), Sb shows higher length and width relative to Pb and Zn and Bi larger dispersion than Zn; however, in Figure 7.8b, Bi shows shorter length relative to Pb.

According to Figures 7.8a to 7.8h, Sb and Bi can be considered as geochemical pathfinders for the Western Mineralisation and similar Pb and Zn ores. By contrast, the amount of length and width of other elements is between moderate and small and they show shorter dispersion in comparison with haloes of Pb and Zn. This situation reduces appreciably their effectiveness and the reliability of their applications as geochemical pathfinders of the respective type of mineralisation. The threshold concentrations of Bi within the mineralisation zone in the Western Mineralisation are estimated to be between 3 and 5 ppm and for Sb, a range between 5.23 and 10 ppm is suggested. Figures 7.8a to 7.8h suggest that in lithogeochemical surveys of Pb and Zn mineralisation targets similar to the Western Mineralisation, the priority should be given to detecting threshold content of Sb and Bi or additive of Sb and Bi (Sb+ Bi) or composite (multiplicative) haloes (Sb × Bi) in surface sampling.

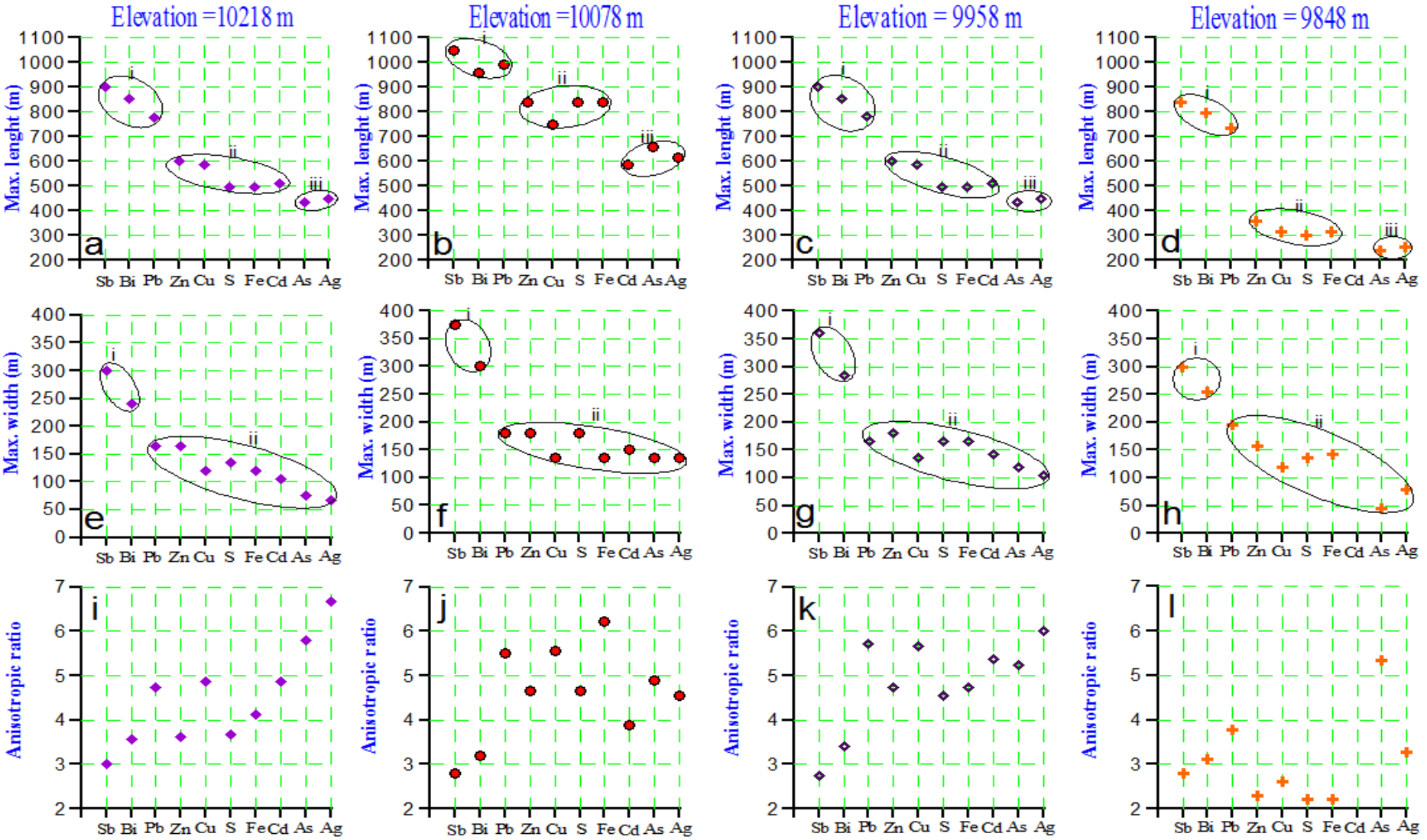

Figure 7.8: Comparison of maximum lengths, maximum widths and anisotropy ratios on the transverse sections at different elevations.

The composite and additive haloes intensify the extent of geochemical haloes and present closer correlations with the structure of the mineralisation relative to monoelement haloes. The application of multi-element haloes is more efficient in the mapping of weak geochemical anomalies particularly, in superficial geochemical fingerprints (Beus & Grigorian 1977). The multi-element haloes are more robust against random and analytical sampling errors and improve the contrast of halo zoning reliability and the geochemical interpretation (Beus & Grigorian 1977). Another important exploration guide for Western Mineralisation type ore is Sb and Bi in the sequence of transverse zonation.

7.4.2 Geometrical characteristics of the axial zoning haloes

Table 7.3: Maximum lengths, maximum widths and anisotropy ratios on the E-W axial sections at N = 2109 m and N = 1639 m (Figure 7.6).

North	E-W axial sections	Length (m)	Width (m)	Anisotropy ratio
2109 m	Sb	630	330	1.91
	Bi	630	240	2.63
	Pb	615	135	4.56
	Zn	525	135	3.89
	Cu	480	105	4.57
	S	465	135	3.44
	Fe	465	120	3.88
	Cd	435	105	4.14
	Ag	345	105	3.29
	As	330	90	3.67
1639 m	Bi	600	240	2.50
	Sb	570	300	1.90
	Pb	555	180	3.08
	Zn	420	150	2.80
	S	360	150	2.40
	Cu	315	105	3.00
	Fe	315	135	2.33
	As	195	60	3.25
	Cd	180	60	3.00
	Ag	180	90	2.00

Table 7.4: The sequence of geochemical haloes based on maximum lengths, maximum widths and anisotropy ratios resulted from Table 7.3.

Zonation sequence along the axial sections	North	Maximum lengths
	2109 m	Sb = Bi > Pb > Zn > Cu > S = Fe > Cd > Ag > As
	1639 m	Bi > Sb > Pb > Zn > S > Cu = Fe > As > Cd > Ag
	North	Maximum widths
	2109 m	Sb > Bi > Pb = Zn = S > Fe > Cu = Cd =Ag > As
	1639 m	Sb > Bi > Pb > Zn = S > Fe > Cu > Ag > As = Cd
	North	Anisotropy ratios
	2109 m	Cu > Pb > Cd > Zn > Fe > As > S > Ag > Bi > Sb
	1639 m	As > Pb > Cu > Cd > Zn > Bi > S > Fe > Ag > Sb

Figure 7.9 show the results of Tables 7.3 and 7.4.

- **Maximum lengths**

In Figures 7.9a and 7.9b, group (i) comprises Sb, Bi and Pb with greater lengths than groups (ii) and (iii). Group (ii) contains Zn, Cu, S and Fe with greater lengths than group (iii) which consists of As and Ag. Cadmium can be attributed to either group (ii) in Figure 7.9a or group (iii) in Figure 7.9b.

- **Maximum widths**

In Figures 7.9c and 7.9d, group (i) includes Sb and Bi with greater widths than group (ii).

- **Anisotropy ratios**

Figures 7.9e and 7.9f show that the anisotropy ratios of Sb and Bi are lower than other elements. Hence, the anisotropic ratio of Sb is 1.90 and for Bi, the anisotropy ratios vary between 2.50 and 2.63. This means distribution of Sb and Bi occurs more easily and is larger than the other eight elements inside and around the mineralisation zone in the Western Mineralisation.

- **Pathfinder**

According to Figures 7.9a, b, c, d the elements of Sb and Bi represent greater spreading relative to other elements. Thus, Sb and Bi can be regarded as geochemical pathfinder for the Western Mineralisation.

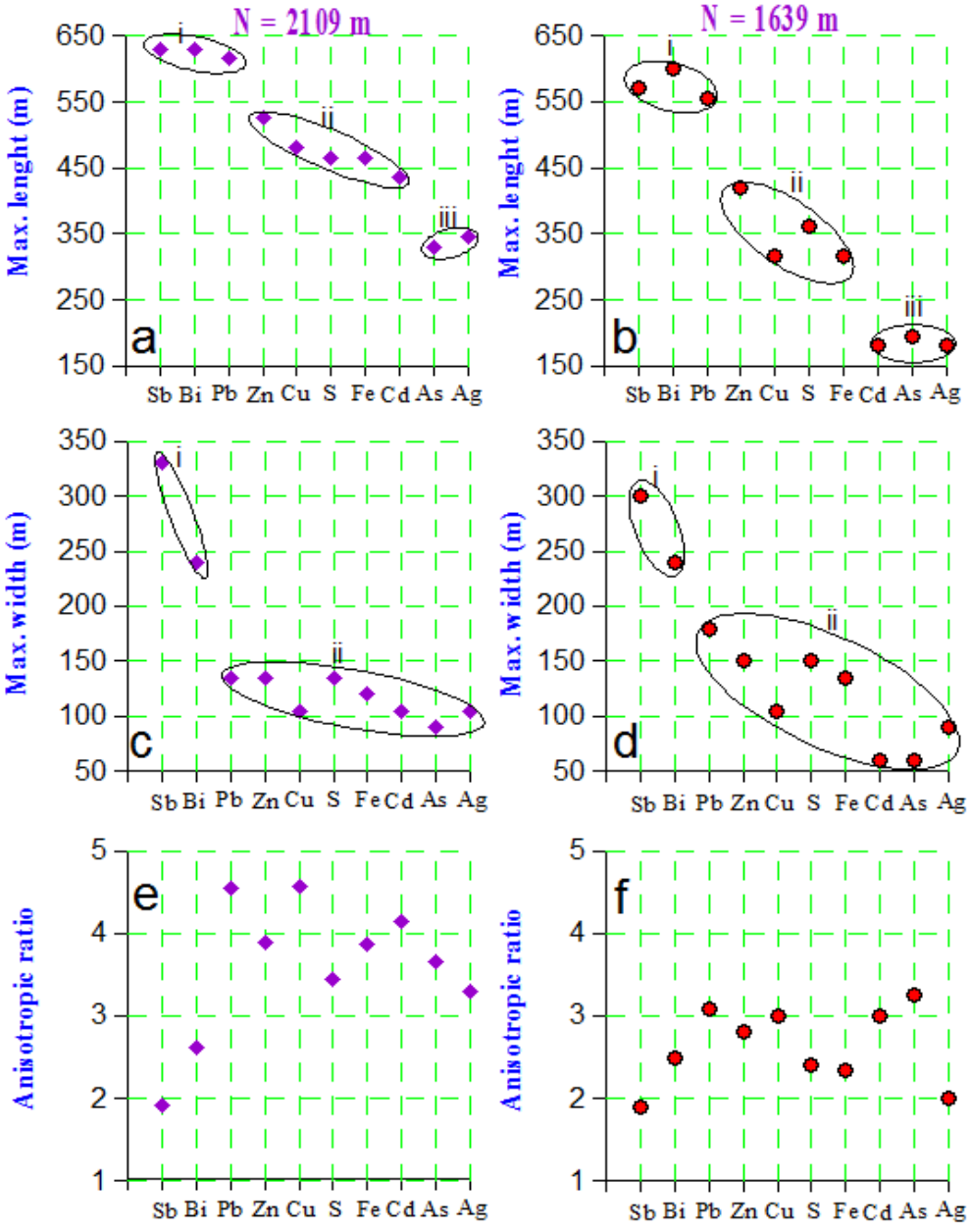

Figure 7.9: Comparison of maximum lengths, maximum widths and anisotropic ratios on the E-W axial sections at N=2109 m and N=1639 m.

7.4.3 Geometrical characteristics of the longitudinal zoning haloes

Table 7.5: Maximum lengths, maximum widths and anisotropy ratios on the N-S longitudinal sections at E = 9467 m and E = 9357 m (Figure 7.7).

East	N-S longitudinal sections	Length (m)	Width (m)	Anisotropy ratio
9467 m	Sb	1100	440	2.50
	Bi	1100	360	3.06
	Pb	1060	200	5.30
	Zn	1000	200	5.00
	S	840	220	3.82
	Cu	840	140	6.00
	Fe	840	200	4.20
	Cd	680	160	4.25
	As	660	100	6.60
	Ag	660	100	6.60
9357 m	Sb	1120	480	2.33
	Bi	1080	340	3.18
	Pb	1080	260	4.15
	Zn	1000	200	5.00
	Cu	960	140	6.86
	Fe	940	220	4.27
	S	940	280	3.36
	Cd	880	120	7.33
	As	640	100	6.40
	Ag	600	100	6.00

Table 7.6: The sequence of geochemical haloes based on maximum lengths, maximum widths and anisotropy ratios resulted from Table 7.5.

Zonation sequence along the longitudinal sections	East	Maximum lengths
	9467 m	Sb = Bi > Pb > Zn > S = Cu = Fe > Cd > As = Ag
	9357 m	Sb > Bi = Pb > Zn > Cu > Fe = S > Cd > As > Ag
	East	Maximum widths
	9467 m	Sb > Bi > S > Pb = Zn = Fe > Cd > Cu > As = Ag
	9357 m	Sb > Bi > S > Pb > Fe > Zn > Cu > Cd > As = Ag
	East	Anisotropy ratios
	9467 m	As = Ag > Cu > Pb > Zn > Cd > Fe > S > Bi > Sb
	9357 m	Cd > Cu > As > Ag > Zn > Fe > Pb > S > Bi > Sb

Figure 7.10 shows the results of Tables 7.5 and 7.6.

- **Maximum lengths**

In Figures 7.10a and 7.10b, group (i) includes Sb, Bi, Pb and Zn with greater lengths relative to groups (ii) and (iii). Group (ii) contains Cu, S and Fe with greater lengths than group (iii) which consists of As and Ag. Cadmium can be attributed to either group (ii) in Figure 7.10a or group (iii) in Figure 7.10b.

- **Maximum widths**

In Figures 7.10c and 7.10d, group (i) includes Sb and Bi with greater widths relative to groups (ii) and (iii). Group (ii) encompasses Pb, Zn, Cu, S and Fe with greater widths than group (iii) which consists of As and Ag. Cadmium can be attributed to either group (ii) in Figure 7.10c or the group (iii) in Figure 7.10d.

- **Anisotropy ratios**

The dispersal elements (Sb and Bi) show very low anisotropy ratios in comparison with other dispersal elements (Figures 7.10e and 7.10f) thus, indicating that the elements' distribution is widespread within the mineralisation zone. The anisotropy ratios of Sb range between 2.33 and 2.5 and, for Bi, vary between 3.06 and 3.18.

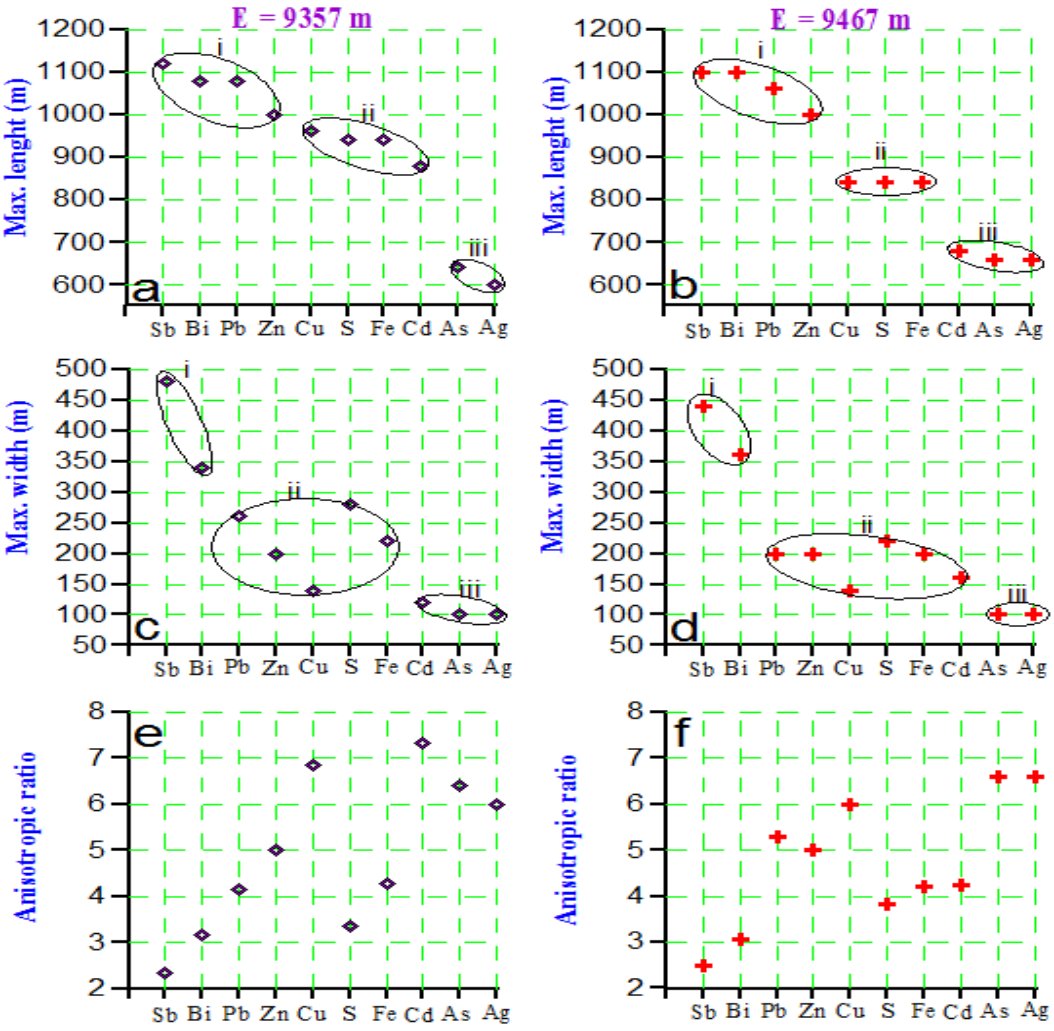

Figure 7.10: Comparison of maximum lengths, maximum widths and anisotropic ratios on the N-S longitudinal sections at E=9357 m and E=9467m.

- **Pathfinder elements**

In the longitudinal sections, Sb and Bi represent higher length and width or distribution shape relative to other elements in the Western Mineralisation (Figures 7.10a, b, c, d). Therefore, they can be introduced as geochemical pathfinders of Pb and Zn for the Western Mineralisation.

7.5 Evaluation of similarity levels among the geometrical patterns of haloes

Although the geometrical similarities of the geochemical haloes can be identified visually in Figures 7.4 to 7.7, one of the useful quantitative methods for identification of the similarity level is cluster analysis. The maximum lengths and widths of all geochemical haloes within all corresponding sections were used as entry data for the cluster analysis (Tables 7.1, 7.3 and 7.5). The cluster algorithm in Figure 7.11 classified the geochemical haloes into a number of groups to ensure that the similarity of haloes based on maximum length and maximum width inside each group is as greater as possible, while at the same time within the groups, the differences are as large as possible. The method of average linkage and correlation coefficient distance was used for amalgamation steps of the cluster algorithm using Minitab software.

Figure 7.11 shows the amount of similarities among the spatial distribution of geochemical haloes in the Western Mineralisation. For example, S and Fe show very similar dispersal shape, orientation and dimension in 8 different cross-sections (Figures 7.4 to 7.7) and they show maximum similarity level in Figure 7.11 with 99.89 % as well.

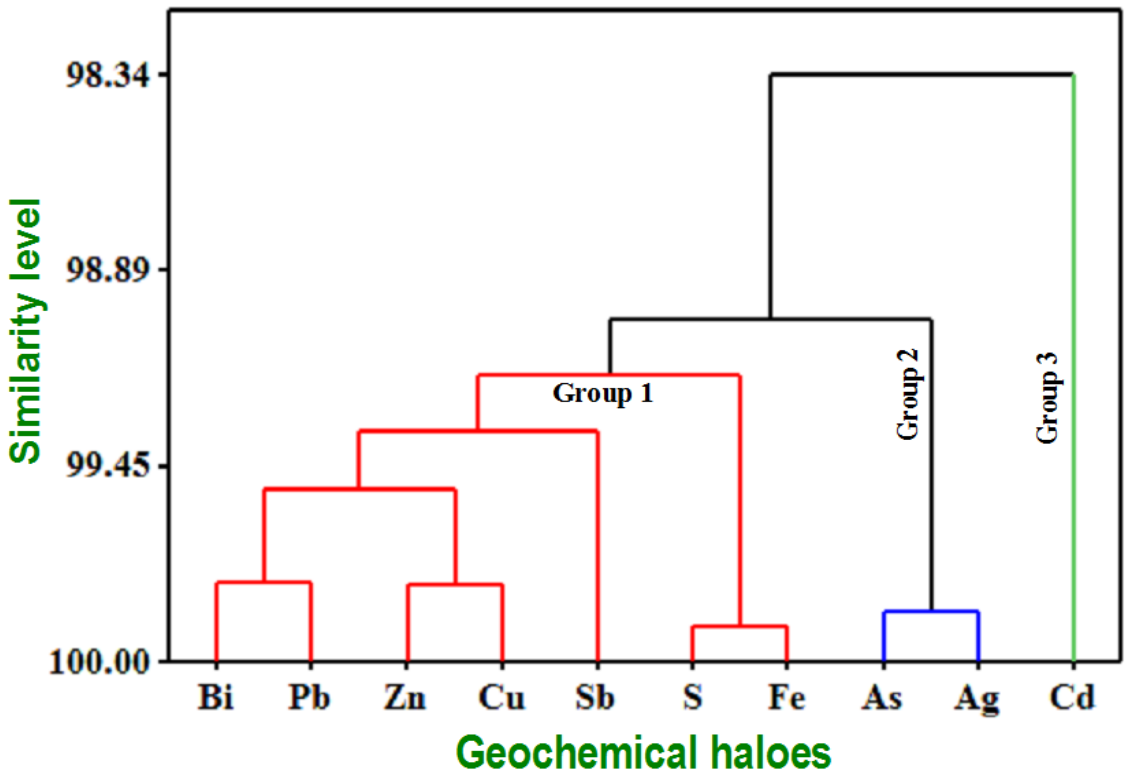

Figure 7.11: The percent of similarity among 10 elements based on the maximum lengths and the maximum widths of their geochemical haloes.

According to Figure 7.11, there are high geometrical similarity among pair geochemical haloes of Bi-Pb, Zn-Cu, S-Fe and As-Ag and the dispersal shape of Cd has the lowest similarity level (98.33 %) with other geochemical haloes followed by the geochemical halo pair As-Ag with 99.02 %.

Final partitions based on three groups are:

1. Group 1 (red lines): Bi, Sb, Pb, Zn, S, Fe and Cu,
2. Group 2 (blue line): As and Ag, and
3. Group 3 (green lines): Cd.

7.6 Summary

This chapter quantitatively evaluates the spatial distribution and geochemical variability of the Western Mineralisation using image processing of 80 cross-sections for 10 three-dimensional block models. Apart from this research, no spatial modelling has been used for identification of the geochemical zonation haloes for any of the orebodies in the Broken Hill deposits.

The first aim of this study was to evaluate the spatial distribution of primary geochemical haloes in the Western Mineralisation. The results show that the distribution shape of Sb and Bi are stronger and broader than other elements at different depths and the elements produced very strong primary haloes in all cross-sections. By contrast, Ag, As and Cd revealed only weak haloes.

Secondly, this study used a combination of spatial analysis and concentration-area method to separate the threshold concentrations from the geochemical background levels for 10 elements. The outcome can be used for tracking anomalous area by surface geochemical sampling and mapping of the element concentrations.

Finally, the geometrical properties (shape, orientation and dimension) and the scale of spatial continuity of the geochemical haloes were compared quantitatively to delineate distinct current zonation sequence in the Western Mineralisation. The results also suggest Bi and Sb as potential pathfinder elements for the Western Mineralisation.

CHAPTER 8

Spatial Models for Geochemistry, Geology and Geophysics of the Western Mineralisation

8.1 Introduction

Selection of appropriate exploration techniques for distinguishing a hidden and blind anomaly (true anomaly) from a false anomaly has always been difficult. In these cases, exploration techniques can be improved by quantitative geological, geochemical and geophysical studies of similar known types of ore deposits. In this chapter, in order to improve exploration methods and geological information associated with the Western Mineralisation, the following methods are conducted:

1. The spatial geochemical models of Chapter 7 are developed for:

   1.1 Assessment of zonation sequence of 10 elements in axial sections.
   1.2 Construction of an empirical formula of "Zonality Coefficient" (ZC) for the Western Mineralisation type deposit in order to improve exploration techniques for a hidden anomaly, and
   1.3 Classification of anomalous concentrations for elements.

2. Different sections of sulphide minerals are studied for appraisal of their structural variation, mineral zonation and alteration. The sections are also used to find their similarities with the geochemical haloes of the orebody,

3. Different sections of magnetic susceptibility are studied to evaluate their spatial relationships with the abundance of magnetic and non-magnetic pyrrhotite, other sulphide minerals and geochemical haloes,

4. The average chemical composition of garnet samples collected from the Broken Hill orebodies are analysed by correspondence analysis to show the relationship of the Broken Hill orebodies with the chemical composition of garnet types,

5. 3D biplots are constructed for garnet samples of the Western Mineralisation to show the chemical variation of garnet types in a spatial geometrical model,

6. Different sections of silicate minerals are studied for appraisal of their structural variation and mineral zonation. The sections are also used to find their similarities with the sulphide minerals, magnetic susceptibility and geochemical haloes of the orebody,

7. Different sections of rock types are studied for appraisal of their structural variation. The sections are also used to find their spatial relationships with the silicate and sulphide minerals, magnetic susceptibility and the geochemical haloes of the orebody, and

8. Different sections of sulphide textures are studied to evaluate their probability of occurrence within the orebody. The sections are also used to find their spatial relationships with the silicate and sulphide minerals, magnetic susceptibility, the rock types and the geochemical haloes of the orebody.

8.2 Appraisal of sequence of the element concentrations in the axial halo zoning

The information about axial halo zoning for each mineralisation can be used for the evaluation of the exposed level of the erosion for similar types of mineralisation associated with depth (Beus & Grigorian 1977). Beus and Grigorian (1977) introduced several empirical methods developed by Russian scientists for quantifying the zonation of haloes in axial (vertical) sections.

One of the methods mostly used in geological research is the evaluation of the average variations of element concentration ratios (e.g. Pb/U or Mo/U) as a function of depth in vertical sections (e.g. Large, Bull & McGoldrick 2000). In this method, the distribution shape of geochemical halos with depth is not considered.

Another method consists of a calculation of "Linear Productivity" (LP) that has been given more emphasis, by calculating the LP, the width of haloes at different depths is considered when characterising the relationship of geochemical haloes with the depth of mineralisation. The LP is calculated as the product of width (in metres) of a geochemical halo at a certain elevation and average element content (as percentage) at the same elevation of the halo (Beus & Grigorian 1977).

In this chapter, Figure 7.6 was used for the calculation of LP of each element at different depths of mineralisation (Appendix E). For this purpose, a number of elevations are selected which are shown as intersecting straight lines on the east-west (E-W) vertical cross-sections at northing (N)=2109 (Figure 8.1) and N=1639. It is unlikely that drill holes were exact on the cross-sections so a tolerance of ± 10 m was used to project intersections on to the cross-section to increase the number of samples on the section. The element concentrations of intersected points of the sample cores with blue lines were averaged for each selected elevation.

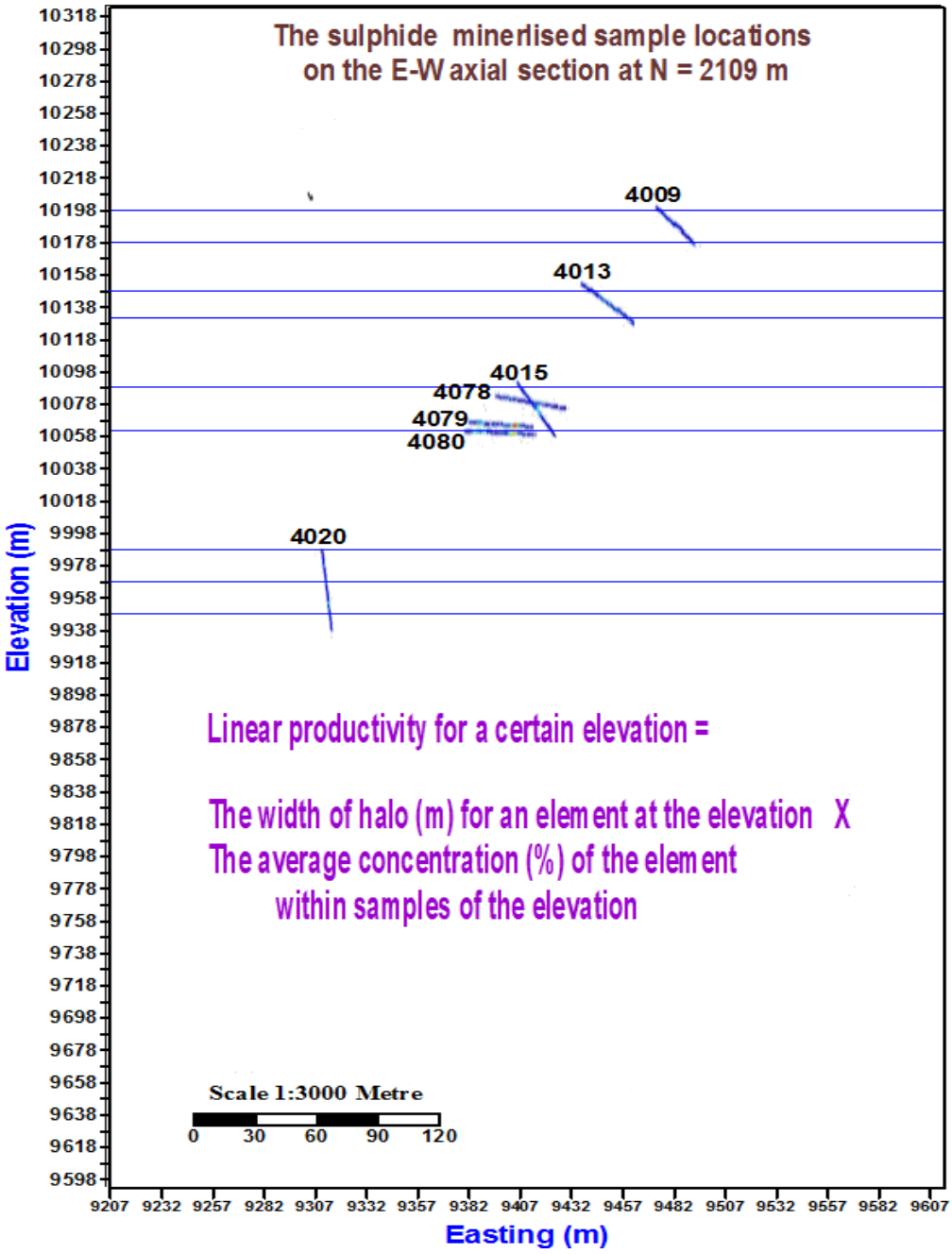

Figure 8.1: Location of the mineralised samples on the E-W axial section at N=2109 and their intersections with the selected elevations (blue lines).

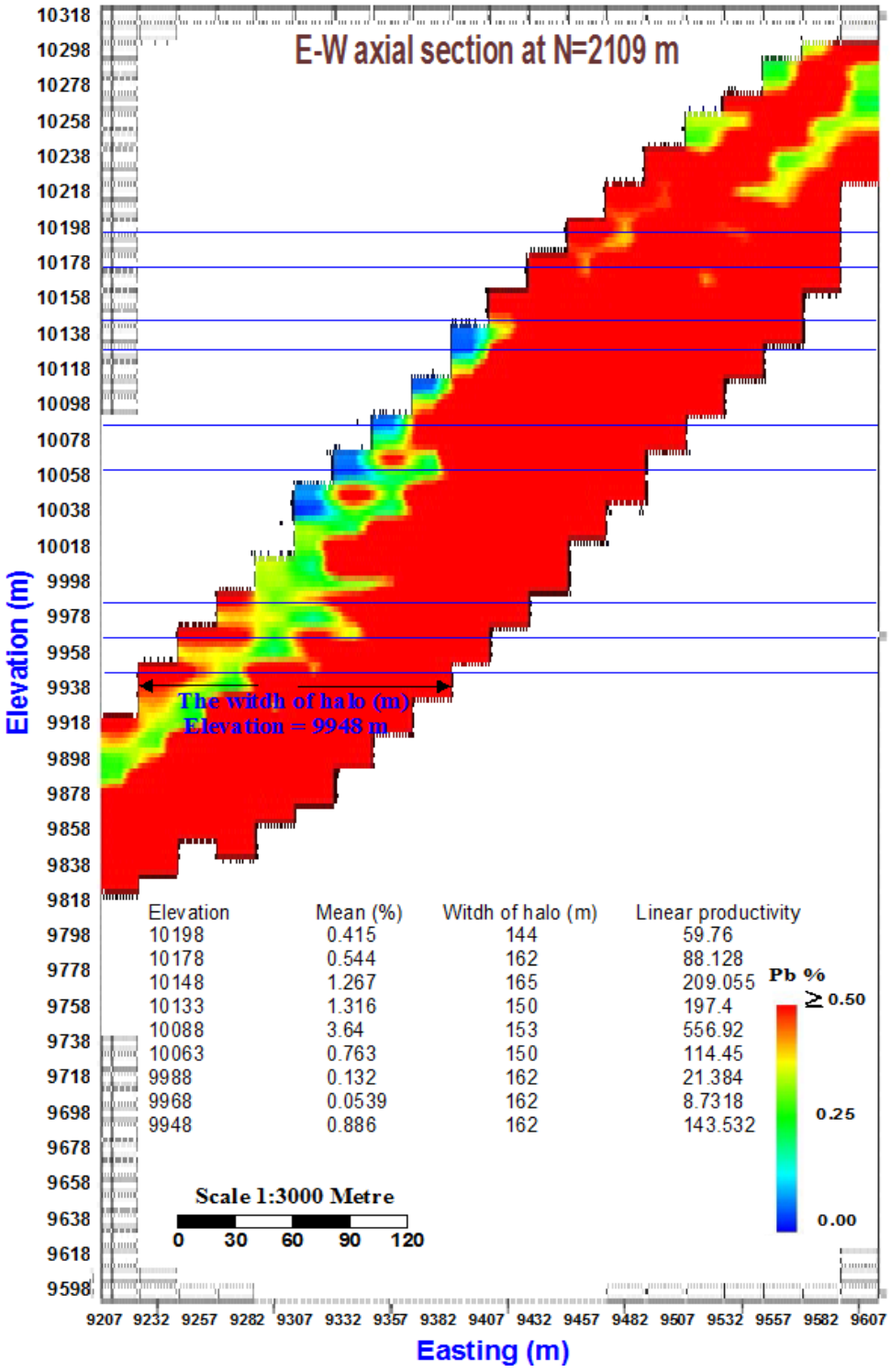

Figure 8.2: The intersections of halo of Pb with the blue lines at the selected elevations on the E-W axial section at N=2109 and calculations of the LP for the elevations.

In Figure 8.2, the length of blue lines inside the dispersion halo (width of the halo) at different elevations was measured in part of the threshold concentration range (from green to red colour). Appendix E shows the zonation of 10 geochemical haloes along the E-W axial sections at N=1639 and N=2109 and their values of LP.

In order to compare LPs of geochemical haloes at different depths, Beus and Grigorian (1977) suggested using the ratio of individual LP of the geochemical halo element at a given elevation to the sum of LPs of the geochemical haloes of all elements at that elevation to determine "Zonality Index" (ZI). In the next sections, the procedure for calculating the ZI of geochemical haloes is outlined. The ZI represents the relative concentration of elements at each elevation.

8.2.1 Calculations of ZI for the 10 geochemical haloes on the E-W axial sections at N=2109 m

Tables 8.1 to 8.4 show procedures of computing of "Normalisation Coefficient" (Cn), ZI and evaluating the zonation sequence of primary geochemical haloes for 10 element concentrations on the E-W axial section at N=2109 m.

The Cn is determined to normalise the values of LP of different element concentrations so that their maximum LP values have the same order of magnitude basis. For example, Pb has maximum LP value of 556.92 and Zn, Fe and S also have similar orders of magnitude of LP (Table 8.1). However, the maximum LP values of Cd, Ag and Sb need to be multiplied by 1000 to find the same order of magnitude of LP. Table 8.2 shows the amount of Cn for maximum LP values of 10 element concentrations. In order to normalise LP values of each element at different elevations, the Cn value of each element given in Table 8.2, should be multiplied by the LP values of the elements in all elevations (Table 8.3).

The ZIs in Table 8.4 were calculated by dividing the normalised LP value of each element in Table 8.3 at a certain elevation to the sum of LPs of that elevation. For example, the ZI of Pb at level of 10198 is calculated by ratio of 59.76 to 909.771 (Table 8.3). Table 8.4 shows that the highest ZI of As occurs at elevation 10178 or at the upper level of the geochemical haloes, whereas the maximum ZIs of Cu, Ag and Sb are at the lowest level of the haloes. In these cases where in the zonation of haloes the order of elements with the same position in a zonation sequence is not clear (e.g. Zn and S are both at the same elevation of 10063 m in Table 8.4), the variability gradient[1] [Equation (8.1)] of the elements should be calculated to determine their real position in the sequence (Beus & Grigorian 1977).

[1]**Variability Index**

Table 8.1: LP values of 10 element concentrations at the selected elevations and maximum LP values for each element shown in red text (Appendix E).

Drill hole	Elevation	Pb	Zn	Cd	Ag	Sb	S	Fe	Cu	As	Bi
4009	10198	59.76	46.818	0.132	0.048	0.2256	94.185	132.192	2.43	4.524	1.0167
4009	10178	88.128	146.4	0.3564	0.036	0.1818	200.121	165.954	3.24	11.151	1.215
4013	10148	209.055	25.38	0.1053	0.06	0.324	127.728	235.62	2.43	2.28	1.17
4013	10133	197.4	291.6	0.7089	0.0588	0.4536	333.33	292.842	9.18	0.3552	1.125
4015	10088	556.92	158.552	0.6324	0.1613	0.9373	277.911	357.93	5.1	0.4753	1.2171
4015-80	10063	114.45	258.552	0.1326	0.0816	0.3096	257.094	513.648	1.02	1.755	0.600
4020	9988	21.384	45.87	0.2706	0.102	0.366	98.34	400.95	4.32	0.8874	1.7442
4020	9968	8.7318	54.108	0.204	0.02772	0.1138	61.38	295.2	2.46	0.612	1.425
4020	9948	143.532	177.017	0.4575	0.2016	0.7776	256.41	253.749	16.32	2.1465	1.425

Table 8.2: Selective Cn values for maximum LP values of each element and their normalised LP results.

Element	Max. LP	Cn	(Max. LP) × Cn	Element	Max. LP	Cn	(Max. LP) × Cn
Pb	556.92	1	556.92	Fe	513.65	1	513.65
Zn	258.55	1	258.55	Cu	16.32	10	163.2
Cd	0.7089	1000	708.9	As	11.151	10	111.51
Ag	0.2016	1000	201.6	Bi	1.7442	100	174.42
Sb	0.93733	1000	937.33	S	333.33	1	333.33

Table 8.3: Normalised LP values* for 10 element concentrations at the selected elevations.

Elements	Cn	10198	10178	10148	10133	10088	10063	9988	9968	9948
Pb	1	59.76	88.128	209.055	197.4	556.92	114.45	21.384	8.7318	143.532
Zn	1	46.818	146.4	25.38	291.6	158.552	258.552	45.87	54.108	177.017
Cd	1000	132	356.4	105.3	708.9	632.343	132.6	270.6	204	457.56
Ag	1000	48	36	60	58.8	161.343	81.6	102	27.72	201.6
Sb	1000	225.6	181.8	324	453.6	937.326	309.6	366	113.85	777.6
S	1	94.185	200.121	127.728	333.33	277.911	257.097	98.34	61.38	256.41
Fe	1	132.192	165.954	235.62	292.842	357.93	513.648	400.95	295.2	253.749
Cu	10	24.3	32.4	24.3	91.8	51	10.2	43.2	24.6	163.2
As	10	45.24	111.51	22.8	3.552	0.473	17.55	8.874	6.12	21.46
Bi	100	101.676	121.5	117	112.5	121.716	60.03	174.42	142.5	142.5
Sum of LP values		909.771	1440.213	1251.183	2544.324	3259.851	1755.327	1531.638	938.209	2594.628

*Normalised LP value of each element = LP value of the element (Table 8.1) × Cn value of the element (Table 8.2) for a certain elevation.

Table 8.4: ZI values for 10 element concentrations and maximum ZI values highlighted in red text.

	Elevation								
Elements	10198	10178	10148	10133	10088	10063	9988	9968	9948
Pb	0.065687	0.061191	0.167086	0.077584	0.170842	0.065202	0.013962	0.009307	0.055319
Zn	0.051461	0.101652	0.020285	0.114608	0.048638	0.147296	0.029948	0.057672	0.068225
Cd	0.145091	0.247463	0.084160	0.278620	0.193997	0.075541	0.176674	0.217435	0.176349
Ag	0.052761	0.024996	0.047955	0.023110	0.049494	0.046487	0.066595	0.029546	0.077699
Sb	0.247974	0.126231	0.258955	0.178279	0.287536	0.176377	0.238960	0.121348	0.299696
S	0.103526	0.138952	0.102086	0.131009	0.085253	0.146467	0.064206	0.065422	0.098823
Fe	0.145302	0.115229	0.188318	0.115096	0.109799	0.292622	0.261779	0.314642	0.097798
Cu	0.026710	0.022497	0.019422	0.036080	0.015645	0.005811	0.028205	0.026220	0.062899
As	0.049727	0.077426	0.018223	0.001396	0.001458	0.009998	0.005794	0.006523	0.008271
Bi	0.111760	0.084363	0.093512	0.044216	0.037338	0.034199	0.113878	0.151885	0.054921
Zonation sequence		As		Cd	Pb	Zn-S		Fe-Bi	Ag-Sb-Cu

Beus and Grigorian (1977, p. 96) suggested the empirical Equation (8.1) to determine the order of the elements with the same sequence subject to their maximum ZI being found at the upper or lower level (elevation) of the zonation of haloes:

$$\mathbf{G} = \sum_{\mathbf{i}}^{\mathbf{n}} \frac{\mathbf{ZI}_{\mathbf{max}}}{\mathbf{ZI}_{\mathbf{i}}} \qquad \textbf{(8.1)}$$

Where G is the variability gradient, ZI_{max} is the maximum value of the zonality index of a given element, ZI_i is the value of the zonality index in the i^{th} elevation and n is the number of elevations (exclusive of the elevations of maximum concentration of ZI_{max}). In Table 8.5, the G of Cu, Ag and Sb were calculated by Equation (8.1). Because the elements are at the lowest elevation in Table 8.4, their sequence of elements was arranged in the order of increasing G and this would be the other way round if the elements occurred in the highest elevations (Beus & Grigorian 1977). The result of $\mathbf{G_{Sb} < G_{Ag} < G_{Cu}}$ suggests the order of Sb-Ag-Cu from upward to downward direction of the zonation sequence along the E-W axial section at N=2109 m.

Table 8.5: Calculations of G for Cu, Ag and Sb.

$$\mathbf{G_{Cu}} = \frac{\mathbf{0.062899}}{\mathbf{0.026220}} + \frac{\mathbf{0.062899}}{\mathbf{0.028205}} + \frac{\mathbf{0.062899}}{\mathbf{0.005811}} + \frac{\mathbf{0.062899}}{\mathbf{0.015645}} + \frac{\mathbf{0.062899}}{\mathbf{0.036080}} + \frac{\mathbf{0.062899}}{\mathbf{0.019422}} + \frac{\mathbf{0.062899}}{\mathbf{0.022497}} + \frac{\mathbf{0.062899}}{\mathbf{0.026710}}$$

$$\mathbf{G_{Ag}} = \frac{\mathbf{0.077699}}{\mathbf{0.029546}} + \frac{\mathbf{0.077699}}{\mathbf{0.066595}} + \frac{\mathbf{0.077699}}{\mathbf{0.046487}} + \frac{\mathbf{0.077699}}{\mathbf{0.049494}} + \frac{\mathbf{0.077699}}{\mathbf{0.023110}} + \frac{\mathbf{0.077699}}{\mathbf{0.047955}} + \frac{\mathbf{0.077699}}{\mathbf{0.024996}} + \frac{\mathbf{0.077699}}{\mathbf{0.052761}}$$

$$\mathbf{G_{Sb}} = \frac{\mathbf{0.299696}}{\mathbf{0.121348}} + \frac{\mathbf{0.299696}}{\mathbf{0.238960}} + \frac{\mathbf{0.299696}}{\mathbf{0.176377}} + \frac{\mathbf{0.299696}}{\mathbf{0.287536}} + \frac{\mathbf{0.299696}}{\mathbf{0.178279}} + \frac{\mathbf{0.299696}}{\mathbf{0.258955}} + \frac{\mathbf{0.299696}}{\mathbf{0.126231}} + \frac{\mathbf{0.299696}}{\mathbf{0.247974}}$$

$\mathbf{G_{Cu} = 29.60}$
$\mathbf{G_{Ag} = 16.60}$
$\mathbf{G_{Sb} = 12.88}$

$$\mathbf{G_{Sb} < G_{Ag} < G_{Cu}}$$

According to Beus and Grigorian (1977), if the maximum ZI of several elements occurs at a certain level **in the middle horizon**, then the difference between variability gradients ($\Delta G = G_2 - G_1$) between downward and upward directions are calculated where:

1. G_2 is calculated for the downward direction from the level of the maximum ZI, and
2. G_1 is calculated for the upward direction from the level of the maximum ZI.

The order of elements in zonation of haloes depends on the magnitude of ΔG. Each element that contains a greater positive ΔG, will be placed further upward (to the left) in the zonation of halo sequence and each element that contains lesser positive ΔG will be located further downward (to the right) in the zonation of halo sequence. This will be the other way round if the ΔG is a negative value. In this case, each element that contains a greater negative ΔG will be placed further downward (to the right) in the zonation. Table 8.6 shows the calculations of ΔG for pairs of S, Zn and pairs of Fe and Bi in order to evaluate the sequence of primary zonation of the haloes in this axial section.

Table 8.6: Calculations of ΔG for pairs S, Zn and pairs Fe and Bi.

$$G_{S1} = \frac{0.146467}{0.085253} + \frac{0.146467}{0.131009} + \frac{0.146467}{0.102086} + \frac{0.146467}{0.138952} + \frac{0.146467}{0.103526}$$

$$G_{S2} = \frac{0.146467}{0.064206} + \frac{0.146467}{0.065422} + \frac{0.146467}{0.098823}$$

$$G_{S2} - G_{S1} = 6.0020971 - 6.7396202 = -0.737523$$

$$G_{Zn1} = \frac{0.147296}{0.048638} + \frac{0.147296}{0.114608} + \frac{0.147296}{0.020285} + \frac{0.147296}{0.101652} + \frac{0.147296}{0.051461}$$

$$G_{Zn2} = \frac{0.147296}{0.029948} + \frac{0.147296}{0.057672} + \frac{0.147296}{0.068225}$$

$$G_{Zn2} - G_{Zn1} = 9.631351 - 15.886293 = -6.254942$$

$$\Delta G_S > \Delta G_{Zn}$$

$$G_{Fe1} = \frac{0.314642}{0.261779} + \frac{0.314642}{0.292622} + \frac{0.314642}{0.109799} + \frac{0.314642}{0.115096} + \frac{0.314642}{0.188318} + \frac{0.314642}{0.115229} + \frac{0.314642}{0.145302}$$

$$G_{Fe2} = \frac{0.314642}{0.097798}$$

$$G_{Fe2} - G_{Fe1} = 3.217267 - 14.443330 = -11.226062$$

$$G_{Bi1} = \frac{0.151885}{0.113878} + \frac{0.151885}{0.034199} + \frac{0.151885}{0.037338} + \frac{0.151885}{0.044216} + \frac{0.151885}{0.093512} + \frac{0.151885}{0.084363} + \frac{0.151885}{0.111760}$$

$$G_{Bi2} = \frac{0.151885}{0.054921}$$

$$G_{Bi2} - G_{Bi1} = 2.76550 - 18.061560 = -15.296051$$

$$\Delta G_{Fe} > \Delta G_{Bi}$$

Table 8.7: The zonation sequence of geochemical haloes on the E-W axial section at N=2109 m (from top to bottom of orebody).

Elevation	10178	10148	10133	10088	10063	9988	9968	9948
Zonation sequence	As		Cd	Pb	S-Zn		Fe-Bi	Sb-Ag-Cu

8.2.2 Calculations of ZI for 10 geochemical haloes along the E-W axial section at N=1639 m

Tables 8.8 to 8.11 display procedures of calculation of the Cn, ZI and evaluating the sequence of primary geochemical zoning haloes for 10 elements along the E-W axial section at N=1639 m.

Table 8.8: LP values of 10 element concentrations at the selected elevations and maximum LP values for each element shown in red text (Appendix E).

Drill hole	Elevation	Pb	Zn	Cd	Ag	Sb	S	Fe	Cu	As	Bi
4042	9948	100.224	93.534	0.3402	0.0336	1.725	88.452	206.793	2.52	0.588	1.215
4042	9928	314.028	228.27	1.1016	0.0273	1.725	323.812	302.226	1.8	0.588	1.32
4050	9888	14.616	3.112	No data	0.0228	1.62	20.328	282.846	0.81	0.105	1.32
4050	9868	313.785	368.01	No data	0.0966	1.515	390.382	375.501	11.34	0.329	1.531
4050	9848	100.435	18.216	No data	0.02436	1.636	76.507	436.089	3.06	0.730	1.215

Table 8.9: Selective Cn values for maximum LP values of each element and their normalised LP results.

Elements	Max. LP	Cn	(Max. LP) × Cn	Elements	Max. LP	Cn	(Max. LP) × Cn
Pb	314.03	1	314.028	S	390.3822	1	390.3822
Zn	368.01	1	368.01	Fe	436.0896	1	436.0896
Cd	1.1016	100	110.16	Cu	11.34	10	113.4
Ag	0.0966	10000	966	As	0.7308	1000	730.8
Sb	1.725	100	172.5	Bi	1.5312	100	153.12

Table 8.10: The normalised LP values* for the 10 element concentrations at the selected elevations.

		Elevations				
Elements	**Cn**	**9948**	**9928**	**9888**	**9868**	**9848**
Pb	**1**	**100.22**	**314.03**	**14.61**	**313.78**	**100.44**
Zn	**1**	**93.534**	**228.27**	**3.1122**	**368.01**	**18.216**
Cd	**100**	**34.02**	**110.16**	**N/A**	**N/A**	**N/A**
Ag	**10000**	**336**	**273**	**228**	**966**	**243.6**
Sb	**100**	**172.5**	**172.5**	**162**	**151.5**	**163.62**
S	**1**	**88.45**	**323.81**	**20.33**	**390.38**	**76.507**
Fe	**1**	**206.79**	**302.22**	**282.85**	**375.50**	**436.09**
Cu	**10**	**25.2**	**18**	**8.1**	**113.4**	**30.6**
As	**1000**	**588**	**588**	**105**	**319.2**	**730.8**
Bi	**100**	**121.5**	**132**	**132**	**153.12**	**121.5**
Sum of LP values		**1766.223**	**2461.996**	**956**	**3150.899**	**1921.368**

***Normalised LP value of each element = LP value of the element (Table 8.8) × Cn value of the element (Table 8.9) for a certain elevation**

The values of ZI in Table 8.11 were calculated by dividing the normalised LP value of each element in Table 8.10 at a certain elevation to the sum of LP values of that elevation. For example, the ZI of Pb at level of 9948 was calculated as $\frac{100.22}{1766.22}$ (Table 8.10).

Table 8.11: The values of ZI for 10 element concentrations and maximum ZI values highlighted in red text.

Elements	**9948**	**9928**	**9888**	**9868**	**9848**
Pb	**0.0567448**	**0.1275501**	**0.0152886**	**0.0995858**	**0.0522729**
Zn	**0.0529570**	**0.0927174**	**0.0032554**	**0.1167952**	**0.0094807**
Cd	**0.0192614**	**0.0447441**	**No data**	**No data**	**No data**
Ag	**0.1902364**	**0.1108856**	**0.2384931**	**0.3065791**	**0.1267846**
Sb	**0.0976660**	**0.0700650**	**0.1694556**	**0.0480815**	**0.0851580**
S	**0.0500797**	**0.1315244**	**0.0212635**	**0.1238954**	**0.0398191**
Fe	**0.1170820**	**0.1227564**	**0.2958633**	**0.1191729**	**0.2269682**
Cu	**0.0142677**	**0.0073111**	**0.0084727**	**0.0359897**	**0.0159261**
As	**0.3329137**	**0.2388305**	**0.1098323**	**0.1013044**	**0.3803539**
Bi	**0.0687908**	**0.0536150**	**0.1380749**	**0.0485956**	**0.0632361**
Zonation sequence		**S-Pb-Cd**	**Sb-Bi-Fe**	**Ag-Cu-Zn**	**As**

Tables 8.12 and 8.13 show the calculations of ΔG for elements S, Pb and Cd at level of 9928 m and Sb, Bi at level of 9888 m and Ag, Cu and Zn at level of 9868 m in order to evaluate the sequence of primary zonation of the haloes in this axial section. The results are given in Table 8.14.

Table 8.12: Calculations of ΔG for (a): S, Pb and Cd, (b): for Sb, Bi and Fe.

(a)

$$G_{S1} = \frac{0.131524}{0.050079}$$

$$G_{S2} = \frac{0.131524}{0.021263} + \frac{0.131524}{0.123895} + \frac{0.131524}{0.039819}$$

$$G_{S2} - G_{S1} = 10.550065 - 0.5862637 = 9.9638021$$

$$G_{Pb1} = \frac{0.127550}{0.056744}$$

$$G_{Pb2} = \frac{0.127550}{0.015288} + \frac{0.127550}{0.099585} + \frac{0.127550}{0.052272}$$

$$G_{Pb2} - G_{Pb1} = 12.06367 - 2.247784 = 9.815890$$

$$G_{Cd} = \frac{0.044744}{0.019261} = 2.322991$$

$$\Delta G_S > \Delta G_{Pb} > \Delta G_{Cd}$$

(b)

$$G_{Sb1} = \frac{0.1694556}{0.0700650} + \frac{0.1694556}{0.0976660}$$

$$G_{Sb2} = \frac{0.1694556}{0.0480815} + \frac{0.1694556}{0.0851580}$$

$$G_{Sb2} - G_{Sb1} = 5.5142374 - 4.1535991 = 1.3606382$$

$$G_{Bi1} = \frac{0.1380749}{0.0536150} + \frac{0.1380749}{0.0687908}$$

$$G_{Bi2} = \frac{0.1380749}{0.0485956} + \frac{0.1380749}{0.0632361}$$

$$G_{Bi2} - G_{Bi1} = 5.024784 - 4.582475 = 0.442309$$

$$G_{Fe1} = \frac{0.2958633}{0.1227564} + \frac{0.2958633}{0.1170820}$$

$$G_{Fe1} = \frac{0.2958633}{0.1191729} + \frac{0.2958633}{0.2269682}$$

$$G_{Fe2} - G_{Fe1} = 3.786183 - 4.9371396 = -1.1509559$$

$$\Delta G_{Sb} > \Delta G_{Bi} > \Delta G_{Fe}$$

Table 8.13: Calculations of ΔG for Ag, Cu and Zn.

$$G_{Ag1} = \frac{0.3065791}{0.2384931} + \frac{0.3065791}{0.1108856} + \frac{0.3065791}{0.1902364}$$

$$G_{Ag2} = \frac{0.3065791}{0.1267846}$$

$$G_{Ag2} - G_{Ag1} = 2.418109 - 5.661876 = -3.243767$$

$$G_{Cu1} = \frac{0.0359897}{0.0084727} + \frac{0.0359897}{0.0073111} + \frac{0.0359897}{0.0142677}$$

$$\Delta G_{Ag} > \Delta G_{Cu} > \Delta G_{Zn}$$

$$G_{Cu2} = \frac{0.0359897}{0.0159261}$$

$$G_{Cu2} - G_{Cu1} = 2.2597882 - 11.692730 = -9.4329422$$

$$G_{Zn1} = \frac{0.1167952}{0.0032554} + \frac{0.1167952}{0.0927174} + \frac{0.1167952}{0.0529570}$$

$$G_{Zn2} = \frac{0.1167952}{0.0094807}$$

$$G_{Zn2} - G_{Zn1} = 12.319206 - 39.342193 = -27.0229867$$

Table 8.14: The zonation sequence of geochemical haloes on the E-W axial section at N=1639 m.

Elevation	9948	9928	9888	9868	9848
Zonation sequence		S-Pb-Cd	Sb-Bi-Fe	Ag-Cu-Zn	As

8.2.3 Comparison of the ZIs between the E-W axial sections at N=2109 m at N= 1639 m

Figure 8.3 was constructed by comparing the two ZIs in the above two axial sections in order to evaluate the zonation sequence of the element concentrations from elevation 10198 m to 9848 m (350 m depth) in the Western Mineralisation. The results are outlined in Table 8.15.

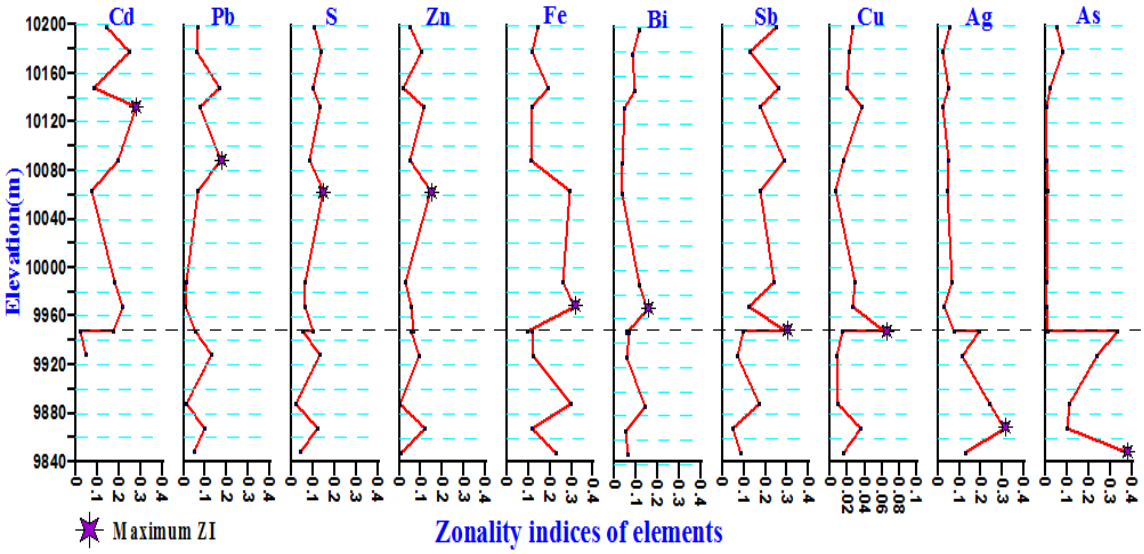

Figure 8.3: Variation of the ZIs for 10 elements at different elevations and their maximum ZI.

Table 8.15: The zonation sequence of geochemical haloes on the E-W axial sections from 10178 to 9840 m in the Western Mineralisation.

Elevation	10148	10133	10088	10063	9968	9948	9868	9848
Zonation sequence		Cd	Pb	S-Zn	Fe-Bi	Sb-Cu	Ag	As

The cluster analysis (Figure 8.4) classifies the geochemical haloes into a number of similar groups based on their ZIs on the E-W axial sections at elevations of N=10198 m and N=9848 m within the Western Mineralisation. The cluster algorithm was calculated by the average linkage and correlation coefficient distance. Figure 8.4 shows the following three main groups for 10 elements:

1. Group 1 (red colour): Pb, Zn and S,
2. Group 2 (blue colour): Ag and As, and
3. Group 3 (green colour): Cd, Sb, Fe, Cu and Bi.

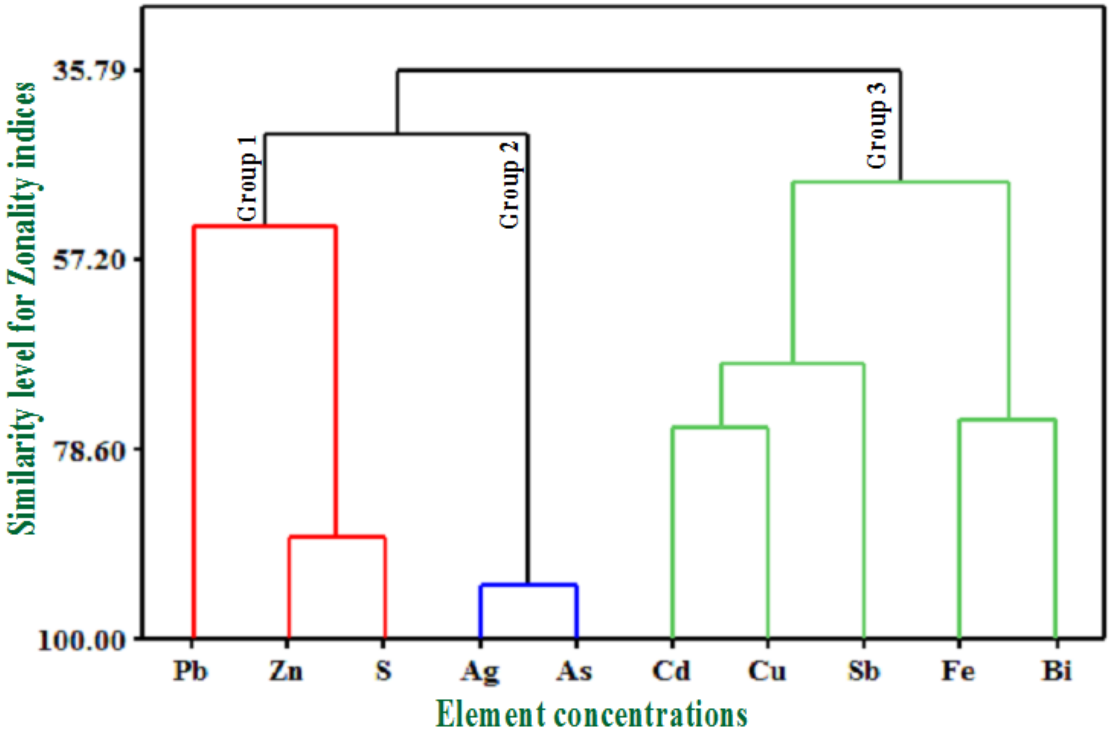

Figure 8.4: Cluster analysis for ZI values of 10 elements.

From Figure 8.4, some high percentage of similarities in the ZIs of 10 elements can be outlined below:

1. Ag and As with 94 % similarity level,
2. Zn and S with 88.60 % similarity level,
3. Cd and Cu with 76.15 % similarity level, and
4. Fe and Bi with 75.29 % similarity level.

Figure 8.4 suggests that the ZI of Cd is more similar to the ZI of Cu and Sb that tend to concentrate in the lower part of mineralisation. This may be because of decreasing of the ZIs of Pb, Zn and S after level of 10063 m (Figure 8.3), while the ZI of Cd is increasing after this level the same as Cu and Sb.

8.3 Exploration significance of the axial (vertical) zoning sequence (ZC)

The product of the indicator element concentrations in the lower part of the Western Mineralisation over those of the upper part of the mineralisation can be used as vertical ZC (Huang & Zhang 1989; Ziaii, Pouyan & Ziaei 2009) for the Western Mineralisation or similar orebodies. The orientation of the ZC may be affected by

other factors, such as primary depositional zoning, secondary remobilisation or reorientation due to folding and faulting.

The empirical product-ratios of ZC can be applied to the following issues:

1. Estimating the degree of denudation level of an anomaly,
2. Evaluating the exposure level of geochemical anomalies,
3. Recognising the upper anomalous halo from the lower anomalous halo, and
4. Predicting the presence of deeply buried Pb and Zn blind or hidden mineralisation in potential areas where the concentrations of elements are more than their local background levels.

According to Table 8.15, Cd, Pb, S, and Zn tend to concentrate in the upper part of the mineralised zone, whereas As, Ag, Cu, Sb and Bi have a tendency to concentrate in the lower part of the mineralisation. Based on the sequence of zonation in Table 8.15, Equation (8.2) is suggested for the Western Mineralisation as ZC.

$$\mathbf{ZC}_1 = \frac{\mathbf{Ag} \times \mathbf{Cu} \times \mathbf{Bi} \times \mathbf{As}}{\mathbf{S} \times \mathbf{Pb} \times \mathbf{Zn} \times \mathbf{Cd}} \qquad \textbf{(8.2)}$$

In Equation (8.2), Cd can be excluded from this calculation because three levels of 9888 m, 9868 m and 9848 m had no concentration values for Cd. Therefore, Equation (8.2) is modified to take into account this situation for the calculation of mean element concentrations at different levels [Equation (8.3)].

$$\mathbf{ZC}_2 = \frac{\mathbf{Ag} \times \mathbf{Cu} \times \mathbf{Bi} \times \mathbf{As}}{\mathbf{S} \times \mathbf{Pb} \times \mathbf{Zn}} \qquad \textbf{(8.3)}$$

If it is considered that Bi is not a suitable element for the Equation (8.2) because of its position in the middle of elevation in Table 8.15, Bi can be removed from Equation (8.3) which can be modified to:

$$\mathbf{ZC}_3 = \frac{\mathbf{Ag} \times \mathbf{Cu} \times \mathbf{As}}{\mathbf{S} \times \mathbf{Pb} \times \mathbf{Zn}} \qquad \textbf{(8.4)}$$

The ZC values can also be interpreted as "Denudation Index" (DI) for a potential deposit. Both Equations (8.3) and (8.4) can be considered as empirical product-ratios of DI for Pb and Zn sulphide ore deposit similar to the Western Mineralisation. This is of value for exploration because the Western Mineralisation does not crop out. The value of a DI can be interpreted according to the following situations for a potential deposit:

1. If the DI < 1, it indicates the erosion level has not affected the upper part of the anomaly. In this case, we have access to the upper part of anomaly and the concentration of Pb, Zn and S will be higher in this part relative to concentrations of As, Bi, Cu and Ag, therefore the value of DI will be less than one,

2. If the DI = 1, it shows that the erosion level has removed the upper part of the anomaly or mineralisation and the rest of mineralisation may appear in depth, and

3. If the DI > 1, it means the erosion level has removed the upper and middle portion of the anomaly. In this case, the lower part of anomaly is exposed and the concentration of As, Bi, Cu and Ag will be greater than concentrations of Pb, Zn and S. Therefore the DI will be more than one and any expectation of mineralisation for that given area is very low if it was at the same erosional level.

Table 8.16 shows the variation of ZC_2 and ZC_3 at different elevations of the Western Mineralisation. It is obvious that the values of ZC (or DI) are very much lower than one, because the Western Mineralisation is an Zn and Pb sulphide orebody which contains very much higher concentrations of S, Pb and Zn in comparison with the concentrations of Ag, Cu, As and Bi.

According to Table 8.16, ZC_2 (DI_2) values vary between 0.01×10^{-10} and 317×10^{-10} in all levels and ZC_3 (DI_3) values vary between 0.002×10^{-7} and 64×10^{-7} in all levels. The product-ratio of ZC or DI for the Western Mineralisation can be used for evaluating similar Zn and Pb mineralisation in other parts of the Broken Hill Domain.

.

Table 8.16: Variations of ZC_2 and ZC_3 at different elevations for the mean percentage of 10 element concentrations of the Western Mineralisation.

	Elevation	Ag	Cu	Bi	As	S	Pb	Zn	$ZC_2 \times 10^{-10}$	$ZC_3 \times 10^{-7}$
The E-W axial sections at N=2109 m	10198	0.0008	0.03	0.0046	0.0754	0.897	0.415	0.459	17.60	3.84
	10178	0.0006	0.04	0.005	0.177	1.627	0.544	1.22	86.64	17.33
	10148	0.001	0.03	0.005	0.038	0.887	1.267	0.18	14.66	2.93
	10133	0.0014	0.09	0.005	0.0074	2.71	1.316	1.8	40.75	8.15
	10088	0.00256	0.05	0.0058	0.0046	1.971	3.64	0.976	63.24	10.76
	10063	0.0008	0.01	0.0029	0.0325	1.587	0.763	1.596	5.79	2
	9988	0.001	0.03	0.0057	0.0087	0.596	0.132	0.278	0.92	0.16
	9968	0.00033	0.02	0.005	0.006	0.372	0.054	0.334	0.10	0.02
	9948	0.0024	0.16	0.005	0.0265	1.554	0.886	1.0927	316.98	63.40
The E-W axial sections at N=1639 m	9948	0.0008	0.03	0.005	0.014	1.134	0.696	0.917	9.46	1.89
	9928	0.00065	0.03	0.005	0.014	2.248	1.716	2.174	22.65	4.53
	9888	0.00038	0.01	0.005	0.005	0.193	0.087	0.0247	0.01	0.002
	9868	0.0023	0.14	0.0058	0.0076	3.336	1.835	2.61	203.74	35.13
	9848	0.00058	0.03	0.005	0.0174	0.531	0.608	0.126	2.19	0.44

Table 8.16 shows maximum ZC_2 and ZC_3 values at an elevation of 9948 m (the greatest depth) of the cross-section of N=2109 m and maximum ZC_2 and ZC_3 values at an elevation of 9868 m of the cross-section of N=1639 m. It should be noted that the distinct (axial) vertical zonation sequence for the Western Mineralisation may not completely reflect the complexity of the vertical zonation structure of the entire Broken Hill deposit.

In cross-sectional analysis, identification of the elements that tend to concentrate below and above the mineralisation zone allow us to calculate an "Additive Index" (AI) [Equation (8.5)] to improve exploration of other similar mineralisations (Beus & Grigorian 1977; Chen & Zhao 1998). Equation (8.5) is calculated by the ratio of the additive concentration of elements that are higher in the zonation of halo (e.g. S, Pb, Zn and Cd as numerator) to the additive concentration of elements that are lower in the zonation of halo (e.g. As, Bi, Cu and Ag as denominator), i.e.

$$\mathbf{AI} = \frac{\mathbf{S} + \mathbf{Pb} + \mathbf{Zn}}{\mathbf{Ag} + \mathbf{Cu} + \mathbf{Bi} + \mathbf{As}} \qquad \textbf{(8.5)}$$

The AI of the Western Mineralisation for elevations of Table 8.16 varies between 5.24 and 348.74. The AI also can be used for detection of a blind or deeply buried mineralisation.

The Broken Hill Domain contains the world's largest Zn-Pb-Ag deposit, the area has undergone at east 12 km of denudation between the Palaeoproterozoic and the Neoproterozoic and Phanerozoic denudation (Plimer 1984). There are hundreds of small Broken Hill type deposits in the Domain in the Cues Formation, Parnell Formation, Freyers Metasediments and Hores Gneiss. Compared with other major metallogenic provinces (e.g. Mount Isa), it is inconceivable that the Broken Hill deposit is an orphan and that other super-large Broken Hill-type deposits were also in the Willyama Supergroup. Because the Western Mineralisation does not crop out, it is ideal for the study of the ZC or DI and AI. If other large Broken Hill-type deposits are not exposed, these indices will be useful for anomalous evaluation of an area where there may only be minor sulphides or even quartz-gahnite and quartz-garnet lode horizon rocks. The closest analogue to Broken Hill is the Cannington deposit (Queensland) in the Eastern Fold Belt. An unmined exposed Broken Hill-type Zn-Pb-Ag deposit is known (i.e. Pegmont). Cannington has the following characteristics (Davidson et al. 1989; Giles & Nutman 2003; Laing 1998; Oliver et al. 2008):

1. Cannington is the same age as Broken Hill and occurs in the same lithological suite of rocks including quartz-gahnite and quartz-garnet rocks suggesting the same ore-forming processes,

2. It is far richer in silver and lead but lower in tonnage than Broken Hill,

3. It has abundant magnetite, a mineral absent from the Broken Hill deposit, and

4. It was discovered beneath Mesozoic cover rocks using gravity and magnetic surveys.

Since discovery, a large geochemical dispersion halo has been detected at the Mesozoic-Palaeoproterozoic unconformity and in Mesozoic sediments. If there is a Broken Hill or Cannington-type deposit in the Broken Hill Domain at a depth of 400 m, it would not be seen by the current geochemical, geological and geophysical methods used in mineral exploration at Broken Hill. Such a deposit may be seen by using the DI or ZC and AI developed in this study combined with deep electrical geophysics (e.g. Zeus method[2]). If another Broken Hill orebody had been removed by weathering and erosion, the tail of a geochemical anomaly may be present at the current level of erosion and may be expressed in the DI or ZC and AI.

8.4 Classification of anomalous concentrations

For anomalous separation, eight different cross-sections are mapped for each element of interest and the concentrations of each group of the cross-sections are shown by colour indices (Figures 8.5 to 8.12). It should be noted that the major differences between Figures 8.5 to 8.12 with the corresponding Figures 7.4 to 7.7 are their colour indices (their range of element concentrations) and the scale of the diagrams, but the geometrical characteristics of the corresponding geochemical haloes within the two groups of cross-sections are the same.

[2]**A proprietary induced polarization (IP) and resistivity technology.**

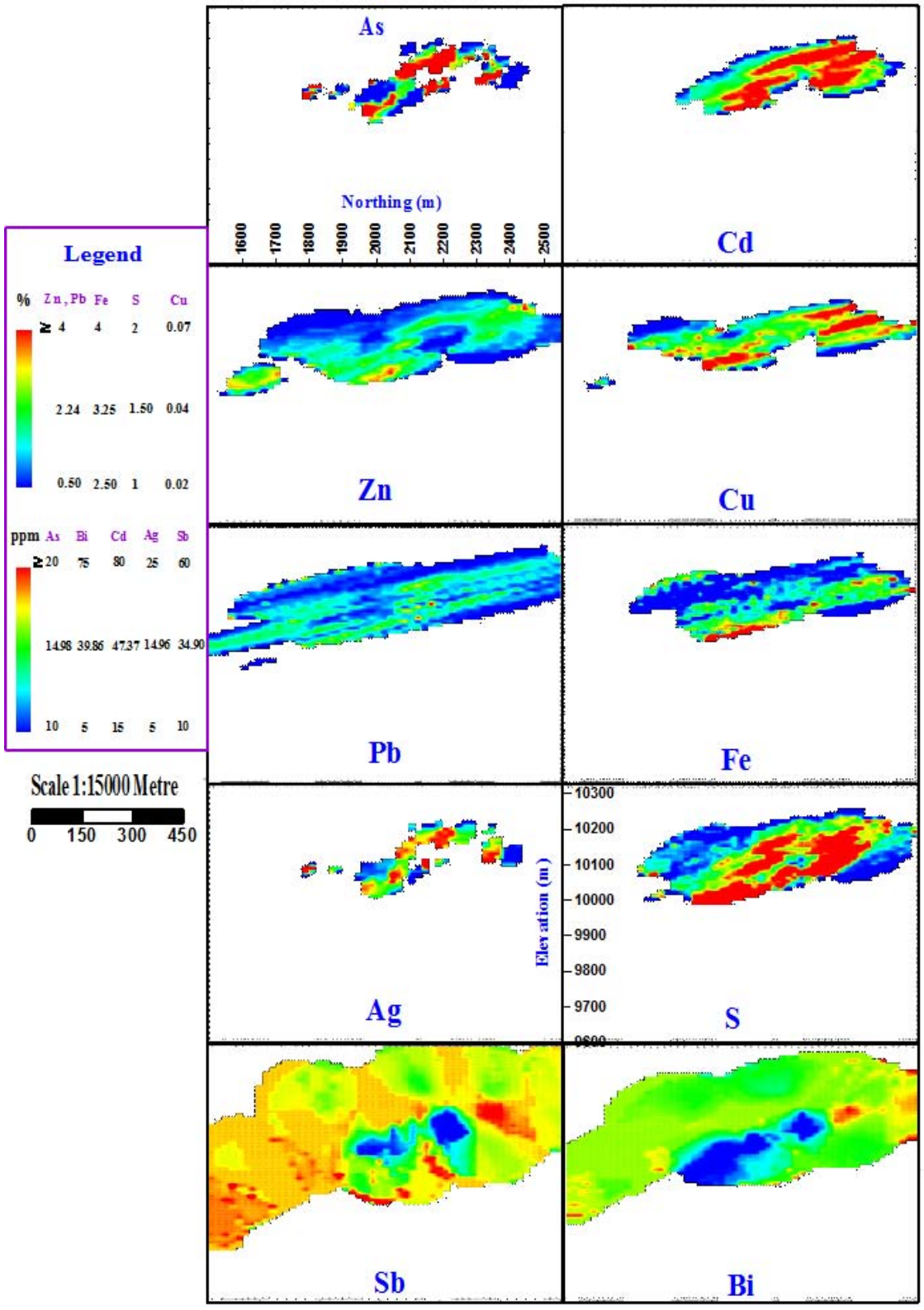

Figure 8.5: The longitudinal sections of 10 geochemical haloes between local threshold and anomalous levels at E=9467 m.

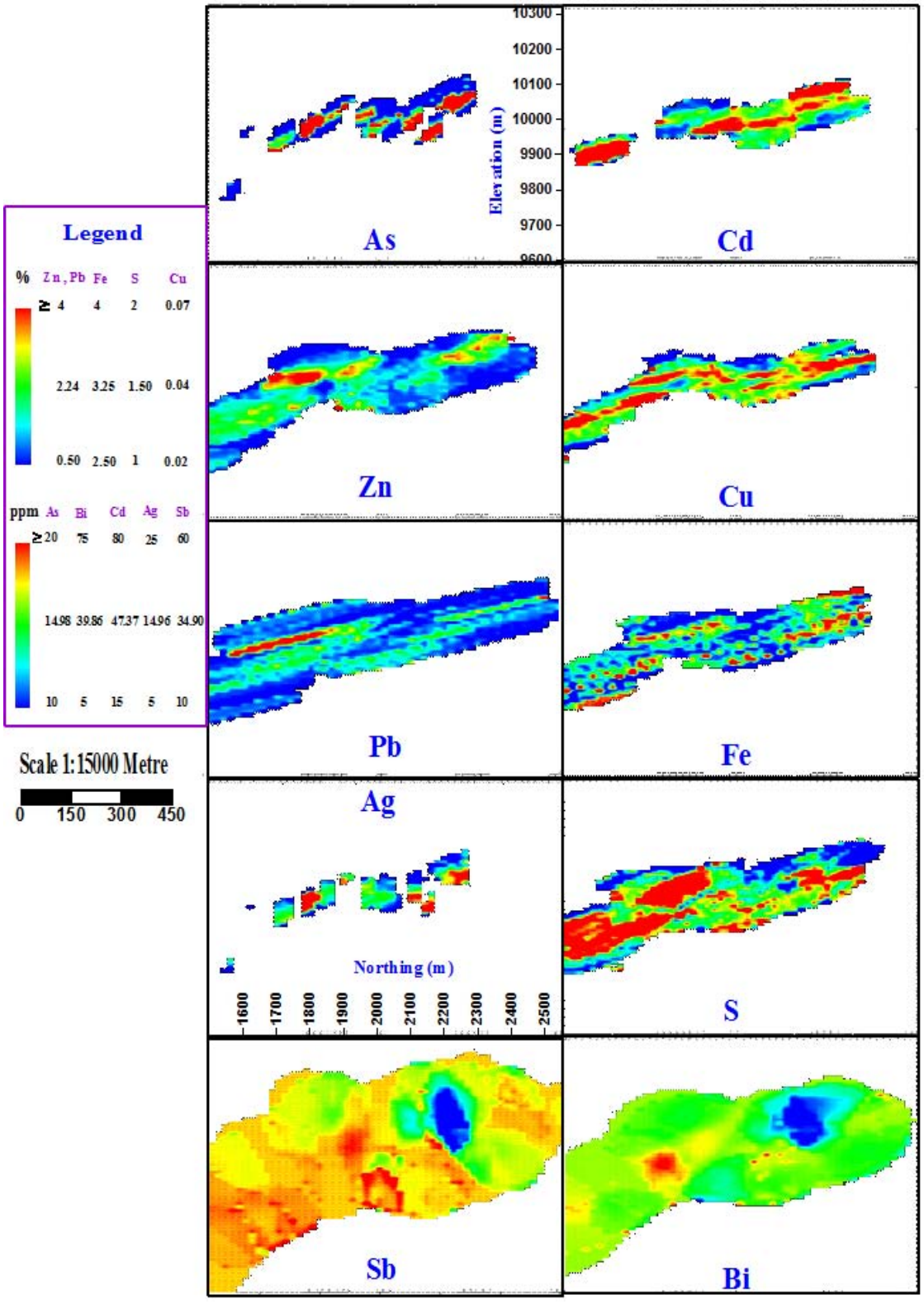

Figure 8.6: The longitudinal sections of 10 geochemical haloes between local threshold and anomalous levels at E= 9357 m.

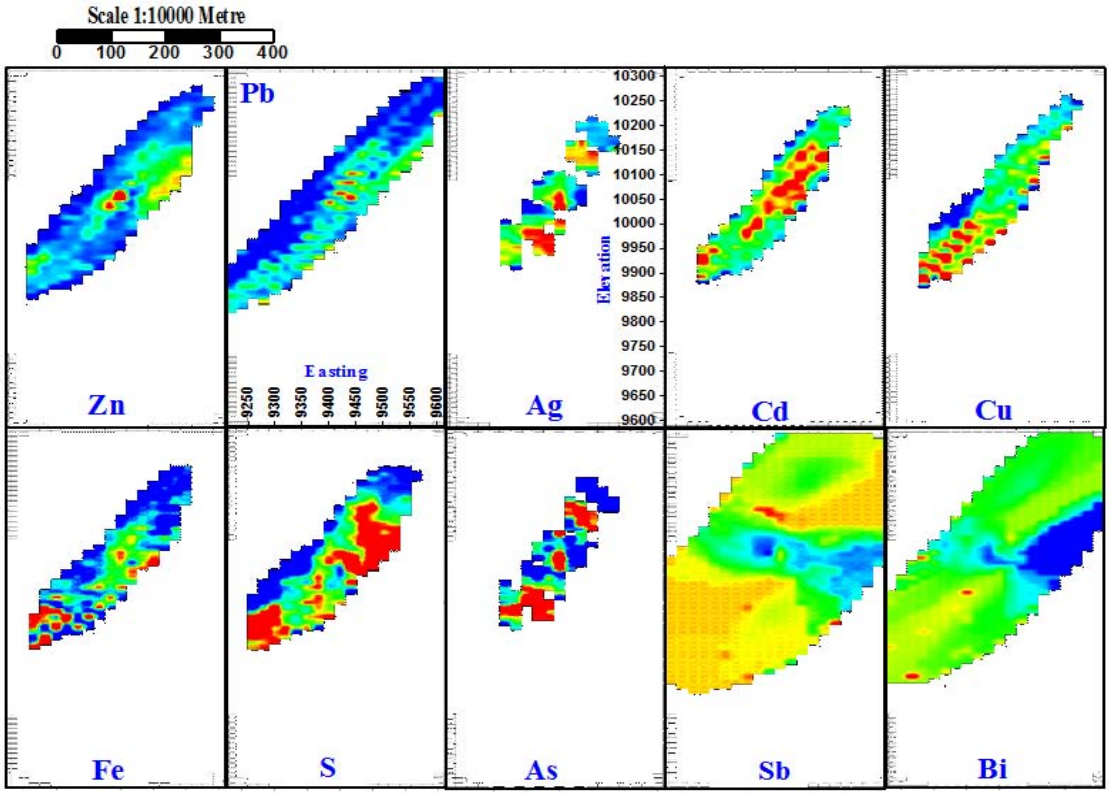

Figure 8.7: The E-W axial sections of 10 geochemical haloes between local threshold and anomalous levels at N=2109 m. (Colour indices of Figure 8.7 are the same as those shown in Figures 8.5 or 8.6).

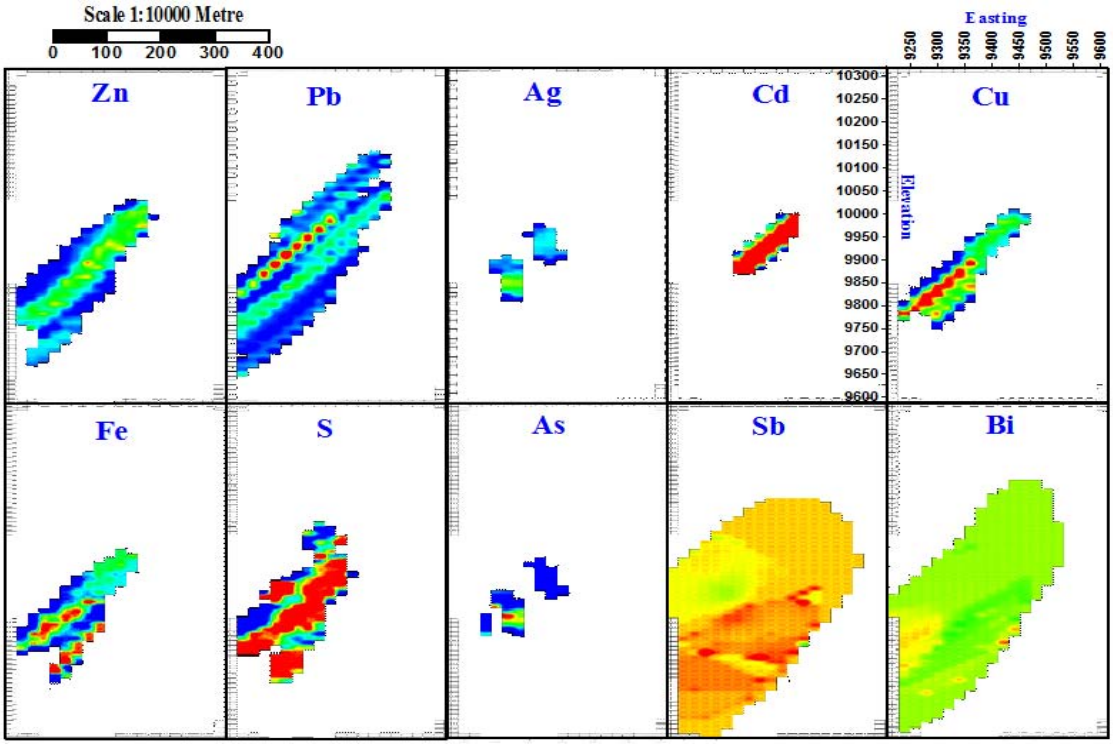

Figure 8.8: The E-W axial sections of 10 geochemical haloes between local threshold and anomalous levels at N=1639 m. (Colour indices of Figure 8.8 are the same as those shown in Figures 8.5 or 8.6).

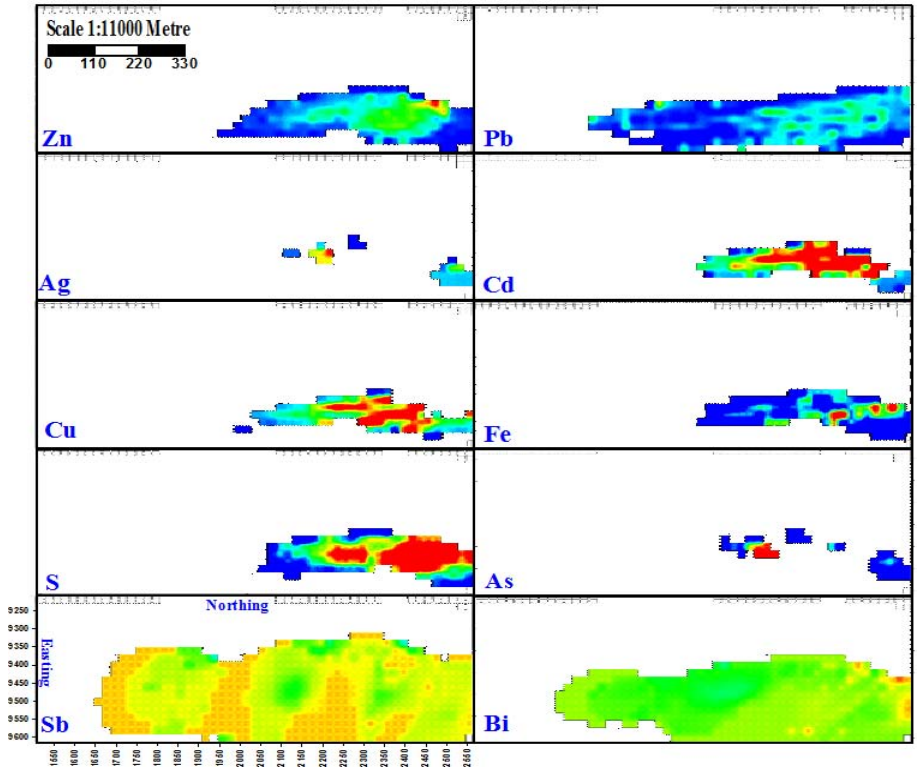

Figure 8.9: The transverse sections of 10 geochemical haloes between local threshold and anomalous levels at elevation=10218 m. (Colour indices of Figure 8.9 are the same as those shown in Figures 8.5 or 8.6).

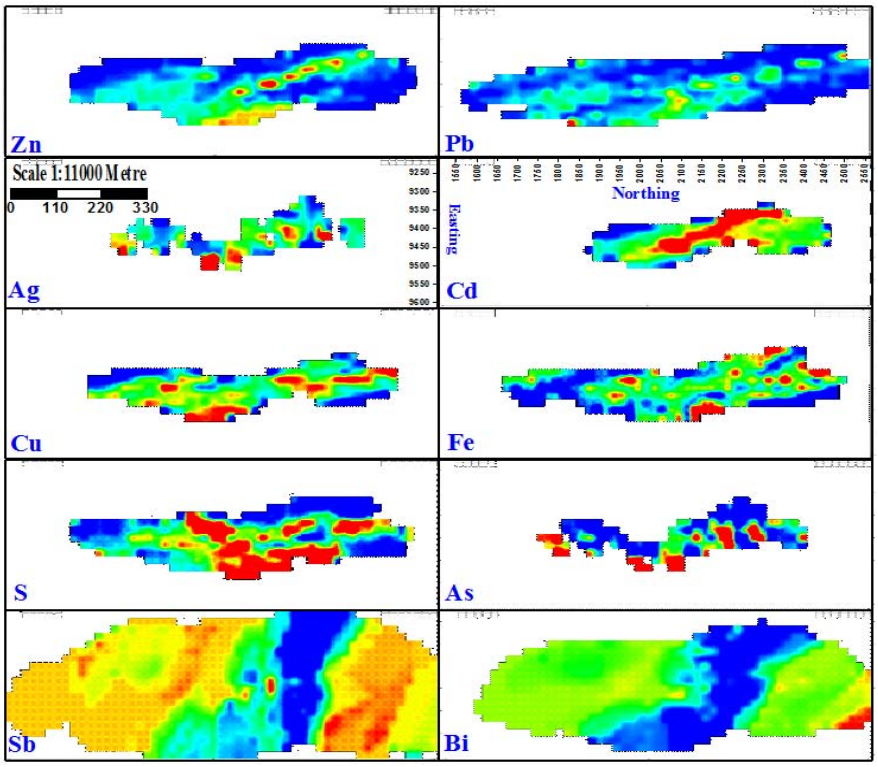

Figure 8.10: The transverse sections of 10 geochemical haloes between local threshold and anomalous levels at elevation=10078 m. (Colour indices of Figure 8.10 is the same as those shown in Figures 8.5 or 8.6).

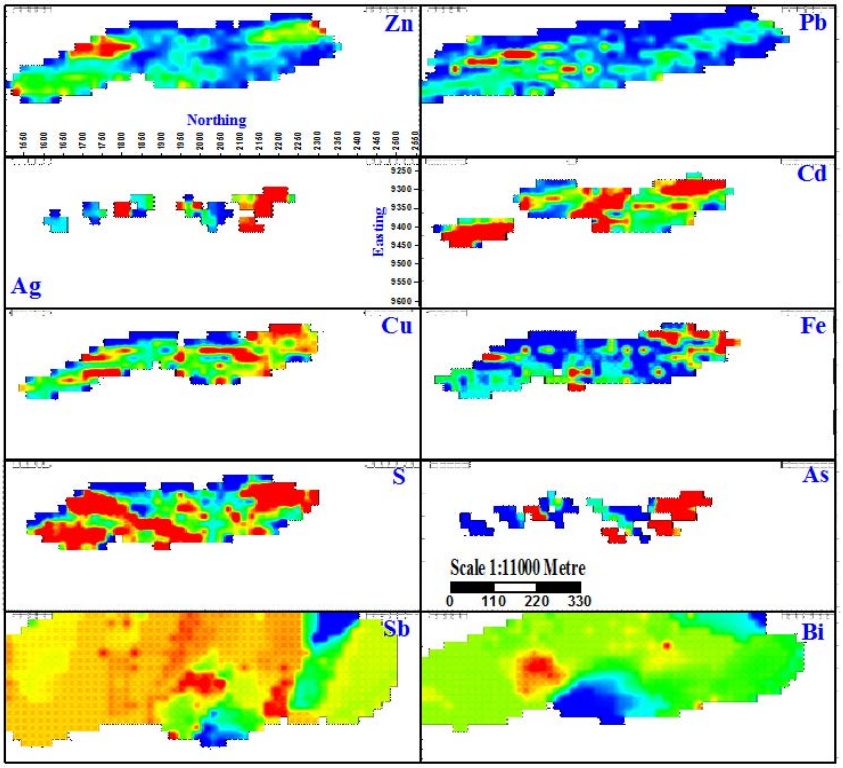

Figure 8.11: The transverse sections of 10 geochemical haloes between local threshold and anomalous levels at elevation=9958 m. (Colour indices of Figure 8.11 are the same as those shown in Figures 8.5 or 8.6).

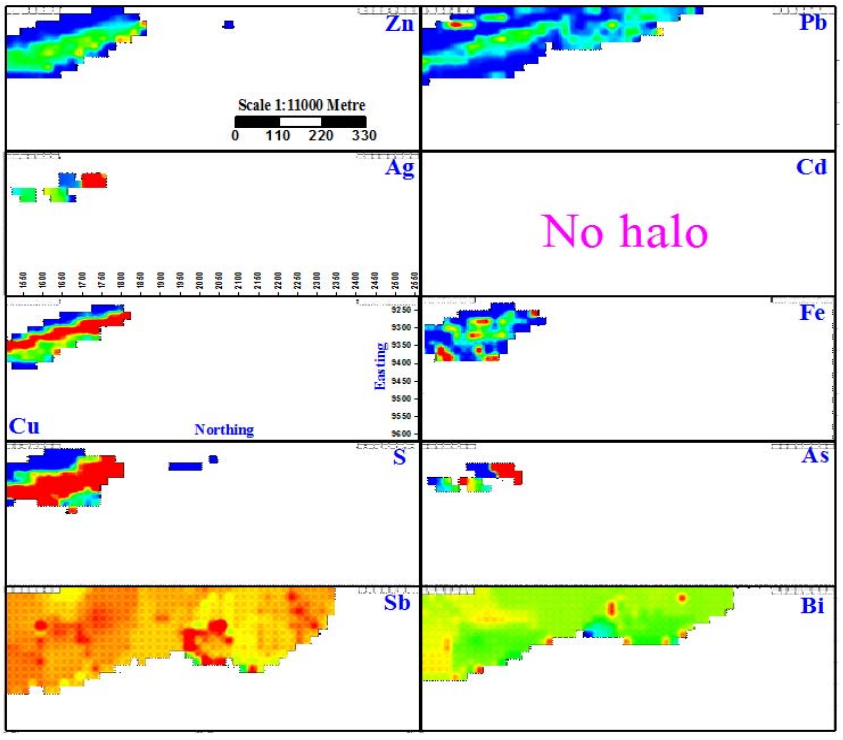

Figure 8.12: The transverse sections of 10 geochemical haloes between local threshold and anomalous levels at elevation=9848 m. (Colour indices of Figure 8.12 is the same as those shown in Figures 8.5 or 8.6).

The colour indices in Figures 8.5 or 8.6 classify anomalous concentrations for 10 elements. The anomalous range starts with a local threshold concentration to a relative high concentration value within the plots. In order to enhance the contrast of colour resolution within images, the relative maximum concentrations of each element were considered instead of their respective absolute maximum concentrations. A deviation from lower grade towards higher grade corresponds to concentration (enrichment) and from higher grade toward lower grade means dispersion (depletion) for each element concentration.

The spatial classification of anomalous concentration of 10 elements provides the opportunity to identify enrichment and depletion patterns for all elements simultaneously for each portion of the Western Mineralisation and for detecting their underlying structural relationships. In general, among Figures 8.5 to 8.12, there are some similarities between concentration variations and anomalous areas among the following geochemical haloes:

1. As and Ag,
2. Sb and Bi, and
3. S, Fe, Cd, Cu and Zn.

In the Western Mineralisation, the extent and intensity of geochemical alteration can be explained by diverse element concentrations in a different locus of anomaly in Figures 8.5 to 8.12. The variations of anomalous concentrations within the plots express the amount of mobility of the elements from depleted zones to an enriched area within the Western Mineralisation. The different mobility of elements of the Western Mineralisation may be attributed to various internal factors, including inherent physical and chemical properties of the elements and numerous external factors such as:

1. Lithostratigraphy,
2. Chemical behaviour of the elements,
3. Variable chemical environments, and
4. Structural geology.

Because the Western Mineralisation will be concurrently mined from a number of stopes, ore blending will minimise the high Bi and Sb in lead concentrate. Both these elements are penalty elements. However, this study provides a prediction of concentration and depletion of the ore elements (Pb and Zn), penalty elements (Bi, Sb and As) and bonus

elements (Ag, Cd and Au). The zonation from Zn-rich to Pb-rich at depth (Figures 8.5 to 8.12) is an important conclusion. The mill design at Broken Hill is for "average" Western Mineralisation ore derived from one down dip PQ hole. Although the behaviour of Broken Hill ores in crushing, grinding and froth flotation mills has been documented after some 200 Mt tonnes of sulphide ore treatment, this study shows that the early mill feed will have a higher $\frac{Zn}{Pb}$ ratio than mill feed later in the mining operation. This may affect recoveries as froth flotation circuits are specifically designed to treat ore of constant mineralogy and chemistry. Figures 8.5 to 8.12 also show that the concentrations of Cu and Fe have been elevated with depth and halo of Sb has higher concentration relative to Bi.

The variation of geochemical anomalies in different cross-sections (Figures. 8.5 to 8.12) may be used to distinguish different underlying geological structures (e.g. faults) transgressing the Western Mineralisation. In geochemical plots, a fault may appear a linear pattern or chained structure, or intrusive rocks may produce an arcuate shape (Cheng, 1999), or changes in rock type and geophysical properties may result in changes of the overall shape of the mineralised zone. Table 8.17 outlines a range of concentrations for anomaly; threshold and background for 10 elements in the Western Mineralisation resulted from the colour indices of Figure 8.5 and Figure 7.4.

Table 8.17: The range of concentrations for anomaly, threshold and background for 10 elements of the Western Mineralisation.

Elements	Background range	Threshold range	Anomalous range
Pb % , Zn %	X* < 0.25	0.25 ≤ X ≤ 0.50	0.50 < X
Fe %	X < 2	2 ≤ X ≤ 2.5	2.5 < X
S %	X < 0.75	0.75 ≤ X ≤ 1	1 < X
Cu %	X < 0.01	0.01 ≤ X ≤ 0.02	0.02 < X
Sb (ppm)	X < 5	5 ≤ X ≤ 10	10 < X
Ag (ppm)	X < 2.5	2.5 ≤ X ≤ 5	5 < X
Cd (ppm)	X < 10	10 ≤ X ≤ 15	15 < X
Bi (ppm)	X < 3	3 ≤ X ≤ 5	5 < X
As (ppm)	X < 7	9 ≤ X ≤ 10	10 < X

*Concentration

8.5 Spatial variations of the sulphide minerals, magnetic susceptibility and specific gravity in the Western Mineralisation

Figures 8.13 to 8.20 show the variation of sulphide mineral (vol. %), magnetic susceptibility (SI) and specific gravity for the different sections of the Western Mineralisation. Those Figures show some similarities in distribution patterns and spatial continuity of sphalerite, AMS, MMS, chalcopyrite and pyrrhotite. Visual zonation of pyrrhotite shows that the Western Mineralisation has a weak halo of pyrrhotite (Plimer 2006b) and this is consistent with the zonation of pyrrhotite in Figures 8.13 to 8.20 that is narrower than the zonation of sphalerite.

The distribution pattern of galena is wider than that of sphalerite in all sections of Figures 8.13 to 8.20 and this is comparable with distribution halo patterns of Pb and Zn. Galena was distinctly enriched in the southern parts of the Western Mineralisation between N=1550 m and N=1900 m whereas sphalerite is pronounced in the northern section of the Western Mineralisation between N=1900 m and N=2350 m. Figures 8.13 and 8.14 further support the dispersal pattern of elevated galena (vol. %) at the N=1639 m in comparison with the N=2109 m and an antithetic pattern for sphalerite (vol. %). The variation of specific gravity in the different cross-sections is small because there is not enough data for reliable estimation. Since the sulphide-bearing rocks also contain dense minerals such as garnet and gahnite, it is unlikely that changes in Western Mineralisation specific gravity are correlated with grade.

The tonnage and grade of Broken Hill ores along the Main Line of Lode is in the hinges of F3 folds and sulphide masses along axial plane cleavages or droppers are common. Remobilisation and redistribution of sulphides during the Olarian and Delamerian Orogenies at Broken Hill is well documented (Plimer 1984). The scale of this local redistribution is not known. However, because the Western Mineralisation is on a downward-facing F1 limb and has been folded in the F2 Broken Hill Antiform, Figures 8.13 to 8.20 show that the scale of remobilisation is less than the drill spacing for the Western Mineralisation otherwise zoning would be spatially-related to structure.

Tables 8.18 and 8.19 outline the variation in abundance and dispersion of the sulphide minerals and magnetic susceptibility from surface to the depth of the Western Mineralisation based on observations of Figures 8.17 to 8.20.

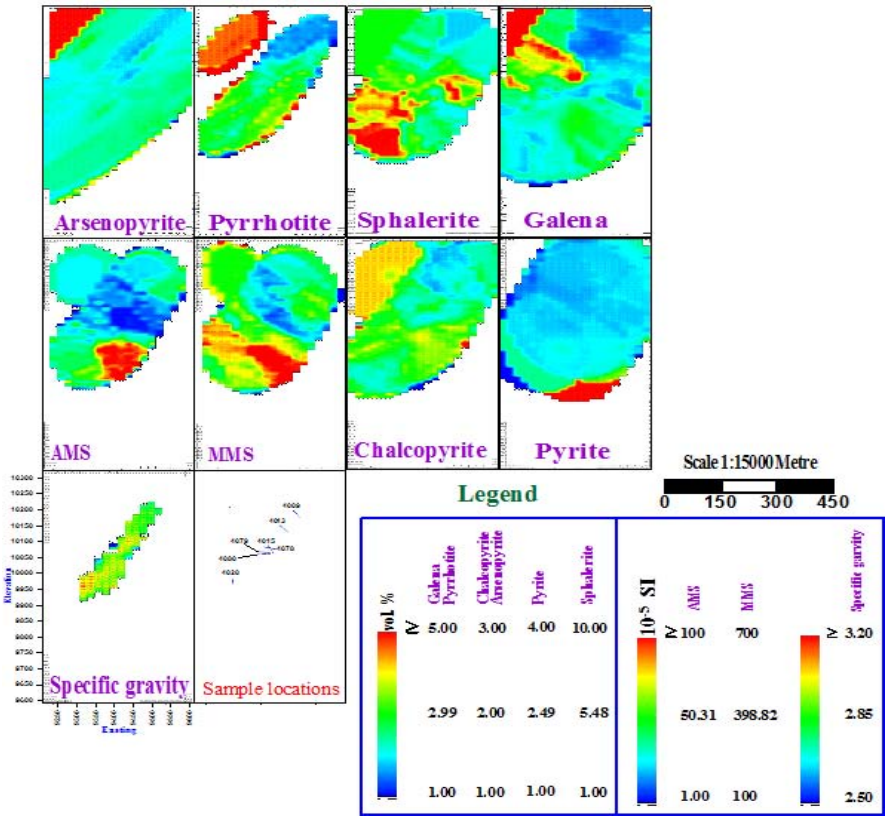

Figure 8.13: Variations of the sulphide minerals, magnetic susceptibility and specific gravity on the E-W axial sections at N=2109 m.

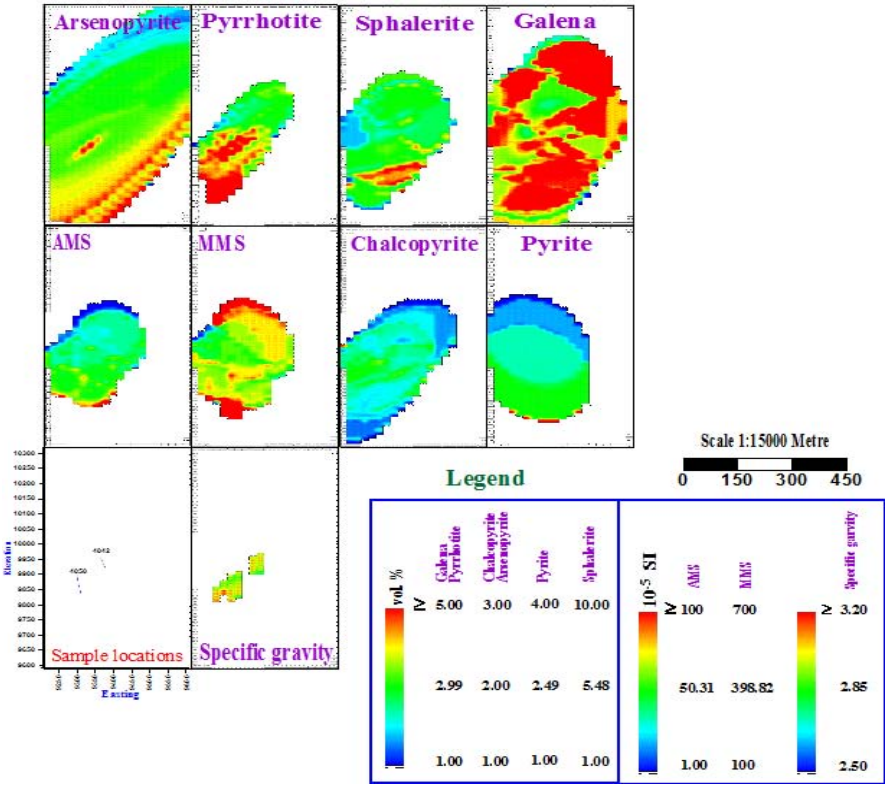

Figure 8.14: Variations of the sulphide minerals, magnetic susceptibility and specific gravity on the E-W axial section at N=1639 m.

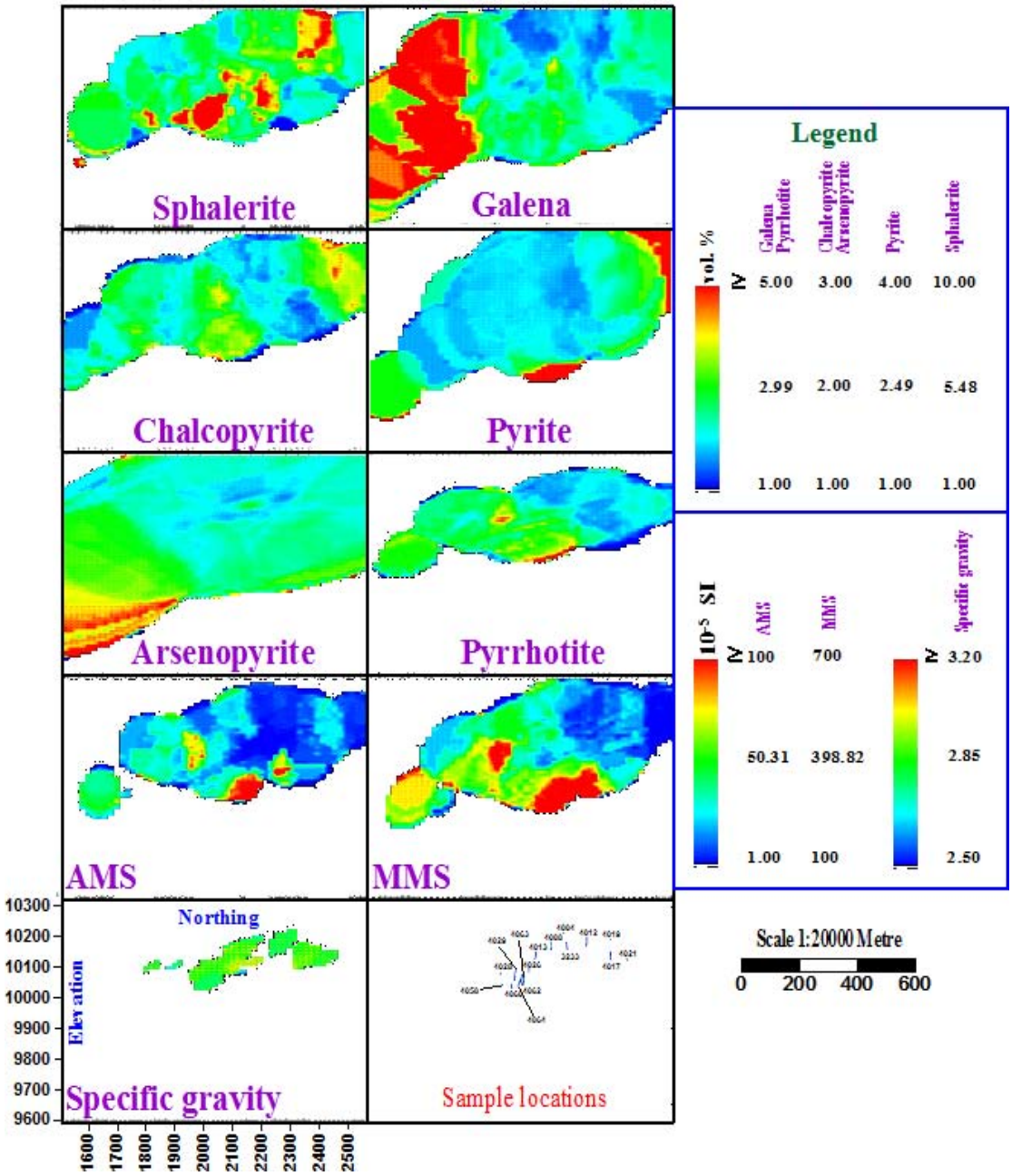

Figure 8.15: Variations of the sulphide minerals, magnetic susceptibility and specific gravity on the N-S longitudinal sections at E=9467 m.

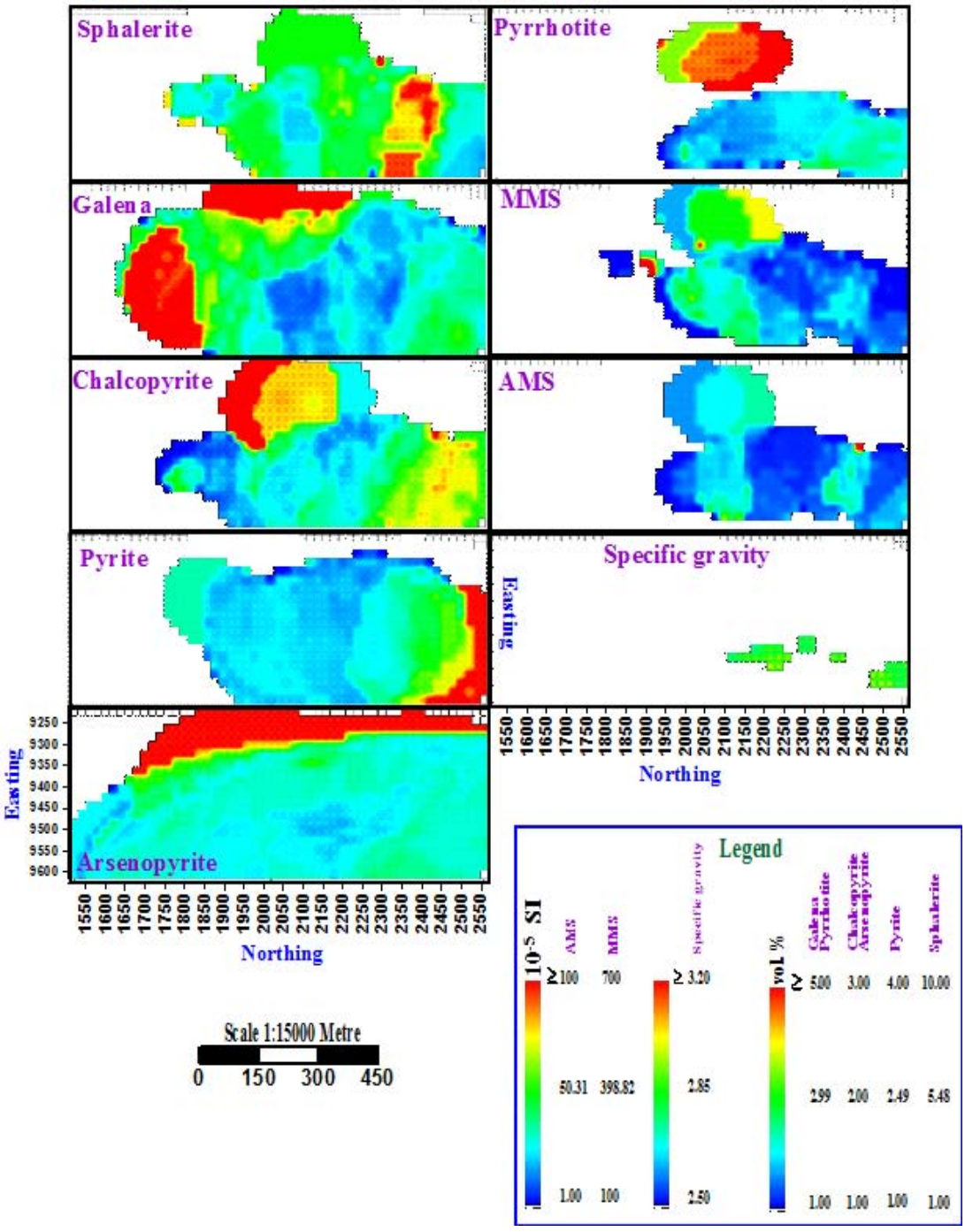

Figure 8.16: Variations of the sulphide minerals, magnetic susceptibility and specific gravity on the N-S longitudinal sections at E=9357 m.

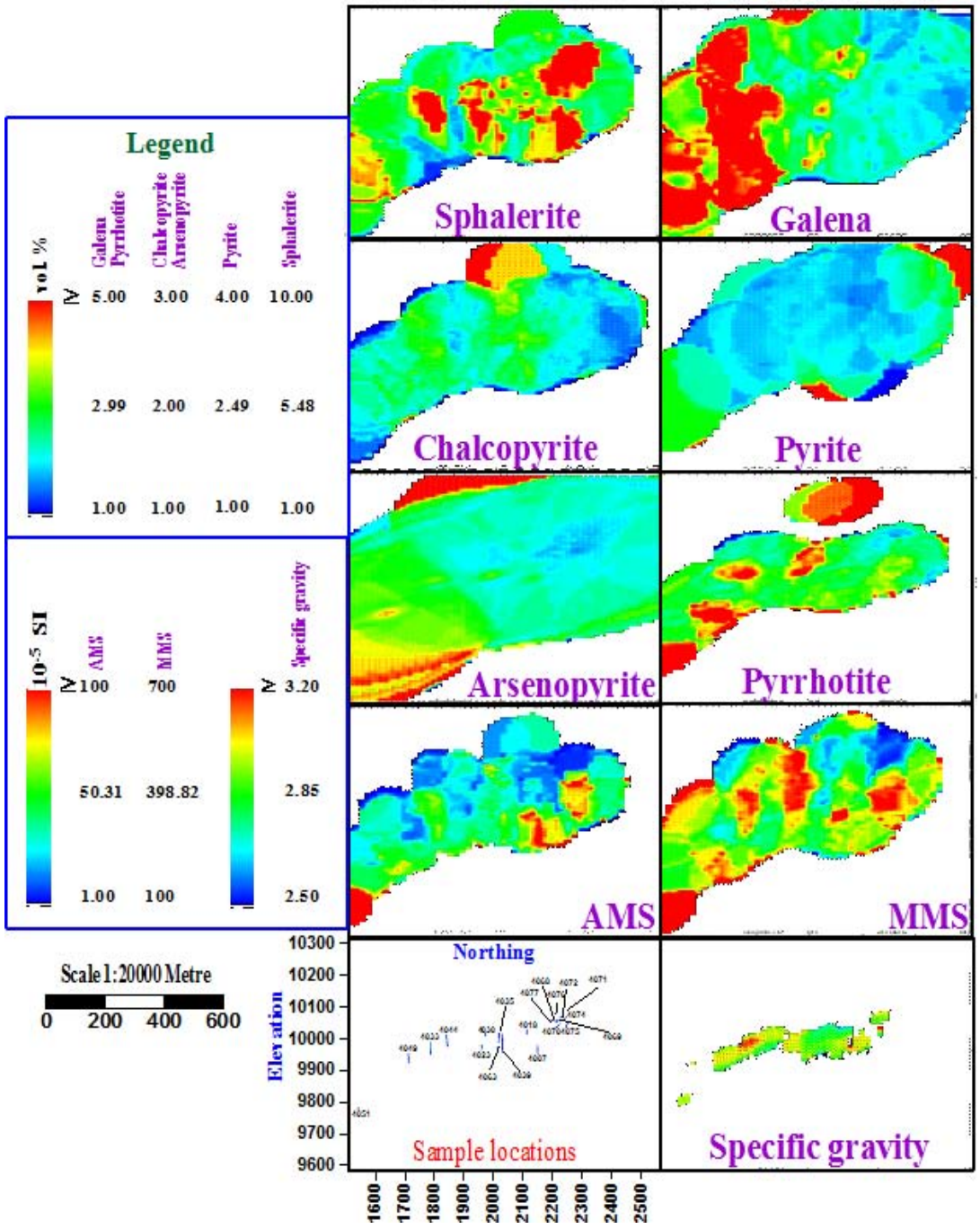

Figure 8.17: Variations of the sulphide minerals, magnetic susceptibility and specific gravity on the transverse sections at elevation=10218 m.

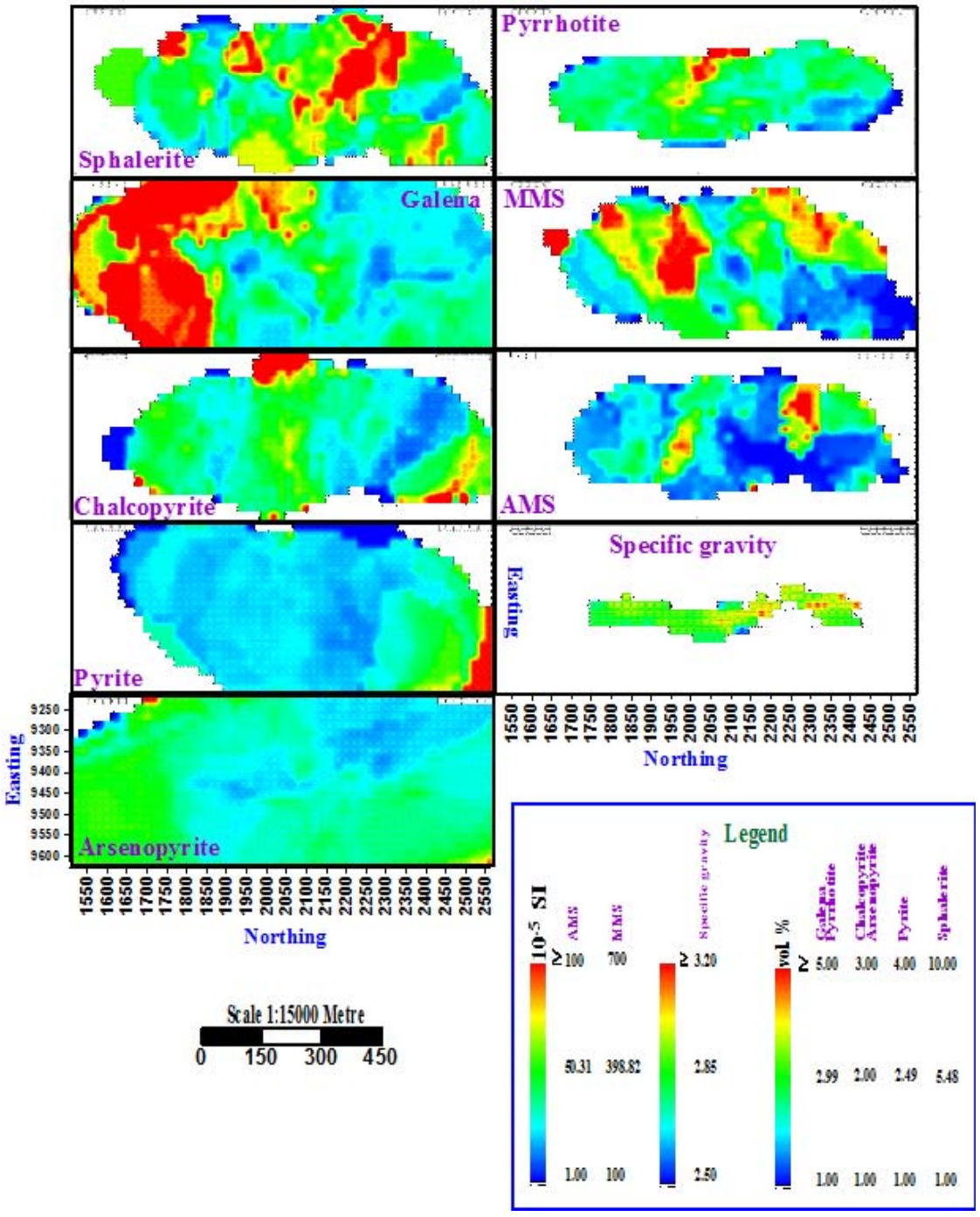

Figure 8.18: Variations of the sulphide minerals, magnetic susceptibility and specific gravity on the transverse sections at elevation=10078 m.

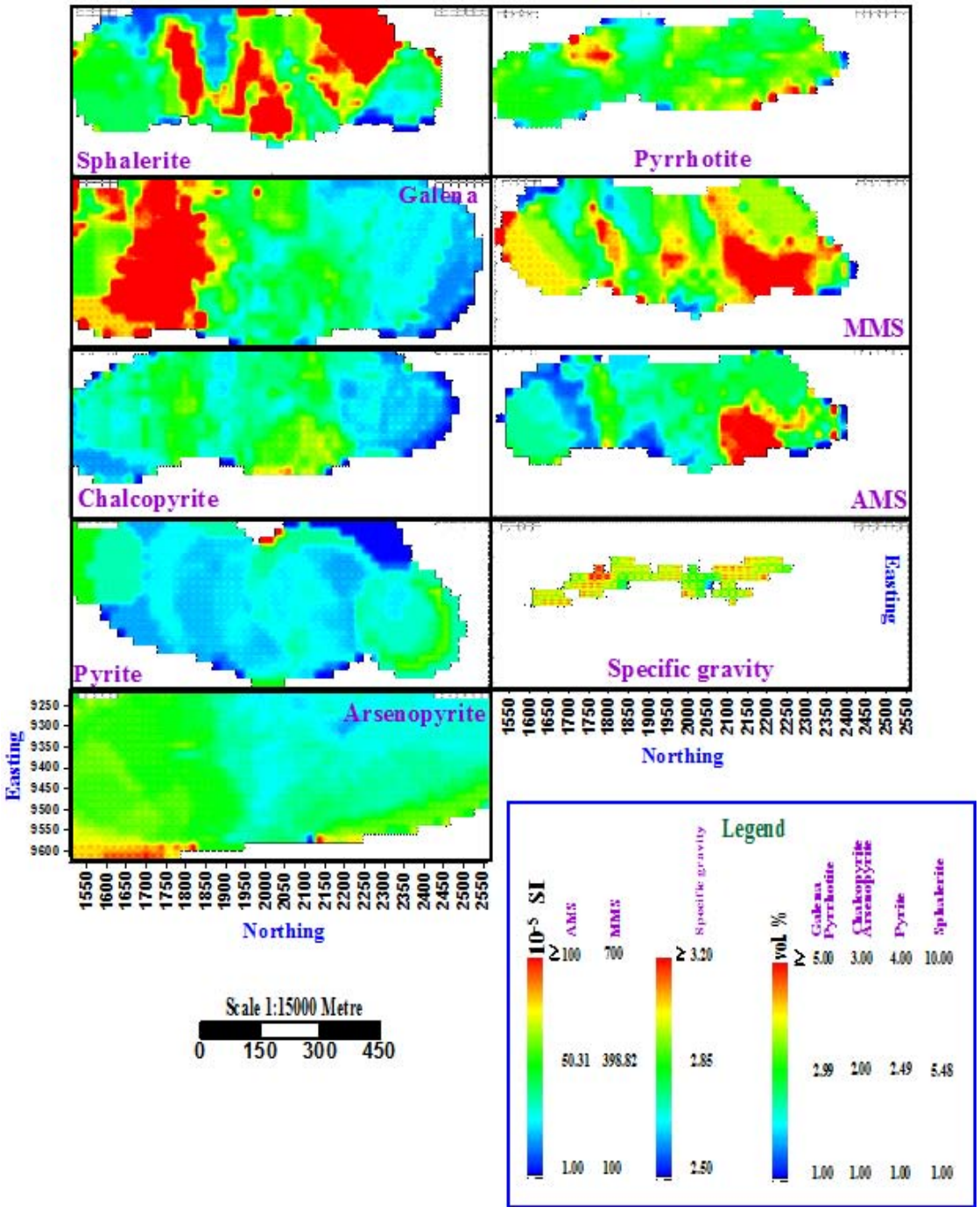

Figure 8.19: Variations of the sulphide minerals, magnetic susceptibility and specific gravity on the transverse sections at elevation=9958 m.

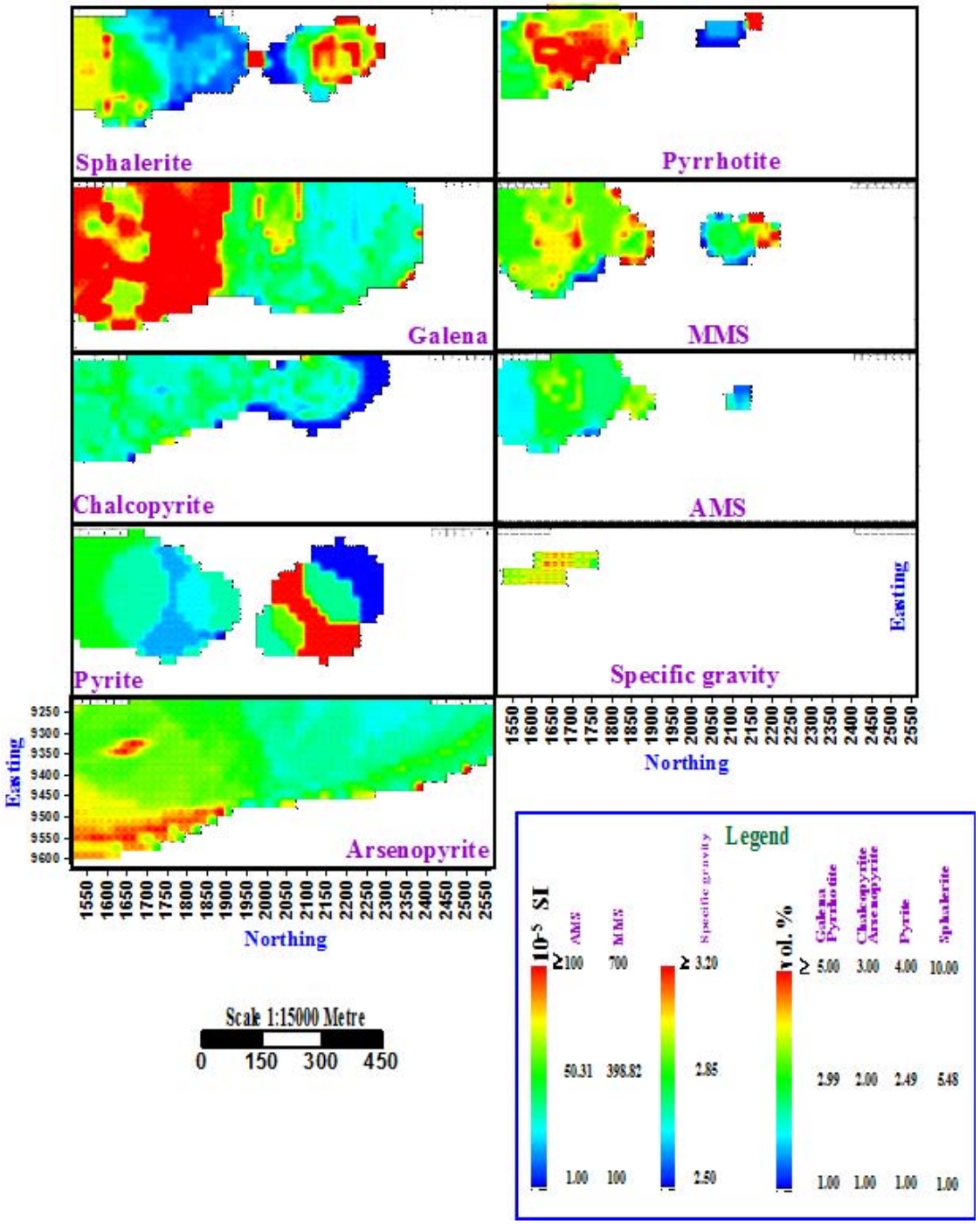

Figure 8.20: Variations of the sulphide minerals, magnetic susceptibility and specific gravity on the transverse sections at elevation=9848 m.

Table 8.18: Variation model for sulphide minerals.

Sulphide minerals	Variation
Sphalerite	Enrichment at the middle depth section
Chalcopyrite	Depletion with depth and decrease of distribution
Pyrite	Enrichment with depth

Table 8.19: Variation model for magnetic susceptibility.

Magnetic susceptibility	Variation	Comments
AMS & MMS	Increase of the magnetic susceptibility at the middle section of depth	Increase of conversion of pyrrhotite with depth (i.e. changing from non-magnetic pyrrhotite to the magnetic pyrrhotite)

8.6 Correspondence analysis for garnet samples of the Broken Hill orebodies

In this section, before the study of spatial variation of silicate minerals in the Western Mineralisation, the previous data sets of garnet samples were analysed statistically and the results were interpreted. Garnet is conducted because it is one of the most common accessory silicate minerals in the Broken Hill deposit. It has a grain size of 0.05-3 cm and can be lilac, red, pink, orange and brown. General formula of garnet is $A_3B_2 (SiO_4)_3$ and at Broken Hill, it is a solid solution of the six common garnet end-members [almandine (Fe, Al), grossular (Ca, Al), pyrope (Mg, Al), spessartine (Mn, Al), andradite (Ca, Fe) and uvarovite (Ca, Cr)].

The Broken Hill garnet samples were collected by Kitchen (2001), Sproal (2001), Tully (2002), Groombridge (2003), Patchett (2003) and Munyantwali (2006) and they were analysed by EMPA. All samples were analysed on the same machine. Average compositions of garnet types within the Broken Hill orebodies are presented in Table 8.20. In this section, the Broken Hill orebodies are categorised based on their relation to the average percent of garnet types using simple correspondence analysis. Table 8.20 shows that the average percentage of almandine in the Western Mineralisation is higher than that of the other orebodies.

There are significant differences between average percent of garnet types in Table 8.20, and this will produce significant differences between variance of the average percent of garnet types and outcome of correspondence analysis. Therefore, the data set of Table 8.20 needs to be standardised using z-transformation [Equation (4.1)]. The z-transformed values of Table 8.20 produce some negative values (Table 8.21) and because correspondence analysis are performed only with positive values, a constant value of 2 was added to the all z-transformed values of Table 8.21 in order to change them to positive values (Table 8.22). The reason for this was explained before in the Section 4.3.1.2. The result of decomposition of data set of Table 8.22 into five dimensions is given in Table 8.23.

Table 8.20: Average percentage of garnet types in garnet samples collected from the Broken Hill orebodies.

Researcher	The number of Samples	Garnet types / Orebody	Almandine $Fe_3Al_2(SiO_4)_3$	Spessartine $Mn_3Al_2(SiO_4)_3$	Pyrope $Mg_3Al_2(SiO_4)_3$	Grossular $Ca_3Al_2(SiO_4)_3$	Andradite $Ca_3Fe_2(SiO_4)_3$	Uvarovite $Ca_3Cr_2(SiO_4)_3$
Tully (2002)	75	A Lode	62.195	21.024	8.912	4.53	3.298	0.051
Tully (2002)	50	B Lode	48.409	34.225	7.131	9.168	0.986	0.082
Sproal (2001)	27	C Lode	63.506	22.987	8.33	1.821	3.332	0.039
Tully (2002)	50	1 Lens	74.403	11.971	12.281	0.059	1.242	0.059
Sproal (2001)	54	2 Lens	27.5173	28.567	3.4348	34.448	5.8213	0.2163
Groombridge (2003)	8							
Groombridge (2003)	31	3 Lens	5.93	76.44	2.32	15.31	0.0001	0.0001
Patchett (2003)	74	The Western Mineralisation	66.22	16.5297	11.8577	2.6927	2.6597	0.051
Kitchen (2001)	19							

Table 8.21: The z-transformed values of Table 8.20.

Garnet types / Orebody	Almandine $Fe_3Al_2(SiO_4)_3$	Spessartine $Mn_3Al_2(SiO_4)_3$	Pyrope $Mg_3Al_2(SiO_4)_3$	Grossular $Ca_3Al_2(SiO_4)_3$	Andradite $Ca_3Fe_2(SiO_4)_3$	Uvarovite $Ca_3Cr_2(SiO_4)_3$
A Lode	0.505710284	-0.426097607	0.303529	-0.42962	0.42389748	-0.2945
B Lode	-0.05404451	0.183642614	-0.16264	-0.04557	-0.7698516	0.157457
C Lode	0.558940992	-0.335428714	0.151194	-0.65394	0.44145262	-0.46946
1 Lens	1.001393335	-0.844246098	1.185344	-0.79984	-0.6376718	-0.17787
2 Lens	-0.90231299	-0.077694419	-1.13009	2.047719	1.72674661	2.115465
3 Lens	-1.77882501	2.133508793	-1.42189	0.46301	-1.2788989	-1.03659
The Western Mineralisation	0.669137895	-0.633684568	1.074548	-0.58176	0.09432565	-0.2945

Table 8.22: The z-transformed values+2 of Table 8.21.

Garnet types / Orebody	Almandine $Fe_3Al_2(SiO_4)_3$	Spessartine $Mn_3Al_2(SiO_4)_3$	Pyrope $Mg_3Al_2(SiO_4)_3$	Grossular $Ca_3Al_2(SiO_4)_3$	Andradite $Ca_3Fe_2(SiO_4)_3$	Uvarovite $Ca_3Cr_2(SiO_4)_3$
A Lode	2.50571	1.57390	2.30353	1.57038	2.42390	1.70550
B Lode	1.94596	2.18364	1.83736	1.95443	1.23015	2.15746
C Lode	2.55894	1.66457	2.15119	1.34606	2.44145	1.53054
1 Lens	3.00139	1.15575	3.18534	1.20016	1.36233	1.82213
2 Lens	1.09769	1.92231	0.86991	4.04772	3.72675	4.11547
3 Lens	0.22117	4.13351	0.57811	2.46301	0.72110	0.96341
The Western Mineralisation	2.66914	1.36632	3.07455	1.41824	2.09433	1.70550

Table 8.23: The results of decomposition of Table 8.22 into five dimensions.

Dimensions	Inertia	Proportion of inertia	Percentage of proportional inertia (PPI)	Percentage of cumulative inertia (PCI)
1	0.1307	0.6640	66.40	66.40
2	0.0565	0.2871	28.71	95.11
3	0-0083	0.0422	4.22	99.33
4	0.0013	0.0065	0.65	99.98
5	0.0000	0.0002	0.02	100.00
Total	0.1968			

8.6.1: Correspondence map for garnet samples of the Broken Hill orebodies

Figure 8.21 shows 95.11 percent[3] of the total variation of garnet types within the Broken Hill orebodies. Figure 8.21 shows that chemical composition of garnet types for A, B and C Lodes, 1 Lens and the Western Mineralisation are more associated with almandine and pyrope in comparison with other orebodies. Chemical composition of garnet types in 3 Lens is more related to spessartine and 2 Lens shows a greater relationship with chemical composition of uvarovite and andradite relative to other garnet types.

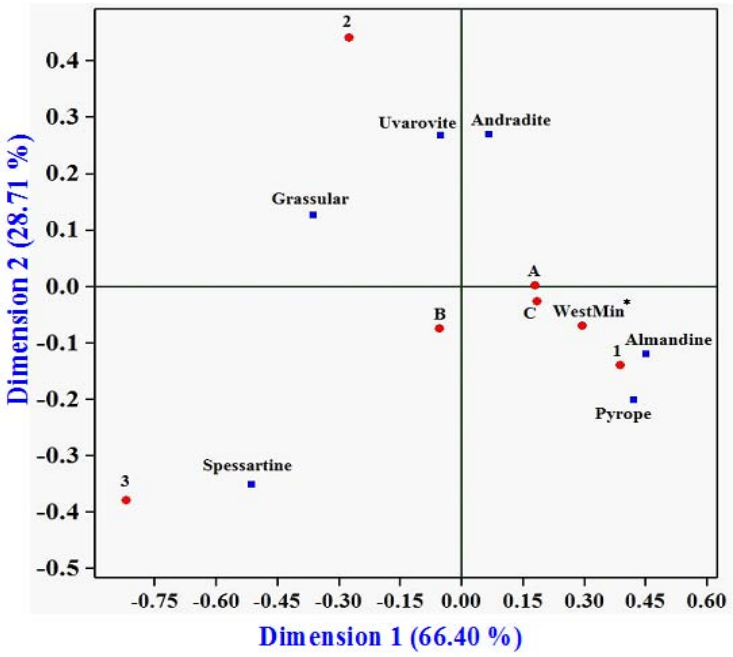

Figure 8.21: Correspondence map in relation to dimensions 1 and 2 for garnet (*the Western Mineralisation)

8.7: The 3D biplot of garnet types and samples of the Western Mineralisation

In this section, 543 garnet samples of Kitchen (2001), Patchett (2003) and Munyantwali (2006) are visualized using 3D biplot model of the CoDaPack3D. The information of introducing data into CoDaPack3D has been explained in Section 5.8.1 and the data set of this section has been provided in supplementary file to this thesis. The 3D biplot models (Figures 8.22 and 8.23) enable us to distinguish distribution patterns and the major chemical composition of garnet types in the Western Mineralisation. Figures 8.22 and 8.23 show the distribution of 543 garnet samples (points) among three groups including grossularite, andradite and the other four garnet types (i.e. spessartine, almandine, uvarovite and pyrope).

[3] **Calculated by PPI (dimension 1) + PPI (dimension 2) from Table 8.23**

The rotation of 3D biplot model in the CoDaPack3D software indicates that garnet samples from the Western Mineralisation were affected highly by chemical variation of Ca and Al (grossular), Ca and Fe (andradite) as well as Ca and Cr (uvarovite).

The following observations can be drawn from Figures 8.22 and 8.23:

1. Strong positive correlation between pyrope and almandine
2. Strong negative correlation between andradite and the other garnet types
3. Strong negative correlation between grossular and the other garnet types

Table 8.24: A summary of decomposition garnet samples of the Western Mineralisation into three PCs based on chemical composition of six garnet types.

PCs	PPI	PCI
PC_1	68	68
PC_2	19	87
PC_3	11	98

According to Table 8.24, a combination of the three PCs[4] explains 98 % of chemical variation of garnet types in the Western Mineralisation.

[4] **Calculated by PPV (PC_1) + PPV (PC_2) + PPV (PC_3) from Table 8.24**

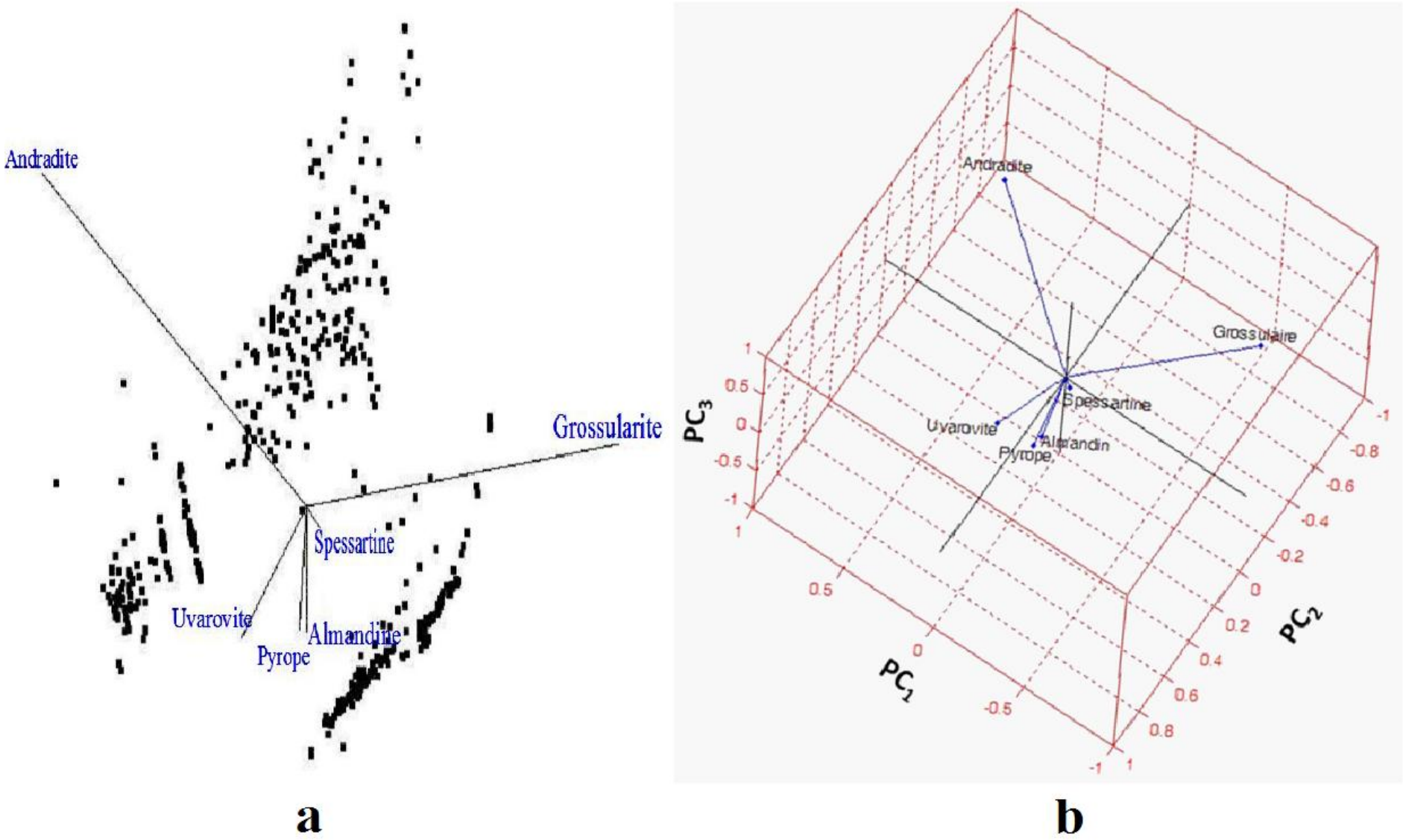

Figure 8.22: (a) the 3D biplot of garnet samples of the Western Mineralisation and (b) the axes of the 3D biplot in relation to three PCs.

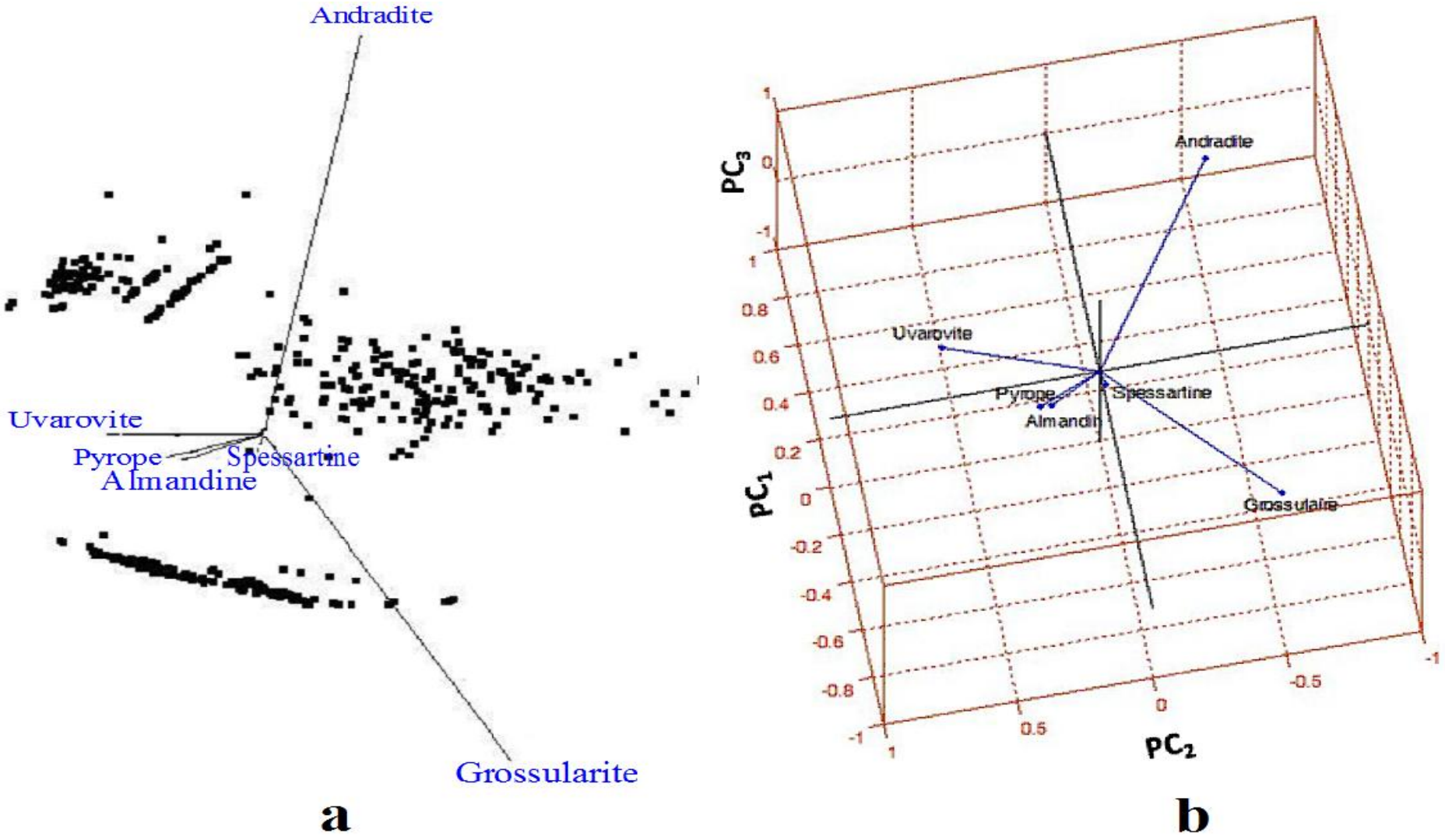

Figures 8.23: (a) the same plot as that of Figure 8.22, but viewing from a different angle and (b) the axes of the 3D biplot in relation to three PCs.

8.8: Spatial variations of the silicate minerals in the Western Mineralisation

Figures 8.24 to 8.31 display the variation of silicate mineral in different cross-sections. In those Figures, the following minerals show great similarities in their distribution patterns:

1. Gahnite and pink garnet, and
2. Blue quartz, green feldspar and hedenbergite.

In Figures 8.24 to 8.31, the following minerals show some similarities in their distribution patterns:

1. Orange garnet and rhodonite, and
2. Red garnet and white quartz.

Some silicate minerals (Figures 8.24 to 8.31) have distribution patterns similar to sulphide minerals, AMS, MMS and specific gravity (Figures 8.13 to 8.20). They are:

1. Green feldspar and arsenopyrite,
2. Rhodonite and pyrite,
3. Blue quartz, hedenbergite and galena,
4. Pink garnet, gahnite, sphalerite, pyrrhotite, AMS and MMS, and
5. White quartz and specific gravity.

Variations in abundance and dispersion of the silicate minerals from surface to depth based on observations of Figures 8.28 to 8.31 are given in Table 8.25.

Table 8.25: Variation models for silicate minerals.

Silicate minerals	Variations	Comments
Orange garnet	Enrichment with depth	Between N=1550 m and N=1950 m
Gahnite	Depletion with depth and decrease of distribution size with depth	
Red garnet	Enrichment at the middle portion of depth	Between N=1850 m and N=2100 m
Hedenbergite	Enrichment with depth	Between N=2150 m and N=2450 m

Each orebody at Broken Hill has slight mineralogical and chemical differences (as shown in this study by the variations in garnet chemistry. Zonation of silicate minerals (e.g. orange garnet, hedenbergite) and sulphides (galena, sphalerite) shows that the Western Mineralisation is not a homogeneous mass.

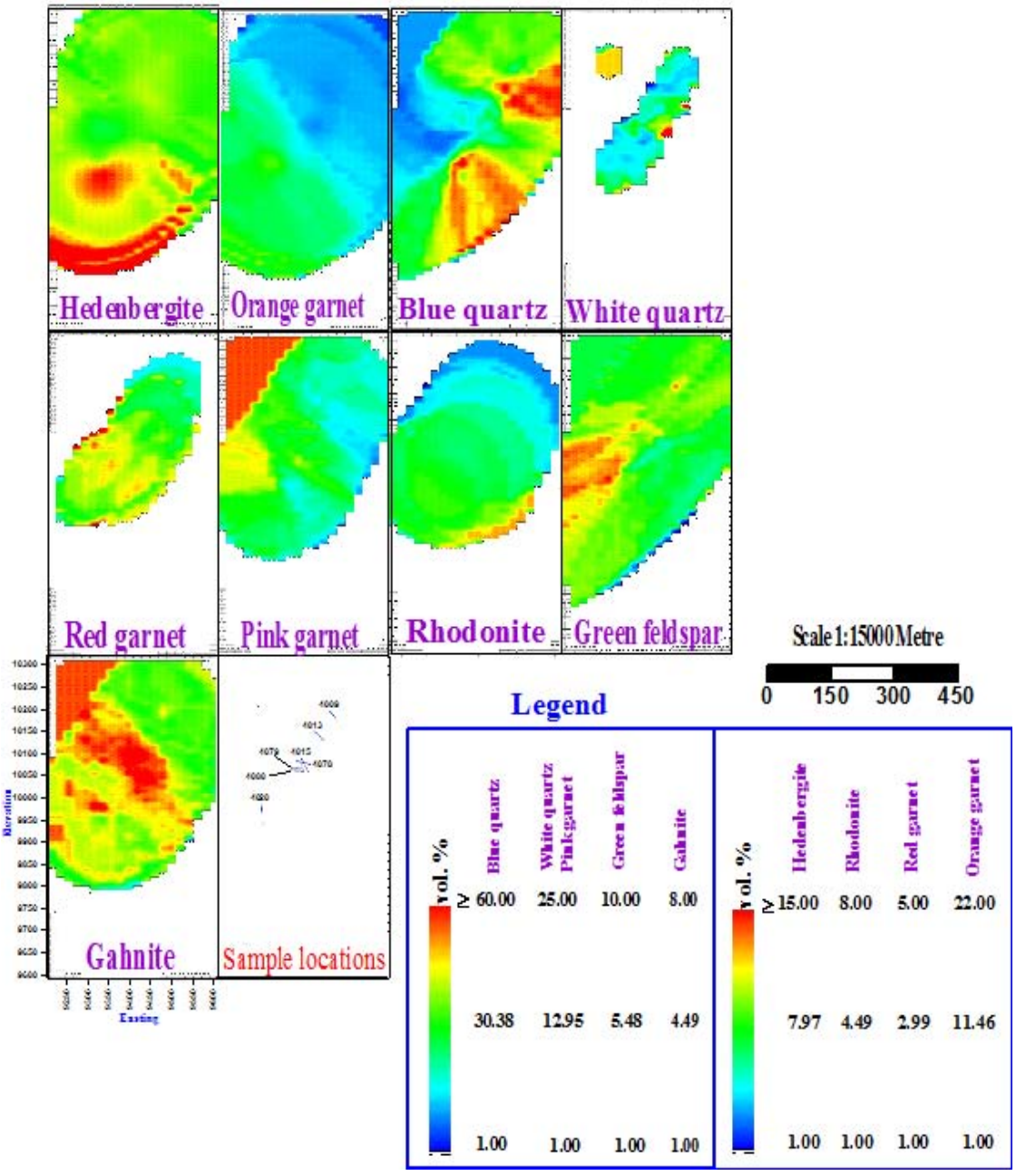

Figure 8.24: Variations of the silicate minerals on the E-W axial sections at N=2109 m.

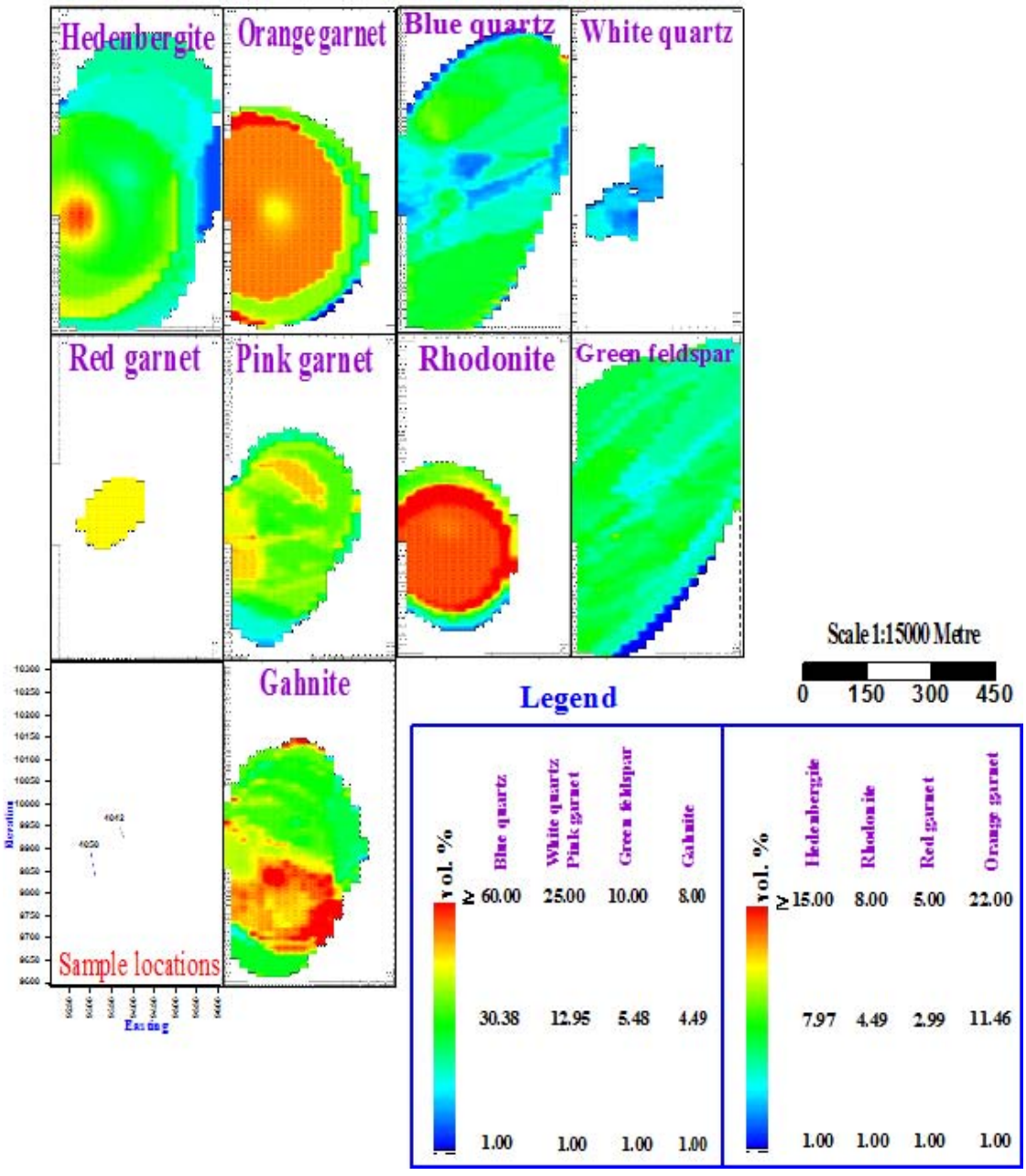

Figure 8.25: Variations of the silicate minerals on the E-W axial sections at N=1639 m.

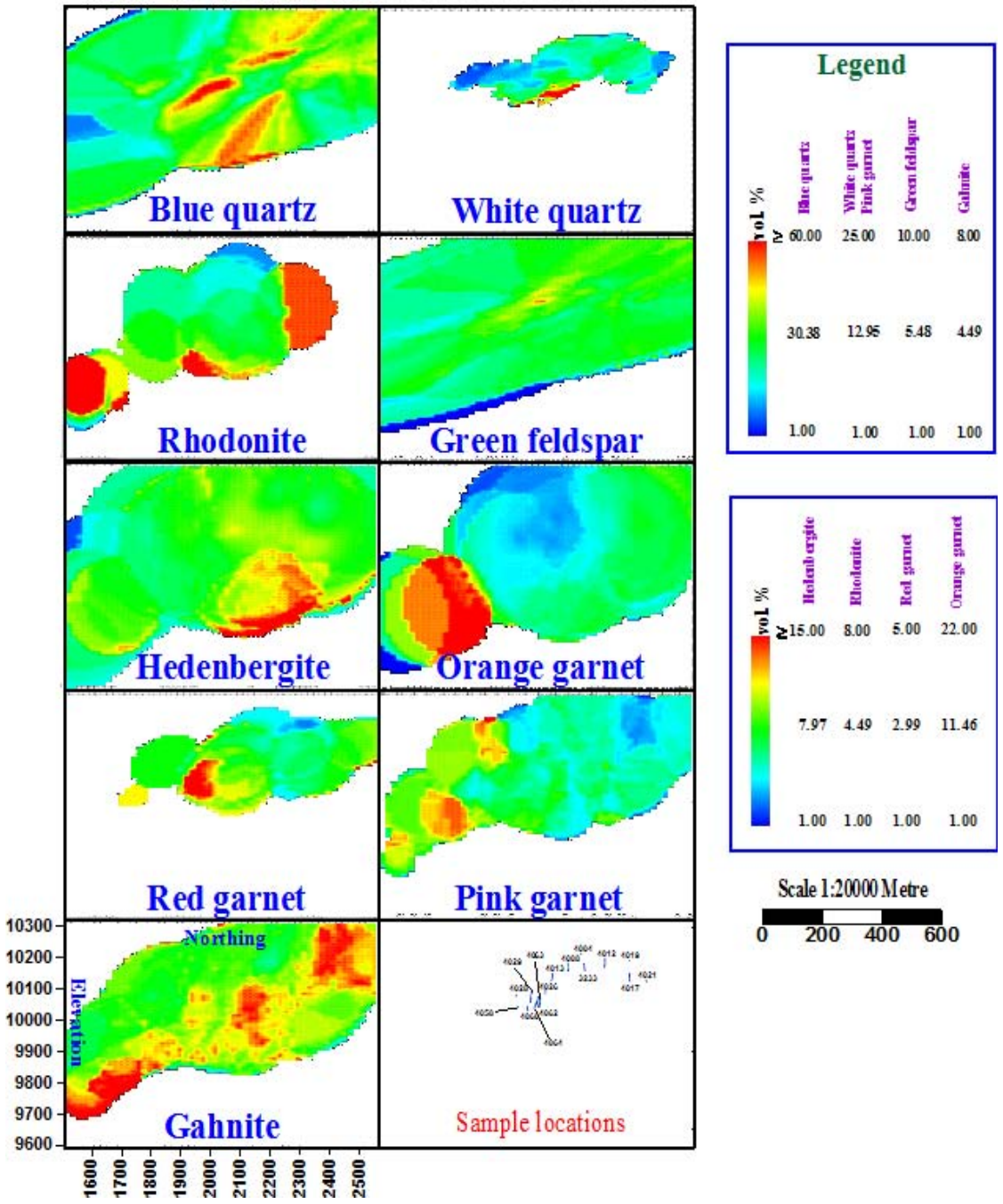

Figure 8.26: Variations of the silicate minerals on the N-S longitudinal sections at E=9467 m.

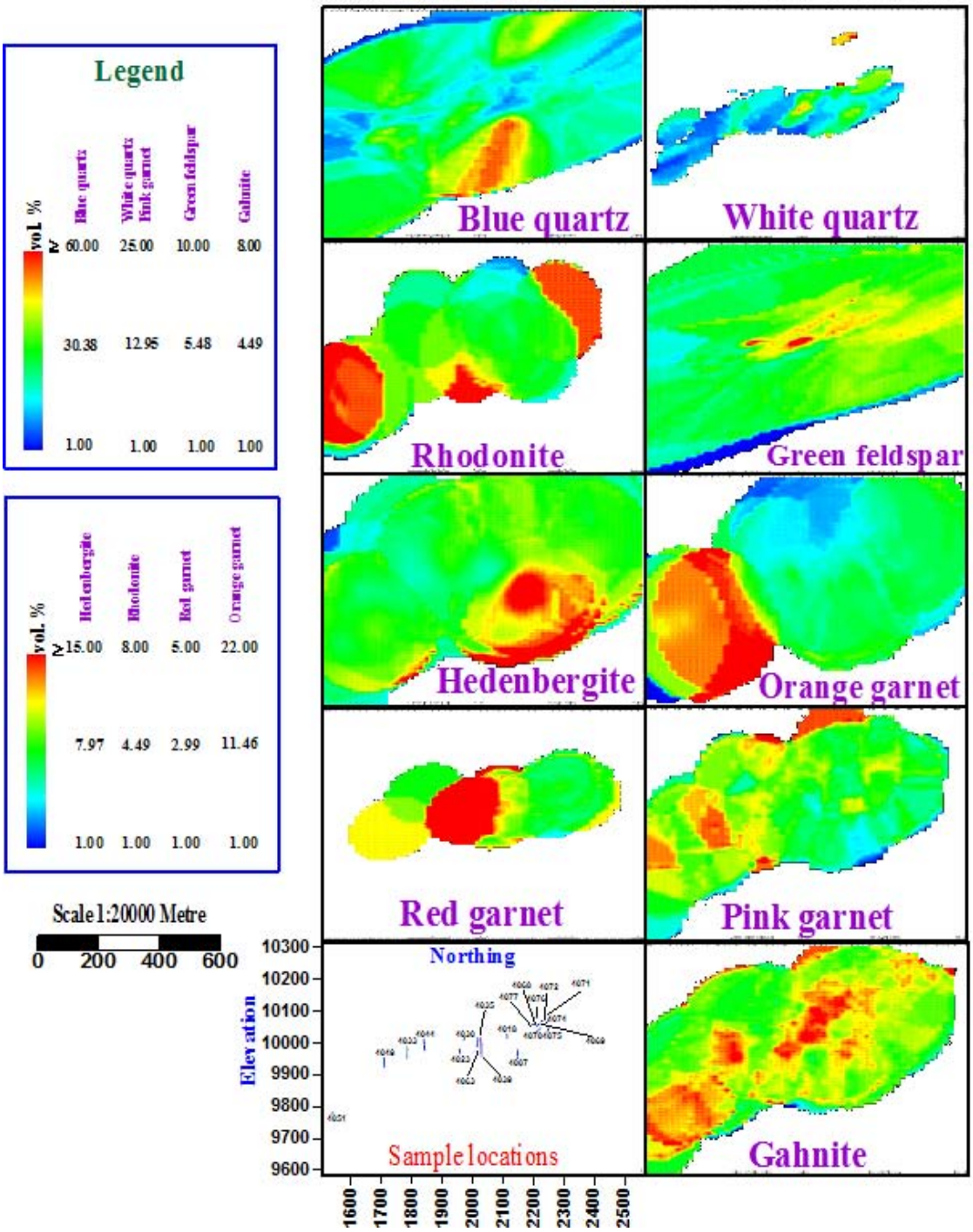

Figure 8.27: Variations of the silicate minerals on the N-S longitudinal sections at E=9357 m.

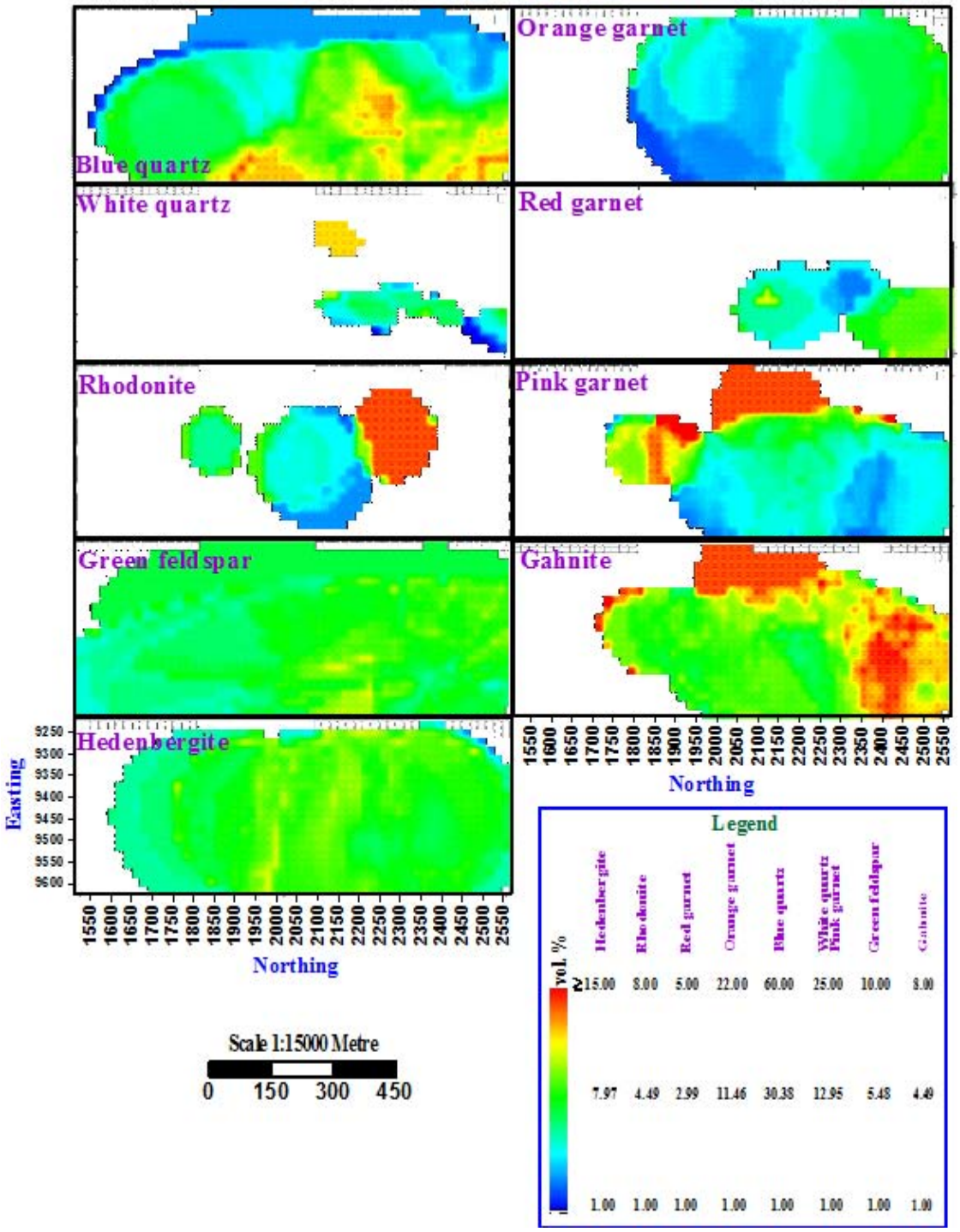

Figure 8.28: Variations of the silicate minerals on the transverse sections at elevation=10218 m.

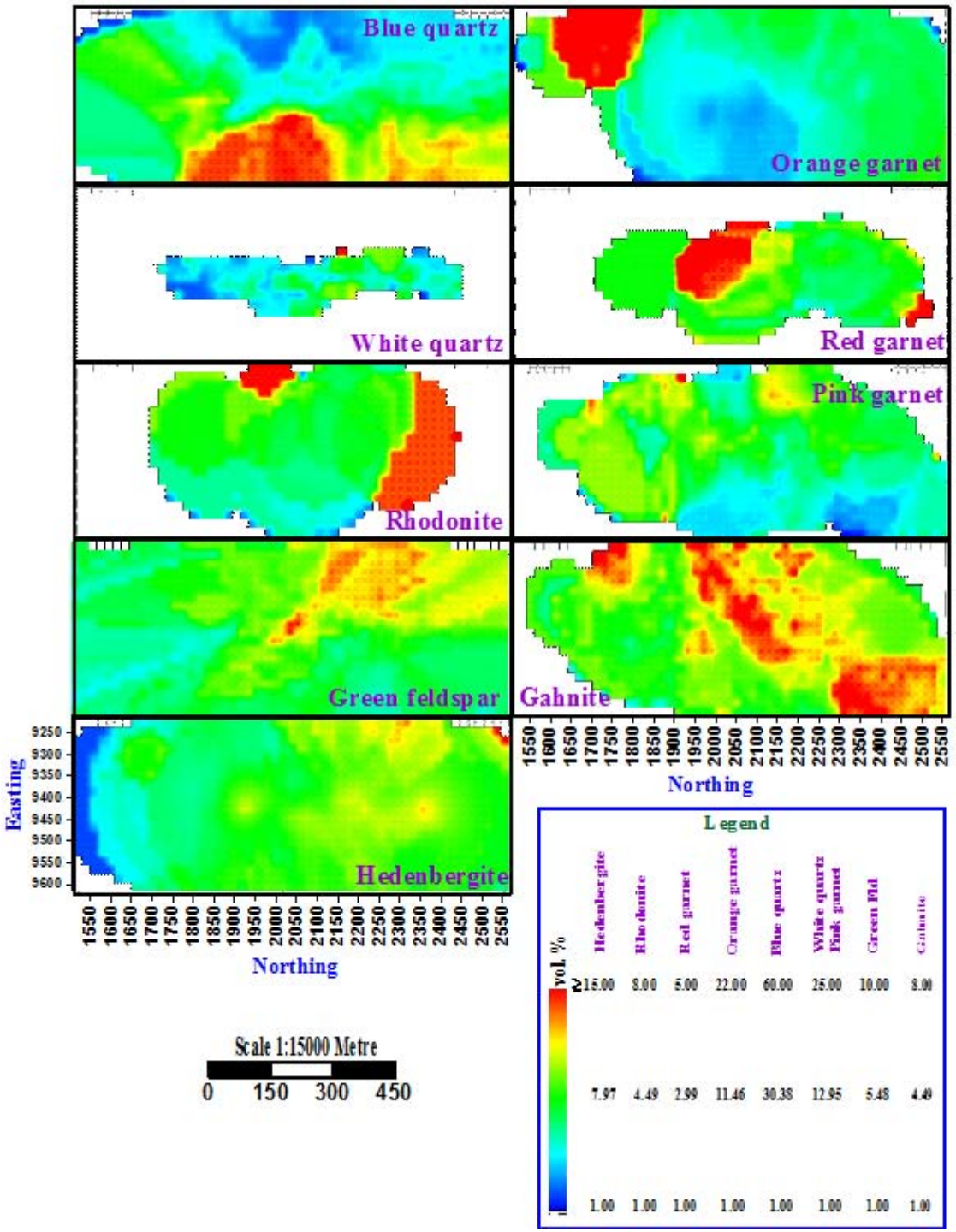

Figure 8.29: Variations of the silicate minerals on the transverse sections at elevation=10078 m.

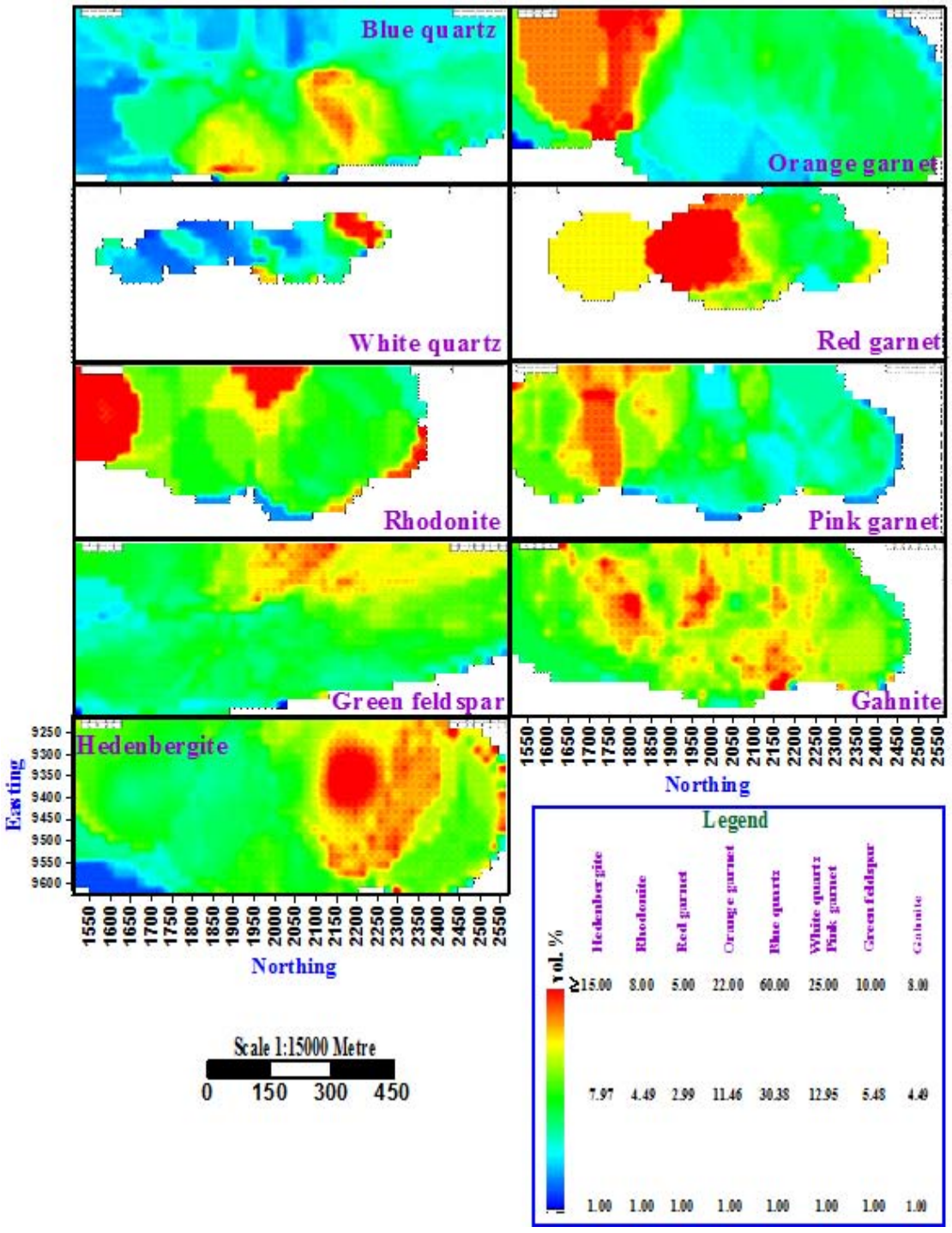

Figure 8.30: Variations of the silicate minerals on the transverse sections at elevation=9958 m.

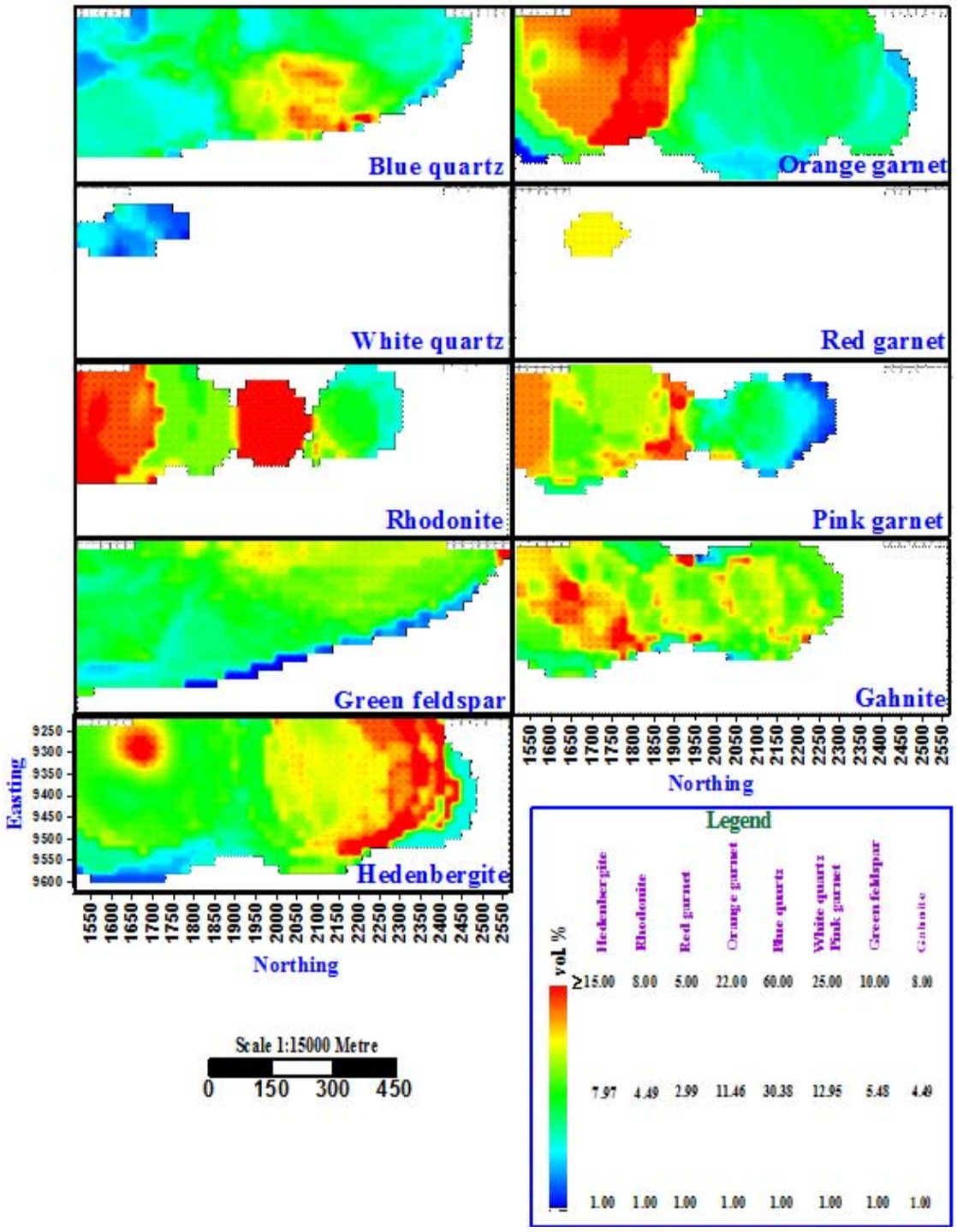

Figure 8.31: Variations of the silicate minerals on the transverse sections at elevation=9848 m.

8.9 Spatial variations of the rock types in the Western Mineralisation

Figures 8.32 to 8.36 display dispersion patterns and variation of rock type in different cross-sections in the Western Mineralisation. There are some similarities in the distribution patterns of the following rock types:

1. Garnet quartzite, pegmatite and blue quartz lode, and
2. Psammite and psammopelite.

There are some similar distribution patterns among garnet quartzite, pegmatite, blue quartz lode (Figures 8.32 to 8.36), AMS, MMS and pyrrhotite (Figures 8.13 to 8.20).

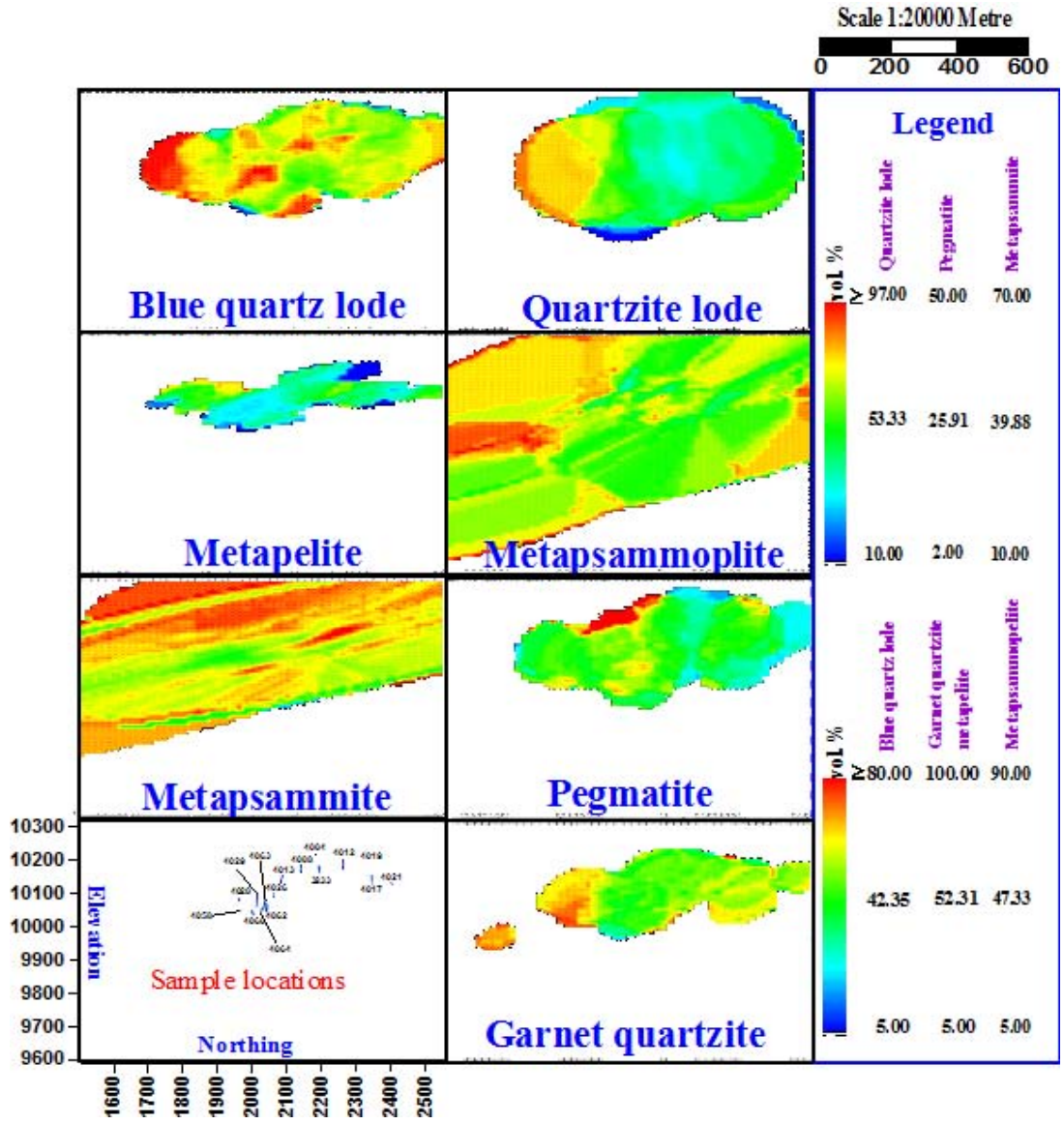

Figure 8.32: Variations of the rock types on the N-S longitudinal sections at E=9467 m.

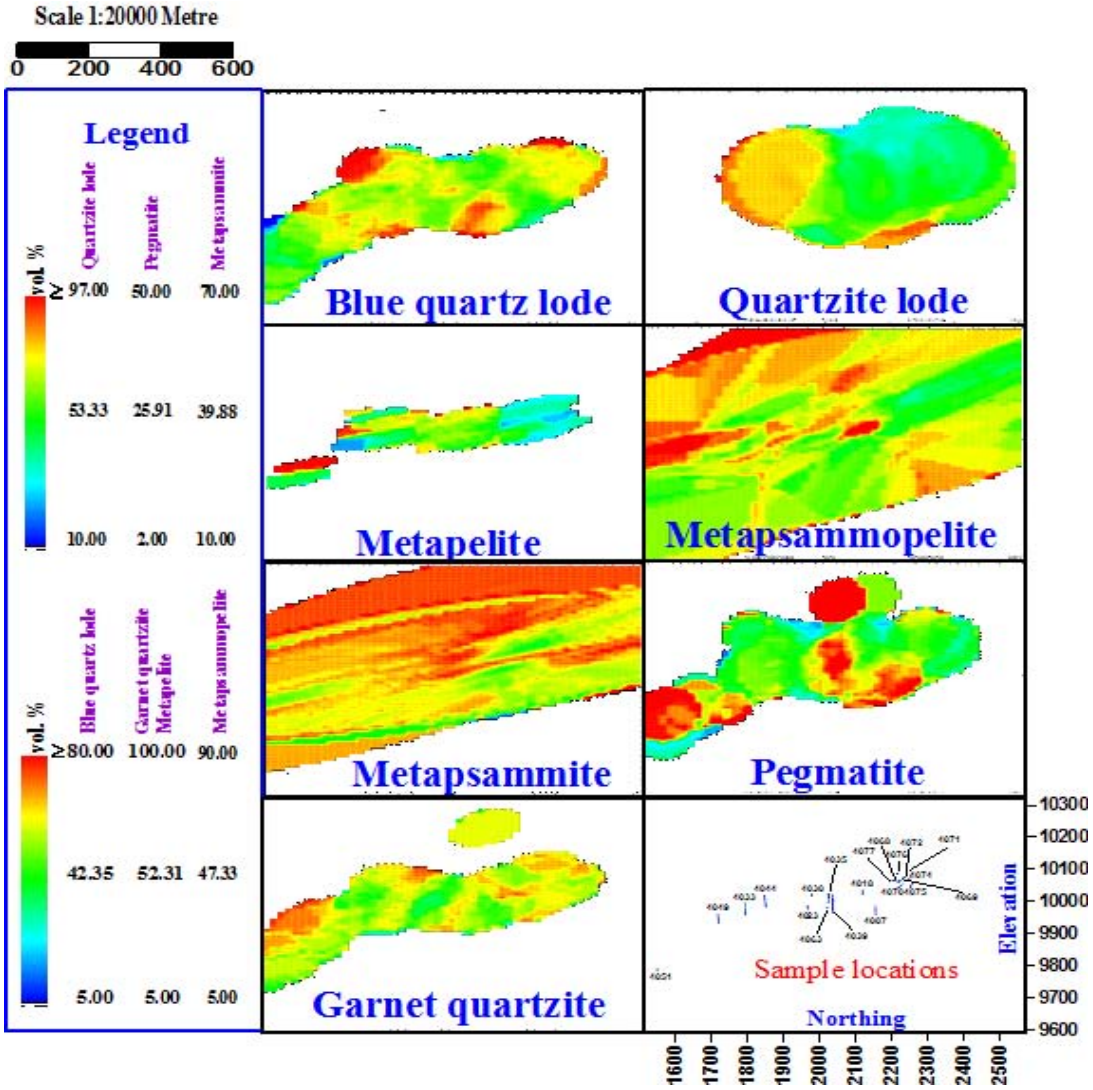

Figure 8.33: Variations of the rock types on the N-S longitudinal sections at E=9357 m

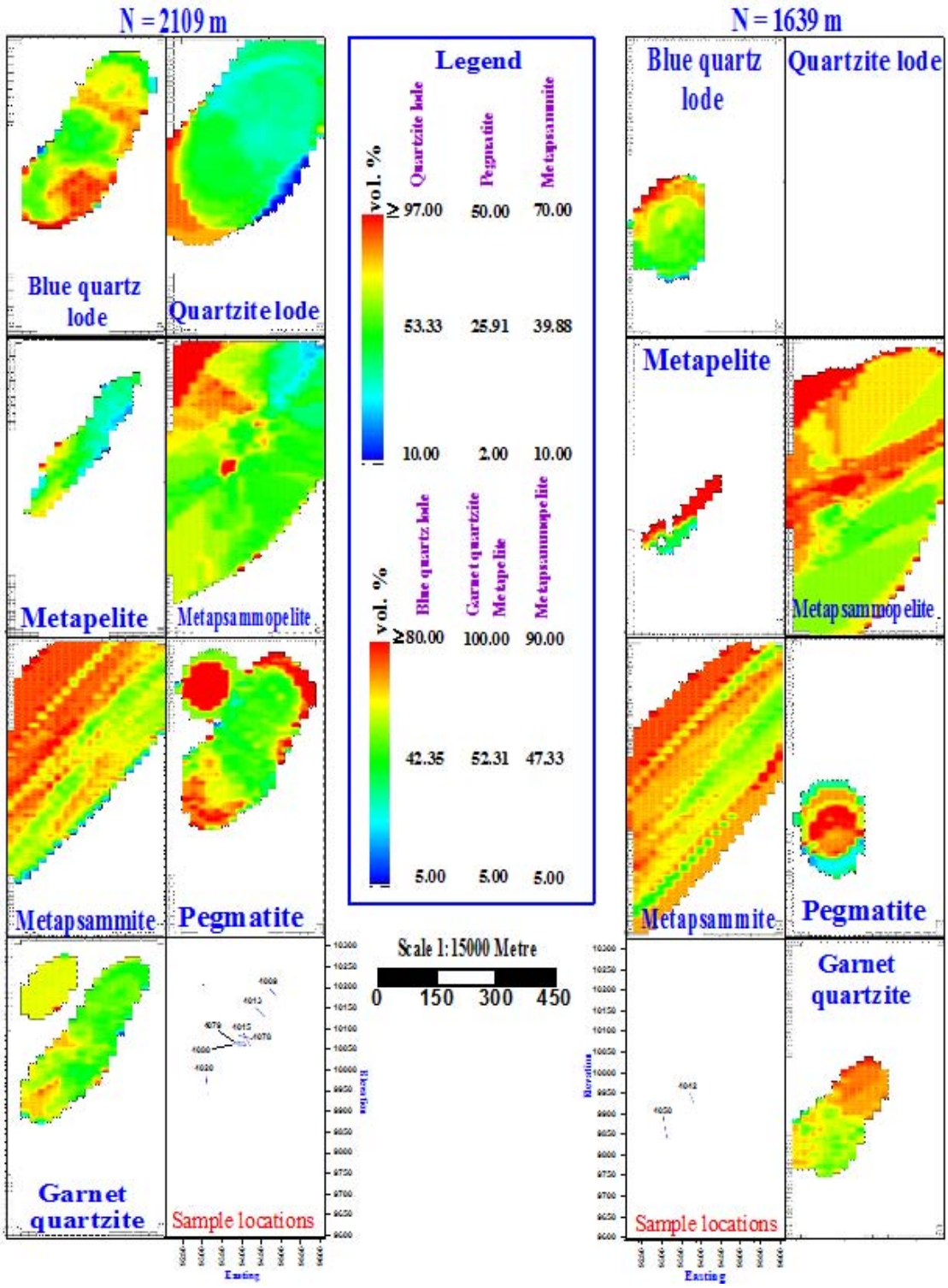

Figure 8.34: Variations of the rock types on the E-W axial sections at N=2109 m and N=1639 m.

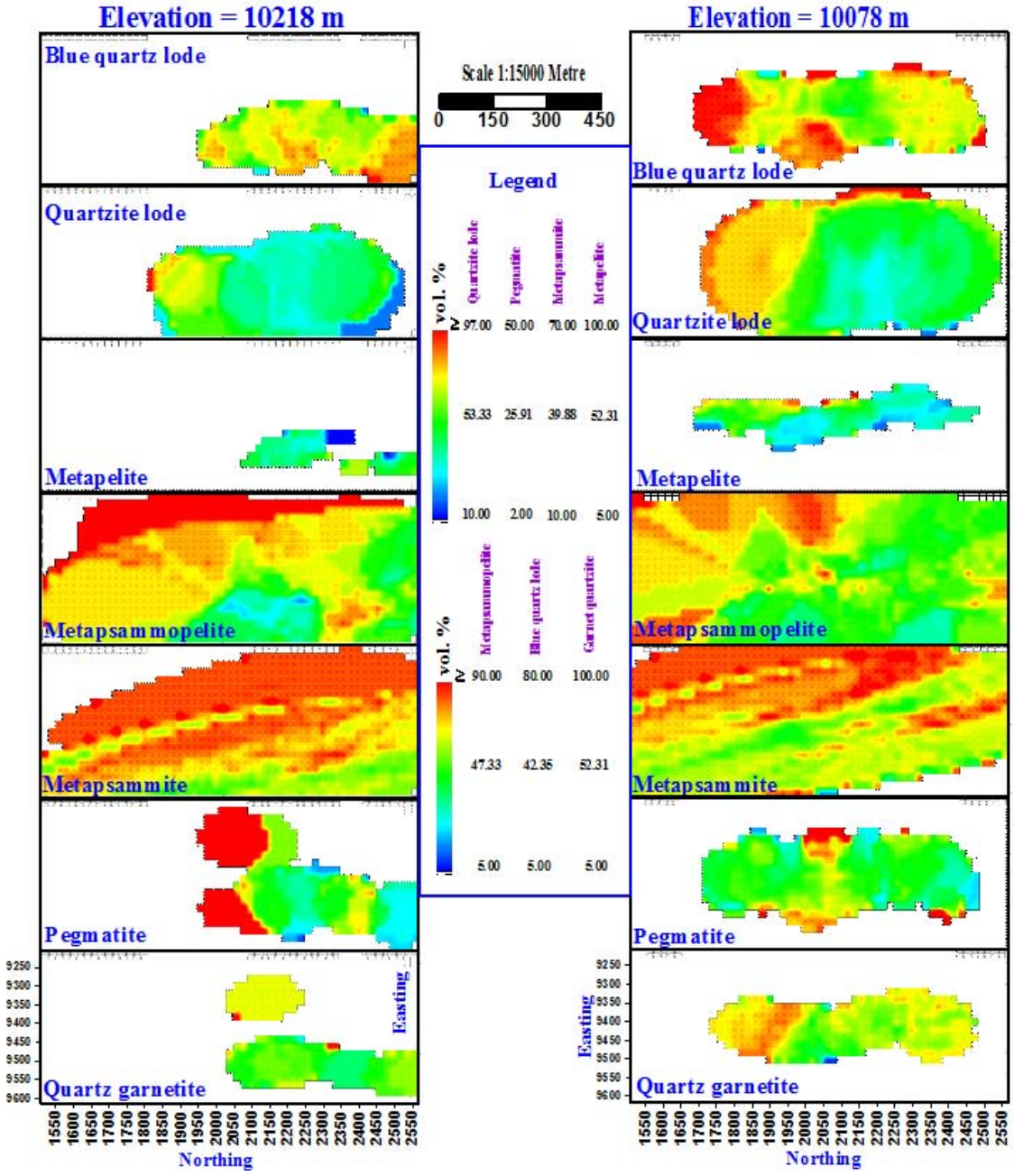

Figure 8.35: Variations of the rock types on the transverse sections at elevation=10218 m and elevation=10078 m.

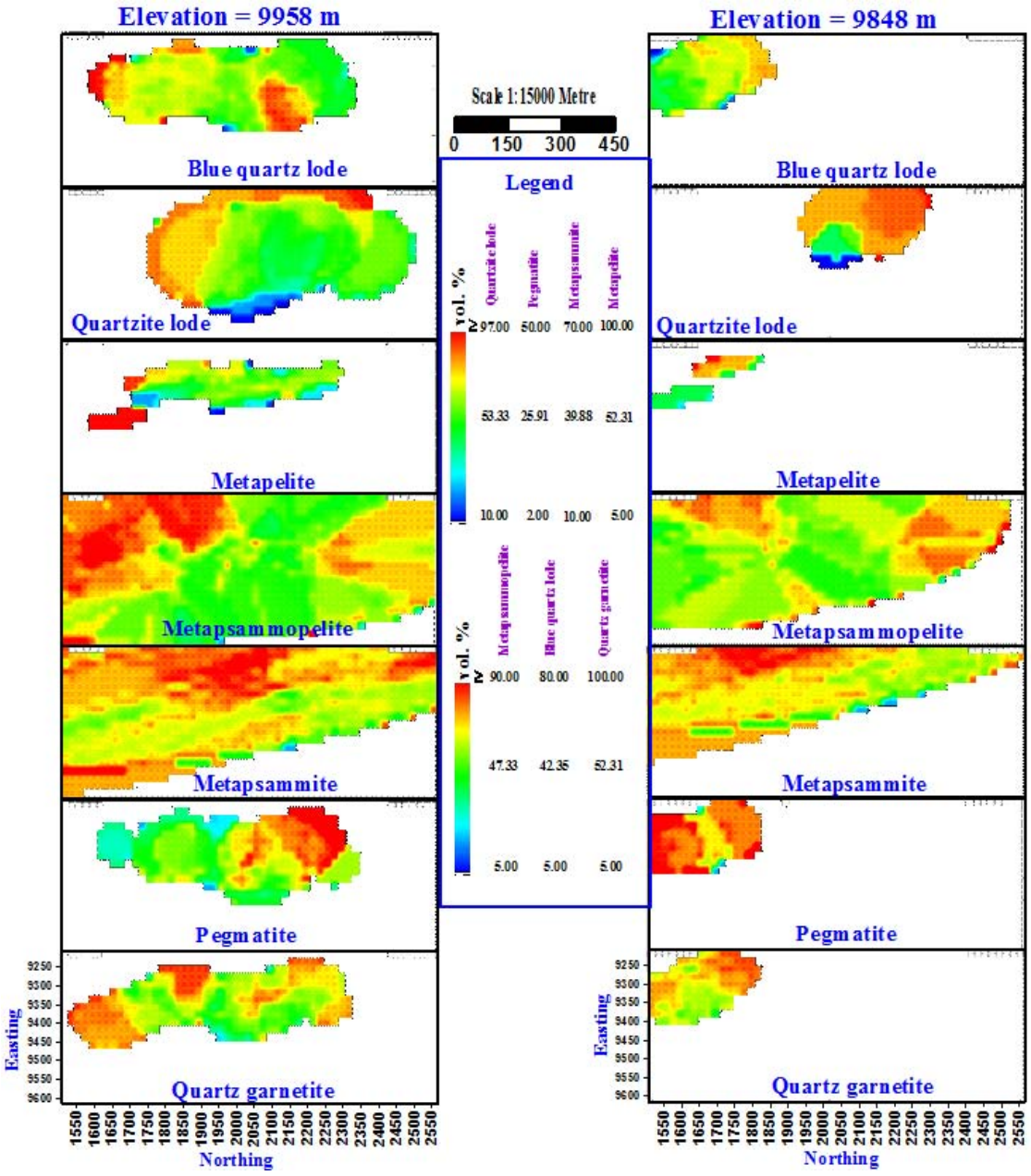

Figure 8.36: Variations of the rock types on the transverse sections at elevation=9958 m and elevation=9848 m.

8.10 Spatial variations of the sulphide textures in the Western Mineralisation

Figures 8.37 to 8.41 display the probability of occurrence of different textures within sulphide minerals in different cross-sections. The probability of occurrence for all textures except for brecciated texture is less than 50 % and for brecciated texture is less than 30 %. This low probability of occurrence is related to lack of textural data for a reliable estimation. In Figures 8.37 to 8.41, the following textures have similar distribution patterns:

1. Stringer, massive and laminated textures, and
2. Vein, network and brecciated textures.

There are some similarities in the structural distribution of the following sulphide textures, silicate minerals (Figures 8.24 to 8.31), sulphide minerals and magnetic susceptibility (Figures 8.13 to 8.20):

1. Massive, stringer, laminated, sphalerite, pyrite, pyrrhotite, chalcopyrite, AMS and MMS,
2. Brecciated, network, vein, galena and arsenopyrite,
3. Massive, stringer, laminated, rhodonite, gahnite and pink garnet, and
4. Disseminated and white quartz.

There are some similarities in the structural distribution of the following textures and rock types (Figures 8.32 to 8.36):

1. Massive, stringer, laminated, pegmatite and quartz garnetite,
2. Vein, network and brecciaed, metapsammite and metapsammopelite, and
3. Disseminated and metapelite.

Plimer (1984) stated that high-grade ores at Broken Hill have invariably brecciated texture. In the Western Mineralisation, there is a visual correlation between brecciated ore and high Pb and this has been used to design stope shapes. In this study, the distribution pattern of vein, network and brecciated textures (Figures 8.37 to 8.41) show some similarities with distribution shape of Pb (Figures 8.5 to 8.12). This indicates that the textures control the grade of Pb in the Western Mineralisation. The distribution pattern of stringer, massive and laminated textures (Figures 8.37 to 8.41) show some similarities with distribution shape of Zn (Figures 8.5 to 8.12). This indicates that the textures control the grade of Zn in the Western Mineralisation.

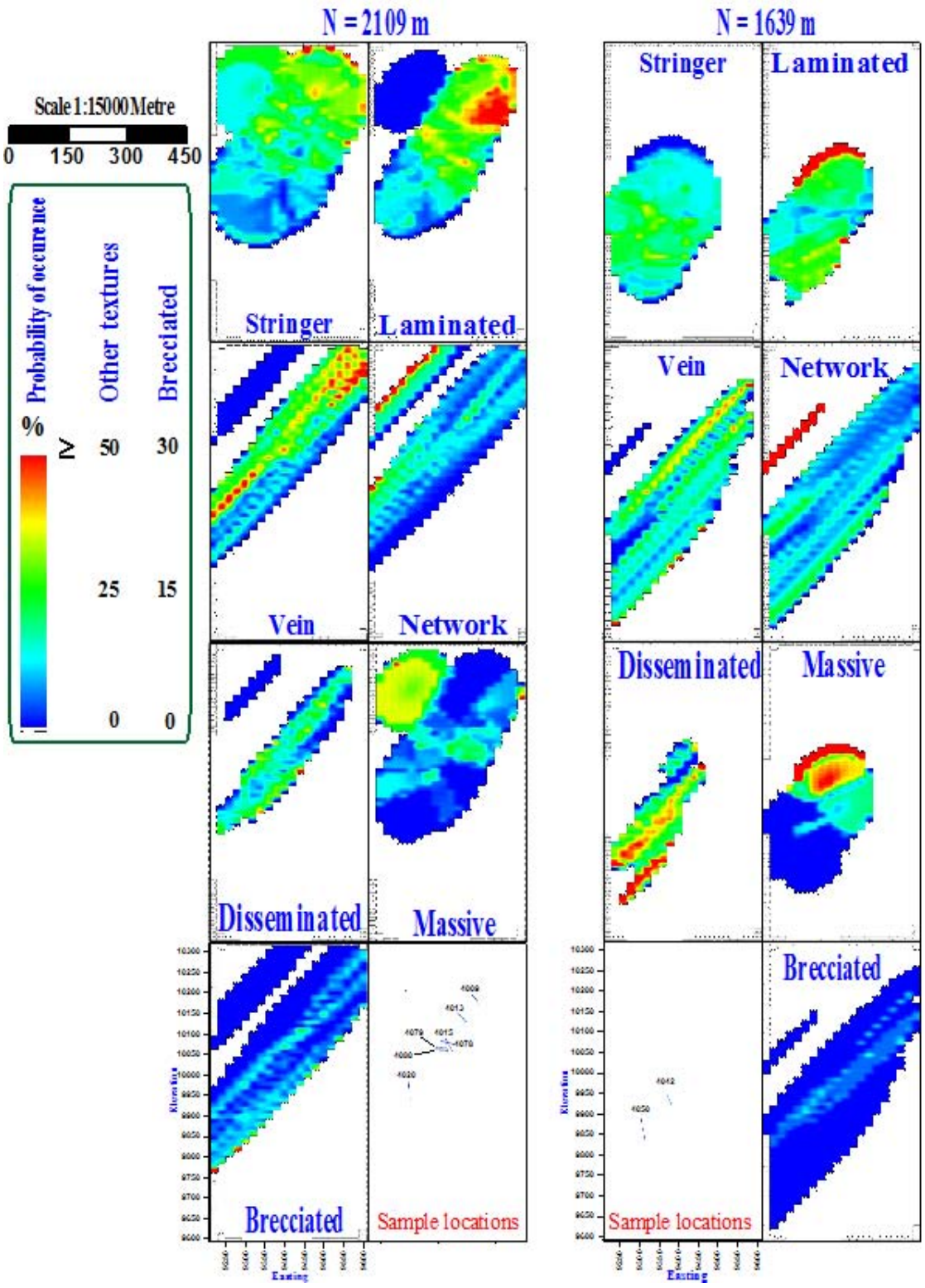

Figure 8.37: Probability of occurrence of sulphide textures on the E-W axial sections at N=2109 m and N=1639 m.

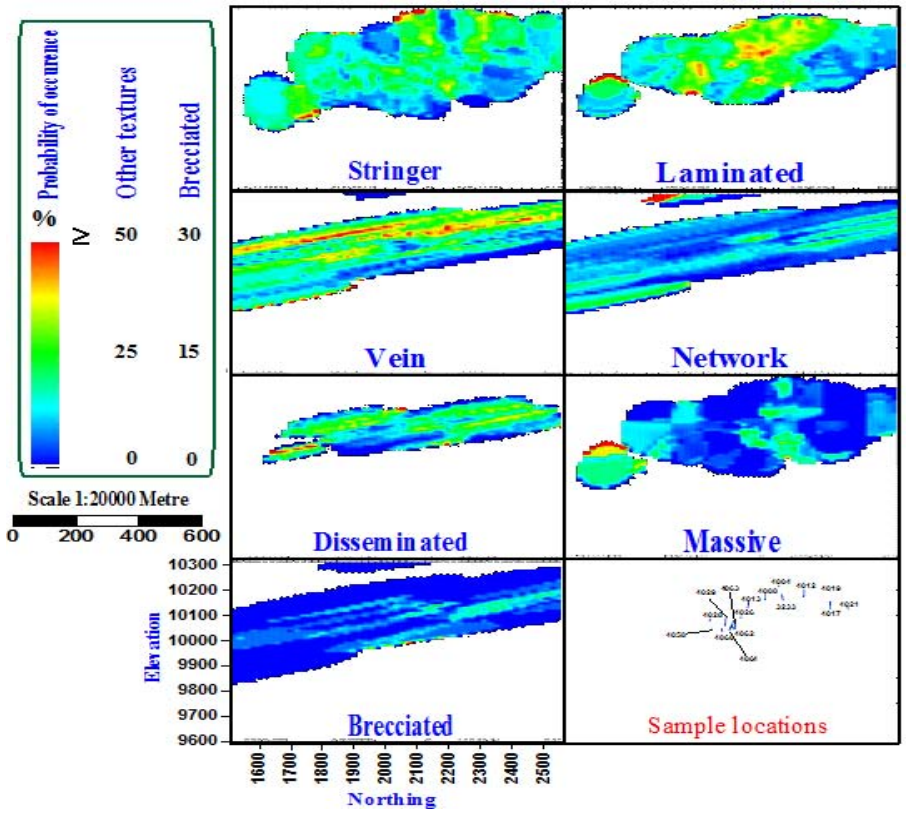

Figure 8.38: Probability of occurrence of sulphide textures on the N-S longitudinal sections at E=9467 m.

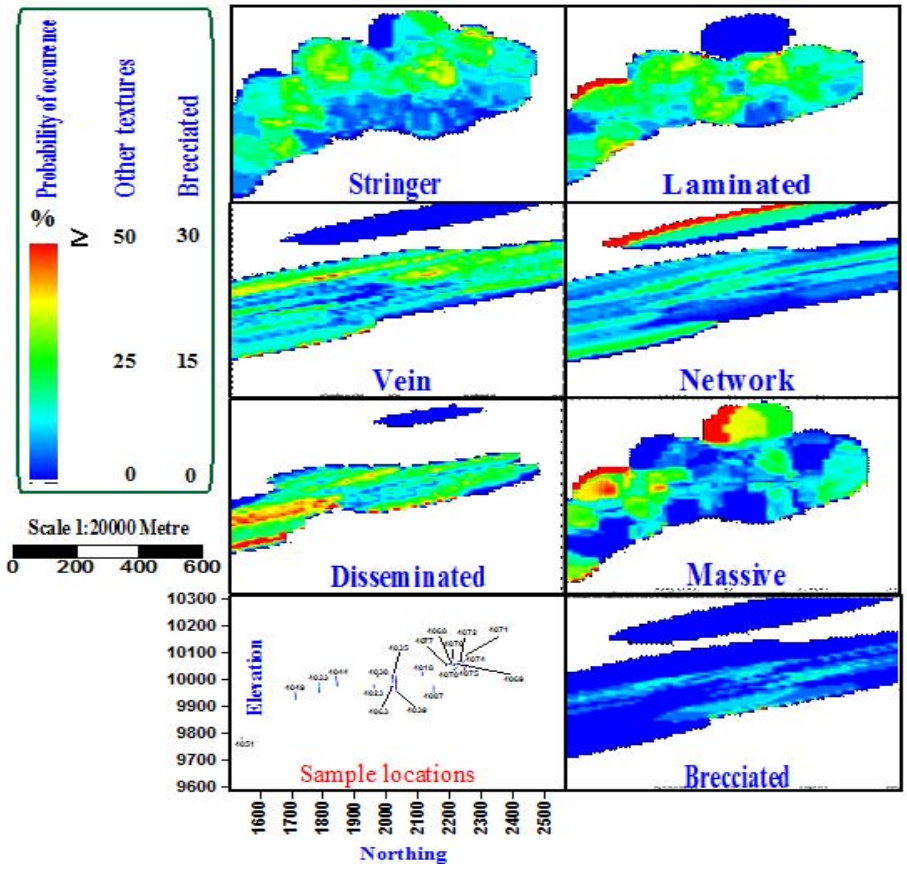

Figure 8.39: Probability of occurrence of sulphide textures on the N-S longitudinal sections at E=9357 m.

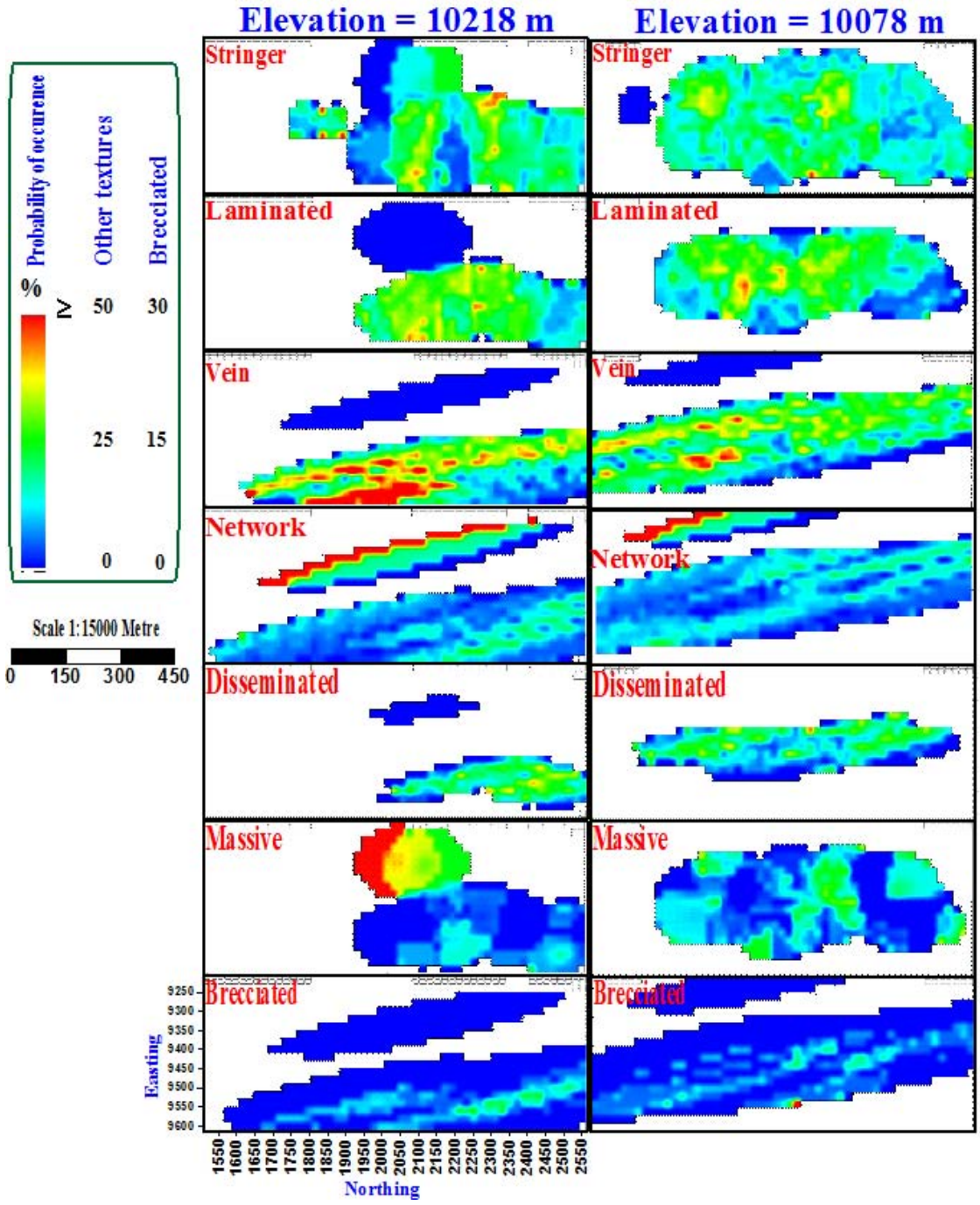

Figure 8.40: Probability of occurrence of sulphide textures on the transverse sections at elevation=10218 m and elevation=10078 m.

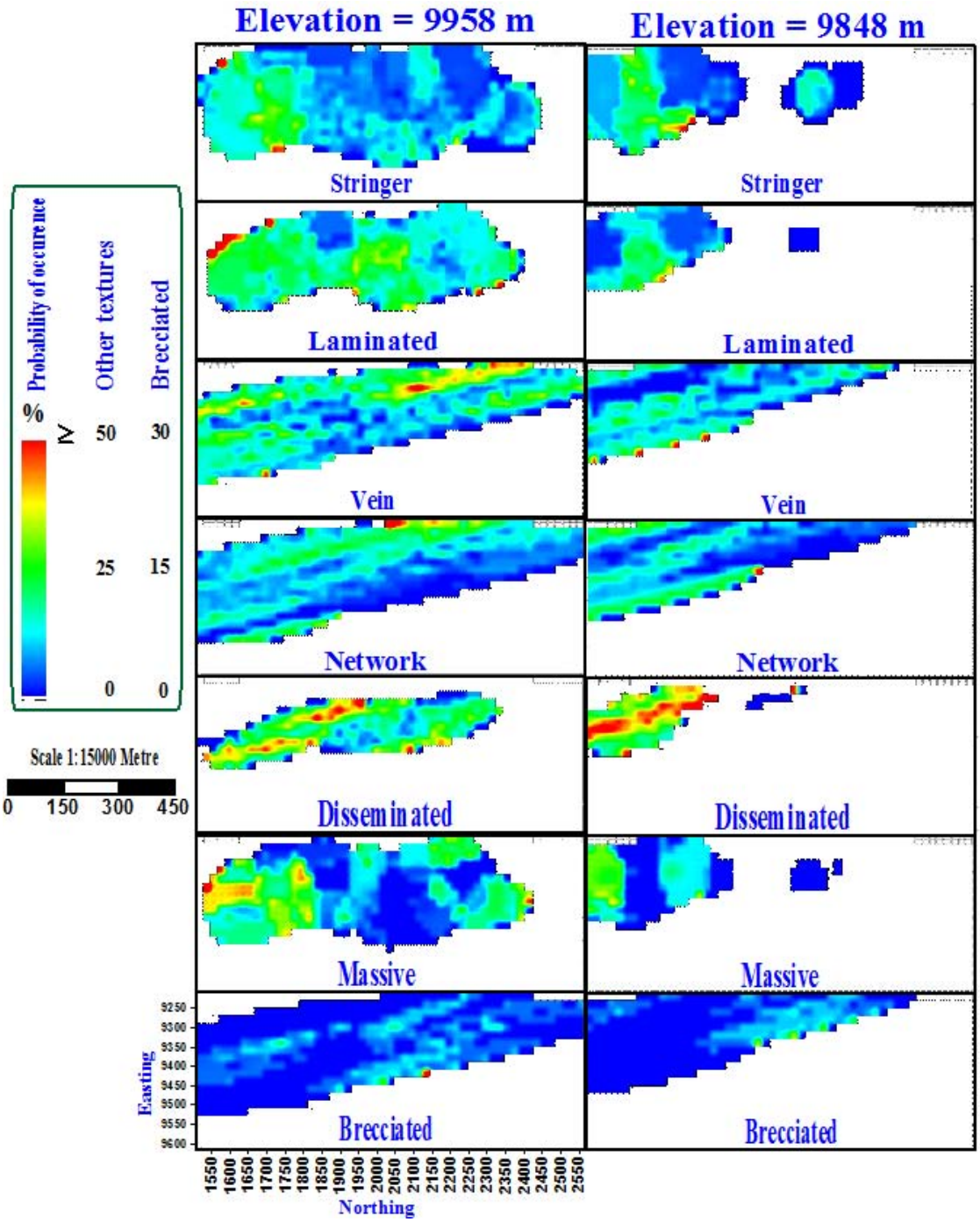

Figure 8.41: Probability of occurrence of sulphide textures on the transverse sections at elevation=9958 m and elevation=9848 m.

8.11 Summary

This chapter evaluates quantitatively the zonation sequence of the 10 element concentrations and provides spatial models for major minerals, rock types, textures and magnetic susceptibility of the Western Mineralisation using image processing of 336 cross-sections for 43 three-dimensional block models. Spatial modelling has not been used for

identification of the geochemical halo, spatial mineralogical and lithological variation for any of the Broken Hill orebodies.

The first aim of this chapter was to calculate the LP, ZI and ΔG of 10 elements in axial sections of the Western Mineralisation in order to evaluate the zonation sequence of the element concentrations as a function of depth. The final result shows that Cd, Pb, S and Zn tend to concentrate in the upper part of the mineralised zone, whereas As, Ag, Cu and Bi have a tendency to concentrate in the lower part of the mineralisation (Table 8.15). Consequently, the empirical product-ratio of $\frac{\mathbf{Ag}\times\mathbf{Cu}\times\mathbf{Bi}\times\mathbf{As}}{\mathbf{S}\times\mathbf{Pb}\times\mathbf{Zn}}$ was suggested as ZC or DI for lead and zinc sulphide ore deposit similar to the Western Mineralisation. The value of ZC for the Western Mineralisation varies between 0.01×10^{-10} and 317×10^{-10} that can be compared with similar Zn and Pb ore mineralisation in other area.

The second aim of this chapter was to use structural analysis to provide a range of colour indices between threshold level and relative local maximum anomaly for the 10 element concentrations. The result of anomalous separation shows several similarities between anomalous areas of some group of elements including:

1. As and Ag,
2. Sb and Bi, and
3. S, Fe, Cd, Cu and Zn.

The correspondence map of average percent of garnet types within the Broken Hill orebodies shows a close relationship of the Western Mineralisation to pyrope and almandine end members in garnet. The 3D biplot shows the garnet samples of the Western Mineralisation were affected highly by chemical variation of Ca and Al (grossular), Ca and Fe (andradite) as well as Ca and Cr (uvarovite).

In final, the distribution patterns of elements, minerals, textures, rock types, magnetic susceptibility and specific gravity were presented in different sections and they were grouped based on their similar distribution patterns.

CHAPTER 9

Conclusions

9.1 Introduction

This final chapter provides a summary of responses to unsolved problems and the research questions of this dissertation that were presented in Chapter 1. It also covers the significance of this research study and some suggestions for future similar research.

9.2 Responses to research questions of this dissertation

9.2.1 Maximizing information of core logging

The first purpose of this research was to maximize information of core logging in the Western Mineralisation (unsolved problem "a" in Section 1.7). In order to solve this problem, all available geological and geochemical data sets about these characteristics from previous studies of the Broken Hill orebodies including the Western Mineralisation were compiled and prepared for multivariate statistical analysis of this research. Moreover, in this study, 30 important geological variables including sulphide and silicate minerals, rock types and sulphide textures were investigated and quantified visually for 1,928 Western Mineralisation samples. The average and maximum magnetic susceptibility were also measured and their specific gravity was recalculated for each metre sample.

Through this quantitative core logging and data processing, 63,624[1] new points of data information were generated and added to the previous assays of the Western Mineralisation. However, because the assays of the Western Mineralisation had been reported for different sample sizes, the theory of sample volume-variance relationship was applied to all HQ and LTK60 assayed samples size in order to convert them to NQ sample size. Also different lengths of measured assayed samples were recalculated for one metre samples. This process of sample compositing performed for all assays of surface and underground drill cores. In final, all quantitative geological, geochemical and geophysical data sets were presented in a large data base (Excel format) named the "quantitative core log data".

[1] **33 ×1928**

9.2.2 Characteristics of the quantitative core log data of the Western Mineralisation

The second unsolved problem was about the conventional descriptive core logging of the Western Mineralisation that is separate from mineral chemistry and geophysical data as well as the processes undertaken at the Rasp Mine which did not allow integration of the data for performing different statistical methods (unsolved problem "b" in Section 1.7). The quantitative core logs data of this study incorporated 44 quantitative variables including 24 geological variables (minerals and rocks), 7 textural variables, 3 geophysical variables and 10 geochemical variables (element concentrations) for 1,928 samples of surface drill cores and 8 geochemical variables for 1,231 samples of underground drill cores.

The data set was defined for equal sample size that is a fundamental prerequisite for performing statistical analyses. The spatial coordination of start, middle and end of each metre core sample has been calculated regarding collar, survey and inclination of drill hole. The quantitative core log data can be visualized directly in any 3D graphs and mining software such as Micromine^{TM}, Vulcan^{TM} and Surpac^{TM} without the requirement of the azimuth (bearing), dip and collar elevation of each drill core.

The quantitative core data was also used for providing high quality core log diagrams with resolution of one metre. The first group of diagrams assists simultaneous evaluation of the variation of 44 variables as a function of depth (Figures 2.8 to 2.13). The second group shows simultaneous variation of Pb+Zn, galena+sphalerite; pyrrhotite, magnetic susceptibility, specific gravity and sulphide textures as a function of depth (Figures 4.13 to 4.17). The diagrams were used to detect internal-consistency among variations of minerals, rock types, assays and sulphide textures in the Western Mineralisation. The quantitative core log data allows the easy use of bar diagrams to evaluate the trend variation of statistical parameters of each variable (e.g. element concentration) within all surface and underground drill cores simultaneously. For example, in bar diagrams of Chapter 3, the trend variation of mean and median values of galena, sphalerite (Figure 3.11) and galena+sphalerite (Figure 3.12) in each sample were compared by those of parameters in bar diagrams of Pb, Zn (Figure 3.3) and Pb+Zn (Figure 3.12) respectively.

9.2.3 Application of classic statistics for the Western Mineralisation

The CBH Resources Ltd has been using geostatistics to determine if there is enough ore at a sufficient grade to warrant economic extraction of the Western Mineralisation, but these processes are unable to evaluate the scientific geological, geochemical and geophysical characteristics by classic statistical analysis (unsolved problem "c" in Section 1.7). The third purpose of this research study was to apply a variety of standard univariate, bivariate and multivariate statistical methods to improve quantitative understanding of mineral chemistry, mineral generations, geochemical, geophysical and geological variations and their relationships.

Since the Broken Hill ore deposit has been well known already in terms of geology, the geological, geochemical and geophysical features of the Western Mineralisation is better understood at the conception of statistical models and numerical exploration methodology. Moreover, the statistical results will be useful to determine potential areas where ore awaits discovery.

In this dissertation, the univariate analyses of descriptive statistics were used to understand which type of statistical parameters are important for each variable and compare and contrast the descriptive statistical parameters of variables with each other (Chapter 3).

Bivariate analyses including different parametric and non-parametric correlation coefficients (Chapters 3, 4 and 5) were applied to measure the degree of relationships and internal consistency among galena+sphalerite, pyrrhotite, magnetic susceptibility and Pb+Zn or between rock types and Pb+Zn. These processes were not possible with conventional core log information.

Statistical tests were used to evaluate significant differences of magnetic susceptibility and pyrrhotite between two group samples containing galena+sphalerite and other samples. Log-ratio transformation was used to open the closed percentage assays into an unconstrained form of the real space. After the transformation, the initial skewed distribution of elements changed to normal distribution. This process is useful for detection of non-linear relationships using bivariate correlation coefficient.

The linear multiple regressions were calculated for Pb and Zn concentrations separately in order to identify their best predictor elements. The predictor elements can be used as geochemical exploration guides for Pb and Zn ore sulphide types similar to the Western Mineralisation (Section 5.5). Those predictor elements suggested by the linear multiple regressions were calculated by geostatistical methods (Chapters 6 and 7) to understand which of them are the most appropriate pathfinder elements of Pb and Zn in the Western Mineralisation.

Cluster analysis was used to classify elements based on their percent of similarities in concentration values or variogram parameters. The agglomerative algorithm and correlation coefficient were used in this process and the results are useful for comparison of the Western Mineralisation with other orebodies.

PCA was applied to 10 element concentrations to quantify the theories behind ore sulphide genesis of the Western Mineralisation. The results of PCA showed strong consistency with existing mineral paragenesis of the Western Mineralisation. PCA reduced geochemical complexity of variation of ten elements into four multi-elemental relationships (Section 5.7).

Simple correspondence analysis was applied to demonstrate in different maps the relationships of different chemical composition of pyrrhotite, galena and sphalerite samples with the Broken Hill orebodies. Simple correspondence analysis was also used to visualize the relationships between the average percent of different garnet types and the Broken Hill orebodies (Section 8.6).

The biplot of chemical composition of pyrrhotite, galena and sphalerite samples were constructed to understand their mineral chemistry generations or their alterations in the Western Mineralisation. The 3D biplot of average percent of garnet types was constructed to understand major chemical compositions of garnet in the Western Mineralisation (Section 8.7).

9.2.4 Application of geostatistics for the Western Mineralisation

There is a lack of spatial models for geological, geochemical and geophysical features of the Western Mineralisation. This is because CBH Recourses Ltd uses

geostatistics to make spatial models for combination of Pb, Zn and Ag to estimate tonnage and grade of the orebody (unsolved problem "d" in Section 1.7). This information alone does not make an effective exploration tool for finding look-alike ore deposit styles within similar prospective areas.

Although, the information of this part of the study may not result directly in a decision to mine, it can be useful to find near-mine repetitions, extensions and continuity of the existing orebody and the detection of primary geochemical haloes. Furthermore, it is of use in regional exploration to evaluate a near miss or to use the AI, ZC and DI to evaluate prospectively.

In order to address this problem, 136 directional variogram and down-hole variogram models were calculated for 43 variables of the quantitative core logs. Their variogram parameters were applied to construct 43 spatial block models using ordinary kriging. The variogram models of the Western Mineralisation were validated using the cross-validation technique. A few investigated minerals such as pyrite, arsenopyrite and red garnet showed low variogram validation because the number of samples were very low and their volume percentage changed between two or three numbers (e.g. between 1 % and 3 %).

The strike direction, plunge and plunge direction, dip and dip direction of the Western Mineralisation was estimated by variogram analysis and geological observations. From the variogram parameters, the optimal sampling grid was determined as an exploration guide for tracking extension of geochemical haloes with surface sampling. The variogram parameters of the Western Mineralisation were also compared with available variogram parameters of the other lead and zinc sulphide ore deposits in order to classify the ore styles (i.e. Sedex, MVT, vein and Irish deposit).

A block size of 20×20×10 m (with the volume of 4000 m^3) was calculated as the most suitable block size for kriging estimation of lead and zinc in the Western Mineralisation. This block size also was considered for construction of the other 41 geological, geochemical and geophysical variables to enable comparison. For better demonstration and interpretation of the 3D block models in this dissertation, each 3D block model was intersected at different horizontal and vertical directions and during this process, 424 cross-sections were generated from 43 spatial block models.

The 80 cross-sections of 10 element concentrations were used for evaluating dimension, orientation and anisotropies of geochemical halo (Chapter 7). For this purpose, maximum lengths and widths of the haloes were measured in transverse, longitudinal and axial sections in order to find the zonation sequence of the geochemical haloes through the orebody. The results showed that Bi and Sb have greater dispersion of haloes relative to the other 8 elements and they can be considered as geochemical pathfinders of the Western Mineralisation.

The 10 geochemical haloes of the Western Mineralisation were plotted into two groups of 80 cross-sections. One group of the cross-sections was distinguished by colour indices between background and threshold levels and another group was distinguished by colour indices between threshold and anomalous values. The colour index of individual element within each group was adjusted by trial and error through the Geostatistics for Windows software. In Chapter 8, the axial sections of geochemical haloes were used for calculation of empirical formulas of the LP, ZI and ΔG (Beus & Grigorian 1977).

From this process, it was concluded that in axial sections, S, Pb, Zn and Cd tend to concentrate in the upper part of the mineralised zone whereas Ag, Cu, Bi and As have a tendency to concentrate in the lower part of the mineralisation. The result was used for construction of an empirical formula of ZC^2 or DI^2 that has various exploration applications (Section 8.3). The spatial distribution pattern of silicate and sulphide minerals, rock types, sulphide textures and magnetic susceptibility were compared and contrasted with each other to find their similarities and variations within the orebody.

9.3 Significance of this kind of research study

Numerical evaluation of geological, geochemical and geochemical characteristics of the Western Mineralisation in the Broken Hill mine has great potential in the following areas:

1. Extraction of more useful and quantitative geological and geophysical information from core samples and integration of the information with assays,

---

2 $\frac{\mathbf{Ag} \times \mathbf{Cu} \times \mathbf{Bi} \times \mathbf{As}}{\mathbf{S} \times \mathbf{Pb} \times \mathbf{Zn}}$

2. Evaluation of previous mineral chemistry data with multivariate statistical methods,

3. Numerical mineralogy and petrology in this study were used to generate spatial models similar to spatial geochemical models,

4. Information of geometrical distribution of the primary geochemical haloes can be used in terms of tracking of secondary geochemical haloes, studies of regolith, geobotany, hydrogeochemistry and biogeochemistry around the Broken Hill orebodies,

5. Providing numerical information for abundant pyrrhotite, magnetic pyrrhotite and magnetic signatures of the orebody,

6. Providing strong documentations based on the quantitative core log data, classic and spatial statistical analysis, geological investigation, geochemical and geophysical measurements which can be updated every time when new data is available. This documentation can be used as numerical exploration guidance for similar types of ore deposits or comparison of different characteristics of orebodies for purposes of ore classification,

7. Providing sustainable information for an orebody because it uses the information of core samples which have been preserved in core storage for a long time which can be referred to in order to validate previous information or start of a new research,

8. The quantitative core log analysis is applicable and repeatable for the other Broken Hill orebodies or other orebodies in other areas,

9. This kind of study does not add mining cost because it deals with previous information and existing core samples of an orebody, and

10. This study also provides environmental information about the mechanism of distribution and penetration of elements that may be released into groundwater and soils in vicinity of the Broken Hill City because of its proximity to the Western Mineralisation. A previous study by De Caritat et al. (2005) showed that groundwater in the Broken Hill district contained lead content matching the Broken Hill lead isotope signature.

9.4 Suggestions for future research

This study was limited to the Western Mineralisation. Additional quantitative core logging is needed for other orebodies of the Broken Hill Mine to identify specific geochemical and mineralogical zonation patterns and spatial relationships of the orebodies in a numerical framework. Future research in this area for the Broken Hill ore deposit can develop the quality of numerical models in relation to geological and geochemical information. Further research could investigate:

1. What the extent of association is among the Broken Hill orebodies in terms of geochemical haloes, sulphide metal and magnetic mineral distribution, and

2. What the mineral/chemical zonation patterns are and which geochemical factors control the Broken Hill orebodies.

This study was constrained to silicate mineral chemistry of a few samples collected from limited drill cores within the Broken Hill orebodies. It is suggested that silicate minerals such as garnet and gahnite are collected from a large range of drill holes within the Broken Hill field and their chemical compositions are determined for construction of spatial mineral chemistry models. Although gahnite and garnet are associated with Broken Hill-types deposits, it is yet to be shown that the chemistry of these minerals can be used as a vector for mineralisation.

References

Adachi, K. 2003, 'Correspondence analysis, multiple correspondence analysis, and joint correspondence analysis', *Japanese Psychological Review*, vol. 46, no. 4, pp. 547-563.

Ahmad, R. & Wilson, C.J.L. 1982, 'Microstructure relationship of sillimanite and 'fibrolite' relationships at Broken Hill', Australia, *Lithos,* vol. 15, no. 1, pp. 49-58.

Aitchison, J. 1986, *The statistical analysis of compositional data, monographs on statistics and applied probability*, Chapman and Hall, London.

Aitchison, J. & Greenare, M. 2002, 'Biplots of compositional data', *Applied Statistics*, vol. 51, no. 4, pp. 375-392.

Anderson, T.W. 1984, *An introduction to multivariate statistical analysis*, 2nd edn, John Wiley & Sons, New York.

Andrews, E.C. 1922, *The geology of the Broken Hill district*, Geological Survey of New South Wales, Memoirs 8, Sydney.

Arabie, P., Hubert, L.J. & De Soete, G. 1996, *Clustering and classification*, World Scientific Singapore.

Armstrong, M. 1998, *Basic linear Geostatistics*, Springer, Berlin.

Arnold, R.G. 1967, 'Range in composition and structure of 82 natural terrestrial pyrrhotites', *The Canadian Mineralogist,* vol. 9, pp. 31-50.

Bellehumeur, C. & Jébrak, M. 1993, 'Regional heavy mineral survey in the exploration for gold using regression: Grenville Province, southwestern Quebec.', *Journal of Geochemical Exploration*, vol. 47, no. 1-3, pp. 45-61.

Benzercri, J.P. 1992, *Correspondence analysis hand book*, Marcel Dekker, New York.

Beus, A.A. & Grigorian, S.V. 1977, *Geochemical exploration methods for mineral deposits*, Illinois, USA.

Blainey, G. 1968, *The rise of Broken Hill*, Macmillan Australia, Melbourne.

Blampain, P. & Plimer, I.R. 2006, 'The Western Mineralisation-Rasp Mine', *Broken Hill Exploration Initiative*, vol. 21, ed. R.J. Korsch, Barnes, R.G., Geoscience Australian Record, Broken Hill, pp. 8-14.

Breiman, L. 2001, 'Random forests', *Machine Learning,* vol. 45, no. 1, pp. 5-32.

Brick, R.A. 2005, 'Pre-metamorphic hydrothermal alteration at Corruge No 1 workings, Broken Hill, New South Wales, Australia', BSc (Honours) thesis, The University of Melbourne, Melbourne.

Brown, R.E., Stevens, B.P.J., Willis, I.L., Stroud, W.J., Bradley, G.M. & Barnes, R.G. 1983, '3. Quartzofeldspathic rocks', in B.P.J. Stevens & W.J. Stroud (eds), *Rocks of the Broken Hill Block: Their classification, nature, stratigraphic distribution and origin*, vol. 21 Geology Survey Record, New South Wales, pp. 127-226.

Bryndzia, L.T., Scott, S.D. & Spry, P.G. 1988, 'Sphalerite and hexagonal pyrrhotite geobarometer; experimental calibration and application to the metamorphosed sulfide ores of Broken Hill, Australia ', *Economic Geology*, vol. 83, no. 6, pp. 1193-1204.

Burton, G. 1998, 'Stratiform Pb-Zn-Ag mineralisation in the Broken Hill and Eurowie Blocks', *Broken Hill Exploration Initiative, Fourth annual meeting,* vol. 25, ed. G.M. Gibson, Australian Geological Survey Organisation Record, Broken Hill, pp. 1-4.

Carpenter, R.H. & Bailey, A.C., 1973, 'Application of Ro and Ar measurements to the study of pyrrhotite and troilite', *American Mineralogist*, vol. 58, pp. 440-443.

Carras, S. 2001, 'Let the orebody speak', in A.C. Edwards (ed.), *Mineral resource and ore reserve estimation-The AusIMM guide to good practice* The Australasian Institute of Mining and Metallurgy, Melbourne, pp. 199-206.

Carrasco, P.C. 2010, 'Nugget effect, artificial or natural?', *The Journal of the Southern African Institute of Mining and Metallurgy,* vol. 110, pp. 299-305.

CBH Resources Ltd., 'Open pits on CML7', unpublished.

Chen, Y., Huang, J. & Liang, Z. 2008, 'Geochemical characteristics and zonation of primary halos of Pulang porphyry copper deposit, North-western Yunnan province, South-western China', *Journal of China University of Geosciences*, vol. 19, no. 4, pp. 371-377.

Chen, Y. & Zhao, P. 1998, 'Zonation in primary halos and geochemical prospecting pattern for the Guilaizhuang gold deposit, eastern China', *Natural Resources Research*, vol. 7, no. 1, pp. 37-44.

Cheng, Q. 1999, 'Spatial and scaling modelling for geochemical anomaly separation', *Journal of Geochemical Exploration*, vol. 65, no. 3, pp. 175-194.

Cheng, Q., Agterberg, F.P. & Ballantyne, S.B. 1994, 'The separation of geochemical anomalies from background by fractal methods', *Journal of Geochemical Exploration*, vol. 51, no. 2, pp. 109-130.

Cheng, Q., Agterberg, F.P. & Bonham-Carter, G.F. 1996, 'A spatial analysis method for geochemical anomaly separation', *Journal of Geochemical Exploration*, vol. 56, no. 3, pp. 183-195.

Cheng, Q., Xu, Y. & Grunsky, E.C. 2000, 'Integrated spatial and spectrum method for geochemical anomaly separation', *Natural Resources Research*, vol. 9, no. 1, pp. 43-51.

, J.P. & Delfiner, P. 1999, *Geostatistics: Modelling spatial uncertainty* John Wiley & Sons, New York.

Clark, D.A. 1997, 'Magnetic petrophysics and magnetic petrology: Aides to geological interpretation of magnetic surveys', *AGSO Journal of Australian Geology and Geophysics*, vol. 17, no. 2, pp. 83-103.

Clarke, G.L., Burg, J.P. & Wilson, C.J.L. 1986, 'Stratigraphic and structural constraints on the Proterozoic tectonic history of the Olary Block, South Australia', *Precambrian Research*, vol. 34, no. 2, pp. 107-137.

Clausen, S.E. 1998, *Applied correspondence analysis: An introduction, Series: Quantitative applications in the social sciences*, Sage Publications, New Jersey.

Conor, C.H.H., Ashley, P.M., Bierlein, F.P., Cook, N.D.J., Crooks, A.F., Lawie, D.C., Plimer, I.R., Preiss, W.V., Robertson, R.S. & Skirrow, R.G. 2006, *Geology of the Olary Domain, Curnamona Province* Report Number 2006/13, Department of Primary Industries and Resources, South Australia.

Conor, C.H.H. & Preiss, W.V. 2008, 'Understanding the 1720-1640 Ma Palaeoproterozoic Willyama Supergroup, Curnamona province, south-eastern Australia: Implications for tectonics, basin evolution and ore genesis', *Precambrian Research*, vol. 166, no. 1-4, pp. 297-317.

Corbett, G.J. & Phillips, G.N. 1981, 'Regional retrograde metamorphism of a high grade terrain: The Willyama Complex, Broken Hill, Australia', *Lithos*, vol. 14, no. 1, pp. 59-73.

Creative Research Systems 1982, *Significance in Statistics & Surveys,*, Creative Research Systems Inc., viewed 6/11/2009 <http://www.surveysystem.com/signif.htm>.

Damm, S. 2008, 'Sequence stratigraphy of the Western Mineralisation, Broken Hill, Australia', MSc thesis, The University of Bremen, Bremen.

Davidson, G.J., Large, R.R., Kary, G. & Osborne, R. 1989, 'The deformed iron-formation-hosted Starra and Trough Tank Au-Cu mineralisation: A new association from the Proterozoic Eastern Succession of Mount Isa, Australia.', *Economic Geology Monograph*, vol. 6, pp. 135-150.

Davis, J.C. 1973, *Statistics and data analysis in geology*, John Wiley & Sons, New York.

De Caritat, P., Kirste, D., Carr, G. & McCulloch, M. 2005, 'Groundwater in the Broken Hill region, Australia: Recognising interaction with bedrock and mineralisation using S, Sr and Pb isotopes', *Applied Geochemistry,* vol. 20, no. 4, pp. 767-787.

De Geoffroy, J. & Wignall, T.K. 1972, 'A statistical study of geological characteristics of porphyry-copper-molybdenum deposits in the Cordilleran Belt-application to the rating of porphyry prospects', *Economic Geology,* vol. 67, no. 5, pp. 656-668.

De Villiers, J.P.R. & Liles, D.C. 2010, 'The crystal-structure and vacancy distribution in 6C pyrrhotite', *American Mineralogist*, vol. 95, no. 1, pp. 148-152.

Dekkers, M.J. 1988, 'Magnetic properties of natural pyrrhotite Part I: Behaviour of initial susceptibility and saturation-magnetization-related rock-magmatic parameters in a grain size dependent framework', *Physics of the Earth and Planetary Interiors*, vol. 52, no. 3-4, pp. 376-393.

DMTC-The Delta Mine Training Center 2009, *Unit Two-Geochemical methods*, DMTC, viewed18/8/2009 <http://www.dmtcalaska.org/exploration/ISU/unit2/u2lesson1.html>.

Dominy, S.C., Stephenson, P.R. & Annels, A.E. 2001, 'Classification and reporting of mineral resources for high-nugget effect gold vein deposits', *Exploration and Mining Geology,* vol. 10, no. 3, pp. 215-233.

Dowd, P.A. 2006a, 'Introduction to Geostatistics for Master of Geostatistics program', Adelaide.

Dowd, P.A. 2006b, 'Linear Geostatistics for Master of Geostatistics program', Adelaide.

Dowd, P.A. & Xu, C. 2006, *Geostatistics for Windows* 3rd edn, The University of Adelaide, Adelaide, p. A comprehensive mineral resource evaluation tool.

Dutter, R. 2003, 'Regularization by cores along a bore-hole', viewed 25/05/2009 <http://www.statistik.tuwien.ac.at/public/dutt/vorles/geost_03/node97.html>.

Egozcue, J.J. & Pawlowsky-Glahn, V. 2005, 'Groups of parts and their balances in compositional data analysis', *Mathematical Geology,* vol. 37, no. 7, pp. 795-828.

Egozcue, J.J., Pawlowsky-Glahn, V., Mateu-Figueras, G. & Barceló-Vidal, C. 2003, 'Isometric logratio transformations for compositional data analysis', *Mathematical Geology*, vol. 35, no. 3, pp. 279-300.

Ender, P.B. 2010, 'Applied categorical & nonnormal data analysis', viewed 20/2/2009 <http://www.philender.com/courses/categorical/notes2/corres.html>.

Everitt, B.S. 2006, *The Cambridge dictionary of statistics*, vol. 1, Cambridge University Press, London.

Feldman, M. 2004, 'The Palaeo-depositional environment of the Broken Hill Group: Application of basin analysis in a high grade metamorphic terrain', BSc (Honours) thesis, The University of Melbourne, Melbourne.

Filzmoser, P., Hron, K. & Reimann, C. 2009, 'Principal component analysis for compositional data with outliers', *Environmetrics*, vol. 20, pp. 621-632.

Filzmoser, P., Reimann, C. & Garrett, R.G. 2005, 'Multivariate outlier detection in exploration geochemistry', *Computers and Geosciences,* vol. 31, no. 5, pp. 579-587.

Flatman, G.T. & Yfantis, A.A. 1984, 'Geostatistical strategy for soil sampling: The survey and the census', *Environmental Monitoring and Assessment,* vol. 4, no. 4, pp. 335-349.

Fraley, C. & Raftery, A.E. 1988, 'How many clusters? Which clustering method? Answers via model-based cluster analysis', *The Computer Journal*, vol. 41, no. 8, pp. 578-588.

Friendly, M. 1995, 'Categorical data analysis with graphics', *Part 5: Correspondence analysis*, viewed 13/6/2009 <http://www.math.yorku.ca/SCS/Courses/grcat/grc5.html>.

Frost, B.R., Mavrogenes, J.A. & Tomkins, A.G. 2002, 'Partial melting of sulfide ore deposits during medium-and high-grade metamorphism', *The Canadian Mineralogist,* vol. 40, pp. 1-18.

Gabriel, K.R. 1971, 'The biplot graphic display of matrices with application to principal component analysis', *Biometrika*, vol. 58, no. 3, pp. 453-467.

Garson, G.D. 2010, *Reliability Analysis*, North Carolina State University, viewed 25/6/2009 <http://faculty.chass.ncsu.edu/garson/PA765/reliab.htm>.

Gentle, L.V. 1968, 'Geology of the Western Limb and the Western Mineralisation at Broken Hill South Limited', in M. Radmanovich & J.T. Woodcock (eds), *Broken Hill Mines*, 75th Anniversary edn, The Australasian Institute of Mining and Metallurgy, Monograph 3, pp. 179-183.

Giles, D. & Nutman, A. 2003, 'SHRIMP U-Pb zircon dating of the host rocks of the Cannington Ag-Pb-Zn deposit, southeastern Mt Isa Block, Australia.', *Australian Journal of Earth Sciences*, vol. 50, no. 3, pp. 295-309.

Godber, K. & Bishop, J. 2006, 'Geophysics at Broken Hill-what works and what doesn't', *Broken Hill Exploration Initiative*, vol. 21, eds R.J. Korsch & R.G. Barnes, Geoscience Australia Record, Broken Hill, p. 59.

Goovaerts, P. 1997, *Geostatistics for natural resources evaluation*, Oxford University Press, New York.

Gordon, A.D. (ed.) 1999, *Classification, monographs on statistics and applied probability,* 2nd edn, vol. 82, Chapman & Hall / CRC, New York.

Govett, G.J.S., Goodfellow, W.D., Chapman, R.P. & Chork, C.Y. 1975, 'Exploration geochemistry distribution of elements and recognition of anomalies', *Mathematical Geology,* vol. 7, no. 5/6, pp. 415-446.

Gower, J.C. 1966, 'Some distance properties of latent root and vector methods used in multivariate analysis', *Biometrika,* vol. 53, no. 3-4, pp. 325-338.

Graham, G.E., Kelley, K.D., Slack, J.F. & Koenig, A.E. 2009, 'Trace elements in Zn-Pb-Ag deposits and related stream sediments, Brooks Range Alaska, with implications for Tl as a pathfinder element', *Geochemistry: Exploration, Environment Analysis,* vol. 9, pp. 19-37.

Greenacre, M. 1984, *Theory and applications of correspondence analysis*, Academic Press, London.

Greenacre, M. 2007, *Correspondence analysis in practice*, Chapman & Hall / CRC, Barcelona, Spain.

Greenacre, M. 2010, *Biplots in Practice* Fundación BBVA, <http://www.fbbva.es/TLFU/tlfu/ing/publicaciones/libros/fichalibro/index.jsp?codigo=571>.

Grigorian, S.V. 1974, 'Primary geochemical haloes in prospecting and exploration of hydrothermal deposits', *International Geology Review*, vol. 16, no. 1, pp. 12-25.

Grigorian, S.V. & Ziaii, M. 1997, 'Computing methods for determination of geochemical haloes background', paper presented to the *International Symposium, Applied Geochemistry in CIS. IMGRE*, Moscow.

Groombridge, D.L. 2003, 'Remobilisation of the Lead Lodes, Broken Hill, New South Wales, Australia', BSc (Honours) thesis, The University of Melbourne, Melbourne.

Groves, I.M., Groves, D.I., Bierlein, F.P., Broome, J. & Penhall, J. 2008, 'Recognition of the hydrothermal feeder to the structurally inverted, giant Broken Hill deposit, New South Wales, Australia', *Economic Geology*, vol. 103, no. 7, pp. 1389-1394.

Grunsky, E.C. & Agterberg, F.P. 1988, 'Spatial and multivariate analysis of geochemical data from metavolcanic rocks in the Ben Nevis Area, Ontario', *Mathematical Geology*, vol. 20, no. 7, pp. 415-446.

Guibal, D. 2001, 'Variography, a tool for the resources geologist ', in A.C. Edwards (ed.), *Mineral resource and ore reserve estimation-The AusIMM guide to good practice*, The Australasian Institute of Mining and Metallurgy, Melbourne, pp. 85-90.

Gulson, B.L., Porritt, P.M., Mizon, K.J. & Barnes, R.G. 1985, 'Lead isotope signature of stratiform and strata-bound mineralisation in the Broken Hill Block, New South Wales, Australia', *Economic Geology*, vol. 80, no. 2, pp. 488-496.

Gundobin, G.M. 1984, 'Peculiarities in the zoning of primary haloes', *Journal of Geochemical Exploration*, vol. 21, no. 1-3, pp. 193-200.

Gustafson, J.K., Burrell, H.C. & Garretty, M.D. 1950, 'Geology of the Broken Hill ore deposit, Broken Hill, New South Wales', *Geological Society of America Bulletin,* vol. 61, pp. 1369-1414.

Hand, M., Rutherford, L. & Barovich, K. 2003, 'Garnet Sm/Nd age constraints on the timing of tectonism in the south-western Curnamona Province: Implications for existing models and correlations.' *Broken Hill Exploration Initiative*, vol. 13, ed. M. Peljo, Geoscience Australia Record Broken Hill, pp. 65-68.

Harrison, T.M. & McDougall, I. 1981, 'Excess ^{40}Ar in metamorphic rocks from Broken Hill, New South Wales: Implications for ^{40}Ar / ^{39}Ar age spectra and the thermal history of the region', *Earth and Planetary Science Letters,* vol. 55, no. 1, pp. 123-149.

Hart, R.F. & Hart, M.K. 2010, 'Testing for "near-normality": The probability plot', viewed 1/08/2009 <http://www.statit.com/support/quality_practice_tips/testingfornearnormality.shtml>.

Hartigan, j. 1975, *Clustering algorithms*, John Wiley & Sons, New York.

Haydon, R.C. & McConachy, G.W. 1987, 'The stratigraphic setting of Pb-Zn-Ag mineralisation at Broken Hill', *Economic Geology*, vol. 82, no. 4, pp. 826-856.

Heimann, A., Spry, P.G., Teale, G.S., Conor, C.H.H. & Leyh, W.R. 2009, 'Geochemistry of garnet-rich rocks in the southern Curnamona province, Australia, and their genetic relationship to Broken Hill-Type Pb-Zn-Ag mineralization', *Economic Geology*, vol. 104, no. 5, pp. 687-712.

Hoaglin, D.C., Mosteller, F. & Tukey, J.W. (eds) 1983, *Understanding robust and exploratory data analysis,* John Wiley & Sons, New York.

Hobbs, B.E., Archibald, N.J., Etheridge, M.A. & Wall, V.J. 1984, 'Tectonic history of the Broken Hill Block, Australia', in A. Kroner & R. Greiling (eds), *Precambrian Tectonics Illustrated*, E. Schweizerbart'sche Verlagsbuchhandlung, Stuttgart, pp. 353-368.

Hodgson, C.J. 1974, 'The geology and geological development of the Broken Hill Lode in the New Broken Hill Consolidated Mine, Australia, Part I: Structural Geology', *Geological Society of Australia,* vol. 21, no. 4, pp. 413-430.

Hopkins, W.G. 2000a, *A new view of statistics: Calculations for reliability,* The University of Auckland, viewed 13/5/2009 <http://www.sportsci.org/resource/stats/relycalc.html>.

Hopkins, W.G. 2000b, *A new view of statistics: Measures of validity*, The University of Auckland, viewed 13/5/2009 <http://www.sportsci.org/resource/stats/valid.html>.

Huang, X. & Zhang, D. 1989, 'Geochemical zoning pattern of the Yinyan tin deposit', *Journal of Geochemical Exploration*, vol. 33, no. 1-3, pp. 109-119.

James, S.D., Pearce, J.A. & Oliver, R.A. 1987, 'The geochemistry of the lower Proterozoic Willyama Complex volcanics, Broken Hill Block, New South Wales', in T.C. Pharoah, R.D. Beckisale & D. Rickard (eds), *Geochemistry and Mineralization of Proterozoic Volcanic Suites of Australia*, vol. 33, Geological Society of London Special Publications London pp. 395-408.

Johnson, I.R. & Klingner, G.D. 1975, 'Broken Hill ore deposit and its environment', *Economic Geology of Australia and Papua New Guinea, 1. Metals,* vol. 5, ed. C.L. Knight, The Australasian Institute of Mining and Metallurgy, Monograph Series, Melbourne, pp. 476-491.

Johnson, R.A. & Wichern, D.W. 1992, *Applied multivariate statistical methods*, 3rd edn, Prentice Hall International, Englewood Cliffs, New Jersey.

Kashirtseva, M.K. 1967, 'Mineral and geochemical zonation of infiltration uranium ores', *International Geology Review*, vol. 9, no. 1, pp. 100-109.

Kelkar, M. 2002, 'Applied Geostatistics for reservoir characterization-Accomplishments and Challenges', *Journal of Canadian Petroleum Technology,* vol. 39, no. 7, pp. 25-29.

Kitchen, K. 2001, 'The geology of the Western Mineralisation, Broken Hill, New South Wales', BSc (Honours) thesis, The University of Melbourne, Melbourne.

Kontny, A., De Wall, H., Sharp, T.G. & Pósfai, M. 2000, 'Mineralogy and magnetic behavior of pyrrhotite from a 260° C section at the KTB drilling site, Germany', *American Mineralogist*, vol. 85, pp. 1416-1427.

Kruse, O. & Ericsson, T. 1988, 'A Mössbauer investigation of natural Troilite from the Agpalilik Meteorite', *Physics and Chemistry Minerals*, vol. 15, pp. 509-513.

Labus, M. 2005, 'Compositional data analysis as a tool for interpretation of rock porosity parameters', *Geology Quarterly,* vol. 49, no. 3, pp. 347-354.

Laing, W.P. 1996a, 'The Diamantina Orogen linking the Willyama and Cloncurry Terranes, eastern Australia', in J. Pongratz & G.J. Davidson (eds), *New developments in Broken Hill type deposits*, vol. 1, Centre for ore deposit and exploration studies special publication Hobart, pp. 67-72.

Laing, W.P. 1996b, 'Nappe interpretation, Palaeogeography and metallogenic synthesis of the Broken Hill-Olary Block', in J. Pongratz & D.G.J. (eds), *New developments in Broken Hill type deposits*, vol. 1, Centre for ore deposit and exploration studies special publication Hobart, pp. 21-52.

Laing, W.P. 1998, 'Structural-metasomatic environment of the East Mt Isa Block base metal-gold province.', *Australian Journal of Earth Sciences,* vol. 45, no. 3, pp. 413-428.

Laing, W.P., Marjoribanks, R.W. & Rutland, R.W.R. 1978, 'Structure of the Broken Hill mines area and its significance for genesis of the orebodies', *Economic Geology,* vol. 73, no. 6, pp. 1112-1136.

Lance, G.N. & Williams, W.T. 1966, 'Computer programs for classification', *Australian National Committee on Computing and Automatic Control Conference*, vol. 3, Canberra, pp. 304-306.

Large, R.R., Bull, S.W. & McGoldrick, P.J. 2000, 'Lithogeochemical halos and geochemical vectors to stratiform sediment hosted Zn-Pb-Ag deposits. Part 2. HYC deposit, McArthur River, Northern Territory', *Journal of Geochemical Exploration*, vol. 68, pp. 105-126.

Large, R.R., Bull, S.W., McGoldrick, P.J. & Walters, S.G. 2005, 'Stratiform and strata-bound Zn-Pb-Ag deposits in Proterozoic sedimentary basins, northern Australia', *Economic Geology*, vol. 100th Anniversary, pp. 931-963.

Lawrence, L.J. 1967, 'Sulphide neomagmas and highly metamorphosed sulphide deposits', *Mineralium Deposita,* vol. 2, no. 1, pp. 5-10.

Lawrence, L.J. 1968, 'The mineralogy and genetic significance of a Consols-type vein in the Main Lode Horizon, Broken Hill, N.S.W.', *Proc. The Australasian Institute of Mining and Metallurgy*, vol. 226, no. 1, pp. 47-57.

Lawrie, K.C. & Hinman, M.C. 1998, 'Cobar-style polymetallic Au-Cu-Ag-Pb-Zn deposits', *AGSO Journal of Australian Geology and Geophysics*, vol. 17, no. 4, pp. 169-187.

Le Maitre, R.W. 1982, *Numerical petrology*, Elsevier Scientific, Amsterdam.

Levinson, A.A. 1974, *Introduction to exploration geochemistry*, Applied Publishing, Calgary.

Leyh, W.R. 2000, 'Detailed lithostructural mapping of the Broken Hill type mineralisation in the Broken Hill Block, NSW', *Broken Hill Exploration Initiative*, vol. 10, ed. M. Peljo, Australian Geological Survey Organisation Record, Broken Hill, pp. 4-7.

Li, C., Ma, T. & Shi, J. 2003, 'Application of a fractal method relating concentrations and distances for separation of geochemical anomalies from background', *Journal of Geochemical Exploration,* vol. 77, no. 2-3, pp. 167-175.

Li, Z.X., Zhang, L. & Powell, C.M. 1995, 'South China in Rodinia: Part of the missing link between Australia-East Antarctica and Laurentia?', *Geology,* vol. 23, no. 5, pp. 407-410.

Lima, A., De Vivo, B., Cicchella, D., Cortini, M. & Albanese, S. 2003, 'Multifractal IDW interpolation and fractal filtering method in environmental studies: An application on regional stream sediments of (Italy), Campania region', *Applied Geochemistry,* vol. 18, no. 12, pp. 1853-1865.

Liu, C. & Xu, W. 1995, 'Primary geochemical anomalies in the Caijiaying Pb-Zn-Ag deposits, Hebei, China', *Journal of Geochemical Exploration,* vol. 55, no. 1-3, pp. 25-32.

Lloyd, C.D. 2006, *Local models for spatial analysis,* CRC Press, Boca Raton.

Lu, J., Plimer, I.R., Foster, D.A. & Lottermoser, B.G. 1996, 'Multiple post-orogenic reactivation in the Olary Block, South Australia: Evidence for ^{40}Ar / ^{39}Ar dating of pegmatitic muscovite', *International Geology Review,* vol. 38, no. 7, pp. 665-685.

Mackenzie, D.H. 1968, 'Lead Lode at New Broken Hill Consolidated Limited', *The Australasian Institute of Mining and Metallurgy, Monograph Series*, vol. 3, pp. 161-169.

Maiden, K.J. 1975, 'High grade metamorphic structures in the Broken Hill orebody', *The Australasian Institute of Mining and Metallurgy, Proceedings*, vol. 254, pp. 19-27.

Marjoribanks, R.W., Rutland, R.W.R., Glen, R.A. & Laing, W.P. 1980, 'The structure and tectonic evolution of the Broken Hill region, Australia', *Precambrian Research*, vol. 13, no. 2-3, pp. 209-240.

Mark, S.A. & Roger, K.B. 1984, *Cluster Analysis*, Sage Publications, London.

Mavrogenes, J.A., Kalinowski, A., Sparks, H.A., Wykes, J.L. & Frost, B.R. 2004, 'Sulfide melt metasomatism: Metamorphic alteration at Broken Hill, Australia', *EOS Transactions, American Geophysical Union*, vol. 85, no. 17.

Microsoft Corporation 2006, *Microsoft Visual Basic 6.5*, *Visual Basic for Applications*, 6.5.1053 edn, Microsoft Corporation, p. Excel Macros (VBA) <http://msdn.microsoft.com/en-us/vbasic/default.aspx>.

Miesch, A.T. 1981, 'Estimation of the geochemical threshold and its statistical significance', *Journal of Geochemical Exploration*, vol. 16, no. 1, pp. 49-76.

Minitab Inc. 2007, *Minitab* 15 edn, Minitab Inc., Pennsylvania, p. Statistical software for quality improvement <http://www.minitab.com/en-AU/default.aspx>.

Morland, R. & Webster, A.E. 1998, 'Broken Hill lead-zinc-silver deposit', in D.A. Berkman & D.H. Mackenzie (eds), *Geology of Australian and Papua New Guinean Mineral Deposits*, The Australasian Institute of Mining and Metallurgy, Melbourne, pp. 619-626.

Munyantwali, I. 2006, 'Geochemistry of the Western Mineralisation, Broken Hill, New South Wales, Australia', BSc (Honours) thesis, The University of Adelaide, Adelaide.

New South Wales Department of Primary Industries 1995, *Broken Hill Geophysical Survey* New South Wales Department of Primary Industries, Mineral Resources, Broken Hill, pp. Magnetics, Radiometrics, DTM.

Nutman, A.P. & Ehlers, K. 1998, 'Evidence for multiple Palaeoproterozoic thermal events and magmatism adjacent to the Broken Hill Pb-Zn-Ag orebody, Australia', *Precambrian Research*, vol. 90, no. 3-4, pp. 203-238.

Nutman, A.P. & Gibson, G.M. 1998, 'Zircon ages from metasediments, granites and mafic intrusions: Reappraisal of the Willyama Supergroup', *Broken Hill Exploration Initiative: Fourth annual meeting,* vol. 25, ed. G.M. Gibson, Australian Geological Survey Organisation Record Broken Hill, pp. 86-88.

Olea, R.A. 1999, *Geostatistics for engineers and earth scientists*, Kluwer Academic Publishers, Boston.

Oliver, N.H.S., Butera, K.M., Rubenach, M.J., Marshall, L.J., Cleverley, J.S., Mark, G., Tullemans, F. & Esser, D. 2008, 'The protracted hydrothermal evolution of the Mount Isa Eastern Succession: A review and tectonic implications', *Precambrian Research*, vol. 163, no. 1-2, pp. 108-130.

Page, R.W., Conor, C.H.H., Stevens, B.P.J., Gibson, G.M., Preiss, W.V. & Southgate, P.N. 2005, 'Correlation of Olary and Broken Hill Domains, Curnamona Province: Possible relationship to Mount Isa and other Northern Australian Pb-Zn-Ag-bearing successions', *Economic Geology,* vol. 100, no. 4, pp. 663-676.

Page, R.W. & Laing, W.P. 1992, 'Felsic metavolcanic rocks related to the Broken Hill Pb-Zn-Ag orebody, Australia; geology, depositional age, and timing of high-grade metamorphism', *Economic Geology,* vol. 87, no. 8, pp. 2138-2168.

Page, R.W., Stevens, B.P.J. & Gibson, G.M. 2000, 'New SHRIMP zircon results from Broken Hill: Towards robust stratigraphic and event timing', paper presented to the *15th Australian Geological Convention, Understanding planet earth: Searching for a sustainable future*, Sydney.

Page, R.W., Stevens, B.P.J. & Gibson, G.M. 2005, 'Geochronology of the Sequence Hosting the Broken Hill Pb-Zn-Ag Orebody, Australia', *Economic Geology*, vol. 100, no. 4, pp. 633-661.

Parr, J.M. & Plimer, I.R. 1993, 'Models for Broken Hill-type lead-zinc-silver deposits', *Geological Association of Canada Special Paper*, vol. 40, eds R.V. Kirkham, W.D. Sinclair, R.I. Thorpe & J.M. Duke, Mineral Deposit Modelling, pp. 253-288.

Parr, J.M., Stevens, B.P.J. & Carr, G.R. 2003, 'Timing of multiple hydrothermal events in the Broken Hill Terrain - Evidence from lead isotopes', *Broken Hill Exploration Initiative*, vol. 13, ed. M. Peljo, Geoscience Australia Record, pp. 126-129.

Patchett, A. 2003, 'Hydrothermal alteration associated with the Western Mineralisation, Broken Hill, New South Wales, Australia', BSc (Honours) thesis, The University of Melbourne, Melbourne

pbarrett.net 2001, *Skewness and Pearson correlations-Attenuation of coefficient size as a function of skewed data,* pbarrett.net, viewed 25/2/2009 <http://www.pbarrett.net/ techpapers/skewness.pdf>.

Peters, W.C. 1987, *Exploration and mining geology,* John Wiley & Sons, New York.

Phillips, G.N. 1980, 'Water activity changes across an amphibolite-granulite facies transition, Broken Hill, Australia', *Contributions to Mineralogy and Petrology*, vol. 75, pp. 377-386.

Phillips, G.N., Archibald, N.J. & Wall, V.J. 1985, 'Metamorphosed high-Fe tholeiites: Their alteration and relationships to sulphide mineralisation, Broken Hill, Australia', *Transactions of the Geological Society of South Africa,* vol. 88, pp. 49-59.

Phillips, G.N. & Wall, V.J. 1981, 'Evaluation of prograde regional metamorphic conditions: Their implications for the heat source and water activity during metamorphism in the Willyama Complex, Broken Hill, Australia', *Bulletin de la Société française de Minéralogie,* vol. 104 pp. 801-810.

Plimer, I.R. 1975, 'A metamorphogenic alteration zones around the stratiform Broken Hill ore deposits, Australia', *Geochemical Journal*, vol. 9, pp. 211-220.

Plimer, I.R. 1977, 'The origin of albite rocks enclosing the cobaltian pyrite deposit at Thackaringa, NSW, Australia', *Mineralium Deposita,* vol. 12, no. 2, pp. 175-187.

Plimer, I.R. 1979, 'Sulphide rock zonation and hydrothermal alteration at Broken Hill, Australia', *Transactions of the Institution of Mining and Metallurgy, Section B*, vol. 88, pp. B161-B176.

Plimer, I.R. 1984, 'The mineralogical history of the Broken Hill Lode, NSW', *Australian Journal of Earth Sciences,* vol. 31, pp. 379-402.

Plimer, I.R. 1985, 'Broken Hill Pb-Zn-Ag deposit-A product of mantle metasomatism', *Mineralium Deposita,* vol. 20, no. 3, pp. 147-153.

Plimer, I.R. 1986, 'Sediment-hosted exhalative Pb-Zn deposits-products of contrasting ensialic rifting', *Geological Society of South Africa Transactions*, vol. 89, no. 1, pp. 57-73.

Plimer, I.R. 2006a, 'Hydrothermal alteration at Broken Hill', *Broken Hill Exploration Initiative*, vol. 21, eds R.J. Korsch & R.G. Barnes, Geoscience Australia Record Broken Hill, pp. 138-145.

Plimer, I.R. 2006b, 'Manganoan garnet rocks associated with the Broken Hill Pb-Zn-Ag orebody', *Mineralogy and Petrology,* vol. 88, no. 3-4, pp. 443-478.

Plimer, I.R., Blampain, P., Collier, J. & Patchett, A. 2003, 'CML7 (The South Mine), Broken Hill, Australia', *Broken Hill Exploration Initiative,* vol. 13, ed. M. Peljo, Geoscience Australia Record Broken Hill, pp. 132-136.

Raetz, M., Krabbendam, M.J. & Donaghy, A.G. 2002, 'Compilation of U-Pb zircon data from the Willyama Supergroup, Broken Hill region, Australia: Evidence for three tectonostratigraphic successions and four magmatic events?', *Australian Journal of Earth Sciences*, vol. 49, no. 6, pp. 965-983.

Raveggi, M., Giles, D., Foden, J. & Raetz, M. 2007, 'High Fe-Ti magmatism and tectonic setting of the Paleoproterozoic Broken Hill Block, NSW, Australia,' *Precambrian Research*, vol. 156, pp. 55-84.

Reimann, C. & Filzmoser, P. 2000, 'Normal and lognormal data distribution in geochemistry: Death of a myth. Consequences for the statistical treatment of geochemical and environmental data', *Environmental Geology,* vol. 39, no. 9, pp. 1001-1014.

Reis, A.P., Sousa, A.J. & Cardoso, F.E. 2001, 'Soil geochemical prospecting for gold at Marrancos (Northern Portugal)', *Journal of Geochemical Exploration*, vol. 73, no. 1, pp. 1-10.

Rencher, A.C. 1995, *Methods of multivariate analysis*, John Wiley & Sons, New York.

Robertson, R.S., Preiss, W.V., Crooks, A.F., Hill, P.W. & Sheard, M.J. 1998, 'Review of the Proterozoic geology and mineral potential of the Curnamona Province in South Australia', *AGSO Journal of Australian Geology and Geophysics*, vol. 17, no. 3, pp. 169-182.

Rochette, P., Fillion, G., Mattéi, J.-L. & Dekkers, M.J. 1990, 'Magnetic transition at 30-34 Kelvin in pyrrhotite: Insight into a widespread occurrence of this mineral in rocks', *Earth and Planetary Science Letters*, vol. 98, no. 3-4, pp. 319-328.

Rothery, E. 2001, 'Tectonic origin of the shape of the Broken Hill lodes supported by their structural setting in a high grade shear zone', *Australian Journal of Earth Sciences,* vol. 48, no. 2, pp. 201-220.

Ryall, W.R. 1979, 'Mercury in the Broken Hill (NSW, Australia) lead-zinc-silver lodes', *Journal of Geochemical Exploration*, vol. 11, no. 2, pp. 175-194.

Sainisch-Plimer, R.M. 1999, 'The life and times of Charles Rasp', in W.D. Birch (ed.), *Minerals of Broken Hill,* Broken Hill City Council, Broken Hill, pp. 12-33.

SAS Institute Inc. 1999, 'Example 24.3: Simple correspondence analysis of U.S. population', viewed 15/9/2009 <http://www.sfu.ca/sasdoc/sashtml/stat/chap24/sect28.htm>.

Scott, S.D., Both, R.A. & Kissin, S.A. 1977, 'Sulfide petrology of the Broken Hill Region, New South Wales', *Economic Geology*, vol. 72, no. 8, pp. 1410-1425.

Segnit, E.R. 1961, 'Petrology of the zinc lode, New Broken Hill Consolidation Ltd, Broken Hill, New South Wales', *The Australasian Institute of Mining and Metallurgy, Proceedings*, vol. 199, pp. 87-112.

Sinclair, A.J. 1974, 'Selection of thresholds in geochemical data using probability graphs', *Journal of Geochemical Exploration*, vol. 3, no. 2, pp. 129-149.

Sinclair, A.J. 1976, 'Application of probability graphs in mineral exploration', *Association Exploration Geochemists, Special,* vol. 4, p. 95.

Slack, J.F., Palmer, M.R., Stevens, B.P.J. & Barnes, R.G. 1993, 'Origin and significance of tourmaline-rich rocks in the Broken Hill district, Australia', *Economic Geology*, vol. 88, no. 3, pp. 505-541.

Slack, J.F. & Stevens, B.P.J. 1994, 'Clastic metasediments of the early Proterozoic Broken Hill Group. New South Wales, Australia: Geochemistry provenance, and metallogenic significance', *Geochimica et Cosmochimica Acta*, vol. 58, no. 17, pp. 3633-3652.

Smith, M.L. 1999, *Geologic and mine modelling using Techbase and Lynx*, Taylor & Francis, UK.

Social Research Update 1995, 'Correspondence analysis', viewed 22/2/2009 <http://sru.soc.surrey.ac.uk/sru7.html>.

Sparks, H.A. & Mavrogenes, J.A. 2005, 'Sulfide melt inclusions as evidence for the existence of a sulfide partial melt at Broken Hill, Australia', *Economic Geology*, vol. 100, no. 4, pp. 773-779.

Sproal, T. 2001, 'C Lode and 2 Lens, CML7, Broken Hill, Australia', BSc (Honours) thesis, The University of Melbourne, Melbourne.

Spry, P.G., Plimer, I.R. & Teale, G.S. 2008, 'Did the giant Broken Hill (Australia) Zn-Pb-Ag deposit melt?', *Ore Geology Reviews*, vol. 34, no. 3, pp. 223-241.

Spry, P.G., Teale, G.T. & Heimann, A. 2003, 'Speculations concerning the origin and exploration significance of lode rocks in the Curnamona Province', *Broken Hill Exploration Initiative*, vol. 13, ed. M. Peljo, Geoscience Australia Record Broken Hill, pp. 162-165.

Spry, P.G. & Wonder, J.D. 1989, 'Manganese-rich garnet rocks associated with the Broken Hill lead-zinc-silver deposit, New South Wales, Australia', *The Canadian Mineralogist,* vol. 27, pp. 275-292.

SPSS Inc 2009, *Predictive analytics software (PASW) statistics* 17.0.2 edn, IBM Company, Chicago, p. Statistical package for the social sciences <http://www.spss.com>.

Stanley, C.R. 1988, 'Comparison of data classification procedures in applied geochemistry using Monte Carlo simulation', PhD thesis, The University of British Columbia, Vancouver.

Stanley, C.R. & Sinclair, A.J. 1989, 'Comparison of probability plots and gap statistics in the selection of threshold for exploration geochemistry data', *Journal of Geochemical Exploration,* vol. 32, no. 1-3, pp. 355-357.

StatSoft Electronic Statistics Textbook 2010, *Correspondence Analysis*, StatSoft Inc., viewed 18/4/2009 <http://www.statsoft.com/textbook/correspondence-analysis/>.

Stevens, B.P.J. 1986, 'Post-depositional history of the Willyama Supergroup in the Broken Hill Block, NSW', *Australian Journal of Earth Sciences*, vol. 33, no. 1, pp. 73-98.

Stevens, B.P.J. 1998, 'The origins of Broken Hill rock types and their relevance to mineralisation. ', *Broken Hill Exploration Initiative, Fourth annual meeting,* vol. 25, ed. G.M. Gibson, Australian Geological Survey Organisation Record, Broken Hill, pp. 109-114.

Stevens, B.P.J. 1999, 'Evidence for multiple Palaeoproterozoic thermal events and magmatism adjacent to the Broken Hill Pb-Zn-Ag orebody, Australia: Discussion', *Precambrian Research,* vol. 98, no. 1-2, pp. 1-5.

Stevens, B.P.J. 2000, 'Evaluating models for tectonic development of the Willyama Supergroup', *Australian Geological Survey Organisation Record*, vol. 10, pp. 93-96.

Stevens, B.P.J. 2003, 'Understanding the Broken Hill Pb-Zn fluid system', *Broken Hill Exploration Initiative,* vol. 13, ed. M. Peljo, Geoscience Australia Record, Broken Hill, pp. 166-169.

Stevens, B.P.J. 2009, 'New interpretation maps of the Willyama Supergroup, Broken Hill, NSW', *Broken Hill Exploration Initiative*, vol. 28, ed. R.J. Korsch, Geoscience Australia Record, Broken Hill, pp. 201-208.

Stevens, B.P.J., Barnes, R.G., Brown, R.E., Stroud, W.J. & Willis, I.L. 1988, 'The Willyama Supergroup in the Broken Hill and Euriowie Blocks, New South Wales', *Precambrian Research*, vol. 40-41, pp. 297-327.

Stevens, B.P.J. & Barron, L.M. 2002, 'Volcanic textures in the Palaeoproterozoic Hores Gneiss, Broken Hill, Australia. New South Wales', *Geological Survey of New South Wales, Quarterly Notes*, vol. 113, pp. 1-22.

Stevens, B.P.J., Willis, I.L., Brown, R.E. & Stroud, W.J. 1983, 'The Early Proterozoic Willyama Supergroup: Definitions of stratigraphic units from the Broken Hill Block, New South Wales', vol. 21, no. 2, pp. 407-442.

Stevens, G., Prins, S. & Rozendaal, A. 2005, 'Partial melting of the assemblage sphalerite + galena + pyrrhotite + chalcopyrite + sulfur: Implications for high-grade metamorphosed massive sulfide deposits.', *Economic Geology*, vol. 100, no. 4, pp. 781-786.

Stilwell, F.L. 1959, 'Petrology of the Broken Hill lode and its bearing on ore genesis', *The Australasian Institute of Mining and Metallurgy, Proceedings*, vol. 190, pp. 1-84.

Swan, A.R.H. & Sandilands, M. 1995, *Introduction to geological data analysis,* Blackwell Science, Oxford.

Taylor, G.F., Wilmshurst, J.R., Togashi, Y. & Andrew, A.S. 1984, 'Geochemical and mineralogical haloes about the Elura Zn-Pb-Ag orebody, Western New South Wales', *Journal of Geochemical Exploration*, vol. 22, pp. 265-290.

Teale, G.S., '1:10,000 integrated mapping of the Moolawatana Domain by honours students', unpublished, The University of Melbourne.

Teil, H. & Cheminee, J.L. 1975, 'Application of correspondence factor analysis to the study of major and trace elements in the Erta Ale Chain (Afar, Ethiopia)', *Mathematical Geology*, vol. 7, no. 1, pp. 13-30.

Templ, M., Filzmoser, P. & Reimann, C. 2008, 'Cluster analysis applied to regional geochemical data: Problems and possibilities', *Applied Geochemistry*, vol. 23, no. 8, pp. 2198-2213.

Terry, R.D. & Chilingar, G.V. 1955, 'Summary of "concerning some additional aides in studying sedimentary formations" by M.S. Shavetsov', *Journal of Sedimentary Petrology*, vol. 25, no. 3, pp. 229-234.

The MathWorks Inc. 2006, *MATLAB* 7.2 (R2006a) edn, MathWorks Massachusetts, p. The language of technical computing <WWW.mathworks.com/patents>.

Thió-Henestrosa, S. 2008, *CoDaPack3D*, 1st edn, The University of Girona, Girona, p. Compositional data package <http://ima.udg.edu/~thio/>.

Tomkins, A.G., Pattison, D.R.M. & Frost, B.R. 2007, 'On the initiation of metamorphic sulfide anatexis', *Journal of Petrology,* vol. 48, no. 3, pp. 511-535.

Tonelli, M., Woodhead, J. & Hergt, J. 2003, 'Pb-Pb dating of garnet, staurolite and tourmaline by a stepwise dissolution technique', *Broken Hill Exploration Initiative,* vol. 13, ed. M. Peljo, Geoscience Australia Record, Broken Hill pp. 188-191.

Tukey, J.W. 1977, *Exploratory data analysis*, Reading, MA, Addison-Wesley.

Tully, R.B. 2002, 'Geology of the B Lode, A Lode and 1 Lens on CML7, Broken Hill, New South Wales', BSc (Honours) thesis, The University of Melbourne, Melbourne.

UCLA: ATS 2007, *SPSS FAQ, What does Cronbach's alpha mean?*, UCLA: Academic Technology Services, Statistical Consulting Group, viewed 24/8/2009 <http://www.ats.ucla.edu/stat/spss/faq/alpha.html>.

Valenchon, F. 1982, 'The use of correspondence analysis in geochemistry', *Mathematical Geology*, vol. 14, no. 4, pp. 331-342.

Van de Geer, J.P. 1993a, *Multivariate analysis of categorical data: Applications,* vol. 2, Sage Publications, Newbury Park.

Van de Geer, J.P. 1993b, *Multivariate analysis of categorical data: Theory*, Sage Publications, Newbury Park.

Vann, J., Jackson, S. & Bertoli, O. 2003, 'Quantitative kriging neighbourhood analysis for the mining geologist-a description of the method with worked case examples', *5th International Mining Geology Conference,* The Australasian Institute of Mining and Metallurgy, Bendigo, Victoria, pp. 215-223.

Vokes, F.M. 1971, 'Some aspects of the regional metamorphic mobilisation of pre-existing sulphide deposits', *Mineralium Deposita,* vol. 6, no. 2, pp. 122-129.

Walter, A.M., Christensen, S. & Simmelsgaard, S.E. 2002, 'Spatial correlation between weed species densities and soil properties', *Weed Research,* vol. 42, pp. 26-38.

Walters, S.G. 1996, 'From Broken Hill to Cannington-key elements in the discovery of a new Broken Hill type Ag-Pb-Zn deposit in the eastern succession of the Mount Isa Inlier', paper presented to the *13th Australian Geological Convention, Geoscience for the community*, Canberra.

Walters, S.G. 1998, 'Broken Hill-type deposits', *AGSO Journal of Australian Geology and Geophysics*, vol. 17, no. 4, pp. 229-237.

Walters, S.G. & Bailey, A. 1998, 'Geology and mineralization of the Cannington Ag-Pb-Zn deposit: An example of Broken Hill-type mineralisation in the Eastern Succession, Mount Isa Inlier, Australia', *Economic Geology*, vol. 93, no. 8, pp. 1307-1329.

Webster, A.E. 1993, 'Sulphide orebodies and structure: Mapping within an orebody and what it can tell you. An example from Broken Hill, NSW', *4th International Mining Geology Conference*, eds I. Robertson, W. Shaw, C. Arnold & K. Lines, Australian Institute of Mining and Metallurgy and the Australian Institute of Geoscientists, Kalgoorlie-Boulder, Western Australia, pp. 133-141.

Webster, A.E. 1996, 'A detailed description of the Broken Hill deposit: Lessons from the ore fabrics', *New developments in Broken Hill type deposits*, vol. 1, eds J. Pongratz & G.J. Davidson, The University of Tasmania, Centre for ore deposit and exploration studies (CODES) special publication Hobart, pp. 95-103.

Webster, R. & Oliver, M.A. 2007, *Geostatistics for environmental scientists* 2nd edn, John Wiley & Sons, Chichester.

Wellmer, F.W. 1998, *Statistical evaluations in exploration for mineral deposits,* Springer-Verlag Berlin Heidelberg, New York.

White, S.H., Rothery, E., Lips, A.W. & Barclay, T.J.R.B. 1995, 'Broken Hill base-metal deposit: A tectonically transported and modified basinal deposit within the Proterozoic Willyama Fold and Thrust Belt', *Transactions of the Institution of Mining and Metallurgy,* vol. 104, pp. B1-B17.

Wilcoxon, F. 1945, 'Individual comparisons by ranking methods', *Biometrics Bulletin*, vol. 1, pp. 80-83.

Willis, I.L., Brown, R.E., Stroud, W.J. & Stevens, B.P.J. 1983, 'The early Proterozoic Willyama supergroup: Stratigraphic subdivision and interpretation of high to low-grade metamorphic rocks in the Broken Hill Block, New South Wales', *Australian Journal of Earth Sciences,* vol. 30, no. 1-2, pp. 195-224.

Wonder, J.D., Spry, P.G. & Windom, K.E. 1988, 'Geochemistry and origin of manganese-rich rocks related to iron-formation and sulfide deposits, western Georgia', *Economic Geology,* vol. 83, no. 5, pp. 1070-1081.

Xu, C. & Dowd, P.A. 2001, 'Orebody modelling by optimal surface reconstruction', *Transactions of the Institution of Mining and Metallurgy Section B-Applied Earth Science*, vol. 110, no. 2, pp. B110-B120.

Yaffee, R.A. 2003, 'Common Correlation and Reliability Analysis with SPSS for Windows', viewed 22/4/2008 <http://www.nyu.edu/its/statistics/Docs/correlate.html>.

Yamashita, K., Creaser, R.A. & Villeneuve, M.E. 2000, 'Integrated Nd isotopic and U-Pb detrital zircon systematics of clastic sedimentary rocks from the Slave Province, Canada: Evidence for extensive crustal reworking in the early-to mid-Archean', *Earth and Planetary Science Letters*, vol. 174, no. 3-4, pp. 283-299.

Yarus, J.M. & Chambers, R.L. (eds) 1994, *Stochastic modelling and Geostatistics*: *Principles, methods, and case studies*: *Computer applications in geology,* vol. 3, American Association of Petroleum Geologists, Tulsa, Oklahoma.

Yund, R.A. & Hall, H.T. 1969, 'Hexagonal and monoclinic pyrrhotites', *Economic Geology,* vol. 64, pp. 420-423.

Zapletal, K. 1992, 'Self-reversal of isothermal remnant magnetization in a pyrrhotite (Fe_7S_8) crystal', *Physics of the Earth and Planetary Interiors*, vol. 70, no. 3-4, pp. 302-311.

Zhao, J. & McCulloch, M.T. 1993, 'Sm-Nd mineral isochron ages of Late Proterozoic dyke swarms in Australia: Evidence for two distinctive events of mafic magmatism and crustal extension', *Chemical Geology*, vol. 109, no. 1-4, pp. 341-345.

Ziaii, M., Pouyan, A.A. & Ziaei, M. 2009, 'Neuro-fuzzy modelling in mining geochemistry: Identifications of geochemical anomalies', *Journal of Geochemical Exploration*, vol. 100, pp. 25-26.